

Peter R. Hoskins · Patricia V. Lawford
Barry J. Doyle *Editors*

Cardiovascular Biomechanics

 Springer

Editors

Peter R. Hoskins, Patricia V. Lawford and Barry J. Doyle

Cardiovascular Biomechanics

 Springer

Editors

Peter R. Hoskins

Centre for Cardiovascular Science, Queens Medical Research Institute,
University of Edinburgh, Edinburgh, UK

Patricia V. Lawford

Department of Infection, Immunity and Cardiovascular Disease/Insigneo
Institute for in silico Medicine, University of Sheffield, Sheffield, UK

Barry J. Doyle

School of Mechanical and Chemical Engineering, University of Western
Australia, Perth, WA, Australia

ISBN 978-3-319-46405-3 e-ISBN 978-3-319-46407-7

DOI 10.1007/978-3-319-46407-7

Library of Congress Control Number: 2016950902

© Springer International Publishing Switzerland 2017

This work is subject to copyright. All rights are reserved by the Publisher, whether the whole or part of the material is concerned, specifically the rights of translation, reprinting, reuse of illustrations, recitation, broadcasting, reproduction on microfilms or in any other physical way, and transmission or information storage and retrieval, electronic adaptation, computer software, or by similar or dissimilar methodology now known or hereafter developed.

The use of general descriptive names, registered names, trademarks, service marks, etc. in this publication does not imply, even in the absence of a specific statement, that such names are exempt from the relevant protective laws and regulations and therefore free for general use.

The publisher, the authors and the editors are safe to assume that the advice

and information in this book are believed to be true and accurate at the date of publication. Neither the publisher nor the authors or the editors give a warranty, express or implied, with respect to the material contained herein or for any errors or omissions that may have been made.

Printed on acid-free paper

This Springer imprint is published by Springer Nature
The registered company is Springer International Publishing AG
The registered company address is: Gewerbestrasse 11, 6330 Cham,
Switzerland

Preface

This book is concerned with cardiovascular biomechanics; this is the study of the function and the structure of the cardiovascular system using the methods of mechanics. It has become clear that this area lies at the heart of all the major cardiovascular diseases such as atherosclerosis and aneurysms; diseases which are responsible for some one-third of world's deaths. The underpinning principle which will be referred to several times in this book is that the cardiovascular system adapts in order to normalise its own mechanical environment. The cardiovascular system is able to do this because mechanical forces are sensed by tissues, and deviations from 'normal' result in biological changes which affect structure. The study of cardiovascular biomechanics therefore requires an interdisciplinary approach involving biology, medicine, physics, engineering and mathematics. This book is an introductory text suitable for students and practitioners in all these different fields. The book is suitable as a textbook to accompany a final-year undergraduate or masters (M.Sc.) course with roughly one or two lectures per chapter. It is also suitable as a first text for researchers and practitioners in cardiovascular biomechanics. The book is divided into four main sections; introductory Chaps. 1 – 2, Chaps. 3 – 8 on biomechanics of different components of the cardiovascular system, Chaps. 9 – 13 on methods used to investigate cardiovascular biomechanics (in clinical practice and research), and Chaps. 14 – 17 written from a perspective of diseases and interventions. There are two appendixes; one with questions for each chapter (multiple-choice questions, short-answer and long-answer questions), one with a glossary of 900+ terms. In order that the book is accessible by a mixed audience the text concentrates on explanations of physical principles without the use of complex mathematics. A few simple equations are used and there are no derivations of equations. The book is heavily illustrated with examples drawn from modern investigative techniques including medical imaging and computational modelling. Cardiovascular biomechanics is a field that continues to evolve. Each chapter includes a number of key references so that the interested reader can use this book as a bridge to the research literature.

Peter R. Hoskins
Patricia V. Lawford
Barry J. Doyle

Edinburgh, UK, Sheffield, UK, Perth, WA, Australia
Summer 2016

Contents

1 Introduction to Solid and Fluid Mechanics

Peter R. Hoskins

2 Introduction to Cardiovascular Biomechanics

Peter R. Hoskins

3 Blood and Blood Flow

Peter R. Hoskins and David Hardman

4 The Arterial System I. Pressure, Flow and Stiffness

Peter R. Hoskins and D. Rodney Hose

5 The Arterial System II. Forces, Adaptability and Mechanotransduction

Peter R. Hoskins

6 Excitation-Contraction in the Heart

Richard H. Clayton and D. Rodney Hose

7 The Venous System

Andrew J. Narracott

8 The Microcirculation

Peter R. Hoskins

9 Medical Imaging

Peter R. Hoskins, Stephen F. Keevil and Saeed Mirsadraee

10 Modelling of the Cardiovascular System

D. Rodney Hose and Barry J. Doyle

11 Patient Specific Modelling

Peter R. Hoskins, Noel Conlisk, Arjan J. Geers and Barry J. Doyle

12 Flow Phantoms

Peter R. Hoskins

13 Measurement of the Mechanical Properties of Biological Tissues

Barry J. Doyle, Ryley A. Macrae and Peter R. Hoskins

14 Hypertension

Peter R. Hoskins and Ian B. Wilkinson

15 Atherosclerosis

Peter R. Hoskins and Patricia V. Lawford

16 Aneurysms

Barry J. Doyle and Peter R. Hoskins

17 Cardiovascular Prostheses

Patricia V. Lawford

Appendix A: Questions

Appendix B: Glossary

Index

Contributors

Richard H. Clayton

University of Sheffield, Sheffield, UK

Noel Conlisk

Edinburgh University, Edinburgh, UK

Barry J. Doyle

University of Western Australia, Perth, WA, Australia

Arjan J. Geers

Edinburgh University, Edinburgh, UK

David Hardman

Castlebrae Community High School, Edinburgh, UK

D. Rodney Hose

University of Sheffield, Sheffield, UK

Peter R. Hoskins

Edinburgh University, Edinburgh, UK

Stephen F. Keevil

Guy's and St Thomas' NHS Foundation Trust, Kings College London,
London, UK

Patricia V. Lawford

Sheffield University, Sheffield, England, UK

Ryley A. Macrae

University of Western Australia, Perth, WA, Australia

Saeed Mirsadraee

Royal Brompton Hospital London, London, UK

Andrew J. Narracott
Sheffield University, Sheffield, UK

Ian B. Wilkinson
Cambridge University, Cambridge, UK

1. Introduction to Solid and Fluid Mechanics

Peter R. Hoskins¹✉

(1) Edinburgh University, Edinburgh, UK

✉ **Peter R. Hoskins**
Email: P.Hoskins@ed.ac.uk

Learning outcomes

1. Explain the difference between a solid and a fluid.
2. Describe features of stress–strain behaviour of a solid measured using a tensile testing system.
3. Explain stress–strain behaviour of biological and non-biological materials in terms of their composition.
4. Define Young’s modulus.
5. Describe the measurement of Young’s modulus using a tensile testing system.
6. Discuss values of Young’s modulus for non-biological and biological materials.

7. Define Poisson ratio and discuss values for different materials.
8. Describe viscoelasticity, its effect on stress–strain behaviour, and models of viscoelasticity.
9. Discuss linear elastic theory and its applicability to biological tissues.
10. Define hydrostatic pressure and values in the human.
11. Define viscosity in terms of shear stress and shear rate.
12. Describe different viscous behaviours.
13. Describe measurement of viscosity.
14. Describe typical measures of viscosity for different fluids.
15. Discuss Poiseuille flow: pressure-flow relationships for flow of Newtonian fluid through a cylinder.
16. Discuss Reynolds number and flow states.
17. Discuss pressure-flow relationships in unsteady flow in cylindrical tubes.
18. Discuss energy considerations in flow including the Bernoulli equation.

An understanding of the functioning of the cardiovascular system draws heavily on principles of fluid flow and of the elastic behaviour of tissues. Indeed, much of the cardiovascular system consists of a fluid (blood), flowing in elastic tubes (arteries and veins). This chapter will introduce basic principles of fluid flow and of solid mechanics. This area has developed over many centuries and Appendix 1 provides details of key scientists and their

contribution.

The concept of a fluid and a solid is familiar from everyday experience. However, from a physics point of view, the question arises as to what distinguishes a fluid from a solid? For a cubic volume element there are two types of forces which the volume element experiences (Fig. 1.1); a force perpendicular to a face and a force in the plane of a face. The forces perpendicular to the face cause compression of the material and this is the case whether the material is liquid or solid. The force parallel to the face is called a shear force. In a solid, the shear force is transmitted through the solid and the solid is deformed or sheared. The shear force is resisted by internal stresses within the solid and, provided the force is not too great, the solid reaches an equilibrium position. At the nano level the atoms and molecules in the solid retain contact with their neighbours. In the case of a fluid, a shear force results in continuous movement of the material. At the nano level the atoms and molecules in the fluid are not permanently connected to their neighbours and they are free to move. The key distinction between a fluid and a solid is that a solid can sustain a shear force whereas a fluid at rest does not.

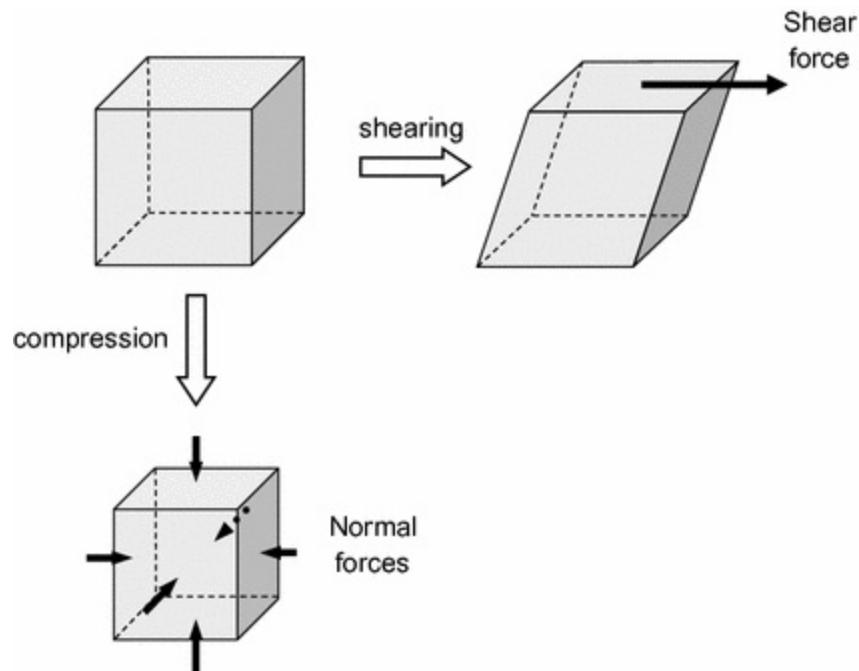


Fig. 1.1 A cube of material is subject to force parallel to a face which cause shearing and forces normal to each face which cause compression

1.1 Solid Mechanics

Solid mechanics is concerned with the relationship between the forces applied to a solid and the deformation of the solid. These relationships go by the name of the ‘constitutive equations’ and are important in areas such as patient-specific modelling discussed in Chap. 11. In general, these relationships are complex. For small deformations many materials deform linearly with applied force, which is fortunate as both experimental measurement and theory are relatively straightforward. This section on solid mechanics will start with 1D deformation of a material, develop linear elastic theory, then describe more complex features including those of biological materials.

1.1.1 1D Deformation

The elastic behaviour of a material is commonly investigated using a tensile testing system. A sample of the material is clamped into the system and then stretched apart. Both applied force and deformation are measured and can be plotted. Figure 1.2 shows the force-extension behaviour for steel. For many materials, such as steel and glass, the initial behaviour is linear; a doubling of applied force results in a doubling of the extension. In this region the material is elastic in that it will follow the same line on the force-extension graph during loading or unloading. The material is elastic up to the point Y, which is called the ‘yield point’ but, after the yield point, the slope of the line decreases. The material is softer in that small changes in force result in large changes in extension. Beyond the yield point the material becomes plastic in that the material does not return to its original shape after removal of the force but is permanently deformed. In Fig. 1.2 further increase in force eventually leads to fracturing of the material at the point U, called the ‘ultimate tensile strength’ (UTS).

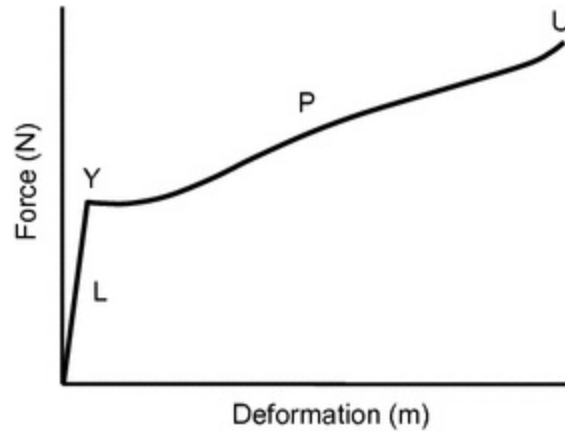


Fig. 1.2 Force-extension curve for steel. *L* linear behaviour; *Y* yield point; *P* plastic deformation; *U* (uniaxial) ultimate strength. Redrawn from Wikipedia under a GNU free documentation licence; the author of the original image is Bbanerje. <https://commons.wikimedia.org/wiki/File:Hyperelastic.svg>

The force-deformation behaviour can be understood at the atomic level. The chemical bonds between atoms and molecules are deformable and small deformations from the equilibrium position can be tolerated without change in structure. The equations governing the force-extension behaviour at the atomic level demonstrate linear behaviour and the macroscopic behaviour of a material is the composite of a multitude of interactions at the atomic and molecular level. In the plastic region there are changes in structure at the atomic and molecular level. In many materials this arises through slip processes involving the movement of dislocations or through the creation and propagation of cracks.

Biological materials are generally composite in nature. From a mechanical point of view the most important components are collagen fibres, elastin, reticulin and an amorphous, hydrophilic, material called ‘ground substance’ which contains as much as 90 % water. The elastic behaviour of the biological tissue is determined by the proportion of each component and by their physical arrangement. For example, collagen fibres in the wall of arteries are arranged in a helical pattern. Collagen is especially important in determining mechanical properties of soft biological tissues. Collagen is laid down in an un-stretched state. These unstressed fibres have a wavy, buckled shape, referred to as ‘crimp’. On application of a force, the fibres begin to straighten and the ‘crimp’ disappears and, as a result, the tissue deforms relatively easily. With increasing extension the fibres straighten fully and resist the stretch. This leads to collagen having a non-linear force-extension behaviour, which explains the non-linear force-extension behaviour of most

biological soft tissues.

A simple 1D tensile testing system can also be used to demonstrate viscoelasticity. It was stated above that in elastic behaviour the loading and unloading curves are the same. For a viscoelastic material they are different. In elastic behaviour the application of a force results more or less immediately in deformation of the material. Viscoelastic behaviour is associated with a time-lag between the applied force and the resulting deformation. The term 'viscoelastic' implies that the material has a mix of elastic and viscous properties. If the tensile testing system stretches the material in a cyclic manner, then as the tissue is loaded and unloaded, the resulting force-deformation curve will be in the shape of an ellipse (Fig. 1.3). During loading the force increases but the extension increases more slowly. During unloading the force decreases but the extension decreases more slowly. If the viscous component is low compared to the elastic component then the loading and unloading curves will be close together. For materials with a higher viscous component the curves are more separated and the width of the ellipse is larger.

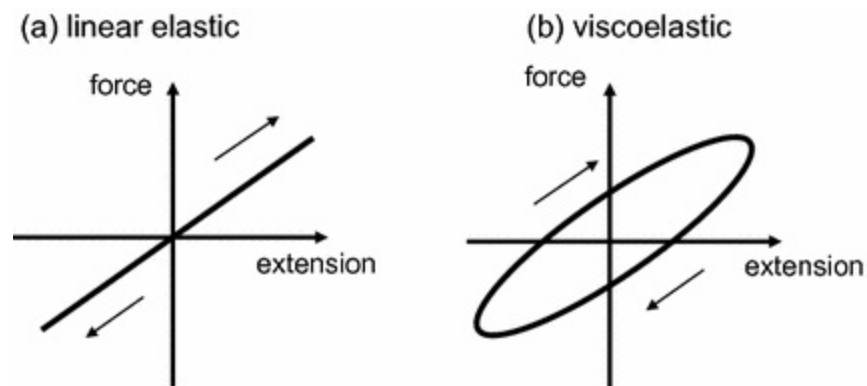


Fig. 1.3 Force-extension curves for cyclically varying force. **a** For a pure linear elastic material the loading and unloading curves are identical. **b** For a viscoelastic material the loading and unloading curves are different and are part of a loop

1.1.2 Young's Modulus

In Sect. 1.1.1 the discussion of elastic behaviour was in terms of applied force and deformation. However the quantities stress and strain are more widely used in theory and experiment. The stress, σ , is the force, F , per unit area, A , and has units of pascals. The strain, ϵ , is the ratio of the extension, δl , divided by the original length, l , and is a dimensionless quantity.

$$\sigma = \frac{F}{A} \quad (1.1)$$

$$\varepsilon = \frac{\delta l}{l} \quad (1.2)$$

The Young's modulus, E , is a measure of the elastic behaviour of a material and is a fundamental mechanical property. Young's modulus is the ratio of stress divided by strain (Eq. 1.3). The units of E are pascals (Pa) or newtons per square metre (N m^{-2}).

$$E = \frac{\sigma}{\varepsilon} \quad (1.3)$$

Young's modulus is commonly measured using a tensile testing system. The value E is equal to the slope of the line on the stress–strain plot. For a linear elastic material the slope is constant over much of the range of stress/strain and the mechanical properties of the material may be described by a single value of E . For non-linear materials such as rubber or soft biological tissues, the value of E is dependent on the strain. For such materials the 'incremental elastic modulus' may be defined as the change in stress over the change in strain over a small section of the stress–strain curve (Eq. 1.4).

$$E_{\text{inc}} = \frac{\Delta\sigma}{\Delta\varepsilon} \quad (1.4)$$

Figure 1.4 shows the Young's modulus of a number of common materials. Note that the scale is logarithmic with a range of 9 orders of magnitude. Hard materials such as ceramics, metals and glasses have very high values of elastic modulus. These are usually quoted in gigapascals (GPa). Wood and wood products have lower values of elastic modulus, but still have a very wide range from very hard woods such as oak, to very soft woods such as balsawood. Rubbers also have a very wide range from the hard vulcanised rubber used in tyres to the soft silicone rubber used in baby's dummies. The lowest elastic moduli values on the graph are for materials that mimic soft tissue used in phantoms for testing medical imaging systems. These are designed to mimic key properties of soft biological tissues, such as fat and muscle, and have low elastic modulus values in the range 2–500 kPa. Figure 1.5 shows the Young's modulus of a number of different biological tissues, taken from Sarvazyan et al. (1998). Again, there is a huge range of values. Bone and tooth enamel have the highest values of elastic modulus; liver, muscle and fat the lowest values.

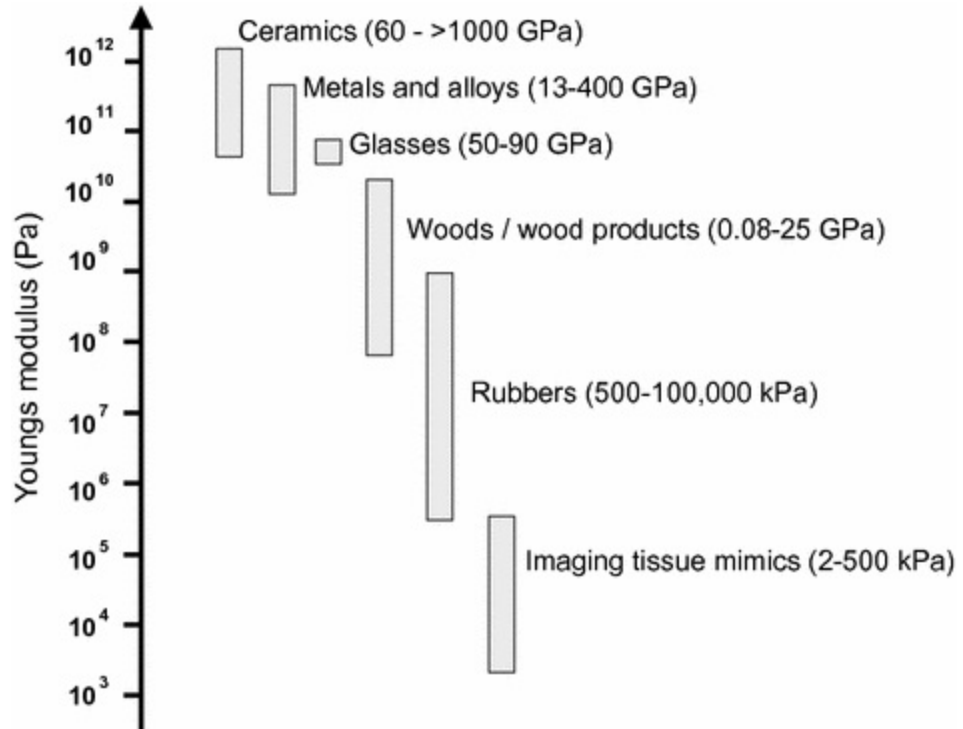


Fig. 1.4 Young's modulus E of common materials

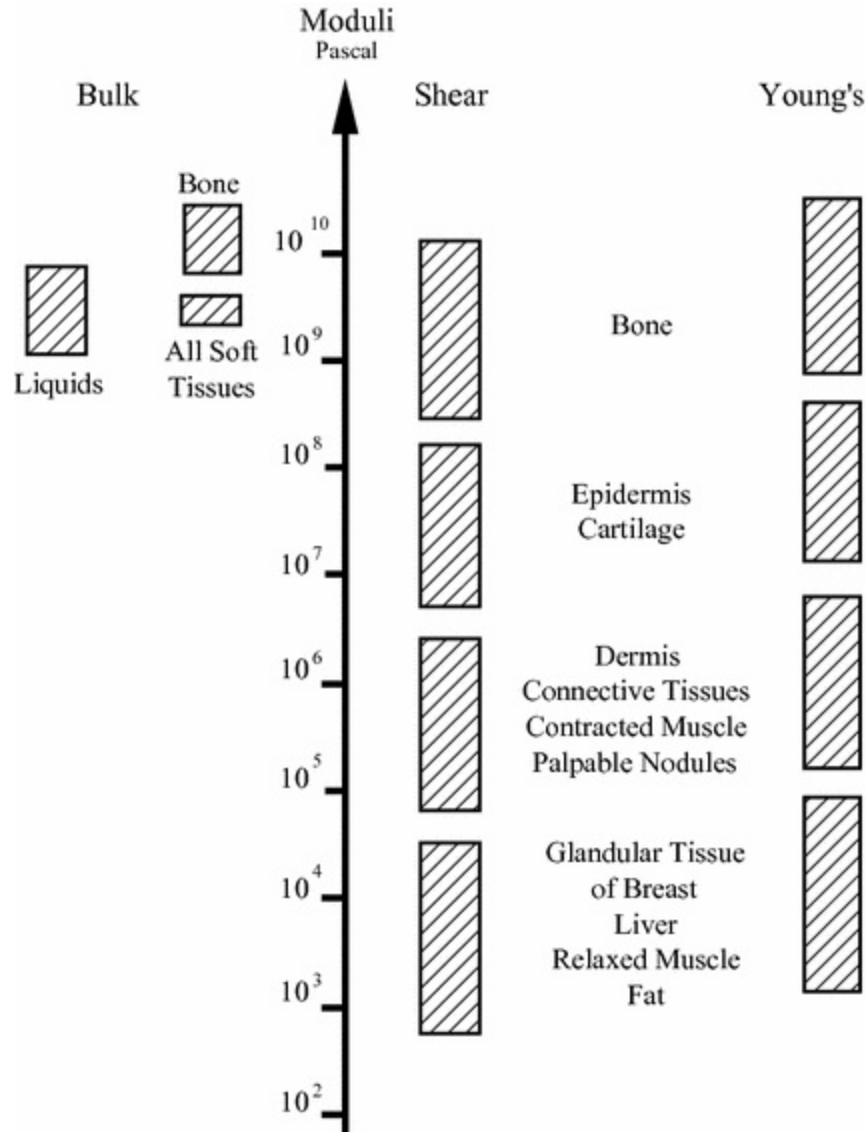


Fig. 1.5 A summary of data from the literature concerning the variation of the shear modulus, Young's modulus and bulk modulus for various materials and body tissues. Reproduced from Sarvazyan et al. (1995), with permission of Springer

The observant reader might have noted that it has been stated that the constitutive equations for soft biological tissues are complex and that the stress–strain behaviour is non-linear. How then is it justified in reporting Young's modulus, which generally applies to simple materials with linear stress–strain behaviours? This question will be addressed in Sect. 1.1.8; after more complex constitutive models have been considered.

1.1.3 Poisson's Ratio

When a material is stretched in the z direction there is usually compression in the x and y directions, and when a material is compressed there is usually expansion in the other two directions. This is called the Poisson effect. The Poisson ratio ν is given by the fractional change in length in the x direction divided by the fractional change in length in the z direction (Eq. 1.5).

$$\nu = \frac{\delta x/x}{\delta z/z} \quad (1.5)$$

For incompressible materials, that is, materials where the volume does not change when loaded, the Poisson ratio has a value of 0.5. Soft biological tissues contain large amounts of water and have Poisson values close to 0.5. For many materials such as metals, glasses and concrete, the Poisson value is in the range 0.2–0.4.

1.1.4 Models of Viscoelastic Behaviour

Elasticity and viscosity can be represented by a spring and a dashpot. The spring responds immediately to being stretched, which represents the purely elastic behaviour of a material. For a dashpot, there is a delay between the stretching force and the extension, which represents the viscous behaviour of a material. A viscoelastic material can be represented as a combination of a spring and a dashpot and there are various configurations, three of which are shown in Fig. 1.6. These are; the Maxwell model where the spring and the dashpot are in series, the Voigt model where the spring and the dashpot are in parallel and a model consisting of two springs and a dashpot. Figure 1.6 also shows the behaviour of each of these models. For the Maxwell model there is a sudden extension which corresponds to the spring stretching immediately followed by a linear increase caused by the dashpot slowly extending. For the Voigt model there is a gradual increase in the deformation. For the 3-parameter model, there is a sudden extension followed by a gradual extension. In practice, for a particular material, the model which best describes the experimentally determined behaviour of the material is chosen.

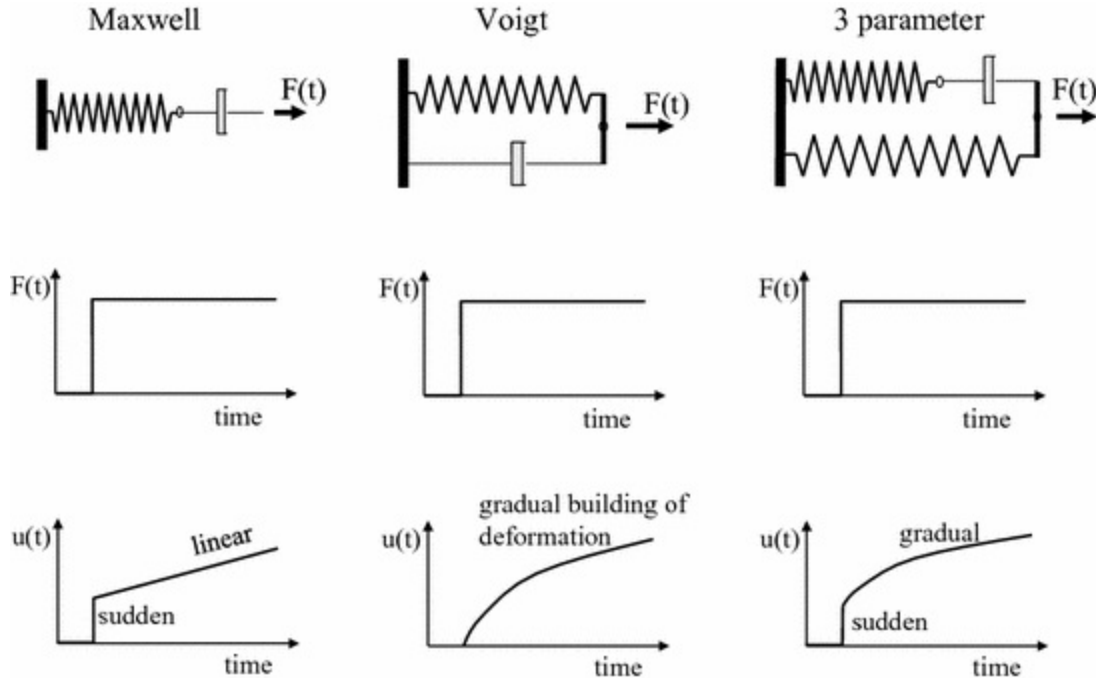


Fig. 1.6 Top row models of viscoelastic behaviour using combinations of a spring (elasticity) and dashpot (viscosity); Maxwell model, Voigt model, 3-parameter model. Middle row a sudden force is applied to the tissues. Bottom row The distension u is shown as a function of time for each model

1.1.5 Linear Elastic Theory (Isotropic)

The Young's modulus and the Poisson ratio are two examples of parameters which describe the elastic behaviour of materials. In this section other parameters will be defined. In order to simplify things, the approach is taken of assuming that the material is linear elastic with no viscous components. It will also be assumed that the material is isotropic (having the same behaviour in all directions).

The bulk modulus, B , describes the ability of the material to resist a change in volume. A cube of material of volume, V , is subjected to a pressure, P , (Fig. 1.7a). The pressure increases by a small amount, δP . This leads to a reduction in volume by a small amount, δV . The bulk modulus is the change in pressure divided by the change in volume.

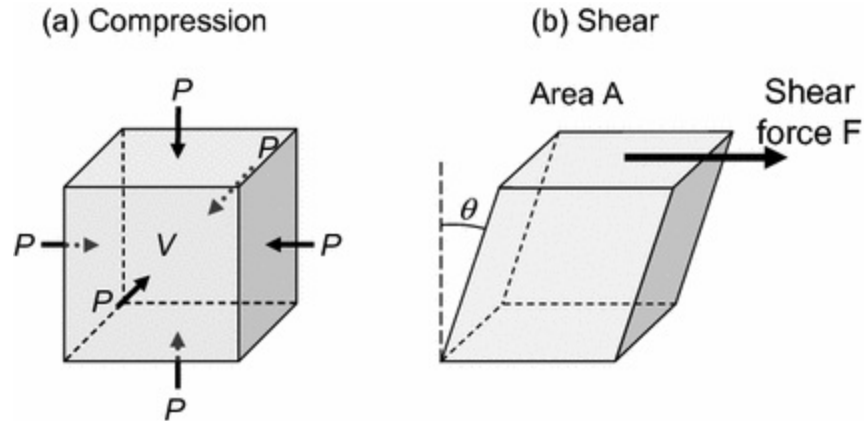


Fig. 1.7 **a** Compression—the cube of volume V is subject to a pressure P on all faces. **b** Shear—the cube is subject to a force F on one face which causes the cube to shear by an angle θ

$$B = -\frac{\delta P}{\delta V} \quad (1.6)$$

The shear modulus, G , describes the ability of a material to withstand a shearing force (Fig. 1.7b). The shear modulus is the shear stress divided by the shear strain.

$$G = \frac{F/A}{\tan(\theta)} \quad (1.7)$$

For the simple elastic material described in this section, G and E are related by Eq. (1.8) which involves both E and the Poisson ratio ν . If the material is also incompressible, then Poisson's ratio ν is 0.5 and the equation simplifies (Eq. 1.9).

$$G = \frac{E}{2(1 + \nu)} \quad (1.8)$$

$$G = \frac{E}{3} \quad (1.9)$$

Figure 1.5 shows values of G and B , along with E , for biological tissues. The range of values for bulk modulus is about one order of magnitude, whereas those for shear modulus and Young's modulus range over 7 orders of magnitude.

For the material described in this section, linear elastic isotropic, there are four parameters which describe elastic behaviour; Young's modulus E , Poisson ratio ν , bulk modulus B and shear modulus G . However, only 2 of these are independent. In other words knowledge of 2 of these quantities (for example Poisson ratio and bulk modulus) allows estimation of the other 2

(Appendix 2).

1.1.6 Linear Elastic Theory (Generalised)

The theory described in the previous section will be developed further, but without the constraint of isotropy. So far the theory has been developed by considering mainly stress and deformation in 1D. However in most cases, the behaviour applies in 3D and the solid will deform in all three directions.

Figure 1.8 shows the forces in 1 dimension for stretching of a column of material, in 2D for a square of material and in 3D for a cube. For the column of material there is a single extension force. For the square, each face has a force perpendicular to the face and also a shear force. For the cube, each face has a perpendicular force and two shear forces. The types of deformation which result are shown in the lower images. The number of stress and strain components needed to describe behaviour increases from 1D to 3D. For 1D it is just one stress and one strain. For 2D four components are needed and for 3D nine components are needed. Much more data is needed to describe behaviour in 3D than in 2D or 1D.

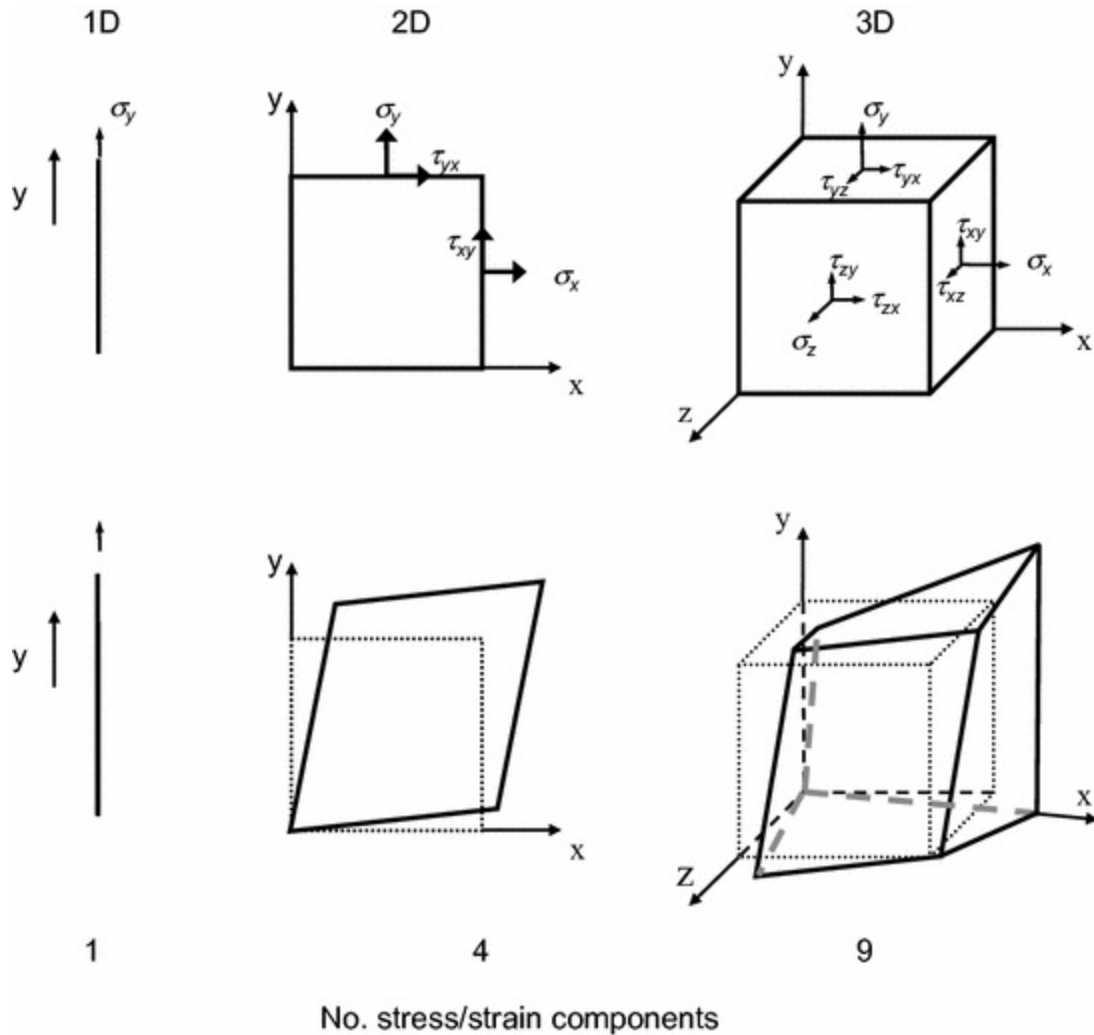


Fig. 1.8 Forces on a solid in 1D, 2D and 3D, and typical deformations. The number of stress and strain components needed to fully describe behaviour is 1 for 1D, 4 for 2D and 9 for 3D

Table 1.1 shows the number of elastic constants required for the constitutive model as a function of the number of dimensions and of the degree of anisotropy. The most general case is a material which is fully anisotropic; behaviour in x , y and z is different. An orthotropic material has at least two planes of symmetry. An example of an orthotropic material might be a section of tree showing concentric rings. The third case is an isotropic material. The table shows the number of elastic constants that are needed for 1D, 2D and 3D constitutive models. For 1D deformation only one constant is needed, the Young's modulus E . The number of constants needed increases as the model becomes more complex and as the number of dimensions increases so that for a 3D anisotropic constitutive model, 21 elastic constants

are needed. Complex constitutive models require measurements of many elastic constants, which is challenging.

Table 1.1 Number of elastic constants required as a function of the number of physical dimensions and the degree of isotropy

	1D	2D	3D
Anisotropic	1	9	21
Orthotropic	1	5	9
Isotropic	1	2	2

1.1.7 Constitutive Models for Non-linear Elasticity

It has been stated above that many biological materials are not described by linear stress–strain behaviour and instead are non-linear. A number of constitutive models have been developed which give non-linear behaviour. Models based on hyperelastic behaviour are widely used (Fig. 1.9); discussed further in e.g. Humphrey (2002). The number of constants varies from one model to the next, one parameter for the Neo-Hookean model, 2 for the Mooney-Rivlin model, three for the Yeoh model and so on. Generally, the constitutive model is developed which fits the experimentally determined data.

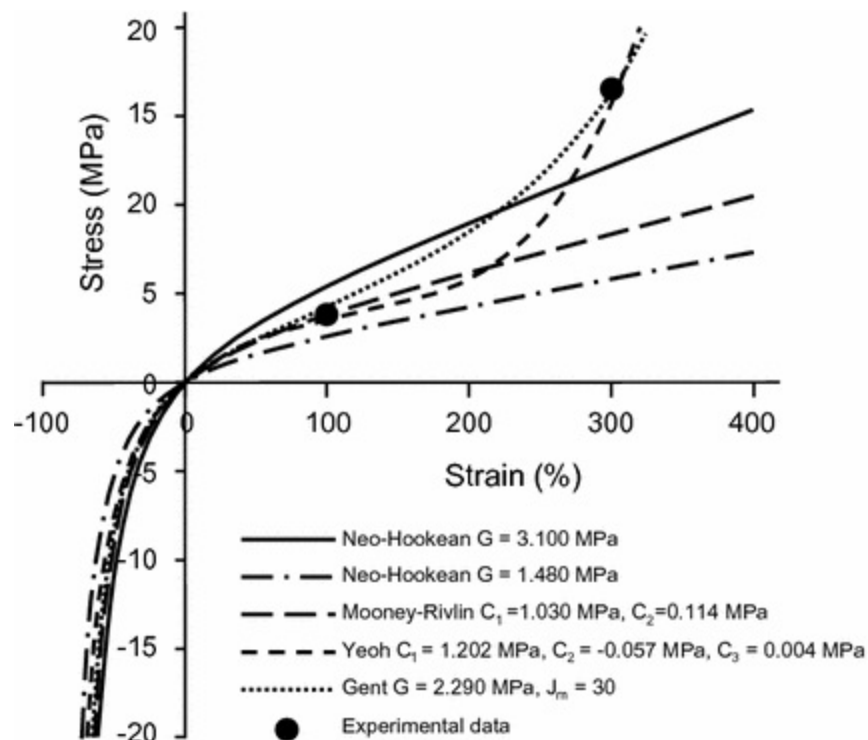


Fig. 1.9 Stress–strain curves for different hyperelastic constitutive models; redrawn from Wikipedia, author Bbanerje, under the GNU free documentation licence

1.1.8 Materials in Practice

The linear elastic constitutive models described in the last two sections are actually relatively simple. Many materials are complex. They may be non-homogeneous and contain internal structures, be anisotropic, or have non-linear elastic, viscoelastic and plastic behaviour depending on the stress and strain. Many biological materials exhibit all of the above characteristics. In general constitutive equations are complex. Constitutive models such as these require advanced mathematics and are not covered in this book. The interested reader is referred to texts by Humphrey (2002), Cowin and Humphrey (2001), Cowin and Doty (2007) and Holzapfel and Ogden (2006). In practice, simplified constitutive models are often used, especially in medical use. There are various reasons for this; most importantly being the reduced number of necessary parameters, which in turn are easier to measure experimentally and make the models computationally less expensive and easier to understand.

An example of this simplification is the reporting of Young's modulus values for biological tissues (as shown in Fig. 1.5) even when the linear elastic constitutive model is recognised as being inappropriate compared to more complex models, such as, for example, a hyperelastic model. There may be several reasons for this simplification. Linear elastic theory is easy to understand whereas hyperelastic theory is more difficult. There are many different hyperelastic models, whereas there is only one linear elastic theory. There is only one constant, Young's modulus, which allows comparison of results between different papers. Different viscoelastic models use different constants so it is harder to compare data from different studies. Young's modulus is easy to measure experimentally, whereas viscoelastic models with several parameters require more complicated measurements.

An important consideration, which will be discussed in Chaps. 10 and 11, is the complexity of constitutive models required for estimation of data from computational modelling. When idealised tissue geometries are used, it is possible to specify in microscopic detail the microstructure of the arterial wall, including collagen fibre orientation and the associated mechanical properties. In this case, it is possible to use more complex constitutive models. However when data from the individual patient is used, it is not

possible to obtain detailed information on geometry at the microscopic level from medical images, and it is not possible to measure, in the individual patient, the many different elastic constants. In this case, it is common practice to use quite simple constitutive models in which only 1–2 elastic constants are used.

1.2 Fluid Mechanics

Fluid mechanics is the study of fluids and the forces acting on them. It is divided into fluid statics, which is the study of fluids at rest and fluid kinematics, which is the study of fluids in motion. The principle fluid of interest in the cardiovascular system is blood, and later chapters will deal specifically with blood and blood flow. This section will describe the general principles of fluid mechanics, using illustrations from blood flow where relevant.

1.2.1 Hydrostatic Pressure

The pressure in a fluid is dependent on depth within the fluid

$$P_d = P_o + \rho g d \quad (1.10)$$
where, P_d is the pressure at depth d , P_o is the pressure at the surface, g is the gravitational constant and ρ is the density of the fluid. The excess pressure, $\rho g d$, is called the hydrostatic pressure. Hydrostatic pressure arises because of the effect of gravity; the weight of the fluid produces a force which operates in a downward direction. This produces a pressure gradient, which operates in an upward direction. In the case of a static fluid (e.g. a puddle or water in a bath) these two forces balance each other.

The average person is some 1.8 m tall and, when standing, there will be a variation in pressure in the cardiovascular system arising from the hydrostatic pressure. The overall pressure difference from the head to the toes is 136 mmHg; from the heart to the toes is around 100 mmHg. This is the minimum pressure (for a person of 1.8 m height) which the heart must provide in order to lift blood from the toes to the heart. It will be seen in later chapters that the maximum pumping pressure of the heart (systolic pressure) in a healthy individual is typically just slightly more than this minimum value at around 120 mmHg (but increasing with age). This pressure gradient arising from gravity is considerably reduced when the person lies down, where the

head, heart and toes are all in the same vertical plane.

1.2.2 Shear Force and Strain Rate

A fluid is unable to retain an unsupported shape. A fluid will flow, taking up the shape of the container and coming to rest. Deformation of the fluid occurs as a result of shear forces. It was noted above that a solid can sustain a shear force whereas a fluid deforms under the action of a shear force. In a fluid at rest, there is no movement and hence no shear forces are present.

For a solid, a shear force will cause a strain (represented by the angle θ in Fig. 1.7); the larger the shear force then the larger the strain. The constitutive model for a solid concerns the relationship between shear force and strain. In contrast, for a liquid, application of a shear force results in an increase in the strain with time (larger angle θ —Fig. 1.10). The constitutive equations for a liquid concern the relationship between shear force and rate of change of strain (strain rate).

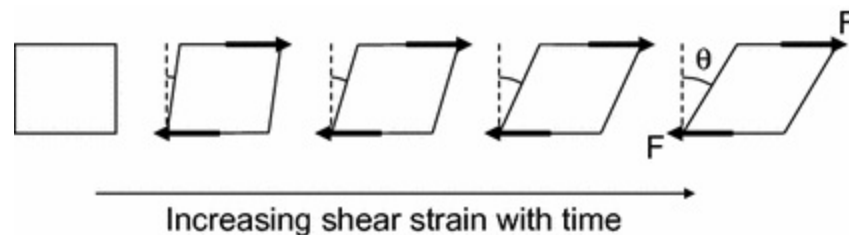


Fig. 1.10 In a liquid a shear force results in increasing strain with time; i.e. increase in the angle θ

1.2.3 Viscosity

Usually fluid motion is of interest with respect to a boundary or wall (Fig. 1.11). The velocity v of the fluid alters with distance y from the wall due to frictional forces within the fluid and between the fluid and the boundary. At the wall, the fluid velocity is zero and the velocity increases with distance from the wall. The variation in velocity with distance is called the shear rate (dv/dy). The viscosity μ is defined as the ratio of the shear stress τ to the shear rate (Eq. 1.11).

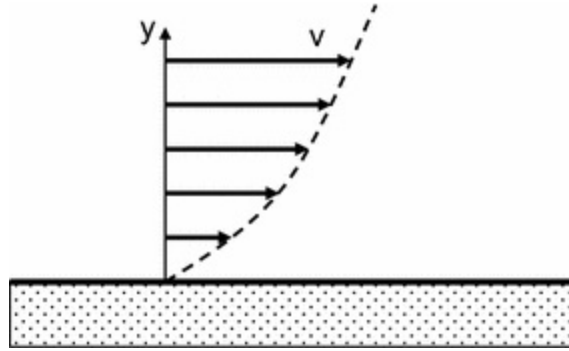


Fig. 1.11 Effect of a surface (wall) on fluid velocity. The velocity at the wall is zero and there is a change in velocity with distance from the wall

$$\mu = \frac{\tau}{dv/dy} \quad (1.11)$$

Viscosity is a fundamental property of a fluid. It describes the ability of the fluid to resist deformation by a shear force, and the viscosity has a major role in defining the velocity values near to surfaces.

The viscosity of a fluid may be measured using a variety of techniques with instruments called ‘viscometers’. Commonly, a cone plate viscometer is used which consists of a flat circular plate and a moving circular plate in the shape of a cone positioned above the flat plate. The fluid is introduced into the space between the plates and the upper plate is spun at increasingly high speeds. From the rotational speed the shear rate is calculated. Figure 1.12 shows plots of shear stress versus shear rate for a variety of different fluids along with the corresponding plots of viscosity versus shear rate. The different types of fluid behaviours are listed below

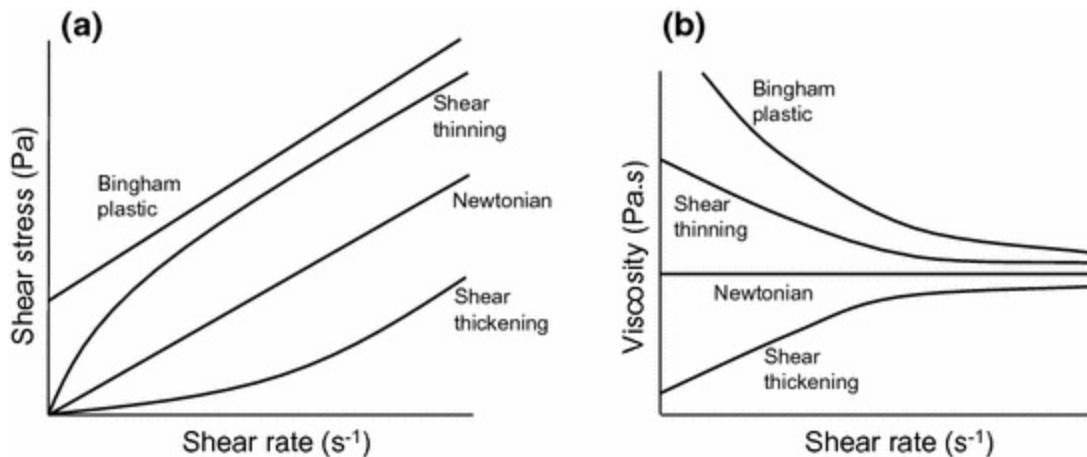


Fig. 1.12 Behaviour of different types of fluid with shear rate; **a** shear stress–shear rate plots, **b**

viscosity shear rate plots

- Newtonian. The shear stress increases linearly with shear rate, and consequently the viscosity is a constant and independent of shear rate. Examples are water and motor oil.
- Non-Newtonian
 - Bingham plastic. A yield stress must be exceeded before the fluid will flow. Examples are toothpaste and mayonnaise.
 - Shear thinning (also called ‘dilatant’). The viscosity decreases with increasing shear rate. Examples are tomato ketchup, blood and latex paint.
 - Shear thickening (also called ‘pseudoplastic’). The viscosity increases with increasing shear rate. Examples are silly putty and cornstarch solution.

Any fluid which does not have a linear stress–shear rate behaviour is a non-Newtonian fluid. Bingham plastic fluids, shear thinning fluids and shear thickening fluids are all examples of non-Newtonian fluids. Blood is a shear thinning fluid and the viscous behaviour of blood will be discussed in detail in Chap. 3. For many materials the viscosity reaches a constant value at higher shear rates and one way of comparing different liquids is to quote the high-shear rate viscosity.

A simple and inexpensive way to measure fluid viscosity is to fill a funnel with the fluid and time how long it takes for the fluid to drain out. This method is commonly used in drilling, for example, to check the quality of drilling mud. The viscosity is approximately proportional to the emptying time from the funnel. Table 1.2 gives rough values of emptying time for different fluids, though it is noted that the calculated values are for illustration only and are not claimed to be accurate. Fluids such as water, blood and oil take 2 min or less to drain out. Thicker fluids such as glycerol and honey take minutes to hours whereas peanut butter can take days. The calculated time for window putty is 3 years, and the longest calculated time is for pitch at 1000s of years. Pitch is an example of a fluid with a viscosity so high that initial inspection would suggest it to be a solid; a block of pitch shatters like glass when hit with a hammer. However, it is a liquid and it will flow given sufficient time. The longest running viscosity measurement is on a

funnel filled with pitch, which was set up in 1927 (Edgeworth et al. 1984). The funnel was filled and allowed to settle for 3 years after which the end of the funnel was cut. After 80 years only 8 drops of pitch had fallen from the funnel.

Table 1.2 High-shear viscosity of different liquids

Fluid	High-shear viscosity (Pa s)	Time to drain
Water	0.001	26 s
Blood	0.004	29 s
Olive oil	0.08	2 min
Glycerol	1	17 min
Honey	5	2 h
Peanut butter	250	3 days
Window putty	100,000	3 years
Pitch	230,000,000	1000s years

Calculated time for different fluids to empty from a funnel (for illustrative purposes only)

1.2.4 Steady Flow in a Tube

The flow of fluids in tubes was investigated by the French physicist Poiseuille. Figure 1.13 shows the basic parameters needed to describe flow in a cylinder. The pressure at the right side of the tube is P and at the left $P + \Delta P$. The pressure drop across the tube, ΔP , gives rise to a flow, Q . The formula derived by Poiseuille relating these variables is shown in Eq. (1.12).

$$Q = \frac{\Delta P \pi D^4}{128 L \mu} \quad (1.12)$$

where, L is the tube length, D is the diameter and μ is the viscosity. For any given tube of constant cross-section the flow rate is proportional to the pressure difference. The formula also shows that the pressure difference required to sustain a certain flow rate Q , is inversely proportional to the 4th power of the diameter. In other words a decrease in diameter by a factor of 2 requires a 16-fold increase in pressure to maintain the same flow rate.

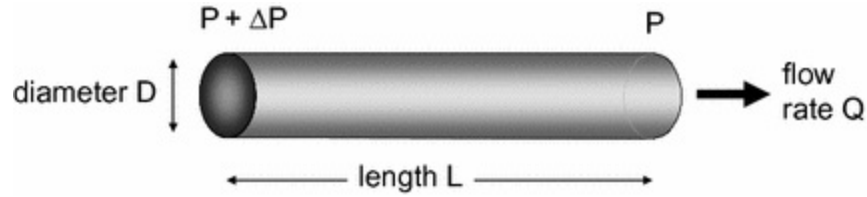


Fig. 1.13 Quantities relevant to flow in a cylindrical tube

For flow in a cylinder the resistance to flow R is defined as the pressure difference divided by the flow rate (Eq. 1.13). For Poiseuille flow this gives Eq. (1.14). The resistance is proportional to the length of the tube and to viscosity and is inversely proportional to diameter to the fourth power.

$$R = \frac{\Delta P}{Q} \quad (1.13)$$

$$R = \frac{128L\mu}{\pi D^4} \quad (1.14)$$

The velocity as a function of position across the diameter is called the ‘velocity profile’. For steady flow of a Newtonian fluid in a long straight tube it can also be shown that the velocity profile has the shape of a parabola (Fig. 1.14). For a parabolic velocity profile the velocity is maximum in the middle of the tube and is zero at the tube wall. The shape is not dependent on the viscosity.

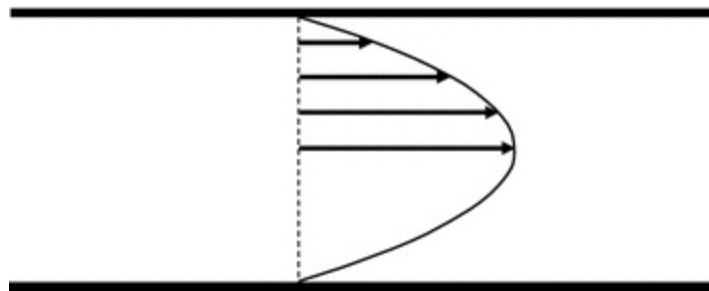


Fig. 1.14 Parabolic velocity profile for flow of a Newtonian fluid in a long straight tube

When the tube is not long and straight the velocity profile will vary, depending on the shape and length of the vessel. At the entrance to a long pipe the velocity profile is initially flattened but after a certain length (called the ‘inlet length’) the velocity profile becomes parabolic, and it remains parabolic after this point (Fig. 1.15). This stable region of flow is called ‘fully developed flow’. Equation (1.15) shows a formula for calculating inlet length

IL (from MacDonald 1974). In this case the velocity profile at a specific point in the vessel is dependent on the viscosity.

$$IL = 0.04dRe \tag{1.15}$$

where, d is diameter and Re is Reynolds number.

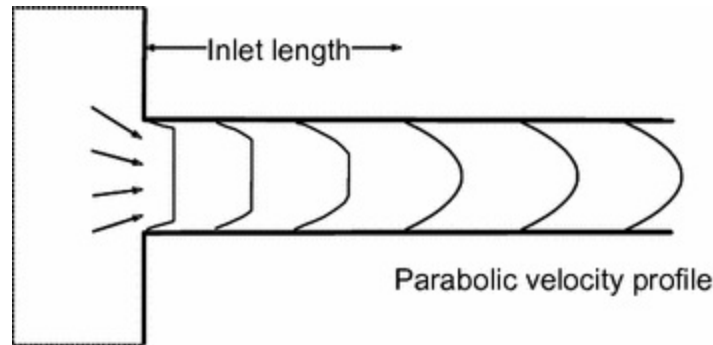


Fig. 1.15 Velocity profiles at the entrance to a long straight tube. The length after which the velocity profile is stable is called the inlet length

1.2.5 Reynolds Number and Flow States

We will continue with consideration of flow at the entrance to a straight pipe. The flow can be divided into two regions (Fig. 1.16). Flow near the entrance is dominated by inertial forces and the velocity profile in the region is flat. Flow further along the tube is dominated by viscous forces and the velocity profile changes with distance from the vessel wall. The interface between these two regions is called the boundary layer.

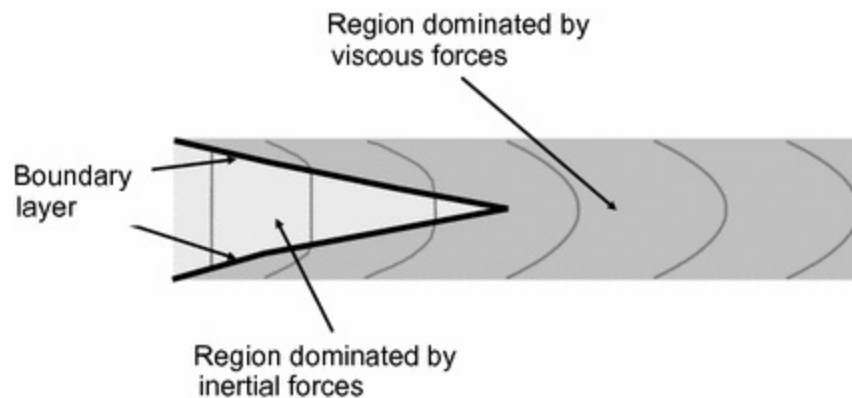


Fig. 1.16 Regions of flow at the entrance to a long straight tube and the boundary layer

The Reynolds number Re of a fluid is defined as the ratio of inertial to

viscous forces. For flow in a tube the Reynolds number is given by Eq. (1.16). The Reynolds number is dimensionless.

$$Re = \frac{\rho V D}{\mu} \quad (1.16)$$

where V is velocity, ρ is density, D is diameter and μ is the viscosity. As the velocity of a fluid increases its behaviour will change. There are three flow states which are related to the Reynolds number, and also the velocity. At low Reynolds numbers and low fluid velocities the flow is laminar. Fluid elements follow clearly defined paths. This behaviour is associated with Reynolds numbers of less than about 2300. In turbulent flow fluid elements follow erratic paths which randomly vary with time. This occurs at high Reynolds numbers greater than about 2500. Between these two states the flow is termed transitional. The fluid is considered to be 'disturbed' with intermittent periods of turbulence and laminar flow.

Figure 1.17 shows the different flow types. Ink is injected into a tube to visualise features within the flow. At low Reynolds numbers there is laminar flow and the dye moves along a single path. At Reynolds numbers just above the critical value there are intermittent periods of laminar flow and turbulence. The dye has periods where it follows a clearly defined straight path and periods where it has an erratic path. For higher Reynolds numbers there is turbulent flow and the dye follows multiple erratic paths.

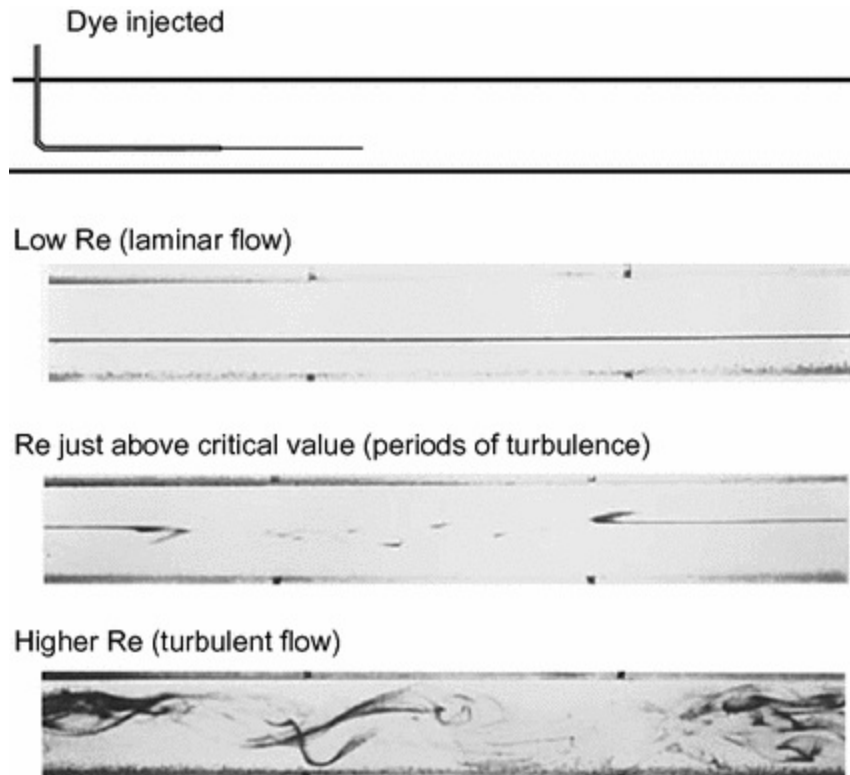


Fig. 1.17 Flow states demonstrated by injection of dye. At low Re the flow is laminar and the dye moves along a straight path. At values of Re just above a critical value the flow oscillates between laminar and turbulent. At higher Re the flow is turbulent and the dye follows multiple erratic paths. Reprinted with permission from: Caro CG, Pedley TJ, Schroter RC, Seed WA, assisted Parker KH; *Mechanics of the circulation* 2nd edition, 2011, Cambridge University Press

1.2.6 Unsteady Flow in Tubes

When the pressure varies in a tube, so will the flow rate. A time-varying pressure gradient results in a time-varying flow (Fig. 1.18). The inertia of the fluid gives rise to a time lag between the flow and pressure.

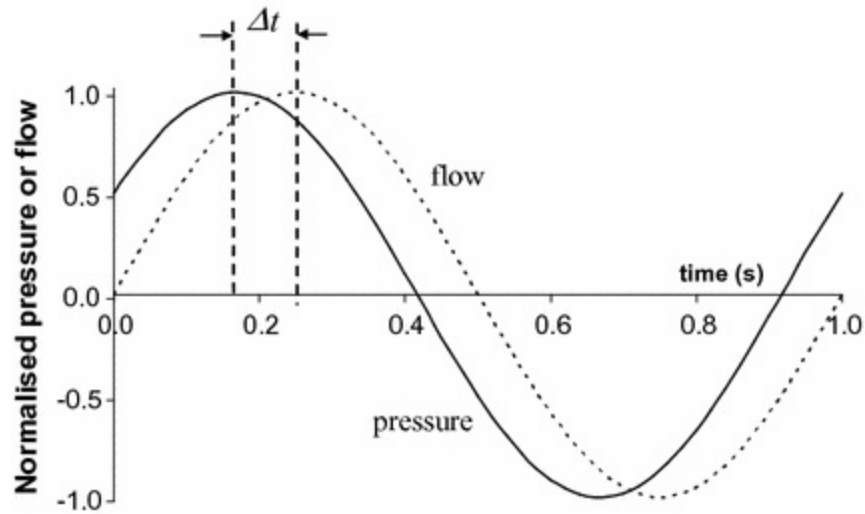


Fig. 1.18 Time-varying sinusoidal pressure in a tube will result in time varying sinusoidal flow. There is a time lag between flow and pressure as a result of the inertia of the fluid

When flow in a tube varies with time, velocity profiles are not parabolic (Fig. 1.19); velocity profiles for a sinusoidal pressure gradient are shown. The inertia of flow in the central core prevents the flow following the pressure gradient, whereas lower velocities at the wall can follow the pressure gradient. This results in complex velocity profiles. In some cases there is both forward flow and reverse flow present at the same time.

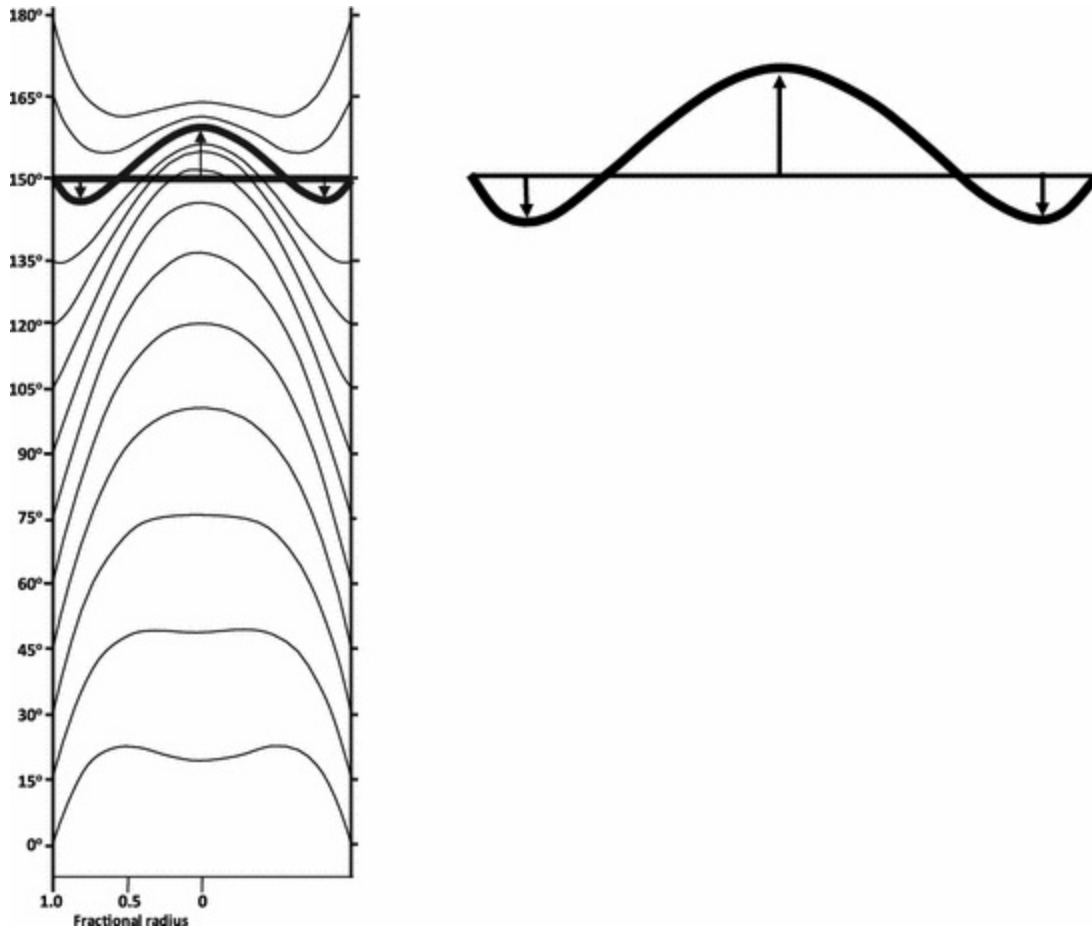


Fig. 1.19 Calculated velocity profiles as a function of phase for a sinusoidal pressure in a straight tube containing a Newtonian fluid

1.2.7 Energy Considerations and the Bernoulli Principle

The Bernoulli principle is that an increase in fluid velocity is associated with a decrease in pressure. In general, for flow along a streamline in which there are no energy losses (i.e. no viscosity), the energy is constant at all points along the streamline and is distributed between gravitational potential energy, pressure energy and kinetic energy. Bernoulli's Eq. (1.17) is simply a statement of conservation of energy.

$$P + h\rho g + \frac{\rho v^2}{2} = \text{constant} \quad (1.17)$$

where P is pressure, h is height, ρ is density, g is the gravitational constant and v is velocity.

Assuming that the effects of gravity can be ignored, Bernoulli's equation can be simplified as shown in Eq. (1.18).

$$P + \frac{\rho v^2}{2} = \text{constant} \quad (1.18)$$

Bernoulli's equation is considered further in Chap. 15 with respect to the pressure of blood in a diseased artery in which there is lumen reduction. In practice viscosity leads to energy losses and this is also considered in Chap. 15.

Appendix 1: Scientists Involved in the Development of Fluid and Solid Mechanics

Many of the scientists below have made contributions in many scientific areas. Only the areas relevant to fluid mechanics and solid mechanics as mentioned in this chapter are described below.

Bernoulli, Daniel

1700–1782. Proposed an inverse relationship between fluid velocity and pressure which came to be known as the Bernoulli principle and an equation which described this, known as the Bernoulli equation.

Bingham, Eugene

1878–1945. Proposed a mathematical form for the behaviour of fluids which have a yield stress before flowing. Subsequently the fluids were referred to as 'Bingham plastics'.

Hagen, Gotthilf

1797–1884. Formulated a law relating pressure drop and flow rate for flow of a fluid in pipes. This was independently discovered by Jean Poiseuille. Subsequently called the Hagen–Poiseuille law, or just the Poiseuille law.

Hooke, Robert

1635–1703. Discovered the law of elasticity (extension proportional to force). Subsequently called Hooke's law.

Maxwell, James

1831–1879. Proposed a model which described the stress–strain behaviour of

materials with viscous and elastic behaviour. Subsequently called the Maxwell model.

Newton, Issac

1642–1727. Developed a theory of mechanics for which the second law states that a force acting on a mass will produce an acceleration. The unit of force, the newton (N), is named after him. Newton also derived the equation for fluids relating shear stress to shear strain rate. Fluids which have a linear stress–strain rate behaviour are said to be Newtonian.

Pascal, Blaise

1623–1662. Undertook studies of pressure, demonstrating that hydrostatic pressure is governed by elevation difference, not on the weight of the fluid. The unit of pressure, the pascal (Pa), is named after him.

Poiseuille, Jean

1797–1869. Formulated a law relating pressure drop and flow rate for flow of a fluid in pipes. This was independently discovered by Gotthilf Hagen. Subsequently called the Hagen–Poiseuille law, or just the Poiseuille law.

Poisson, Simeon

1781–1840. Defined a ratio to express the contraction of a material in the direction transverse to the direction of stretching. Subsequently called Poisson’s ratio.

Reynolds, Osborne

1842–1912. Investigated flow in pipes, deriving a dimensionless quantity to describe the transition from laminar to turbulent flow. Subsequently called Reynold’s number.

Voigt, Woldemar

1850–1919. Studied the elastic behaviour of materials formulating a model which could be used to describe the stress–strain behaviour. Subsequently called the Voigt model.

Young, Thomas

1773–1829. Performed experiments on the stretching of materials. Originated the concept of the elastic modulus as a fundamental property of a material.

The elastic modulus was subsequently called the Young's modulus.

Appendix 2: Relationships Between the 4 Elastic Constants for a Linear Isotropic Material

Input constants	Output equations			
	$E =$	$\nu =$	$G =$	$B =$
E, ν	–	–	$\frac{E}{2(1+\nu)}$	$\frac{E}{3(1-2\nu)}$
E, G	–	$\frac{E-2G}{2G}$	–	$\frac{EG}{3(3G-E)}$
E, B	–	$\frac{3B-E}{6B}$	$\frac{3BE}{9B-E}$	–
ν, G	$2G(1 + \nu)$	–	–	$\frac{2G(1+\nu)}{3(1-2\nu)}$
ν, B	$3B(1 - 2\nu)$	–	$\frac{3B(1-2\nu)}{2(1+\nu)}$	–
G, B	$\frac{9BG}{3B+G}$	$\frac{3B-2G}{6B+2G}$	–	–

References

Caro CG, Pedley TJ, Schroter RC, Seed WA, Parker KH. Mechanics of the circulation. 2nd ed. Cambridge University Press; (2011).

Cowin SC, Doty SB. Tissue mechanics. New York: Springer; 2007.
[CrossRef]

Cowin SC, Humphrey JD. Cardiovascular soft tissue mechanics. Dordrecht: Kluwer; 2001.

Edgeworth R, Dalton BJ, Parnell T. The pitch drop experiment. Eur J Phys. 1984;5:198–200.
[CrossRef]

Holzapfel GA, Ogden RW, editors. Mechanics of biological tissues. New York: Springer; 2006.

Humphrey JD. Cardiovascular solid mechanics. New York: Springer; 2002.
[CrossRef]

McDonald DA. Blood flow in arteries. London: Edward Arnold; 1974.

Sarvazyan AP, Skovoroda AR, Emelianov SY, Fowlkes JB, Pipe JG, Adler RS, Buxton RB, Carson PL. Biophysical bases of elasticity imaging. In: Acoustical imaging. Springer: US; 1995. p. 223–40.

Sarvazyan AP, Rudenko OV, Swanson SD, Fowlkes JB, Emelianov SY. Shear wave elasticity imaging: a new ultrasonic technology of medical diagnostics. *Ultrasound Med Biol.* 1998;24:1419–35.
[\[CrossRef\]](#)[\[PubMed\]](#)

2. Introduction to Cardiovascular Biomechanics

Peter R. Hoskins¹✉

(1) Edinburgh University, Edinburgh, UK

✉ **Peter R. Hoskins**
Email: P.Hoskins@ed.ac.uk

Learning outcomes

1. Describe the main components of the cardiovascular system.
2. Describe the organisation of the cardiovascular system into pulmonary and systemic circulations.
3. Describe the main functions of the cardiovascular system.
4. Describe the change in relevant physical quantities in different vessels of the circulation.
5. Discuss the control of blood pressure in capillaries.

This chapter will explore the biomechanics of the cardiovascular system as a whole. Other chapters discuss in more detail the biomechanics of cardiovascular system components, including the heart, arteries, veins and the

microcirculation.

2.1 Components and Function

2.1.1 Organisation of the Cardiovascular System

The human cardiovascular system is illustrated in Fig. 2.1. This shows two sub-systems; the systemic circulation and the pulmonary circulation. The pulmonary circulation is concerned with obtaining oxygen from the lungs, as well as discharging carbon dioxide (a waste product of metabolism) from the blood into the alveoli of the lungs where it can be breathed out. Blood is ejected from the right ventricle into the pulmonary artery and returns to the left atrium via the pulmonary veins. The systemic circulation transports oxygenated blood to the rest of the body, returning deoxygenated blood via the veins. Blood is ejected from the left ventricle into the aorta, the largest artery in the body and returns via two large veins (the inferior and superior vena cava) to the right atrium.

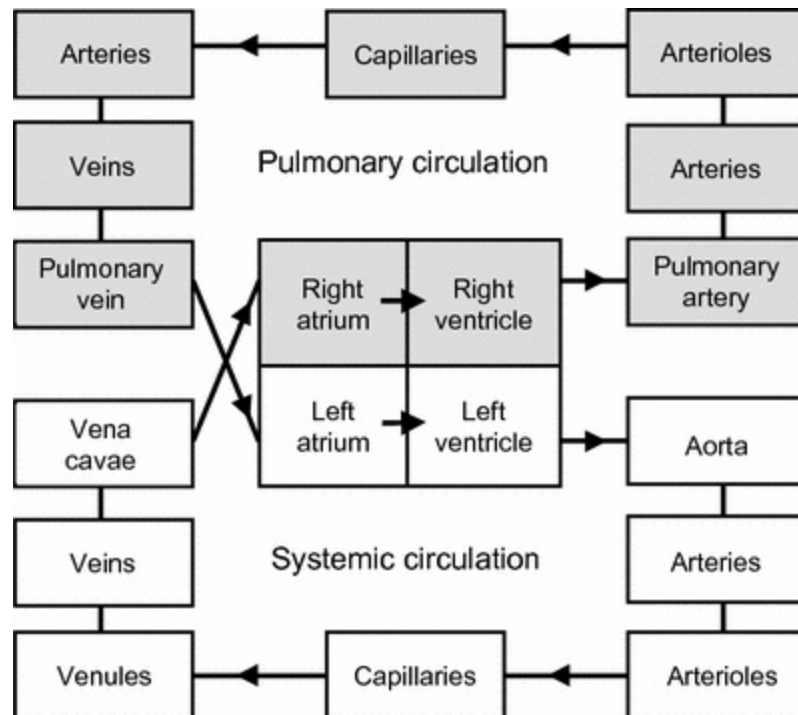


Fig. 2.1 Components of the cardiovascular system; systemic circulation is shown in *white*, pulmonary circulation in *grey*

2.1.2 Components of the Cardiovascular System

Heart

The structure of the heart is illustrated in Fig. 2.2. The heart has two main phases; a contraction phase when blood is ejected from the left and right ventricles, and a relaxation phase when the chambers fill with blood returning via the venous system. The heart valves prevent backflow and operate in a passive manner associated with pressure differences. During ejection, the aortic and pulmonary valves are open and the tricuspid and mitral valves closed. During filling, the aortic and pulmonary valves are closed and the other two valves are open. The left ventricle ejects blood into the relatively high-pressure systemic system, hence has a much thicker wall than the right ventricle, which ejects blood into the low-pressure pulmonary system.

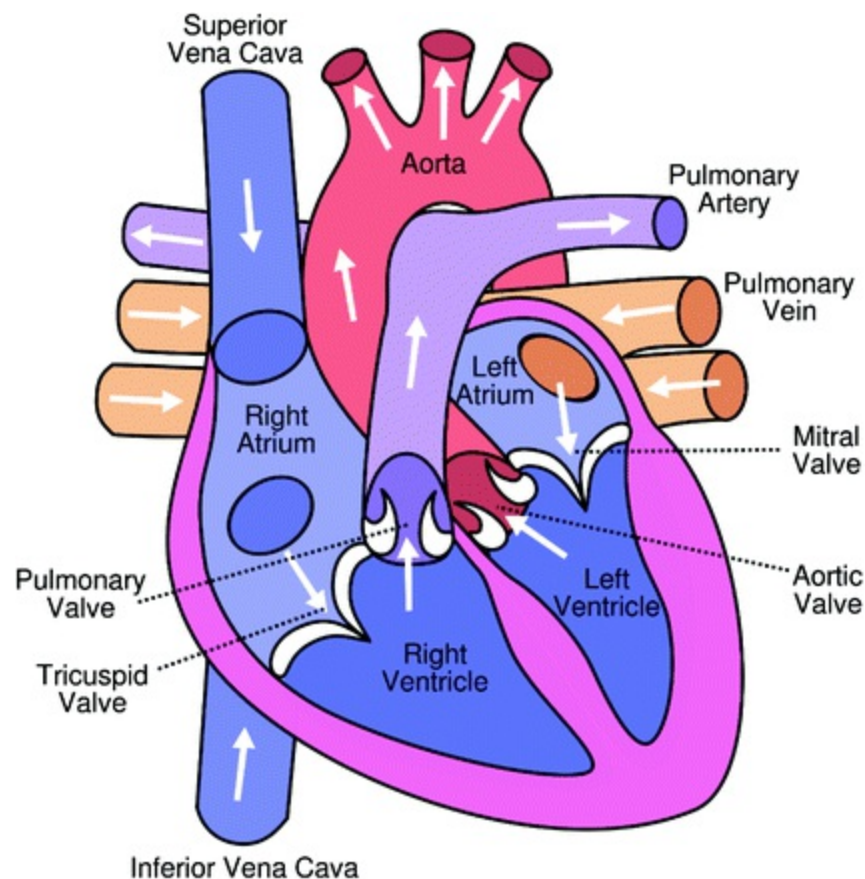


Fig. 2.2 Principal components of the heart. Reproduced from Wikipedia according to the GNU Free Documentation License; diagram authored by Wapcaplet and Yaddah. [https://commons.wikimedia.org/wiki/File:Diagram_of_the_human_heart_\(cropped\).svg](https://commons.wikimedia.org/wiki/File:Diagram_of_the_human_heart_(cropped).svg)

Composition of vessels

The vessels are composed of three layers, as shown in Fig. 2.3. These layers are:

- *Adventitia*. The outermost layer, primarily consisting of collagen fibres layered in a spiral fashion.
- *Media*. A layer consisting of smooth muscle, elastin sheets (layered circumferentially) and collagen fibres.
- *Intima*. The innermost layer consisting of a single layer of endothelial cells. These line the lumen, and hence are in contact with flowing blood. There is also a basement membrane immediately beneath the endothelium.

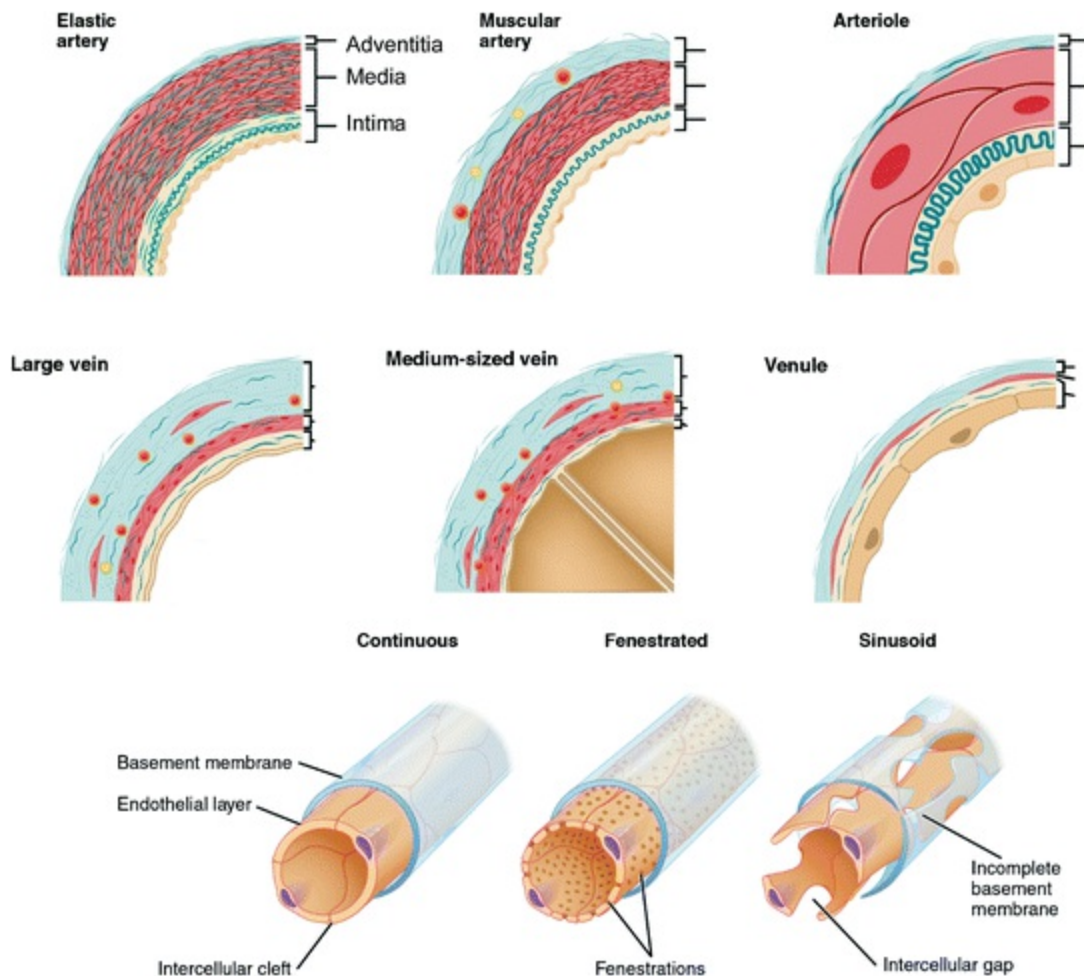


Fig. 2.3 Principal components of vessel wall. Note that vessel curvature is not to scale. Images reproduced from ‘Structure and function of blood vessels’ Openstar; under a creative commons licence <http://creativecommons.org/licenses/by/3.0/legalcode>. Download for free at <http://cnx.org/contents/58db2cce-b3d9-4904-9049-80a6cd89264b@4>

From a mechanical perspective, the two main constituents of the vessel wall are elastin and collagen. These are considered further in Chap. 4. Elastin is highly deformable with a low Young's modulus whilst collagen has a nonlinear behaviour with high values of Young's modulus and a high breaking strength. The ratio of elastin to collagen is the principal determinant of the overall elastic behaviour of a vessel. If the ratio is high, the vessel is elastic and deforms under increasing pressure. If the ratio is low, the vessel does not deform much under pressure.

Types of vessel

The vessels shown in Fig. 2.3 can be grouped and are described in this section. The microscopic structures of the different types of vessel are closely linked to the vessel's specific function.

- *Arteries (diameter 1–30 mm)*. Arteries carry blood away from the heart. Systemic arteries must withstand relatively high pressures and so have thick walls consisting of the three basic layers described earlier. Arteries are subcategorised, on the basis of their wall composition, into elastic and muscular arteries. Elastic arteries such as the aorta and its major branches are low resistance vessels and have a high elastin/collagen ratio. The high elastin content results in high distensibility. This allows them to accommodate the volume of blood ejected from the heart and also enables the storage of energy. More distal arteries, such those supplying the organs and those in the leg and arms, are muscular in nature. Muscular arteries have a thicker medial layer which has less elastin and more smooth muscle than that of elastic arteries. These vessels are also known as distributive arteries.
- *Arterioles (diameter 10–100 μm)*. Arterioles have all three layers (adventitia, media and intima) but of much reduced thickness compared to arteries. Proportionally, the thickness of the media is large consisting mainly of smooth muscle cells. These enable the lumen size to be controlled over a wide range. Constriction and dilatation of the arterioles controls the flow to capillaries. Diameter ranges from 100 μm to around 10 μm for the smallest (terminal) arterioles.
- *Capillaries (diameter 4–40 μm)*. These have a very thin wall consisting of only endothelium and basement membrane. There are three types of capillary. The most common are the continuous capillaries; these are

found in skin and muscle. Whilst the endothelial cells of these capillaries are closely coupled by tight junctions, small gaps are present which control the passage of fluids and small molecules. Fenestrated capillaries have pores (fenestrations), which give greater permeability to fluids and allow certain small molecules to pass through. They are found in the intestine and kidney. Sinusoidal capillaries are the least common and have large gaps allowing greater volume of materials to pass through. These are found in the liver, spleen and endocrine glands, for example. The diameter of continuous and fenestrated capillaries is in the range 4–10 μm , however sinusoidal capillaries can have much larger diameters of up to 40 μm . Capillaries are around one mm in length.

- *Venules (diameter 10–200 μm)*. These have all three layers but are much thinner than arterioles with an almost absent medial layer.
- *Veins (diameter 1–25 mm)*. Veins return the blood to the heart. The venous system has a much lower pressure than the arterial system and consequently the wall thickness of veins is much less than that of arteries. Intermediate sized veins contain valves, which prevent backflow of blood. Larger veins including the vena cava do not. The adventitial layer is thicker than the medial layer and the elastin/collagen ratio is small compared to arteries. This makes veins relatively stiff when fully distended, but when veins are under low or negative pressure they may collapse.

2.1.3 Functions of the Cardiovascular System

The cardiovascular system has several functions; transport of molecules, defence and healing, thermoregulation and maintenance of fluid balance between different tissues in the body.

Transport of molecules

The cardiovascular system transports molecules from one vascular bed to another. Entry and exit of molecules into the cardiovascular system occurs through the walls of the capillaries. For example, oxygen is transported from the pulmonary vascular bed to vascular beds all over the body where oxygen is needed for metabolism. Carbon dioxide is a waste product of metabolism and is made in tissues all over the body. Carbon dioxide is transported from vascular beds to the lungs, where it is discharged into the alveoli. Glucose,

amino acids, vitamins and minerals are discharged into the blood from the vascular beds of the gastrointestinal tract. As far as transport of molecules is concerned, the function of the rest of the cardiovascular system is to provide passage of molecules from one capillary bed to another.

Defence and healing

The cardiovascular system has two main safety systems; the immune system and the tissue repair system. These systems involve particles transported in blood, especially white cells, platelets and macromolecules such as fibrinogen.

Thermoregulation

In order to help maintain a constant core body temperature of 37 °C, the amount of blood flowing close to the skin surface can be controlled. Under normal conditions, only some 4 % of blood flows near the skin, however, this can be increased to almost half of the cardiac output under conditions of excessive heat. Combined with sweating, the aim is to remove heat from the body.

Fluid balance

Fluid in the body is partitioned between fluid within cells (intracellular fluid) and fluid outside the cells (extracellular fluid). Extracellular fluid consists of the fluid between cells (interstitial fluid), blood (in the cardiovascular system) and lymph (in the lymphatic system). These volumes need to keep within a narrow range and also their electrolyte concentration needs to be kept within a narrow range. The cardiovascular system has a major role in control of these fluid volumes and electrolyte concentration.

2.2 Physical Quantities

This section discusses basic physical quantities relevant to cardiovascular mechanics. Table 2.1 provides data for the different components of the systemic cardiovascular system. Definitive data covering all quantities for the human is hard to come by. Table 2.1 is based on work by Dawson (2005, 2008). These are data for the human systemic circulation extrapolated (using scaling laws) from data in the dog (Green 1944). A simplified approach is taken in which the main arteries and veins are divided into 3 sizes. For the

arteries these are the aorta (the largest artery), arteries of 6 mm diameter which branch from the aorta, and arteries of 2 mm diameter. For the veins, these are veins of 2 mm diameter, veins of 10 mm diameter and the vena cava. These data allow us to explore the change in different physical quantities in the circulation.

Table 2.1 Values of various physical quantities for the systemic circulation

Vessel	Diameter (mm)	Length (mm)	Number	Volume (mL)	Cross sectional area (cm ²)	Mean velocity (cm s ⁻¹)	Mean pressure (mmHg)
Aorta	22	600	1	228	4	25	95
Large arteries	6	300	40	339	11	8.3	93
Small arteries	2	50	2400	377	75	1.2	87
Arterioles	0.02	3	1.1×10^8	104	346	0.3	54
Capillaries	0.01	1	3.3×10^9	259	2592	0.04	25
Venules	0.04	3	2.2×10^8	829	2765	0.03	7
Small veins	2	50	2400	377	75	1.2	4
Large veins	10	300	40	943	31	3	2
Venae cava	22	500 ^a	2	228	4	25	0

Data is taken and adapted from Dawson (2008). Data on pressure is taken from other sources

^aCombined length of inferior and superior vena cava

2.2.1 Dimensions of the Systemic Circulation

The design of the cardiovascular system follows the need for exchange of oxygen and other molecules through capillaries. Oxygen can travel by diffusion over a distance of about 100 μm and, in practice, virtually all cells within the body lie no further than 100 μm from a capillary. The systemic cardiovascular system starts with a single vessel, the aorta and progressively divides, increasing the number of vessels and overall cross-sectional area. Beyond the capillary beds the vessels progressively unite, decreasing in number and overall cross-sectional area until there are just two vessels (the

inferior and superior vena cava) which then connect back with the heart. Figures 2.4, 2.5 and 2.6 are based on the data in Table 2.1 and show the change in the number, diameter and cross-sectional area for the vessels of the systemic circulation.

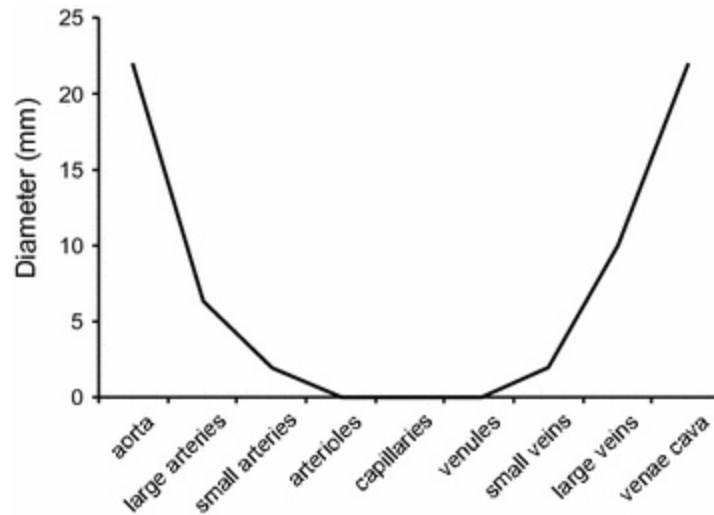


Fig. 2.4 Vessel diameter for vessels of the systemic circulation (see Table 2.1)

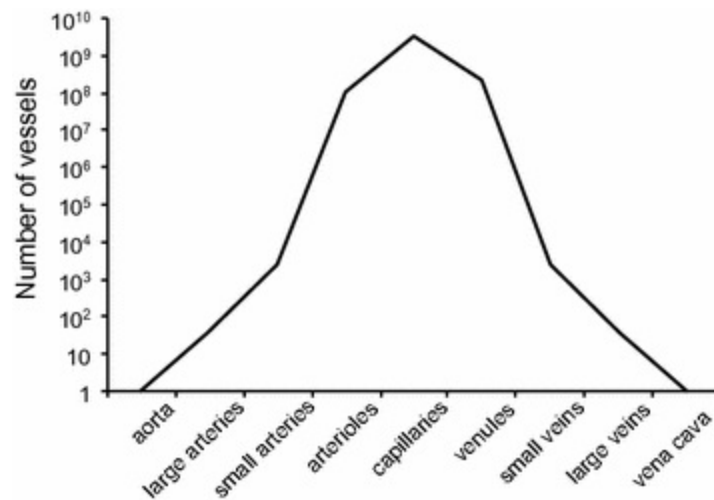


Fig. 2.5 Number of vessels of the systemic circulation (see Table 2.1)

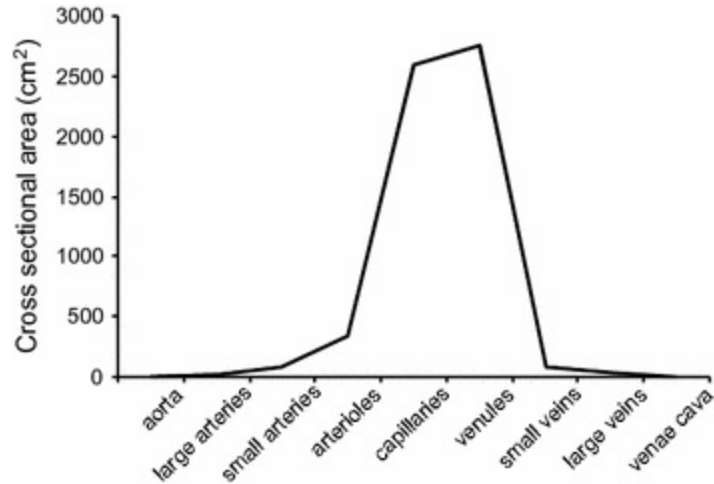


Fig. 2.6 Total cross-sectional area of vessels of the systemic circulation (see Table 2.1)

The blood volume is not uniformly distributed within the systemic vessels. The venous system contains 65 % of the volume, almost two-thirds, the arterial system contains 28 % and the remaining 7 % is in capillaries.

2.2.2 Pressure in the Systemic Circulation

Figure 2.7 illustrates the pressure in the vessels of the systemic circulation. The heart ejects its contents from the left ventricle into the aorta. The aorta expands and the pressure rises. With increasing distance from the heart the pulse pressure (difference between maximum and minimum pressure) increases due to the stiffening of arteries with distance from the heart. Mean pressure falls through the remainder of the cardiovascular system, reaching its lowest value at the entrance to the right atrium. It was thought for many years that pressure (and flow) in the capillaries was steady however (as discussed below and in Chap. 8) there is some pulsatility occurring as a result of upstream pressure variation which is transmitted to the capillaries. Pressure in the venules and veins does not vary much, apart from the action of the muscles as discussed in Chap. 7. In veins nearer the heart, especially in the vena cava, pressure will have some variation during the cardiac cycle and, as explained below, is also influenced by pressure changes in the thorax related to breathing.

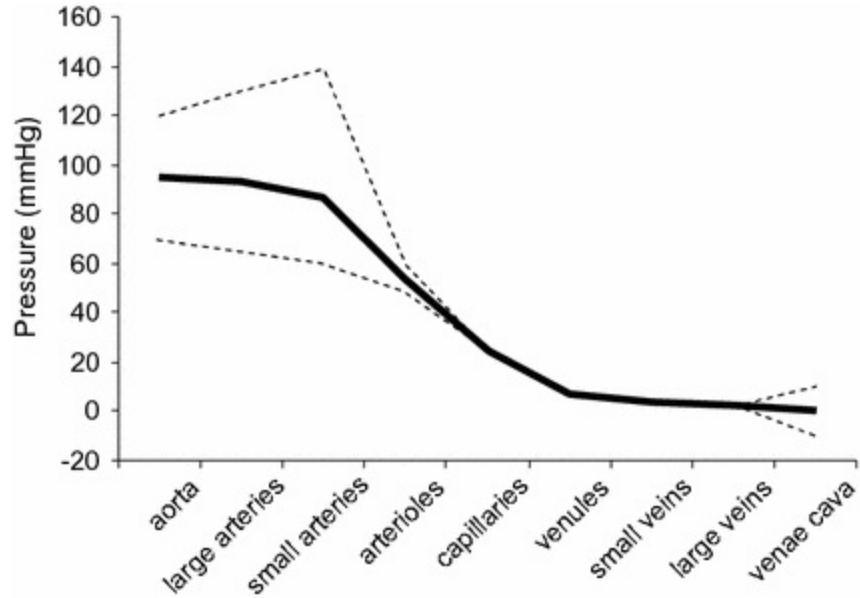


Fig. 2.7 Mean blood pressure of vessels of the systemic circulation (see Table 2.1). Also shown are the maximum and minimum blood pressure

The pressure gradient in the arteries is caused by the force of ejection of blood into the aorta from the left ventricle. In the venous system, two mechanisms operate to move blood along the veins; the respiratory pump and the musculo-venous pump. Breathing in (inspiration) causes an increase in pressure in the abdomen and a reduction in pressure in the thorax. This creates a suction pressure, which sucks blood along the veins towards the heart. This suction effect leads to negative pressures (pressures below zero mmHg) in the larger veins. This negative pressure can give rise to temporary venous collapse (reduction of the cross-sectional area of the vein to zero). The second main mechanism driving blood through the veins is venous compression by the musculature, as a result of walking and general movement. Blood is prevented travelling back along the veins in the limbs by valves which are present at regular intervals.

2.2.3 Pressure in Capillaries

Pressure in the capillaries is controlled to a high degree. Water is able to flow freely from blood to tissues through small gaps ('tight junctions') in the endothelium but the net flow rate depends on the balance between the hydrostatic pressure and the colloid osmotic pressure within the capillary (Fig. 2.8). At the arterial end of the capillary, there is a net flow of water from

the capillary into the tissue whilst at the venous end, there is a net flow of water from the tissue into the capillary. In the absence of a control mechanism, the blood pressure in the capillaries would vary by huge amounts from lying down to standing up, from resting to exercising, and also with fluid intake. One of the principle regulatory functions in the microcirculation is to ensure that, no matter what the body is doing, the pressure in the capillaries is maintained at a level, which exactly balances the colloid osmotic pressure (that is, about 22 mmHg). This means that, from a mechanical point of view, the venous and arterial systems are largely decoupled and can be considered as independent systems.

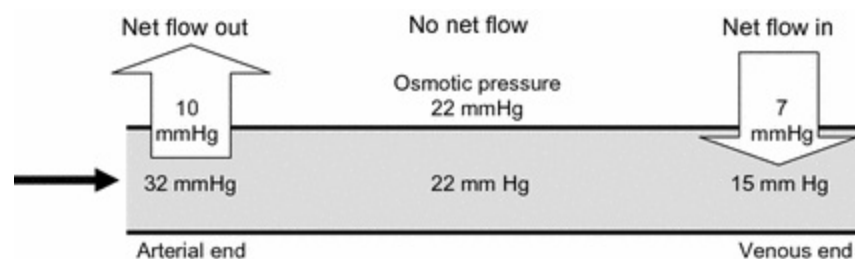


Fig. 2.8 Pressure and cross-wall flow in the capillary. The net flow across the capillary wall is driven by the balance between blood pressure and osmotic pressure. At the arterial end the blood pressure is greater than the osmotic pressure and there is net flow outwards. At the venous end the blood pressure is less than the osmotic pressure and there is net flow inwards

2.2.4 Flow and Velocity in the Systemic Circulation

If it is assumed that the circulation is a bifurcating system then the total flow rate at each level in the systemic circulation remains constant. Therefore, as the total cross-sectional area of vessels increases, the mean velocity decreases (Fig. 2.9). Mean velocity can be measured using a variety of techniques as discussed in later chapters. In order to provide consistency, mean velocity in Table 2.1 has been calculated by assuming a cardiac output of 5.6 L min^{-1} (average for a male) and dividing by the cross-sectional area. This provides values for mean velocity, ranging from 25 cm s^{-1} in the largest vessels, down to $0.3\text{--}0.4 \text{ mm s}^{-1}$ in the smallest. The assumption of a bifurcating system allows quick estimation of velocities and flow rates, giving values which are reasonably representative of actual velocities and flow rates, even down to the capillary. The blood velocity varies through the cardiac cycle in arteries and arterioles (and to some extent in capillaries) as a result of variation in pressure during the cardiac cycle; this is considered in detail in Chaps. 4 and

8.

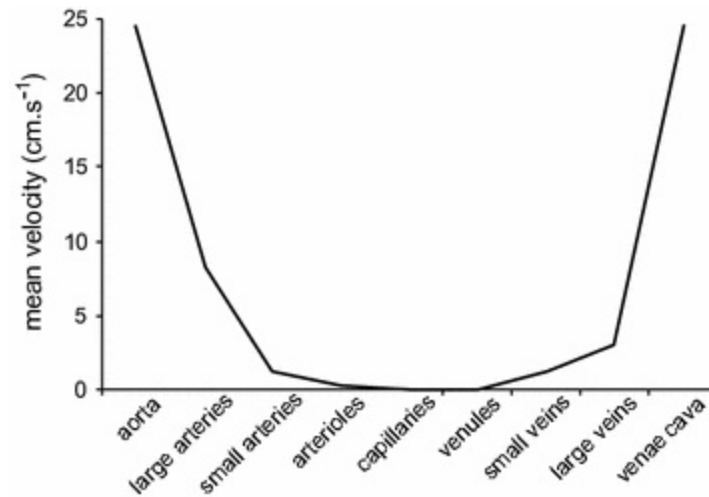


Fig. 2.9 Mean blood velocity of vessels of the systemic circulation (see Table 2.1)

References

Dawson TH. Modeling of vascular networks. *J Exp Biol.* 2005;208:1687–94.
[CrossRef][PubMed]

Dawson TH. Modeling the vascular system and its capillary networks. In: Yim PJ, editor. *Vascular hemodynamics: bioengineering and clinical perspectives.* New Jersey: John Wiley; 2008. p. 1–35.

Green HD. Circulation: physical principles. In: Glasser O, editor. *Medical physics, vol. 1.* Chicago: Year-book Publishers; 1944. p. 208–32.

3. Blood and Blood Flow

Peter R. Hoskins¹✉ and David Hardman²

- (1) Edinburgh University, Edinburgh, UK
- (2) Castlebrae Community High School, Edinburgh, UK

✉ **Peter R. Hoskins**
Email: P.Hoskins@ed.ac.uk

Learning outcomes

1. Describe the constituents of blood and discuss their function.
2. Describe the main forces acting on blood particles.
3. Describe the Segre-Silberberg effect and discuss its origin in terms of forces.
4. Describe Rouleaux formation and discuss its origin in terms of forces.
5. Describe leukocyte adhesion and discuss the role of forces in adhesion.
6. Discuss the effect of particle deformability on the viscosity—volume fraction curve.
7. Describe the role of spectrin in maintaining red cell shape.

8. Describe the effect of shear rate on the shape of the individual red cell.
9. Describe the shape of red cells when flowing in tubes of different diameter.
10. Describe the viscosity–wall shear rate curve for whole blood.
11. Discuss the shape of the viscosity–wall shear rate curve for whole blood in terms of red cell behaviour.
12. Describe the Fahreaus effect and the Fahraeus–Linqvist effect.
13. Discuss the Fahreaus effect and the Fahraeus–Linqvist effect in particle depletion at the wall.
14. Describe and discuss the viscous behaviour of blood in arteries.
15. Describe the viscous behaviour of blood in the heart, veins and microcirculation.

Blood is the fluid which flows in the cardiovascular system. It is, however, not a pure fluid but rather a suspension of a number of different particles (cells, cell fragments and macromolecules) in a fluid base. This chapter explores the fluid behaviour of blood including the impact of the particles on this behaviour. The study of blood flow has developed over many decades and blood rheology continues to be a highly active area of research. Ideally knowledge would be based on data collected in vivo, however, this is difficult to obtain. In practice, an understanding of blood rheology is obtained from many sources; the general area of flow of particle suspensions (important in other areas such as microfluidics and transport of chemicals), experiments involving particles which simulate blood cells, in vitro and in vivo observations and computational modelling. In the absence of definitive in vivo data this chapter draws on all of these sources to help create understanding of blood and blood flow.

3.1 Constituents of Blood

The constituents of blood are considered in this section and include the fluid base ‘plasma’ and a number of particles listed in Table 3.1. Figure 3.1 shows a ‘blood smear’ which shows blood cells from a sample of human blood photographed using an optical microscope.

Table 3.1 Components of blood

Blood component	% By volume	Principle function	Low %volume	High %volume
Plasma	50–60	Fluid base for blood, carbon dioxide and nutrient transport	Dehydration Blood loss Excess salt loss (e.g. after sport)	Kidney disease
Red cells	40–50	Carrying oxygen	Blood loss Sickle cell anaemia Enlarged spleen Cancer	Polycythaemia Chronic hypoxia Blood doping Dehydration
White cells	0.7	Immune system	Medication and radiation treatment Immune dysfunction (e.g. AIDS) Toxins including alcohol Major surgery	Infection (normal) Genetic disorders Leukaemia Spleen removal
Platelets	0.3	Clotting of blood	Medication and chemotherapy HELLP syndrome Haemolytic-uremic syndrome Snakebite	Thrombocytosis
Macromolecules: albumin	2	Maintenance oncotic pressure	Reduced production (various diseases)	Dehydration
Other	1.5	Various		

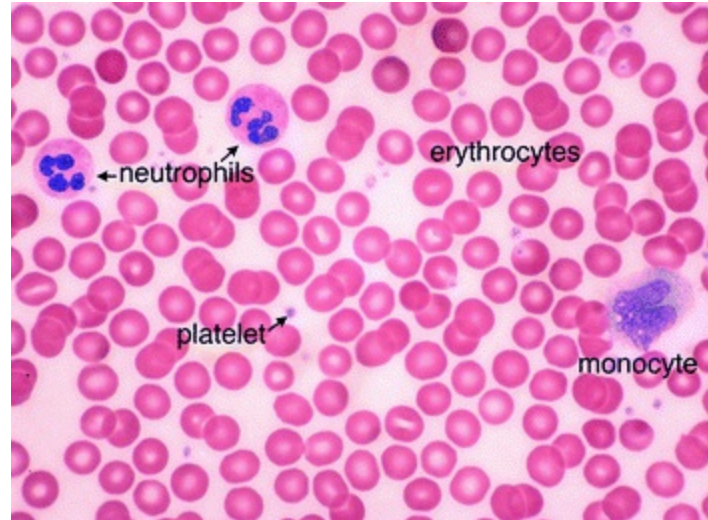


Fig. 3.1 Blood cells. Several types of blood cells are shown including red cells (erythrocytes), two different white cells (neutrophils and a monocyte) and platelets. Image kindly provided by Karen Hart, Peninsula College, Port Angeles, WA, USA. © 2006–2010 Karen Hart

3.1.1 Plasma

Plasma is a straw coloured fluid and consists of 90 % water and 1 % electrolytes, with various molecules making up the remainder. Electrolytes play an important role in ensuring the correct fluid content within cells; consequently, electrolyte concentration is subject to several control mechanisms. Low plasma volume may arise from a number of causes including dehydration, salt depletion (e.g. following sport), or blood loss. High plasma volume can occur as a result of inadequate salt excretion associated with kidney disease.

3.1.2 Macromolecules and Other Molecules

Macromolecules make up around 9 % of the plasma volume. The majority of molecules are proteins, such as globulins (part of the immune system), albumin (important for maintenance of oncotic pressure) and fibrinogen (part of the clotting system). Also present are a number of molecules in transit such as vitamins, hormones, waste products (urea, ammonia), carbon dioxide and oxygen. After a meal there is an increase in volume of fatty acids, amino acids and peptides arising from digestion in the blood. Some of these molecules such as LDL (low density lipoprotein) cholesterol play important roles in arterial disease.

Albumin is important in regulating the balance of fluids in the body. Low levels of albumin in blood are due to lack of protein in the diet or due to impaired production from the liver or to kidney disease. Low albumin levels result in an imbalance of fluids resulting in generalised swelling of tissues as a result of water retention, known as 'oedema'. A high level of albumin may arise from excess protein in the diet, but are usually caused by dehydration where the fluid levels in the tissues are low.

3.1.3 Red Cells

The principle particle in blood is the red cell or erythrocyte. The percent by volume of red cells is called the haematocrit, the packed cell volume or the erythrocyte volume fraction. The haematocrit has a normal range of 41–52 % in men and 36–48 % in women. The red cell is unique as, unlike other cells it has no nucleus and it has a biconcave shape (Fig. 3.2). Human red cells, have a diameter of 7.5 μm , a thickness of 2.0 μm and an effective diameter (i.e. the diameter if the red cell contents were formed into a sphere) of 5.5 μm . The size and shape of red cells is remarkably similar across all mammals; the diameter of a red cell in a mouse and an elephant is about the same. Red cells are involved in the transport of oxygen from the lungs to the tissues, for which the iron in the red cell plays an important role. Low haematocrit has a number of causes, including blood loss and various diseases. High haematocrit leads to an increase in the oxygen carrying ability of the blood, which is the reason why some athletes involved in endurance events have blood transfusions before the race. However it is also risky, as the viscosity of blood is higher, leading to greater resistance to flow and increased risk of clinical events such as heart attack and stroke. Sickle cell disease is associated with abnormally shaped red cells in the form of a sickle rather than a disc. While the oxygen carrying capability is impaired, the presence of sickle cells gives immunity against malaria, a deadly disease which operates through destruction of red cells.

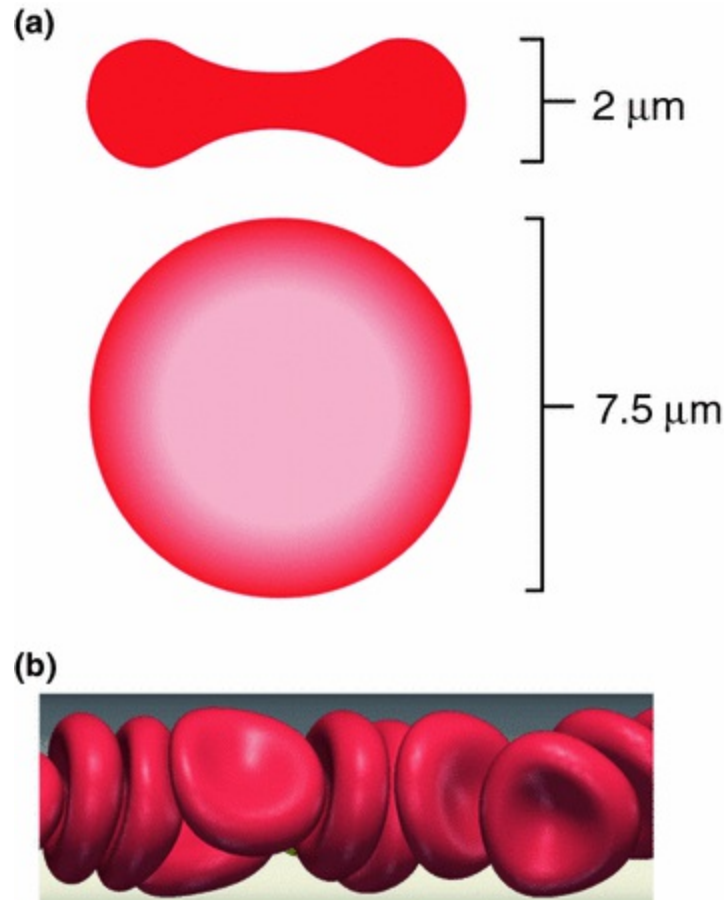


Fig. 3.2 Red cells. **a** Red cell shape and dimensions. **b** Red cells at low shear. (**b**) from; Krüger (2015); © Springer-Verlag Berlin Heidelberg 2015, with permission of Springer

3.1.4 White Cells

White cells, or leukocytes, occupy some 0.7 % of the blood volume in health. There are a number of different leukocytes as shown in Fig. 3.3, each with a different role. Neutrophils (diameter 10–12 μm) ingest and digest bacteria and fungi. Eosinophils (diameter 10–12 μm) attack larger parasites and are involved in allergic responses. Monocytes (diameter 15–30 μm) are carried by the cardiovascular system to different tissues where they transform into cells called macrophages. Lymphocytes (diameter 7–15 μm) attack invading bacteria and viruses and also help destroy cells in the body which have become diseased through virus infection or cancer. Basophils (diameter 12–15 μm) are involved in response to allergic symptoms including histamine release. An increase in the volume fraction of white cells is a normal response to infection and is not usually harmful. However abnormal increases

occurring in diseases such as leukaemia may be fatal. Low white cell volumes are due to decreased production or increased destruction arising from various diseases and lead to impaired functioning of the immune system.

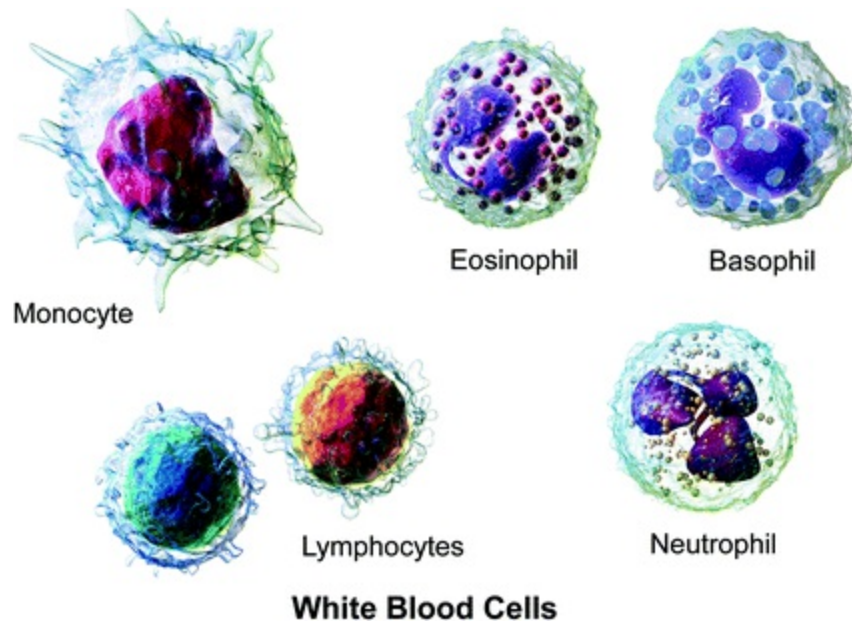


Fig. 3.3 White cells; illustration of various types of white cell. Image reproduced from wikipedia with permission. Original image authored by Bruce Blausen: Wikiversity Journal of Medicine. doi:10.15347/wjm/2014.010. ISSN 20018762.—Own work, CC BY 3.0, <https://commons.wikimedia.org/w/index.php?curid=28223981>

3.1.5 Platelets

Platelets are fragments of much larger cells called megakaryocytes and occupy 0.3 % of the blood volume in health. Platelets exist in unactivated and activated forms (Fig. 3.4). The majority of circulating platelets are unactivated and their shape is plate-like (hence the name ‘platelet’). These have a greatest diameter of 2–3 μm . Once activated, they become sticky and more spherical with projections (pseudopods). These projections are important in enabling activated platelets to clump together. Platelets are involved in blood clotting and in the repair of damaged endothelium. If the endothelium is damaged, underlying collagen fibres are exposed. Unactivated platelets coming into contact with collagen become activated and will stick to the collagen sealing off the damaged area after which repair of the area ensues. Platelets can also be activated by increases in wall shear in narrowed

vessels. Low platelet volume fraction can arise from a number of diseases and lead to impaired clotting ability, leading to potentially life-threatening blood loss from minor wounds. Increased platelet volume fraction arising from disease leads to increased risk of thrombosis which in turn may lead to potentially life-threatening clinical events such as heart attack and stroke.

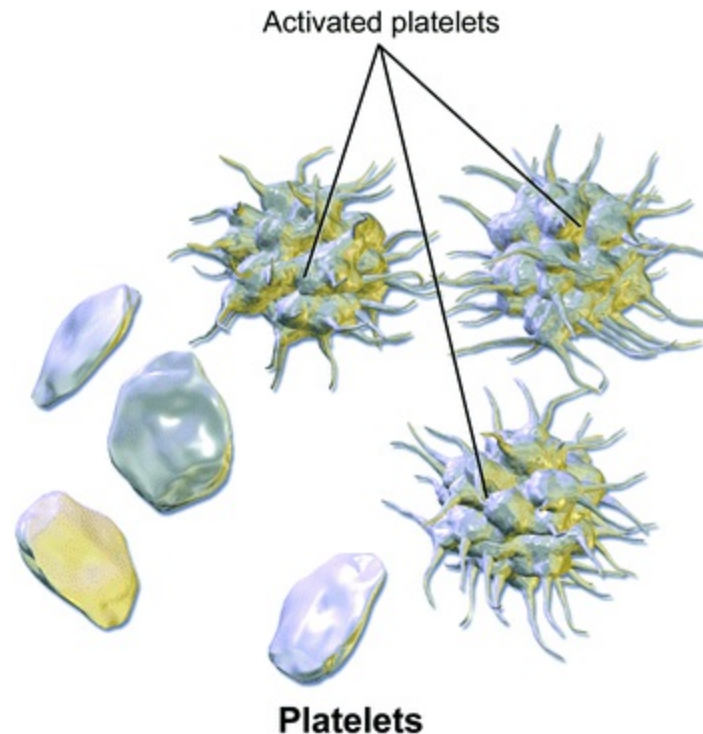


Fig. 3.4 Platelets; illustration of unactivated and activated platelets. Image reproduced from wikipedia with permission. Original image authored by Bruce Blausen: Wikiversity Journal of Medicine. doi:[10.15347/wjm/2014.010](https://doi.org/10.15347/wjm/2014.010). ISSN 20018762.—Own work, CC BY 3.0, <https://commons.wikimedia.org/w/index.php?curid=28223979>

3.2 Forces on Blood Particles

This section examines the forces on particles and discusses these in the context of blood viscosity and blood flow. The examples below are drawn from a variety of sources including in vitro experimental flow systems, computational modelling and in vivo measurements.

3.2.1 Forces Associated with Gravity

Gravity is a long-range force affecting all particles in a fluid in the lab and in the human body on planet earth (and any other planet or moon humans

choose to live on). The forces on a particle arising from gravity are:

- *Gravitational force*. The weight of the particle will tend to make the particle fall in a gravitational field.
- *Buoyant force*. The hydrostatic pressure (difference in pressure in the fluid due to height difference) tends to make the particle rise in a gravitational field.

These forces are illustrated in Fig. 3.5. If the particle density is greater than the fluid density then the overall force will cause the particle to sink. Conversely if the particle density is less than the fluid density, then the particle will rise. When the particle density is the same as the density of surrounding fluid, there is no net force on the particle and the particle is said to be 'neutrally buoyant'. The density of an average red cell, at 1125 kg m^{-3} , is slightly higher than that of plasma at 1025 kg m^{-3} , and so red cells have a slight tendency to sink.

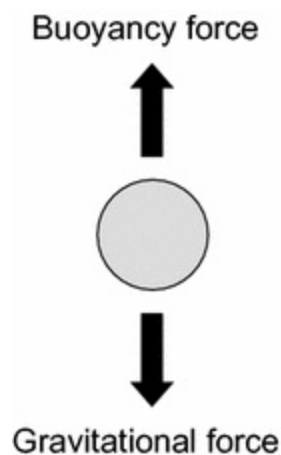


Fig. 3.5 Forces on a particle initially at rest in a stationary fluid

3.2.2 Forces Associated with the Velocity and Shear Field at High Reynolds Number

Forces arising from the velocity and shear field have different effects depending on the flow conditions in the vessel. In the following sections the forces will be based on Reynolds number. It will be recalled that Reynolds number (Re) is the ratio of inertial to viscous forces. Effects due to inertia of the fluid (present at high Re) are most prevalent in larger vessels and will be

considered in this section. Effects relevant at lower Re (<1) where viscous forces dominate, are most prevalent in the microcirculation and will be considered in the next section. Figure 3.6 shows the principal forces arising from motion of the fluid. The forces are as follows:

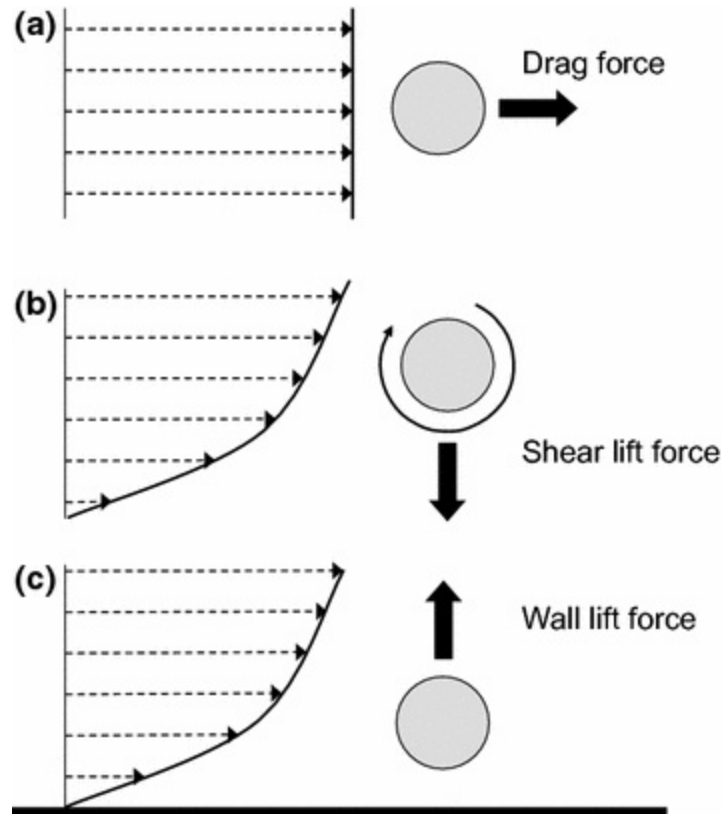


Fig. 3.6 Inertial forces arising from motion of the fluid with respect to the particle. **a** Drag force. **b** Shear induced lift. **c** Wall induced lift. Note that lateral motion of the particle will also give rise to a drag force

- *Drag force.* When there is relative motion between the fluid and the particle, the particle experiences a force in the direction of the flow as a result of the inertia of the particle. If a fluid is at rest and is subject to a pressure gradient, the fluid will accelerate. The particle experiences a force in the direction of the fluid motion which accelerates the particle until there are no forces in the direction of motion. If there is lateral motion of the particle (i.e. across streamlines) then this relative motion will also lead to a drag force.
- *Shear-induced inertial lift.* When a particle is in a shear field the difference in shear on either side of the particle causes the particle to

spin. There is an associated force perpendicular to the direction of fluid motion which causes the particles to migrate to higher shear rate regions. The force originates from inertial effects in the fluid surrounding the particle. Ho and Leal (1974) provided one of the first theoretical formulations which gave good agreement with experimental data.

- *Wall-induced inertial lift forces.* A number of different inertial forces are present on a particle near a wall or a particle touching a wall. All these forces are directed away from the wall leading to motion of the particle away from the wall. These include lift on a non-spinning particle near a wall (Cherukat and McLaughlin 1994), lift on a spinning particle near a wall (called the Magnus effect), and lift on a particle touching the wall (Leighton and Acrivos 1985).

In 1962, Segre and Silberberg published a paper on flow of neutrally buoyant solid particles in a vertical tube. The particles were uniformly distributed at the inlet to the tube but, further along, they located in a ring of particles at a distance of 0.6 of the tube radius from the centre. This was termed the ‘tubular pinch effect’ and subsequently became known as the Segre-Silberberg effect. The pinch effect was strongest for Re numbers of less than about 30. For higher Re the width of the particle-free region near the wall increased and there was spreading of the particles throughout the whole cross section of the tube. The explanation for this effect concerns inertial forces which push the particle across the streamlines (di Carlo 2009). Particles experience a shear-induced lift force which pushes the particles away from the centre. Particles near the wall experience a lift force as a result of the presence of the wall which pushes them away from the wall. The particles locate at a distance where these 2 forces balance each other (Fig. 3.7). At higher Reynolds numbers, the balance of lift forces changes and the equilibrium position moves towards the wall. Higher Reynolds number flows of 500–2000 is associated with an inner annulus and a more uniform distribution (Matas and Morris 2004). These effects are seen at low volume concentrations, less than 20 %, where particle–particle interaction can be neglected. However, any particle suspension at $Re > 1$ will be subject to these lift forces to some degree, which will lead first, to particle depletion at the wall and second, to inhomogeneity in particle concentration.

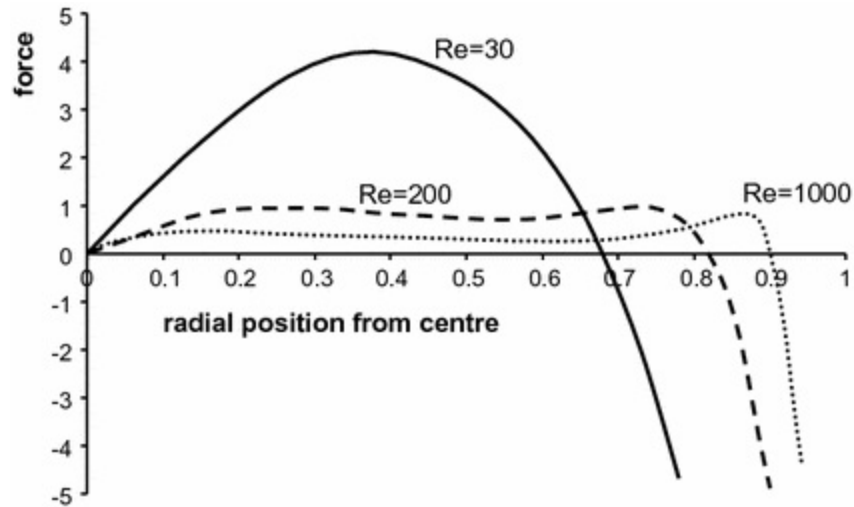


Fig. 3.7 Overall inertial lift force on a particle in Poiseuille flow in a cylinder for a dilute suspension of particles; at low shear the equilibrium position is at 0.68 of the diameter corresponding roughly to the Segre-Silberberg position. At higher shear the equilibrium position moves nearer to the wall. From Matas and Morris (2004); reproduced with permission

3.2.3 Forces Associated with the Velocity and Shear Field at Low Reynolds Number

At low Reynolds numbers < 1 , flow is dominated by viscous effects. Forces arising from inertial effects, such as the lift forces discussed in Sect. 3.2.2, do not occur. A formal explanation for this is that at very low Re , fluid flow is governed by Stokes flow which is time reversible for spherical objects meaning that viscous forces cannot operate (see, e.g. Cantat and Misbah 1999). Inertial-based lateral motion of a particle is therefore impossible. However, viscous lateral motion is possible and mainly relevant to deformable particles. The forces leading to lateral motion are described here. For further reading see Vlahovska et al. (2009).

- *Drag force.* Relative motion between the particle and the fluid will result in a drag force due to the viscous forces between the fluid and the particle surface.
- *Lift due to loss of particle symmetry.* An initially spherical particle which is deformable will become elongated as a result of the difference in drag on the particle from the wall and the non-wall side. In particular, the particle will have upstream–downstream asymmetry resulting in a viscous lift force (Olla 1997; Cantat and Misbah 1999).

- *Lift due to tank-treading.* A deformable particle undergoing tank-treading (see Sect. 3.3) near a wall will experience a lift force which causes it to move away from the wall (Olla 1997; Kaoui et al. 2008).

These forces contribute to the creation of a cell-free layer in the microcirculation where viscous flow dominates, discussed further in Chap. 8.

3.2.4 Chemical and Electrical Forces

These forces generally operate at close range and arise through interaction between particles, rather than through the dynamic behaviour of the fluid in which the particles are suspended. Figure 3.8 illustrates these two forces.

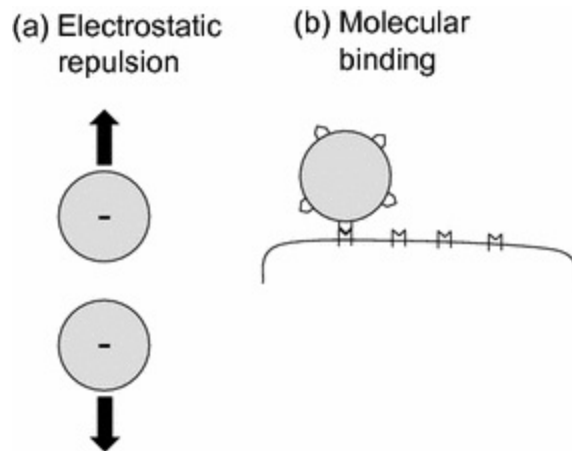


Fig. 3.8 Electrostatic and chemical forces on a particle in a fluid

- *Electrostatic forces.* Electrically charged particles will repel similarly charged particles and attract particles of opposite charge. Some particles may have overall neutral charge but the charge can be split in the form a dipole with a positive and negative end. In this case the positive and negative ends of adjacent particles attract and the similarly charged ends repel.
- *Molecular binding forces.* These concern the binding of one biological cell or molecule with another biological cell or molecule.

Electrostatic forces are important in that red cells, white cells and platelets all have a negative charge. This helps to keep them apart and helps prevent thrombus formation in the normal circulation. Electrostatic forces are also the origin of a lift force on deformable particles near a wall. If a particle

deforms in shear flow near a wall, an electrostatic dipole will be produced which interacts with the mirror of the dipole in the wall producing a lift force (Leal 1980).

Molecular binding forces are especially relevant in blood flow and three phenomena will be considered in more detail; Rouleaux formation, leukocyte adhesion and platelet aggregation and adhesion.

Rouleaux formation

Red cells at low shear clump together face to face to form rouleaux (Fig. 3.13). A review by Wagner et al. (2013) considers two explanations for this; the bridging model and the depletion model. Rouleaux formation in vivo is thought to require the presence of albumin and fibrinogen. If plasma is replaced with an isotonic saline solution then rouleaux formation does not take place. In the bridging model, albumin and fibrinogen are adsorbed onto the surface of the red cell. There is chemical bonding between the molecules on the surfaces of adjacent red cells, which is sufficient to overcome the electrostatic repulsion resulting in adhesion of red cells and rouleaux formation. In the depletion model, a randomly low concentration of albumin and fibrinogen concentration gives rise to a depletion force (see Sect. 3.2.5), which results in red cell adhesion and rouleaux formation.

Leukocyte adhesion

Activated white cells travelling close to the vessel wall form molecular links with endothelial cells. These links are formed through bonding between ligands on the white cell and selectin molecules on the endothelium. If other forces (e.g. related to particle inertia and shear) are greater than the molecular binding force then the link is broken, the white cell rolls along the endothelium until a link is re-established. This repeatedly happens and the white cell rolls along the endothelium until either the shear forces are sufficient to detach the white cell or the molecular links are strong enough to prevent the cell from rolling further. Leukocyte adhesion is a necessary step in the migration of leukocytes through the endothelium.

Platelet aggregation and adhesion

Activated platelets chemically bond to each other via macromolecules (fibrinogen and von Willebrand factor) present in plasma. Platelets also adhere to collagen exposed by damaged endothelium. These are important

steps in thrombus formation.

3.2.5 Forces Arising from Collision

Particles in a fluid are subject to collisions from both fluid molecules and other particles. These collisions give rise to a number of different forces (Fig. 3.9).

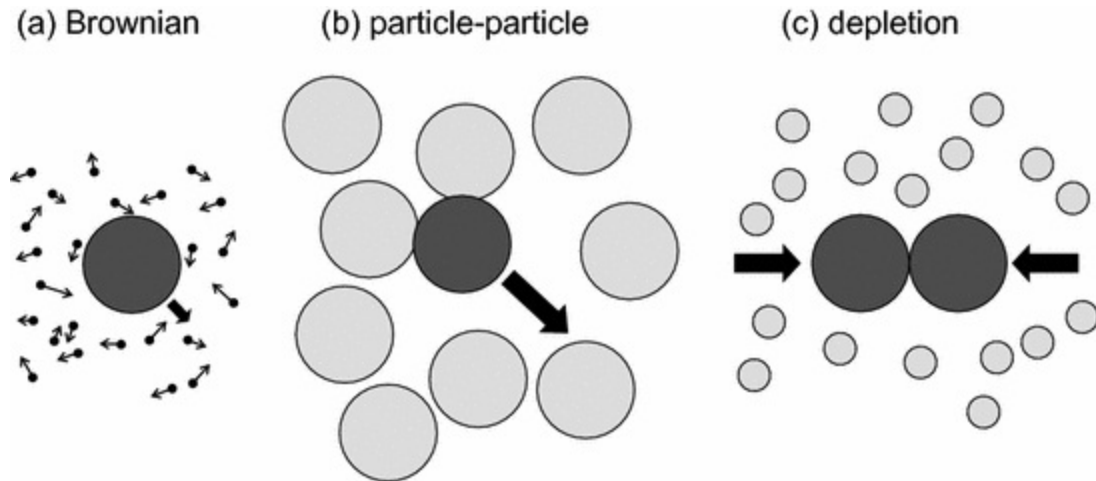


Fig. 3.9 Forces arising from collision of particles. **a** Forces arising from collisions from fluid molecules leading to a small force whose magnitude varies randomly in time and magnitude leading to small random movements of the particle (Brownian motion). **b** Forces arising from collisions between particles. **c** Depletion force. Where the large particles touch there is a region where small particles are excluded. This produces an attractive force between the two large particles

- *Fluid-particle forces (Brownian motion).* Random variations in the number of fluid molecules impacting on the particle will produce small random forces which vary in magnitude and direction. This results in a particle suspended in the fluid having random erratic movements, called Brownian motion. This motion is more significant for particles with small mass, such as LDL cholesterol, and less so for heavier particles such as blood cells.
- *Particle-particle forces.* When the volume fraction of particles is small, collisions between particles are rare and the particles can be considered to be independent in that their main interaction is with the surrounding fluid and not with other particles. As the volume fraction increases collisions which are more common and becomes a major factor in determining the distribution of particles within the fluid volume and the

viscous behaviour.

- *Depletion force.* If a fluid contains macromolecules such as albumin then these act to keep larger particles such as red cells apart. Where there is a local deficiency in macromolecules, occurring through random changes in their distribution, this will allow the larger particles to be in close contact. This is equivalent to a force and is called a ‘depletion force’ (Asakura and Oosawa 1958).

Whether the particle is solid or deformable is a key determinant of viscous behaviour. For a suspension of solid particles, the viscosity increases with volume fraction, linearly at first, but then non-linearly, finally reaching an infinite value at about 64 % volume fraction (Gondret 1997). At this concentration the fluid no longer flows as the particles cannot flow past each other due to the close proximity of their neighbours and the fluid behaves as a solid. For a suspension of deformable particles, the viscosity is lower than for a suspension of solid particles of the same volume fraction, and flow is maintained at higher volume fractions. It has been reported that a suspension of red cells will continue to flow for volume fractions up to 98 %. Figure 3.10 illustrates the viscosity—shear rate behaviour for idealised solid spheres and red cells.

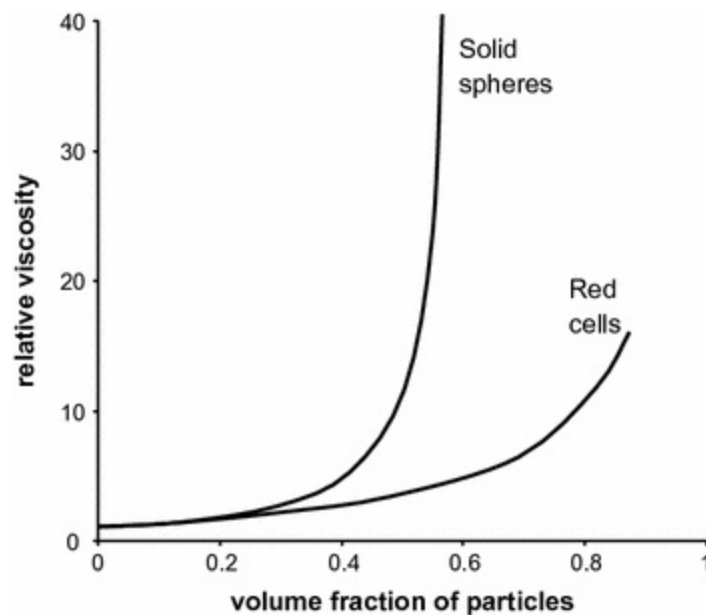


Fig. 3.10 Viscosity as a function of particle volume fraction for idealised solid particles and red cells at a shear rate of 200 s^{-1} . Red cell data from Goldsmith (1972). Solid particle data from Gondret (1997)

In a suspension of identical particles, there is movement of particles across streamlines so that the particle distribution is non-homogeneous and consequently the local viscosity is also non-homogeneous. The collision rate is dependent on the local shear gradient. A higher shear gradient means more particles flowing past each other, which results in more collisions. The collisions give rise to lateral displacement of the particles towards regions of lower collision rate and lower shear gradient. For steady flow in a tube, the shear gradient is zero at the centre of the tube increasing to a maximum at the wall. This can lead to higher particle concentrations at the tube centre than at the tube wall and blunting of the velocity profile (Lyon and Leal 1998; Kumar and Graham 2012a). This phenomenon is generally described with respect to low Reynolds number flows (<1), however in principle it is also applicable to higher Reynolds number flows including at physiological values seen in large arteries. For example, the study below by Aarts et al. (1988) reports decreased red cell concentration at the vessel walls in a 3 mm vessel with a Reynolds number of between 280 and 1150, which is comparable to that in arteries.

For flow of a suspension of particles of different size there are, in addition to the interactions described above, interactions between the different types of particles. The 1988 study by Aarts investigated the distribution of platelets and red cells in a suspension of red cells at 45 % haematocrit. This was undertaken in a glass tube of 3 mm diameter at wall shear rates from 240 to 1260 s^{-1} ; comparable to physiological flow in a small artery such as the brachial or anterior tibial arteries. The platelets were suspended in a saline fluid and also in a suspension of red cell ghosts at 45 % volume fraction. Red cell ghosts are red cells rendered optically transparent by removal of their haemoglobin. During preparation, the red cells are made to burst spilling the haemoglobin contents. After washing and immersion in saline, the red cell membranes reform in a biconcave shape. Figure 3.11a shows the distribution of platelets when immersed in saline. There is accumulation roughly midway between the wall and the centre of the tube, as expected from the Segre-Silberberg effect. When immersed in ghosts, the platelets mostly accumulate near the vessel wall (Fig. 3.11b). The phenomenon of cell accumulation near the vessel wall is called 'margination'. Blood cell margination has been studied using both experimental techniques and computational modelling (see reviews by Kumar and Graham 2012a, b). Cell stiffness rather than cell size is thought to

be the principle determinant of cell margination. Platelets, white cells and diseased red cells arising from malaria and sickle cell disease are all stiffer than normal red cells and all marginate. The process of margination is further enhanced by rouleaux formation (Nash et al. 2008). Margination of stiff particles by red cells looks to be a design feature of the cardiovascular system. Platelets are pushed to the wall so that they can be available for endothelial repair and thrombus formation. White cells are pushed to the wall so that they can be available for combating infection in tissues by crossing the endothelium.

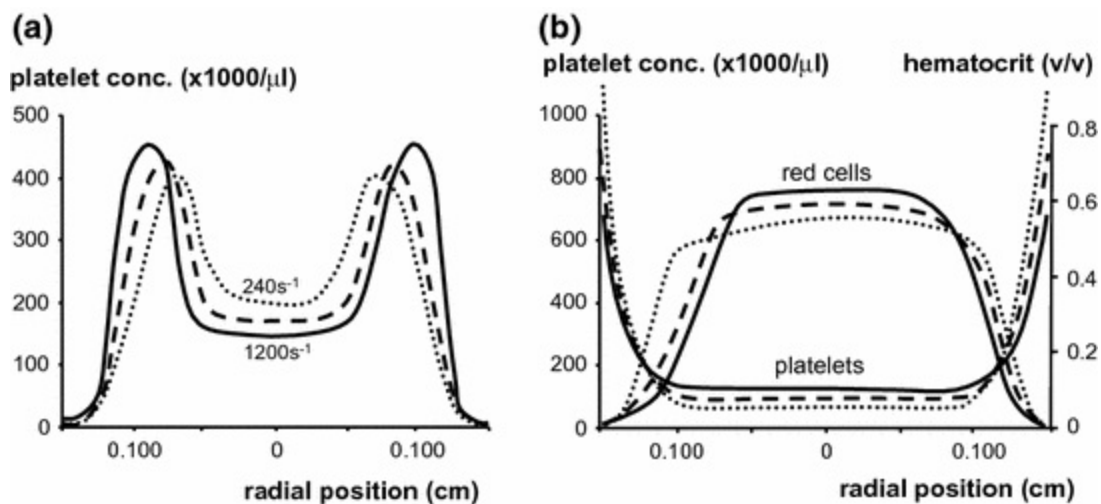


Fig. 3.11 Red cell and platelet distribution with radial position for blood flowing in a tube of 3 mm internal diameter. **a** Platelets in saline at wall shear rates of 1200 s^{-1} (solid line), 760 s^{-1} (dashed line), 240 s^{-1} (dotted line). **b** platelets in ghosts (optically transparent red cells); same wall shear rates as (a). From Aarts PAMM, van den Broek SA, Prins GW, Kuiken GDC, Sixma JJ, Heethaar RM; Blood platelets are concentrated near the wall and red blood cells, in the center in flowing blood; *Arteriosclerosis* 1988;8(6):819–824, reproduced with permission

3.3 Viscous Behaviour of Blood

This section provides a discussion on the viscous behaviour of blood including variations in viscosity within the vessel. The viscous behaviour of blood is almost entirely dominated by the behaviour of red cells, so this section will focus on the behaviour of red cells with shear rate and vessel diameter, and their effect on white cells and platelets.

3.3.1 Behaviour of Single Blood Cells

A mammalian biological cell consists of a lipid bilayer (the cell membrane), intracellular fluid (cytoplasm) and a skeletal structure (cytoskeleton) which gives the cell rigidity and through which cell movement is effected, and various internal structures (organelles). The lipid bilayer is some 6 nm thick and acts like an incompressible 2D fluid in that the surface area is difficult to increase but the elements of the bilayer may flow over the surface of the cell. When a cell is subject to shear the bilayer may flow around the cell in the same way that the tracks of a tank rotate around the drive wheels (hence the term ‘tank treading’). The cytoskeleton consists of filaments and tubules which are anchored at proteins floating within the lipid bilayer.

A number of methods exist for measuring the viscoelastic properties of cells and the reader is referred to the article by Yamada et al. (2000) for a review of some of these methods. Reported values of stiffness and viscosity for blood cells are provided by Tran-Son-Tay and Nash (2007). For the purpose of this chapter it is sufficient to note that platelets and white cells are much stiffer than red cells and this qualitative description will allow us to explore their behaviour in flow.

In the red cell, the cytoskeletal network (‘spectrin’) is immediately below the lipid bilayer and is coupled to it at various points. The spectrin network determines the biconcave shape of the red cell. Spectrin has shape-memory so after deformation the red cell reassumes its biconcave shape.

The biconcave disc shape allows the red cells to undergo considerable deformation without a change of surface area, and more importantly, without rupture of the cell. At low shear ($\sim 3 \text{ s}^{-1}$) the red cell will undergo tumbling but still maintains its biconcave shape. At slightly higher shear ($\sim 6 \text{ s}^{-1}$), the red cell will experience tank-treading (Dupire et al. 2012). As the shear rate increases, the red cell deforms, becoming stretched with the long axis aligned at an angle with respect to the flow. The degree of stretching increases with shear rate (Fig. 3.13). In small diameter tubes at low Reynolds numbers (comparable to flow in the microcirculation) the red cell deforms and a number of characteristic shapes are seen (Fig. 3.12). For diameters of 4–7 μm the red cell resembles a bullet; for diameters of 7–10 μm , where red cells travel in a single line, the cell resembles a parachute, for higher diameters the red cells interact and may assume a slipper shape. In the extreme case, the deformability of the red cell allows it to squeeze through an orifice of only 3 μm in diameter.

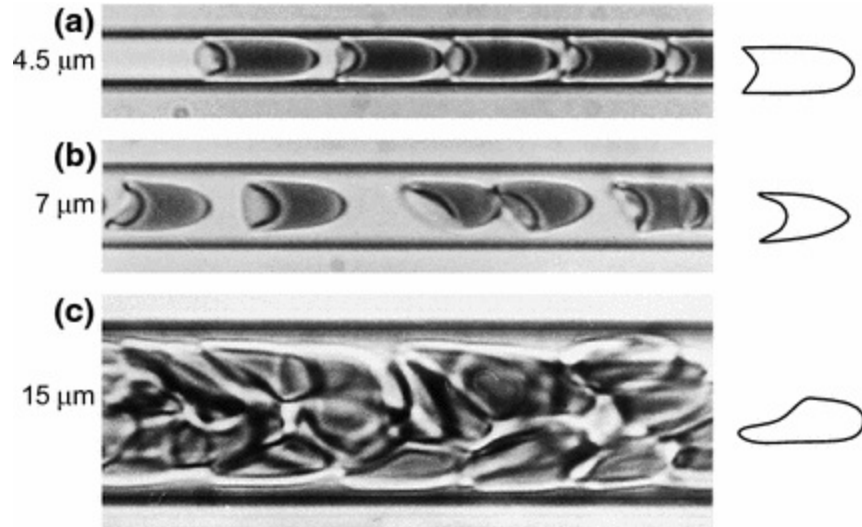


Fig. 3.12 Flow of blood in small diameter tubes; **a** 4.5 μm —the red cell distorts to a *bullet shape*, **b** 7 μm , the red cell distorts to a *parachute shape*, **c** 15 μm —some of the red cells have *slipper shapes*. Reprinted from Pries AR, Secomb TW. Blood flow in microvascular networks. In: Tuma RF, Duran WN, Ley K, editors. Handbook of Physiology: Microcirculation. pp. 3–36, Copyright (2008) with permission from Elsevier

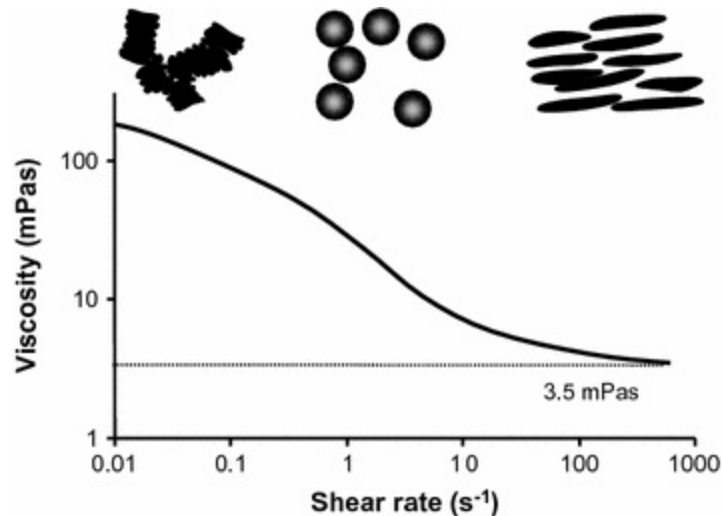


Fig. 3.13 Schematic of whole-blood viscosity as a function of shear rate and of the appearance of red cells at different shear rates. There is rouleaux formation at low shear; independent red cells at intermediate shear; elongation at high shear. The high-shear viscosity is 3.5 mPa s

White cells are observed to take much longer than red cells in traversing capillaries and this is put down to the increased stiffness of white cells. White cells contribute significantly to resistance in microvascular beds. If there is increased white cell stiffness as a result of cell activation, or if there is decreased perfusion as a result of disease, then white cells can get stuck in the

capillary bed with local occlusion of blood flow (Tran-Son-Tay and Nash 2007).

3.3.2 Viscosity—Shear Rate Behaviour of Whole Blood

A cone plate viscometer is typically used to measure the change in viscosity of blood as a function of shear rate. Figure 3.13 shows that blood is a shear-thinning fluid in which the viscosity decreases with increasing shear rate. This behaviour can be explained entirely through changes in the red cell behaviour. In other words the viscous behaviour of whole blood is dominated by the red cell behaviour, not that of white cells or platelets.

At low shear, the high viscosity results from the presence of rouleaux. At very low shear, the rouleaux will form an interlocking structure which requires a small yield stress before flow occurs. As shear rate increases rouleaux formation decreases and viscosity decreases. At shear rates above about 10 s^{-1} rouleaux do not form. Red cell deformation occurs for a shear rate above about 1 s^{-1} . As shear rate increases, red cells elongate and partially align themselves with the flow direction causing decrease in viscosity. At the highest shear rates, there may be layering of red cells with plasma rich regions, which further decreases viscosity. Figure 3.14 is a schematic of the contribution of red cell aggregation and deformation to the viscous behaviour of blood with varying shear rate. If it is assumed that red cells are stiff then the viscosity is roughly constant with shear rate. Adding aggregation results in an increase in viscosity at low shear. Adding deformation results in a reduction in viscosity at higher shear. Further details on the effect of aggregation and deformation can be found in Chien (1970). Table 3.2 summarises the behaviour of red cells in whole blood at increasing shear rate.

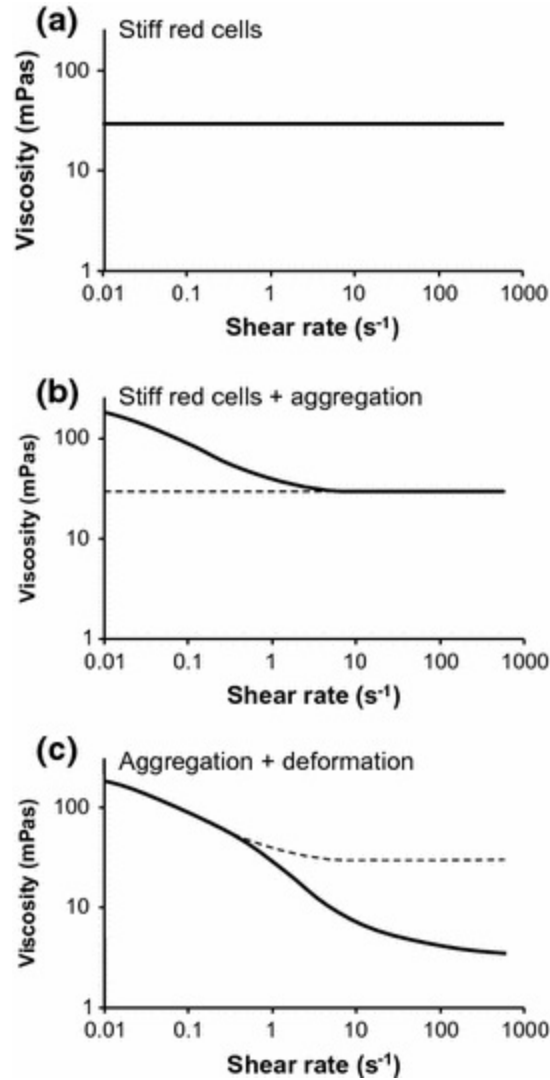


Fig. 3.14 Schematic of the contribution of various components to the viscosity of whole blood. **a** Viscosity for red cells which are stiff and independent. **b** Viscosity when red cell aggregation is included. **c** Viscosity when red cell deformation is included

Table 3.2 Summary of red cell behaviour at different shear rate

Shear rate (s ⁻¹)	Red cell behaviour
0–0.01	Virtually all red cells form rouleaux Rouleaux tangle forming an interlocking structure like a solid There is a very small yield stress
0.01–1	Rouleaux length decreases Chains align themselves with respect to flow direction
1–100	Very few rouleaux present; none above about 5 s ⁻¹ Red cells begin to deform, elongating and aligning with flow direction
100–1000	Red cells are elongated

3.3.3 Viscosity—Diameter Behaviour of Whole Blood

Two historical studies are commonly used to illustrate phenomena involving flow of blood in small diameter vessels; one by Fahraeus in 1929 and the other by Fahraeus and Lindqvist in 1931, and in each case the effects observed have been named after the authors (Fig. 3.15). The Fahraeus effect is that the haematocrit of blood in a tube of small diameter is less than the haematocrit of blood in the receiving tank. The effect is most pronounced at a tube diameter of 12–13 μm . The Fahraeus–Lindqvist effect is that the viscosity in the tube (measured from pressure and flow) depends on tube diameter, reaching a minimum viscosity at a tube diameter of 7 μm . The key feature is the presence of a layer near the wall which is free of red cells. Observations of a cell-free layer were made by Pouiseulle in the mesenteric circulation of the frog in the nineteenth century. Fahraeus and Lindqvist hypothesised that the reduced viscosity in the plasma layer near the wall (1.8 mPa s as opposed to 3–4 mPa s for whole blood) meant that the effective viscosity for flow of whole blood was reduced. The presence of a cell-free layer also explains the Fahraeus effect. The plasma layer near the wall moves at low velocity and the red cells in the centre of the vessel move at high velocity. The overall result is that the relative volume of red cells to plasma is greater in the discharge fluid than for the fluid in the tube. Both these effects have been extensively investigated by others, extending the range of diameters and the range of haematocrit values. Figure 3.15 is based on best-fit equations to experimental data obtained by Pries et al. (1990, 1992). These effects are most relevant for the microcirculation where vessel diameter varies from 5 to 10 μm in capillaries to a maximum diameter of around 200 μm in arterioles.

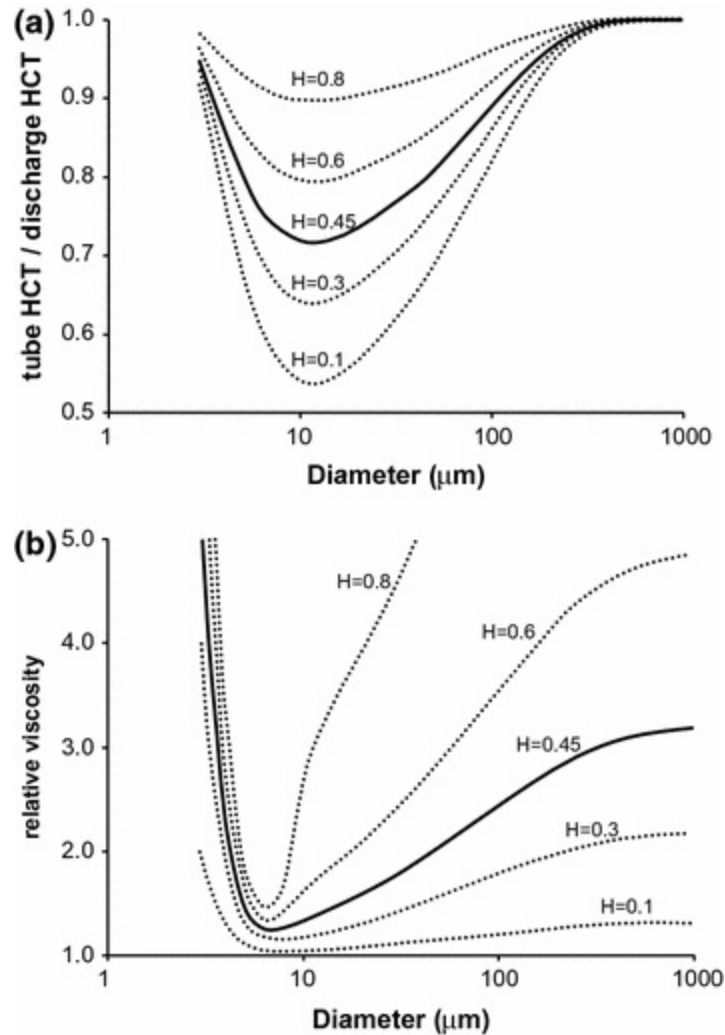


Fig. 3.15 Flow of blood in glass tubes at different haematocrit. **a** Fahraeus effect; the ratio of tube haematocrit (H) to discharge haematocrit is less than 1 and has a minimum value at 12–13 μm diameter. **b** Fahraeus–Lindqvist effect; the relative viscosity is dependent on diameter with a minimum value at 7 μm diameter. Best-fit equations were used taken from Pries et al. (1990, 1992)

We will now examine the origin of the plasma free layer seen in the Fahraeus and Fahraeus–Lindqvist effects. From Sect. 3.2 we have seen that there are several wall lift forces which could potentially give rise to a cell-free layer, and some of these are dependent on Reynolds number. For Fahraeus–Lindqvist experiments, Reynolds numbers may be calculated from the data provided by Pries et al. (Table 1, 1992). These show a range of Re values from 0.001 to 360 (Fig. 3.16). There are therefore several causes of the plasma-free layer seen for flow of blood in glass tubes. For low $Re < 1$, viscous effects will dominate and so viscous lift forces are relevant. For high $Re > 1$, inertial lift forces are relevant. Where the diameter is sufficient to

allow several red cells adjacent to each other, there will be collisions and red cell migration towards the tube centre. For low diameters, only one red cell at a time can travel along the pipe and there is a lift force associated with asymmetry of the particle.

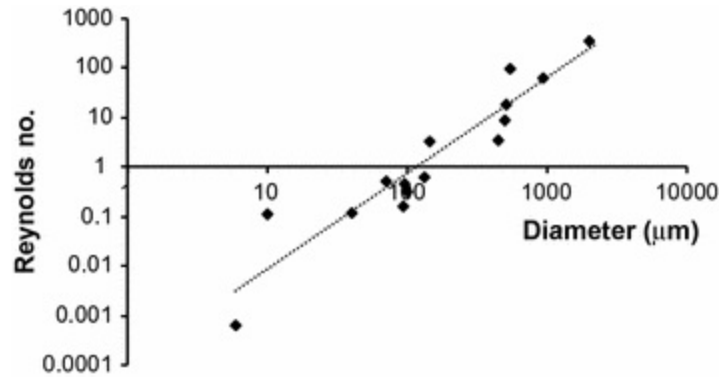


Fig. 3.16 Reynolds number versus tube diameter for experimental data exploring the Fahraeus–Lindqvist effect (calculated from data in Pries et al. 1990)

The themes explored in this section, axial accumulation of red cells, the presence of a cell-free layer, forces arising from deformation of particles, reduction of viscosity in small vessels and local variations in haematocrit are all relevant to the microcirculation and are explored further in Chap. 8.

3.3.4 Viscous Behaviour in Arteries

This section discusses viscous behaviour in vivo in the human arterial system. Table 3.3 summarises the main feature of viscous behaviour for the different cardiovascular system components, including arteries.

Table 3.3 Flow and red cell behaviour in the components of the cardiovascular system

Component	Peak Reynolds number	Turbulence?	Red cell aggregation?	Homogeneous distribution of red cells?
Heart	5000–20,000	Yes	No	Yes
Arteries	5000 (ascending aorta) 500 (smallest arteries)	In ascending aorta (post-systole)	No	Yes
Microcirculation	0.5 (largest arterioles) 0.0003 (capillaries)	No	Yes	No

Veins	100 (smallest veins) 3000–4000 (vena cavae)	No	Yes	No
-------	--	----	-----	----

Arteries in the human have a diameter from 25 to 30 mm for the ascending aorta down to 1 mm for the smallest arteries. The heart acts to mix blood thoroughly so that the red cell distribution leaving the heart is homogeneous. Peak Reynolds numbers (Re) are below 2000 apart from the ascending aorta during ejection of blood where values of 4000–5000 regularly occur. Flow in healthy arteries is therefore laminar apart from a brief period immediately post-systole in the ascending aorta. One might expect that flow would be described by laminar streamlines and effects concerning lateral migration across streamlines should be considered. It was noted above that forces leading to lateral migration across streamlines are always present in suspensions of particles. The study by Aarts in a 3 mm vessel with physiological Reynolds number did show depletion of red cells near the wall. It is, however, generally thought that in arteries, red cells are uniformly distributed apart from a small cell-free region near the wall, which has no effect on overall viscosity. At the time of writing, there does seem to be a lack of definitive studies on which to base this conclusion. Most of the discussion above on force and effects has considered straight tubes and axial flow. In the arterial system, it is recognised that there is a strong helical flow component in most arteries so that flow is not axial. It has been shown that helical flow has a strong mixing effect (Caro et al. 2005; Cookson et al. 2009), though these studies were on spiral flow in grafts. It is possible that the helical flow in arteries acts to mix the red cells leading to a greater homogeneity than would be the case if there were no helical flow.

In Sect. 3.2.2, it was noted that the viscosity of whole blood in arteries is shear dependent reaching a plateau value for shear rates above about 200 s^{-1} . The measured mean shear rate in large arteries is $200\text{--}300 \text{ s}^{-1}$ and the maximum shear is $800\text{--}1000 \text{ s}^{-1}$ (Wu et al. 2004). The assumed homogeneous distribution of red cells and the high mean and maximum shear rates in arteries has led to the conclusion that most of the time it is reasonable to treat blood as a Newtonian fluid with a viscosity equal to that from the high-shear region, commonly taken as $3\text{--}4 \text{ mPa s}$ (e.g. see Pedley 1980). Most of the theoretical, experimental and computational studies on blood

flow have assumed that blood is a Newtonian fluid. However most large arteries, especially those supplying muscle, have periods of reverse flow where the mean velocity passes through zero, and some arteries have no flow for a period during diastole. In this case the wall shear rate will be much less than 200 s^{-1} and it is likely that non-Newtonian effects are present. Evidence for non-Newtonian behaviour in vivo comes from simulation studies performed using computational modelling. These investigate velocity profile and wall shear stress distributions using a Newtonian viscous model, and then using a non-Newtonian model. Figure 3.17 is taken from Johnston et al. (2004) showing wall shear stress in the coronary artery estimated using computational fluid dynamics using a Newtonian model and a Power law model of viscosity. There are clear differences in wall shear stress, especially at the low velocities of 0.02 m s^{-1} . Figure 3.18 shows velocity profiles in an idealised bifurcation estimated using a Newtonian and a non-Newtonian model (Gijssen et al. 1999), again showing clear differences in the estimated flow field data. Non-Newtonian behaviour in arteries is therefore relevant to both the bulk flow field and wall shear stress. The non-Newtonian behaviour in arteries is due to red cell deformation, not aggregation. Ideally non-Newtonian behaviour should be taken into account in blood flow modelling studies, but mostly is not.

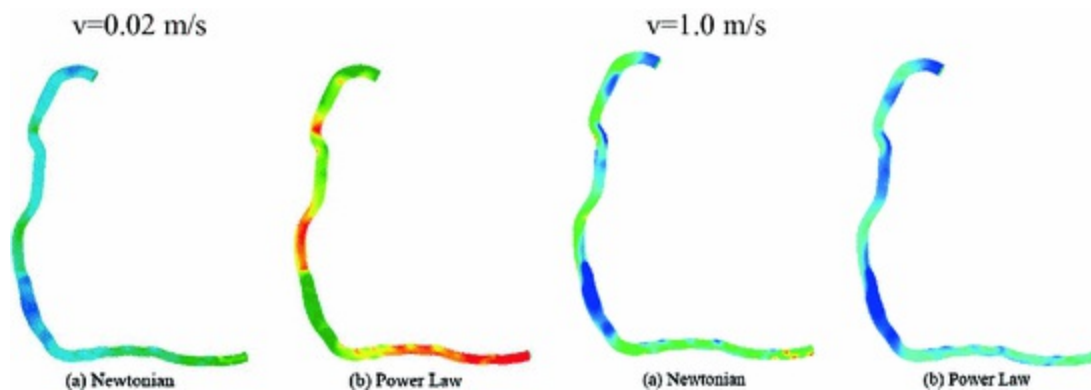


Fig. 3.17 Effect of non-Newtonian viscosity model on wall shear stress. Simulated flow was undertaken in a coronary artery with Newtonian and Power Law non-Newtonian viscous models. Differences are most pronounced at the lower velocity of 2 cm s^{-1} . Reprinted from Journal of Biomechanics Vol. 37, Non-Newtonian blood flow in human right coronary arteries: steady state simulations, Johnston BM, Johnston PR, Corney S, Kilpatrick D; pp. 709–720; Copyright (2004) with permission from Elsevier

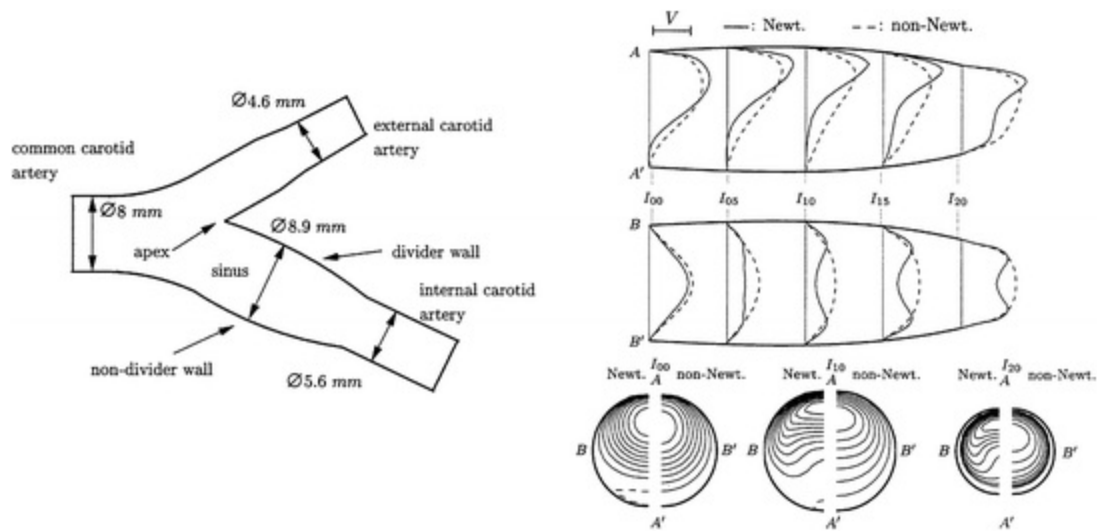
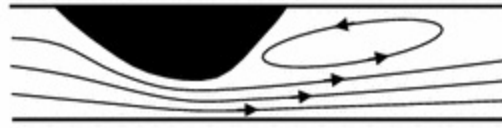


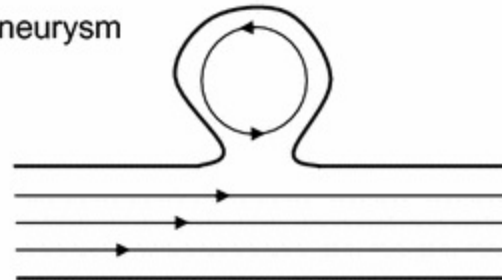
Fig. 3.18 Effect of non-Newtonian viscosity model on the bulk flow field. Simulated flow in the carotid bifurcation was undertaken using a Newtonian and non-Newtonian viscous model. There are differences in velocity profile and in iso-velocity contours. Reprinted from Journal of Biomechanics, Vol. 32, Gijzen FJH, van de Vosse FN, Janssen JD; The influence of the non-Newtonian properties of blood on the flow in large arteries: Steady flow in a carotid bifurcation model; pp. 601–608, Copyright (1999), with permission from Elsevier

Diseased arteries are associated with reduction in local diameter for atherosclerotic plaque and increase in local diameter for an aneurysm. In both cases, there are regions where low shear rate may persist for substantial proportions of the cardiac cycle (Fig. 3.19). If there is a local vortex, then shear will be low and the conditions are suitable for red cell aggregation. There is also evidence from experimental flow studies (Shuib et al. 2011) and from computational modelling (Jung and Hassanein 2008) which suggest that there may be local reductions in red cell concentration (Fig. 3.20). These effects may be relevant in vivo and are the subject of research at the time of writing.

(a) atherosclerotic plaque



(b) saccular aneurysm



(c) fusiform aneurysm

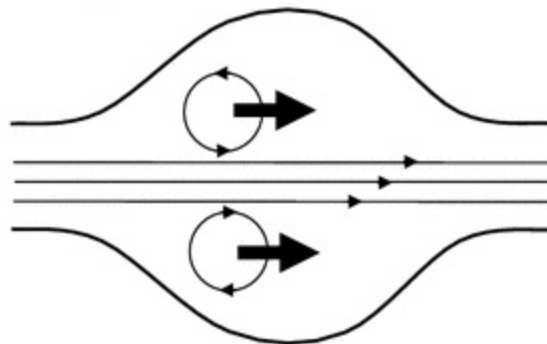


Fig. 3.19 Vortex production in arterial disease which is associated with low shear and can provide suitable conditions for red cell aggregation. **a** Atherosclerotic plaque—a vortex is present in the post-stenotic region which may be stable or which may be shed downstream. **b** Berry aneurysm—a stable vortex is present. **c** Fusilar aneurysm—a vortex ring may be generated which propagates downstream during the cardiac cycle

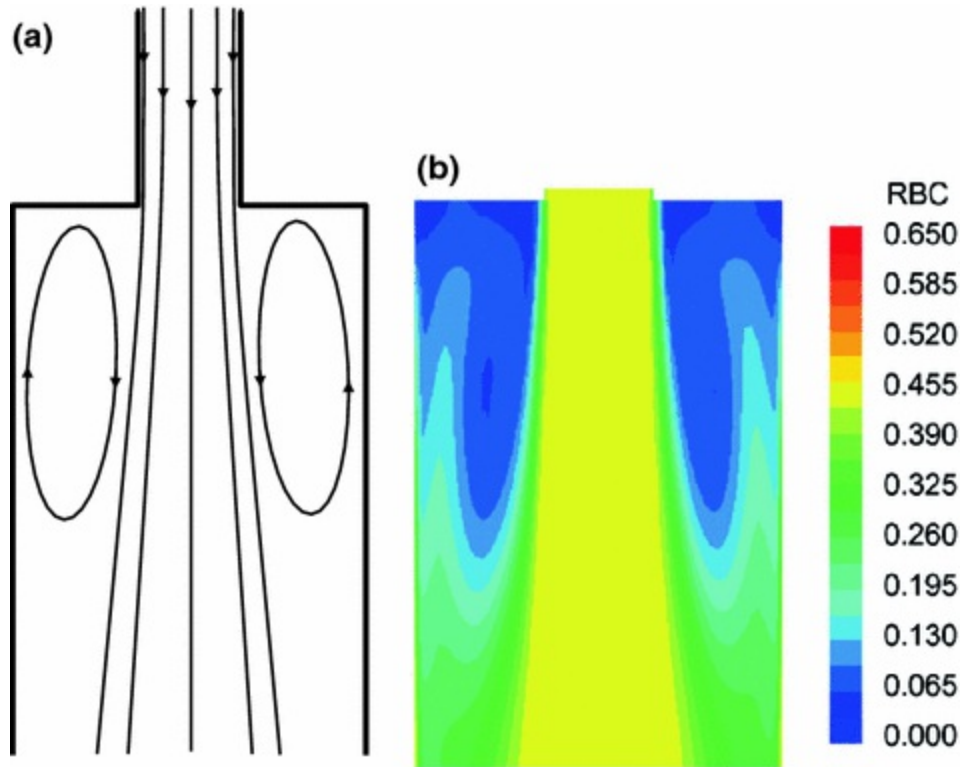


Fig. 3.20 Reduction in red cell volume fraction in low shear regions. Simulated flow of red cells was undertaken for an expansion with volume fraction of 45 % and a maximum velocity of 70 cm s^{-1} at the inlet. **a** Schematic of geometry and flow streamlines. Flow in the inlet has a maximum velocity in the centre of the tube. In the expansion regime there are stable vortices either side of the main flow. **b** Volume fraction of red cells. In the core this is 45 % however in the low shear side regions the volume fraction is as low as 5 %. This suggests that particles may not be distributed uniformly in the region downstream of stenoses in vivo. Reprinted from Medical Engineering and Physics, Vol. 30, Jung J, Hassanein A; Three-phase CFD analytical modeling of blood flow; pp. 91–103, Copyright (2008), with permission from Elsevier on behalf of IPEM

3.3.5 Viscous Behaviour in Other Parts of the Cardiovascular System

From a rheological point of view, the cardiovascular system may be divided into the heart, arteries, microcirculation and veins. Table 3.3 summarises the viscous features of blood in these various compartments. The heart is associated with high Reynolds number flow involving considerable mixing and the treatment of blood as a homogeneous Newtonian fluid with a high-shear viscosity is usually reasonable. Flow in the veins is generally of low Reynolds number (<500), so flow is mostly laminar. In vivo evidence from ultrasound identifies the presence of rouleaux in venous flow (Cloutier et al.

1997; Wang and Shung 2001) suggesting that the non-Newtonian properties of blood are important. Flow in the microcirculation is complex and covered in detail in Chap. 8, building on the discussions of the Fahraeus and Fahraeus–Lindqvist effects covered in Sect. 3.3.3.

References

Aarts PAMM, van den Broek SA, Prins GW, Kuiken GDC, Sixma JJ, Heethaar RM. Blood platelets are concentrated near the wall and red blood cells, in the center in flowing blood. *Arteriosclerosis*. 1988;8:819–24.

[CrossRef][PubMed]

Asakura S, Oosawa F. Interactions between particles suspended in solutions of macromolecules. *J Polym Sci*. 1958;33:183–92.

[CrossRef]

Blausen B. Wikiversity J Med. 2014. doi:10.15347/wjm/2014.010. ISSN 20018762.

Cantat I, Misbah C. Lift force and dynamical unbinding of adhering vesicles under shear flow. *Phys Rev Lett*. 1999;83:880–3.

[CrossRef]

Caro CG, Cheshire NJ, Watkins N. Preliminary comparative study of small amplitude helical and conventional ePTFE arteriovenous shunts in pigs. *J R Soc Interface*. 2005;2:261–6.

[CrossRef][PubMed][PubMedCentral]

Cherukat P, McLaughlin JB. The inertial lift on a rigid sphere in a linear shear-flow field near a flat wall. *J Fluid Mech*. 1994;263:1–18.

[CrossRef]

Chien S. Shear dependence of effective cell volume as a determinant of blood viscosity. *Science*. 1970;168:977–9.

[CrossRef][PubMed]

Cloutier G, Weng XD, Roederer GO, Allard L, Tardif F, Beaulieu R. Differences in the erythrocyte aggregation level between veins and arteries of normolipidemic and hyperlipidemic individuals. *Ultrasound Med Biol*. 1997;23:1383–93.

[CrossRef][PubMed]

Cookson AN, Doorly DJ, Sherwin SJ. Mixing through stirring of steady flow in small amplitude helical tubes. *Ann Biomed Eng*. 2009;37:710–21.

[CrossRef][PubMed]

Di Carlo D. Inertial microfluidics. *Lab Chip*. 2009;9:3038–46.

[CrossRef][PubMed]

Dupire J, Socol M, Viallat A. Full dynamics of a red blood cell in shear flow. *Proc Natl Acad Sci USA*. 2012;109:20808–13.

[CrossRef][PubMed][PubMedCentral]

Fahraeus R. The suspension stability of the blood. *Physiol Rev.* 1929;9:241–74.

Fahraeus R, Lindqvist T. The viscosity of the blood in narrow capillary tubes. *Am J Physiol.* 1931;96:562–8.

Gijssen FJH, van de Vosse FN, Janssen JD. The influence of the non-Newtonian properties of blood on the flow in large arteries: steady flow in a carotid bifurcation model. *J Biomech.* 1999;32:601–8.

[CrossRef][PubMed]

Goldsmith HL. The flow of model particles and blood cells and its relation to thrombogenesis. *Prog Hemost Thromb.* 1972;1:97–127.

[PubMed]

Gondret P. Dynamic viscosity of macroscopic suspensions of bimodal sized solid spheres. *J Rheol.* 1997;41:1261–74.

[CrossRef]

Ho P, Leal LG. Inertial migration of rigid spheres in two-dimensional unidirectional flows. *J Fluid Mech.* 1974;65:365–400.

[CrossRef]

Johnston BM, Johnston PR, Corney S, Kilpatrick D. Non-Newtonian blood flow in human right coronary arteries: steady state simulations. *J Biomech.* 2004;37:709–20.

[CrossRef][PubMed]

Jung J, Hassanein A. Three-phase CFD analytical modeling of blood flow. *Med Eng Phys.* 2008;30:91–103.

[CrossRef][PubMed]

Kaoui B, Ristow GH, Cantat I, Misbah C, Zimmermann W. Lateral migration of a two-dimensional vesicle in unbounded Poiseuille flow. *Phys Rev E.* 2008;77: article number: 021903.

Krüger T. Effect of tube diameter and capillary number on platelet margination and near-wall dynamics. *Rheol Acta.* 2015. Doi:10.1007/s00397-015-0891-6.

Kumar A, Graham MD. Margination and segregation in confined flows of blood and other multicomponent suspensions. *Soft Matter.* 2012a;8:10536–48.

[CrossRef]

Kumar A, Graham MD. Mechanism of margination in confined flows of blood and other multicomponent suspensions. *Phys RevLett.* 2012b;109:108102.

Leal LG. Particle motions in a viscous fluid. *Ann Rev Fluid Mech.* 1980;12:435–76.

[CrossRef]

Leighton D, Acrivos A. The lift on a small sphere touching a plane in the presence of a simple shear-flow. *Z Angew Math Phys.* 1985;36:174–8.

[CrossRef]

Lyon MK, Leal LG. An experimental study of the motion of concentrated suspensions in two-

dimensional channel flow. Part 1. Monodisperse systems. *J Fluid Mech.* 1998;363:25–56.
[\[CrossRef\]](#)

Matas JP, Morris JF. Inertial migration of rigid spherical particles in Poiseuille flow. *J Fluid Mech.* 2004;515:171–95.
[\[CrossRef\]](#)

Nash GB, Watts T, Thornton C, Barigou M. Red cell aggregation as a factor influencing margination and adhesion of leukocytes and platelets. *Clin Hemorheol Microcirc.* 2008;39:303–10.
[\[PubMed\]](#)

Olla P. The lift on a tank-treading ellipsoidal cell in a shear flow. *J Phys.* 1997;7:1533–40.

Pedley TJ. *The fluid mechanics of large blood vessels.* Cambridge: Cambridge University Press; 1980.
[\[CrossRef\]](#)

Pries AR, Secomb TW. Blood flow in microvascular networks. In: Tuma RF, Duran WN, Ley K, editors. *Handbook of physiology: microcirculation.* 2008. p. 3–36.

Pries AR, Secomb TW, Gaehtgens P, Gross JF. Blood flow in microvascular networks. Experiments and simulation. *Circ Res.* 1990;67:826–34.
[\[CrossRef\]](#)[\[PubMed\]](#)

Pries AR, Neuhaus D, Gaehtgens P. Blood viscosity in tube flow: dependence on diameter and haematocrit. *Am J Physiol.* 1992;263:H1770–8.
[\[PubMed\]](#)

Segre G, Silberberg A. Behaviour of macroscopic rigid spheres in Poiseuille flow. Part 2. Experimental results and interpretation. *J Fluid Mech.* 1962;14:136–57.
[\[CrossRef\]](#)

Shuib AS, Hoskins PR, Easson WJ. Experimental investigation of particle distribution in a flow through a stenosed artery. *J Mech Sci Technol.* 2011;25:357–64.
[\[CrossRef\]](#)

Tran-Son-Tay R, Nash GB. Mechanical properties of leukocytes and their effects on the circulation. In: Baskurt OK et al., editors. *Handbook of hemorheology and hemodynamics.* IOS Press; 2007. p. 137–49.

Vlahovska PM, Podgorski T, Misbah C. Vesicles and red blood cells in flow: from individual dynamics to rheology. *C R Phys.* 2009;10:775–89.
[\[CrossRef\]](#)

Wagner C, Steffen P, Svetina S. Aggregation of red blood cells: from rouleaux to clot formation. *C R Phys.* 2013;14:459–69.
[\[CrossRef\]](#)

Wang SH, Shung KK. In vivo measurements of ultrasonic backscattering in blood. *IEEE Trans Ultrason Ferroelec Freq Control.* 2001;48:425–31.
[\[CrossRef\]](#)

Wu SP, Ringgaard S, Oyre S, Hansen MS, Rasmus S, Pedersen EM. Wall shear rates differ between the normal carotid, femoral, and brachial arteries: an in vivo MRI study. *JMRI J Magn Res Im.* 2004;19:188–93.

[\[CrossRef\]](#)

Yamada S, Wirtz D, Kuo SC. Mechanics of living cells measured by laser tracking microrheology. *Biophys J.* 2000;78:1736–47.

[\[CrossRef\]](#)[\[PubMed\]](#)[\[PubMedCentral\]](#)

4. The Arterial System I. Pressure, Flow and Stiffness

Peter R. Hoskins¹✉ and D. Rodney Hose²

- (1) Edinburgh University, Edinburgh, UK
- (2) Sheffield University, Sheffield, UK

✉ **Peter R. Hoskins**
Email: P.Hoskins@ed.ac.uk

Learning outcomes

1. Describe the main constituents of an artery.
2. Describe the organisation of elastin and collagen in the artery.
3. Describe the stress–strain (pressure–diameter) behaviour of arteries.
4. Discuss the stress–strain behaviour of arteries in terms of the mechanical properties of elastin and collagen.
5. Describe pressure–time and velocity–flow waveforms in different arteries.
6. Describe the Windkessel model.

7. Discuss how the Windkessel model produces velocity–time and pressure–time waveforms.
8. Describe pressure wave propagation.
9. Define the Moens–Korteweg equation for pressure wave velocity.
10. Discuss how pressure–time and velocity–time waveforms in arteries arise from pressure wave propagation and reflected waves.
11. Describe laminar, turbulent and disturbed flow in arteries.
12. Describe axial and rotating flow in arteries.
13. Discuss fully developed flow and non-fully developed flow in arteries.

This chapter will explore basic biomechanics of arteries concentrating on pressure, flow and stiffness. Here the emphasis will be on normal function. Abnormal function and disease will be considered in later chapters. In the appendix at the end of the chapter is a table of the values of key quantities in different arteries.

4.1 Stiffness of Arteries

This section describes the stiffness and stress–strain behaviour of arteries in relation to their biological composition.

4.1.1 Structure and Composition of Arteries

Figure 4.1 shows the main structures present within an artery. The endothelium, the basement membrane and the internal elastic lamina (a thin sheet of elastin) together make up the intima on which endothelial cells are attached. The internal elastic membrane allows the endothelium to move independently of the media. The media contains elastin fibres which provide

elasticity, collagen fibres which provide strength, and smooth muscle cells. The outermost layer is the adventitia which contains mainly collagen fibres.

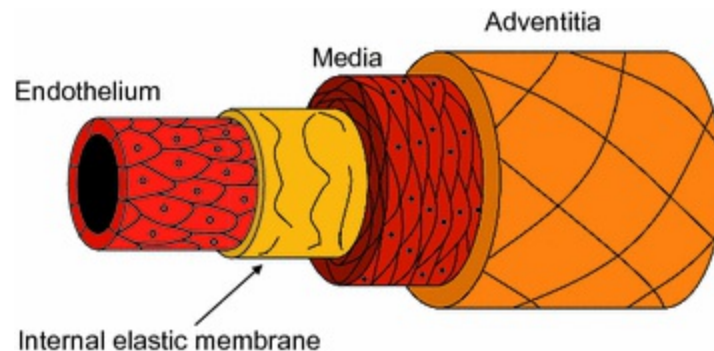


Fig. 4.1 The main components of an artery

From a mechanical point of view the two most important constituents of arteries are collagen and elastin. These are arranged in layers around the artery. The number of sheets increases during gestation but is fixed at birth. The molecules are arranged in a helical pattern around the artery, with a different pitch for different layers within the artery. The collagen molecules are present in a loose, wavy network in the adventitia. As the artery expands so the molecules unfurl to reach their straightened lengths at which point they become extremely stiff. This behaviour protects the smooth muscle cells from acute over-distension.

Elastin is a stable protein with a long half-life of around 50 years, so that the elastin sheets laid down in early life remain in place into later life. Collagen, on the other hand, has a half-life of 2 weeks, and thus is in a continuous state of turnover.

4.1.2 Stress–Strain Behaviour in Arteries

The stress–strain behaviour of an artery may be characterised by a plot of pressure versus diameter. Figure 4.2 shows pressure–diameter behaviour in an excised artery subject to an inflation pressure. The diameter–pressure behaviour is nonlinear, though over a restricted range (e.g. 80–120 mmHg) it is approximately linear. Within the physiologic range Fig. 4.2 shows a 10 % increase in diameter which is typical of the variation found in vivo during the cardiac cycle.

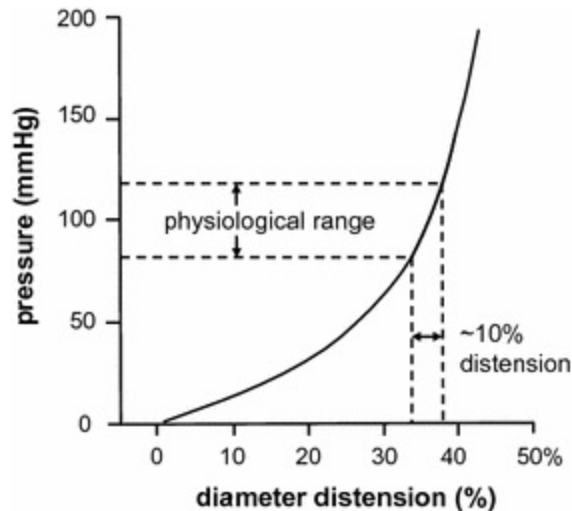


Fig. 4.2 Pressure-distension for an artery. The behaviour is nonlinear; the physiologic range of 80–120 mm Hg produces a 10 % variation in diameter

The contribution of elastin and collagen to the stress–strain behaviour was explored by Roach and Burton (1957). Figure 4.3 shows the tension-radius behaviour for 3 samples of artery. In the left curve the elastin has been removed by a chemical process so that the mechanical behaviour of the artery is governed by the collagen. The artery is quite stiff so that high stress has to be provided to stretch the vessel. In the right trace the collagen has been digested so that mechanical behaviour is governed by the elastin. The artery is now quite elastic so that that small changes in stress result in large changes in diameter. The elastic behaviour of the untreated artery can be explained by the different behaviours of collagen and elastin. At small distensions the collagen fibres are quite crimped and the behaviour is dominated by elastin. At high extensions the collagen fibres have straightened out; these now dominate mechanical behaviour and the artery becomes very stiff. This may be likened to a balloon in a net. Blowing up the balloon is easy until it is the same size as the net, at which point it is difficult to blow up the balloon much further.

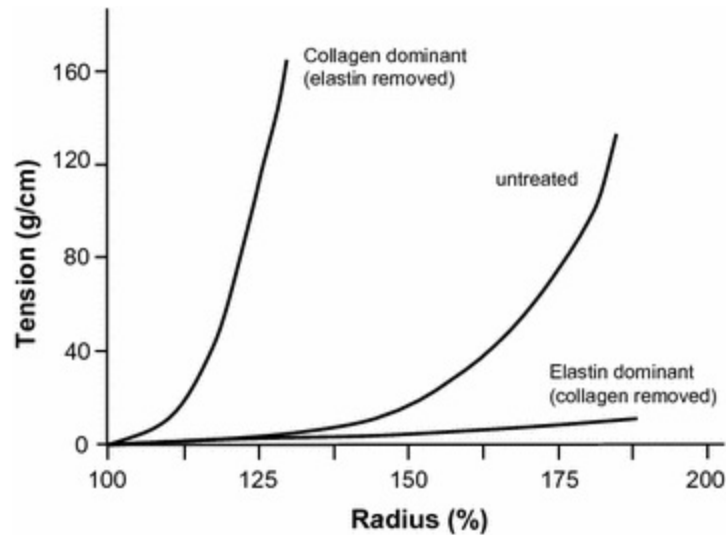


Fig. 4.3 Effect of collagen and elastin on the tension-radius behaviour for an artery. Removal of elastin leads to stiffening; removal of collagen leads to more elastic behaviour. From: Roach MR, Burton AC; The reason for the shape of the distensibility curve of arteries; *Can J Biochem Physiol.* 1957;35:681–690; © Canadian Science Publishing or its licensors; redrawn with permission

As introduced in Chap. 1, the elastic modulus of elastin, collagen and arteries may be measured in a tensile testing system. The elastic modulus for elastin is low at 0.4–0.6 MPa but for collagen is much higher at 100 MPa. Arteries have intermediate values of 1–5 MPa (Ryan and Foster 1997). Note that, in the case of collagen and artery, incremental elastic modulus values are reported as the stress–strain behaviour is nonlinear. The Young’s modulus for an artery describes the composite behaviour.

The artery is a multi-layer structure and each layer has different mechanical properties. However to describe the overall stress–strain or diameter–pressure behaviour for an artery it is not necessary to know the elastic moduli of the different layers. This approach assumes that the artery is uniform and homogeneous; i.e. that the wall thickness and elastic composition are the same for different positions around the circumference. This assumption is valid in healthy arteries although it may not be true in disease due to 3D changes in geometry, wall thickness and wall composition (see later chapters).

4.2 Pressure and Flow Waveforms in Arteries

Figure 4.4 shows pressure–time waveforms from various arteries in the systemic circulation. The baseline or diastolic pressure in this example is

about 80 mm Hg. The peak or systolic pressure increases with distance from the heart; in this example from 110 mm Hg at the aortic outflow to 160 mm Hg at the tibial arteries. There is also some change in shape of the pressure waveform with distance from the heart. Figure 4.4 also shows velocity–time waveforms taken using Doppler ultrasound. The waveforms are all similar in that they have a period of forward flow followed by a period of reverse flow. Figure 4.5 shows more time–velocity waveforms, taken from arteries supplying the brain and kidney. These organs have a low vascular resistance and the time–velocity waveforms have flow throughout the cardiac cycle. In this section we will be looking at the origins of the shape of the pressure and flow waveforms in different arteries.

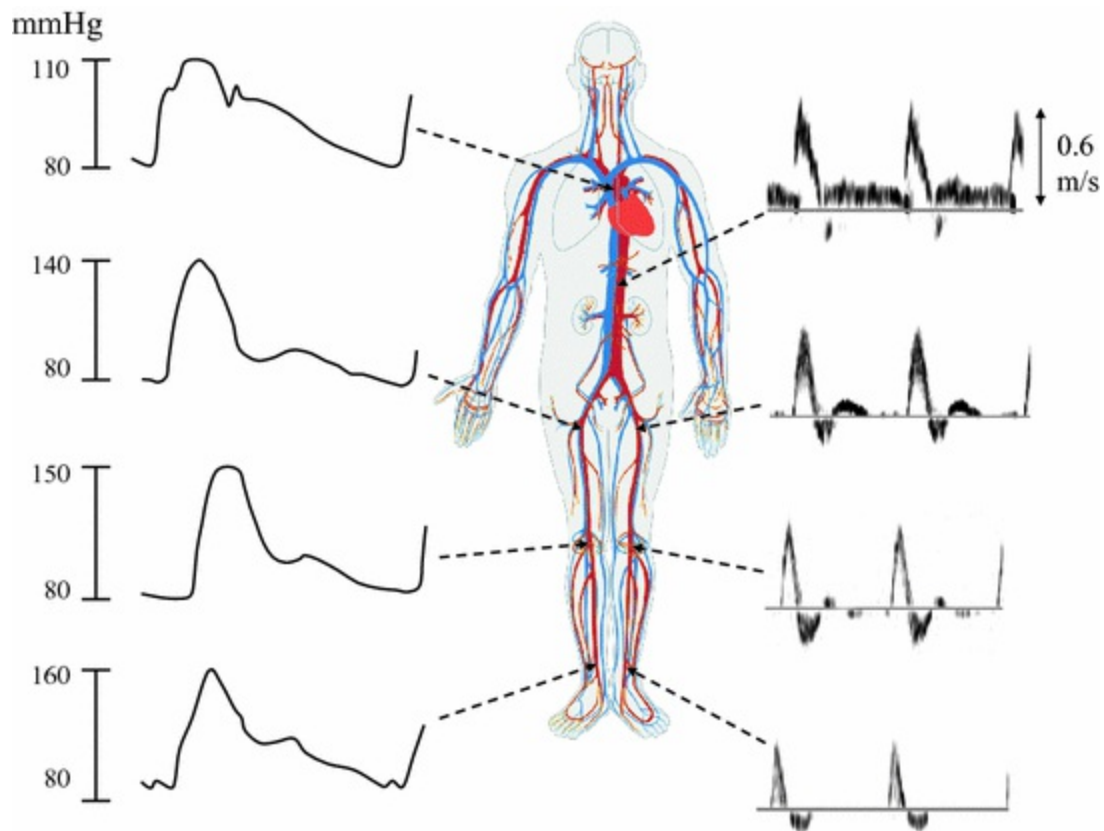


Fig. 4.4 Blood pressure–time and velocity–time waveforms at increasing distance from the heart. There is a baseline (diastolic) pressure of 80 mm Hg; the peak (systolic) pressure increases with distance and there are changes in the overall shape. The flow waveforms are taken from Doppler ultrasound. The waveforms are pulsatile with a period of forward flow followed by a period of reverse flow then more forward flow. Circulation figure reproduced from Wikipedia; https://commons.wikimedia.org/wiki/File:Circulatory_System_en.svg. This image is in the public domain and was authored by Mariana Ruiz Villarreal

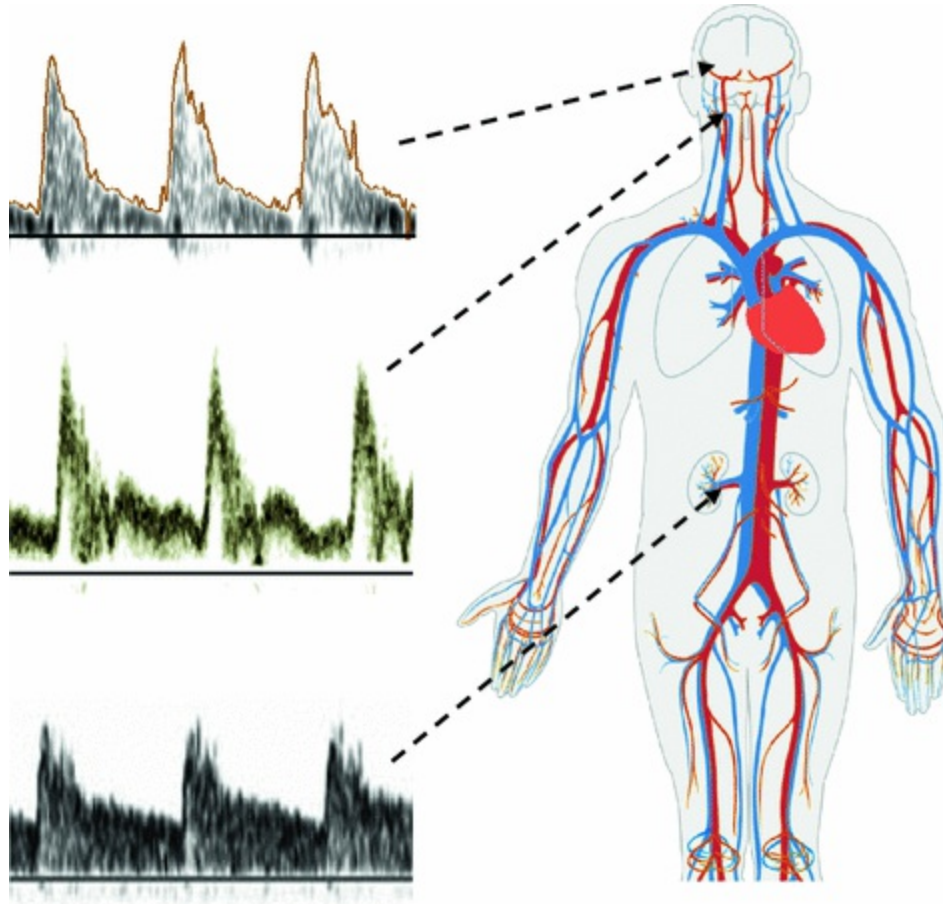


Fig. 4.5 Velocity–time waveforms from arteries supplying organs (brain and kidney) with high metabolic demand. Waveforms demonstrate a high baseline of flow. Circulation figure reproduced from Wikipedia; https://commons.wikimedia.org/wiki/File:Circulatory_System_en.svg. This image is in the public domain and was authored by Mariana Ruiz Villarreal

4.2.1 Windkessel Model

Models of pressure and flow in the arterial system generally only consider the arteries. The pressure at the capillaries (as noted in Chap. 2) is a fixed value close to zero so the venous system does not need to be taken into account when modelling the arterial system. An early model which tried to explain the pressure–time and flow–time waveforms is the Windkessel model. This comes from the German word ‘Windkessel’ meaning ‘air chamber’. The Windkessel model of the systemic circulation consists of three elements (Fig. 4.6); a pump representing the heart, an elastic chamber representing the arteries, and an outflow resistance representing flow through the arterioles. The process can be broken into 3 phases:

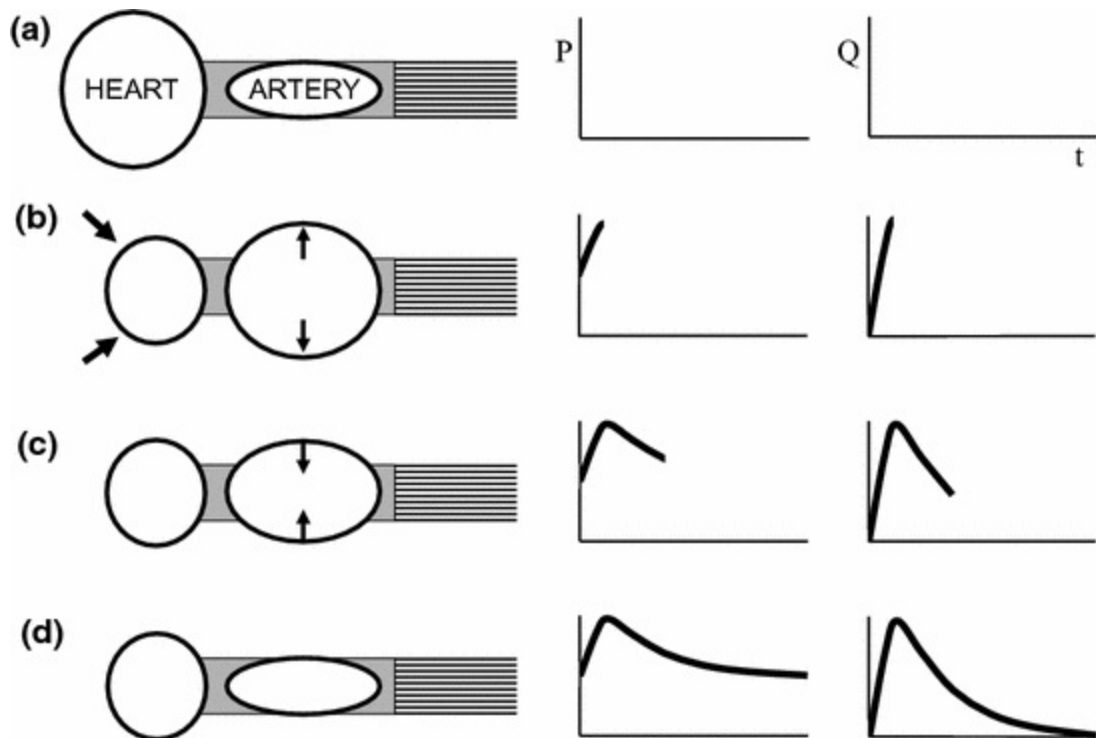


Fig. 4.6 Windkessel model consisting of a pump (heart), an elastic chamber (artery) and an outflow resistance (arteriolar bed). **a** Pre-ejection phase where the heart is full of blood. **b** In the ejection phase the heart contracts ejecting blood into the compliant chamber. The ejection takes about 100 ms. The tension in the wall of the chamber causes a pressure on the blood, which is forced out through the resistance vessels. Pressure and flow reach a maximum at the end of the ejection phase. **c** The ejection of blood from the heart stops. This is the relaxation phase. As the chamber gradually returns to its resting position the pressure on the blood decreases. As a result of the decrease in pressure, the flow also reduces. **d** The chamber returns to its resting position. The pressure reduces to its resting value and the flow reduces to zero

- *Ejection phase.* The heart contracts ejecting blood into the compliant chamber. The ejection takes about 100 ms. The tension in the wall of the chamber causes a pressure on the blood, which is forced out through the resistance vessels. Pressure and flow reach a maximum at the end of the ejection phase.
- *Relaxation phase.* The ejection of blood from the heart stops. This is the relaxation phase. As the chamber gradually returns to its resting position the pressure on the blood decreases. As a result of the decrease in pressure, the flow also reduces.
- *Resting phase.* The chamber returns to its resting position. This is the completion of the relaxation phase. The pressure reduces to its resting value and the flow reduces to zero.

There are some similarities between the pressure waveforms from the Windkessel model and those seen in Fig. 4.4, in that pressure reaches a peak and gradually reduces. The Windkessel flow waveforms also have a peak and gradually reduce in value thereafter, similar to those in Fig. 4.5 for arteries supplying brain and kidney. However, the Windkessel flow waveforms bear little resemblance to the flow waveforms seen in Fig. 4.4 which have a period of reverse flow.

4.2.2 Wave Propagation Model

The Windkessel model is useful in basic understanding but it omits a key feature of the arterial system which is wave propagation. Ejection of blood from the left ventricle leads to expansion of the aorta in order to accommodate the ejected volume. The increase in circumference leads to an increase in tension within the arterial wall and hence an increase in pressure within the blood. The pressure passes down the artery in the form of a wave. This phenomenon can be demonstrated by recording the pressure with time at various locations from the heart. Figure 4.7 shows the pressure–time waveform at different distances from the heart up to 60 cm. The increase in pressure at the beginning of the waveform occurs at later times. This is consistent with the idea that the pressure pulse propagates down the artery as a wave. The pressure wave propagation speed is usually called the ‘pulse wave velocity’ or PWV. The typical PWV in the thoracic aorta is about 5 m s^{-1} and increases, with distance from the heart, to about 15 m s^{-1} in the arteries of the lower leg. An important point is that pressure wave speed is not the same as blood speed. The pressure wave speed is the speed at which the pressure wave propagates and is typically $5\text{--}15 \text{ m s}^{-1}$. The blood speed is the speed at which the blood moves which is typically $0\text{--}1 \text{ m s}^{-1}$ in health.

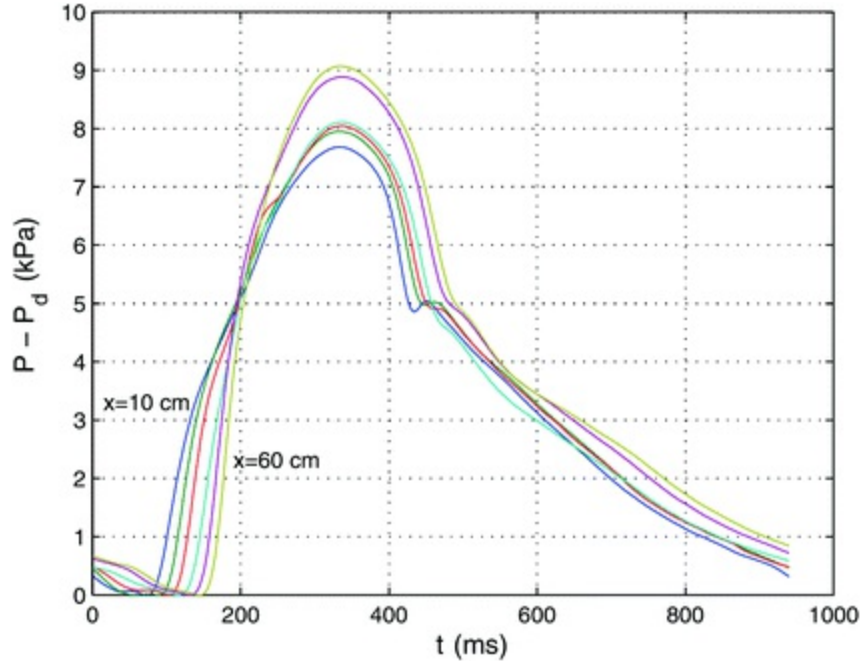


Fig. 4.7 Aortic pressure measured 10, 20, 30, 40, 50 and 60 cm downstream from the aortic valve plotted on as a function of time at different distances. The increase in pressure at the beginning of the waveform occurs at increasingly later times with distance demonstrating that the pressure propagates as a wave down the arterial tree. From *Medical and Biological Engineering and Computing, An introduction to wave intensity analysis*, Vol. 47, 2009, pp. 175–180, Parker KH, © International Federation for Medical and Biological Engineering 2009, with permission of Springer

An early attempt to formulate an equation for PWV was made in 1878 by Moens and Korteweg. This states that PWV is related to the elastic modulus E of the artery, the wall thickness h , the diameter d and the density ρ of blood. This simple equation in practice predicts the correct PWV to within about 10 % in healthy arteries.

$$\text{PWV} = \sqrt{\frac{Eh}{d\rho}} \quad (4.1)$$

4.2.3 Propagation Model with Reflected Waves

For propagation of any wave, in any medium, the wave will be scattered or reflected where there is a change in local impedance and this is also true for pressure waves in arteries. A change in impedance occurs as a result of change in diameter, shape or elastic properties. Common sites of reflected waves are at bifurcations; that is when a single parent artery splits into 2 or more daughter arteries. However, by far the largest contribution to reflected

waves comes from the change in impedance which occurs between arteries and arterioles. The pressure–time waveform at a particular location in an artery is therefore a composite of the forward-going pressure wave, and a reverse-going pressure wave arising from downstream reflections at the level of the arterioles (Fig. 4.8a). The flow-time waveform can be considered in the same manner as a combination of a forward-going flow wave and a reverse-going flow wave (see e.g. Murgo et al. 1981). However, the flow waves combine in a subtractive manner (Fig. 4.8b). In the example shown in Fig. 4.8b the composite flow waveform has a period of reverse flow, similar to that seen in Fig. 4.4.

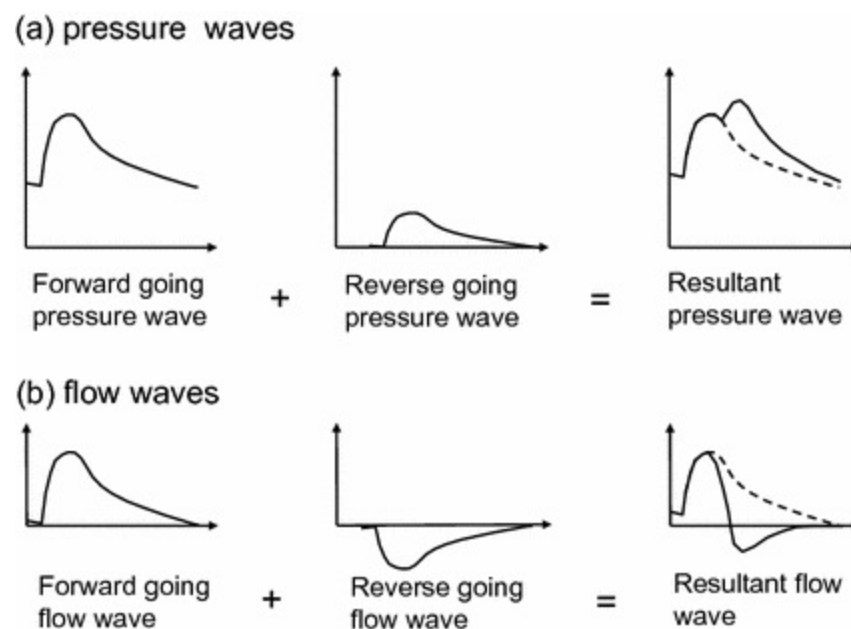


Fig. 4.8 Pressure and flow as a composite of forward-going waves and reverse-going waves; reverse waves are due to reflections, mainly from the distal arteriolar bed. **a** Forward and reverse pressure waves combine in an additive manner, producing an increase in maximum pressure. **b** Forward and reverse flow waves combine in a subtractive manner, in this case producing a period of reverse flow

A simple model can help explain these features in more detail (Fig. 4.9). The components of the model are the heart, a block representing the large arteries, a block representing the arterioles, with a fixed value of pressure (22 mm Hg) at the level of the capillaries. The flow rate of blood is determined by the overall pressure difference between the heart and the capillaries and by the overall resistance to flow. The overall resistance to flow is the sum of the resistance in the arteries and the arterioles. In practice it is the arteriolar resistance which is used to control the flow rate. The

arterioles are lined with smooth muscle which can constrict the diameter of the arterioles to create high resistance, such as may occur for muscles at rest which have low metabolic demands. When metabolic demands are high and a high flow rate is needed the smooth muscle in the arterioles relaxes, the diameter increases and the resistance drops. Local changes in flow rate are effected in the first instance by this mechanism, followed by associated increase in cardiac output. This then explains the features of flow waveforms seen in Figs. 4.4 and 4.5. In Fig. 4.4 the arteries are mostly supplying the buttocks and lower limbs. Since the bulk of this tissue is muscle at rest, the arteriolar resistance is high, the amplitude of reflected waves is high, and there is a large reverse flow component. In Fig. 4.5 the arteries are supplying the brain and the kidney which have high metabolic demand. The arteriolar resistance is low, the amplitude of reflected waves from the arteriolar bed is low and the flow is mainly dominated by the forward flow wave which has a high baseline of flow.

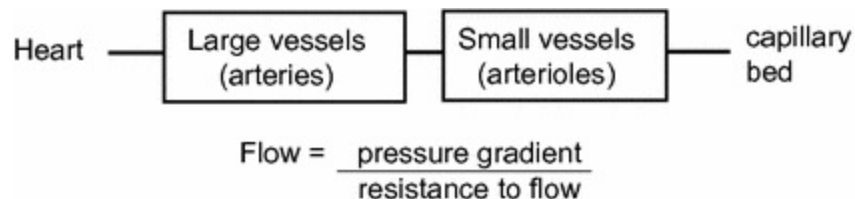


Fig. 4.9 A simple model of flow in arteries. The heart pumps blood through large vessels (arteries) and small vessels (arterioles) to the capillary bed. The large and small arteries each has a resistance to flow. The overall flow rate is the ratio of the pressure gradient divided by the resistance to flow

The above changes can be illustrated using a simple experiment; reactive hyperaemia in the arm (Fig. 4.10). In this example the hand is clenched while monitoring the flow in the brachial artery. During hand clenching blood is expelled from the hand and fingers. Metabolic demand build up and arterioles dilate but flow is unable to increase due to pressure constriction from the clenching. On release of the fist there is no pressure constriction and there is a sudden increase in flow rate due to arteriolar dilation. After unclenching the reverse flow waves have small amplitude and there is a large baseline of flow. Over 30–60 s the metabolic demands of the tissues are met and the flow waveform gradually returns to its resting state. During this time the arterioles become more constricted; the resistance in the arteriolar bed gradually increases, the amplitude of reverse-going waves increases and eventually the baseline of flow is lost with return of the reverse flow component.

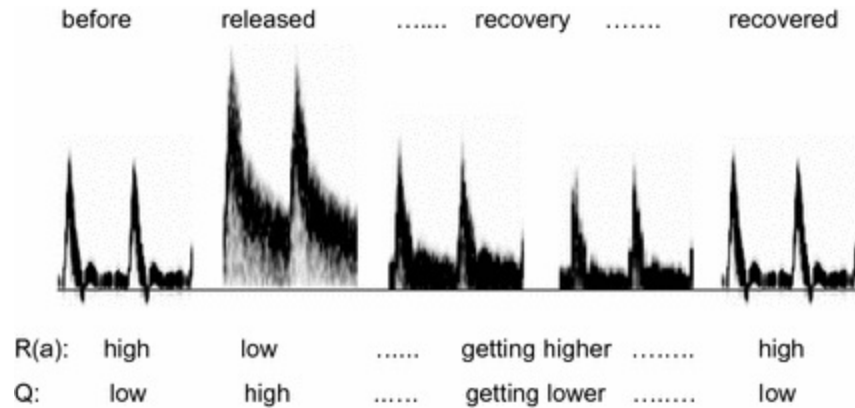


Fig. 4.10 Relationship between distal resistance and waveform shape illustrated by reactive hyperaemia. Doppler velocity–time waveforms are shown in the brachial artery. The hand is clenched for 2–3 min to increase metabolic activity. Clenching causes local compression; during clenching arterioles fully dilate but without increase in flow. On release of the hand there is a dramatic decrease in overall resistance leading to a huge increase in flow rate. The reflected waves have low amplitude and the velocity–time waveforms demonstrate flow throughout the cardiac cycle. During the recovery phase the arteriolar resistance increases, flow is reduced and the velocity–time waveforms become more pulsatile returning to a normal shape with reverse flow after 1–2 min

4.2.4 Pressure and Flow Waveforms at Different Distances from the Heart

With increasing distance from the heart, pressure waveforms in arteries change shape. In young adults there is increase in the pulse-pressure (systolic-diastolic) with distance from the heart (Nichols et al. 1993). This is seen in Fig. 4.4 where the peak pressure increases from 110 mm Hg in the ascending aorta to 160 mm Hg in the posterior tibial artery. Increase in pulse-pressure arises from increase in stiffness of arteries with increasing distance from the heart. This phenomenon continues down to very small arteries. Figure 4.11 shows increase in pulse-pressure from the brachial artery (3–4 mm diameter in the arm) to the digital artery (1–1.2 mm diameter in the finger).

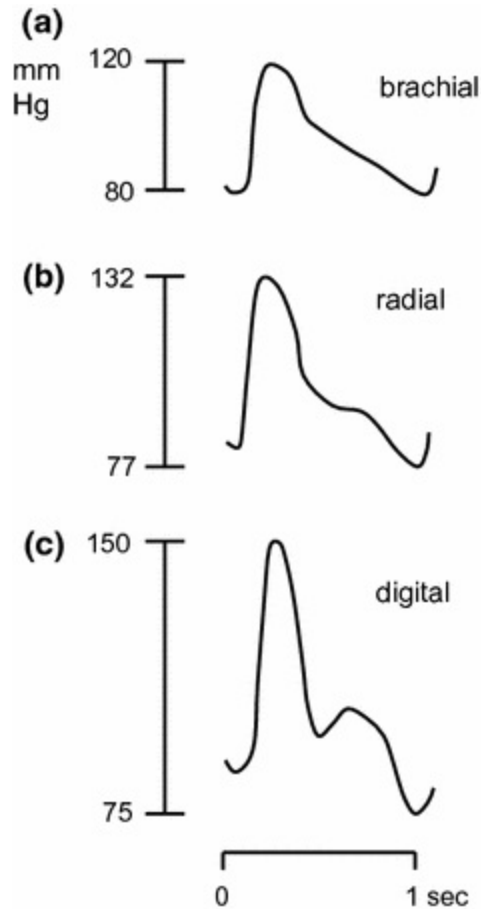


Fig. 4.11 Pressure–time waveforms from arteries in the arm and hand showing pressure augmentation in small arteries; **a** brachial, **b** radial, **c** digital

For peak flow, velocity invasive measurements demonstrate decrease in peak velocity with distance from the heart (McDonald 1974). Peak velocity is easy to measure using Doppler ultrasound and Fig. 4.4 shows velocity–time waveforms from mid-aorta to the posterior tibial artery.

4.3 Flow in Arteries

This section discusses characteristics of the flow-field, i.e. the local 3D distribution of blood velocities, within arteries.

4.3.1 Turbulence, Disturbed and Laminar Flow

The principal flow characteristics of laminar and turbulent flow are determined by the Reynolds number. In the arterial system the mean

Reynolds number decreases with distance from the heart. The highest Reynolds numbers are seen in the aorta, mainly in the systolic phase where values greater than 2000 regularly occur in the ascending aorta. This leads to periods of turbulent flow in the post-systolic phase of the flow waveform (Nerem et al. 1972). In the remainder of the arterial circulation in healthy individuals flow is laminar. In addition to laminar and turbulent flow it is useful to define a third flow state called 'disturbed flow' which relates to vortices and vortex shedding. Vortices or eddies are regions of circulating flow. These typically occur in the low shear region downstream of obstructions and are a common feature of vessel disease. They can also occur in healthy vessels and the one place where they are regularly seen is in the carotid sinus (Fig. 4.12). This is a dilated region at the entrance to the internal carotid artery and is associated with the location of sensors which monitor blood pressure in the body. Disturbed flow may also be seen in aneurysms, which are pathological bulges which can affect both the cerebral circulation and the aorta.

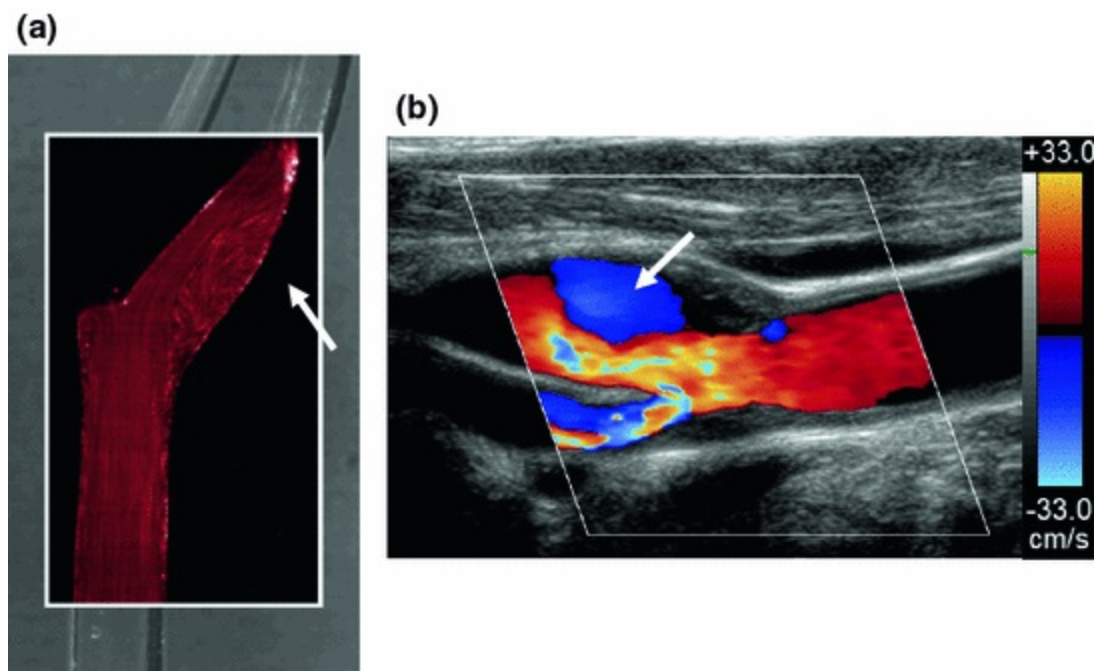


Fig. 4.12 Recirculation of flow in the carotid bulb. **a** An anatomical model of the carotid bifurcation with flow visualisation. **b** Colour flow ultrasound with recirculation shown in blue

4.3.2 Rotating Versus Axial Flow

Flow in a long straight pipe will become axial after a certain distance, no

matter what the flow conditions at the inlet. Rotation of flow is induced in a curved pipe and in the daughter arms of branching tubes. Though these phenomena are well known in fluid mechanics, evidence for rotation of flow in arteries only arose in the 1990s using both ultrasound and MRI (Kilner et al. 1993; Hoskins et al. 1994). Curvature and bifurcations in arteries will induce rotational flow; the fluid at the centre of the flow moves to the outer curve returning along the wall to the inner curve, hence creating a double spiral. In addition to these passive mechanisms, it is also clear that there is active induction of rotational flow. The left ventricle in the heart twists during contraction which induces a rotational flow component in the aorta. Figure 4.13 shows example of rotational flow observed in different arteries. It has been hypothesised that the presence of rotational flow acts to stabilise flow in the arterial system by reducing shear stress differences (Shipkowitz et al. 2000). Rotational flow also acts to mix blood (Caro et al. 2005; Cookson et al. 2009) which may lead to a more uniform distribution of red cells in arteries. In arteries which are relatively straight and far distant from an upstream branching point it is likely that the rotational component will have diminished and that flow will mainly be axial, for example flow in distal arteries in the legs and arms.

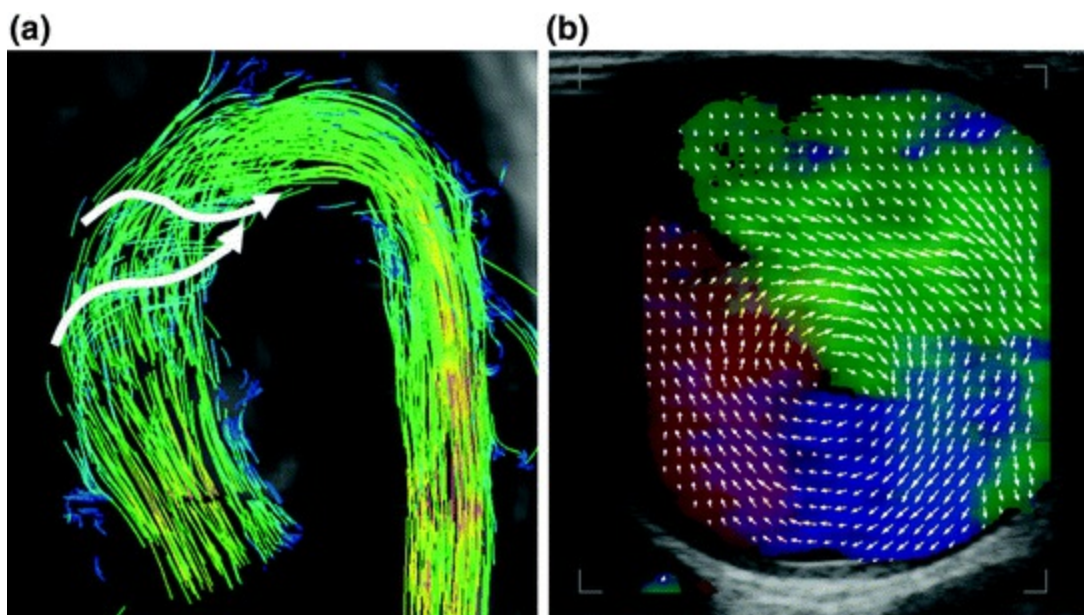


Fig. 4.13 Spiral flow. **a** Typical secondary flow patterns depicted by streamline visualisation in a systolic time frame for the ascending aorta using MRI. **b** Ultrasound colour vector image of spiral flow in the descending aorta. Image (a) from European Radiology; Interdependencies of aortic arch secondary flow patterns, geometry, and age analysed by 4-dimensional phase contrast magnetic

4.3.3 Fully Developed Flow Versus Non-fully Developed

From Chap. 2 the inlet length for flow in a straight pipe is the distance from the inlet beyond which flow is stable ('fully developed'). Under the assumption that the arterial system consists of segments which are straight then the inlet length can be calculated and compared to the length of the segment to get some idea whether flow has any chance of being fully developed. Equation 4.2 is from McDonald (1974, p. 111) and gives the inlet length L_s for the steady-flow component which requires knowledge of the diameter and Reynolds number based on mean velocity through the cardiac cycle.

$$L_s = 0.04d Re_m \quad (4.2)$$

The data in Appendix 1 show calculated inlet lengths for steady flow for selected arteries. For the aorta the steady-flow inlet length is greater than the length of the aorta, however, for distal vessels such as the radial and posterior tibial arteries it is less than 2 % of the artery length.

Flow in arteries is pulsatile rather than steady, however as noted by van de Vosse (1998) the pulsatile inlet length is less than the steady-flow inlet length in arteries, so there is no need to consider this. Equations for pulsatile inlet length are provided by Caro et al. (1978, p. 321) and Wood (1999).

On this basis, for most of the larger arteries (aorta, carotid, femoral) flow is not fully developed. For more distal smaller arteries in the leg and arm flow is fully developed, provided it can be assumed that arteries are straight between branching points. This has implications for measurement of flow rate and related quantities using medical imaging where assumptions of fully developed flow are often made (see Chap. 9). The implications are that assumptions of fully developed flow are unlikely to be valid in the larger arteries but may be valid in smaller distal arteries.

4.3.4 Symmetric Versus Asymmetric Velocity Profiles

Velocity profiles in a long straight tube beyond the inlet length are symmetric with respect to the radius. The maximum velocity profile is located centrally

within the tube (except in pulsatile flow when the flow passes through zero in which case the maximum velocity is located off-centre). Asymmetric velocity profiles occur when the vessel is curved or immediately downstream of a branching point. In these cases it is necessary to measure the 2D velocity profile. Figure 4.14 shows example of velocity profiles in vivo.

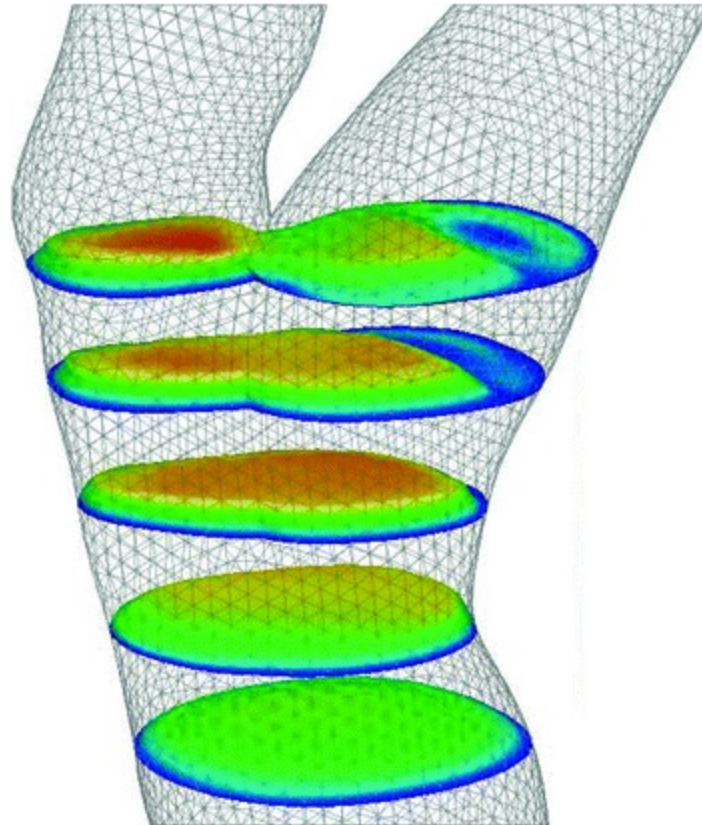


Fig. 4.14 2D velocity profiles in the carotid bifurcation derived from patient-specific modelling. Profiles are symmetric in the common carotid, but asymmetric just below the point of branching and in the internal carotid

4.3.5 Considerations for Measurement of Blood Velocity and Related Quantities

The above features of blood flow are relevant to estimation of blood velocity profiles using imaging and modelling as will be seen in later chapters. Full 3D flow-field estimation is complex and is generally performed using patient-specific modelling (Chap. 11), though MRI may also provide 3D flow-field data. Simpler methods using ultrasound may rely on assumptions of axial flow for estimation of blood velocity, or on velocity profile

symmetry for estimation of flow rate (Chap. 9).

Appendix 1: Physical Quantities for Selected Arteries

Data are indicative and taken from various sources including Caro et al. (1978), Marshall et al. (2004) and Reymond et al. (2009). L (length), D (diameter), V_m (mean velocity averaged over time and area), V_p (peak velocity), Re_m (Reynolds number from mean velocity), Re_p (Reynolds number from peak velocity), α (Womersley parameter), L_s (inlet length for the steady-flow component), L_s/L (ratio steady-flow inlet length to arterial length).

	L (cm)	D (cm)	V_m (cm/s)	V_p (cm/s)	Re_m	Re_p	α	L_s (cm)	L_s/L
Descending aorta	21	1.9	22	70	1100	3600	17	86	4.1
Abdominal aorta	13	1.4	13	60	500	2300	15	28	2.1
External iliac/common femoral	14	0.8	16	60	350	1300	5	11	0.8
Superficial femoral/popliteal	44	0.6	15	60	250	1000	4	6	0.1
Posterior tibial	32	0.3	5	50	50	400	3	0.5	0.02
Common carotid	9	0.7	17	80	320	1500	4	9	1.0
Internal carotid	18	0.5	23	75	310	1000	4	6	0.3
External carotid	41	0.4	12	80	130	900	4	2	0.1
Brachiocephalic	42	0.5	8	75	110	1000	8	2	0.1
Radial	24	0.2	5	60	30	300	4	0.2	0.01

References

Caro CG, Cheshire NJ, Watkins N. Preliminary comparative study of small amplitude helical and conventional ePTFE arteriovenous shunts in pigs. *J R Soc Interface*. 2005;2:261–6.

[CrossRef][PubMed][PubMedCentral]

Caro CG, Pedley TJ, Schroter RC, Seed WA. *The mechanics of the circulation*. Oxford: Oxford University Press; 1978.

Cookson AN, Doorly DJ, Sherwin SJ. Mixing through stirring of steady flow in small amplitude helical tubes. *Ann Biomed Eng*. 2009;37:710–21.

[CrossRef][PubMed]

Hoskins PR, Fleming A, Stonebridge P, Allan PL, Cameron DC. Scan-plane vector maps and secondary flow motions. *Euro J Ultrasound*. 1994;1:159–69.

Kilner PJ, Yang GZ, Mohiaddin RH, Firmin DN, Longmore DB. Helical and retrograde secondary flow patterns in the aortic-arch studied by 3-directional magnetic-resonance velocity mapping. *Circulation*. 1993;88:2235–47.

[CrossRef][PubMed]

Marshall I, Papathanasopoulou P, Wartolowska K. Carotid flow rates and flow division at the bifurcation in healthy volunteers. *Physiol Meas*. 2004;25:691–7.

[CrossRef][PubMed]

McDonald DA. *Blood flow in arteries*. 2nd ed. London: Edward Arnold; 1974.

Murgo JP, Col MC, Westerhof N, et al. Manipulation of ascending aortic pressure and flow waveform reflections with the Valsalva manoeuvre: relationship to input impedance. *Circulation*. 1981;63:122–32.

[CrossRef][PubMed]

Nerem RM, Seed WA, Woods NB. An experimental study of the velocity distribution and transition to turbulence in the aorta. *J Fluid Mech*. 1972;52:137–60.

[CrossRef]

Nichols WW, Avolio AP, Kelly RP, O'Rourke MF. Effects of age and hypertension on wave travel and reflections. In: O'Rourke M, Safar M, Dzau V, editors. *Arterial vasodilation: mechanisms and therapy*. Sevenoaks: Edward Arnold; 1993. p. 23–40.

Reymond P, Merenda F, Perren F, Fenacht DR, Stergiopoulos N. Validation of a one-dimensional model of the systemic arterial tree. *Am J Physiol Heart Circ Physiol*. 2009;297:H208–22.

[CrossRef][PubMed]

Roach MR, Burton AC. The reason for the shape of the distensibility curve of arteries. *Can J Biochem Physiol*. 1957;35:681–90.

[CrossRef][PubMed]

Ryan LK, Foster FS. Tissue equivalent vessel phantoms for intravascular ultrasound. *Ultrasound Med Biol*. 1997;23:261–73.

[CrossRef][PubMed]

Shipkowitz T, Rodgers VGJ, Frazin LJ, Chandran KB. Numerical study on the effect of secondary flow in the human aorta on local shear stresses in abdominal aortic branches. *J Biomech*. 2000;33:717–28.

[CrossRef][PubMed]

van de Vosse FN. Cardiovascular fluid mechanics—lecture notes. 1998. <http://www.mate.tue.nl/people/vosse/docs/cardio.pdf>

Wood NB. Aspects of fluid dynamics applied to the larger arteries. *J Theor Biol*. 1999;199:137–61.

[CrossRef][PubMed]

5. The Arterial System II. Forces, Adaptability and Mechanotransduction

Peter R. Hoskins¹✉

(1) Edinburgh University, Edinburgh, UK

✉ **Peter R. Hoskins**
Email: P.Hoskins@ed.ac.uk

Learning outcomes

1. Describe the forces on the arterial wall and the typical magnitude of forces.
2. Describe Murray's law.
3. Discuss historical work on the variation of wall shear stress with arterial diameter.
4. Describe the Law of Laplace.
5. Describe the lamellar unit of structure in the arterial wall.
6. Describe arterial system design principles in terms of normalisation of stress; wall shear stress, longitudinal stress and circumferential stress.
7. Discuss the role of forces in growth and adaptability of arteries at

different stages of life from embryogenesis to old age.

8. Define the term 'mechanotransduction'.
9. Discuss the 4 principles steps of mechanotransduction: mechanotransmission, mechanosensing, mechanosignalling and mechanoreponse.
10. Describe the effects of changes in wall shear stress on the endothelium.
11. Describe the decentralised model of endothelial mechanotransduction.
12. Describe potential endothelial mechanosensors.

This chapter is the second on arterial biomechanics and will explore the forces on arteries and their effect. The emphasis will be on normal function in this chapter. Arterial disease is considered in Chaps. 14–16. There are three main principles which underpin this chapter:

- The arterial wall is subject to forces which arise from blood flow and from blood pressure.
- The arterial wall is able to sense forces.
- The arterial wall will alter its structure and geometry in an attempt to maintain these forces within a narrow range of values.

5.1 Introduction

5.1.1 Historical Introduction

This introduction will start by referencing a study performed by Thoma (1893). His study concerned the developing chick embryo and three observations were made concerning the relationship between forces and arteries which provide a useful indication of key ideas in the text below. These observations (quoted in Wagenseil et al. 2009) are:

- Vessel inner diameter (i.e. the luminal diameter) depends on blood flow.
- Vessel length depends on longitudinal forces exerted by surrounding tissues.
- Vessel wall thickness depends on blood pressure.

It will be seen below that it is wall shear stress (WSS) that determines mean vessel diameter, longitudinal stress that determines vessel length and circumferential stress that determines mean wall thickness.

5.1.2 Forces on Arteries

The arterial wall is subject to two forces from the blood; pressure and shear stress (Fig. 5.1). The blood pressure acts on the arterial wall and is balanced by circumferential stress (also called hoop stress) within the wall (Fig. 5.2). Typical average values of these forces in the aorta are 90 mmHg (12,000 Pa) for pressure, 1 Pa for WSS and 12,000 Pa for circumferential stress.

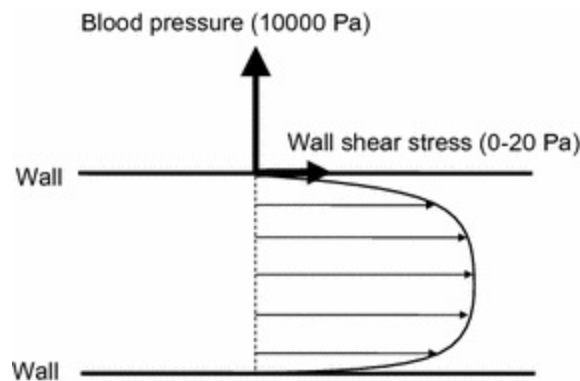


Fig. 5.1 Forces on an artery wall, blood pressure and wall shear stress

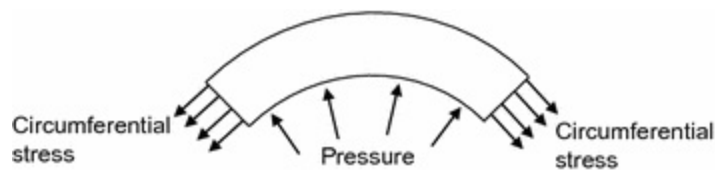


Fig. 5.2 Cross section of an artery wall. The pressure acts on the arterial wall. This is balanced by a circumferential stress within the wall

The cyclic variation in pressure gives rise to a cyclic variation in the diameter and circumference of the artery. Each cell within the wall therefore

undergoes a cyclic stretching and un-stretching. An artery diameter typically varies by 10 % over the cardiac cycle so each cell will typically be stretched and un-stretched by the same amount in the circumferential direction. The expansion in the circumferential direction is accompanied by a decrease in thickness in the radial direction. This can be seen as a cyclic variation in the thickness of the intima-media layer measured using ultrasound imaging (Meinders et al. 2003).

The WSS is the viscous drag of blood on the wall and acts in the plane of the wall. The WSS changes in a cyclic manner with changes in blood flow during the cardiac cycle (Fig. 5.3). If overall flow is axial then the WSS vector will also be axial. However in regions of complex flow such as near bifurcations the WSS vector may have a large non-axial component (Fig. 5.4).

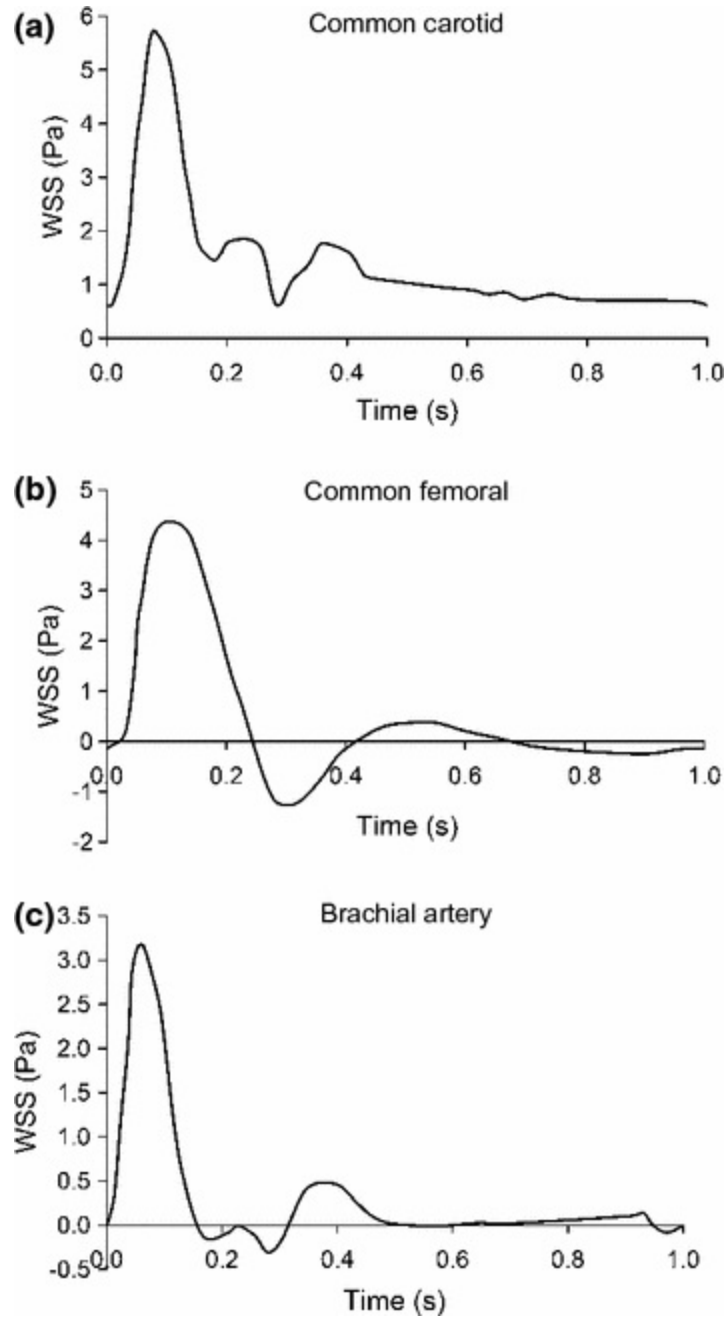


Fig. 5.3 Variation of WSS magnitude with time in the common carotid, common femoral and brachial arteries. Reprinted from *Atherosclerosis*, Vol. 191; Stroev PV, Hoskins PR, Easson WJ; Distribution of wall shear rate throughout the arterial tree: a case study; pp. 276–280, Copyright (2007), with permission from Elsevier

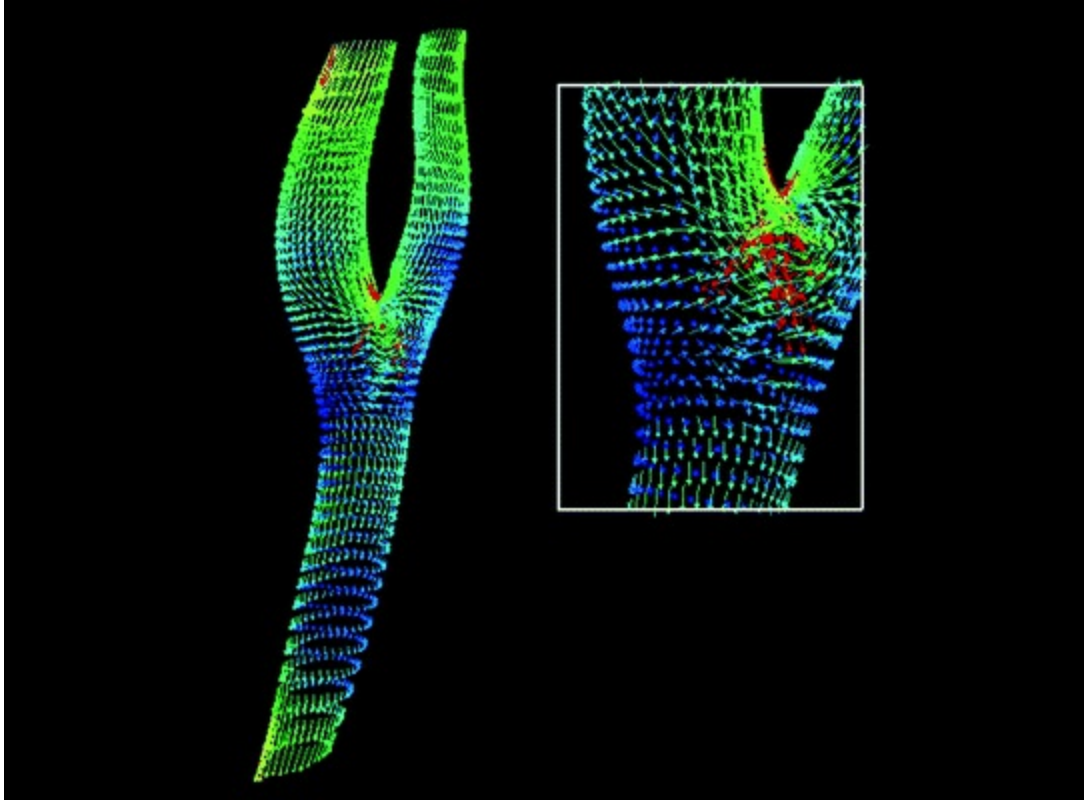


Fig. 5.4 WSS vector orientation in the carotid arteries at peak systole with large non-axial components close to the bifurcation. Image kindly provided by Prof Yun Xu, Imperial College

If an artery is excised from the body its length will decrease by about 40 % implying that in vivo there is longitudinal tension; that is the artery is pre-stressed in the longitudinal direction (Fig. 5.5). If the excised artery is sliced open longitudinally it will partially spring open implying that the artery wall is also pre-stressed from the inner to the outer lumen. Arteries do not exist an unloaded state in vivo. In vivo, arteries are always in a longitudinally stretched state and are always subject to pressure. In the unloaded state this pre-stressing gives rise to an uneven stress distribution from inner to outer wall. However, in vivo under blood pressure, the stress distribution becomes more uniform (Fig. 5.6).

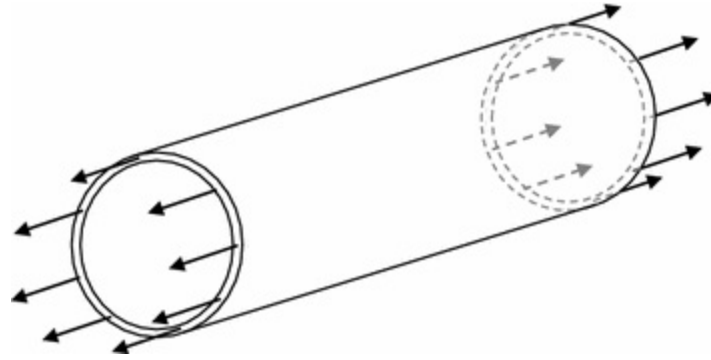


Fig. 5.5 Arteries in vivo are in a pre-stressed state in the longitudinal direction

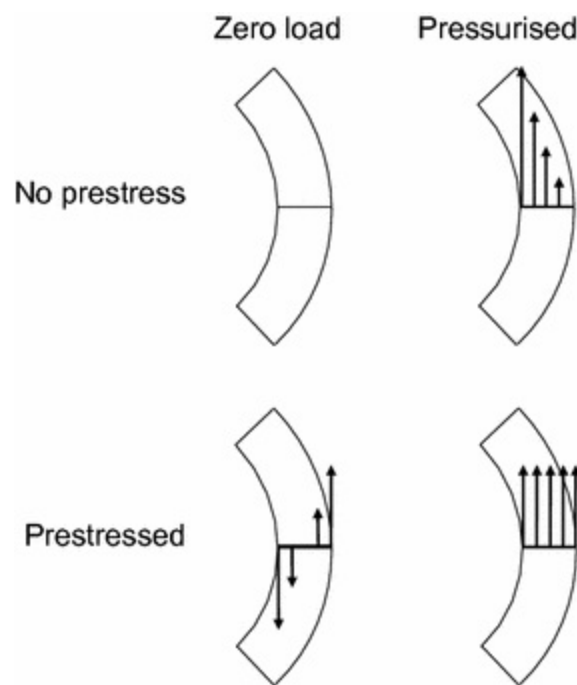


Fig. 5.6 Circumferential stress distribution in an artery with no blood pressure and with blood pressure, with and without pre-stressing. The stress distribution is uniform for the pressurised artery with pre-stressing

In the above analysis the artery is treated as a homogenous material. However, in reality, the presence of several layers (intima, media and adventitia) leads to a more complicated stress distribution due the different mechanical properties and the different amounts of pre-stressing in each layer (Holzapfel and Ogden 2010; Karsaj and Humphrey 2012).

5.1.3 Murray's Law

The arterial system is a branching network; the number of vessels increases with each branching and the diameters decrease. An early attempt to investigate the design of the branches was performed by Murray (1926a, b). He hypothesised that the arterial system is designed so that the heart needs to expend the minimum amount of effort in order to pump the blood along the arteries. From this he derived that the diameter d_1 of the parent artery to the third power is equal to the sum of the diameters d_2 and d_3 of the daughter arteries to the third power (Eq. 5.1, Fig. 5.7).

$$d_1^3 = d_2^3 + d_3^3 \quad (5.1)$$

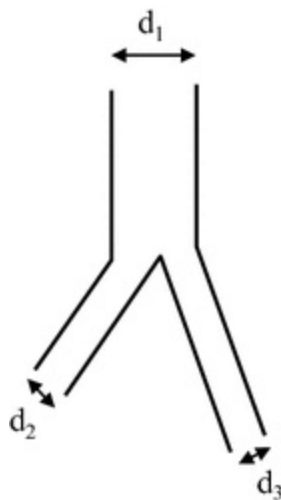


Fig. 5.7 Diameters of parent artery (d_1) and daughter arteries (d_2 and d_3) used in Eq. 5.1

This is known as Murray's law and has been widely quoted in publications on the structure of the arterial system. Though Murray did not concern himself with WSS it follows from Murray's law that the mean WSS is constant for all arteries from the largest to the smallest (Sherman 1981). It is also worth saying that if Murray's law applies to all mammals, which have basically the same design of cardiovascular system, then the WSS in all arteries in the whale should be the same, and the WSS in all arteries in the mouse should be the same.

The work of Murray is concerned with the principles by which the arterial system is designed. It follows that there must then be a mechanism for controlling arterial diameter according to some design principle. The mechanism suggested here is that the arterial system is designed to maintain WSS at a constant value (Zamir 1977). This is further considered below.

5.1.4 Brief Review of Wall Shear Stress

It was described in Sect. 5.1.3 that Murray's law predicts that the mean WSS is constant in all arteries. This section looks at experimental data on WSS and whether Murray's law has been confirmed to apply in vivo.

Early studies which estimated WSS in arteries assumed a parabolic velocity profile in the vessel. With this assumption an equation can be derived which relates wall shear rate to the flow rate and the diameter. In invasive studies flow rate can be measured using a variety of techniques including electromagnetic flow probes and thermodilution. Diameter can be measured using X-ray imaging or from calliper measurements in exposed vessels. These measurements need not even be made at the same time. Once the wall shear rate is calculated it is multiplied by viscosity to give the WSS. An early summary of WSS data is provided by Giddens et al. (1993) which demonstrated that mean WSS lies within the narrow range of 1–2 Pa in a range of arteries in the human and dog. This finding of a constant mean WSS is consistent with Murray's law and seemed to provide good confirmation that Murray's law was correct.

It is worth restating the situation in the early 1990s concerning WSS; Murray's law suggested that WSS is constant within a species; experimental findings suggested that WSS was similar in several different arteries in the human in the dog.

The constancy of WSS was challenged by later studies which used in vivo techniques based on MRI and ultrasound. The spatial resolution and functionality of in vivo imaging gradually improved to the point where it was possible to obtain reliable measurements of WSS in vivo. Advances in computing power and the availability of computational fluid dynamics also meant that by the 1990s it was possible to estimate WSS in realistic geometries (rather than in simple straight tubes). This combination of imaging and modelling data came up with a slightly different story concerning WSS which is summarised by Cheng et al. (2007). Figure 5.8 illustrates findings in 3 arteries, the common carotid, brachial and femoral. There are clear differences, with the common carotid having a higher mean WSS than the brachial or femoral arteries. It was also found that there are differences in WSS between species with smaller species having high WSS. An MRI study by Greve et al. (2006) demonstrated a dependence of mean WSS on body-mass to the power of -0.38 , which is in excellent agreement with the dependence of -0.375 predicted by Weinberg and Ethier (2007)

from scaling laws.

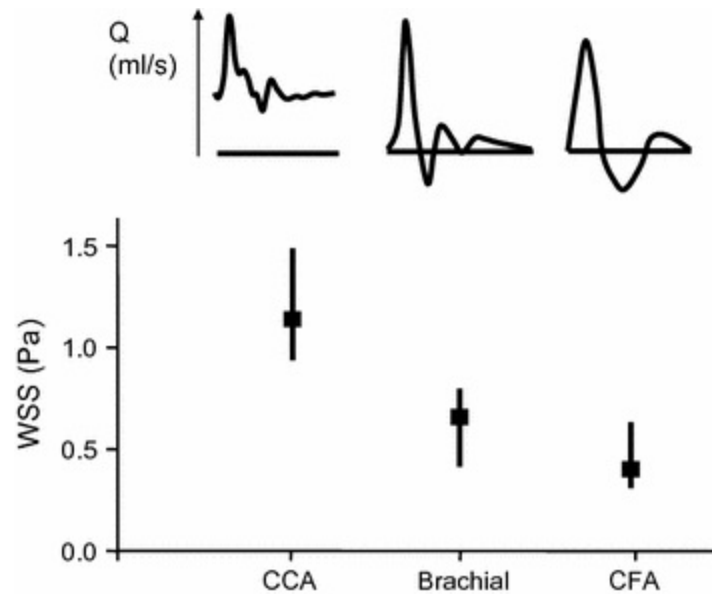


Fig. 5.8 Variation of mean WSS in the common carotid, femoral and brachial arteries. The differences are due to differences in the pulsatility of the flow waveform, with higher values of mean WSS for the carotid and lower values for the femoral and brachial. Data from Cheng et al. (2007)

The evidence above points to a control mechanism which attempts to maintain WSS within a narrow bound (Langille 1996). The ‘set point’ for WSS in human arteries is around 1–2 Pa and deviation from this value will result in change in diameter; this is called ‘arterial remodelling’. If the mean WSS is greater than the set-point, the diameter increases to reduce WSS until its value lies at the set-point. Conversely if the mean WSS is less than the set-point the diameter decreases until the mean WSS value lies at the set-point. It is noted that temporary increases in mean WSS, such as occur during a few minutes exercise, will not result in long-term change in diameter. The control mechanism comes into play when the changes are longer term.

The discussion around Murray’s law above suggests that it was initially thought that the value of the set-point for WSS was the same in all arteries. It has become clear that the set-point is different for different arteries. One possible explanation for this was offered by Reneman et al. (2006). He noted that the flow waveform is not the same in all arteries. This is illustrated in Fig. 5.8; the common carotid has a high degree of flow throughout the cardiac cycle (and higher mean WSS) whereas the brachial and femoral (which supply blood to muscle) have high pulsatility (and low-mean WSS).

However during exercise the flow waveforms in arteries supplying muscle change significantly; the waveforms have a much higher component of flow and a much higher mean WSS. Reneman's observation was that *during exercise* the mean WSS is similar in different arteries, implying that the set-point may be relevant for conditions of high flow, not resting flow (for which most measurements are taken).

5.1.5 The Law of Laplace

It was noted above that blood pressure is opposed by a tension within the arterial wall. The relationship between pressure and tension was investigated by the French physicist Pierre de Laplace in the eighteenth century in the context of surface tension in water. Approximating an artery as a thin-walled cylinder gives the 'law of Laplace' as shown in Eq. 5.2.

$T = P \cdot r$ (5.2)
This states that, for a fixed pressure P , as the radius r increases the tension T in the wall increases. An alternative formulation of the law of Laplace is in the context of stress (force per unit area). The circumferential stress or hoop stress H is shown in Eq. 5.3 where w is wall thickness.

$H = \frac{Pr}{w}$ (5.3)

Figure 5.9 shows wall stress as a function of age in the aorta and carotid artery (from Åstrand et al. 2005). Values range from 3000 to 16,000 Pa.

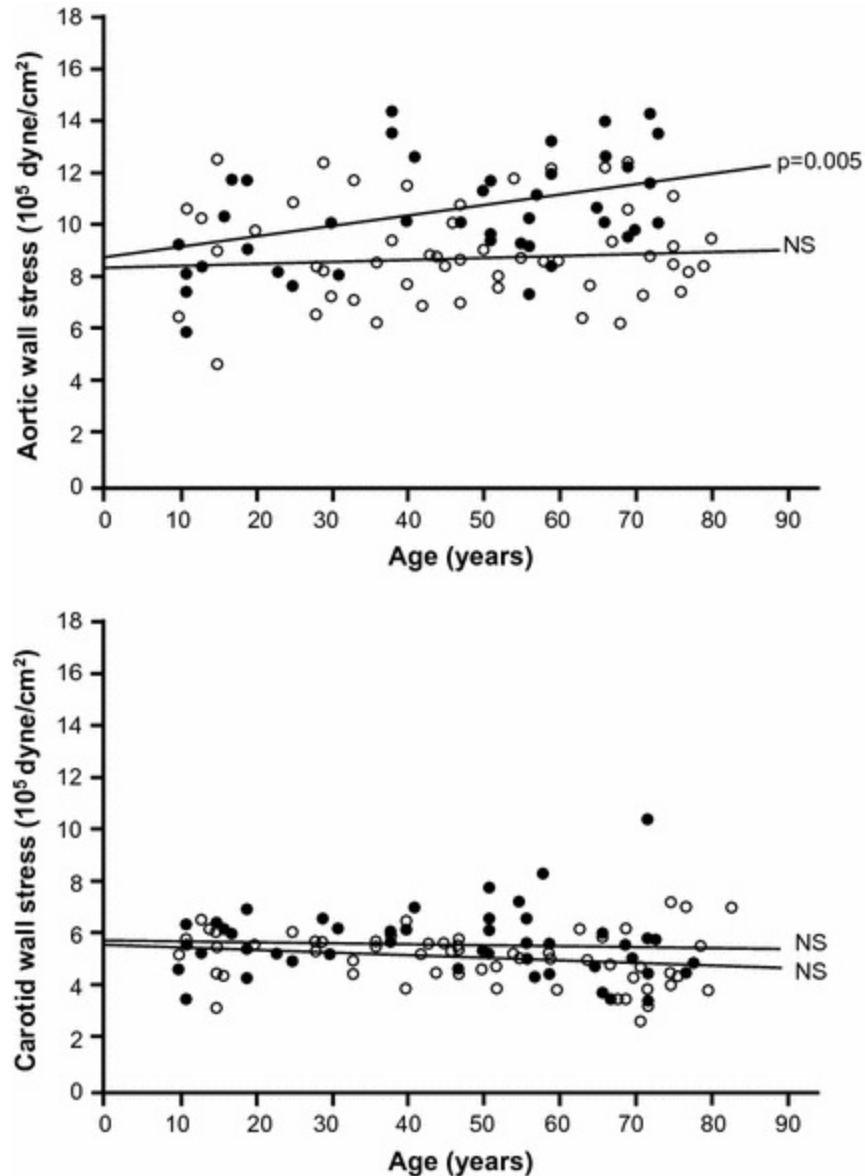


Fig. 5.9 Plots of circumferential stress as a function of age in the aorta and common carotid arteries. *Closed circles* are male, *open circles* female. Reprinted from Journal of Vascular Surgery, Vol. 42; Åstrand H, Rydén-Ahlgren A, Sandgren T, Länne T; Age-related increase in wall stress of the human abdominal aorta: an in vivo study; pp. 926–931, Copyright (2005), with permission from The Society for Vascular Surgery

5.1.6 Brief Review of Circumferential and Longitudinal Wall Stress

The mechanical strength of an artery is governed primarily by the elastin and collagen fibres which are laid down in a concentric fashion. The idea of a lamellar unit of structure consisting of muscle, elastin and collagen was

formulated by Wolinsky and Glagov (1967). During fetal development the number of lamellar units increases and remains constant after birth. The number of lamellar units in the adult aorta of different species was studied by Wolinsky and Glagov (1967). In decreasing order of animal size there are around 70 units in the pig, 60 in the human, 45 in the dog, 13 in the guinea pig and 5 in the mouse. The circumferential tension in the wall of the aorta increases with animal size (5 N m^{-1} for the mouse increasing to 190 N m^{-1} for the pig). However the significant finding reported in the Wolinsky paper was that the tension per lamellar unit was similar across all species at $1\text{--}3 \text{ N m}^{-1}$. Wall thickness therefore adjusts in order to maintain circumferential stress within a narrow range. Thickening of the wall during embryonic development occurs by increase in the number of lamellar units. Post-birth increases in wall thickness arise through thickening of each lamellar unit. In healthy individuals this is achieved by an increase in smooth muscle content, however in disease such as in hypertension thickening is accompanied by increasing collagen deposition and the changes become irreversible (Hayashi and Naiki 2009). Conversely, where there is decrease in circumferential stress, possibly as a result of disease, this leads to atrophy of the wall (Bomberger et al. 1980).

It was noted above that arteries are pre-stretched; that is there is longitudinal wall stress. Arteries are surrounded by a fibrous adventitia which is attached to tissues surrounding the other organs of the body. These organs will exert forces on the arteries via the adventitia which can be referred to as 'tethering forces'. The main determinant of structure within the body is the skeleton. As the skeleton grows the arteries will be subject to stretching which will increase the longitudinal stress. The response of the artery is to lengthen in order to normalise the longitudinal stress. However, where an artery is decreased in length it does not shorten to normalise the longitudinal stress and the result is a tortuous artery (Wagenseil and Mecham 2009).

5.2 Arterial System Growth and Adaptability

This section examines the role of forces in the growth and remodelling of arteries from the embryo through birth into old age. It is noted that there are gaps in the evidence base and the literature comes from several different mammals including chick, sheep and human. Further detail is provided in review articles (Langille 1996; Pries et al. 2005; Humphrey 2008; Hayashi

and Naiki 2009; Wagenseil and Mecham 2009). This section is mostly not concerned with disease. The underpinning process governing growth and remodelling is termed ‘mechanotransduction’ and is described in detail in Sects. 5.3 and 5.4.

5.2.1 Embryogenesis

Following fertilisation of the mother’s egg with the father’s sperm the offspring begins to develop. The process starts with a single cell which quickly subdivides into many cells. During the initial few weeks of this development the offspring is called an ‘embryo’ and the formation of the embryo is called ‘embryogenesis’. Over time, a few days and weeks, organs form and a vascular system is laid down. The initial laying down of the vascular system, though fascinating, does not concern us. However once the earliest vessels are formed then these grow and develop into the vascular system; arteries, veins, capillaries etc. These immature simple vessels consist of a tube of endothelial cells without any surrounding smooth muscle, very similar to capillaries. The rudimentary heart pumps blood along the early vascular system and as the flow rate increases the arteries increase in diameter. Studies on the chick embryo (le Noble et al. 2005) estimated ‘reduced-velocity’ which is the ratio of blood velocity to diameter, as an index which was easy to calculate and proportional to WSS. They showed that reduced-velocity was similar for embryonic arteries greater than 40 μm in diameter (Fig. 5.10).

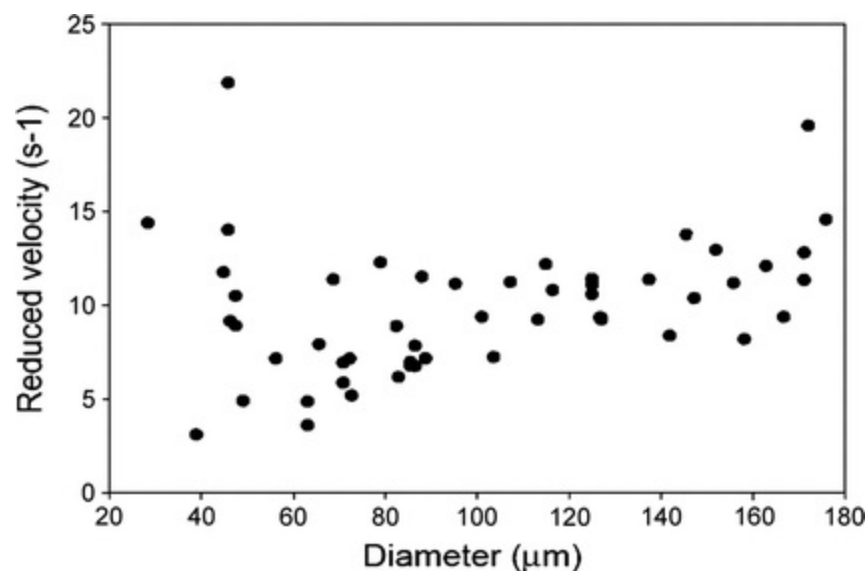


Fig. 5.10 Reduced-velocity (a measure of wall shear stress) versus diameter in embryonic arteries of the chick. Reduced-velocity is constant for arteries from 60–160 microns indicating the presence of a control mechanism. From; le Noble F, Fleury V, Pries A, Corvol P, Eichmann A, Reneman RS; Control of arterial branching morphogenesis in embryogenesis: go with the flow; *Cardiovasc Res.* 2005;65(3);619–28; by permission of the European Society of Cardiology

Even at this extremely early stage in the development of the arterial system 2 things emerge. First the constancy of reduced-velocity with diameter suggests a control mechanism in which diameter is adjusted to maintain reduced-velocity (i.e. shear stress) within a narrow bound; secondly that the endothelium (in the absence of any other cell types) is responsible for this control.

5.2.2 Fetal Growth

By the end of 8 weeks most of the major organs in the human embryo are in place and the remaining 32 weeks in the womb are spent growing. The embryo is now referred to as a fetus. Over this period the fetus grows from 3 g to 3 kg in weight, and the arterial system also grows. The diameter of the aortic root (where the aorta emerges from the left ventricle) is 1 mm at 11 weeks increasing linearly with time to 9 mm at 40 weeks (Cartier et al. 1987; Achiron et al. 1998; Haak et al. 2002). There is very little literature on WSS in the fetus. Struijk et al. (2005) used ultrasound imaging in the descending aorta in fetuses with gestational age from 18 to 39 weeks, demonstrating that there was no change in mean WSS which had an average value of 2.2 Pa.

During the period from 8 weeks to birth the development of the arterial system can be described as follows; as the fetus grows, the cardiac output increases and the blood pressure increases. The arteries will increase in diameter in an attempt to maintain WSS at a constant value. The increase in pressure will result in an increase in wall thickness in an attempt to maintain circumferential stress at a constant value. This increase in thickness is associated with an increase in the number of lamellar units. The general enlargement of the skeleton and organs gives rise to an increase in longitudinal stress and the arteries will lengthen in an attempt to maintain longitudinal stress at a constant value.

5.2.3 Birth

The fetus is supplied with oxygen from the mother via the placenta and the umbilical cord. The left and right sides of the heart are connected via a hole (the foramen ovale) between the left and right atria, and the pulmonary and systemic circulations are connected via a bridging vessel (the ductus arteriosus) which links the pulmonary artery and the aorta. After birth the umbilical supply is cut and there are a number of plumbing changes which occur. The foramen ovale closes separating the left and right sides of the heart and there is closure of the ductus arteriosus separating the pulmonary and systemic circulations. The loss of the umbilical supply leads to an increase in pressure in the aorta and the reduction in pulmonary resistance leads to a decrease in pressure in the pulmonary artery. Before birth the aorta and pulmonary artery carry similar flow rate, have similar diameter and similar wall thickness. After birth the flow rate and diameter remain similar. However, there is increase in wall thickness of the aorta and decrease in wall thickness in the pulmonary artery. These changes in wall thickness are consistent with the renormalisation of circumferential stress following changes in pressure immediately following birth (Leung et al. 1977).

5.2.4 Childhood

Human life post-birth may be divided into two phases; birth to adulthood (childhood) at around 20 years when height no longer increases, then 20 years to death at age up to around 100 years.

In childhood the arterial system dimensions increase along with the dimensions of the rest of the body. Cardiac output increases and flow in each artery increases. There is an absence of literature in this area in childhood so what follows is conjecture based on the control theory described above. It is likely that the increase in arterial diameter is driven by the need to maintain WSS constant. The increase in pressure and diameter of arteries leads to increase in wall thickness. This is associated with an increase in the thickness of each lamellar unit, noting that the number of units in each artery is fixed at birth. Growth of the skeleton and organs leads to stretching of the arteries, and in response to the increase in longitudinal stress these elongate in an attempt to maintain longitudinal stress at a constant value.

5.2.5 Adulthood

During the second phase of ageing, from 20 years to death the arterial system

does not remain of fixed dimensions. The aorta in particular increases in diameter. Figure 5.11a shows the diameter of the abdominal aorta as a function of age. From age 25 to 70 years the diameter increases by 20–25 % (Sonesson et al. 1993). As the adult is no longer growing the increase in diameter is not driven by increase in flow rate. The relevant fact is that the aorta increases in stiffness with age (Fig. 5.11b).

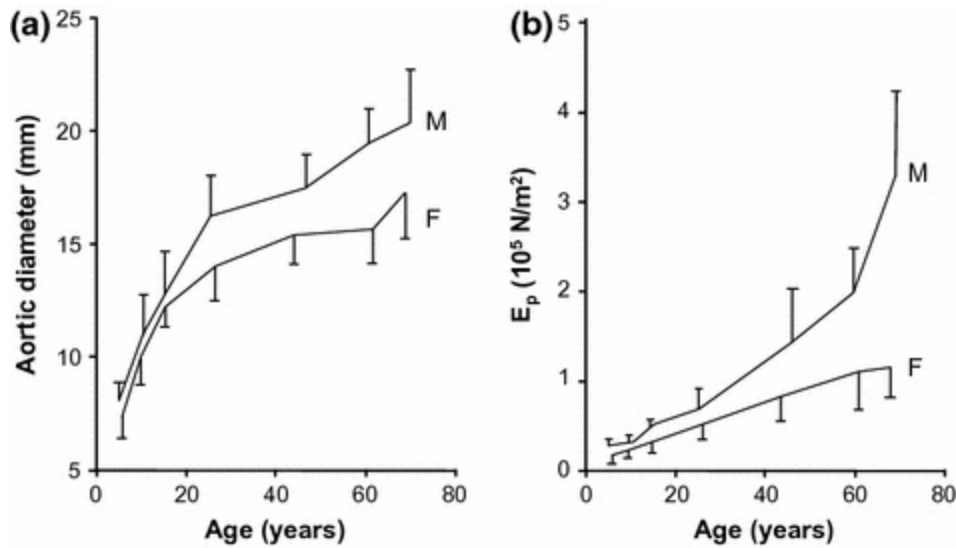


Fig. 5.11 Aorta diameter and stiffness as a function of age in the human. Reprinted from European Journal of Vascular Surgery, Vol. (7); Sonesson B, Hansen F, Stale H, Lanne T; Compliance and diameter in the human abdominal aorta - the influence of age and sex; pp. 690–697, Copyright (1993), with permission from Elsevier

In Chap. 4 it was explained that ejected blood from the heart passes into the aorta, which is elastic and increases in diameter during the cardiac cycle in order to accommodate the blood ejected from the heart. If the aorta is stiffer then the diameter expands by a smaller amount. This in turn gives rise to increased blood velocity and increased WSS. Over time the aorta increases in diameter in an attempt to normalise WSS. Increase in blood pressure, arising through ageing and disease leads to increase in wall thickness. Chapter 14 discusses, in more detail, stiffening of arteries with ageing where it is noted that there are two principal mechanisms; loss of elastin due to cyclic stress fracturing and pathological changes associated with disease.

After age 40 there is loss in height mainly due to thinning of the intervertebral discs. Typically 1 cm is lost each decade with a total loss of up to around 10 cm. There will be shrinkage of associated arteries such as the aorta. In principle this could lead to tortuosity as noted above. Whilst age-

related increased arterial tortuosity has been reported in regions subject to significant flexure (close to the knee, for example) (Wensing 1995) it is thought that increases in arterial tortuosity is mainly associated with a genetic defect which also leads to hyperflexible skin and hypermobility of joints.

5.2.6 Intervention and Disease

If mean flow rate is increased on a long-term basis then arterial diameter will gradually increase, reaching a maximum value at around 1–2 months. The change in diameter is called ‘remodelling’. This is observed, for example in the human when dialysis fistulae are created. This involves direct connection of an artery and a vein in the arm in order to create a high-flow region from which blood can be drawn for passage through a dialysis system. The diameter of the radial artery increases during the post-operative maturing process which typically takes 6 weeks (Girerd et al. 1996). Similar changes occur in animals when fistulae are created (Masuda et al. 1999; Sho et al. 2004). Conversely, a decrease in flow rate over the long term will lead to reduction in diameter of the artery. For example in paraplegia there is severe muscle wasting and reduced blood flow in major arteries followed by reduction of arterial diameter (Reneman et al. 2006).

5.2.7 Summary of the Control of Arterial Structure

The key concepts which have been described above are summarised in this section. Figure 5.12 shows the three forces and their effect on the artery. These are

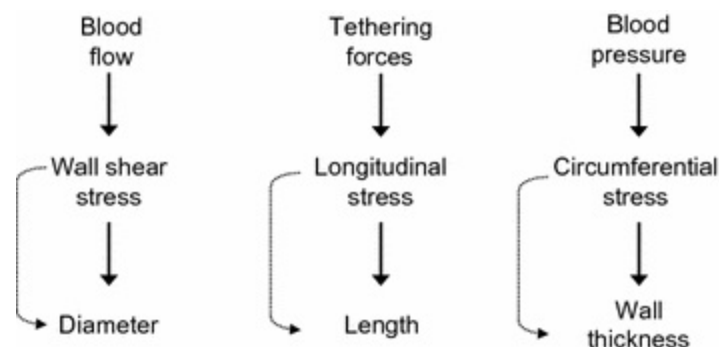


Fig. 5.12 The main control mechanisms relating to arterial structure

- *Arterial diameter and wall shear stress.* Long-term change in flow rate

leads to change in WSS. The response of the artery is to change the diameter in order to renormalise WSS to a value around 1–2 Pa (though this value is different in different parts of the arterial system). Increase in WSS leads to increase in diameter. Conversely a decrease in WSS leads to decrease in diameter.

- *Arterial length and longitudinal stress.* Arteries are pre-stressed in the longitudinal direction, that is, there is a baseline longitudinal stress. Increase in tethering forces, which occur for example during growth, will lead to increase in longitudinal stress. The response of the artery is to lengthen to normalise the longitudinal stress. This mechanism only operates during growth. Decreases in tethering forces do not lead to shrinkage in the length of the artery; instead the artery will lengthen. This can lead to a tortuous geometry in experiments on animals, but tortuosity in humans is mainly thought to be associated with genetic defects.
- *Wall thickness and circumferential stress.* Long-term changes in blood pressure lead to changes in wall thickness in order to normalise circumferential stress. The response differs pre-birth and post-birth. Pre-birth wall thickness increases through an increase in the number of lamellar units. Post-birth the number of lamellar units is fixed and wall thickness increases by increase in the thickness of each unit. Initially wall thickening is associated with increased smooth muscle content. Post-birth, decrease in circumferential stress will lead to a decrease in wall thickness, and *vice versa*. In disease, for example hypertension, thickening is also accompanied by an increase in collagen which is irreversible.

Figure 5.12 shows these control mechanisms operating independently. In terms of developing a basic understanding of arterial biomechanics this assumption is sufficient. However, as noted by Pries et al. (2005), there is a level of interdependence.

5.3 Principles of Mechanotransduction

Virtually every cell in the human body is aware of its mechanical environment to some degree and will respond to changes in the mechanical environment. Mechanotransduction is the process whereby mechanical forces

are translated into biological behaviour and vice versa. Mechanotransduction can be divided into four steps

- *Mechanotransmission*. A force is transmitted to mechanosensitive elements within the cell.
- *Mechanosensing*. The mechanosensitive elements detect the transmitted force.
- *Mechanosignalling*. The detected force results in events which are transmitted elsewhere in the cell.
- *Mechanoresponse*. A biological change is effected as a result of the detected signal.

This section explores general principles of mechanotransduction including each of the four steps listed above. This area is the subject of considerable research at the time of writing and the details of many of the steps below remain unresolved. The reader may wish to explore reviews of this area (Orr et al. 2006; Hoffman et al. 2011; Schwartz 2009).

5.3.1 Mechanotransmission

Cells are subject to external forces which result in stretching and displacement of the cell membrane and of its internal constituents. Some cells in contact with fluid, such as endothelial cells, are subject to shear stress on the surface of the cell adjacent to the moving fluid. These forces are transmitted to the mechanosensitive apparatus. In the case of endothelial cells, where mechanosensors are located on the cell surface, the force is applied directly to the mechanosensors (this is discussed further in Sect. 5.4). Force transmission through the cell is effected by the cytoskeleton. This intracellular structure is composed of filaments and microtubules which are stiff over a time period of microseconds and are capable of transmitting force from one part of the cell to another.

5.3.2 Mechanosensing

Within cells specialised units (mechanosensors) exist which are capable of detecting changes in their mechanical environment. If activated, mechanosensors can signal to other parts of the cell that there has been a change in the mechanical environment. The underlying physical basis for

much of mechanosensing is the change in protein shape arising from force applied to the protein (Orr et al. 2006). Proteins are complex molecules which will adopt a shape ('conformation') corresponding to the lowest free energy. If a physical force is applied to one part of the protein then the shape will change in order to accommodate the applied force. In energy terms the protein moves to a different energy state. There are several types of protein conformation changes relevant to mechanotransduction (Ingber 2006). These are:

- *Stretch-sensitive ion channel*. This is the most widely studied mechanosensor. Increase in the pressure within the cell during osmotic swelling will result in increase in tension in the lipid bilayer which opens allowing ions to either leave the cell or enter the cell (Sukharev et al. 2001) (Fig. 5.13). Alternatively tensional forces are transmitted direct from the cytoskeleton resulting in channel opening.

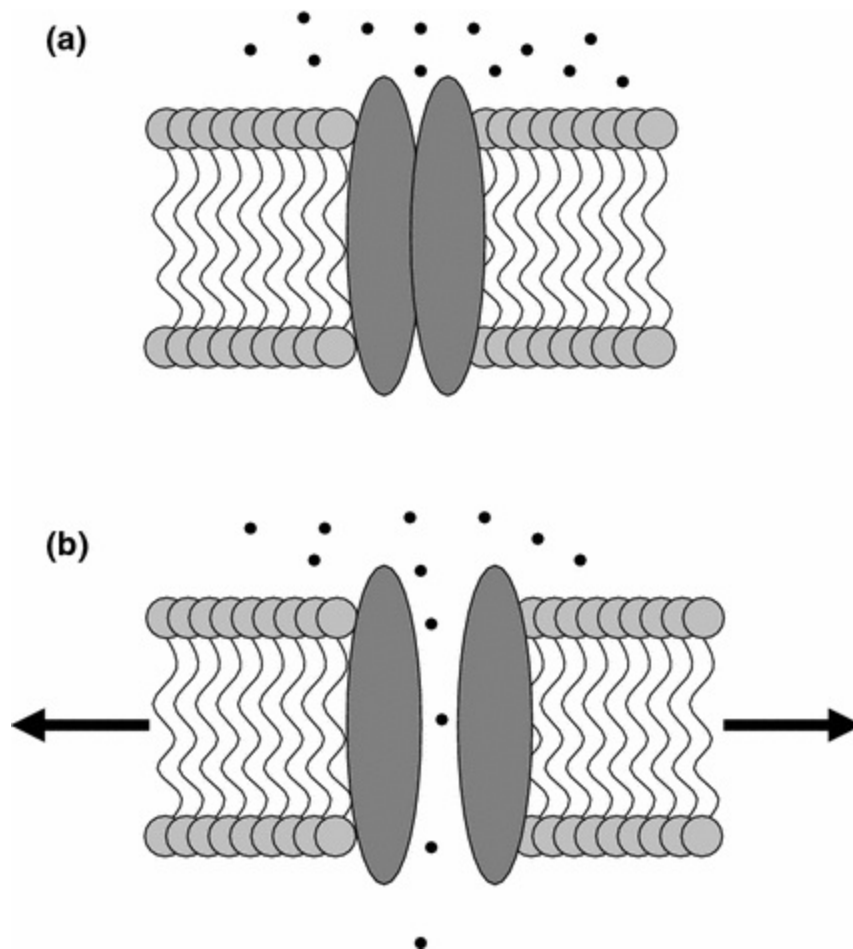


Fig. 5.13 Stretch sensitive ion channel. Increase in tension within the lipid membrane, arising

from increase in pressure within the cell, leads to opening of the ion channel allowing passage of molecules in or out of the cell

- *Tension dependent distortion of an enzyme.* In the un-stretched state the enzyme acts to cleave the molecule it binds to. When a force is applied the enzyme is stretched and is unable to cleave the molecule.
- *Binding site exposure.* In the un-stretched state a binding site is hidden within the protein. Application of a force changes the shape of the protein revealing the binding site, in this example by stretching of the protein. The binding site is then available to bind local molecules.

5.3.3 Mechanosignalling

Mechanosensing is followed by triggering of events, the mechanoreponse. If the mechanosensors and the mechanoreponse occur in separate parts of the cell then the signal must be transmitted between the sensor and the area where the response can be affected. Mechanisms for signal transmission are referred to as 'mechanosignalling' and there are two main mechanisms. The first is force transmission via the cytoskeleton, the second is release of chemicals which then diffuse through the cell. Mechanosignalling via the cytoskeleton is fast, with typical response times of a few hundred milliseconds. Chemical signalling is much slower with response times of the order of 10 s of seconds (Na et al. 2008).

5.3.4 Mechanoreponse

The mechanical response may be immediate as in the case of ion channels. More commonly the response involves pathways within the cell involving the nucleus of the cell and also signalling to other cells. In which case, the time-course of events can be days to months. Examples include bone deposition under increased weight bearing, or thickening of the arterial wall under a sustained increased blood pressure.

5.3.5 Switch-Like and Dynamic Models of Mechanotransduction

The description of mechanotransduction above involves the detection of a force as an on/off process. The relevant protein involved in the

mechanosensors changes conformation and the signal and subsequent response is either produced fully or not at all. However, in endothelial cells the response to WSS and to cyclic stretch depends on the frequency and to the detailed time variation, which an on/off model is unable to explain (Hoffman et al. 2011). Hoffmann et al. proposed a model of mechanosensing in which the time variation of the stimulus was accounted for.

5.3.6 Other Mechanosensory Mechanisms

It was noted above that protein conformation change is the dominant mechanism for mechanosensing. Another mechanism is compression of the intercellular space. Forces leading to reduction in the distance between cells will lead to changes in the concentrations of molecules in the gap between cells leading to increased binding at receptors on the cell surface; e.g. autocrine molecules in heart muscle (Maly et al. 2004).

5.4 Endothelial Mechanotransduction

It was noted above that the artery is subject to cyclic pressure which leads to a cyclic circumferential tension and cyclic stretch of all the layers of the artery (endothelium, media and adventitia), and the endothelium is subject to WSS. Of these elements by far the most important in terms of mechanotransduction is the effect of WSS on the endothelium. Most of the discussion below will be in terms of the combination of WSS and endothelium. Reviews of this area are provided by Ando and Yamamoto (2009), Davies (1995, 2009), Chien (2007) and Hahn and Schwartz (2009).

5.4.1 Effect of Wall Shear Stress on Endothelium

Laboratory studies of the effect of flow on arteries have largely concentrated on cultured endothelium; that is endothelial cells which are grown on a glass plate or similar material. Flow is then passed over the endothelium and a range of tests can be performed to investigate cell shape, orientation and the biological behaviour of the cells. Chapter 14 discusses cultured endothelium in more detail. Change in shear stress leads to a wide variety of effects as listed in Table 5.1. These have different timescales from potassium channel activation (seconds) to cell alignment (hours). Figure 5.14 shows cultured bovine endothelial cells before and several hours after a wall shear stress of

10 dyn cm⁻².

Table 5.1 Responses to changes in WSS in cultured endothelium (modified from Davies 1995); glycocalyx significance from Zeng and Tarbell (2014)

Timescale	Response	Significance
Secs	K ⁺ channel activation	Related to vasorelaxation
Secs	NO release	Flow-mediated vasorelaxation
15–40 s	Ca ²⁺ rise	Ca ²⁺ as second messenger
2 min	PGI release	Regulation of vascular tone
Secs–mins	Remodelling of focal adhesion sites	Transmission/transduction stress
Mins–hours	Remodelling of the glycocalyx	Changes in mechanotransduction, selective permeability and leukocyte adhesion
2–3 h	Induction protein kinase C	Regulation protein phosphorylation
>6 h	Cell alignment and direction change	Minimises the drag on cells

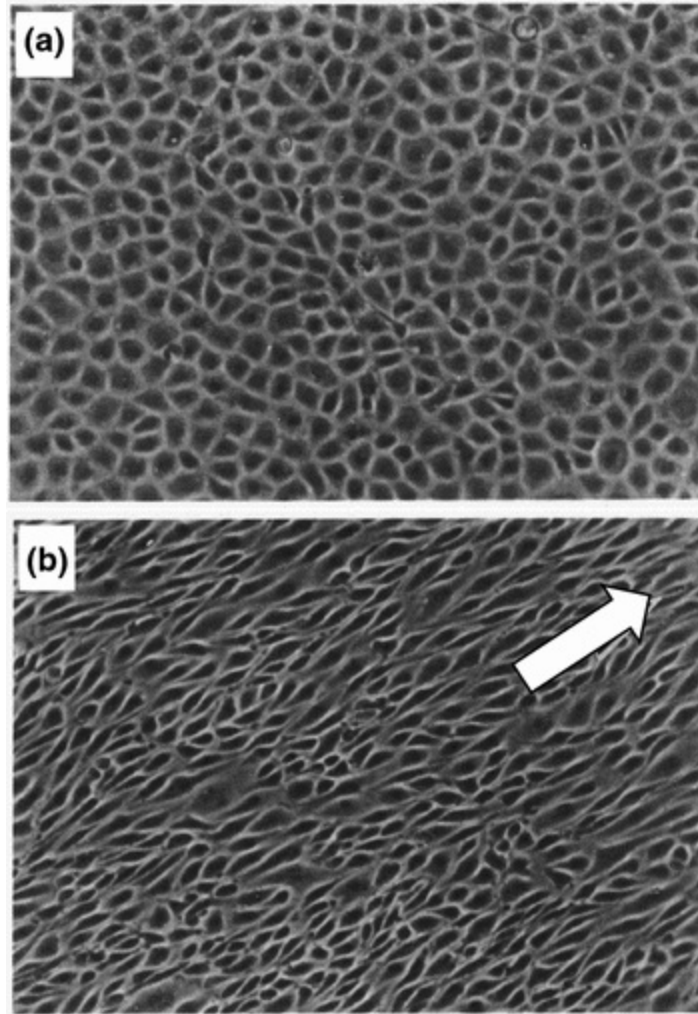


Fig. 5.14 Effect of wall shear stress on endothelial cell alignment using cultured bovine cells. **a** No wall shear stress; cells have a cobblestone appearance with no preferred direction, **b** several hours after wall shear stress of magnitude 10 dyn cm^{-2} ; cells are aligned with the direction of wall shear stress. Images kindly provided by Prof. Peter Davies, University of Pennsylvania, USA

5.4.2 Decentralised Model of Endothelial Mechanotransduction

Mechanosensors can be divided between those on the endothelial surface adjacent to flowing blood and those embedded within the endothelial cell. It is thought that mechanosensors are distributed throughout the endothelial cell rather than just being on the surface. This is called the ‘decentralised model of mechanotransduction’ (Davies 1995; Helmke and Davies 2002).

Figure 5.15 illustrates the main components involved in endothelial mechanotransduction in the decentralised model. In the figure, potential

mechanosensors are located at four locations; (1) on the endothelial surface adjacent to flowing blood, (2) at the junction between cells, (3) at adhesion sites and (4) at the nucleus. Transmission of force between sites is effected by the cytoskeleton such that multiple locations may become activated near-simultaneously.

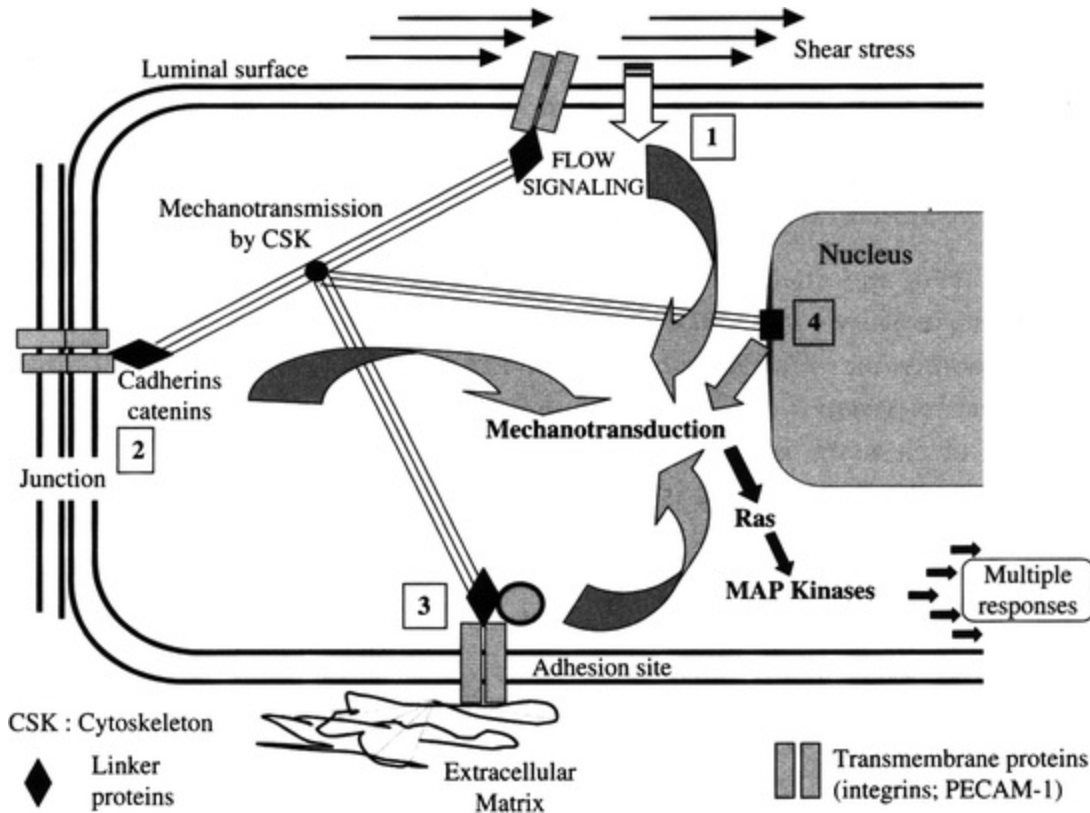


Fig. 5.15 Decentralised model of endothelial mechanotransduction. Reprinted by permission from Macmillan Publishers Ltd.: Nature Clinical Practice in Cardiovascular Medicine, Davies (2009), copyright (2008)

5.4.3 Potential Wall Shear Stress Mechanosensors

This section will describe mechanosensors. This is a highly active research area and understanding of the role of these sensors is continuing to evolve.

Luminal mechanosensors. Figure 5.16 illustrates mechanosensors present on the surface of the endothelium. These include ion channels (ATP, potassium and calcium), protein receptors (tyrosine kinase and G-coupled protein) and larger structures (glycocalyx and primary cilia). The shear force from blood flowing close to the endothelium will pull on the luminal proteins and luminal structures causing these to bend or change conformation.

Potassium (K^+) and calcium (Ca^{2+}) ion channels are known to open in response to increased wall shear stress. Influx of calcium ions through open ion channels travels through the cell like a wave. The primary cilium extends several microns from the surface of the cell where shear force will be higher. The glycocalyx is a layer of glycoproteins which covers the surface of the endothelial cell projecting up to 4.5 microns.

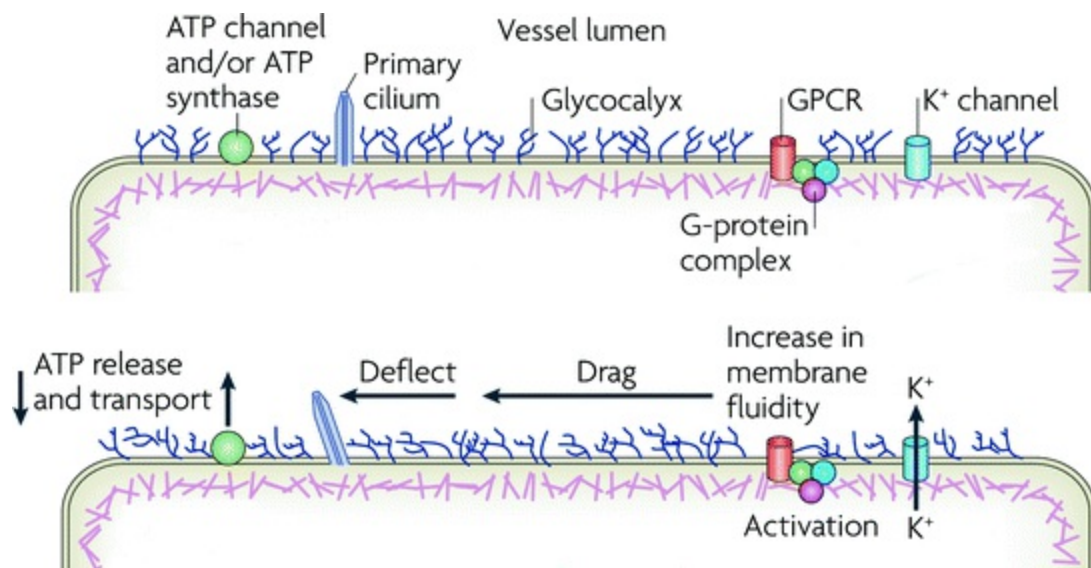


Fig. 5.16 Luminal mechanosensors. Figure adapted by permission from Macmillan Publishers Ltd: Nature Reviews of Molecular and Cellular Biology, Hahn C, Schwartz MA; Mechanotransduction in vascular physiology and atherogenesis, Vol. 10, pp. 53–62, copyright (2009)

Cytoskeleton. It has been proposed (Ingber 1997) that the cytoskeleton itself is constructed to stabilise the shape of the cell and to be able to detect changes in shape. The tensegrity model is one in which a matrix of stiff elements are held in a stable configuration by the tension in elastic elements. Changes in shear will alter the tension distribution within the cell which is sensed by mechanosensors (adhesion proteins) connected to the cytoskeleton.

Adhesion proteins. The cytoskeleton is attached to proteins in the membrane referred to as ‘adhesion proteins’. These adhesion proteins are subject to stress transmitted by the cytoskeleton and respond to this stress.

References

Achiron R, Golan-Porat N, Gabbay U, Rotstein Z, Heggesh J, Mashiach S, Lipit S. In utero

ultrasonographic measurements of fetal aortic and pulmonary artery diameters during the first half of gestation. *Ultrasound Obstet Gynecol.* 1998;11:180–4.

[\[CrossRef\]](#)[\[PubMed\]](#)

Ando J, Yamamoto K. Vascular mechanobiology—endothelial cell responses to fluid shear stress. *Circ J.* 2009;73:1983–92.

[\[CrossRef\]](#)[\[PubMed\]](#)

Åstrand H, Rydén-Ahlgren A, Sandgren T, Länne T. Age-related increase in wall stress of the human abdominal aorta: an in vivo study. *J Vasc Surg.* 2005;42:926–31.

[\[CrossRef\]](#)[\[PubMed\]](#)

Bomberger RA, Zarins CK, Taylor KE, Glagov S. Effect of hypotension on atherogenesis and aortic wall composition. *J Surg Res.* 1980;28:402–9.

[\[CrossRef\]](#)[\[PubMed\]](#)

Cartier MS, Davidoff A, Warneke LA, Hirsh MP, Bannon S, Sutton MS, Doubilet PM. The normal diameter of the fetal aorta and pulmonary-artery—echocardiographic evaluation in utero. *Am J Roentgenol.* 1987;149:1003–7.

[\[CrossRef\]](#)

Cheng C, Helderman F, Tempel D, Segers D, Hierck B, Poelmann R, et al. Large variations in absolute wall shear stress levels within one species and between species. *Atherosclerosis.* 2007;195:225–34.

[\[CrossRef\]](#)[\[PubMed\]](#)

Chien S. Mechanotransduction and endothelial cell homeostasis: the wisdom of the cell. *Am J Physiol Heart Circ Physiol.* 2007;292:H1209–24.

[\[CrossRef\]](#)[\[PubMed\]](#)

Davies PF. Flow-mediated endothelial mechanotransduction. *Physiol Rev.* 1995;75:519–60.

[\[PubMed\]](#)[\[PubMedCentral\]](#)

Davies PF. Hemodynamic shear stress and the endothelium in cardiovascular pathophysiology. *Nature Clin Prac Cardiovasc Med.* 2009;6:16–26.

[\[CrossRef\]](#)

Giddens DP, Zarins CK, Glagov S. The role of fluid mechanics in the localization and detection of atherosclerosis. *J Biomech Eng.* 1993;115:588–94.

[\[CrossRef\]](#)[\[PubMed\]](#)

Girerd X, London G, Boutouyrie P, Mourad JJ, Safar M, Laurent S. Remodeling of the radial artery in response to a chronic increase in shear stress. *Hypertension.* 1996;27:799–803.

[\[CrossRef\]](#)[\[PubMed\]](#)

Greve JM, Les AS, Tang BT, Draney Blomme MT, Wilson NM, Dalman RL, Pelc NJ, Taylor CA. Allometric scaling of wall shear stress from mice to humans: quantification using cine phase-contrast MRI and computational fluid dynamics. *Am J Physiol Heart Circ Physiol.* 2006;291:H1700–08.

Haak MC, Twisk JWR, Van Vugt JMG. How successful is fetal echocardiographic examination in the first trimester of pregnancy? *Ultrasound Obstet Gynecol.* 2002;20: 9–13.

Hahn C, Schwartz MA. Mechanotransduction in vascular physiology and atherogenesis. *Nat Rev Mol*

Cell Biol. 2009;10:53–62.

[CrossRef][PubMed][PubMedCentral]

Hayashi K, Naiki T. Adaptation and remodeling of vascular wall; biomechanical response to hypertension. *J Mech Behav Biomed Mater.* 2009;2:3–19.

[CrossRef][PubMed]

Helmke BP, Davies PF. The cytoskeleton under external fluid mechanical forces: hemodynamic forces acting on the endothelium. *Ann Biomed Eng.* 2002;30:284–96.

[CrossRef][PubMed]

Hoffman BD, Grashoff C, Schwartz MA. Dynamic molecular processes mediate cellular mechanotransduction. *Nature.* 2011;475:316–23.

[CrossRef][PubMed]

Holzapfel GA, Ogden RW. Modelling the layer-specific three-dimensional residual stresses in arteries, with an application to the human aorta. *J Royal Soc Int.* 2010;7:787–99.

[CrossRef]

Humphrey JD. Vascular adaptation and mechanical homeostasis at tissue, cellular, and sub-cellular levels. *Cell Biochem Biophys.* 2008;50:53–78.

[CrossRef][PubMed]

Ingber DE. Tensegrity: the architectural basis of cellular mechanotransduction. *Annu Rev Physiol.* 1997;59:575–99.

[CrossRef][PubMed]

Ingber DE. Cellular mechanotransduction: putting all the pieces together again. *FASEB J.* 2006;20:811–27.

[CrossRef][PubMed]

Karsaj I, Humphrey JD. A multilayered wall model of arterial growth and remodelling. *Mech Mater.* 2012;44:110–9.

[CrossRef][PubMed][PubMedCentral]

Langille BL. Arterial remodeling: relation to hemodynamics. *Can J Physiol Pharmacol.* 1996;74:834–41.

[CrossRef][PubMed]

le Noble F, Fleury V, Pries A, Corvol P, Eichmann A, Reneman RS. Control of arterial branching morphogenesis in embryogenesis: go with the flow. *Cardiovasc Res.* 2005;65:619–28.

[CrossRef][PubMed]

Leung DY, Glagov S, Mathews MB. Elastin and collagen accumulation in rabbit ascending aorta and pulmonary trunk during postnatal growth. Correlation of cellular synthetic response with medial tension. *Circ Res.* 1977;41:316–23.

[CrossRef][PubMed]

Maly IV, Lee RT, Lauffenburger DA. A model for mechanotransduction in cardiac muscle: effects of extracellular matrix deformation on autocrine signaling. *Ann Biomed Eng.* 2004;32:1319–35.

[CrossRef][PubMed]

Masuda H, Zhuang YJ, Singh TM, Kawamura K, Murakami M, Zarins CK, et al. Adaptive remodeling of internal elastic lamina and endothelial lining during flow-induced arterial enlargement. *Arterioscl Thromb Vasc Biol.* 1999;19:2298–307.

[\[CrossRef\]](#)[\[PubMed\]](#)

Meinders JM, Kornet L, Hoeks APG. Assessment of spatial inhomogeneities in intima media thickness along an arterial segment using its dynamic behaviour. *Am J Physiol Heart Circ Physiol.* 2003;285:H384–91.

[\[CrossRef\]](#)[\[PubMed\]](#)

Murray CD: The physiological principle of minimum work. I. The vascular system and the cost of blood volume. *Proc Natl Acad Sci USA.* 1926a;12:207–214.

Murray CD. The physiological principle of minimal work applied to the angle of branching of arteries. *J Gen Physiol.* 1926;9:835–41.

[\[CrossRef\]](#)[\[PubMed\]](#)[\[PubMedCentral\]](#)

Na S, Collin O, Chowdhury F, Tay B, Ouyang M, Wang Y, Wang N. Rapid signal transduction in living cells is a unique feature of mechanotransduction. *Proc Natl Acad Sci USA.* 2008;105:6626–31.

[\[CrossRef\]](#)[\[PubMed\]](#)[\[PubMedCentral\]](#)

Orr AW, Helmke BP, Blackman BR, Schwartz MA. Mechanisms of mechanotransduction. *Dev Cell.* 2006;10:11–20.

[\[CrossRef\]](#)[\[PubMed\]](#)

Pries AR, Reglin B, Secomb TW. Remodeling of blood vessels: responses of diameter and wall thickness to hemodynamic and metabolic stimuli. *Hypertension.* 2005;46:726–31.

[\[CrossRef\]](#)

Reneman RS, Arts T, Hoeks APG. Wall shear stress—an important determinant of endothelial cell function and structure—in the arterial system in vivo. *J Vasc Res.* 2006;43:251–69.

[\[CrossRef\]](#)[\[PubMed\]](#)

Schwartz MA. The force is with us. *Science.* 2009;323:588–9.

[\[CrossRef\]](#)[\[PubMed\]](#)

Sherman TF. On connecting large vessels to small the meaning of Murray’s law. *J Gen Physiol.* 1981;78:431–53.

[\[CrossRef\]](#)[\[PubMed\]](#)

Sho E, Nanjo H, Sho M, Kobayashi M, Komatsu M, Kawamura K, et al. Arterial enlargement, tortuosity, and intimal thickening in response to sequential exposure to high and low wall shear stress. *J Vasc Surg.* 2004;39:601–12.

[\[CrossRef\]](#)[\[PubMed\]](#)

Sonesson B, Hansen F, Stale H, Lanne T. Compliance and diameter in the human abdominal aorta—the influence of age and sex. *Eur J Vasc Surg.* 1993;7:690–7.

[\[CrossRef\]](#)[\[PubMed\]](#)

Struijk PC, Stewart PA, Fernando KL, Mathews VJ, Loupas T, Steegers EAP, Wladimiroff JW. Wall shear stress and related hemodynamic parameters in the fetal descending aorta derived from color Doppler velocity profiles. *Ultrasound Med Biol.* 2005;31:1441–50.

[\[CrossRef\]](#)[\[PubMed\]](#)

Sukharev S, Betanzos M, Chiang CS, Guy HR. The gating mechanism of the large mechanosensitive channel MscL. *Nature*. 2001;409:720–4.

[\[CrossRef\]](#)[\[PubMed\]](#)

Thoma R. Untersuchungen über die Histogenese und Histomechanik des Gefäßsystems. Stuttgart: Ferdinand Enke; 1893.

Wagenseil JE, Mecham RP. Vascular extracellular matrix and arterial mechanics. *Physiol Rev*. 2009;89:957–89.

[\[CrossRef\]](#)[\[PubMed\]](#)[\[PubMedCentral\]](#)

Weinberg PD, Ethier CR. Twenty-fold difference in hemodynamic wall shear stress between murine and human aortas. *J Biomech*. 2007;40:1594–8.

[\[CrossRef\]](#)[\[PubMed\]](#)

Wensing PJ. Arterial tortuosity in the femoropopliteal region during knee flexion. *J Anat*. 1995;186:133–9.

Wolinsky H, Glagov S. A lamellar unit of aortic medial structure and function in mammals. *Circ Res*. 1967;20:99–111.

Zamir M. Shear forces and blood vessel radii in the cardiovascular system. *J Gen Physiol*. 1977;69:449–61.

[\[CrossRef\]](#)[\[PubMed\]](#)

Zeng Y, Tarbell JM. The adaptive remodeling of endothelial glycocalyx in response to fluid shear stress. *PLoS One*. 2014;9:e86249.

[\[CrossRef\]](#)[\[PubMed\]](#)[\[PubMedCentral\]](#)

6. Excitation-Contraction in the Heart

Richard H. Clayton¹✉ and D. Rodney Hose¹✉

(1) University of Sheffield, Sheffield, UK

✉ **Richard H. Clayton (Corresponding author)**

Email: r.h.clayton@sheffield.ac.uk

✉ **D. Rodney Hose**

Email: D.R.Hose@sheffield.ac.uk

Learning outcomes

1. Describe the main anatomical features of the human heart, and explain how each of them behaves during a normal heart beat.
2. Describe the structural relationship between myocytes, myofibrils and sarcomeres.
3. Describe the main ionic currents that underlie a normal action potential.
4. Describe the normal electrical activation sequence of the heart.
5. Explain how the normal electrical activation sequence of the heart is disturbed in an arrhythmia, giving an example.
6. Describe the mechanism by which electrical activation initiates

contraction of a cardiac myocyte.

7. Describe the Frank--Starling law of the heart.
8. Discuss the mechanism of cardiac remodelling, and its consequences for cardiac function.

The mammalian heart is a muscular organ that acts to propel blood through the pulmonary and systemic circulation. It is two pumps in series; the right side of the heart supplies the pulmonary circulation and left side the systemic circulation. The role of the heart is vital in sustaining life, since it delivers oxygen from the lungs to tissues, and removes products of metabolism (principally CO₂).

Each heartbeat is initiated as an electrical depolarisation of cells in the natural pacemaker. Electrical activation then spreads through the whole heart, acting as a signal to both initiate and synchronise mechanical contraction. Abnormal initiation or conduction of the activation sequence is a cardiac arrhythmia. The electrical activity of the heart produces current flow in the torso, which can be registered as the electrocardiogram (ECG).

The electrical activation of each cardiac cell admits a small amount of Ca²⁺, which triggers release of additional Ca²⁺ from intracellular stores. The resulting increase in intracellular Ca²⁺ concentration engages contractile proteins in the cell, producing mechanical force.

Cardiac cells are arranged so that contraction of the tissue acts to increase the pressure in each chamber of the heart in turn, leading to opening of the valves and the pulsatile flow of blood around the circulation. The rate and strength of contractions is regulated so as to balance the delivery of oxygen and removal of CO₂, notably during exercise. When this regulation is disturbed then the heart may not be able to meet metabolic demands, resulting in heart failure.

6.1 Overview of Cardiac Structure and Function

6.1.1 Cardiac Anatomy and the Cardiac Cycle

The mammalian heart is a four-chambered pump, which acts to propel blood

around the pulmonary and systemic circulation (Fig. 6.1). Deoxygenated blood returning from the systemic circulation enters the right atrium (RA), and as the atria contract, this blood is pumped into the right ventricle (RV) through the tricuspid valve. Ventricular contraction follows atrial contraction, and the deoxygenated blood is then pumped through the pulmonary valve and into the pulmonary arteries and pulmonary circulation. Oxygenated blood then returns from the pulmonary circulation through the pulmonary veins and into the left atrium (LA). As the atria contract, this blood is pumped into the left ventricle (LV) through the mitral valve. Contraction of the LV then ejects the oxygenated blood through the aortic valve and into the systemic circulation.

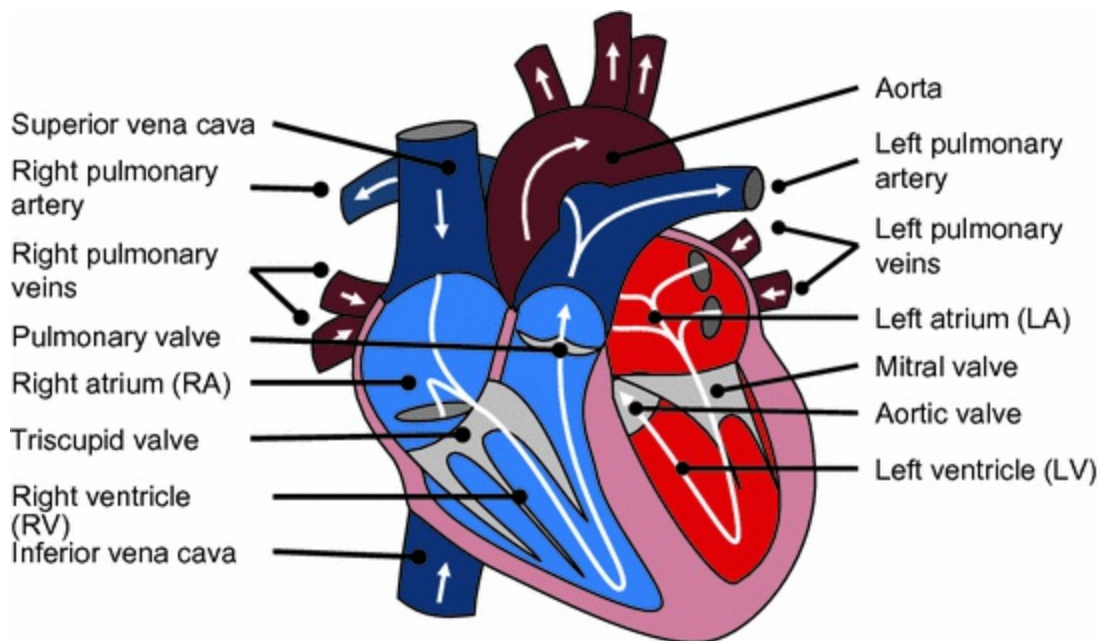


Fig. 6.1 Anatomy of the human heart showing the main structures. *Blue regions* indicate the right side of the heart, which pumps venous blood. *Red regions* indicate the left side of the heart, which pumps arterial blood. *White arrows* show the direction of blood flow

Each heartbeat is therefore reliant on a sequence of events that include mechanical contraction, as well as the opening and closing of the valves in the correct order. The outcome is an increase of pressure in the aorta, which acts to produce flow of blood around the systemic circulation. Figure 6.2 illustrates typical pressures and volume in the left side of the human heart during each beat. Atrial systole (contraction) produces a rise in LA pressure, filling the LV through the open mitral valve. The onset of ventricular systole

results in pressure rise within the LV. Once LV pressure exceeds LA pressure, the mitral valve shuts, and when LV pressure exceeds pressure in the aorta the aortic valve opens. Blood is then ejected through the aortic valve, producing a pressure rise in the aorta. When LV pressure falls below aortic pressure the aortic valve closes, and when LV pressure falls below LA pressure the mitral valve opens.

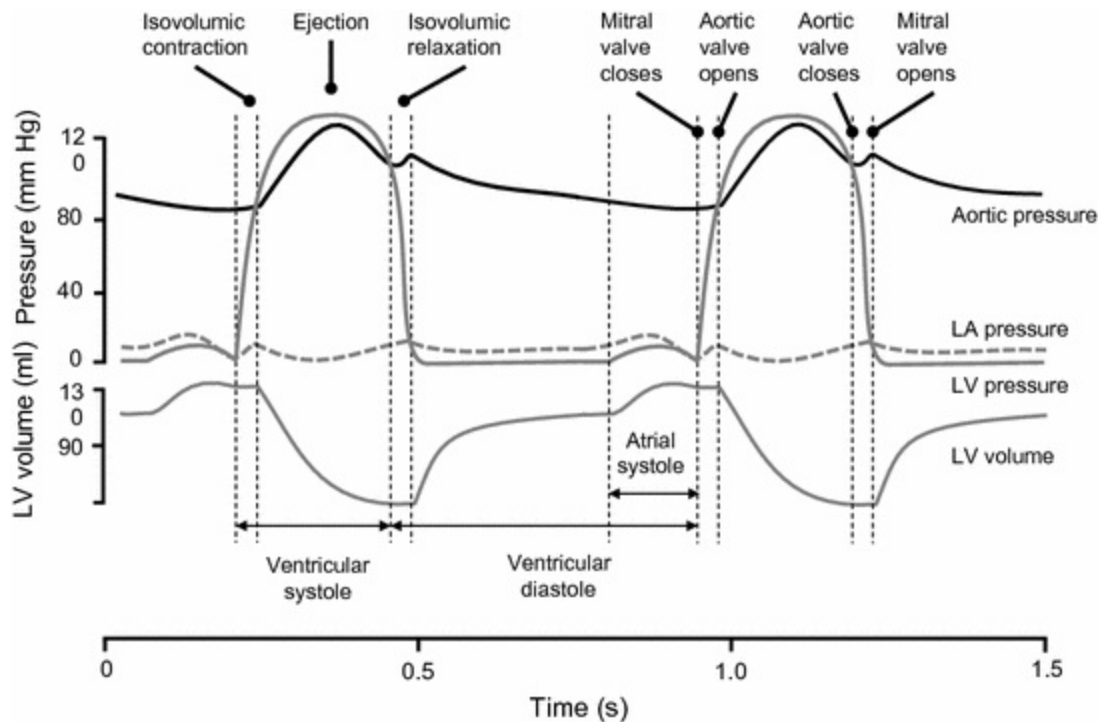


Fig. 6.2 Cardiac cycle, showing changes in pressure and volume in different parts of the heart during two heart beats

6.1.2 Cardiac Cells and Tissue

The myocardium is a composite material, composed primarily of myocytes, fibroblasts and the extracellular matrix. Myocytes generate mechanical tension when stimulated electrically. Fibroblasts are connective tissue cells that act to regulate the extracellular matrix that supports the structures of the heart including the valves.

Cardiac myocytes are rod-shaped cells, 50–150 μm in length and 10–20 μm in diameter. When stimulated electrically, a myocyte generates tension in the direction of its long axis, and individual myocytes are connected end to end into fibres (Fig. 6.3a). The interface between adjacent cells has a characteristic stepped appearance and is called the intercalated disc. The

intercalated discs contain gap junctions, which provide an electrical connection from one cell to its neighbour. Cardiac myocytes may have more than one nucleus, and may also branch, so that an individual cell may have more than two neighbours.

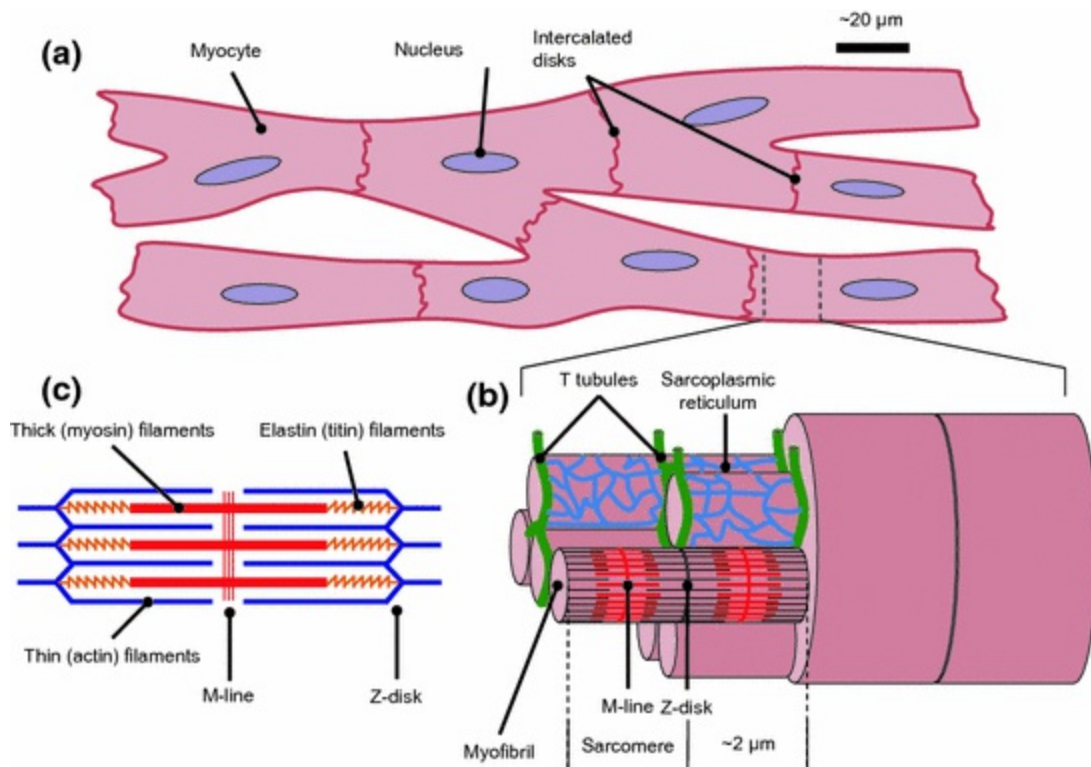


Fig. 6.3 Structure of cardiac tissue and myocytes. **a** Arrangement of cardiac myocytes and connections between them. **b** Internal structure of myocyte. **c** Diagram showing the contractile apparatus within a myofibril

In the ventricles, there is evidence that these fibres are also arranged into sheets, and this orthotropic structure contributes to the passive and active mechanical properties of the tissue (Nielsen et al. 1991). Figure 6.3a illustrates the typical arrangement of myocytes in tissue.

Myocytes are also composed of striated myofibrils (Fig. 6.3b). Each myofibril consists of chains of sarcomeres, each about 2 μm long, which are terminated at each end by a Z-disc. These Z discs provide an anchor for the thin filaments, which engage with thick filaments to generate tension (Fig. 6.3c). The mechanism of tension generation is described in more detail in Sect. 6.3.

A valve plane separates the electrically excitable atria and ventricles. It is composed of connective tissue and provides a mechanical anchor for the

valves. The connective tissue is electrically inexcitable, and is penetrated only by the atrioventricular node (see below).

6.1.3 Myocardial Perfusion and Metabolism

The heart itself requires a supply of oxygenated blood in order for its metabolic needs to be met, and has its own system of arteries and veins. A branching network of coronary arteries is perfused from left and right branches, which connect to the aorta very close to the aortic valve. The main branches of the coronary arteries remain on the epicardial surface, and smaller vessels penetrate the myocardium. If a coronary artery develops a significant stenosis, then the region of myocardium perfused by that artery may become ischaemic. Ischaemia describes the changes in cell metabolism resulting from a reduction or interruption of the supply of oxygenated blood. These changes include altered electrical excitability, and reduced contractility. Prolonged or severe ischaemia resulting from complete blockage of a coronary artery will result in a myocardial infarction. Unless blood flow is restored quickly, the ischaemic region of myocardium will undergo irreversible cell death. Ultimately the region will become scar tissue, with impaired mechanical function.

Venous blood collects in the coronary sinus, which is located around the posterior of the heart, close to the valve plane. The coronary sinus drains into the right atrium.

6.2 Electrical Excitation

6.2.1 The Cardiac Action Potential

The mechanical contraction of cardiac cells and tissue is both initiated and synchronised by electrical excitation that originates in the sinus node, which acts as a natural pacemaker. The sequence of electrical excitation and recovery in a single cell is the cardiac action potential.

Cardiac myocytes are electrically excitable cells with a bilipid membrane that encloses the cell contents and acts as a barrier to the movement of ions. Embedded within the membrane are ion channels, pumps and exchangers, which have a permeability or conductance that depends on the potential difference across the membrane. An example of an ion channel embedded in the cell membrane is shown in Fig. 6.4. These ion channels, pumps and

exchangers act to regulate the intracellular concentration of Na^+ , Ca^{2+} and K^+ .

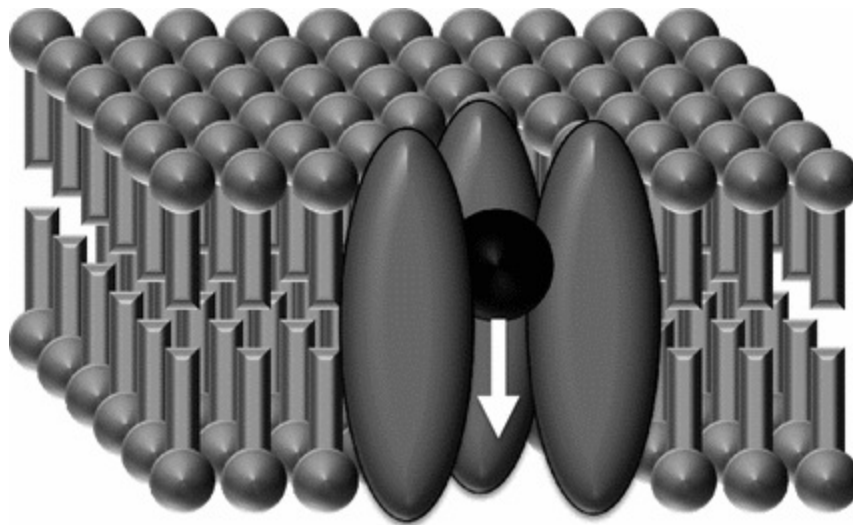


Fig. 6.4 Cartoon of myocyte cell membrane, showing lipid bilayer, with embedded ion channel (elongated ellipsoids) admitting a single ion

At rest, the concentrations of Na^+ and Ca^{2+} outside the cell exceed the concentration inside the cell, and the concentration of K^+ inside the cell exceeds the concentration outside the cell (Table 6.1). At rest, the cell membrane is permeable to K^+ . A single K^+ ion is therefore exposed to a concentration gradient, and so K^+ ions tend to diffuse out of the cell. The effect of this diffusion is to establish a gradient in electrical potential because the K^+ ions that diffuse out of the cell carry an excess positive charge. At equilibrium, the tendency to diffuse out of the cell is balanced by the opposing effect of potential difference. The corresponding voltage across the cell membrane at equilibrium is given by the Nernst equation

$$E = \frac{RT}{zF} \log_e \left(\frac{[\text{K}^+]_o}{[\text{K}^+]_i} \right),$$

Table 6.1 Typical equilibrium concentrations of cations involved in the cardiac action potential

Ionic species	Intracellular concentration (mM)	Extracellular concentration (mM)	Nernst potential (mV)
Na^+	10	140	+70
Ca^{2+}	0.0001	1.2	+124

K^+	140	5	-90
-------	-----	---	-----

where R is the gas constant ($8.316 \text{ J K}^{-1} \text{ mol}^{-1}$), T is absolute temperature (body temperature is 310 K), z the valency of K^+ ions (1), F the Faraday constant (charge carried by one mole of K^+ ions, $96,484 \text{ C mol}^{-1}$), $[K^+]$ concentration of K^+ outside (o) and inside (i) the cell. For normal concentrations of K^+ , the Nernst potential is -90 mV , with the inside of the cell negatively charged relative to the outside. This is close to the resting potential of cardiac myocytes, which are polarised to a voltage typically between -80 and -90 mV . The K^+ Nernst potential is not exactly equal to the resting potential because the membrane retains a very small permeability to Na^+ ions, which acts to slightly reduce the resting potential.

When the potential difference across the cell membrane is perturbed so that it decreases below a threshold of around -65 mV (for example by an action potential in a neighbouring cell), voltage-gated ion channels open to admit Na^+ . There is a large gradient not only in Na^+ concentration but also in electrical potential, which results in an influx of Na^+ into the cell and a rapid depolarisation of the membrane potential towards the Nernst potential for Na^+ ions, which is around $+70 \text{ mV}$.

Almost immediately, the Na^+ ion channels inactivate, shutting off further influx of Na^+ ions. However, the change in membrane potential has two further consequences. First, the change opens voltage-gated Ca^{2+} ion channels, which admit Ca^{2+} into the cell. Second, the change also opens voltage-gated K^+ ion channels, which results in an outward flow of K^+ ions. Initially the influx of Ca^{2+} tends to balance the outflow of K^+ , but then the Ca^{2+} ion channels begin to close and the outflow of K^+ dominates, leading to repolarisation of the cell to the resting potential. Computational and mathematical models have played an important role alongside experimental work in the discovery of these detailed physiological mechanisms, and this story is recounted by Noble and Rudy (2001).

The action potential is an all or nothing response, once the cell is depolarised to its threshold it will respond with a complete action potential. Once a cell begins an action potential, it will not respond to a further stimulus until it has repolarised. The cell is said to be refractory, and the interval between depolarisation and the time at which the cell can produce another action potential is called the refractory period. Typically, the refractory

period is around the same as the action potential duration. Figure 6.5 shows time series generated from a computer model of the human atrial action potential, and includes both the action potential and the main currents that flow throughout the different phases.

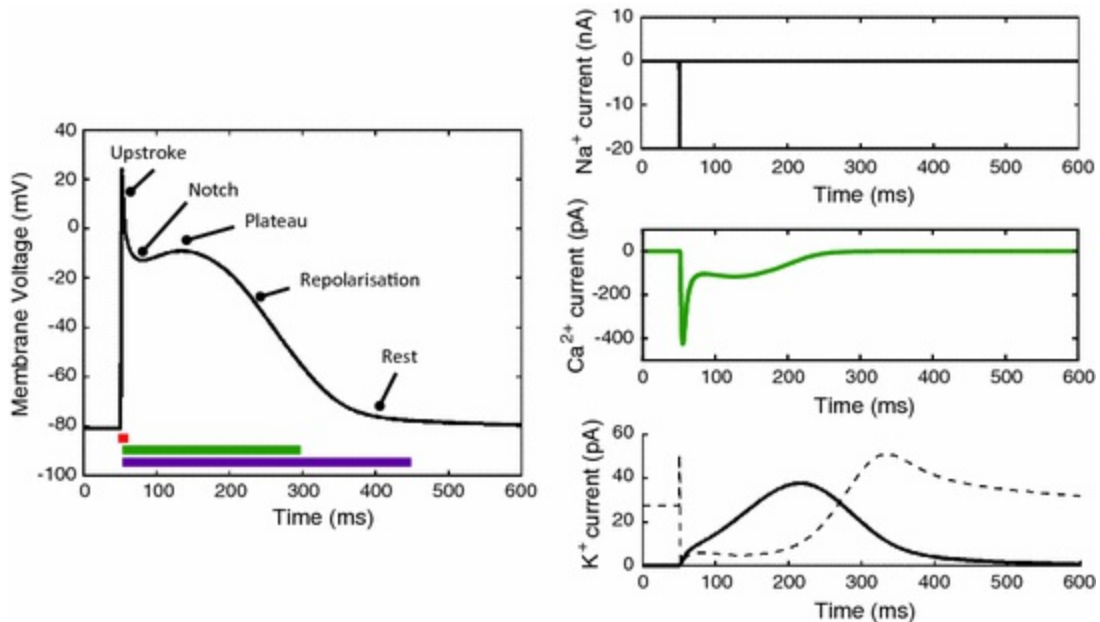


Fig. 6.5 Cardiac action potential, with principal inward (Na^+ and Ca^{2+}), and outward (K^+) currents shown

In cardiac tissue, cells are electrically connected by gap junctions, which enable the action potential to be passed from one cell to its neighbours. Since gap junctions are part of the intercalated discs, the action potential propagates faster along the long axis of cells than across the short axis.

6.2.2 Activation Sequence for Normal Beats

A normal heartbeat begins with the spontaneous depolarisation of pacemaking cells in the sinus node, located in the right atrium. In these specialised cells, there a small inward current gradually brings the membrane potential to threshold during the resting phase. The result is a series of spontaneous beats, and the interval between these beats is modulated by neural activity.

The normal beat initiated in the sinus node propagates through the left and right atrium, and into a further specialised region of tissue called the atrioventricular node. In the normal heart, the atrioventricular node provides

the only pathway for an action potential to propagate through the fibrous tissue that separates the atria and ventricles, and acts as a mechanical support for the valves.

The atrioventricular node is linked to Purkinje fibres, which conduct the action potential very rapidly, and terminate throughout the ventricular tissue. The rapid propagation of the action potential through the Purkinje system ensures synchronised contraction of the ventricular chambers.

This sequence of electrical activation is shown in Fig. 6.6, which includes a representation of the action potential shape in each region.

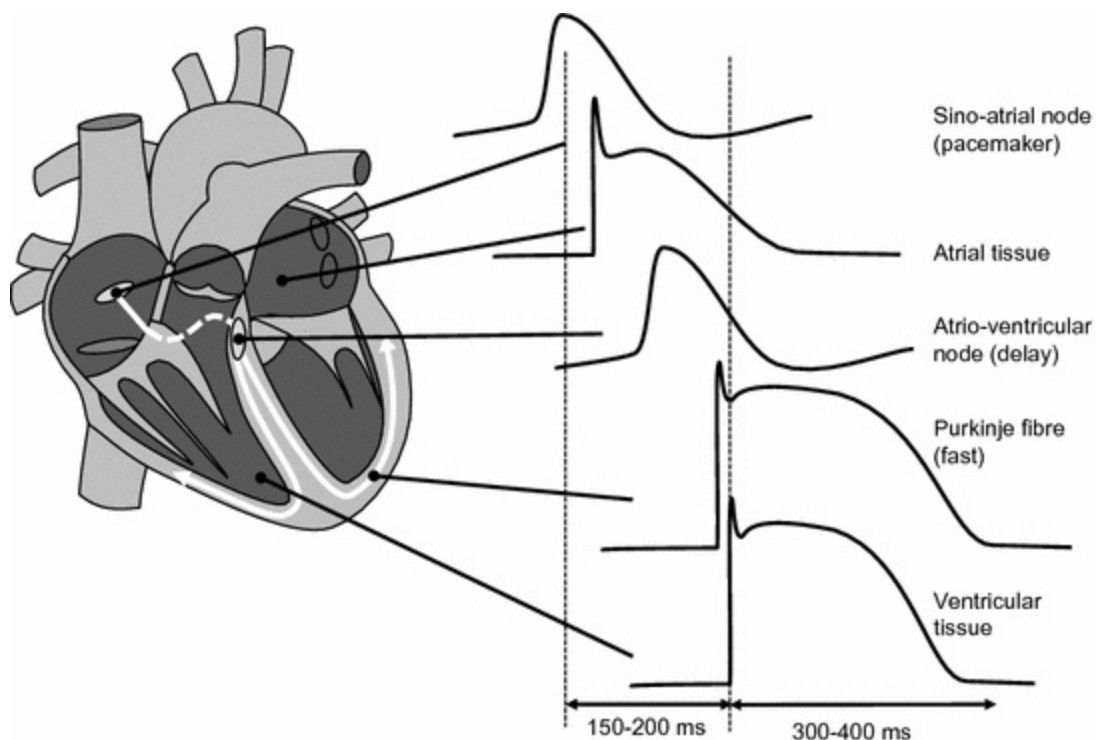


Fig. 6.6 Cardiac action potentials in different regions of the heart

6.2.3 Origin of the Electrocardiogram

The sequence of electrical activation and recovery that acts to initiate and synchronises the mechanical activity of the heart can be observed on the torso surface as the electrocardiogram (ECG). The local electrical potential produced by action potentials in the tissue act to generate current flow within the torso, which behaves as a volume conductor. In turn, this current flow produces a potential on the body surface, and the time course of the potential reflects the sequence of activation and recovery in different parts of the heart.

Since it provides a non-invasive way to assess the function of the heart, the ECG is a powerful and widely used diagnostic tool. The ECG is recorded from electrodes placed on the torso, and the ECG arising from each complete cardiac cycle is composed of three types of deflection, as shown in Fig. 6.7. The size and shape of these deflections depends on the electrode placement.

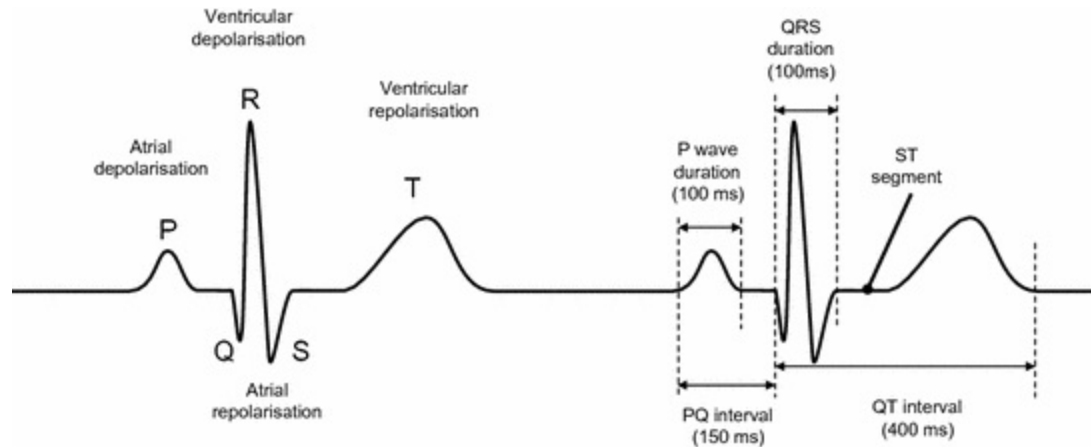


Fig. 6.7 The normal electrocardiogram

Electrical activation of the sinus node and atria is inscribed on the ECG as the P wave. The electrical activation the ventricles is then inscribed as the QRS complex. The Q wave is the first downward deflection, the R wave the upward deflection, and the S wave the second downward deflection. The configuration of the QRS complex is strongly influenced by the location of recording electrodes, and one or more of the Q, R and S waves may be very small. The QRS complex typically obscures any deflection arising from repolarisation of the atria, but repolarisation of the ventricles is inscribed as the T wave. The duration of each deflection, as well as intervals between the deflections, can convey important diagnostic information.

The P wave duration reflects conduction of the action potential through the atria, and the PQ interval (usually referred to, incorrectly, as the PR interval) indicates atrial activation time plus slow conduction through the atrioventricular node. A short PQ interval can indicate an additional and abnormal activation pathway from atria to ventricles, which results in early activation of the ventricles and can provide a substrate for re-entrant arrhythmia (see below). A prolonged PR interval can indicate delays in conduction through the atrioventricular node.

The QRS duration reflects electrical activation of the specialised Purkinje

fibres and both left and right ventricles. A prolonged QRS duration indicates slower than normal conduction in the Purkinje system.

The portion of the ECG between the end of the QRS complex and the start of the T wave is the ST segment, and reflects the state of the ventricles between the end of the activation sequence and the start of recovery. When this segment is displaced above or below the ECG baseline, it is indicative of myocardial ischaemia.

The QT interval reflects the time between the start of ventricular activation, and then end of ventricular recovery. The QT interval duration shortens at elevated heart rates, and may be expressed as a corrected value (denoted QT_C) calculated using Bazett's formula, which gives QT_C as the measured QT divided by the square root of the RR interval. The QT interval is prolonged by any change that acts to increase the action potential duration, or the range of action potential durations, in ventricular myocytes.

6.2.4 Arrhythmias and Conduction Defects

Cardiac arrhythmias disturb the normal activation of the heart, and so influence the ability of the heart to propel blood around the circulation. An arrhythmia can arise from spontaneous action potential formation outside of the sino-atrial node, from abnormal conduction of the action potential, or from a combination of the two. Spontaneous depolarisation can arise in the atria, the atrioventricular node, or the ventricles, and produces an ectopic beat that usually precedes the next natural beat. These extra beats are seen on the ECG, and usually have a different morphology to normal beats because they arise in a different location and produce a different activation sequence. Ectopic beats are often felt as a 'missed beat', and are a common finding in otherwise normal individuals.

Abnormal propagation of the action potential can be more serious. During a normal beat, the cardiac tissue does not begin to recover until all of the tissue has been activated. However, if the duration of electrical activation is short, or the activation wave propagates slowly, then it is possible for the activation to propagate into regions of tissue that have recovered. This leads to circulating waves of electrical activation that are termed re-entry, and are similar to a 'Mexican wave' in a sports stadium. The period of re-entry is usually faster than the normal heart rate, and so an arrhythmia sustained by re-entry will suppress beats arising naturally in the sinus node. The increase

in activation rate is referred to as tachycardia.

Three types of arrhythmia are shown in Fig. 6.8. In atrioventricular node re-entrant tachycardia, activation propagates from the atria to the ventricles through the atrioventricular node. Re-entry occurs because the activation is then able to propagate back into the atria, before re-entering the ventricles. In some individuals, an abnormal region of excitable tissue between atria and ventricles exists, and provides an alternative pathway alongside the atrioventricular node. This condition is called Wolff—Parkinson--White syndrome, and activation of the atrioventricular node and then alternative pathway (or vice versa) provides the substrate for re-entry. Each activation produces a series of deflections on the ECG.

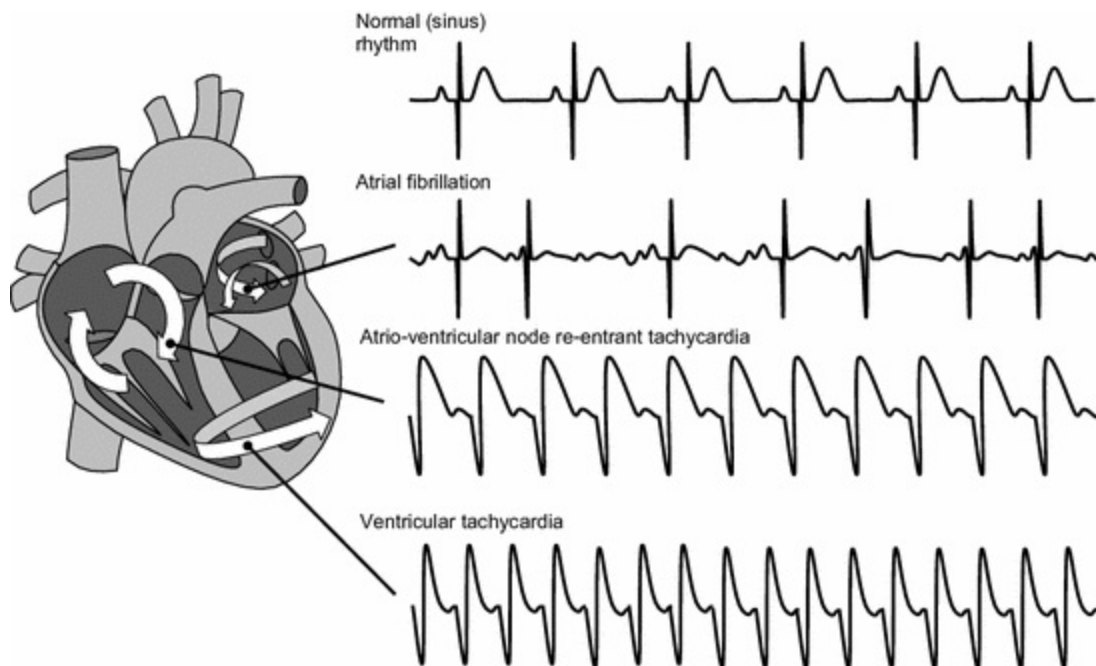


Fig. 6.8 Electrocardiogram of normal beat, atrial fibrillation, atrioventricular node re-entrant tachycardia, and ventricular tachycardia

In the ventricles, damaged tissue following a myocardial infarction can provide a region of slow conduction, which acts as a substrate to set up a re-entrant circuit for ventricular tachycardia. Each activation produces a deflection on the ECG. If the single activation wave breaks up into several re-entrant waves, then ventricular tachycardia can degenerate to ventricular fibrillation.

Multiple re-entrant waves in the atria the mechanism that underlies atrial

fibrillation. The turbulent activity in the atria produces an undulating baseline on the ECG, with no regular and discernible P waves. Activation of the atrioventricular node is irregular, and so ventricular beats occur at irregular intervals.

6.3 Excitation-Contraction Coupling

Contraction of the heart is initiated by electrical activation. It involves the interaction of active tension generation at the cell level with the passive elastic properties of the tissue.

6.3.1 Molecular and Cell Scale Mechanisms

Within each myocyte, the sarcoplasmic reticulum acts as a Ca^{2+} store. During the action potential, Ca^{2+} enters the cell through ion channels (see Fig. 6.5), and this leads to an increase in intracellular $[\text{Ca}^{2+}]$ concentration. The increase in $[\text{Ca}^{2+}]$ concentration is detected by ryanodine receptors on the surface of the sarcoplasmic reticulum, and leads to the release of stored Ca^{2+} . The amount of Ca^{2+} stored in the sarcoplasmic reticulum is much higher than the amount that enters through ion channels, and $[\text{Ca}^{2+}]$ concentration rises around ten times, from a resting value of around 0.0001 to 0.001 mM.

The increase in intracellular $[\text{Ca}^{2+}]$ concentration provides a catalyst for a series of reactions involving the contractile proteins. These reactions result in tension. Pumps in the sarcoplasmic reticulum membrane return the released Ca^{2+} to the store and $[\text{Ca}^{2+}]$ concentration returns to a resting level shortly after repolarisation of the action potential. Figure 6.9 shows a schematic of Ca^{2+} induced Ca^{2+} release, and the contractile proteins that are involved in tension generation.

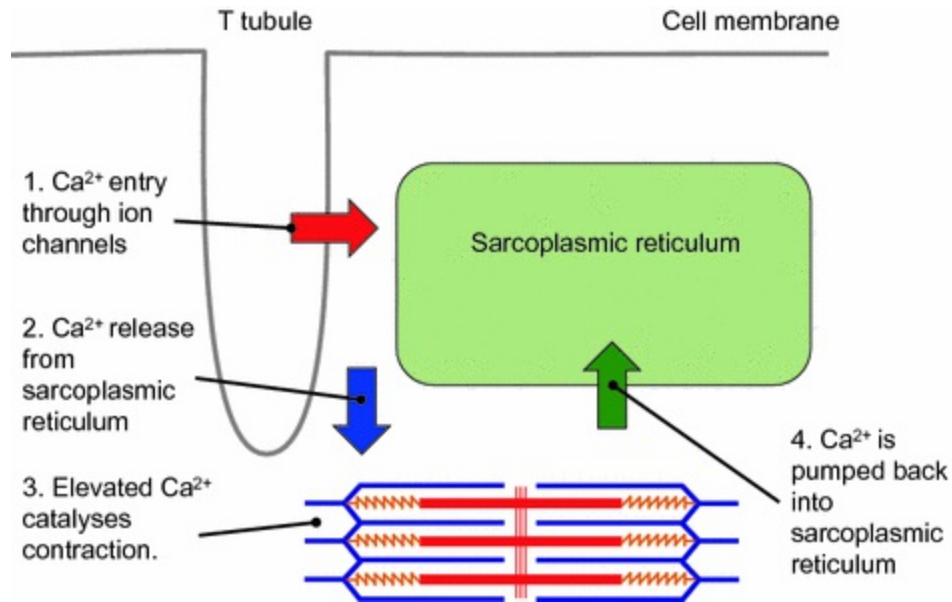


Fig. 6.9 Molecular components of excitation-contraction coupling, showing a numbered sequence of events that occur during a single cardiac cycle

Active tension is produced by extensions that protrude from the myosin (thick) filaments in the sarcomere (Fig. 6.10). Myosin heads can bind to specific locations that are evenly spaced along the actin (thin) filaments. These binding sites are exposed when Ca^{2+} binds to troponin, causing a conformational change. Once the myosin head is bound to the thin filament, it forms a crossbridge, which changes shape in an energy-consuming process. Movement of the cross-bridge advances each myosin head to the next binding site. Repeated cross-bridge cycles produce movement of the thick filaments relative to the thin filaments, and hence generate tension in the sarcomere. As Ca^{2+} concentration falls, Ca^{2+} unbinds from troponin, concealing the myosin binding sites once more, and the sarcomere relaxes.

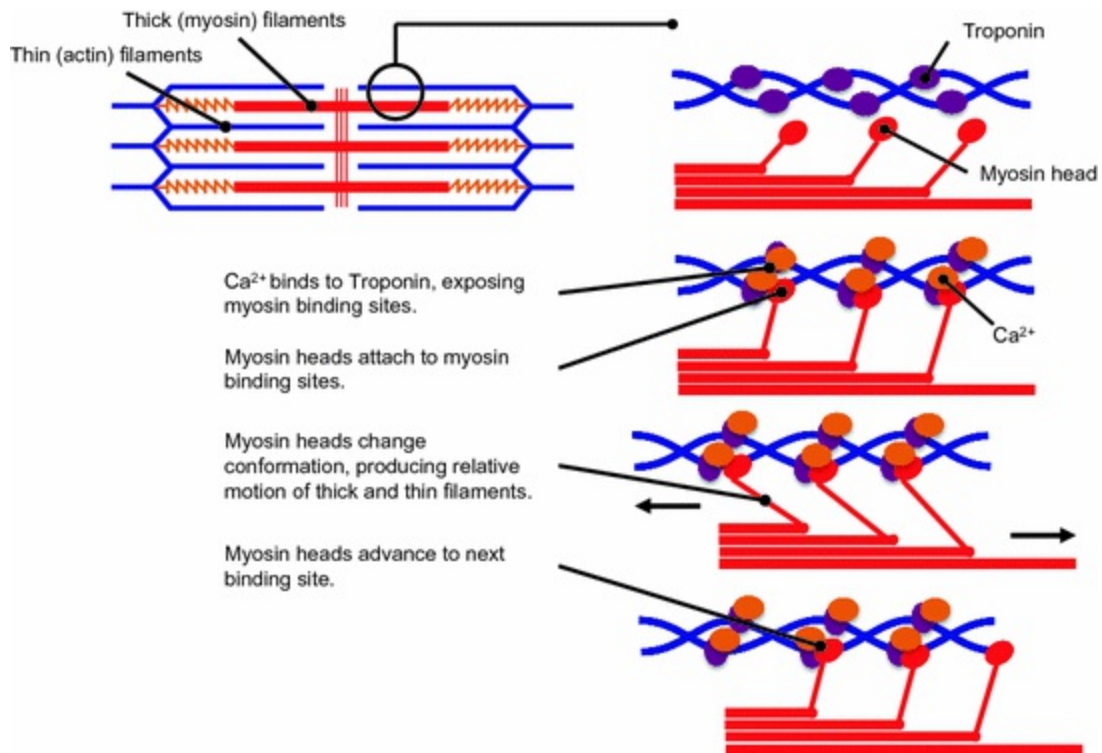


Fig. 6.10 Molecular mechanisms involved in tension generation, showing a single stroke of the actin-myosin complex, catalysed by Ca^{2+}

6.3.2 Biomechanics of Cardiac Cells and Tissue

The configuration of actin and myosin filaments in a sarcomere is important because it provides a mechanistic explanation for observations in both isolated tissue preparations and the intact heart.

If a tissue preparation is held at a fixed length, then the tension developed when it is electrically activated depends on the length of the preparation. Typical behaviour is shown schematically in Fig. 6.11. If the sarcomeres are unstretched, then the passive tension is small, and the active tension is also small because the actin and myosin filaments completely overlap. With modest stretch (corresponding to a sarcomere length of around $1.6 \mu\text{m}$), the thick and thin filaments overlap, more crossbridges can form, and active isometric tension increases with length. As the sarcomere is stretched further, the overlap of thick and thin filaments decreases, and so the number of available cross-bridges decreases. The active isometric tension therefore decreases, but at the same time the passive tension increases.

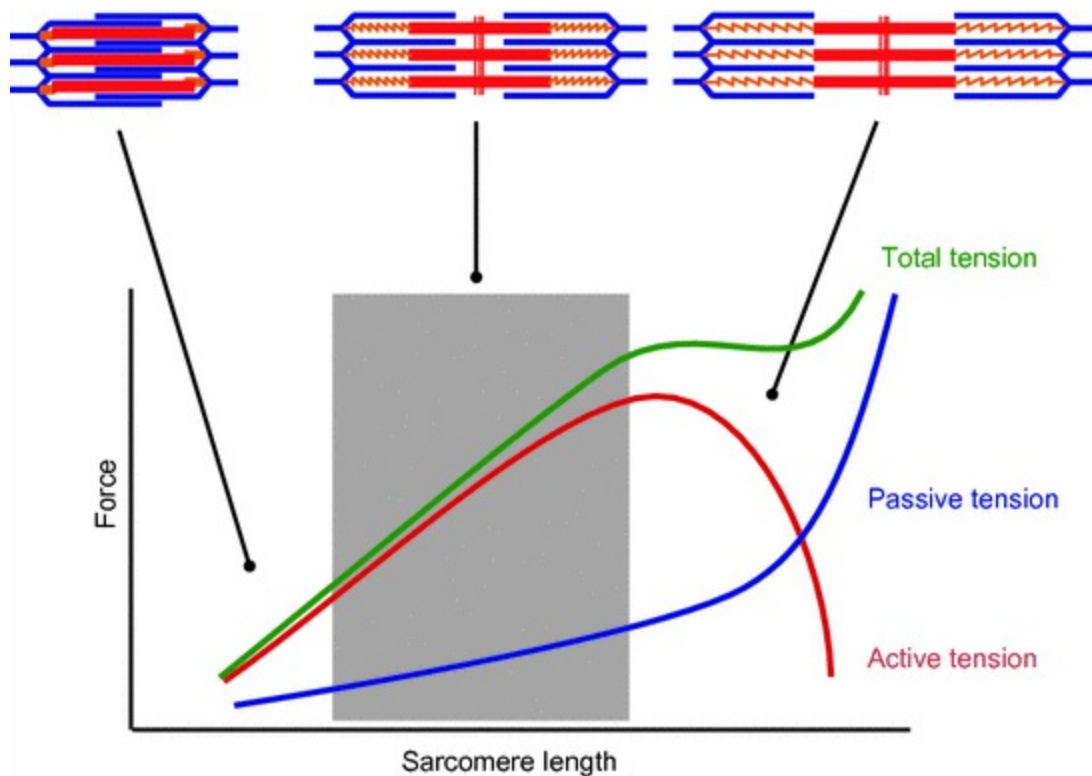


Fig. 6.11 Tension generation in a cardiac myocyte, showing passive and active tension generated at different sarcomere lengths (see text for details)

The grey box in Fig. 6.11 indicates the normal operating range for a cardiac sarcomere. Within this region, the active isometric tension is roughly proportional to sarcomere length. In the whole heart, isometric contraction corresponds to the isovolumetric phase of the cardiac cycle, before the valves open. Once the valves open, the tissue is able to change its length and the contraction becomes isotonic. The mechanical behaviour now depends on the initial stretch (the preload) and the tension under which it contracts (the afterload). In the ventricles, the preload arises from stretch associated with the chamber filling pressure and afterload arises from the hydraulic resistance of the circulation.

In order for the ventricles to contract, contraction of individual myocytes on their long axis should act to produce a reduction in the ventricular volume. This is achieved by myocyte orientations that produce both circumferential (hoop) stress and longitudinal stress. In the middle of the ventricular wall, the myocytes are oriented with their long axis aligned to the circumferential direction and producing a circumferential component to the wall stress. The orientation of myocytes on the inner and outer walls differ by $\pm 60^\circ$ from the

circumferential direction, producing a longitudinal component to the wall stress that results in twisting of the ventricle as it contracts.

6.4 Control of Cardiac Output

6.4.1 Frank--Starling Mechanism

In an experimental system for examining isotonic contraction, a muscle preparation can be stretched by a weight, which provides a preload. When the active tension exceeds the preload the preparation is able to shorten. As the preparation shortens, it suspends an additional weight, which provides the afterload. An increased afterload decreases both the amount of shortening and the velocity of shortening. The effect of increasing the preload is to increase the isometric tension, which for a given afterload results in an increased shortening and velocity of shortening. These relationships are shown schematically in Fig. 6.12.

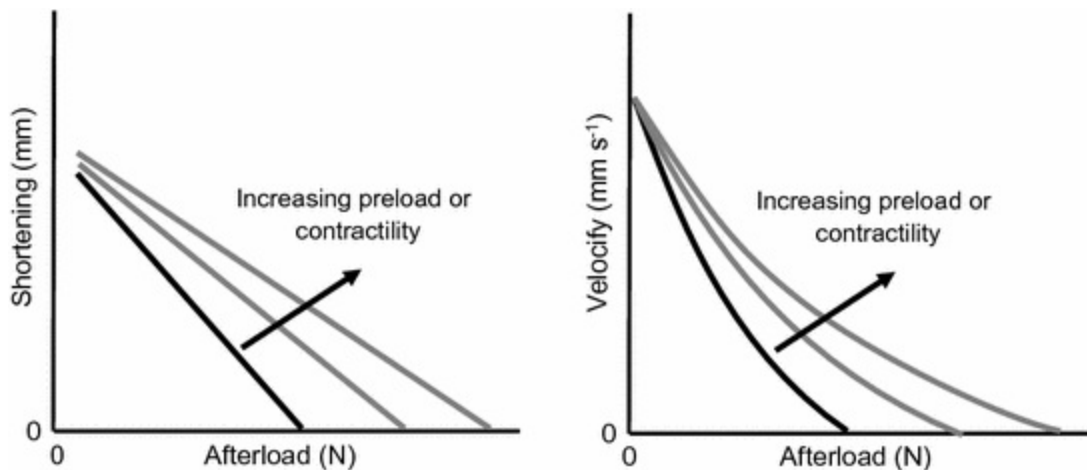


Fig. 6.12 Cartoon showing how both shortening and velocity of shortening of a cardiac muscle preparation depends on both preload and afterload (see text for details)

The impact of these properties of cardiac muscle on the behaviour of the whole heart was investigated in a series of experiments conducted in frog and dog hearts by Otto Frank and Ernest Starling in the late eighteenth and early twentieth century and described in detail by Katz (2002). Frank investigated isovolumetric contraction in a frog heart where the aorta was sewn shut. Increasing ventricular volume produced stronger contractions, and a larger systolic pressure. Starling extended these experiments to an isolated dog heart

with variable filling pressure and output resistance. The findings of these experiments are shown schematically in Fig. 6.13. They are the basis of the Frank--Starling law of the heart, which states that greater stretch of the ventricle in diastole produces greater stroke work in systole, providing all other factors remain constant.

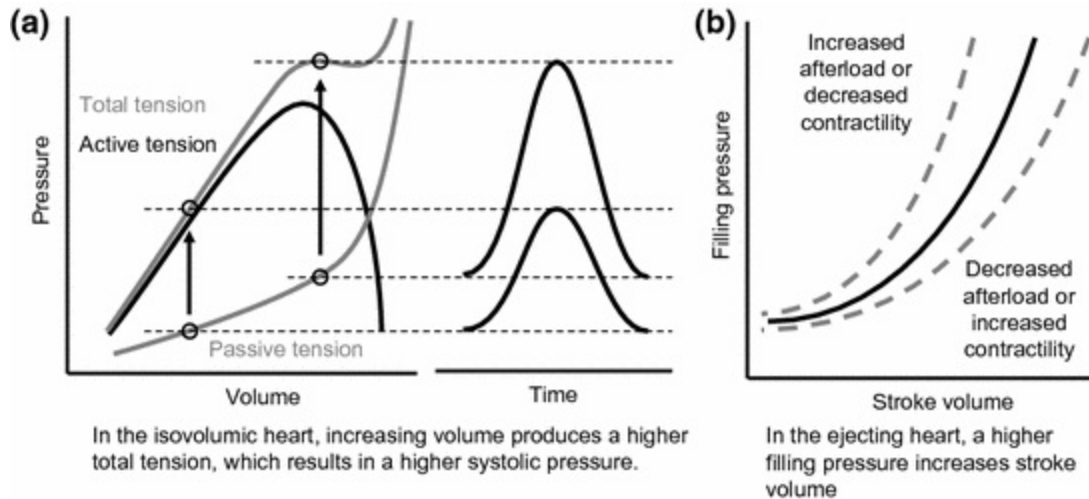


Fig. 6.13 Illustration of the Frank--Starling law, showing the relationship between pressure and volume under isovolumic conditions (a) and during ejection (b)

In Fig. 6.13a, the left-hand graph shows the relationship between pressure and volume, in which the total pressure (green line) arises from passive tension (blue line) and active tension (red line). If the volume of the left ventricle is held constant, as in the experiments of Otto Frank, then at rest the left ventricular pressure will be produced by the passive tension. When stimulated, the left ventricular pressure will increase up to a value given by the sum of pressure due to active and passive tension. This increase is shown for two volumes in the figure. A higher volume results in a higher tension, and hence, a higher pressure is generated. The right-hand graph shows pressure plotted against time for small and large volumes.

In Fig. 6.13b, the idea is extended to the ejecting heart, as investigated by Ernest Starling and colleagues. Note that the volume axis in Fig. 6.13b is stroke volume, which is the volume ejected during each beat. The effect of increased filling pressure is to increase preload, and this results in an increased stroke volume. The curve is shifted upwards and downwards by decreased and increased afterload, respectively.

6.4.2 Work in the Heart

During the cardiac cycle, energy is expended to generate tension. Some of this energy is expended as heat, and some of this energy performs work to eject blood from the chambers.

The change in pressure and volume in the heart during the cardiac cycle has already been illustrated in Fig. 6.2. An alternative way to depict these changes is to plot pressure against volume for the left and right ventricles. In this type of plot, the pressure and volume follows an anticlockwise loop trajectory, once for each cycle. Figure 6.14 illustrates a typical pressure-volume loop for the left ventricle. The initial (isovolumetric) contraction starts on the lower bound (A), which is determined by the end diastolic (passive) pressure-volume relationship in the left ventricle (blue line). Pressure increases until the aortic valve opens (B). The volume then decreases until the loop reaches the upper bound, set by the end systolic (both active and passive) pressure-volume relationship (green line). At this point the aortic valve closes, and the left ventricle relaxes while maintaining a constant volume (C). On opening of the mitral valve, the ventricle fills along the passive pressure-volume curve (D), and then the cycle repeats.

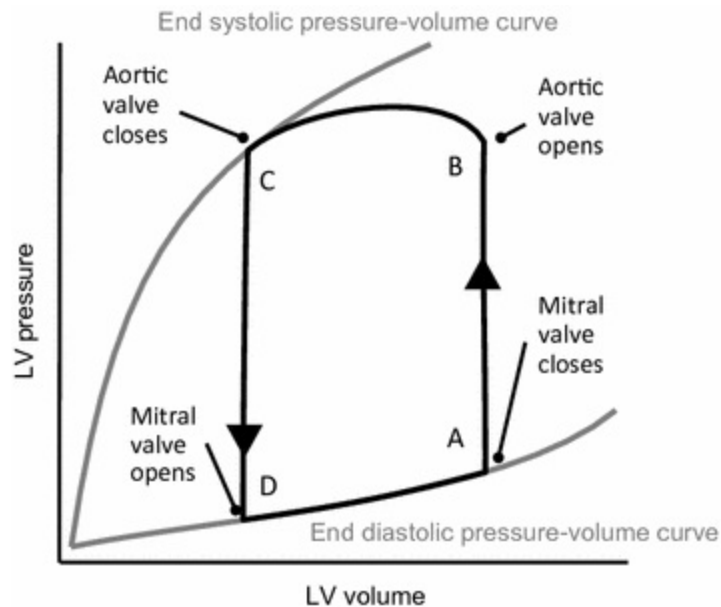


Fig. 6.14 Relationship between LV pressure and LV volume during a single cardiac cycle

As the pressure-volume loop is traversed, the myocardium converts metabolic energy into mechanical work. During each cardiac cycle, the

mechanical work performed, or stroke work, is given by the change in pressure multiplied by the change in volume. Stroke work is often approximated as mean arterial pressure during ejection multiplied by the stroke volume. A more accurate approach is to integrate the change in pressure over the change in volume throughout the cycle, and so stroke work can also be calculated as the area of the pressure-volume loop.

The pressure-volume loop is influenced by changes in preload, afterload and contractility. These changes are illustrated in Fig. 6.15. An increase in preload increases end diastolic volume, and so this is reflected as a rightward shift of the isovolumic contraction phase of the pressure volume loop. An increased afterload (higher systolic arterial pressure) results in earlier closure of the aortic valve, and so the isovolumic relaxation phase of the pressure volume loop is shifted rightwards. Increased contractility shifts the end systolic pressure-volume curve upwards, and so the isovolumic relaxation phase of the pressure-volume loop is shifted leftwards.

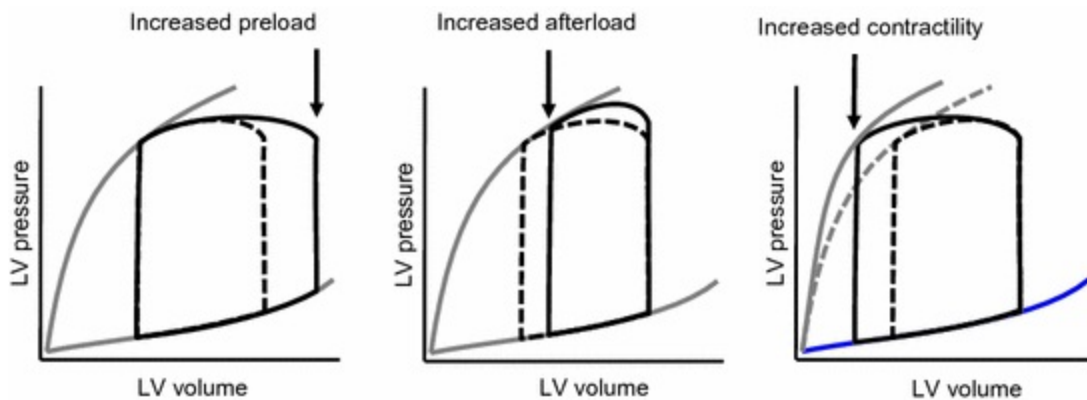


Fig. 6.15 Relationship between LV pressure and LV volume under conditions of increased preload, increased afterload, and increased contractility

6.4.3 Regulation of the Heart

The Frank--Starling mechanism is an important component of the control of the heart, because any change in end diastolic volume (point A on Fig. 6.14) results in a change in cardiac output. This effect is seen very clearly in the way that left ventricular output is balance with right ventricular output. It is crucial that the output from each ventricle is balanced. If there is any sustained difference, then congestion of either pulmonary or systemic circulation follows very quickly.

If there is a transient increase in the output of the right ventricle so that it exceeds the output of the left ventricle, then the volume of blood in the pulmonary circulation increases. This increase results in a rise in pulmonary venous pressure, which in turn acts to increase the preload of the left ventricle. The increase in left ventricular preload then results, through the Frank--Starling mechanism, in a stronger contraction of the left ventricle, and hence an increase in the left ventricular output.

6.5 Cardiac Remodelling

6.5.1 The Remodelling Process

This chapter has described the fundamental mechanics of the electrical activation and conduction in the heart, with the structural sequela associated with the resulting contraction of the fibres of myocardium and ultimately the ejection of blood from the ventricles. The pressure-volume curves, or loops, provide a simple and intuitive representation of ventricular performance. The heart is designed to work most effectively in a particular range, with typical values of characteristic measures indicated in Table 6.2. When the parameters are moved outside this range, for any one of many reasons including long-term hypertension associated with increased afterload or acute events such as myocardial infarction, the wall of the ventricle remodels to try to maintain or restore physiological function. This remodelling might include morphological changes, including size of the ventricle and thickness of the wall, and structural changes including re-orientation of the fibres. Increase in the size of the ventricles associated with the pathological response to changed physiological conditions is commonly referred to as ventricular hypertrophy.

Table 6.2 Typical haemodynamic parameters for a resting 70 kg adult (Levick 2009)

Parameter	Value at rest
Heart rate	65–75 beats min ⁻¹
Stroke volume	70–80 ml
Cardiac output	4.5–6.0 L min ⁻¹
Ejection fraction	0.67
Systemic venous pressure	12–15 mmHg
Pulmonary arterial pressure	20–25 mmHg (systole) 8–12 mmHg (diastole)

Pulmonary venous pressure	5–8 mmHg
Systemic aortic pressure	120 mmHg (systole) 80 mHg (diastole)

There is a large body of clinical literature on ventricular remodelling. A comprehensive introduction by Cohn et al. (2000) includes five key consensus statements on concepts of remodelling, remodelling and heart failure progression, diagnostic tools and their clinical value, the effect of therapeutic intervention and educational implications. The focus is on heart failure, and the appreciation of the potential benefits of candidate therapies, particularly pharmacological intervention, based on physiological diagnostic factors including ventricular volume and ejection fraction data. Although the emphasis is on the pathological remodelling associated with disease progression, already in 2000 there is discussion of reverse remodelling as a target for heart failure therapies. A recent state-of-the-art review by Konstam et al. (2011) focuses on measures of remodelling. Several clinical papers discuss the effect on remodelling of candidate surgical interventions to reduce haemodynamic load, e.g. the review by Villa et al. (2006).

6.5.2 Engineering Mechanics of Ventricular Remodelling

The engineering representation of ventricular remodelling is complex because the process is multifactorial. Although the response is essentially an attempt by the heart to maintain performance in terms of cardiac output, and intimately associated with the maintenance of stresses and strain levels in the ventricular wall, there are many genetic factors and biological responses that are outside the normal scope of engineering mechanics. Generally, we recognise the conditions of pressure overload and volume overload as causative factors in the remodelling of the ventricles. Pressure overload is associated with an excessive afterload on the heart, which means that it has to generate a higher pressure per unit flow. Volume overload is associated with the size of the heart chamber, referring to the fact that there is an excessive volume of blood at the start of contraction. Of course the two are related, and volume overload might result from long-term pressure overload. The Frank-Starling mechanism, which describes a normal physiological process, has already been discussed earlier in this chapter.

An important review of engineering models of cardiac growth and remodelling (G&R), with emphasis on the remodelling of fibre orientation but including an excellent introduction to the overall concepts, is presented by Bovendeerd (Bovendeerd 2012). Bovendeerd's abstract sums up the challenges: 'A continued effort combining information on mechanotransduction at the cellular level, experimental observations on G&R at organ level, and testing of hypotheses on stimulus-effect relations in mathematical models is needed.... Ultimately, models of cardiac G&R seem indispensable for patient-specific modeling, both to reconstruct the actual state of the heart and to assess the long-term effect of potential interventions'. He reviews optimisation models, which compute the cardiac parameters associated with an evolved state of stress and/or strain in end-stage heart failure to characterise the physiological state, and adaptation models which seek to describe the mechanistic relationship between stimulus and effect, describing the evolution in time of tissue and volume properties. Arts et al. (2010) have made major contributions to the development of models of G&R, from the development four decades ago of single fibre models of the ventricle, assuming a homogeneous distribution of stress and strain, through to sophisticated patient-specific models including adaptation mechanisms.

References

Arts T, Lumens J, Kroon W, Donker D, Prinzen F, Delhaas T. Patient-specific models of cardiovascular mechanics with a major role for adaptation. In: Kerckhoffs RCP, editor. Patient specific modeling of the cardiovascular system. New York: Springer; 2010. p. 21–41.

[CrossRef]

Bovendeerd PHM. Modeling of cardiac growth and remodelling of myofiber orientation. *J Biomech.* 2012;45:872–81.

[CrossRef][PubMed]

Cohn JN, Ferrari R, Sharpe N. Cardiac remodeling—concepts and clinical implications: a consensus paper from an international forum on cardiac remodeling. Behalf of an international forum on cardiac remodeling. *J Am Coll Cardiol.* 2000;35:569–82.

[CrossRef][PubMed]

Katz AM. Ernest Henry Starling, his predecessors, and the “Law of the Heart”. *Circulation.* 2002;106:2986–92.

[CrossRef][PubMed]

Konstam MA, Kramer DG, Patel AR, Maron MS, Udelson JE. Left ventricular remodeling in heart failure. *JACC Cardiovasc Imag.* 2011;4:98–108.

[CrossRef]

Levick RJ. An introduction to cardiovascular physiology. 5th ed. Boca Raton: CRC Press; 2009.

Nielsen P, Le Grice I, Smaill B, Hunter P. Mathematical model of geometry and fibrous structure of the heart. *Am J Physiol; Heart Circ Physiol.* 1991;260:H1365–78.

Noble D, Rudy Y. Models of cardiac ventricular action potentials: iterative interaction between experiment and simulation. *Philos Trans R Soc London; Ser A Math Phys Eng Sci.* 2001;359:1127.

[CrossRef]

Villa E, Troise G, Cirillo M, Brunelli F, Dall Tomba M, Mhagna Z, Tasca G, Quaini E, Cohn JN, Ferrari R, Sharpe N. Factors affecting left ventricular remodelling after valve replacement for aortic stenosis. An overview. *Cardiovasc Ultrasound.* 2006;4(25). doi:[10.1186/1476-7120-4-25](https://doi.org/10.1186/1476-7120-4-25).

7. The Venous System

Andrew J. Narracott¹ 

(1) Sheffield University, Sheffield, UK

 **Andrew J. Narracott**
Email: a.j.narracott@sheffield.ac.uk

Learning outcomes

1. Describe the role of the venous circulation in providing storage capacity within the circulation.
2. Describe the variation in compliance of the veins with transmural pressure and the implications of this on the resistance to flow as the veins collapse.
3. Describe the features of venous compliance which allow the veins to act as a blood reservoir.
4. Describe the role of the muscle pumps of the lower limb and the respiratory pump in returning blood from the legs to the heart and the importance of venous valves in this process.
5. Describe how the distribution of venous valves varies throughout the circulation.

6. Describe how changes in posture lead to changes in venous volume with attention to the associated timescales.
7. Define what is meant by venous insufficiency and state complications associated with the condition.
8. Describe the applications of B-mode and Doppler ultrasound in diagnosis of venous disease.
9. Describe the features that characterise varicose veins.
10. Describe the nature of deep vein thrombosis (DVT) and the factors associated with increased risk of DVT.

The role of the venous system is to return blood to the heart under low pressure conditions, compared with the arterial system. In humans the haemodynamics of venous flow is significantly influenced by postural changes, due to venous compliance, and an understanding of the physics associated with changes in hydrostatic pressure in the veins informs discussion of the biomechanics of the venous system. This chapter presents key concepts associated with the role of the venous system in the circulation, how these relate to normal physiological conditions and how these processes may be altered under abnormal conditions.

7.1 Properties and Function of the Venous System

A schematic representation of the venous circulation, focusing on the larger vessels, is provided in Fig. 7.1. In all regions of the body the anatomy of the venous system becomes more complex as the vessel caliber becomes smaller, terminating in branching networks, often mirroring the anatomy of the arterial circulation.

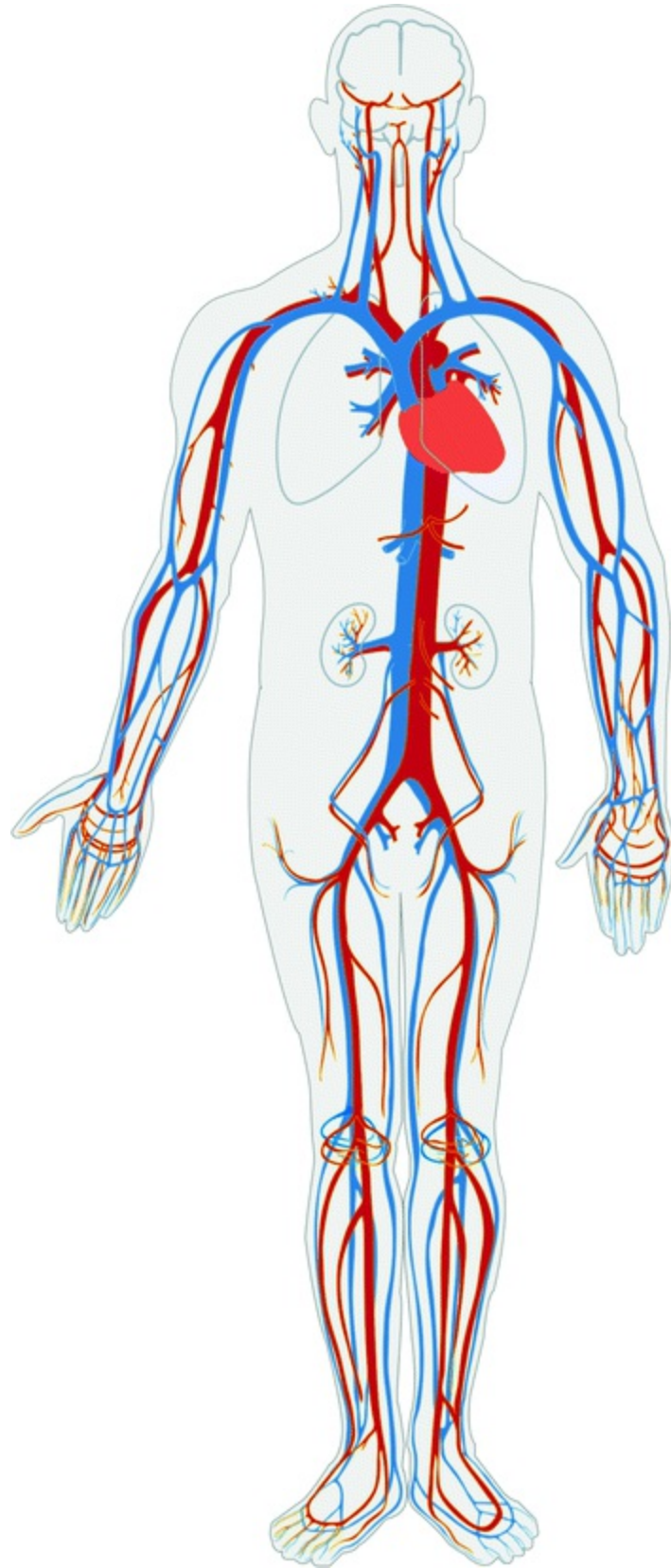


Fig. 7.1 Schematic representation of the circulation, arteries are shown in *red*, veins in *blue*. Reproduced from Wikipedia; https://commons.wikimedia.org/wiki/File:Circulatory_System_en.svg. This image is in the public domain and was authored by Mariana Ruiz Villarreal

These networks are designed to return blood from organ systems and musculature and the complexity of the venous network is particularly pronounced in the peripheral circulation (i.e. hands, feet and cerebral circulation). In general the anatomy of the venous circulation is more variable than the arterial circulation between individuals, particularly in the extremities. This variability may arise from the inherent redundancy associated in the mechanisms for venous return, which are discussed in more detail in the following sections. This aspect of venous anatomy poses particular challenges when considering the biomechanics of the venous circulation in detail for individual subjects, rather than typical behaviour of the overall system.

7.1.1 Venous Composition and Compliance

An important function of the venous circulation is to provide storage capacity within the circulatory loop, typically 60–80 % of the total blood volume is stored within the venous system depending on both posture and activity (Meissner et al. 2007). The storage capacity of the veins arises from the compliance of the vessels, which is related to their geometry, material properties, influence of the surrounding tissue and variation in transmural pressure, defined as the difference between the internal and external pressures acting on the vein.

$$P_{\text{transmural}} = P_{\text{internal}} - P_{\text{external}} \quad (7.1)$$

The vein wall is thinner than that of its companion artery and contains less smooth muscle. Under physiological pressure loading the diameter of the venous lumen is larger than that of neighbouring arteries, particularly in peripheral vessels. The elastic modulus of veins has been shown to vary considerably with vessel location, exhibiting a similar stiffening response to arteries with increase in pressure loading (Wesley et al. 1975). For a particular value of elastic modulus simple linear measures of vessel compliance (Eq. 7.2) predict higher compliance in the venous circulation due to the larger diameter and thinner wall of the veins.

$$C = \frac{dA}{dP} = \frac{2\pi R dr}{Eh dr/R^2} = \frac{2\pi R^3}{Eh} \quad (7.2)$$

where R is the vessel radius, h the wall thickness and E the Young's modulus of the vessel wall. The increase in compliance arises from the higher circumferential stress in a larger, thinner vessel at a given pressure.

In addition to the contribution from passive mechanical properties the pressure–area response of the veins is determined by active processes including metabolic control and pressure and flow-mediated changes in venous tone (Monos et al. 1995).

7.1.2 Vessel Collapse and Nonlinear Pressure–Area Relationship

The linear approximation of Eq. 7.2 neglects the large changes in compliance of the veins which arise over the range of transmural pressures experienced by these vessels. When transmural pressure becomes negative, the compliance of the veins is nonlinear as a result of changes in geometry of the vessel cross-section. Under negative transmural pressure the vein does not remain circular in cross-section, becoming elliptical or adopting a dumbbell shape. The form of the vessel cross section is determined by the support conditions with different forms of response observed in vessels surrounded by muscular tissue (e.g. deep calf veins) than in those with less supporting tissue (e.g. vena cava).

To examine the mechanics of venous collapse the vein can be considered a thin-walled elastic cylinder. The initial circular cross-section of the vein will deform to adopt a non-circular cross section under a uniform pressure load, as illustrated in Fig. 7.2. This arises from the elastic instability of the system and the pressure at which this occurs can be obtained through consideration of small deformations of the tube and a linear analytical approach (Fung 1997), which predicts that the vein will adopt a non-circular form at the transmural pressure given by Eq. 7.3.

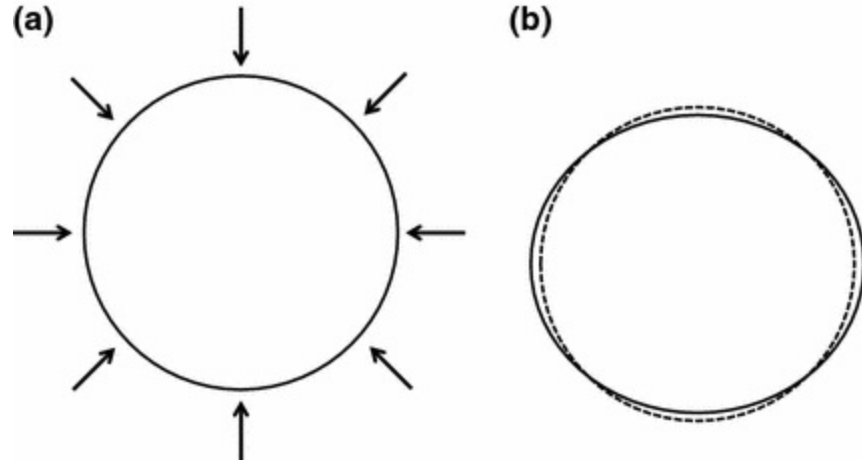


Fig. 7.2 **a** Initial geometry of thin-walled elastic cylinder subject to uniform pressure loading (arrows). **b** Post-buckling geometry of the cylinder (solid line) compared to initial geometry (dashed line)

$$p_e - p = \frac{Eh^3}{4R^3(1 - \nu^2)} \quad (7.3)$$

where p_e is the external pressure, p the internal pressure and ν is the Poisson's ratio of the vessel wall. Extension of the analysis of this deformation into the post-buckling regime was undertaken by Flaherty et al. (1972) using numerical integration. This analysis captures the self-contact of the cylinder and the rapid changes in cross-sectional area that occur with increase in pressure following the initial buckling response. Figure 7.3 illustrates these effects through the solution of a finite element model of a thin cylinder under uniform pressure load. This analysis recognizes the finite thickness of the cylinder and captures the variation of the stress across the wall.

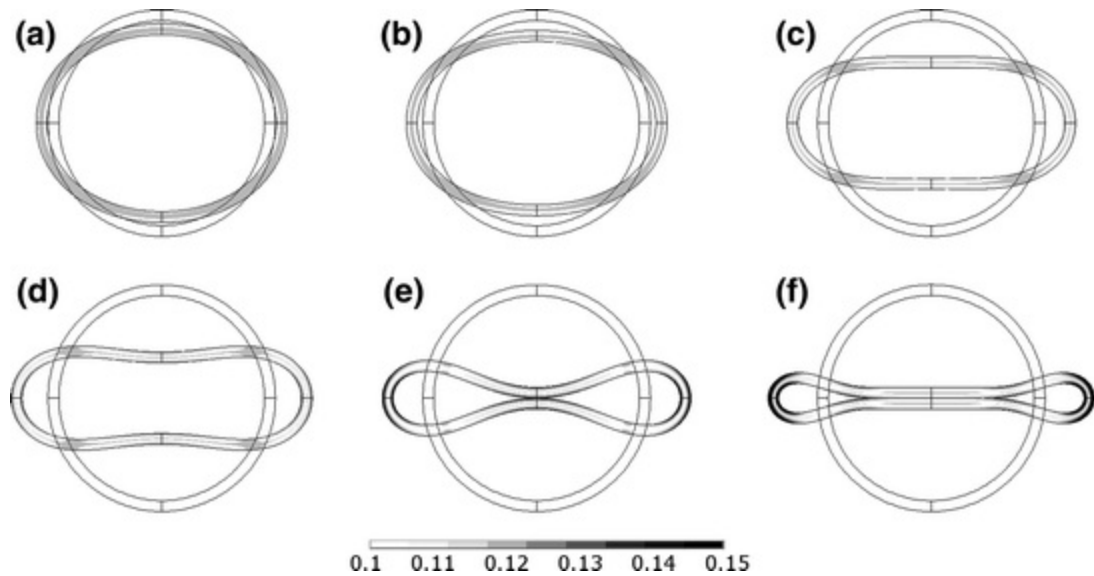


Fig. 7.3 Finite element model of a thin-walled cylinder under uniform pressure loading. The deformation demonstrates the initial buckling of the cylinder (a) and subsequent collapse leading to self-contact (e) and further contact with increasing pressure along the plane of symmetry. The contours in these plots show the equivalent strain values

The response of the finite element model demonstrates significant changes in the geometry of the cross-section as the transmural pressure becomes negative. It should be noted that these deformations arise from nonlinear geometric effects in this analysis and that the strain within the cylinder is relatively low throughout the deformation. These effects are distinct from the nonlinearities observed in both the arterial and venous pressure/area relationship under positive transmural pressure resulting from the nonlinear mechanical response of the vessel to loading due to the vessel wall constituents. For more complex analysis of the deformation of thin-walled elastic tubes, including 3D deformation effects and fluid-structure interaction, the reader is referred to more detailed reports (Grotberg and Jensen 2004).

The results of such analyses provide a description of the nonlinear pressure–area response (compliance) of the venous system, which is generally handled through the definition of a “tube-law” to describe this behaviour. The typical form of an analytical tube-law is shown in Fig. 7.4 along with the response of the vessel computed using the finite element approach for two vessel thicknesses ($h/R = 0.1$ and 0.05). The equation for the tube-law is given below, with K_p the bending stiffness of the vessel, A the cross-sectional area and A_0 the area at zero pressure:

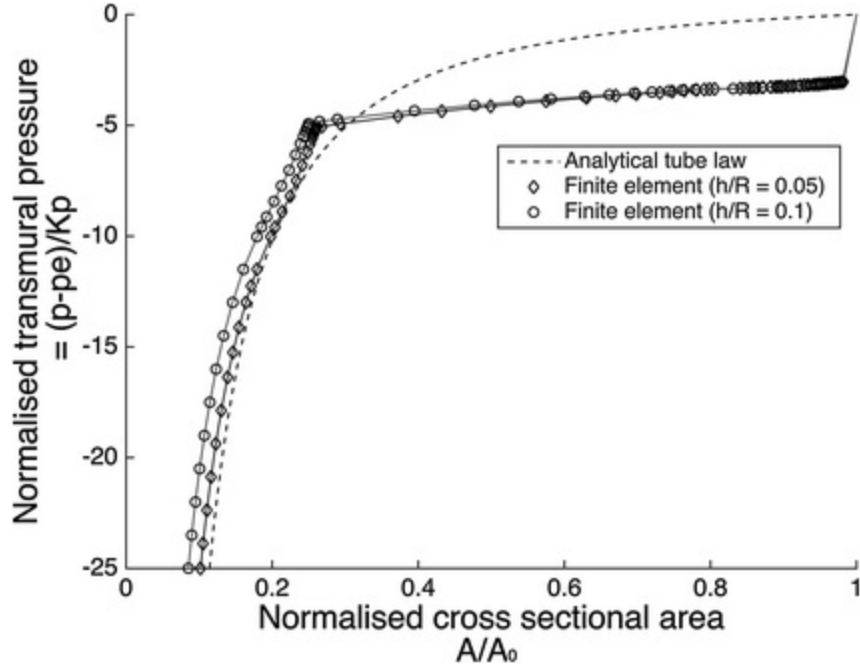


Fig. 7.4 Relationship between the normalized pressure and area obtained from the finite element analysis of vessel collapse along with typical analytical form of tube-law to describe the nonlinear vessel compliance

$$\frac{p - p_c}{K_p} = \left(\frac{A}{A_0} \right)^{-3/2} - 1 \quad (7.4)$$

$$K_p = \frac{Eh^3}{R^3(1 - \nu^2)} \quad (7.5)$$

From Fig. 7.4 it is clear that, as the transmural pressure becomes increasingly negative, small changes in pressure result in large changes in cross-sectional area. This allows the vein to act as a blood reservoir without large increases in venous pressure. With further decrease in transmural pressure the compliance of the vessel reduces, due to the self-contact illustrated in Fig. 7.3e, f which correspond to normalized pressure of -4.86 and -25 respectively.

7.1.3 Resistance to Flow and Supercritical Flow in Collapsed Veins

In addition to the nonlinear form of the pressure–area response, it is also evident that the effective resistance of the vein will change significantly during the collapse phase. As a result, regions of vein which are collapsed

present a high resistance to flow, which provides a dynamic mechanism for flow limitation. This effect is clear from Fig. 7.3 where the flow travels through a small gap and viscous losses are high in the collapsed state (d–f) compared to flow within the vessel as the transmural pressure increases (a–c). This effect is also observed in the operation of a Starling resistor, originally used to control flow rates within a heart-lung machine.

More complex behaviour is observed under conditions where the local speed u of the blood within the vein, exceeds the speed c of propagation of waves along the vessel. Due to significant variations in both cross-sectional area and local compliance of the vein, which determines the wavespeed, it is possible to transition between subcritical ($u < c$) and supercritical ($u > c$) flows within a single vein. Detailed analysis of the implications of these effects has been examined using a 1D numerical model under steady flow conditions (Shapiro 1977).

As wavespeed decreases with increase in compliance, supercritical flow becomes more likely in conditions when the veins are partially collapsed, this occurs in the jugular vein and the superior vena cava when in the standing position and in the superficial circulation when the limb is raised above heart level, as described in Sect. 7.2.4.

7.1.4 Venous Return

Venous return is defined as the volume of blood returning to the right atrium from the systemic venous circulation. Maintaining venous return is important for obvious reasons to ensure that blood is continuously available to prime the pulmonary circulation thus, in turn, providing oxygenated blood to the left ventricle. The storage capacity of the venous system and the subtle relationship between pressure and volume within the veins allows the venous system to act as a ‘buffer’, regulating levels of venous return under transient changes in cardiac output.

Total venous return is determined by a number of contributing factors including; the pressure gradient between the peripheral veins and the right atrium, the resistance of the venous vascular bed, the influence of transient muscle pump activation (in particular the calf muscle pump) and the effects of the respiratory pump. As discussed above, the resistance of the venous bed can be strongly nonlinear due to the increased resistance of collapsed vascular segments, this is particularly notable in the abdomen during collapse of the vena cava under changes of abdominal pressure (Wallace et al. 2010).

The mechanisms underlying the calf muscle pump and respiratory pump are discussed in more detail in the following sections. Both pumping mechanisms rely on the presence of venous valves.

7.1.5 Calf Muscle Pump

During exercise, increased cardiac output requires an associated increase in venous return. Augmentation of venous return from the legs is achieved through the action of the foot, calf and thigh muscle pumps, allowing venous return to be enhanced beyond the level associated with the pressure gradient between the legs and the heart. The anatomy of the calf muscle pump, which provides the most significant contribution, is shown in Fig. 7.5. The calf pump is formed by the action of the gastrocnemius and soleus muscles which contract and force blood out of the deep veins of the calf (anterior tibial, posterior tibial and peroneal veins) which drain into the popliteal vein at the knee.

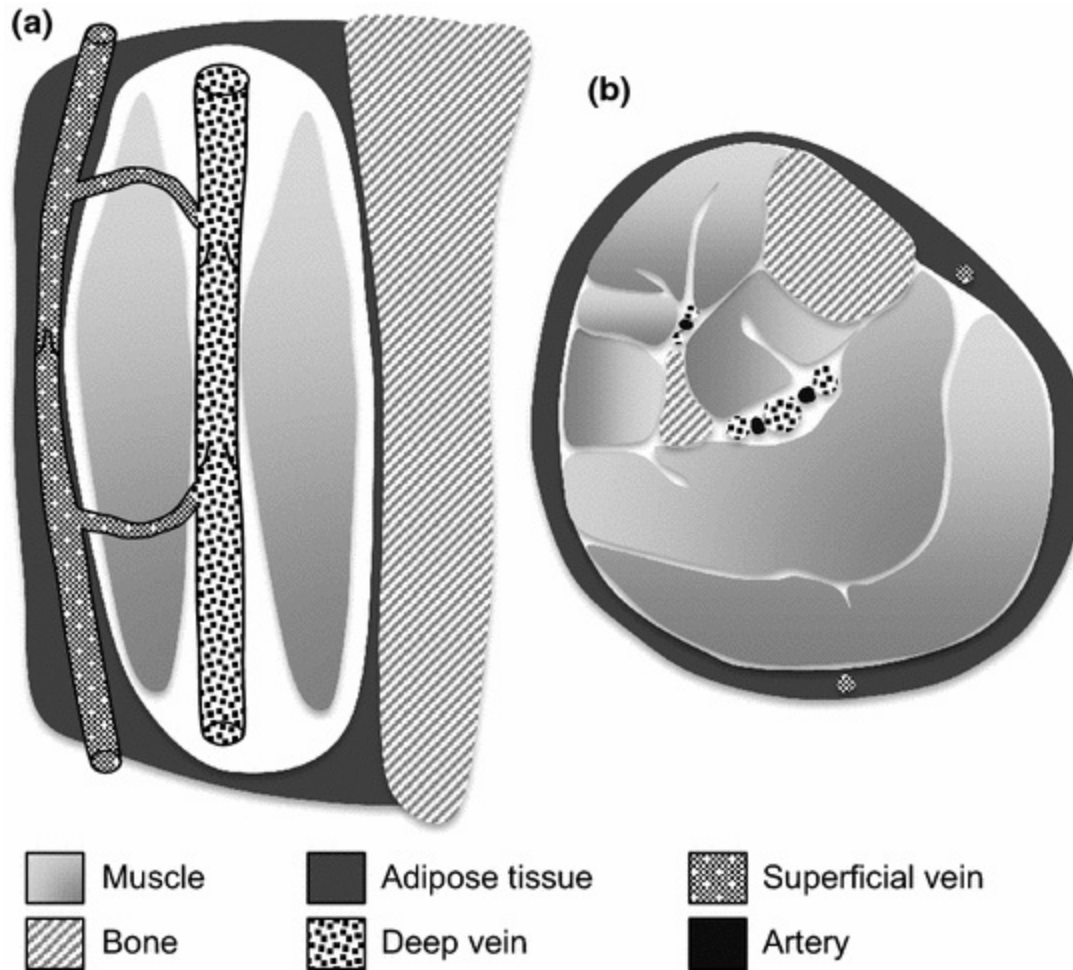


Fig. 7.5 Anatomy of the calf muscle pump in **a** longitudinal plane **b** transverse plane

The presence of competent venous valves within the lower limb ensures that blood ejected from the calf during muscle contraction is not able to return to the calf under the influence of gravity when the muscle relaxes. The refilling of the deep veins is achieved through inflow from the arterial circulation and from flow between the superficial and deep venous systems which is facilitated by the perforating veins. These vessels extend through the fascia to connect the deep and superficial venous circulation. Uni-directional flow from the superficial to the deep veins is dependent on the presence of valves within the perforating veins.

The physiological action of the calf muscle pump has informed design of prophylaxis to reduce incidence of DVT following surgery. This involves the use of an external cuff to apply intermittent compression to the calf, mimicking the contraction and relaxation of the calf muscle. Understanding

of the mechanics associated with the transfer of pressure from the surface of the calf to the veins is important to predict the degree of collapse of the deep veins.

Numerical analysis combined with anatomical characterisation using magnetic resonance imaging (MRI) has provided a methodology to examine this behaviour in detail (Narracott et al. 2009). Figure 7.6a illustrates the deformation of the calf caused by inflation of an external cuff assessed using MRI and simulated using the finite element approach. The deep veins and arteries are arranged with two veins either side of a single artery and are identified as labelled in the figure.

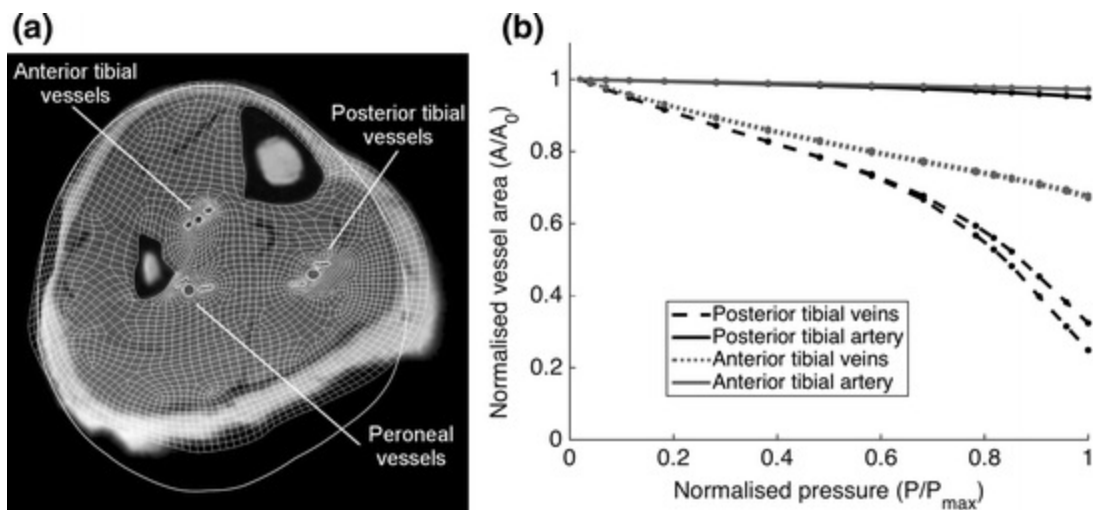


Fig. 7.6 **a** MRI image of calf following cuff inflation. The *solid white* outline shows the calf outline prior to cuff inflation, the mesh overlaid on the MRI image shows the finite element model of the calf following application of the cuff pressure. The deep veins and arteries are arranged with two veins either side of a single artery. **b** Collapse of deep vessels of the calf during cuff inflation, data is shown for six of the vessels labelled in **a**

Whilst MRI provides useful information on the overall calf deformation it is less effective for assessing the detail of vein collapse. This is due to the relatively low spatial resolution of the images and the fact that during the time required to acquire the image (order several minutes) refilling of the vein may occur due to arterial inflow. B-mode ultrasound imaging can be used to dynamically visualize the collapse of the veins during cuff inflation but the depth of the vessels makes this approach challenging. The importance of considering the anatomy of the calf is clear in this case, as the tibia and fibula influence the transfer of pressure from the surface of the calf to the deep vessels, resulting in less collapse of the anterior tibial veins, as shown in

Fig. 7.6b.

Other applications of these techniques include study of the influence of continuous elastic compression on wall shear stress with the deep veins (Downie et al. 2008) and the effect of active muscular contraction on venous collapse (Rohan et al. 2015).

7.1.6 The Respiratory Pump

The respiratory pump enhances venous return through changes in pressure within the abdomen and the thorax. During inspiration the pressure decreases in the thorax and increases in the abdomen. These changes in pressure compress the vena cava in the abdomen and, as the vena cava does not possess valves, blood is expelled from the abdomen to the thorax and the extremity. Both the presence of valves in the veins of the legs and the decrease in thoracic pressure promote flow towards the heart. During expiration the pressure reduces in the abdomen and increases in the thorax. The pressure on the vena cava is reduced and refilling occurs as the valves below the abdomen open, priming the vena cava prior to further inspiration. As the pressure in the thorax is below atmospheric throughout the respiratory cycle, the vena cava is not compressed within this region.

Despite the presence of valves between the abdomen and the periphery, the influence of respiration on venous flow within the lower limbs has been demonstrated using Doppler ultrasound measurements to characterise the frequency of transient changes in flow rate in the common femoral vein (Abu-Yousef et al. 1997).

7.2 The Role of Venous Valves

The venous valves form during development of the cardiovascular system, initially as a bulging in the endothelial layer of the vein wall which covers the valve leaflet surface. The form of the valve is shown, as a longitudinal section, in Fig. 7.7. When developed, the valve leaflet consists of a thin elastic layer on the luminal surface and underlying collagen with very little connective tissue. Smooth muscle cells are only found in the valvular agger, where the valve attaches to the vein wall (Gottlob and May 1986).

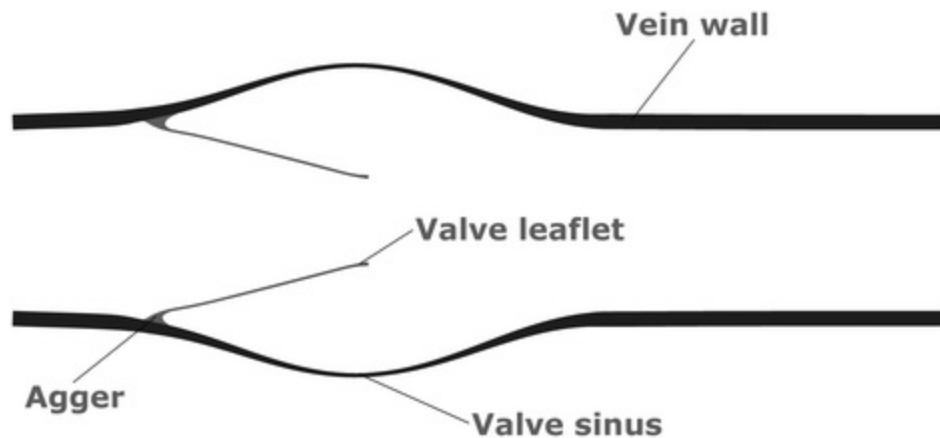


Fig. 7.7 Longitudinal cross-section of the vein showing key features of venous valve geometry

7.2.1 Valve Geometry

Unlike the aortic valve, most venous valves are composed of two valve leaflets (bicuspid), although occasionally tricuspid valves have been observed. In addition to the valve leaflets the valve geometry often also features a pronounced sinus region similar to the aortic sinus, the valve sinus can be visualized during imaging studies such as contrast MR studies or X-ray venograms. The extent of the valve sinus is determined by the unstressed geometry of the vessel wall in this region and the distension of the sinus due to changes in transmural pressure, as the venous wall in the sinus region is thinner than other locations, making it more distensible (Kampmeier and La Fleur Birch 1927).

7.2.2 Valve Locations and Incidence

Valves are found within all components of the venous system (superficial, deep and perforating veins) and in general the number of valves increases from the central circulation to the peripheral circulation of the arms and legs.

The vena cava is reported to be without valves, with valves observed infrequently in the common iliac vein and more frequently in the external and internal iliac veins. Most subjects are observed to have a valve in the femoral vein and the popliteal vein is also reported to contain one or more valves. There is a significant increase in the number of valves in the deep veins below the knee, with at least 8 valves reported in the posterior and anterior tibial and peroneal veins (Gottlob and May 1986). The veins of the upper limb are also reported to contain a significant number of valves (Iimura et al.

2003). This increase in valves towards the periphery is associated with the importance of the skeletal muscle pump in the peripheral circulation.

7.2.3 Dynamic Valve Behaviour

Detailed descriptions of venous valve function in vivo are scarce due to the challenges in imaging the dynamic structure of the valve due to the thinness of the valve leaflets, the relatively small size of the valve and the tissue thickness between the skin and the deep veins. B-mode ultrasound imaging has provided data to characterise valve function in relation to changes in haemodynamics (Lurie et al. 2002, 2003; Nam et al. 2012). This data demonstrates distinct phases to valvular motion, including opening, closing and resting phases. It is notable that the valve leaflets undergo oscillatory motion during the ‘resting phase’ when the volume flow through the valve region is constant, this effect is similar to the observations of self-excited oscillations which occur during steady flow through compliant tubes, due to the strongly coupled interaction between the solid and fluid mechanics in such systems. The valve leaflets do not open fully to the vein wall, resulting in a reduction in the diameter of the vessel as shown in transverse cross-section in Fig. 7.8a. This local stenosis results in velocity augmentation through the valve and fluid recirculation in the valve sinus as shown in Fig. 7.8b. The vortices which form within the valve sinus whilst the valve is open result in a region of recirculating blood, which has implications for the development of valvular thrombosis.

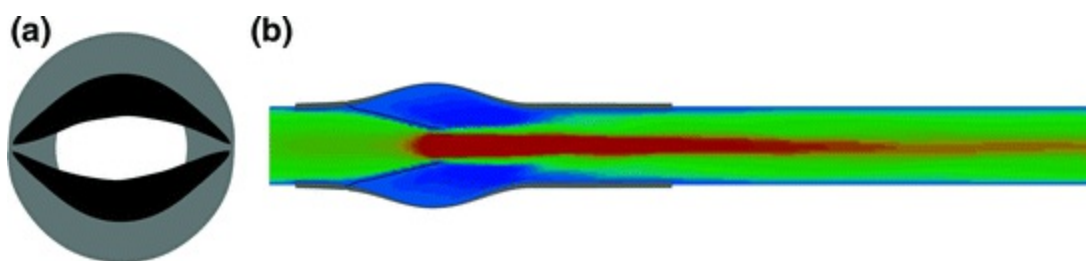


Fig. 7.8 **a** Transverse cross-section of the open valve showing the vein wall (*light*) and the valve leaflets (*dark*). **b** Longitudinal cross-section of the open valve showing velocity augmentation (*red*) through the valve leaflets and recirculation (*blue*) in the valve sinus

The response of the valve under various physiological loading conditions has been described by Lurie et al. (2002); the loading includes normal respiration and simulated walking in both standing and recumbent positions.

Such observations highlight the variability of venous haemodynamics and the changes in the nature of venous flow that occur within individual vascular compartments. The compliance of the venous system acts to reduce the influence of such variability on the overall form of the venous return. Observations of valve motion during quiet respiration along with reports of contraction of the musculature, even during quiet standing, and the influence of this effect on valve motion (Nam et al. 2012), demonstrates the sensitivity of the valves to changes in pressure and flow. Regular valve motion is considered to act as a protective mechanism against the formation of thrombosis behind the valve leaflets.

7.2.4 Influence of Postural Changes

Due to the distensibility of the venous system, changes in hydrostatic pressure lead to significant changes in venous volume. This effect is illustrated in Fig. 7.9 which shows the superficial veins of the hand in three positions (at the level of the head, at the level of the heart and below heart level).

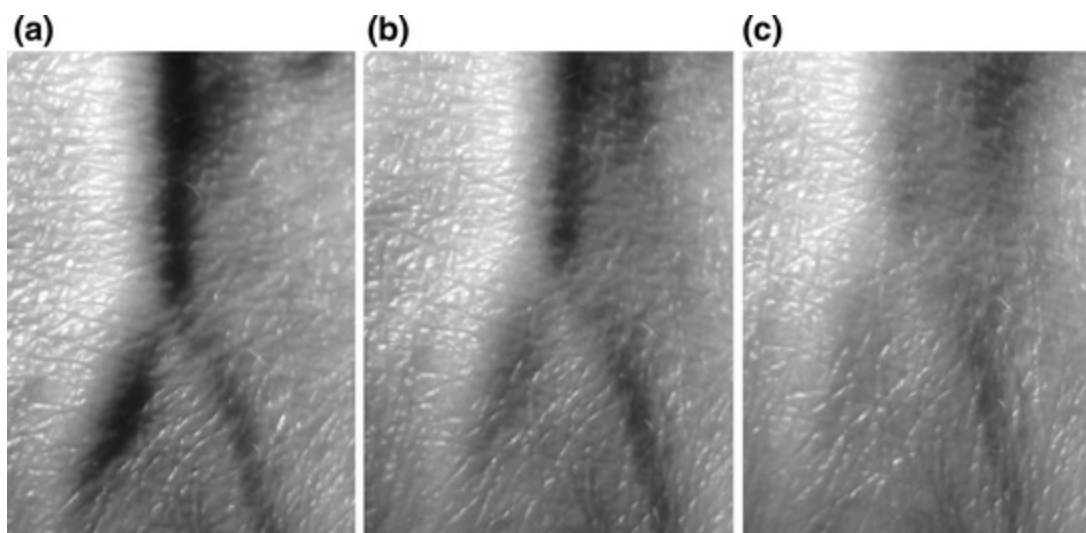


Fig. 7.9 Veins of the hand under varying hydrostatic pressure **a** below heart level **b** level with the heart **c** at head level

The change in pressure in the vein is given by:

$$dP = \rho gh \tag{7.6}$$

where h is the vertical distance from the reference position, g is the gravitational constant and ρ is the density of blood. The distension of the vein

is noticeable under this magnitude of pressure variation. It is evident that the vessel is not collapsed when the hand is at the level of the heart, as the venous pressure is higher than that of the right atrium due to the pressure gradient required to sustain venous return from the periphery. These effects are also reported for veins in the deep circulation under changes in elevation of the leg (Cirovic et al. 2006). Variation in distensibility of the superficial and deep systems arises from the variation in support conditions of the vein as the deep veins do not collapse in the same manner, due to the support of the surrounding muscular tissue.

The hydrostatic pressure does not develop instantaneously upon change in posture, as fluid shifts are required to establish the hydrostatic pressure gradient, which will be impeded by venous valve closure. The changes described above are therefore the steady state conditions once the hydrostatic pressure gradient has developed. The timescale for establishment of the hydrostatic pressure when moving from sitting to standing is of the order 20 s (Pollack and Wood 1949). Similar effects are observed during walking which produces a transient reduction in the pressure within the veins as blood is expelled from the calf. When walking stops the pressure gradually increases to the value associated with the hydrostatic column due to refilling from the arterial circulation.

7.3 Biomechanics of Venous Disease

7.3.1 Venous Insufficiency

Venous insufficiency is defined as the lack of reduction of pressure in the deep veins of the lower limb during exercise and is associated with a range of complications which present clinical symptoms associated with poor venous return from the lower limb. Whilst clinical gradings have been developed to report the severity of disease, the underlying causes of poor venous return can be hard to assess. Chronic venous insufficiency can result in complications including ulceration, oedema and fibrosis (Meissner et al. 2007). Ultrasound imaging has become widely used as a tool to aid understanding of such vascular complications and diagnosis of the cause of venous insufficiency.

B-mode ultrasound can be used to assess venous anatomy and undertake vein mapping in the lower limb. This can be helpful to identify anatomical features in an individual which contribute to poor venous return including

congenital absence of valves, valve incompetence and outflow obstruction. Doppler ultrasound is employed to assess the direction of flow during clinical tests and can provide quantitative measures of haemodynamics. This technique is used to assess the magnitude of reflux in the venous system following manual calf compression, muscle pump activation or the valsalva maneuver. Assessment along the length of a vein aids identification of specific valve sites associated with reflux, which can be used to target intervention. Kotani et al. (2007) report the use of M-mode ultrasound to assess the variation of valve geometry and examine valve incompetence demonstrating clear visualization of the incomplete closure of the valve leaflets.

7.3.2 Varicose Veins

The aetiology of varicose veins remains unclear as a number of mechanisms have been suggested to contribute to the eventual tortuosity of the superficial venous circulation which characterises the pathology. These include the failure or absence of valves leading to distension of the vein wall and alteration of the mechanical properties of the vein wall due to changes in the wall constituents. The biomechanical implications of increase of collagen concentration and reduced elasticity of the vein have been demonstrated using a finite element approach (Badel et al. 2013). This demonstrates the development of vessel tortuosity and the strong dependence of this effect on the axial pre-stretch of the vein.

7.3.3 Deep Vein Thrombosis

DVT is the development of thrombus within the deep veins, typically of the calf or thigh. DVT is often asymptomatic, if symptoms occur they include swelling of the limb and change in skin pigmentation. The most severe outcomes arise when the thrombus detaches from the vein and travels through the circulation. If the thrombus occludes the pulmonary arterial circulation, restricting blood from reaching the lungs, this results in a potentially fatal pulmonary embolism.

Post-mortem studies have indicated a tendency for DVT to form at venous valve sites. This has been linked to the generation of vortices within the valve sinus (Lurie et al. 2003; Karino and Motomiya 1984) whilst the valve remains in the open configuration, resulting in the recirculation of

blood constituents and the potential for cellular damage due to the avascular nature of the valve leaflets and resulting reduction in PO₂ tension (Malone and Agutter 2006). The biological response to this injury includes platelet aggregation and clot formation behind the valve leaflets.

The potential for thrombus formation is increased during periods of prolonged inactivity, such as long haul air travel or bed-rest following surgery, when the transient action of the muscle and respiratory pumps may not be sufficient to open and close the valves. These links between the biomechanics of valve function and the action of the muscle pump have led to the development of intermittent compression techniques to replicate the muscle pump and reduce DVT incidence in surgical patients, as described earlier.

References

Abu-Yousef MM, Mufid M, Woods KT, Brown BP, Barloon TJ. Normal lower limb venous Doppler flow phasicity: is it cardiac or respiratory? *Am J Roentgenol*. 1997;169:1721–5.

[CrossRef]

Badel P, Rohan CP, Avril S. Finite element simulation of buckling-induced vein tortuosity and influence of the wall constitutive properties. *J Mech Behav Biomed Mater*. 2013;26:119–26.

[CrossRef][PubMed]

Cirovic S, Walsh C, Fraser WD, Gulino A. Venous filling and elastance in the calf positioned above and below heart level. *Aviat Space Env Med*. 2006;77:1009–14.

Downie SP, Raynor SM, Firmin DN, Wood NB, et al. Effects of elastic compression stockings on wall shear stress in deep and superficial veins of the calf. *Am J Physiol Heart Circ Physiol*. 2008;294:H2112–20.

[CrossRef][PubMed]

Flaherty JE, Keller JB, Rubinow SI. Post buckling behavior of elastic tubes and rings with opposite sides in contact. *SIAM J Appl Math*. 1972;23:446–55.

[CrossRef]

Fung YC. *Biomechanics*. New York: Springer New York; 1997.

[CrossRef]

Gottlob R, May R. *Venous valves*. Vienna: Springer Vienna; 1986.

[CrossRef]

Grothberg JB, Jensen OE. Biofluid mechanics in flexible tubes. *Ann Rev Fluid Mech*. 2004;36:121–47.

[CrossRef]

Imura A, Nakamura Y, Itoh M. Anatomical study of distribution of valves of the cutaneous veins of adult's limbs. *Ann Anat.* 2003;185:91–5.

[\[CrossRef\]](#)[\[PubMed\]](#)

Kampmeier OF, La Fleur Birch C. The origin and development of the venous valves, with particular reference to the saphenous district. *Am J Anat.* 1927;38:451–499.

Karino T, Motomiya M. Flow through a venous valve and its implication for thrombus formation. *Thromb Res.* 1984;36:245–57.

[\[CrossRef\]](#)[\[PubMed\]](#)

Kotani A, Hirano Y, Yasuda C, Ishikawa K. A new ultrasonographic technique for diagnosing deep venous insufficiency—imaging and functional evaluation of venous valves by ultrasonography with improved resolution. *Int J Cardiovasc Imaging.* 2007;23:493–500.

[\[CrossRef\]](#)[\[PubMed\]](#)

Lurie F, Kistner RL, Eklof B. The mechanism of venous valve closure in normal physiologic conditions. *J Vasc Surg.* 2002;35:713–7.

[\[CrossRef\]](#)[\[PubMed\]](#)

Lurie F, Kistner RL, Eklof B, Kessler D. Mechanism of venous valve closure and role of the valve in circulation: a new concept. *J Vasc Surg.* 2003;38:955–61.

[\[CrossRef\]](#)[\[PubMed\]](#)

Malone PC, Agutter PS. The aetiology of deep venous thrombosis. *Quart J Med.* 2006;99:581–93.

[\[CrossRef\]](#)

Meissner MH, Moneta G, Burnand K, Gloviczki P, et al. The hemodynamics and diagnosis of venous disease. *J Vasc Surg.* 2007;46:4S–24S.

[\[CrossRef\]](#)[\[PubMed\]](#)

Monos E, Berczi V, Nadasy G. Local control of veins: biomechanical, metabolic, and humoral aspects. *Physiol Rev.* 1995;75:611–66.

[\[PubMed\]](#)

Nam KH, Yeom E, Ha H, Lee SJ. Velocity field measurements of valvular blood flow in a human superficial vein using high-frequency ultrasound speckle image velocimetry. *Int J Cardiovasc Imaging.* 2012;28:69–77.

[\[CrossRef\]](#)[\[PubMed\]](#)

Narracott AJ, John GW, Morris RJ, Woodcock JP, Hose DR, Lawford PV. A validated model of calf compression and deep vessel collapse during external cuff inflation. *IEEE Trans Biomed Eng.* 2009;56:273–280.

Pollack AA, Wood EH. Venous pressure in the saphenous vein at the ankle in man during exercise and changes in posture. *J Appl Physiol.* 1949;1:649–62.

[\[PubMed\]](#)

Rohan PY, Badel P, Lun B, Rastel D, Avril S. Prediction of the biomechanical effects of compression therapy on deep veins using finite element modelling. *Ann Biomed Eng.* 2015;43:314–24.

[\[CrossRef\]](#)[\[PubMed\]](#)

Shapiro AH. Steady flow in collapsible tubes. *J Biomech Eng.* 1977;99:126–47.
[\[CrossRef\]](#)

Wallace DJ, Allison M, Stone MB. Inferior vena cava percentage collapse during respiration is affected by the sampling location: an ultrasound study in healthy volunteers. *Acad Emerg Med.* 2010;17:96–9.
[\[CrossRef\]](#)[\[PubMed\]](#)

Wesly RL, Vaishnav RN, Fuchs JC, Patel DJ, Greenfield JC. Static linear and nonlinear elastic properties of normal and arterialized venous tissue in dog and man. *Circ Res.* 1975;37:509–20.
[\[CrossRef\]](#)[\[PubMed\]](#)

8. The Microcirculation

Peter R. Hoskins¹ 

(1) Edinburgh University, Edinburgh, UK

 **Peter R. Hoskins**
Email: P.Hoskins@ed.ac.uk

Learning outcomes

1. Describe the components of the microcirculation.
2. Describe the functions of the different components of the microcirculation.
3. Describe the variation of pressure and velocity with vessel type in the microcirculation.
4. Describe haemodynamic phenomena relevant to the microcirculation including plasma skimming; reduction and variability of viscosity and haemodynamics.
5. Discuss the origins of haemodynamic phenomena relevant to the microcirculation in terms of the behaviour of particles in small diameter tubes.
6. Describe the myogenic effect for arterioles (the Bayliss effect).

7. Discuss the control of blood pressure in the capillary by the Bayliss effect.
8. Describe the stress–strain behaviour of arterioles.
9. Describe pulse wave velocity in arterioles and capillaries.
10. Describe vasomotion and discuss how this may be a feature of the Bayliss effect.
11. Describe reasons for flow pulsatility in arterioles.
12. Describe the variation of wall shear stress for different vessels in the microcirculation.
13. Describe Starling’s equation for diffusion of molecules across the capillary wall.
14. Describe transport of molecules across the capillary wall; diffusion, vesicular transport and bulk flow.
15. Describe ‘flow autoregulation’.
16. Discuss the mechanisms for controlling flow; metabolic control, shear stress control, myogenic control.

8.1 Structure and Function of the Microcirculation

8.1.1 Structure

The microcirculation consists of those vessels of the cardiovascular system between the arteries and the veins; so the arterioles, the capillaries and the venules. Figure 8.1 shows a typical arrangement of vessels which are in the form of a network. The components of the microcirculatory network are

described below. There is variation of values for both upper and lower lumen diameters in the literature; the values below are typical of those quoted in the literature:

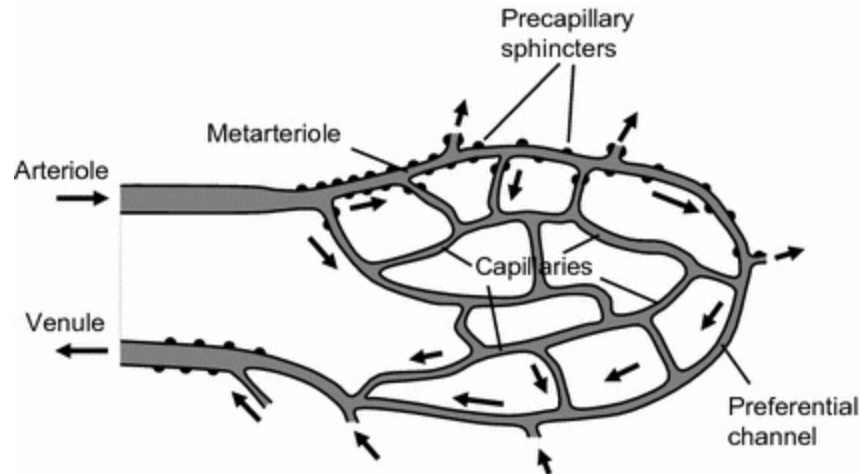


Fig. 8.1 Schematic of key microvessels and their organisation. On the arterial side is the arteriole and metarteriole. The metarteriole connect directly with the venule (on the venous side) forming a route (labelled as the ‘preferential channel’) which bypasses the capillary bed. Capillaries lie between the metarteriole and the venule; the capillary bed resembles a mesh rather than a bifurcating network. Precapillary sphincters are bands of smooth muscle which control flow in the capillary bed

- *Arterioles* (diameter 10–100 μm). These vessels are on the arterial side of the circulation. These branch several times and link the small muscular arteries to the capillaries. Arterioles contain three layers (intima, media adventitia), of which the media is proportionally the largest. The media is primarily comprised of vascular smooth muscle cells (typically, one or two layers in the larger arterioles with only a single spiralling layer in the smaller vessels leading to the capillaries). The residual tension in these cells, their tone, allows for alteration of arteriolar diameter and thus lumen size in response to changes in neural stimuli or in local chemistry. This plays a large part in control of capillary bed flow (see below) as well as the control of vascular resistance and systemic blood pressure.
- *Metarteriole* (diameter 10–20 μm). This term refers to an arteriole which is directly connected to a venule. This provides a vascular shunt which allows the capillary bed to be bypassed. In terms of structure, whilst metarterioles do not have continuous media, smooth muscle cells are present at the distal end of these vessels at the entrance to the

capillary bed forming what are known as ‘precapillary sphincters’. These can constrict to reduce flow into the specific capillary bed.

- *Precapillary sphincter*. The precapillary sphincter is a band of smooth muscle cells which controls flow into the capillary.
- *Preferential channel*. This is the channel between the metarteriole and the connecting venule. Constriction of the precapillary sphincters results in most flow travelling through the preferential channel rather than through the capillary bed.
- *Capillaries (diameter 4–10 μm ; up to 40 μm in sinusoidal capillaries)*. These are the smallest vessels in the cardiovascular system and, structurally are characterised as three types; continuous, fenestrated and sinusoidal. Capillaries consist of an endothelial layer and a basement membrane. Continuous capillaries have an uninterrupted endothelial lining and are the most common type of capillary. Fenestrated capillaries have pores in the endothelium which allow passage of certain molecules and are commonly found in endocrine glands, the gastrointestinal tract and the glomeruli of kidneys. Sinusoidal capillaries have large gaps in the membrane and an incomplete endothelial coverage which allows the flow of fluid and large molecules into the interstitial space. Sinusoidal cells are mostly found in the liver.
- *Venule (10–200 μm)*. These vessels are on the venous side of the circulation, branching several times between the capillaries and the veins. Venules contain three layers (intima, media, adventitia), but these layers are much thinner than for arterioles and the medial layer is almost absent.

The above microcirculation architecture is commonly taught in textbooks. However, it has been pointed out that it is only the GI tract which has metarterioles in the sense of an arteriole with a discontinuous medial layer and precapillary sphincters. In other circulatory beds the term ‘metarteriole’ has come to refer to the smallest arterioles immediately before the capillaries.

It can be seen both from Fig. 8.1 and the discussion above that the capillary bed is not a conventional bifurcating network. There are bypasses in the form of ‘preferential channels’; if precapillary sphincters are activated this can result in almost complete shut down of flow to the capillary bed. The capillary bed itself more resembles a mesh than a bifurcating network, so that

there are multiple possible routes that a red cell can take through the bed.

8.1.2 Functions

The main functions of the microcirculation in terms of its components parts can be summarised as follows:

- *Resistance to flow.* Constriction of smooth muscle in the arterioles and the metarteriole enables control of local vascular resistance. This enables control of the pressure at the level of the capillaries and flow rate through the capillary bed.
 - *Molecular exchange.* The exchange of fluid and of key molecules occurs through the walls of the capillaries. The main mechanism of exchange (diffusion) is pressure driven hence it is important to maintain hydrostatic pressure constant at the level of the capillary.
 - *Flow bypass.* This refers to blood flow in vascular beds where the microcirculation contains a preferential channel controlled by precapillary sphincters. This allows particular capillary beds to be excluded from the microcirculation.
 - *Capacitance.* The venules act as a reservoir of blood; some 22 % of the whole blood volume is contained in the venules.
-

8.2 Haemodynamics and Mechanics

8.2.1 Pressure and Velocity

In Chap. 2, basic concepts of cardiovascular biomechanics were introduced where it was noted that both blood pressure falls and blood velocity falls while travelling from the aorta to the capillaries. Rough estimates were provided in Table 2.1 of mean velocity based on a pure bifurcating model. Data on pressure and velocity in the microcirculation is shown in Fig. 8.2. This shows considerable decrease in pressure in the arteriolar part of the microcirculation, which is due to the high resistance to flow of arterioles. The pressure continues to fall through the capillary bed and the venules. Blood velocity is lowest in the capillaries with a value of around 2 mm s^{-1} . Table 8.1 shows values of mean velocity and other haemodynamic quantities in different vessels of the microcirculation.

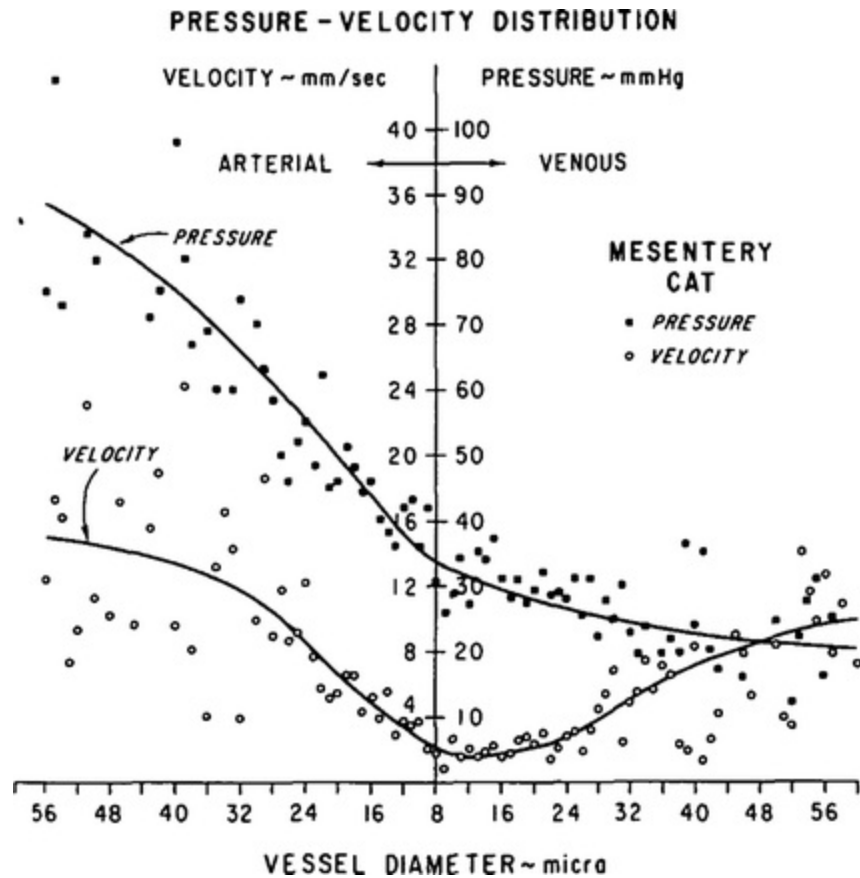


Fig. 8.2 Blood pressure and velocity in the microcirculation from arterioles to venules. From Zweifach BW, Lipowsky HH; Quantitative studies of microcirculatory structure and function. III. Microvascular hemodynamics of cat mesentery and rabbit omentum; Circulation Research; Vol. 41(3), pp. 380–390. Copyright American Heart Association (1977), reprinted with permission from Wolters Kluwer Health, Inc.

Table 8.1 Haemodynamic quantities in the microcirculation

Vessel	Diameter (μm)	Mean velocity (mm s^{-1})	Reynolds number, Re	Womersley parameter, α	Pseudoshear rate (s^{-1})	Wall shear stress (Pa)	Effective viscosity (mPa s)	Haematocrit
Arterioles	60	12	0.2	0.8	200	6	2.8	0.29 ± 0.12
Arterioles	15	7	0.03	0.2	470	14	4.9	
Capillaries	5	0.2	0.0003	0.07	40	12	15	0.23 ± 0.14
Venules	18	0.2	0.001	0.2	10	3	4.2	0.31 ± 0.13
Venules	72	2.4	0.05	0.9	30	10	2.9	

Data taken from Popel and Johnson (2005) from the resting cat sartorius muscle, with data on haematocrit from Pries and Secomb (2008)

8.2.2 Blood Flow

Blood is a suspension of particles, principally red cells. The human red cell dimensions of 7.5 by 2 μm , is tiny in comparison to the diameter of 1–30 mm of the larger arteries and veins. This means that in larger arteries and veins the blood can primarily be considered as a continuous fluid; or in other words, individual red cells can usually be ignored in considering haemodynamics. However in the microcirculation, the dimensions of the vessels are close to the dimensions of the red cell. This is especially true for capillaries where the typical diameter of 4–10 μm is comparable to the 7.5 μm diameter of the red cell. Red cells squeeze through capillaries in single file and are distorted in shape as they do so. Flow in the microcirculation is more complex than flow in larger vessels, and the effect of individual red cells must be considered. Chapter 3 describes a number of phenomena concerning flow of particles in tubes where the ratio of tube-diameter to particle-diameter is low and/or where shear rate is low. These phenomena are relevant to the microcirculation and are briefly summarised here.

- *Cell margination and depletion.* Particles flowing in a cylindrically shaped vessel will experience a number of forces. Some forces will push an individual particle away from the centre of the vessel and others will push the particle away from the vessel wall. This can lead to accumulation of particles in a ring between the vessel centre and the vessel wall. This is known as the Segre–Silberberg effect from the original paper (Segre and Silberberg 1962). Flow in blood is more complicated in that there are several different particle types; red cells are relatively deformable while platelets and white cells are relatively stiff. There is interaction between the particles in flow of whole blood. The red cells have a tendency to move away from the wall, leaving a layer near the wall depleted of red cells, while platelets and white cells are pushed by the red cells to the vessel wall (Aarts et al. 1988) as shown in Fig. 8.3.



Fig. 8.3 Simulation of flow of red blood cells (RBCs) and platelets in a vessel with a diameter of 20 μm . Red cells are aligned with the direction of flow and there is a cell-free region near the wall. Platelets in yellow appear mainly in the cell-free region (having been pushed there by the RBCs). From; Rheologica Acta, Effect of tube-diameter and capillary number on platelet margination and near-wall dynamics, 2015, doi:[10.1007/s00397-015-0891-6](https://doi.org/10.1007/s00397-015-0891-6); Krüger T; © Springer-Verlag Berlin Heidelberg 2015, with permission of Springer

- *Variation of viscosity with vessel diameter.* Due to red cell depletion near the wall, the effective viscosity of the fluid is reduced when the vessel diameter is a few red blood cell diameters. Near the wall, the particle density is reduced and the viscosity is dominated by the underlying fluid. The viscosity mainly arises from flow in the high shear region near the wall, so that the overall viscosity is more akin to that of the fluid base rather than that of the suspension. This is called the Fahraeus–Lindqvist effect after the authors of the original paper (Fahraeus and Lindqvist 1931). Calculations of the Fahraeus–Lindqvist effect shown in Fig. 3.15b demonstrate a minimum viscosity at a vessel diameter of around 7–9 μm depending on haematocrit. In smaller vessels the red blood cell is deformed and hence viscosity is higher.
- *Variation of haematocrit with vessel diameter.* This is concerned with reduction in haematocrit within the vessel compared to that within the receiving reservoir. This is called the Fahraeus effect after the author of the original paper (Fahraeus 1929). The explanation is similar for the Fahraeus–Lindqvist effect in that the red cells in the centre of the vessel move faster than the liquid at the edge of the vessel. Hence the relative volume of red cells to plasma is greater in the discharge fluid than for the fluid in the tube. Figure 3.15a shows that the effect is greatest (i.e. largest reduction in haematocrit) for a vessel diameter of 12–13 μm .
- *Red cell aggregation.* At low shear, red cells aggregate leading to an increase in viscosity and further exacerbating red cell depletion at the wall.

Building on the above understanding we will now look at a number of features of flow in the microcirculation. Further details of flow in the microcirculation are provided in review articles, e.g. Pries et al. (1996), Mchedlishvili and Maeda (2001), Baskurt and Meiselman (2003).

- *Plasma skimming.* This is the phenomenon whereby flow in a side-branch contains few or no red cells as a result of cell depletion at the wall of the parent vessel (Fig. 8.4). Through the microcirculation and in the capillary bed the red cell density will be highly variable depending on a number of factors including the diameter of the vessel, red cell aggregation and the flow rate.

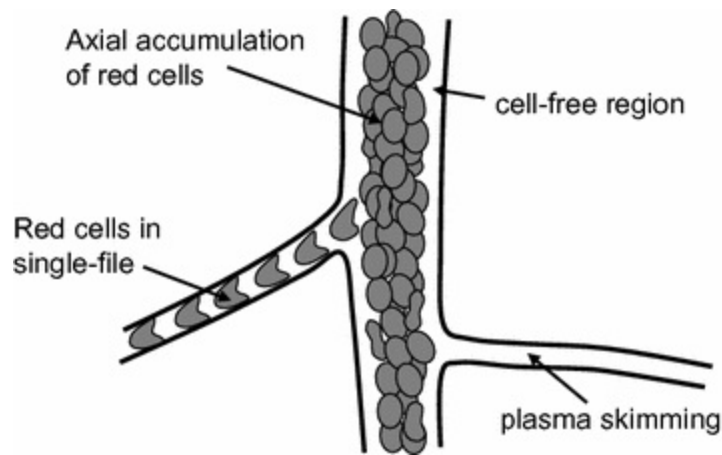


Fig. 8.4 Illustration of the flow of red cells in the microcirculation. There is a tendency to axially accumulate in the main vessel leading to a cell-free region near the wall. In one side-branch this leads to plasma skimming. In another branch red cells travel in single file

- *Viscosity variations.* The effective viscosity is dependent on the red cell density, the diameter of the vessel, red cell aggregation, the flow rate and the exact path which is taken by the red cells through the microcirculation. These factors lead to considerable variation in viscosity in vessels of similar diameter, and variations in viscosity with diameter. Table 8.1 shows the highest viscosity of 15 mPa s for capillaries (compared to 3.5–4 mPa s in large arteries), and low viscosities of 2.8–2.9 mPa s in the large arterioles and venules.
- *Reduced and variable haematocrit.* The haematocrit (red cell concentration by volume) is 0.4–0.5 in the larger arteries and veins, with only a small variation in the value in different arteries and veins in the individual. In the microcirculation the haematocrit is reduced and has a

wide variation in different vessels in the individual subject. Values of haematocrit are 0.29 ± 0.12 in arterioles, 0.23 ± 0.14 in capillaries and 0.31 ± 0.13 in venules (Pries and Secomb 2008).

- *Time dependence of haemodynamic quantities.* The effect of the passage of individual red cells will lead to variations of key quantities such as wall shear over short timeframes. This is at its most pronounced in the smallest vessels, the capillaries, where red cells traverse the capillary in single file.

8.2.3 Myogenic Effect and Bayliss Effect

The myogenic effect is the response of small arteries and arterioles to a change in blood pressure. Following an increase in blood pressure there is decrease in diameter caused by constriction of the smooth muscle cells in the media. Conversely; following a decrease in blood pressure there is an increase in diameter caused by relaxation of smooth muscle. This mechanism is locally controlled and is thought to be associated with a stretch-activated ion channel. This leads to depolarisation of the cells which in turn results in a calcium signal leading to muscle contraction. This effect was originally observed by Bayliss (1902) in arterioles where it is called the 'Bayliss effect'. The myogenic effect is also demonstrated in smaller arteries, especially intracerebral arteries. The Bayliss effect is the principle mechanism by which capillary pressure is maintained within a narrow range. The time course of the Bayliss effect is illustrated in Fig. 8.5. A sudden increase in blood pressure results in an initial increase in diameter as a result of the increased distending pressure. The increase in pressure is sensed by the smooth muscle cells in the media and there is calcium signalling leading to constriction of the smooth muscle cells. The constriction leads to decrease in the diameter. The initial increase in arteriolar pressure also leads to increase in capillary pressure. The decrease in arteriolar diameter is associated with increased resistance to flow, and hence increase in pressure drop across the arterioles. The increase in arteriolar pressure is therefore balanced by pressure loss and the capillary pressure is restored to its normal value.

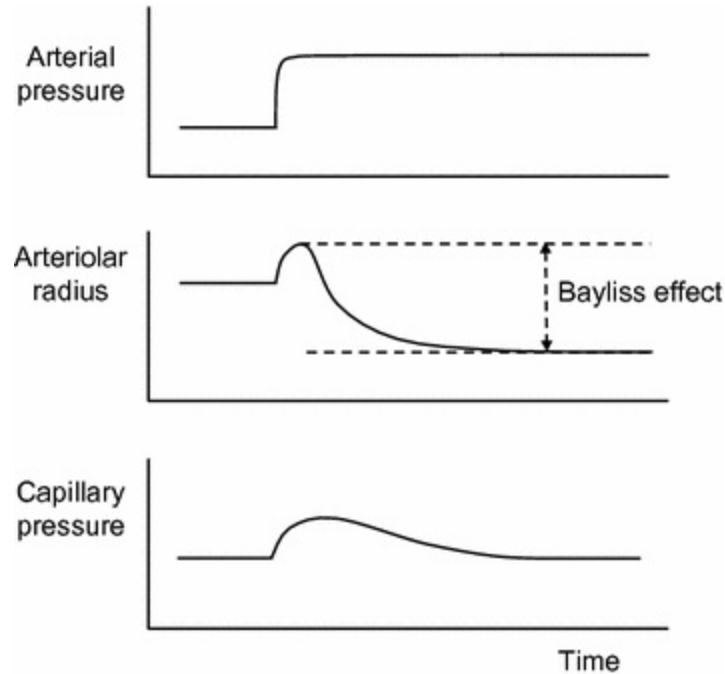


Fig. 8.5 Schematic of the myogenic effect in arterioles (Bayliss effect). A sudden change in blood pressure in an arteriole results initially in increase in diameter associated with passive elastic behaviour of the vessel wall. This is followed by constriction of the smooth muscle cells in the medial layer leading to decrease in diameter over a time period of 1–2 s. Capillary pressure increases following increase in arteriolar pressure but returns to baseline levels following arteriolar constriction

8.2.4 Vessel Wall Mechanics

Studies on the pressure–diameter relationship of microvessels may be undertaken in excised vessels. In larger vessels, such as arteries, the blood pressure is much higher than the pressure in the surrounding tissue so the effect of the pressure on the vessel from the surrounding tissue can largely be ignored. This is not true in the microcirculation where the blood pressure is low. The overall pressure on the vessel wall is the ‘transmural pressure’ which is the difference between pressure acting on the wall from the inside (blood pressure) and the pressure acting on the wall from the outside and experimental data in this area is often presented in terms of transmural pressure. In general a non-linear relationship is exhibited between transmural pressure and diameter, similar to that seen in larger vessels. Figure 8.6 shows area as a function of transmural pressure for capillaries showing a non-linear relationship in which incremental distension reduces as pressure increases. Figure 8.7 shows the corresponding stress–strain curve calculated using a simple elastic model; it can be seen that the stress–strain behaviour also

exhibits a non-linear relationship.

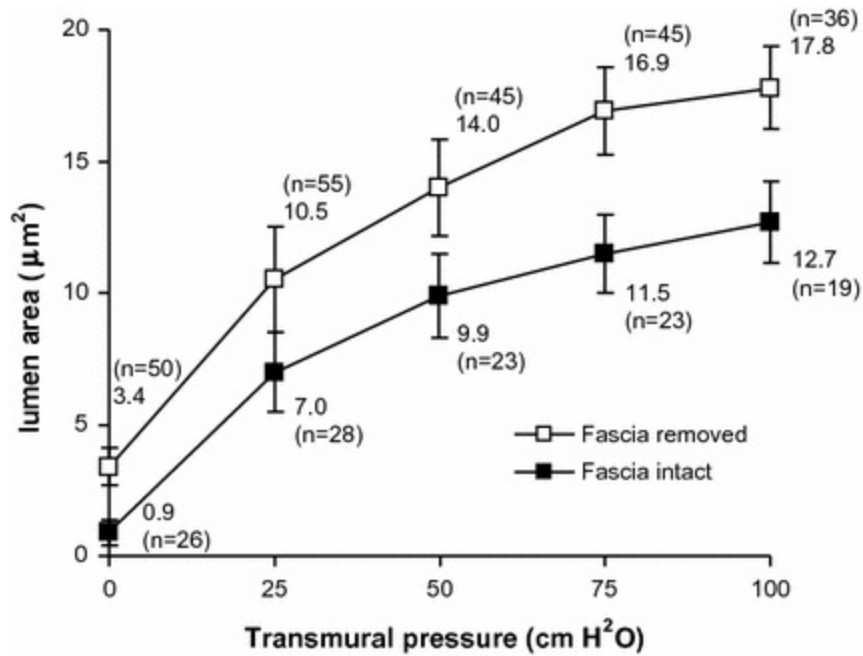


Fig. 8.6 Area-pressure in the capillary from the skeletal muscle of a rat. Average lumen area of the capillaries as a function of the capillary transmural pressure. The numbers indicate mean values (μm^2) and number of observations (n). Standard deviations are shown by the vertical bars. The capillary cross sections were derived from three muscles at each pressure. From; Annals of Biomedical Engineering, Biomechanics of skeletal muscle capillaries: hemodynamic resistance, endothelial distensibility, and pseudopod formation, volume 23, 1995, pp. 226–246; Lee J, Schmid-Schönbein GW; Copyright © 1995 Biomedical Engineering Society, with permission of Springer

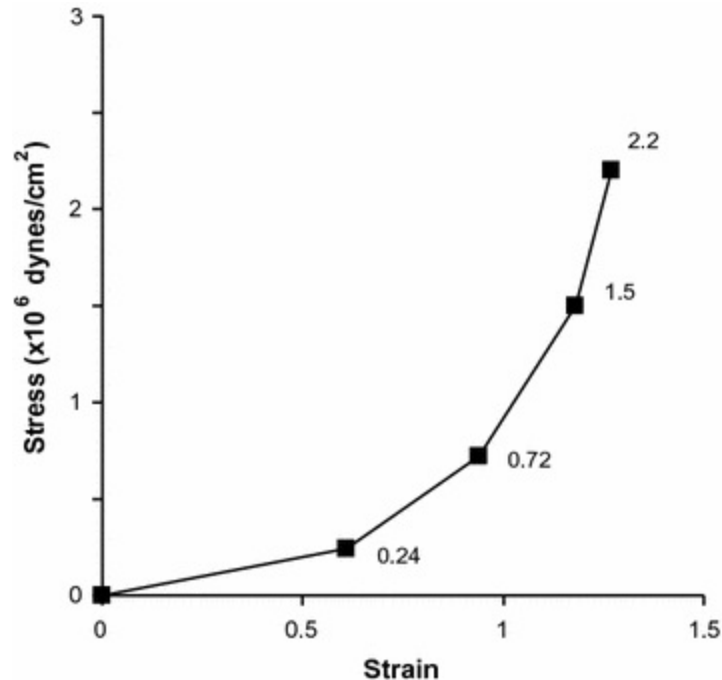


Fig. 8.7 Capillary stress–strain behaviour from the skeletal muscle of a rat. Average circumferential stress–strain curve for isolated capillaries without the wall support provided by surrounding skeletal muscle fibres. From; *Annals of Biomedical Engineering*, Biomechanics of skeletal muscle capillaries: hemodynamic resistance, endothelial distensibility, and pseudopod formation, volume 23, 1995, pp. 226–246; Lee J, Schmid-Schönbein GW; Copyright © 1995 Biomedical Engineering Society, with permission of Springer

For microvessels which have muscular tone (i.e. where the smooth muscle cells cause constriction), the pressure–diameter behaviour has both an active and a passive component (Fig. 8.8). The passive component corresponds to the artery with smooth muscle cells in a state of maximum relaxation. The active component is dependent on vascular tone; i.e. on the level of contraction of the smooth muscle.

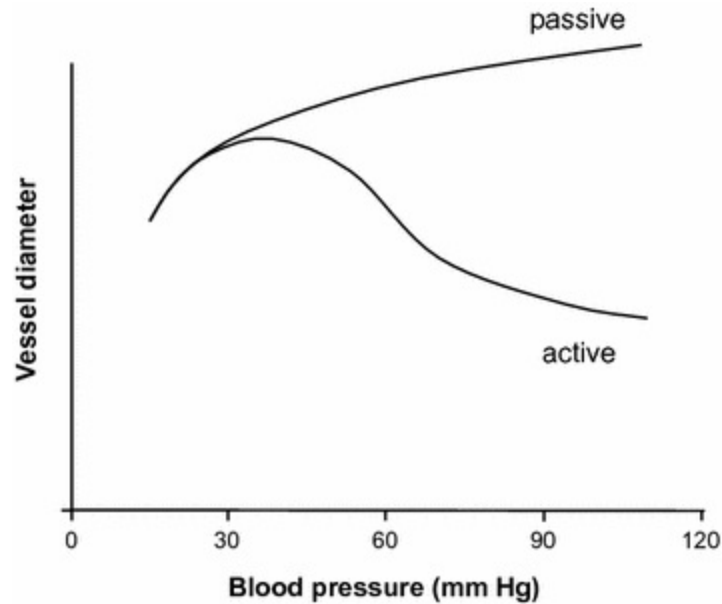


Fig. 8.8 Schematic diagram showing the pressure–diameter relationship in the arteriole when the smooth muscle is relaxed (*passive*) and constricted (*active*)

In the arterial system it was noted that the elastic nature of the vessel wall gave rise to pressure wave propagation, with the speed referred to as the ‘pulse wave velocity’ or PWV. The compliant nature of microvessels also leads to pressure wave propagation. Values of PWV in the range $3.5\text{--}134\text{ cm s}^{-1}$ were found in arterioles of diameter $12\text{--}43\text{ }\mu\text{m}$, with PWV increasing with diameter (Seki 1994). Using acoustic microscopy, Yeh et al. (2012) found mean values of PWV in arterioles of 30 cm s^{-1} ($30\text{ }\mu\text{m}$ diameter) increasing to 110 cm s^{-1} ($60\text{ }\mu\text{m}$ diameter). For pulse propagation in the capillary, a value of about 10 cm s^{-1} was estimated by Caro et al. (1978).

8.2.5 Vasomotion

Vasomotion describes the cyclic variation of vessel tone which is unrelated to the heart beat or to respiration. It has been observed that arterioles may exhibit regular changes in diameter at a frequency of $3\text{--}30\text{ min}^{-1}$. The total change in diameter during vasomotion is large at $50\text{--}100\%$ of the mean diameter (Tuma et al. 2008). The changes in diameter are linked to contraction and relaxation of the smooth muscle in the medial layer of the vessel wall. The function of this motion is uncertain but several possible benefits of vasomotion have been described (Arciero and Secomb 2012):

reduction in hypoxia in resting muscle, improved oxygenation and blood flow in tissues adjacent to muscle, improved filtration through the vessel wall, and improved lymphatic drainage.

A model of vasomotion was developed by Gonzalez-Fernandez and Ermentrout (1994) which predicts its main features. Central to this model is the myogenic effect. The model itself is complex but the key feature involves polarisation of the cell membrane which, as noted above, leads to muscle cell contraction. Calcium influx leads to polarisation hence to vessel constriction. Potassium influx repolarises the membrane leading to muscle relaxation. A delay between calcium influx and potassium influx will lead to oscillations in the contraction of the smooth muscle, and hence to oscillation in diameter. Other theories are explored by Secomb (2008).

8.2.6 Flow Pulsatility

Flow pulsatility in the microcirculation arises from several sources which are described in this section:

- *Arterial pressure pulsation.* Arteries have a high degree of flow-related pulsatility. This variation is damped within the arteriolar system and it was long assumed there was no transmission of this flow pulsatility to the capillaries. In other words, one of the functions of the arteriolar bed is to damp the pressure variation arising from the heart and to produce steadier flow in the capillaries. However, it has been shown that flow may be pulsatile in the most distal arterioles with some component of this pulsatility arising from the undamped blood pressure wave from upstream arteries.
- *Myogenic effect.* The variations in arteriolar diameter described above will lead to some variation in blood velocities.
- *Tissue compression.* Changes in pressure within the tissues will lead to changes in transmural pressure which will affect vessel cross-sectional area and hence blood velocity.

8.2.7 Wall Stress and Adaptability

Wall shear stress (WSS), the viscous drag of the blood on the vessel wall, has been estimated in the microcirculation using both measurement and simulation. The WSS will depend on diameter of the vessel, the flow rate and

on the blood characteristics near the wall. It is noted that in much of the microcirculation there is depletion of red cells at the vessel wall so that haematocrit and viscosity are reduced near the wall. These will impact on WSS (reduced viscosity at the wall leads to reduced WSS, reduced haematocrit at the wall leads to increased WSS). In addition, the passage of individual red cells will give rise to time-varying WSS. Early experimental measurements of WSS are presented in Fig. 8.9. These show high values in the arterial side of the microcirculation with much reduced values in the venous side.

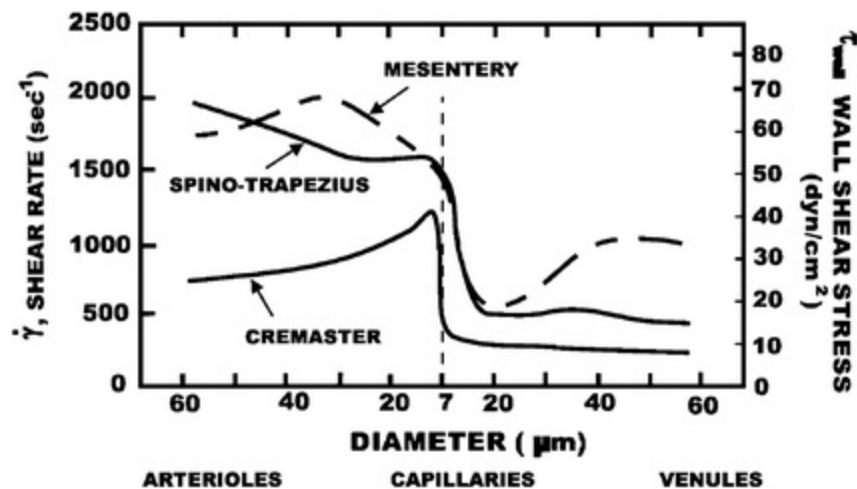


Fig. 8.9 Shear rate and wall shear stress in the microcirculation. Representative arteriovenous distributions of shear rate and wall shear stress from measurements of red cell velocity in the microcirculation of mesentery, spinotrapezius muscle and cremaster muscle. Vessel diameter (abscissa) may be considered as an index of position with the network. Values of wall shear stress were estimated from the product of shear rate and viscosity assuming a viscosity value of 3.5 mPa s. From; Flow-Dependent Regulation of Vascular Function; Shear Stress in the Circulation; 1995, pp. 28-45, Lipowsky HH, Copyright © 1995 by the American Physiological Society, with permission of Springer

In Chap. 5 it was discussed that WSS is a key feature of a control mechanism involving the endothelium, in which arterial diameter is adjusted in order to maintain mean WSS within a narrow range. Figure 8.10a shows WSS as a function of diameter and Fig. 8.10b shows WSS as a function of pressure. In terms of a control mechanism, Pries and Secomb (2008) suggest that a simple Murray's law model of design (based on minimisation of energy leading to independence of WSS with diameter; see Chap. 5) is inappropriate for the microcirculation, but that there is an adaptation process common to all types of vessel involving both wall shear stress and pressure.

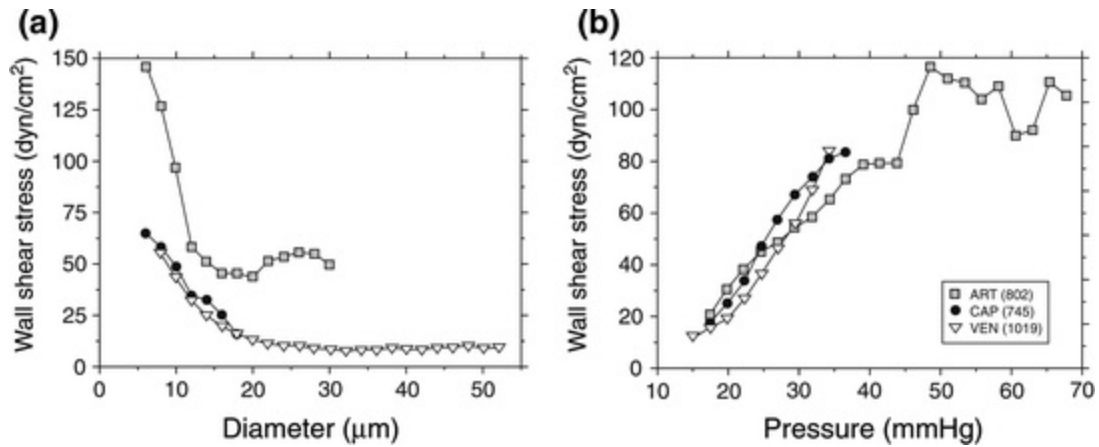


Fig. 8.10 Wall shear stress for arterioles, capillaries and venules as a function of **a** diameter and **b** pressure. Reprinted from Handbook of Physiology: Microcirculation. 2nd ed; Blood flow in microvascular networks; Pries AR, Secomb TW; with permission from Elsevier; pp. 3–36, copyright (2008); with permission from Elsevier

Pries and Secomb (2008) also showed that circumferential stress and vessel diameter are linearly related (Fig. 8.11) suggesting a similar adaptation process common to all vessels.

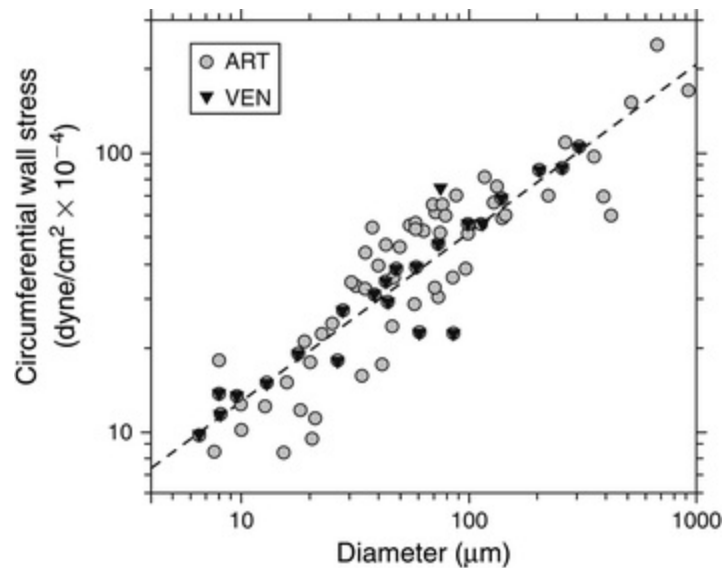


Fig. 8.11 Circumferential wall stress in vessels as a function of diameter. Reprinted from Handbook of Physiology: Microcirculation. 2nd ed; Blood flow in microvascular networks; Pries AR, Secomb TW; with permission from Elsevier; pp. 3–36, copyright (2008); with permission from Elsevier

Following from the above, it is relevant to discuss the relationship between mechanical forces and adaptability (remodelling) of the microcirculation. Secomb and Pries (2011) summarise that the same

principles that occur in the larger arteries apply, but with some modifications. In arteries (Chap. 5), the three main relationships are: wall shear stress and diameter, circumferential stress (related to pressure) and wall thickness, and longitudinal stress and longitudinal length. In addition Secomb and Pries (2011) describe that metabolic demand is a key determinant of vascular structure in the microcirculation.

Microcirculation adaptability also involves the generation of new vessels, a process which is referred to as angiogenesis. As the tissues of the body are under constant change, angiogenesis is an ongoing process which occurs every day. For example, exercise will increase skeletal muscle mass requiring the production of new vessels. Similarly, the increase in adipose (fat) tissue associated with weight gain will also be associated with the development of new vessels and injury is followed by repair and the laying down of new tissue and a new microcirculation. Many diseases are associated with the development of a new microcirculation, especially cancer where the growing tumour establishes its own blood supply.

8.3 Molecular Transport

While the heart and larger vessels are involved in transport of blood from one part of the body to another, the main transport function of the microcirculation concerns the exchange of molecules between the blood and the tissues of the body. This section describes the main transport mechanisms. Most molecular transport involves the diffusion of molecules, in which the delivery of oxygen to the tissues is a key function. Oxygen is a key molecule required for metabolic processes. Within the body the diffusion distance for oxygen is found to range from 20 to 200 μm . This variation is closely linked with metabolic demand; shorter diffusion distances are required for tissues with high metabolic activity such as skeletal muscle during exercise, and longer distances are observed for tissues with low metabolic activity. Most tissues in the body are within about 100 μm of a capillary, presumably in order to ensure adequate delivery of oxygen to tissues.

8.3.1 Starling's Equations

Starling's equation (Eq. 8.1) is concerned with the absorption and filtration of

molecules across the capillary wall. Water is able to flow freely from the blood into tissues through small gaps ('tight junctions' or fenestrations, depending on the type of capillary) in the endothelium. The net flow rate depends on the balance between the hydrostatic pressure and the colloid osmotic pressure (also known as the oncotic pressure) within the capillary (Fig. 8.12). Remembering that pressures in the microcirculation are low and that the tissues may be under some form of pressure due to external or internal compression, the net hydrostatic pressure is the difference between the blood pressure and the pressure in the surrounding tissues. The colloid osmotic pressure derives from the presence of proteins in the blood. The most important protein in this respect is albumin. Water diffuses freely across a porous membrane and there will be a net flow from higher to lower concentrations. As the percent by volume of water is less in blood than in the surrounding tissues there is a net tendency for water to diffuse into the capillary. The additional intravascular pressure which would need to be applied to the blood to stop diffusion is called the 'colloid osmotic pressure'. The two relevant pressures influencing the diffusion of water from the capillaries to the surrounding tissues are therefore:

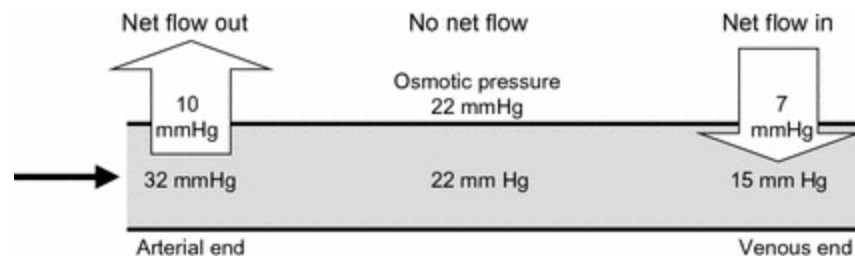


Fig. 8.12 Relationship between blood pressure, osmotic pressure and flow in the capillary

- *net hydrostatic pressure*: difference between pressure p_c in the blood and the pressure p_i in the interstitial fluid, and
- *net colloid osmotic pressure*: difference between osmotic pressure π_c in the blood and the osmotic pressure π_i in the interstitial fluid.

Starling's equation describes trans-capillary flow Q as follows:

$$Q = K_f ([p_c - p_i] - [\pi_c - \pi_i]), \quad (8.1)$$

where K_f is the filtration coefficient (a constant related to the area available for exchange and the capillary wall permeability).

When the net hydrostatic pressure exceeds the net osmotic pressure, which is the situation at the entrance region of the capillary, water will flow from the capillaries into the surrounding tissue. Conversely when the net hydrostatic pressure is less than the net osmotic pressure, water will flow from the surrounding tissues into the capillary. This situation applies at the exit region of the capillary.

The flow of fluid into or out of the capillaries requires that the blood pressure at the level of the capillary is maintained at a stable level. It was noted above that the myogenic effect has a major role to play in maintaining constant blood pressure in the capillaries.

8.3.2 Molecular Movement Across the Capillary Wall

The molecules present within blood which move across the capillary wall are: water; gases such as CO₂, O₂ and NO; electrolytes such as Na⁺ and K⁺; and various larger molecules such as glucose, amino acids and hormones. There are three main methods for movement of molecules across the capillary wall which will be described in this section. Further details may be found in Popel and Pittman (2014).

Diffusion. Diffusion concerns movement of molecules down a concentration gradient. Both CO₂ and O₂ are lipid soluble so can diffuse from the blood to the extracellular space across the lipid bilayer of the endothelium. Larger molecules such as steroid hormones can also diffuse by this method. In contrast, water-soluble molecules diffuse through gaps (fenestrations or larger pores) in the capillary wall. Examples of water-soluble molecules are glucose and amino acids.

Vesicular transport. A vesicle is a fluid-filled structure formed from the membrane of the cell (lipid bilayer). The vesicle is formed on one side of the endothelial cell (e.g. on the luminal side, adjacent to the blood) and moves across to the other side (e.g. on the side adjacent to the basement membrane). The vesicle and its contents are transported across the endothelium. This mode of transport is important for larger molecules such as antibodies that are unable to diffuse readily due to size or lack of lipid solubility.

Bulk flow. The mechanisms concerning bulk flow have been described above under 'Starling's law'. Bulk flow occurs through pores and clefts and is particularly important in fenestrated and sinusoidal capillaries.

8.4 Control of Flow

A simple model of the arterial system from heart to capillaries relating flow, pressure and resistance was described in Chap. 4. It was noted that changes in local flow are mainly effected through changes in arteriolar resistance, achieved by alteration of vessel diameter. Arterioles are vasoactive in that they have smooth muscle which when contracted leads to decrease in vessel diameter and conversely, when relaxed leads to increase in diameter. Some arterioles are capable of constriction to the point of complete shut down of flow. This large range of variation in diameter allows considerable change in local resistance which in turn allows for large variations in local flow rate. For example, in skeletal muscle under exercise, or following release of a tourniquet (where it is called reactive hyperaemia), there is an increase in flow rate by a factor of up to 20.

The ability of the microcirculation to maintain constant perfusion over a wide range of input pressure is referred to as blood flow autoregulation. Figure 8.13 shows schematically the effect of changing arterial pressure on perfusion. At low pressure, arterioles are fully dilated in an attempt to maximise the flow rate. Conversely, at high pressure arterioles are maximally constricted in order to keep the flow rate down. Between these two regions arterioles can constrict/dilate as necessary in order to maintain perfusion within a narrow range.

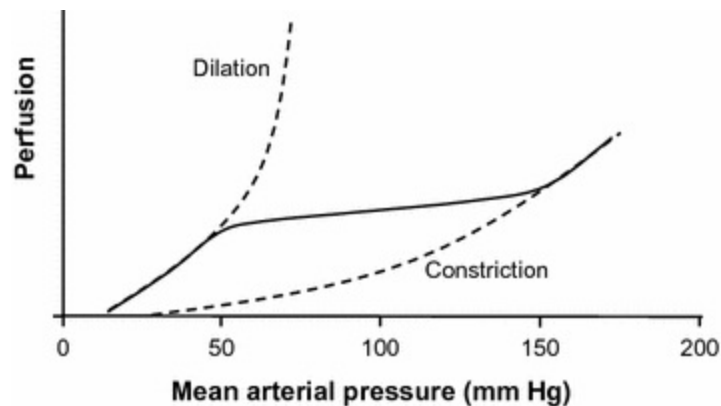


Fig. 8.13 Schematic of flow autoregulation; showing perfusion plotted against mean arterial pressure

The factors involved in control of local flow rate are metabolic control, shear stress control and myogenic control and are described below. Further reading is provided by Carlson et al. (2008) and Secomb (2008). These

control mechanisms interact which is considered in the model of flow autoregulation described by Carlson (2008). Their model, incorporating all three control mechanisms, was able to reproduce the experimentally observed dependence of perfusion on mean arterial pressure.

8.4.1 Metabolic Control

Two of the main functions of the microcirculation are to ensure sufficient supply of oxygen to the tissues for metabolic purposes, and to remove the waste products of metabolism such as carbon dioxide. Local control of blood flow to tissues is initiated by changes in the concentration of oxygen and carbon dioxide in tissues which leads to changes in arteriolar constriction. A decrease in oxygen concentration (occurring as a result of increased metabolism; e.g. muscles at work) leads to arteriolar smooth muscle relaxation and increase in local perfusion. Carbon dioxide has a similar effect in that an increase in CO₂ concentration leads to an increase in local perfusion. For oxygen, the actual mechanism was initially thought to be detection of oxygen concentration at the level of the arteriole but this appears not to be the case. Instead changes in oxygen concentration are detected downstream, possibly at the level of the venules, and information is communicated to the arterioles through cell–cell signalling along the vessel walls via gap junctions (Secomb 2008; Pries and Secomb 2008).

8.4.2 Shear Stress Control

Endothelium responds to changes in wall shear stress as discussed above and in Chap. 5. Increased shear stress is associated with release of NO which is a potent vasodilator, resulting in smooth muscle relaxation and increase in diameter in an attempt to normalise wall shear stress. As with metabolic control it is thought that the wall shear stress is detected downstream and that cell–cell signalling results in dilation at the level of the arterioles (Pries and Secomb 2008).

8.4.3 Myogenic Control

In Sect. 8.2.3 above it was noted that the myogenic effect is concerned with the change in arteriolar diameter arising from a change in pressure, and that this is the principle mechanism by which capillary inlet pressure is

maintained constant. There will be associated changes in flow rate arising from a change in pressure; the flow rate will initially increase due to the raised pressure then normalise as the myogenic effect occurs.

References

Aarts PAMM, van den Broek SA, Prins GW, Kuiken GDC, Sixma JJ, Heethaar RM. Blood platelets are concentrated near the wall and red blood cells, in the center in flowing blood. *Arteriosclerosis*. 1988;8:819–24.

[CrossRef][PubMed]

Arciero JC, Secomb TW. Spontaneous oscillations in a model for active control of microvessel diameters. *Math Med Biol*. 2012;29:163–80.

[CrossRef][PubMed]

Baskurt OK, Meiselman HJ. Blood rheology and hemodynamics. *Semin Thromb Hemost*. 2003;29:435–50.

[CrossRef][PubMed]

Bayliss N. On the local reactions of the arterial wall to changes of internal pressure. *J Physiol*. 1902;28:220–31.

[CrossRef][PubMed][PubMedCentral]

Carlson BE, Arciero JC, Secomb TW. Theoretical model of blood flow autoregulation: roles of myogenic, shear-dependent, and metabolic responses. *Am J Physiol Heart Circ Physiol*. 2008;295:H1572–1579.

Caro CG, Pedley TJ, Schroter RC, Seed WA. *The mechanics of the circulation*. Oxford: Oxford University Press; 1978. p. 383.

Fahraeus R. The suspension stability of the blood. *Phys Rev*. 1929;9:241–74.

Fahraeus R, Lindqvist T. The viscosity of the blood in narrow capillary tubes. *Am J Physiol*. 1931;96:562–8.

Gonzalez-Fernandez JM, Ermentrout B. On the origin and dynamics of the vasomotion of small arteries. *Math Biosci*. 1994;119:127–67.

[CrossRef][PubMed]

Mchedlishvili G, Maeda N. Blood flow structure related to red cell flow: determinant of blood fluidity in narrow microvessels. *Jpn J Physiol*. 2001;51:19–30.

[CrossRef][PubMed]

Popel AS, Pittman RN. The microcirculation physiome. In: Peterson DR, Bronzino JD, editors. *Biomechanics—principles and practices*. Boca Raton: CRC Press; 2014. p. 13-1–13-18.

Popel AS, Johnson PC. Microcirculation and Hemorheology. *Annu Rev Fluid Mech*. 2005;37:43–69.

[CrossRef][PubMed][PubMedCentral]

Pries AR, Secomb TW. Blood flow in microvascular networks. In: Tuma RF, Duran WN, Ley K, editors. Handbook of physiology: microcirculation. 2nd ed. San Diego: Academic Press; 2008. p. 3–36.
[CrossRef]

Pries AR, Secomb TW, Gaehtgens P. Biophysical aspects of blood flow in the microvasculature. Cardiovasc Res. 1996;32:654–67.
[CrossRef][PubMed]

Secomb TW. Theoretical models for regulation of blood flow. Microcirculation. 2008;15:765–75.
[CrossRef][PubMed][PubMedCentral]

Secomb TW, Pries AR. The microcirculation: physiology at the mesoscale. J Physiol. 2011;589:1047–52.
[CrossRef][PubMed][PubMedCentral]

Segre G, Silberberg A. Behaviour of macroscopic rigid spheres in Poiseuille flow. Part 2. Experimental results and interpretation. J Fluid Mech. 1962;14:136–57.
[CrossRef]

Seki J. Flow pulsation and network structure in mesenteric microvasculature of rats. Am J Physiol. 1994;266:H811–21.
[PubMed]

Tuma RE, Duran WN, Ley K. Handbook of physiology: microcirculation. San Diego: Elsevier; 2008.

Yeh C, Hu S, Maslov K, Wang LV. Photoacoustic microscopy of blood pulse wave. J Biomed Opt. 2012;17:070504. doi:10.1117/1.JBO.17.7.070504.
[CrossRef][PubMed][PubMedCentral]

9. Medical Imaging

Peter R. Hoskins¹✉, Stephen F. Keevil² and
Saeed Mirsadraee³

- (1) Edinburgh University, Edinburgh, UK
- (2) Guy's and St Thomas' NHS Foundation Trust, and Kings College London, London, UK
- (3) Royal Brompton Hospital, London, UK

✉ **Peter R. Hoskins**
Email: P.Hoskins@ed.ac.uk

Learning outcomes

1. Discuss the features of structural and functional medical imaging techniques.
2. Describe the principles of image formation of the different types of medical imaging system (X-ray imaging techniques, MRI, ultrasound, PET, gamma camera imaging and SPECT).
3. Define the term 'tracer' and describe the principle of operation of tracers used in nuclear medicine.
4. Define the term 'contrast agent' and describe the principle of operation of contrast agents in X-ray imaging, ultrasound and MRI.

5. Compare imaging characteristics of the different medical imaging systems.
6. Describe the principles of image formation for catheter-based imaging systems; IVUS and OCT.
7. Describe the different physical measurements which may be made using medical imaging systems; geometry and motion, blood velocity and related quantities, strain and stiffness.
8. Discuss different applications of functional imaging.

Medical imaging systems may be used to obtain information related to cardiovascular structure, physiology and mechanics in the individual subject. This information may be used in its own right in research and in health care. Information obtained from medical imaging is also used as input to patient-specific modelling. This chapter will provide a brief introduction to the main principles of medical imaging. Emphasis will be placed on the physical principles of image formation. Issues associated with instrumentation including detector technology and signal processing will not be considered. Texts which provide further details of medical imaging are Allisy-Roberts and Williams (2008), Hoskins et al. (2010) and Flower (2012).

9.1 Principles of Medical Imaging

This section describes the physical principles of medical imaging. Before considering each imaging modality in turn we will look at how different imaging techniques are commonly grouped; into ‘structural imaging’ and ‘functional imaging’.

- *Structural imaging techniques.* These primarily provide information on geometry and motion. This allows visualisation of organ shapes, measurement of organ volumes, characterisation of tissues, visualisation of flow patterns and measurement of blood velocity and related quantities. The main structural imaging techniques use X-ray imaging (including CT), ultrasound and Magnetic Resonance Imaging (MRI).

- *Functional imaging techniques.* These provide information related to physiological function, including regional blood flow (perfusion) and chemical and biological function (Margolis et al. 2007). All of the imaging modalities can, to some extent, be used for functional imaging. One form of functional MRI (or fMRI) provides information on brain activity through measurement of changes in oxygen levels in the brain. Many functional imaging techniques rely on the injection of contrast agents and tracers which can be detected by the imaging system. The tracer mimics particular molecules in the body and its uptake is dependent on how the molecule is processed within the body. Nuclear medicine and PET operate by the use of radioactive tracers. Contrast agents are larger constructs, typically of micron dimensions, commonly used in ultrasound and MRI for imaging of perfusion. Targeted contrast agents allow some measure of biological function.

9.1.1 X-Ray Techniques

X-ray imaging is the oldest form of medical imaging originating in the late 1800s. The German physicist Röntgen was the first to systematically study these rays and he labelled them ‘X-rays’. X-ray imaging involves the generation of X-rays in an X-ray tube, passage of the X-rays through the patient and detection of the X-rays using a detector placed behind the patient. The detected intensity of X-rays is dependent on the degree of attenuation of the rays by the tissues. Tissues containing high atomic number atoms such as calcium (in bone or calcifications) result in high attenuation. Tissues containing air (e.g. lungs) result in low attenuation. There is high image contrast between bone and soft tissue (e.g. as seen in X-rays of bone fractures) and between air and soft tissue (e.g. chest X-ray). The contrast between different types of soft tissue (e.g. fat and muscle) is less. Contrast agents containing high atomic number atoms can be used to improve image contrast. These operate by increasing the attenuation of X-rays. Iodine-based contrast agents are used to help visualise vascular lumen (arteries and veins) while other contrast agents (e.g. barium) are used for visualising the gastrointestinal system. There are several variants of X-ray imaging systems, the main ones relevant to the cardiovascular system are described here.

Projection radiograph. This is the simplest and most widespread X-ray technique. A 2D image is produced with both tube and detector remaining fixed in position during the taking of the X-ray (Fig. 9.1a). Older systems

used film detection of X-rays but modern detection is based on the use of a solid-state detector in which the image is captured digitally.

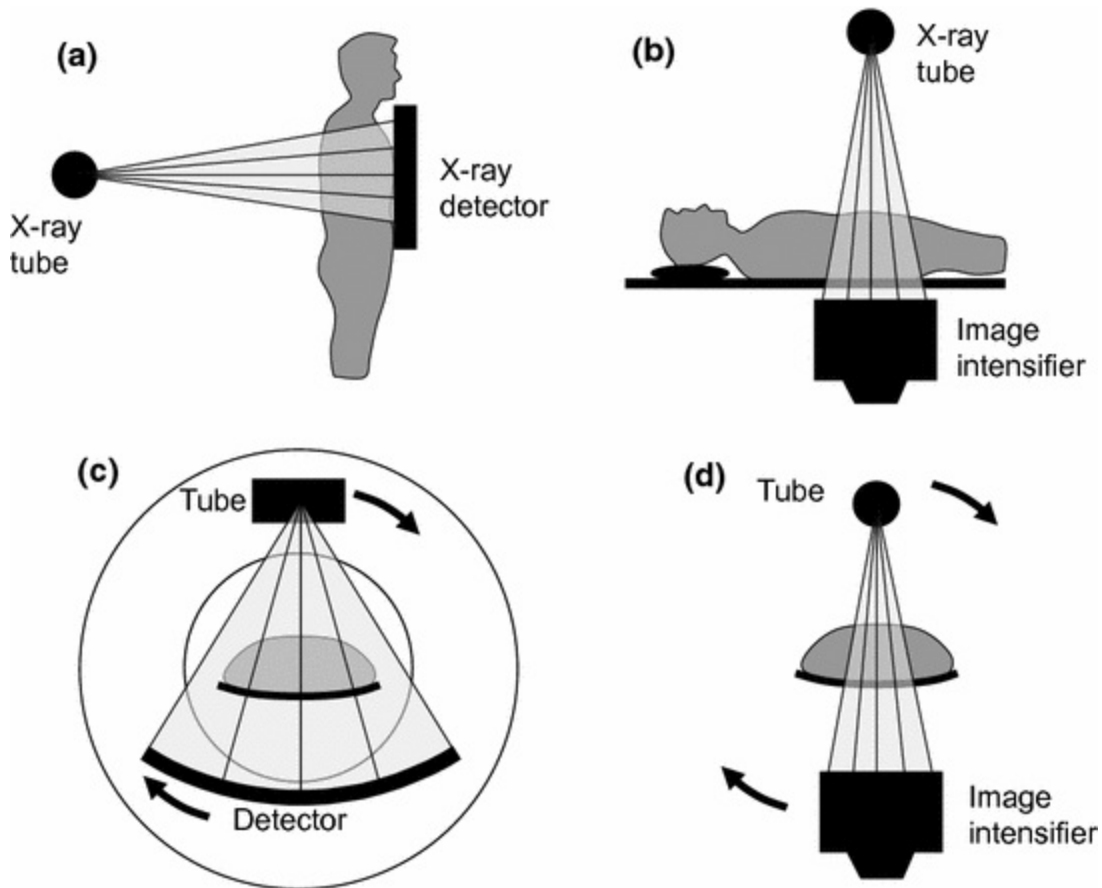


Fig. 9.1 X-ray imaging. X-rays are generated by a tube, travel through the patient and are detected by a detector placed behind the patient. **a** Projection radiography; a 2D image is taken, e.g. a chest X-ray. **b** Fluoroscopy; this is a real-time technique in which low-level X-rays are detected by an image intensifier placed underneath the patient couch. **c** CT scanning; X-rays are taken continuously while the tube/detector travels around the patient. **d** Rotational angiography; a fluoroscopy system rotates around the patient in a similar manner to a CT system

Fluoroscopy. X-rays are produced and detected continuously forming a 2D real-time image sequence (Fig. 9.1b). The X-ray beam intensity is much less than for projection radiography resulting in images which are noisier, but of sufficient quality to allow real-time visualisation. Fluoroscopy is widely used in examination of the arterial and venous systems and the chambers of the heart, where it is called ‘angiography’. As noted above the contrast between soft tissues is low and blood vessels would not show up without the use of an iodine based contrast agent which is injected into a vein or (less commonly) an artery. Fluoroscopy may be used purely for diagnosis, to

investigate the location of any diseased region. More commonly fluoroscopy is combined with intervention in which the diseased area is identified then treated. In balloon angioplasty a catheter is inserted into the artery and directed to the area of stenosis then a balloon is inflated under high pressure (several atmospheres) resulting in increase in local lumen diameter with increase in blood flow. A stent may also be placed to help prevent restenosis.

Computed tomography (CT). In CT, X-ray data is collected at different angles around the patient (Fig. 9.1c). This is achieved by rotation of the tube and detector with typically 1000 datasets collected for a full 360° rotation. The individual projections are combined in the computer using a method called 'back projection' to form a 2D cross-sectional image in which the displayed data is related to the attenuation coefficient of the tissues. Early CT scanners collected 1 slice at a time and a 3D dataset was built up by sequential series of slices with the patient couch moved between each slice. In modern CT scanners data is collected continuously with constant rotation of the tube-detector around the patient and continuous movement of the patient through the CT system; so-called helical scanning. Further decrease in acquisition time is enabled by multi-slice detectors in which several slices can be collected simultaneously. Typically 64 slices are collected continuously. With helical scanning and multi-slice detectors a full thorax and abdominal scan takes a few seconds. This is a sufficiently short time to enable the patient to hold their breath during scanning which helps reduce registration artefacts associated with breathing in by different amounts for each slice. Modern CT scanners can acquire up to 320 slices simultaneously (up to 16 cm coverage in one rotation), or combine very fast imaging techniques with dual-X-ray source technology to significantly improve temporal resolution. These techniques allow collection of a time-gated heart scan in one cardiac cycle and total body angiography with single contrast injection protocol.

Rotational angiography. This is a variant of angiography in which there is rotation of the tube and detector around the patient through 180° (Fig. 9.1d). The data sequence can be used to view the arteries from a series of different angles. Alternatively the data can be reconstructed to produce a 3D image of the vascular system.

9.1.2 Magnetic Resonance Imaging (MRI)

MRI is based on control of the magnetisation of the nuclei of atoms within

tissues. The nuclei in some atoms act as small magnets. This arises from the spin of the protons and neutrons which make up the nucleus. Pairs of spins tend to cancel. However where the atom has an odd number of neutrons or protons (or both) there is a net spin. In the human body the main atoms (by relative number) are: hydrogen (62 %), oxygen (24 %), carbon (12 %) and nitrogen (1.1 %). The most common isotopes of both oxygen and carbon have even numbers of protons and neutrons and hence no spin. Hydrogen has a single proton and has a spin of $1/2$. Nitrogen has 7 neutrons and 7 protons and a spin of 1. Due to its abundance in the body (62 %) it is the hydrogen nucleus which gives rise to the signal in an MRI scanner; or in other words the vast majority of MRI is hydrogen (proton) imaging, and is associated with detection of water (H_2O).

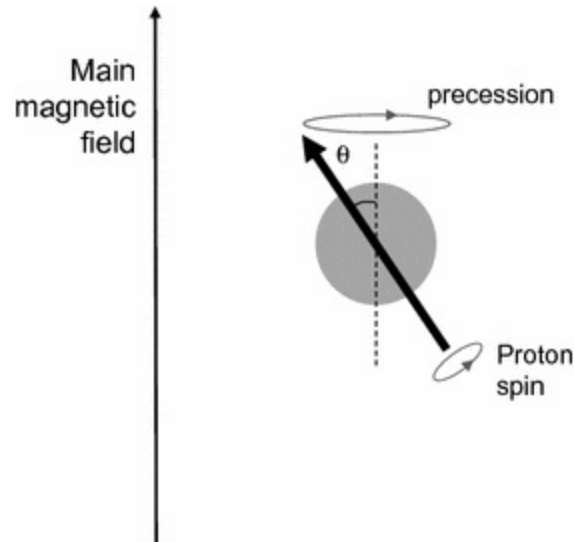


Fig. 9.2 Behaviour of a magnetised nucleus (e.g. hydrogen atom) in a magnetic field. The magnetic moment will precess around the magnetic field

Underpinning Physics. If placed in a magnetic field the proton will precess; that is the magnetic axis of rotation sweeps out a cone around the magnetic field (Fig. 9.2). This is similar to the way a spinning top will behave where the axis of rotation rotates around the gravitational field. The rate of rotation is called the Larmor frequency and is equal to about 43 MHz per tesla (T); tesla is the SI unit of the magnetic field strength. For 1.5 and 3 T fields (the most common in clinical practice) the Larmor frequency is 64 and 128 MHz, respectively, which is in the radiofrequency range (i.e. the frequency range in the electromagnetic spectrum which consist of radio

waves).

The signal used to form the MRI image arises due to the hydrogen nuclei absorbing energy from the MRI scanner then reemitting energy which is detected. A large magnet is used to align the magnetic moments of the hydrogen atoms (Fig. 9.3a). A coil transmitting in the radiofrequency range is used to change the direction of magnetisation of the protons (Fig. 9.3b). The degree of tilt of the magnetic moment depends on the duration and amplitude of the RF pulse. Only those nuclei precessing at the same frequency as the RF frequency are affected (hence the term 'resonance' in MRI). Once the RF pulse is switched off the nuclei will gradually return to their original magnetisation (Fig. 9.3c–f). In energy terms the protons are pushed into a higher energy state by the RF pulse. Once the RF pulse is switched off they transition ('relax') to a lower energy state and in the process emit energy. This energy is detected by the MR system, and this forms the MR signal; which is used to produce the MR image.

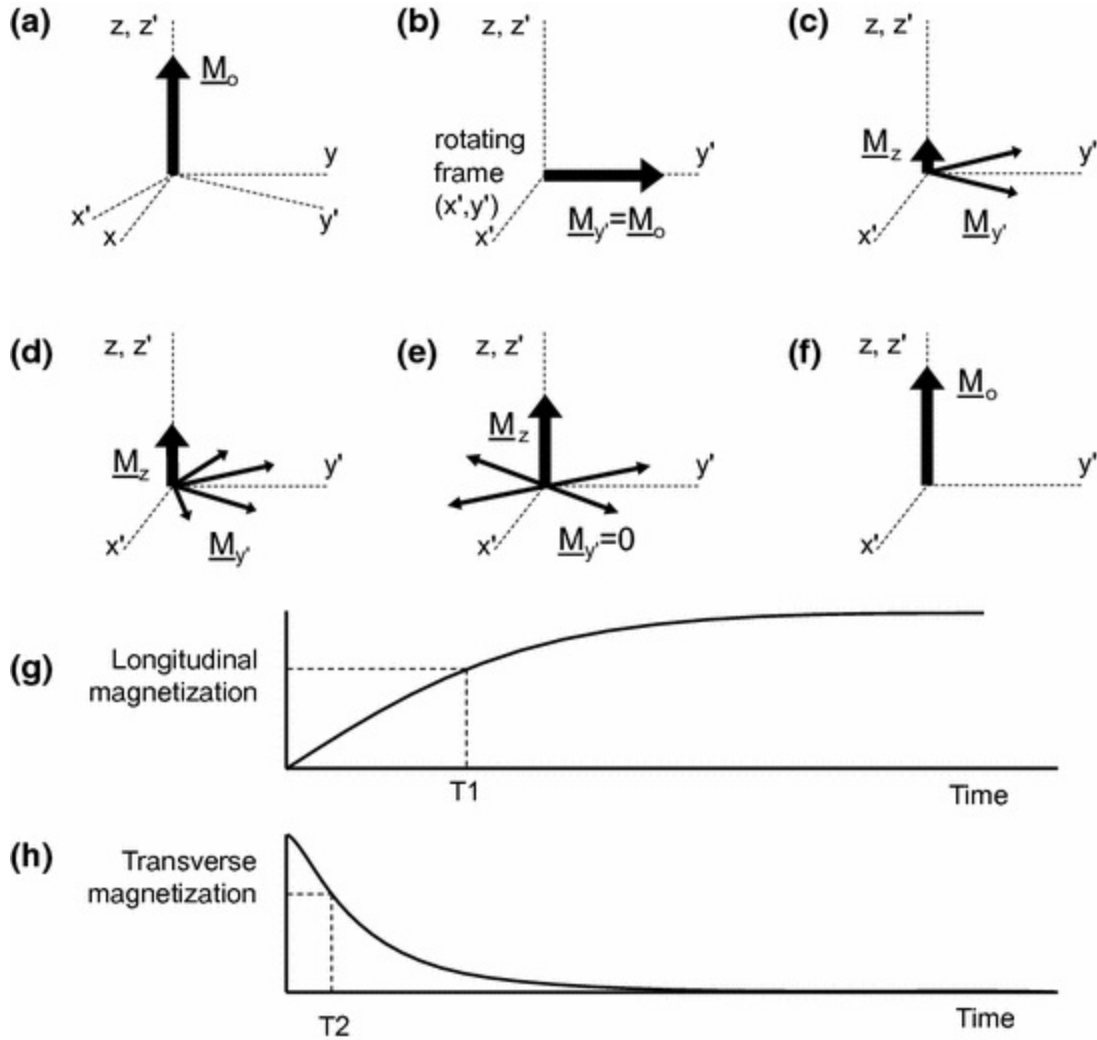


Fig. 9.3 RF pulse and subsequent relaxation. **a** The magnetic moment M_0 is aligned with the main magnetic field. **b** an RF pulse cause a 90° shift in alignment and the magnetic moment precesses; this is taken into account by the use of a rotating (x', y') frame of reference. **c–f** The longitudinal magnetization M_z gradually recovers to its full strength while the transverse magnetization M_y gradually dephases and reduces to zero. **g–h** Change in longitudinal and transverse magnetization with time

The detected signal is the composite of many individual protons relaxing. During relaxation, the magnetisation recovers in the direction of the magnetic field (T_1 or spin-lattice relaxation) (Fig. 9.3g) and decays transverse to the field (T_2 or spin-spin relaxation) (Fig. 9.3h). The T_1 relaxation time is the time for the longitudinal magnetization to achieve 63 % of its equilibrium value. T_1 is a measure of the rate of energy exchange between the protons and the neighbouring molecules. The T_2 relaxation time is the time at which there is 37 % loss of the original transverse magnetization. T_2 is a measure of

the rate of decay of the transverse magnetization. T2 relaxation is associated with gradual loss of phase coherence of the protons. After the initial RF pulse the magnetic moments of the protons are all in phase. Gradually these become out of phase as a result of T2 relaxation. T1 and T2 have different values for different tissues and this provides the principle image contrast in MRI, along with the MRI signal strength which is related to the number of protons imaged (proton density). Values of T1 and T2 in tissues are provided by Selwyn (2014); see Table 12.3. Generally T1 values are longer than T2 values (for the same tissue) by a factor of 10–20.

Operating principles. The MRI scanner usually consists of a large magnet in the shape of a tube capable of generating field strengths of 1.5 or 3 T. The patient is positioned within the magnet. The magnetic field affects the alignment of the hydrogen nuclei so as to produce a net magnetisation along the direction of the field. A transmitting RF coil is used to tilt the magnetic moment of the hydrogen nuclei. When the alternating field is switched off the proton magnetic moments relax to their equilibrium orientation, emitting energy. This energy is detected by receiving coils positioned around the patient. Positional information is obtained by the use of gradient coils. These produce a smooth change in magnetic field strength and hence in Larmor frequency along different directions within the magnet bore. Gradient magnetic fields are switched on and off as needed during the image acquisition process. Information on spatial location is therefore encoded into the received signal because of these differences in Larmor frequency. There are three gradient coils; one for each direction; x , y and z . A full account of spatial encoding in MRI is beyond the scope of this book. However, the process allows acquisition of image slices in any orientation within the magnet bore, and of 3D as well as 2D data sets. These are very useful capabilities for cardiovascular imaging, as they allow for example acquisition of images aligned with the long and short axes of the left ventricle.

The series of radiofrequency pulses and gradients employed during MR image acquisition is known as a ‘pulse sequence’. Different sequences produce images with a variety of geometrical, temporal and contrast properties, and development of new pulse sequences remains a very active research area. It is possible, for example, to produce images of the heart in which blood appears dark (‘black blood imaging’) or bright (‘bright blood imaging’), and these have different clinical applications. It is also possible to image the beating heart in real time (‘MR fluoroscopy’) and to produce

images that are sensitive primarily to flowing blood ('MR angiography'). Contrast agents used in MRI are chosen for their magnetic properties, rather than for high atomic number as in the case of X-ray imaging. These contrast agents can be particularly useful in MR angiography, but also for assessment of myocardial perfusion and viability (see also Sect. 9.1.5). There are also a variety of quantitative MR methods, such as mapping of T1 and T2 relaxation times which has recently undergone something of resurgence particularly for the investigation of diffuse cardiac disease.

9.1.3 Ultrasound

Essential physics: Ultrasound for medical diagnostic use consists of high frequency sound waves in the frequency range 2–20 MHz. Ultrasound is generated by a transducer which is in contact with the patient and the waves pass into the patient along a thin beam. The waves are scattered by the tissues, with some of the energy returning back to the transducer where the waves are detected. The depth D from which the scattered ultrasound arises is calculated from the time T_R between transmission and reception, assuming that the speed of propagation c is 1540 m s^{-1} (Eq. 9.1). This is called the pulse-echo technique (Fig. 9.4).

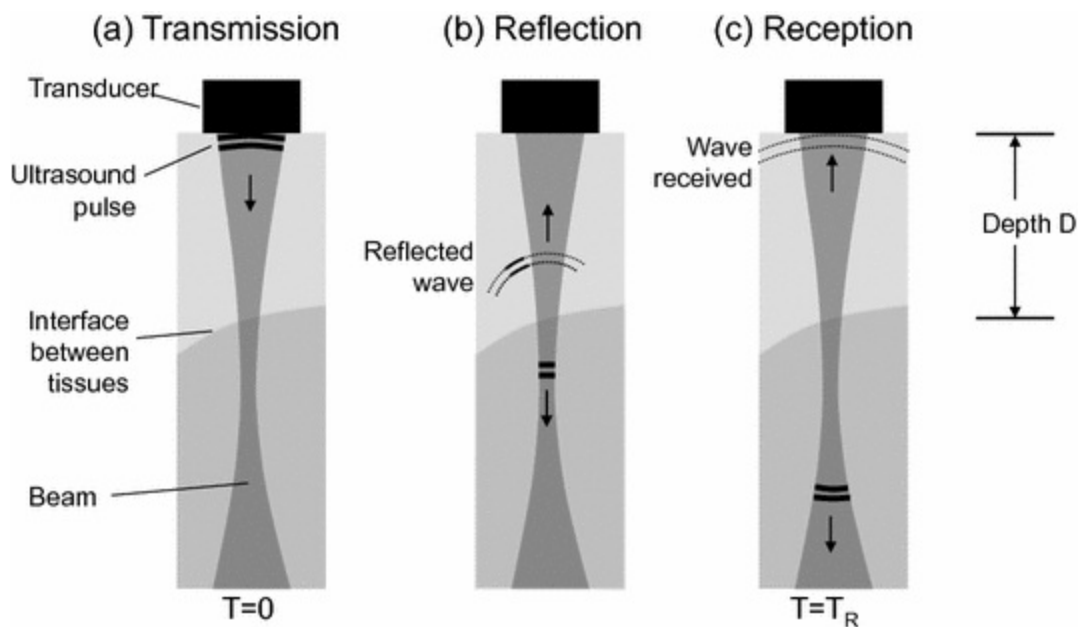


Fig. 9.4 The pulse-echo technique for ultrasound using a simplified model of 2 tissues. **a** Transmission. An ultrasound is transmitted by the transducer at time zero. The pulse travels along a well defined beam. **b** Some of the acoustic energy is reflected at the interface between the tissues and

travels back along the beam. **c** The reflected ultrasound is detected by the transducer and the machine notes the time (T_R). The ultrasound machine calculates the depth D from which the echoes arose as the speed of sound (assumed to be 1540 m s^{-1} multiplied by $T_R/2$)

$$D = cT_R \quad (9.1)$$

The amplitude of scattered ultrasound is determined by local differences in acoustic impedance within the tissues. These differences are especially high at the boundaries of organs resulting in high amplitude scattering.

Image formation: The amplitude of the received ultrasound is displayed in grey scale on the image; called a B-mode (brightness mode) image. The transducer sweeps the beam through the tissues and the image is built up line by line (Fig. 9.5). A 2D image typically is collected in 15–50 ms which is equivalent to 20–70 frames/second. This frame rate is sufficiently high for the image display to appear in real time. Higher frame rates can be achieved by collecting several scan lines simultaneously.

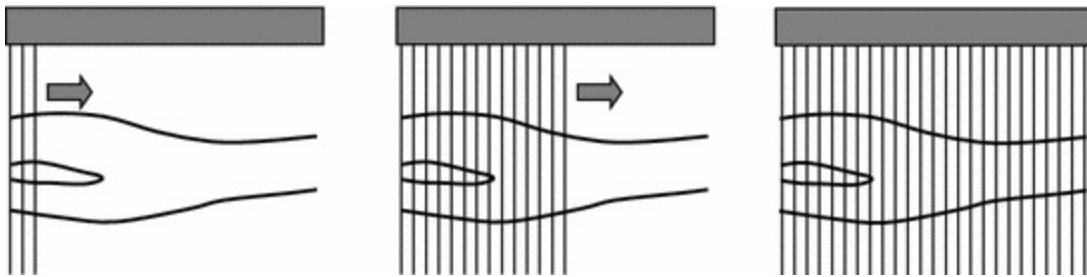


Fig. 9.5 Building up a single ultrasound frame line by line

Most ultrasound in clinical practice is based on the acquisition of real-time 2D images as described above. It is also possible to collect 3D ultrasound data (Prager et al. 2010; Fenster et al. 2011). This may be achieved through collection of a series of 2D images which from a technical point of view is the easiest way. The existing transducers for 2D scanning are adapted to enable them to collect 3D data. Typically this involves mechanical oscillation of the transducer to and fro to build up the 3D image. Dedicated transducers designed specifically for 3D imaging are able to steer the ultrasound beam within a 3D volume enabling collection of 3D data without the need for mechanical components. Using a single-beam system the number of volumes collected is low at 1–2 per second. Applications where real-time visualisation of 3D movement is required include cardiac scanning. Commercial ultrasound systems for cardiac scanning can achieve over a

hundred volumes per second by simultaneous collection of many scan lines simultaneously.

Doppler ultrasound: Information on motion of blood may be obtained by Doppler ultrasound. The Doppler effect is familiar within everyday living; it is the difference between the transmitted and perceived frequency of sound when there is motion of either the source or the observer. An everyday example is the change in pitch of the siren from an ambulance as it passes the observer. In ultrasound if the transmitted ultrasound has a frequency f_t and the tissue is moving with a velocity v then the ultrasound received by the transducer will have a slightly different frequency f_r . The difference in frequency ($f_r - f_t$) is called the Doppler shift f_d . The Doppler shift is related to the velocity and the direction of motion as illustrated in Fig. 9.6 and shown in Eq. 9.2.

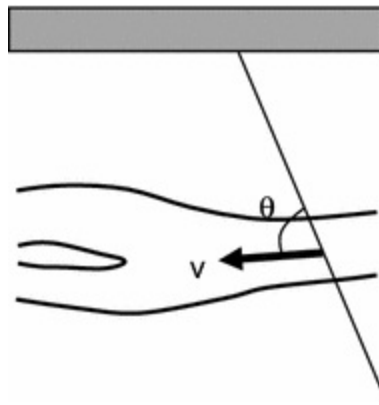


Fig. 9.6 Schematic for Doppler ultrasound estimation of blood velocity. Blood of velocity v travels in a direction which makes an angle θ with respect to the Doppler beam

$$f_d = \frac{2f_t v \cos \theta}{c} \quad (9.2)$$

$$v = \frac{c f_d}{2f_t \cos \theta} \quad (9.3)$$

where θ is the angle between the Doppler beam and the direction of motion.

The Doppler shift can be used to measure velocity of the tissues (Eq. 9.3). This requires measurement of the Doppler frequency shift f_d and of the angle θ . Commercial systems adopt 2 main display modes which use Doppler shift data. Spectral Doppler is a real-time display of Doppler frequencies versus

time from blood flow; essentially this is the time–velocity waveform. Colour flow is a real-time display of the pattern of blood flow with the mean Doppler frequency displayed at each pixel.

Endoscopy: In clinical practice the vast majority of ultrasound examinations involve the use of transducers placed on the skin, so-called transcutaneous imaging. It is also possible to collect ultrasound images from inside the patient. Intravascular ultrasound involves a miniature ultrasound system at the distal end of a catheter inserted in the blood stream via an arterial puncture, and is described in the section on ‘catheter based imaging’ (9.1.7). An endoscope is a long flexible instrument which is inserted into a body orifice such as the oesophagus for examination of the tissues from the inside. An ultrasound transducer may be incorporated at the distal end of the endoscope allowing ultrasound imaging of the tissues. For cardiovascular imaging the most widespread endoscopic technique is TOE or transoesophageal echocardiography. The oesophagus passes very close to the heart, so that very high quality cardiac images can be obtained using TOE compared to transcutaneous imaging. Clinically TOE is most commonly used to help guide surgical procedures such as cardiac valve replacement and in haemodynamic monitoring during surgery.

9.1.4 Gamma Camera Imaging and Positron Emission Tomography

The term ‘nuclear medicine’ refers to techniques used to diagnose and treat clinical disorders using radioactive isotopes. The two main imaging techniques in nuclear medicine are gamma camera imaging and positron emission tomography (PET). Both of these imaging techniques involve the injection or inhalation of radioactive chemicals containing a radioactive atom. The radioactive atoms subsequently decay resulting in the production of gamma rays (high energy electromagnetic particles). It is the detection of the gamma rays which forms the basis for imaging in gamma camera imaging and PET.

Radioisotopes used in nuclear medicine have short half-lives so do not occur naturally. Some, particularly those used in PET, are produced in a cyclotron. If there is no on-site cyclotron then radioisotopes must be transported from the cyclotron to the nuclear medicine department where the imaging takes place. In some cases a parent radioisotope is produced with a

relatively long half-life which decays into the isotope of interest; this is referred to as a ‘generator’. By far the most common radioisotope used in gamma camera imaging is technetium 99m (or Tc-99m) which has a half life of 6 h. In practice a molybdenum-99 generator is produced; Mo-99 is a fission product from nuclear reactors and has a half life of 66 h and decays to Tc-99m allowing Tc-99m to be drawn off over a period of several days. Tc-99m may be bound to several different molecules and used for imaging of different organs (e.g. lung, bone, heart, liver, thyroid). Other isotopes used in gamma camera imaging include iodine (I-123 or I-131) for thyroid imaging, indium (In-111) for white cell imaging and gallium (Ga-67) for imaging of inflammation. Typical radioisotopes used in PET are oxygen (O-15), carbon (C-11), nitrogen (N-13) and fluorine (F-18). These have short half-lives of 2–100 min. These radioisotopes may be used unaltered in PET or they may be incorporated into molecules for use in scanning; for example water (O-15), ammonia (N-13), acetate or carbon dioxide (C-11) and, the most commonly used PET tracer, fluorodeoxyglucose (FDG) (F-18).

In gamma camera imaging gamma rays from the patient are detected one gamma ray at a time using a 2D detector (Fig. 9.7a). Over time, typically a few minutes, an image is built corresponding to the distribution of radioactivity within the patient. If the camera is rotated around the patient then the data acquired may be used to generate a 3D image in a similar manner to CT scanning; this is called SPECT (single-photon emission computed tomography) (Fig. 9.7b). The article by Rahmima and Zaidib (2008) compares PET and SPECT.

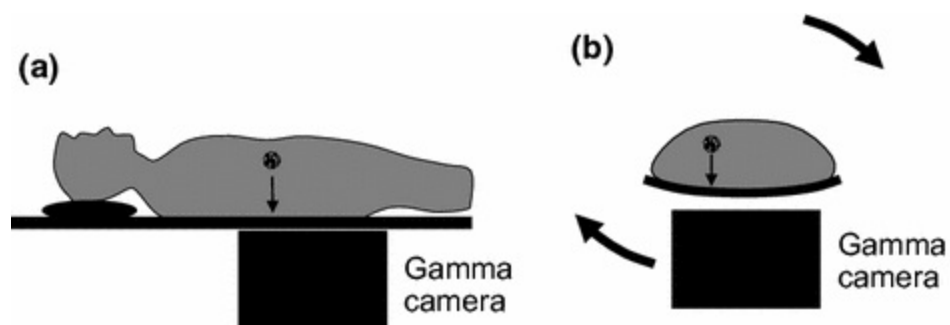


Fig. 9.7 **a** Gamma camera imaging; radionuclides in the patient decay producing gamma rays which are detected by the camera. **b** SPECT; the gamma camera is rotated around the patient and from the acquired data a 3D reconstructed image is produced

In PET, the decay of each radioactive atom produces a positron. The

positron is the anti-particle of the electron so has a positive charge. The positron travels for a short distance from its point of creation gradually slowing down until it collides with an electron. The mass of the positron and electron is completely converted into energy ('annihilation') resulting in the formation of two gamma rays which travel in opposite directions (Fig. 9.8a). In PET the gamma ray pair is detected by sensors which surround the subject (Fig. 9.8b). A line may then be drawn between the two detection points and the gamma rays must have originated somewhere along this line. Data is collected over many millions of annihilation events and is reconstructed in the computer in a similar manner to CT imaging to obtain a 2D cross-sectional image of the number of events occurring at each location within the image. In practice a 3D dataset is collected. A whole body dataset may be collected if the patient/volunteer is passed slowly through the detectors. Typical scan times are 20–60 min. The distance the positron travels before annihilation is 1–3 mm. This places an inherent limitation on the accuracy of localisation of the origin of the positron, and hence on the achievable spatial resolution which is typically 4–6 mm in the human. In practice a low radiation dose PET scan is followed immediately by a CT scan (delivered within the same imaging system) for the purposes of attenuation correction and localisation of PET uptake to local anatomy.

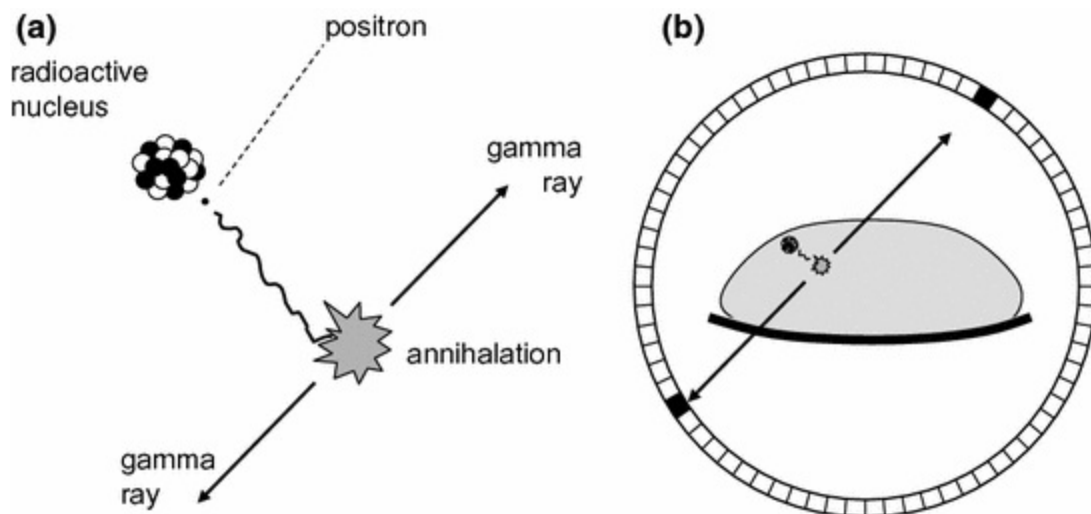


Fig. 9.8 Principles of PET imaging. **a** A radioactive nucleus decays releasing a positron. This travels a short distance then collides with an electron undergoing annihilation and two gamma rays are produced which travel in opposite directions. **b** In a patient a radioactive nucleus decays and the gamma rays are detected by the detector

9.1.5 Contrast Agents for Ultrasound and MRI

The term 'contrast agent' is used to refer to a material which when injected into the patient provides a significant change (increase or decrease) in the imaged quantity enabling improved visualisation of particular structures; or in other words an agent which improves image contrast. Often a contrast agent is simply associated with an increase or decrease in received signal strength. Contrast agents for X-ray imaging were noted above where an iodinated compound is injected into the vascular system to enable visualisation of arteries and veins, and where barium is swallowed by mouth or pumped into the rectum to enable visualisation of the gastrointestinal system.

Ultrasound contrast agents. For ultrasound, contrast agents are based on microbubbles (Fig. 9.9) (Sboros 2008). These are spherical consisting of a gas encapsulated by a thin shell. These are usually injected into a vein in the arm; they pass through the lung capillary bed; enter the systemic arterial system and travel to the organ of interest where they are imaged using ultrasound. Microbubbles are commonly manufactured with diameters in the range 2–6 μm in order that they can pass through the capillaries in the lung. The behaviour of the microbubble in the acoustic field depends on the peak acoustic pressure (Fig. 9.10). At low pressure the bubble behaves in a linear manner with small oscillation. At higher peak pressure the bubble will oscillate with non-linear motion including resonance. This non-linear motion induces additional (harmonic) frequencies in the scattered ultrasound. At very high peak pressure the bubble shell will burst. A number of display modes are designed to take advantage of these different behaviours; examples are as follows.

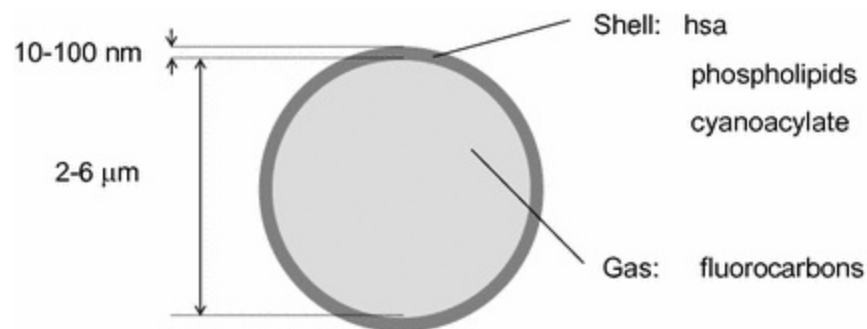


Fig. 9.9 An ultrasound contrast agent

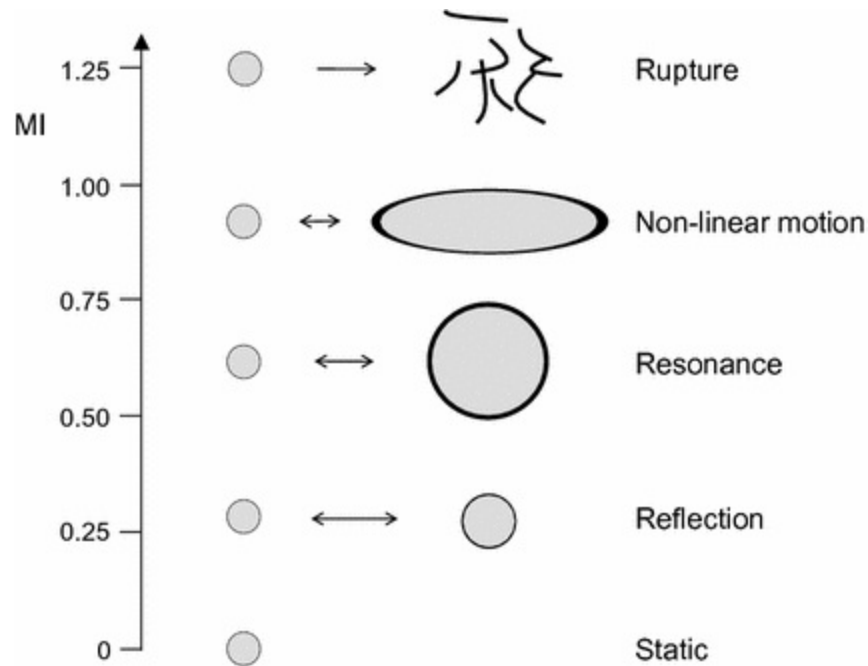


Fig. 9.10 Behaviour of an ultrasound contrast agent with increasing acoustic power

- *Non-linear imaging.* Intermediate acoustic pressure is used which induces bubble resonance and non-linear behaviour. The scattered ultrasound contains harmonic frequencies which are detected and displayed.
- *Destruction imaging.* After injection of contrast agents, low acoustic pressure is used and bubble concentration increases. A high pressure acoustic pulse (flash pulse) is swept across the field of view destroying all bubbles. The bubble destruction causes small changes in the detected acoustic field which can be detected (e.g. appearing as a pseudo Doppler effect). Quantification of acoustic intensity after the flash pulse may be used to estimate local perfusion.

MRI contrast agents. MRI contrast agents are based on heavy metals such as gadolinium or iron (Strijkers et al. 2007; Bashir et al. 2015). These operate by reducing one of the relaxation times, T1 or T2. Gadolinium-based contrast agents are low molecular weight molecules such as Gd-DTPA (Magnevist) and Gd-DOTA (Dotarem). Gadolinium is strongly paramagnetic and leads to relaxation of nearby protons resulting in a fall of T1. Iron based contrast agents are usually in the form of superparamagnetic iron oxide (SPIO) particles with a core diameter of 4-50 nm. These are classified according to

size; ultrasmall SPIO (USPIO) with diameter of 10–40 nm, SPIO nanoparticles (50–200 nm) and micron-sized particles of iron oxide (MPIOs) (0.75–1.75 μm). These contain many thousands of iron atoms which are magnetised by the MRI field. This results in a relatively large local magnetic moment, which in turn produces strong local field gradients resulting in loss of phase coherence in surrounding protons and a lowering of T2 (Fig. 9.11). In addition to conventional contrast-enhanced imaging and MR angiography, gadolinium-based MR contrast agents can be used for quantitative imaging of blood perfusion in tissues by injecting a bolus of contrast agent and using rapid imaging to track changes in signal intensity as the agent washes through the tissue. MR perfusion imaging can be used to assess myocardial perfusion, including stress testing. Gadolinium-based agents are also used in assessment of myocardial viability, for example following an infarct.

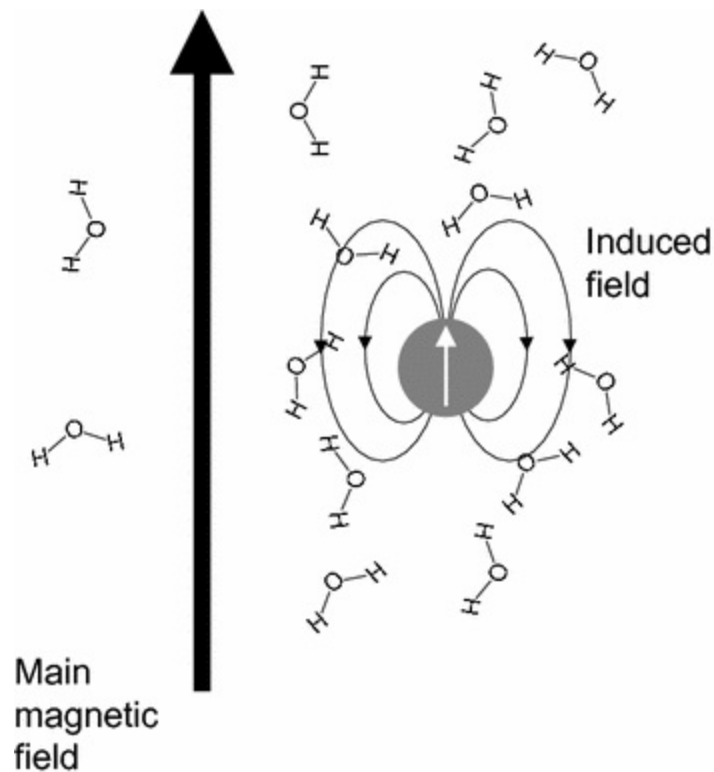


Fig. 9.11 Mechanism of reduced T2 relaxation due to iron oxide particles. The main magnetic field magnetises the iron atoms and there is an associated induced field which causes dephasing of hydrogen nuclei and reduction in T2

Targeted contrast agents for MRI and ultrasound. A targeted contrast agent is one which will bind to specific biological sites (Huang 2008;

Gessner and Dayton 2010). For both MRI and ultrasound agents this has been achieved through a bridging construct. At one end of the bridge is attached the contrast agent. At the other end of the bridge is attached a molecular probe such as an antibody, a peptide or a polysaccharide. These will attach to cells on the vascular wall which have receptors for these probes. In the context of MRI, targeted agents are beginning to be used to visualise a range of physiological and pathological processes, including inflammation and apoptosis.

9.1.6 Comparison of Medical Imaging Systems

A brief comparison is presented in this section of the different imaging systems, focussing on 3D capability (Table 9.1).

Table 9.1 Comparison of 3D medical imaging systems, data is given with reference to an abdominal scan

	CT	MRI	3D ultrasound	SPECT	PET
Typical capital cost	£200k	£1.2 million	£100k	£300–500 k	£2–3 million
Imaged quantity	X-ray attenuation coefficient	Proton density, magnetic relaxation times	Acoustic impedance	Tracer concentration	Tracer concentration
Full body cross section	Yes	Yes	No	Yes	Yes
Spatial resolution (mm)	0.4–0.8 mm; x, y, z	1 mm x, y; 2–5 mm z	1 mm x, z; 2 mm y	10 mm	4–6 mm
Acquisition time 1 volume	3–5 s	15–20 min	0.1 s	30 min	30 min
Real-time mode (guidance in intervention)	No	Yes	Yes	No	No
Ability to image perfusion	Yes	Yes	Yes	Yes	Yes
Ability to image biological processes	No	Yes	Yes	Yes	Yes
Radiation dose	Yes	No	No	Yes	Yes
Patient acceptance (%)	99–100	95	99–100	99–100	99–100

2015 Guide price for; 64 slice CT, 3T MRI, high-end ultrasound, PET-CT

CT, SPECT and PET are examples of photon-limited imaging systems. These rely on acquisition of a large number of photons in order to produce a low noise image; the larger the number of photons, the lower the image noise. The acquisition time is determined by the minimum number of photons which must be detected in order to produce an image with noise below a certain threshold. This results in long imaging times for PET in particular. In CT the X-ray tube can generate a very large number of X-ray photons per unit time so short imaging times are achievable. Ultrasound is not based on imaging of photons. Ultrasound images have a structured noise called 'speckle' which is independent of imaging time. The noise arises as an interference pattern from scattering of ultrasound within the ultrasound beam. In MRI, image quality is limited ultimately by the fact that the magnetisation induced in the patient's body by the static magnetic field is very small, so relatively long imaging times are needed to achieve sufficient signal to noise (SNR). There is a trade off between SNR and other performance parameters such as temporal and spatial resolution. Good pulse sequence design can optimise SNR subject to other constraints, and high field strength magnets result in a larger magnetisation vector which explains the trend from 1.5 to 3 T and now to 7 T in some research applications.

When quoting spatial resolution it should be noted that there are three different values along the x , y and z axes. For 2D MRI the resolution in the cross-sectional (x , y) plane is typically 1 mm, however the slice thickness is more typically 3–5 mm. In this case the voxel (the unit element of an image) is long and thin. For ultrasound the axial resolution for abdominal imaging is also around 1 mm, but the lateral and elevation resolutions are 2–3 mm. CT systems have the same resolution in all directions (isotropic) at 0.4–0.8 mm. PET has a much lower spatial resolution of 4–6 mm.

Both PET and CT use ionising radiation and are associated with a radiation dose to the patient. There is a small but quantifiable risk of cancer induction. The use of CT and PET must therefore be justified medically, and the dose received optimised relative to the clinical information obtained. Repeated use of CT and PET is generally avoided unless the medical benefit outweighs the risk from radiation. MRI and ultrasound are classified as non-invasive in that there is no known long-term damage to tissues arising from the imaging (although MRI in particular has some short-term hazards that are well understood and well managed in clinical practice). This makes MRI and ultrasound more suitable for repeated follow up studies and for use in

volunteers. There are contraindications for the use of MRI due to the effect of the strong magnetic field on metals. Patients with most pacemakers and surgical clips are precluded.

In terms of patient acceptance this is close to 100 % for CT, ultrasound and PET. A large minority of patients, some 5–10 %, experience claustrophobia in an MRI scanner and cannot be imaged (although specially designed open MRI systems may be suitable).

In general there is no perfect imaging system and the imaging system is chosen which best matches either the clinical question or the research need.

9.1.7 Catheter-Based Imaging—IVUS and OCT

In catheter-based imaging, a miniature imaging system is mounted on the end of a catheter which is passed along the arterial system to the point of interest. Two imaging methods have been used in research and are emerging into clinical practice; intravascular ultrasound (IVUS) and optical coherence tomography (OCT). This section briefly describes these two invasive imaging modalities.

An IVUS system produces a cross-sectional image of an artery using a high frequency ultrasound transducer mounted on the distal end of a catheter. The principles of construction of a B-mode image are the same as for clinical imaging involving the pulse-echo technique and building up the image line by line. Typically the IVUS transducer produces frequencies in the range 20–60 MHz, much higher than for clinical use. In ultrasound imaging the spatial resolution is inversely proportional to the frequency; a 10-times increase in frequency results in a 10 times improvement in spatial resolution. Whereas, the spatial resolution (along the beam axis) of a clinical transducer operating at 5 MHz is around 0.5 mm, the spatial resolution of an IVUS transducer operating at 50 MHz is around 50 μm . IVUS imaging therefore produces the most detailed images of any ultrasound technique (Fig. 9.12a). The simplest and most widely used transducer design consists of a single-element attached to the side of the catheter. The catheter is rotated (using an external drive) and the beam is swept around in a circle. An array transducer consisting of a number of elements wrapped around the catheter allows sweeping of the beam in a circle without rotation of the transducer. 3D images may be collected by gradual pullback of the catheter. Analysis of the RF data allows different types of plaque components to be distinguished (Nair et al. 2002). In commercial use this is called ‘virtual histology’ (Volcano, Sand Diego,

USA).

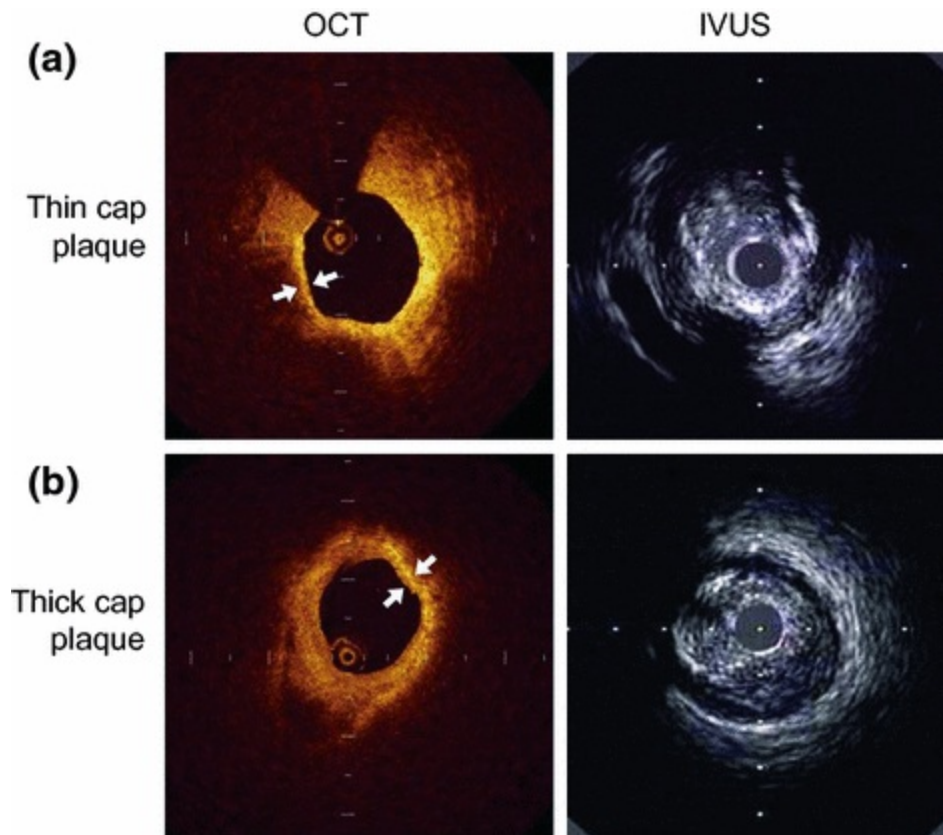


Fig. 9.12 Catheter-based imaging of arteries using OCT and IVUS. **a** thin-cap plaque. **b** Thick cap plaque. From; Maejima N, Hibi K, Saka K, Nakayama N, Matsuzawa Y, Endo M, Iwahashi N, Okuda J, Tsukahara K, Tahara Y, Kosuge M, Ebina T, Umemura S, Kimura K; Morphological features of non-culprit plaques on optical coherence tomography and integrated backscatter intravascular ultrasound in patients with acute coronary syndromes; *European Heart Journal - Cardiovascular Imaging*. 2015;16(2):190–197; paper published on behalf of the European Society of Cardiology; © The Author 2014, with permission from Oxford University Press

An OCT system uses infrared light to produce images. There is high absorption of light in tissue for the visible frequency range (violet-red). However infrared light in the wavelength range 650–1350 nm has low absorption and there is penetration of 2–3 mm in most tissues. The typical resolution of a catheter-based OCT system is 10–20 μm . It is noted that optical imaging in general (i.e. microscopy) is high resolution and this is the reason that high resolution is achievable using OCT. OCT operates in a similar manner to ultrasound in that the time of flight of light is estimated between transmission from the laser, scattering from the tissue and reception at the detector. As the speed of light is so large, it is not possible to measure

the time of flight directly. Instead an interference method is used to obtain time (and hence depth) information. This involves interference between the light scattered from the tissues and a reference beam; the details of the methodology and instrumentation are described in review papers (Fujimoto et al. 2000; Terashima et al. 2012). For use in arterial imaging the light source and the light detector are placed externally and light travels to and from the catheter tip along an optical fibre. Figure 9.12b shows a typical image obtained using an OCT system. The spatial resolution of OCT (10–20 μm) is by far the best of any medical imaging system.

Chapter 15 covers atherosclerosis and it is noted that plaque rupture occurs when the fibrous cap is thin and a critical thickness of 65 μm is noted. This is far lower than the best spatial resolution available for clinical imaging. It is at about the resolution limit of IVUS. It is only OCT with spatial resolution of 10–20 μm that has the ability to provide accurate measurements of a cap thickness of 65 μm .

9.2 Measurements and Applications

This section describes the measurements and applications that can be made using imaging systems, with examples drawn from cardiovascular applications.

9.2.1 Geometry and Motion

It was noted above that CT, MRI and ultrasound are principally structural imaging techniques; that is the images provide information about structure and geometry. The basic measurements related to structure are distance, area and volume; in other words measurements related to 1, 2 and 3 spatial dimensions. In addition there is change in geometry with time (4D).

1D. Information in 1D is mostly of interest in terms of measurement of distance. This may be performed manually in which the operator locates two points and the machine calculates the distance between the points. An example here is the measurement of the diameter of an artery. For an abdominal aortic aneurysm the maximum diameter as measured from ultrasound is used as the criterion for surgical repair; if the diameter is greater than 5.5 cm the patient is offered repair. The change in diameter with time may be measured automatically using ultrasound.

2D. Measurement of area requires the boundary of a structure to be identified. The process of boundary identification is called segmentation. This may be performed manually by the operator selecting points along the boundary which the machine will then join together, calculating the area prescribed by the points. Alternatively the boundary may be identified automatically by the machine. Examples of area measurement include the cross-sectional area of an artery, which may be used for estimation of volumetric blood flow from the product of cross-sectional area and mean velocity.

3D/4D. Segmentation of a 3D geometry can be undertaken manually. The volume is divided into a number of slices, the operator identifies points around each slice, and software is used to join the dots forming a surface. This is very time consuming for the operator. The use of automated segmentation for identifying the boundary is much preferred. If time-varying imaging data is available then a time-varying segmented geometry can be obtained. 3D surface geometries are required for patient-specific modelling (Chap. 11). 3D geometry data is used in heart scanning to visualise and make measurements on the left ventricle such as the change in volume with time (Fig. 9.13). Abnormal patterns of motion can be identified automatically from the segmented data.

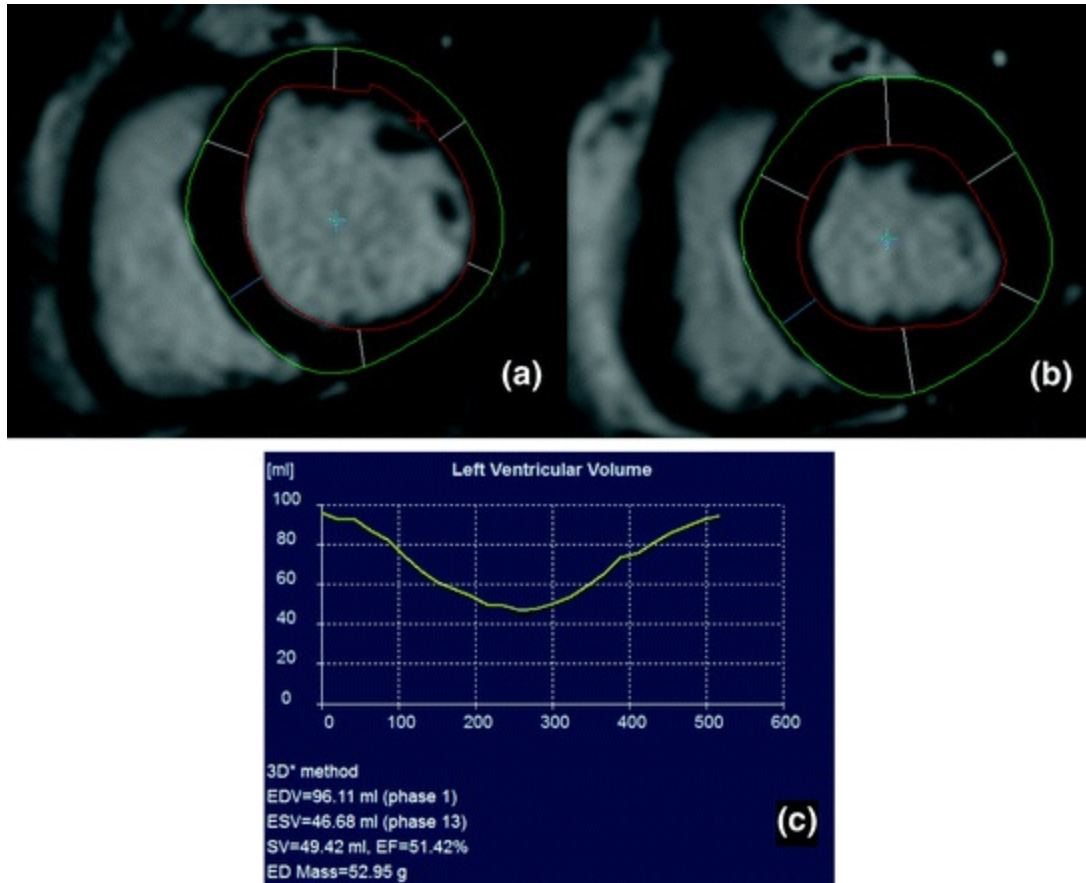


Fig. 9.13 Measurement of ventricular volume with time from CT

9.2.2 Blood Velocity and Related Quantities

Information on blood velocity may be obtained from MRI and ultrasound. From velocity a number of other quantities may be estimated including volumetric flow and wall shear rate. A complex flow field, such as occurs in for example the carotid bifurcation, is fully described by three spatial components (x, y, z), three velocity components (v_x, v_y, v_z) and one time component, which is seven components in all. Imaging of all seven velocity components is rarely undertaken. In practice measurement of some much reduced subset is undertaken as described below.

Ultrasound. Commercial ultrasound systems are limited in their ability to measure velocity (Hoskins 2011). The main measurement is the maximum velocity as a function of time from spectral Doppler (Fig. 9.14). Other measurements are made using a number of assumptions. The principle assumptions are that flow is axial (travels parallel to the vessel wall), the

vessel is straight and flow is fully developed (see Chap. 1). These assumptions describe a simple flow which is axisymmetric and where the maximum velocity is located at the centre of the vessel. Importantly the time-average velocity profile is parabolic from which it follows that the mean velocity (averaged over the cardiac cycle) is exactly half the maximum velocity (averaged over the cardiac cycle). Volumetric flow Q is calculated as the product of cross-sectional area A and time-averaged mean velocity $v_{mean-ta}$:

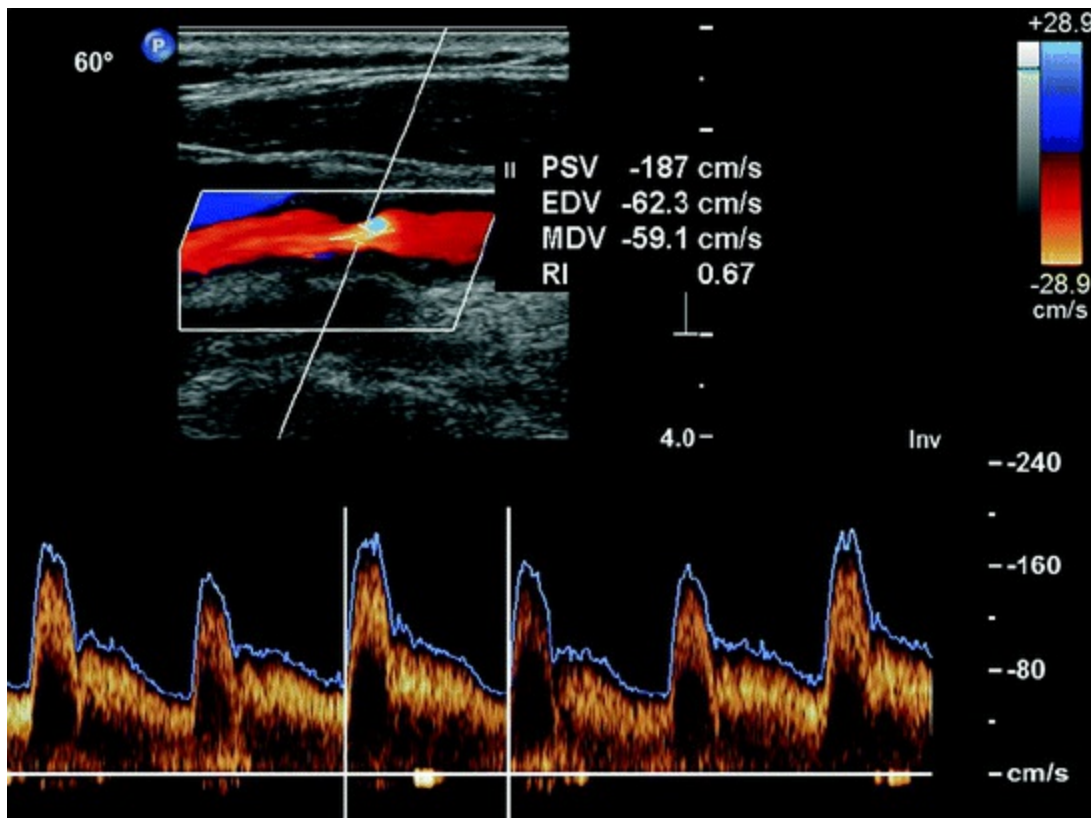


Fig. 9.14 Measurement of maximum velocity using spectral Doppler

$$Q = Av_{mean-ta} \quad (9.4)$$

Mean velocity $v_{mean-ta}$ is half the measured maximum velocity v_{max-ta} . Area is estimated from the diameter d measured from B-mode imaging. Time-averaged maximum velocity is measured from spectral Doppler. Volume flow is then measured according to Eq. 9.5.

$$Q = \frac{\pi d^2 v_{\max-ta}}{8} \quad (9.5)$$

With the assumption of parabolic velocity profile the mean wall shear rate $WSR_{mean-ta}$ over the cardiac cycle may be estimated using Eq. 9.6. The mean wall shear stress is then obtained by multiplying the mean wall shear rate by the viscosity (commonly assumed to be 3.5 or 4 mPa s).

$$WSR_{mean-ta} = \frac{4v_{\max-ta}}{d} \quad (9.6)$$

Estimation of time-varying wall shear rate and volumetric flow requires a slightly more complex approach, reported in Blake et al. (2008). The input data is again the maximum velocity obtained from spectral Doppler and diameter obtained from the B-mode image. The Womersley equations (Chap. 1) are used to estimate the change in velocity profile with time. From the velocity profiles the instantaneous wall shear rate and volumetric flow can be calculated.

In practice flow in main arteries is rarely fully developed (see Chap. 4) so that measurements of flow rate and wall shear rate above have errors. Dedicated ultrasound systems in the research literature have been used to estimate velocity profiles enabling measurement of wall shear rate and volumetric flow without the assumption of fully developed flow (reviewed in Hoskins 2012).

Spectral Doppler in commercial ultrasound systems is based on measurement of one velocity component; that along the ultrasound beam. Measurement of two or three velocity components is possible and involves the use of multiple beams (Hoskins 2015). This approach has been adopted commercially by BK Medical. This allows measurement of the time-varying velocity profile, from which volume flow may be estimated (Fig. 9.15). It is noted that this is five components; two spatial, two velocity and one time.

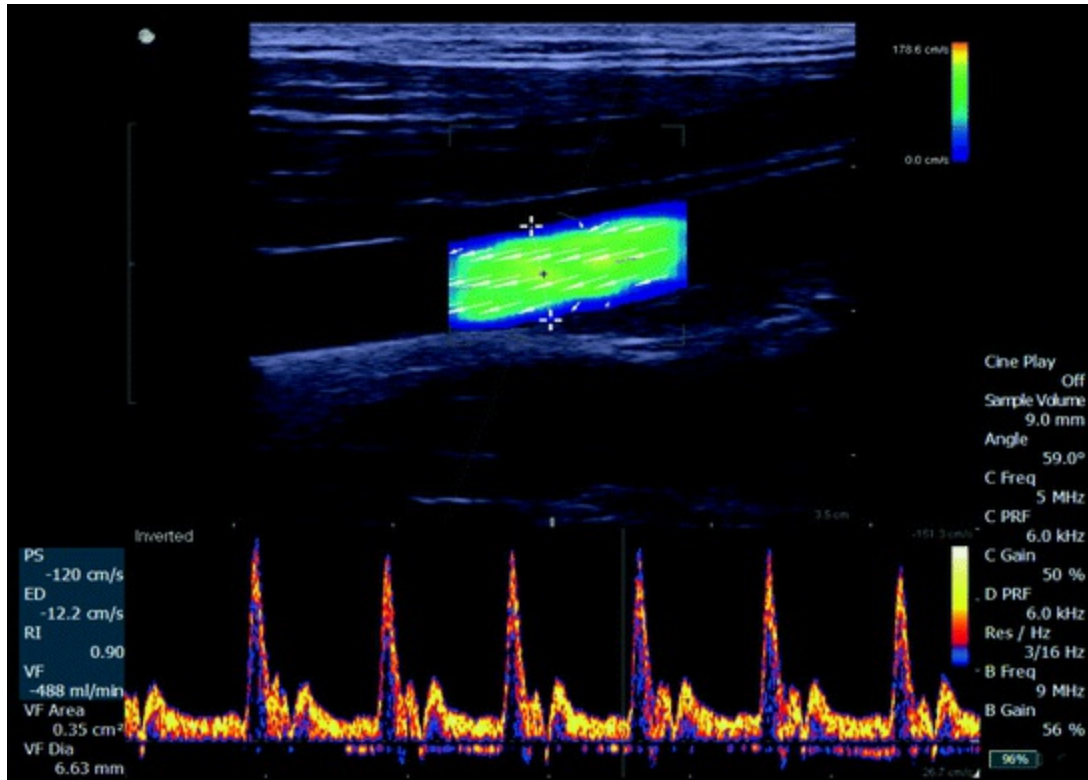


Fig. 9.15 Measurement of volumetric flow using the BK Medical system which displays true velocity magnitude. Image kindly provided by BK Medical

MRI. MRI systems have much increased flexibility for measurement of velocity compared with ultrasound. It is possible to acquire full 7D imaging through use of gated studies with measurements of v_x , v_y and v_z (Papathanasopoulou et al. 2003; Boussel et al. 2009; Markl et al. 2014; Stankovic et al. 2014). These techniques allow measurement of the 2D velocity profile as a function of time (Fig. 9.16) and visualisation of complex flow patterns, such as the helical flow of blood in the aorta (Fig. 4.13). Where 2D velocity profile data is available, flow rate is estimated as the sum of the velocity data over the cross-sectional area of the vessel (Olufsen et al. 2000).

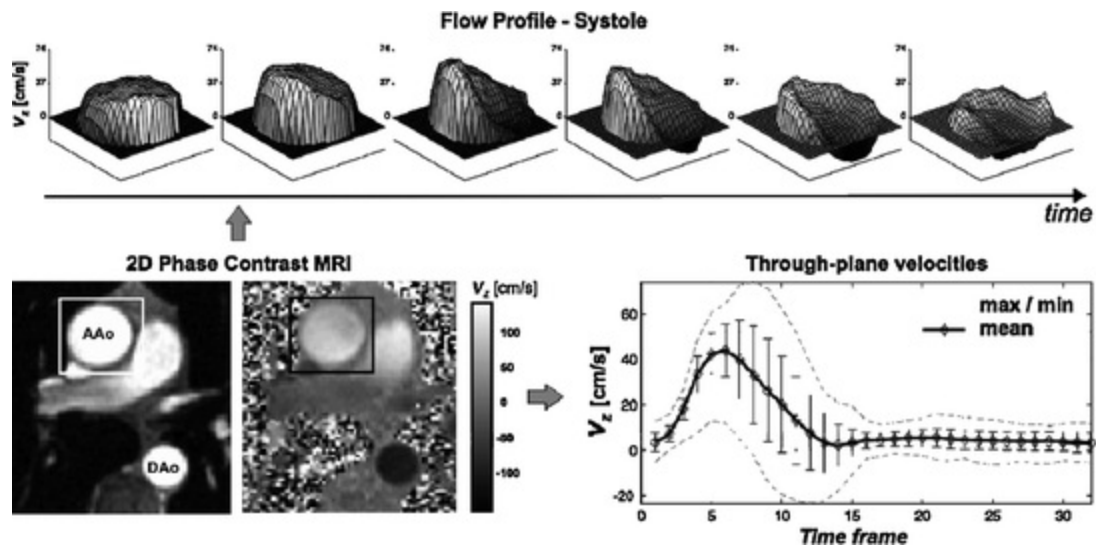


Fig. 9.16 Estimation of 2D velocity profiles using MRI. Reproduced with kind permission from Springer Science+Business Media: Markl M; Techniques in the assessment of cardiovascular blood flow and velocity. In: Kwong RY (editor); ‘Cardiovascular magnetic resonance imaging’: Totowa, NJ; Human Press Inc.; 2008, pp. 195–210; Fig. 6, © Humana Press Inc., Totowa, NJ

While MRI is able to estimate the 3D velocity field with good accuracy, estimation of wall shear rate in complex geometries is challenging for two reasons. The first reason is the difficulty in measuring low velocities near to the vessel wall. The second reason is estimation of the location of the wall. It has become common practice to use computational fluid dynamics to estimate the 7D flow field and wall shear stress as described in Chap. 11.

9.2.3 Strain

As noted in Chap. 1, strain is the fractional change in length following change in applied load. Strain imaging therefore is concerned with imaging of the fractional change in dimensions of tissues with change in load. Measurement of strain requires images taken before and after the load is applied. The images record the change in dimensions. Image processing is undertaken to estimate the local change in image dimensions, and then local strain is calculated. Strain imaging may be undertaken using MRI, CT and ultrasound as described below, with an emphasis on cardiovascular applications.

MRI. In myocardial tagging, specialised pulse sequences are used to magnetically tag the myocardium, and these tags can be tracked over the course of the cardiac cycle so that normal or abnormal motion can be

visualised and biomechanical parameters such as strain and torsion can be extracted (Dornier et al. 2004).

CT. 3D time-varying data from the aorta may be acquired allowing measurement of the change in vessel diameter and length through the cardiac cycle. This has been used to calculate the aorta circumferential and longitudinal strain (Morrison et al. 2009).

Ultrasound. There are two main strain-imaging techniques used in ultrasound based on use of geometry data (RF or B-mode) and the second based on the use of Doppler ultrasound. Comparison of two consecutive RF A-lines may be undertaken using cross-correlation techniques (Kanai et al. 2003). This allows estimation of local tissue displacements with an accuracy of 1–10 μm . It is noted that this is far below the typical axial spatial resolution of 300–600 μm . These and related techniques have been used to estimate strain within atherosclerotic plaque (Kanai et al. 2003). Cardiac strain imaging has been widely adopted in clinical practice. Typically Doppler tissue imaging provides information on local myocardial velocities. From the velocity field the velocity gradient is calculated and then from this the local strain is calculated. Following myocardial infarction local strain is reduced compared to normal myocardium. Cardiac strain imaging may also be undertaken by tracking of image points from the 2D B-mode data using a technique called ‘speckle tracking’ (Perk et al. 2007).

Strain imaging is also widely used in elastography which is concerned with the measurement of the stiffness of tissues (Hoskins 2012). The rationale here is that stiff tissues generally experience lower strain than soft tissues under the application of a load. However, strain is used only as a surrogate for stiffness, whereas true measurement of stiffness may be undertaken using shear wave elastography as described in the next section.

9.2.4 Stiffness

The measurement of the stiffness of tissues using imaging is referred to as elastography. We will consider shear wave elastography in this section; further consideration of elastography is given in Chap. 13. Shear waves are transverse waves (Chap. 1). These travel at relatively slow velocities in soft tissues of typically 1–20 m s^{-1} . There are four steps in the estimation of stiffness using shear wave elastography

1. Induction of shear waves.
2. Imaging of shear wave propagation through soft tissue.
3. Estimation of shear wave velocity c_s .
4. Conversion of shear wave velocity data to elastic modulus E using Eq. 9.7.

$$E = 3\rho c_s^2 \quad (9.7)$$

where ρ is the local tissue density (the manufacturers assume a value for density).

Approaches to shear wave elastography which have been adopted in ultrasound and MRI are described below.

9.2.4.1 Ultrasound Shear Wave Elastography

In commercial ultrasound systems induction of shear waves is performed through use of a high-power acoustic beam called a ‘pushing beam’. Ultrasound is associated with a radiation force in the direction of the beam. When a high-power beam is used this results in displacements of the tissue in the direction of the beam by 10–20 μm over a period of a few ms. This displacement is then transmitted through the tissues in the form of a shear wave. In practice several high-power pulses are generated, each focussed at a different depth within the beam. The result is a high amplitude shear wave which propagates further through the tissue. Following transmission of the pushing beam the ultrasound transducer switches into reception mode. The propagation of the shear wave is tracked by the ultrasound system. This requires an imaging frame rate of several thousand per second which is much higher than can be achieved in conventional B-mode imaging. The details of high frame rate imaging are beyond the scope of the current text; the interested reader is referred to Chap. 3 in Hoskins (2012) for further information. Equation 9.7 is used to estimate the Young’s modulus from the local shear wave velocity. Further reading is provided by Hoskins (2012) and Gennisson et al. (2013).

9.2.4.2 *Magnetic Resonance Elastography*

An external actuator is used to generate shear waves of frequency 100–500 Hz. The actuation device is designed with any metallic components located at a distance from the MRI magnet. A loudspeaker has been used to generate sound waves which are transmitted through a long pole which is attached to the subject via a flexible cuff. A more flexible arrangement is a pneumatic approach involving transmission of sound waves via an air column within a stiff pipe. Shear waves produced by the actuator travel through the tissues of the body.

Dedicated MRI pulse sequences are used to image the shear waves as they pass through the tissues and wave-inversion estimates local shear wavelength, and from this shear wave velocity. Local stiffness is then estimated using Eq. 9.5. Further reading is provided by Glaser et al. (2012) and Venkatesh et al. (2013).

9.2.5 *Functional Imaging in Cardiovascular Disease*

This section briefly describes applications of functional imaging systems in cardiovascular disease. Some of these techniques are still at the research stage and are yet to enter clinical practice. This is necessarily a brief and selective overview: readers are referred to more specialist literature for more information on these areas.

Perfusion. Quantitative measurement of local perfusion in units of $\text{ml min}^{-1} \text{g}^{-1}$ may be performed by PET using O-15 incorporated into water. Other imaging modalities provide images related to perfusion. The method most widely adopted in clinical practice is gamma camera imaging using Tl-201 whose uptake in the myocardium is proportional to local perfusion. Typically imaging is performed after some form of cardiac stress (e.g. exercise) and then again at rest, with the two patterns of uptake compared. As noted above contrast agents for MRI and ultrasound can also be used to image perfusion.

Myocardial architecture. Specialised MRI techniques provide unique windows on aspects of myocardial microstructure and mechanical function. Diffusion tensor imaging (DTI) permits non-invasive investigation of the muscle fibre architecture of the myocardium, which promises to be a useful clinical tool.

Inflammation. It is known that inflammation is a key component of cardiovascular disease. Inflammation is associated with high concentrations

of macrophages; these are a type of white cell that engulf and digest damaged or dead cells. Both PET and MRI have been used to image inflammation. PET imaging involves the use of F-18 in Fluorodeoxyglucose (FDG). FDG contains glucose which is taken up in higher concentration by highly metabolic pathologies such as inflammation or tumours. Increased uptake in atherosclerotic plaque is indicative of metabolic activity of macrophages (Tarkin et al. 2014) (Fig. 9.17). MR imaging of inflammation involves the use of USPIOs (ultrasmall paramagnetic iron oxide particles). In abdominal aortic aneurysms these are taken up by macrophages (Richards et al. 2011) (Fig. 9.18).

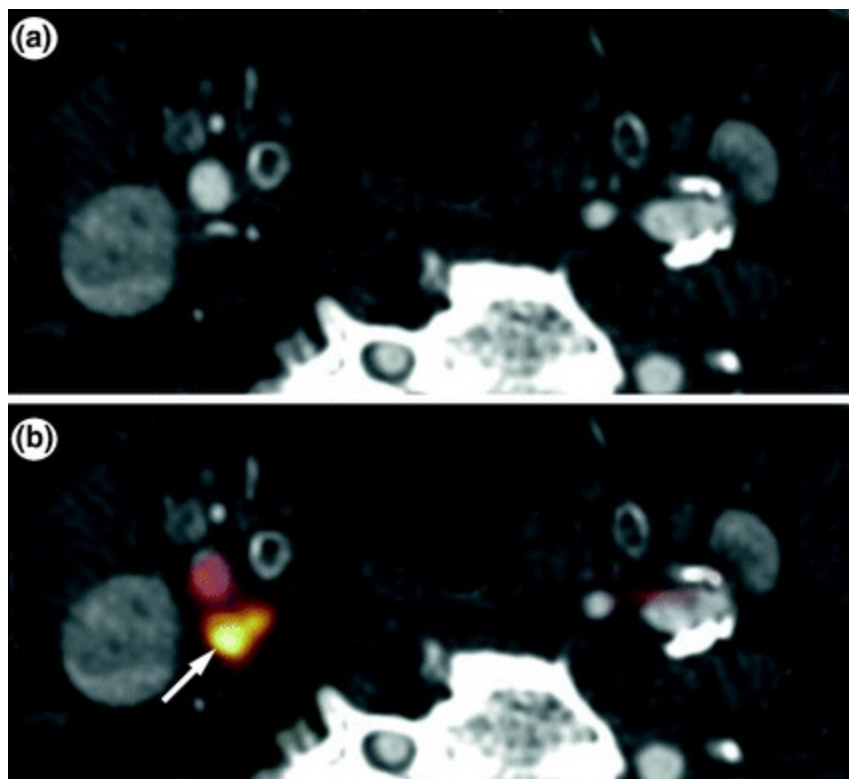


Fig. 9.17 PET FDG image of the carotid arteries. **a** CT angiogram. **b** 18F-FDG uptake (*arrow*) in the right carotid artery on fused 18F-FDG PET–CT images. From; Tarkin et al. (2014), © 2014 Macmillan Publishers Limited, with permission from Walters Kluwer Health, Inc.

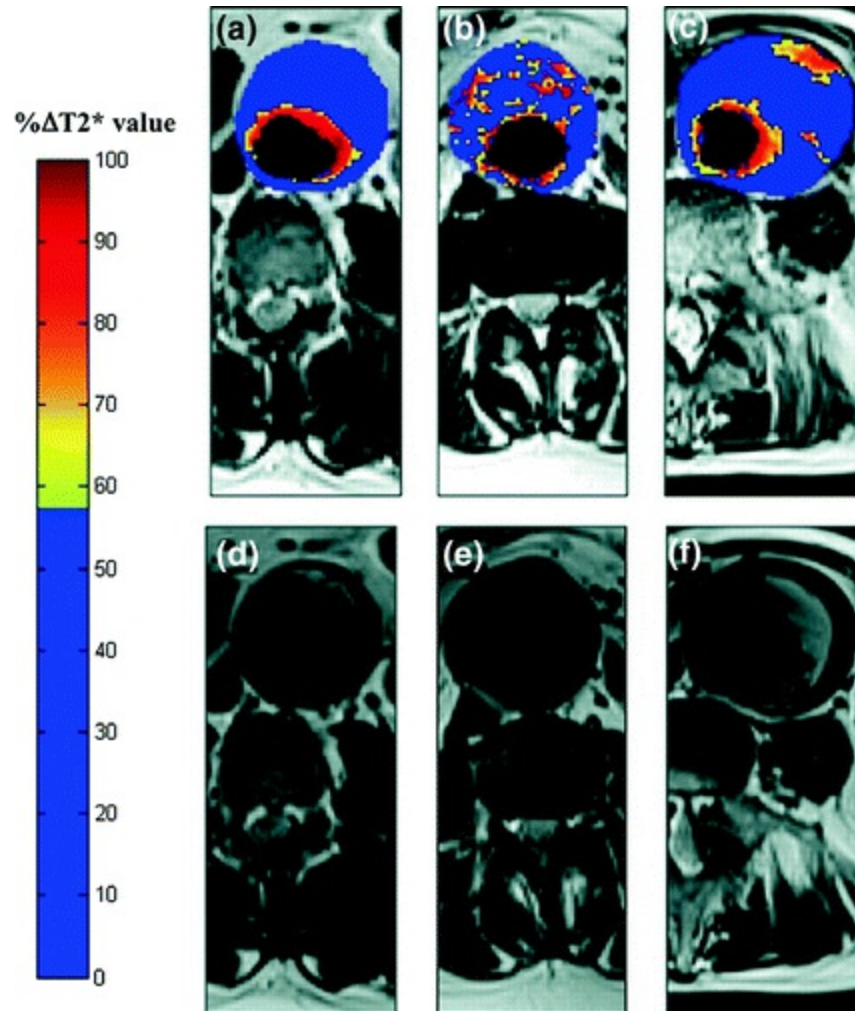


Fig. 9.18 USPIO uptake in patients with abdominal aortic aneurysm. **a:** USPIO uptake around the lumen. **b** Diffuse patchy uptake throughout the intraluminal thrombus. **c** Discrete focal area of USPIO involving the wall of the AAA that is distinct from the periluminal region. **d, e;** corresponding MRI T2 weighted anatomic images. The focal uptake seen in **c** is thought to represent focal inflammation and to be an indicator of increased risk of rupture. Reprinted by permission from Macmillan Publishers Ltd: Richards et al. (2011); copyright (2011)

Micro-calcification. In the early stages of atherosclerosis, micro-calcifications occur in response to inflammation. This is thought to be a defensive response in an attempt to seal off the affected area. PET imaging of micro-calcification involves the use of F-18 sodium fluoride where it has been used in the coronary arteries to detect early disease (Dweck et al. 2012).

References

- Allisy-Roberts P, Williams JR. Farr's physics for medical imaging. London: WB Saunders; 2008.
- Bashir MR, Bhatti L, Marin D, Nelson RC. Emerging applications for ferumoxytol as a contrast agent in MRI. *J Magn Reson Imaging*. 2015;41:884–98.
[\[CrossRef\]](#)[\[PubMed\]](#)
- Blake JR, Meagher SC, Fraser KH, Eason WJ, Hoskins PR. A method to estimate wall shear rate with clinical ultrasound scanners. *Ultrasound Med Biol*. 2008;34:760–74.
[\[CrossRef\]](#)[\[PubMed\]](#)
- Boussel L, Rayz V, Martin A, Acevedo-Bolton G, Lawton MT, Higashida R, Smith WS, Young WL, Saloner D. Phase-contrast magnetic resonance imaging measurements in intracranial aneurysms in vivo of flow patterns, velocity fields, and wall shear stress: comparison with computational fluid dynamics. *Magn Reson Med*. 2009;61:409–17.
[\[CrossRef\]](#)[\[PubMed\]](#)[\[PubMedCentral\]](#)
- Dornier C, Somsen GA, Ivancevic MK, Osman NF, et al. Comparison between tagged MRI and standard cine MRI for evaluation of left ventricular ejection fraction. *Eur Radiol*. 2004;14:1348–52.
[\[CrossRef\]](#)[\[PubMed\]](#)
- Dweck MR, Chow MW, Joshi NV, Williams MC, Jones C, Fletcher AM, Richardson H, White A, McKillop G, van Beek EJ, Boon NA, Rudd JH, Newby DE. Coronary arterial ¹⁸F-sodium fluoride uptake: a novel marker of plaque biology. *J Am Coll Cardiol*. 2012;59:1539–48.
[\[CrossRef\]](#)[\[PubMed\]](#)
- Fenster A, Parraga G, Bax J. Three-dimensional ultrasound scanning. *Int Foc*. 2011;1:503–19.
[\[CrossRef\]](#)
- Flower MA, editor. Webb's physics of medical imaging. 2nd ed. Boca Raton: CRC Press; 2012.
- Fujimoto JG, Pitris C, Boppart SA, Brezinski ME. Optical coherence tomography: an emerging technology for biomedical imaging and optical biopsy. *Neoplasia*. 2000;2:9–25.
[\[CrossRef\]](#)[\[PubMed\]](#)[\[PubMedCentral\]](#)
- Gennisson JL, Deffieux T, Fink M, Tanter M. Ultrasound elastography: principles and techniques. *Diagn Interv Imaging*. 2013;94:487–95.
[\[CrossRef\]](#)[\[PubMed\]](#)
- Gessner R, Dayton PA. Advances in molecular imaging with ultrasound. *Mol Imaging*. 2010;9:117–27.
[\[PubMed\]](#)[\[PubMedCentral\]](#)
- Glaser KJ, Manduca A, Ehman RL. Review of MR elastography applications and recent developments. *J Magn Reson Imaging*. 2012;36:757–74.
[\[CrossRef\]](#)[\[PubMed\]](#)
- Hoskins PR. Measurement of blood velocity, volumetric flow and wall shear rate. *Ultrasound*. 2011;19:120–9.
[\[CrossRef\]](#)
- Hoskins PR. Principles of ultrasound elastography. *Ultrasound*. 2012;20:8–15.
[\[CrossRef\]](#)

Hoskins PR. Recent developments in vascular ultrasound technology. *Ultrasound*. 2015;23:158–65.
[CrossRef][PubMed][PubMedCentral]

Hoskins PR, Martin K, Thrush A, editors. *Diagnostic ultrasound: physics and equipment*. 2nd ed. Cambridge: Cambridge University Press; 2010.

Huang SL. Liposomes in ultrasonic drug and gene delivery. *Adv Drug Deliv Rev*. 2008;60:1167–76.
[CrossRef][PubMed]

Kanai H, Hasegawa H, Ichiki M, Tezuka F, Koiwa Y. Elasticity imaging of atheroma with transcutaneous ultrasound preliminary study. *Circulation*. 2003;107:3018–21.
[CrossRef][PubMed]

Kwong RY, editor. *Cardiovascular magnetic resonance imaging*. Totowa, NJ; Humana Press Inc.; 2008, p. 195–210

Margolis DJ, Hoffman JM, Herfkens RJ, Jeffrey RB, Quon A, Gambhir SS. Molecular imaging techniques in body imaging. *Radiology*. 2007;245:333–56.
[CrossRef][PubMed]

Markl M, Schnell S, Barker AJ. 4D flow imaging: current status to future clinical applications. *Curr Cardiol Rep*. 2014;16:481.
[CrossRef][PubMed]

Maejima N, Hibi K, Saka K, Nakayama N, Matsuzawa Y, Endo M, Iwahashi N, Okuda J, Tsukahara K, Tahara Y, Kosuge M, Ebina T, Umemura S, Kimura K; Morphological features of non-culprit plaques on optical coherence tomography and integrated backscatter intravascular ultrasound in patients with acute coronary syndromes. *Eur Heart J Cardiovasc Imaging*. 2015;16(2):190–197

Morrison TM, Choi G, Zarins CK, Taylor CA. Circumferential and longitudinal cyclic strain of the human thoracic aorta: age-related changes. *J Vasc Surg*. 2009;49:1029–36.
[CrossRef][PubMed][PubMedCentral]

Nair A, Kuban BD, Tuzcu EM, Schoenhagen P, Nissen SE, Vince DG. Coronary plaque classification with intravascular ultrasound radiofrequency data analysis. *Circulation*. 2002;106:2200–6.
[CrossRef][PubMed]

Olufsen M, Peskin C, Kim W, Pedersen E. Numerical simulation and experimental validation of blood flow in arteries with structured-tree outflow conditions. *Ann Biomed Eng*. 2000;28:1281–99.
[CrossRef][PubMed]

Papathanasopoulou P, Marshall I, Robertson MB, Köhler U, Hoskins P, Zhao S, Xu XY. MRI measurement of time-resolved wall shear stress vectors in a carotid bifurcation model, and comparison with CFD predictions. *J Magn Reson Imaging*. 2003;2003(17):153–62.
[CrossRef]

Perk G, Tunick PA, Kronzon I. Non-Doppler two-dimensional strain imaging by echocardiography—from technical considerations to clinical applications. *J Am Soc Echocardiogr*. 2007;20:234–43.
[CrossRef][PubMed]

Prager RW, Ijaz UZ, Gee AH, Treece GM. Three-dimensional ultrasound imaging. *J. Eng Med*.

2010;H2:193–223.

[\[CrossRef\]](#)

Rahmima A, Zaidib H. PET versus SPECT: strengths, limitations and challenges. *Nucl Med Commun.* 2008;29:193–207.

[\[CrossRef\]](#)

Richards JM, Semple SI, MacGillivray TJ, Gray C, Langrish JP, Williams M, Dweck M, Wallace W, McKillop G, Chalmers RT, Garden OJ, Newby DE. Abdominal aortic aneurysm growth predicted by uptake of ultrasmall superparamagnetic particles of iron oxide: a pilot study. *Circ Cardiovasc Imaging.* 2011;4:274–81.

[\[CrossRef\]](#)[\[PubMed\]](#)

Sboros V. Response of contrast agents to ultrasound. *Adv Drug Deliv Rev.* 2008;60:1117–36.

[\[CrossRef\]](#)[\[PubMed\]](#)

Selwyn R. Phantoms for magnetic resonance imaging. In: DeWerd LA, Kissick M, editors. *The phantoms of medical and health physics: devices for research and development.* New York: Springer-Verlag; 2014. p. 181–200.

[\[CrossRef\]](#)

Stankovic Z, Allen BD, Garcia J, Jarvis KB, Markl M. 4D flow imaging with MRI. *Cardiovasc Diagn Ther.* 2014;4:173–92.

[\[PubMed\]](#)[\[PubMedCentral\]](#)

Strijkers GJ, Mulder WJ, van Tilborg GA, Nicolay K. MRI contrast agents: current status and future perspectives. *Anticancer Agents Med Chem.* 2007;7:291–305.

[\[CrossRef\]](#)[\[PubMed\]](#)

Tarkin JM, Joshi FR, Rudd JH. PET imaging of inflammation in atherosclerosis. *Nat Rev Cardiol.* 2014;11:443–57.

[\[CrossRef\]](#)[\[PubMed\]](#)

Terashima M, Kaneda H, Suzuki T. The role of optical coherence tomography in coronary intervention. *Korean J Intern Med.* 2012;27:1–12.

[\[CrossRef\]](#)[\[PubMed\]](#)[\[PubMedCentral\]](#)

Venkatesh SK, Yin M, Ehman RL. Magnetic resonance elastography of liver: technique, analysis, and clinical applications. *J Magn Reson Imaging.* 2013;37:544–55.

[\[CrossRef\]](#)[\[PubMed\]](#)[\[PubMedCentral\]](#)

10. Modelling of the Cardiovascular System

D. Rodney Hose¹ and Barry J. Doyle²✉

- (1) Sheffield University, Sheffield, UK
- (2) University of Western Australia, Perth, Australia

✉ **Barry J. Doyle**
Email: barry.doyle@uwa.edu.au

Learning outcomes

1. Describe the purpose of a cardiovascular computational model.
2. Understand the complexity of such a model.
3. Understand the difference between zero, one, three and multi-dimensional models.
4. Understand the role of rigid and compliant-wall models of the cardiovascular system.
5. Understand how to apply a computational model to represent a specific region of the cardiovascular system.

This chapter introduces the process of modelling of the cardiovascular

system. Modelling incorporates the representation of the fundamental mechanics of the cardiovascular system, as well as the determination of important features needed to ensure that the model captures the essential information relevant to the problem.

10.1 Introduction to Cardiovascular Modelling

10.1.1 Model Definition

A model is a simplified version of reality designed to answer a specific question. In the cardiovascular system, typical questions are:

- What are the overall distributions of pressure and flow in the arterial system, and how would they change under different states of physical activity, or in the presence of pathology?
- What is the load on the heart in a particular physiological state?
- Is there a risk that this artery (e.g. aneurysm) will rupture?
- What is the prognosis for this individual? Will the pathology get worse, and what will be the consequences?
- How will things change, both in the short and the long-term, if there is an intervention?

The aim of a model can often be categorised as diagnostic or prognostic. Diagnostic models seek to quantify a characteristic of a system that determines the current health or disease. Prognostic models seek to predict how health or disease might evolve in the future. In the case of the cardiovascular system, a comprehensive model might determine the diagnosis of a specific disease, predict the prognosis after a specific treatment and enable a range of different treatments to be compared.

10.1.2 Model Complexity

The complexity of the model depends on the needs of the problem to be solved. A complex model will be computationally large with many parameters and require long run-times. If used in a patient-specific sense the model may require physiological input data which is not readily available or requires invasive tests or data from medical imaging at a resolution which is

not available from modern medical imaging systems (see Chap. 11). If the model is too simple then it may not adequately describe key features which are relevant to the specific question that the model has been designed to address. In general a model should be sufficiently complex to address the question, and no more complex than that. It is the responsibility of the analyst to identify the purpose of the model and the level of complexity needed to determine relevant data.

An example of a specific question is the determination of the distribution of pressure and flow in the arterial system. The model must be capable of determining the relationship between flow and pressure in branching vessels. This requires information on the diameter of each vessel (which may be available from medical images), information as to where and how the vessels branch (which also may be available from imaging), information on the compliance of the vessel wall, and information on the characteristics of the blood itself. These data constitute the minimum that would be needed to build a model for this purpose. Other features of the system that it might not be necessary to model in the context of this specific question might be, for example, details at a microscopic level such as the interaction between individual red cells (which would be taken into account using a viscosity term) or the detailed cellular and matrix composition of the artery wall (which would be taken into account using a stress–strain function).

When localised features such as wall shear stress are not required, a lower dimensional model (one which does not account for variations in space, or does so only in fewer dimensions) may be sufficient. On the other hand, when concerned with the interaction between blood forces and the endothelium in a highly irregular geometry, a 3D model that accounts for blood–wall interaction may be better suited.

10.1.3 Modelling

Generally, the process of modelling takes a series of inputs and transforms them through a series of operations into a series of outputs. For the applications that are the focus of this chapter the model describes relationships between the parameters in a quantitative sense, usually by equations, based on an understanding of the underlying physical processes. Other types of model represent associations between parameters based on multiple observations together with machine learning and/or statistical operations. An overview of the operation of a model of heart valve

physiology, based on a Computational Fluid Dynamics (CFD) work flow developed by EurValve (Horizon 2020, Project Number 689617), is presented in Fig. 10.1. The modelling elements are illustrated in green. An analysis protocol is chosen based on the specific question and then a model is constructed using input parameters from a range of possible sources. The work flow element is discussed more extensively in Chap. 11. Most models compute the variation of parameters in a local domain, which is bounded by other domains and other structures. One of the most challenging parts of the modelling process is to set the correct boundary conditions on the domain of interest. The combination of the domain inputs, which generally include a representation of the geometry and of the rheological properties, together with the boundary conditions and the description of the operations to be performed specifies the model. The operation produces outputs which are the result of the model. Sometimes the outputs will be very large, for example full descriptions of pressure and velocity fields varying in time and space, and it is not unusual for these data to run to tens or even hundreds of GB of storage. Almost always some data reduction operation is performed to evaluate characteristics that are easy to understand and to compare.

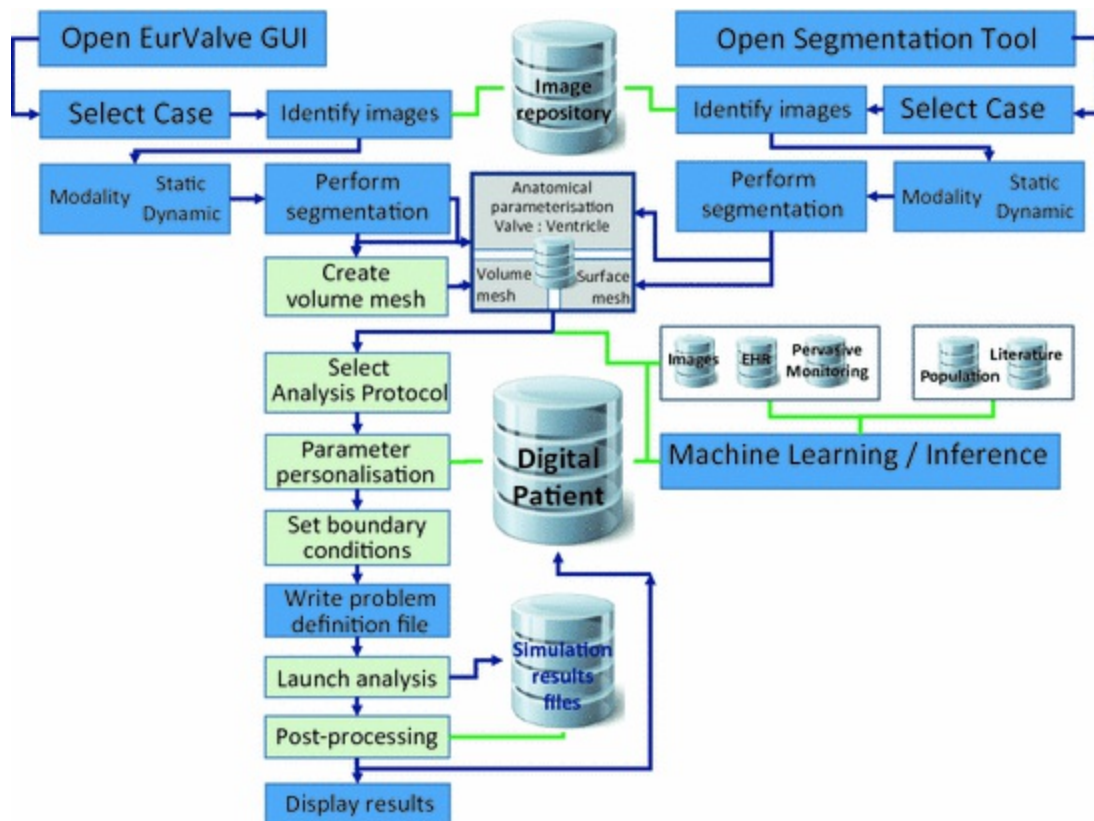


Fig. 10.1 Overview of the operation of a model of heart valve physiology, based on a Computational Fluid Dynamics (CFD) work flow developed by EurValve (Horizon 2020, Project Number 689617)

The model is a set of mathematical equations. These equations are relevant to the question the model has been designed to answer. They describe the governing dynamics (e.g. stress–strain behaviour of the wall, shear–shear-rate behaviour of the blood). In the real-world things exist in four dimensions; x , y , z and t . The model may also exist in four dimensions but lower dimensional models might be able to represent the system with sufficient accuracy, and might even produce additional insight that is obscured in a more complex model. There is some inconsistency in the description of the dimensionality of models. Generally 0D, 1D, 2D and 3D indicate the number of spatial dimensions in the model. For 0D models variation in time is implicit, for the higher dimensions, transient analyses are sometimes described for example as 3D + t and sometimes as 4D. There are even references, particularly in the medical imaging community, to higher dimensions such as ‘7D’. This refers to the three-dimensional field of the three components of velocity, changing in time.

Additional constraints relevant to the problem being solved are needed which are applied to the model in order that a solution can be obtained from the equations which make up the model. It is useful to separate these additional constraints into ‘boundary conditions’ and ‘input data’. For example, in a 3D flow model one might be interested in the variation in wall shear stress for different input flow waveforms. In this case the boundary conditions would be the 3D geometry and the pressure which would be set the same for all simulations. The input data would be the flow-time waveform which would vary from one simulation to the next.

The output data is the data which arises from the simulation. For the example above this would be a 3D time-varying dataset of blood velocity from which wall shear stress could be calculated.

10.2 Zero Dimensional Models

Zero dimensional (0D) models are a reduced order abstraction of reality. In these models it is assumed that there is no spatial variation of a quantity within any individual compartment of the model. The system within any compartment is described by a series of ordinary differential equations, with only time derivatives. Zero-D models can be powerful tools to describe

system-level interactions between components. Characteristics such as ventricular pressure-volume loops, systolic-diastolic pressure ratios, temporal pressure gradients, cardiac output, ejection fractions, ventricular work, etc., can all be computed using 0D models. The most commonly used 0D model of a chamber of the heart is the *variable elastance model*. In this model, a relationship is described between elastance, which is specified as a function of time, chamber volume and chamber pressure. The elastance terms describe the active contraction of the heart. The 0D vascular components lump all of the inertia, resistance and compliance of a portion of the vasculature into simple electrical analogue representations. A very simple model of the left side of the heart and the systemic circulation, including a snapshot of the model representation from the CellML repository (www.cellml.org), is presented in Fig. 10.2. Despite its simplicity, a typical implementation of this model actually has 23 input parameters. It is a real challenge to select appropriate parameters and parameter ranges for the study of the mechanics of the system, and an even greater challenge to personalise them to represent an individual.

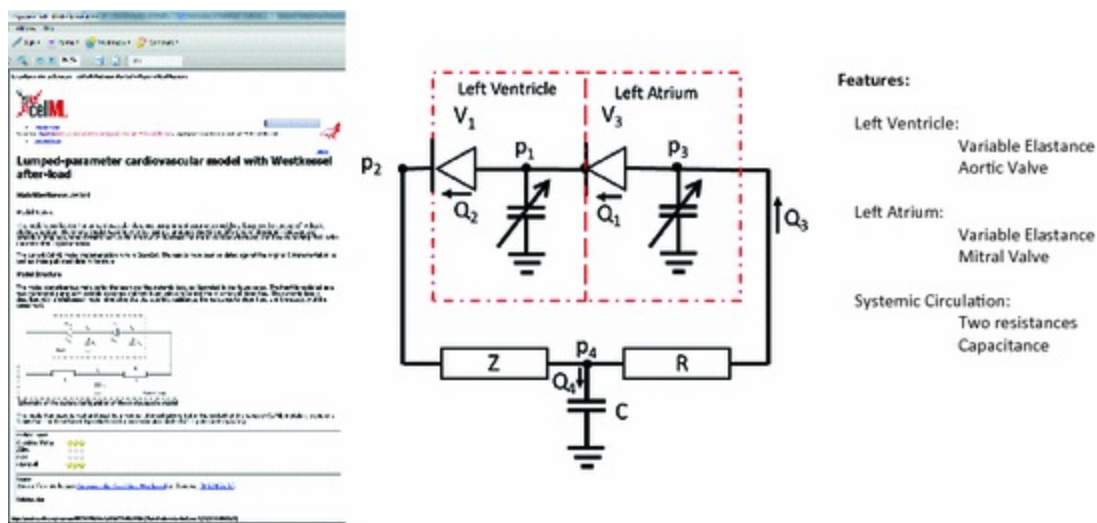


Fig. 10.2 Simple model of the *left side* of the heart and the systemic circulation ('Westkessel'), including a *snapshot* of the model representation from the CellML repository (www.cellml.org)

One important class of applications of 0D models includes the representation of changes under prospective interventions. As the human system is not passive, but is actively regulated by both central and local control systems, it is necessary to model control mechanisms if the model is to accurately represent the effects of interventions (pharmacological or

surgical), or changes of physiological state (e.g. exercise). Such control models can describe regulation, neural signals to control pressure, volume and flow fluctuations, physiological and interventional changes, as well as haemorrhage. The CellML repository contains a wealth of curated models that are freely available for download. For further reading on all the above aspects of 0D models of the cardiovascular system, please see Shi et al. (2011).

10.3 One Dimensional Models

One dimensional (1D) models are useful to capture gross features of the circulation and are particularly useful downstream of the heart. They are described by partial differential equations that relate pressure and the axial component of velocity and their spatial and temporal derivatives. The 1D equations can be derived directly from the full 3D Navier-Stokes equations (see for example Landau and Lifshitz 1959), represented in polar coordinates, by making the assumption of axisymmetry. The characteristics of these equations are studied in detail by Canic and Kim (2003), who show for example that, if the radius of the vessel is small relative to a characteristic length, the pressure is constant over the radius of the vessel. This is an important practical result for flow in arteries. A radial distribution of the axial velocity is assumed, the form of which depends on the flow regime that is to be represented. One-D models are particularly useful to capture wave transmission in the cardiovascular system without the computational expense of a 3D model. Wave transmission arises from the elasticity of the vessels and their capacity to store fluid as they are pressurised.

A 1D representation of the circulation can be important in the use of system models that characterise, for example, cardiac load under a range of physiological conditions, or the impact of disease on the elevation of cardiac and vascular pressures. An example of the application of state-of-the-art branching tree models to the physiology of the pulmonary circulation is presented by Qureshi et al. (2014). In some applications, particularly in the context of coronary and pulmonary physiology, 1D models are used to describe and to characterise the relationship between forward and backward travelling waves in the circulation. Analysis might be conducted in the frequency domain or in the time domain: for the latter the concept of wave intensity analysis, reviewed by Hughes et al. (2008) is a useful device. The

healthy system maximises the efficiency of blood transmission and minimises the load on the heart by matching the impedance of different branching vessels. In disease, this impedance matching can be diminished, with measurable differences in power of the forward and backward travelling waves. For a comprehensive review of 1D models including theoretical considerations, see van de Vosse and Stergiopulos (2011).

10.4 Three-Dimensional Models

Three-dimensional (3D) models aim to incorporate 3D geometry. A 3D model requires geometry, which can either be created using computer aided design (CAD) software, or can be obtained from medical images (described in Chap. 11). For the heart and the larger arteries and veins, blood is usually assumed to be a fluid continuum, ignoring its microscopic make-up, and incompressible. Under these conditions there are:

- Two fundamental variables of interest, pressure (p) and velocity (v), and, since velocity is a vector with three direction components (u, v, w), there are four degrees of freedom (p, u, v, w) that together describe the physical state at each point within the fluid domain.
- Two governing equations accurately describe the variation of the fundamental variables (p, u, v, w) throughout the domain, given material properties and boundary conditions. The first is based on the conservation of mass and the second is based on the conservation of momentum. Since the velocity has three component directions, there are three momentum equations. The equation of conservation of mass is often called the continuity equation and the equations of conservation of momentum are called the Navier–Stokes equations.

10.4.1 Rigid Wall Models

A rigid wall model is one in which the vessel walls do not move during the cardiac cycle. This is opposed to the reality in vivo where the vessel wall in an artery typically changes in diameter by 5–10 % during the cardiac cycle. Rigid wall analysis is suited to applications where the purpose of the model is to evaluate flow characteristics that are not strongly influenced by shape changes. It is a necessary, but not sufficient, condition that the fractional volume change of the domain of interest over the cardiac cycle is small.

Examples in which the rigid wall assumption might be adequate include the modelling of flow separation and of vortical structures, wall shear stress distributions in the region of bifurcations, aneurysms, stenoses or anastomoses. In particular, wall shear stress in arteries is relatively insensitive to the motion of the vessel wall, and therefore, it is often adequate to assume a rigid wall model.

The boundary conditions for a rigid walled arterial flow model are typically described by the wall itself together with one proximal (upstream) boundary where the blood enters and multiple distal (downstream) boundaries through which the blood leaves. The fundamental variables are pressure and velocity. It is usually assumed that the velocity at all points on the wall of the vessel is equal to zero (as the wall is stationary). This is called the 'no slip boundary condition'. If the pressure at the outlets, or the pressure gradient across the domain, is known, a pressure boundary condition will often be assigned to an outlet. This information might be measured invasively via a catheter. Care is needed when the outlet of the domain cuts through an area in which complex flow features, such as recirculation, are expected. It is often advised to extend the domain so that flow is in only one direction at the boundary.

The boundary condition at the inlet of a vascular domain might be velocity, flow (an integral measure of velocity) or pressure. As discussed above, the outlet boundary condition is often pressure, and generally then it is preferred, for reasons of computational stability, to define the inlet as a velocity or flow condition. On a plane the inlet flow field data is defined by a 2D velocity profile with 3 velocity components. For patient-specific models inlet flow data may be obtained using MRI or ultrasound as described in Chap. 11. In the absence of explicit data on velocity distribution, the following are the most commonly used assumptions.

- *Plug flow or parabolic flow.* In this approach it is assumed that the velocity profile remains unchanged through the cardiac cycle. In plug flow the velocity is the same at all points of the cross-section. As noted in Chap. 1 plug flow is a feature of inertial flow where viscous effects are minimal. Plug flow is found in large arteries where flow is pulsatile, especially at the beginning of the cardiac cycle. Parabolic flow is a feature of steady flow where the velocity profile is dominated by viscous effects, with maximum velocity in the centre of the vessel. In arteries which supply organs with high-flow demand there is a large baseline

component of flow; for example in the carotid arteries supplying the brain, the renal arteries supplying the kidneys and in the uterine and arcuate arteries supplying the placenta. In this case flow is mainly viscous in nature and flow profiles will be more parabolic than plug. However, all arteries have some form of pulsatile flow, and some component of viscous flow, so that the use of purely plug flow or parabolic flow is too simplistic to be used directly at the inlet. In practice one of these simple inlet flows may be applied in combination with a short development length of typically one to five times the inlet diameter.

- *Womersley flow.* In Chap. 1 Womersley flow was introduced. It was noted that this is the flow which is pulsatile and fully developed. The velocity profile changes during the cardiac cycle. When overall flow changes direction, the flow close to the wall is in the opposite direction to the flow in the centreline. These equations allow estimation of the 2D time-varying velocity profile from the flow-time waveform. The flow-time waveform may be estimated in the person or patient from ultrasound or MRI, so that the Womersley method provides an easy way for obtaining inlet flow data useful for modelling. This may be applied directly at the inlet or, more commonly, in combination with a short length of one to five times the inlet diameter.
- *Measured 2D velocity profile.* While the above methods provide 2D time-varying inlet data, they do not easily account for flow which is non-axial (helical), asymmetric or not fully developed. As noted in Chap. 4 arteries may exhibit all of these features. If it is necessary to model these features then the full 2D 3-component time-varying velocity field is required, which may be measured using MRI (see Chap. 11).

10.4.2 Compliant-Walled Models

If a cardiac model is used to determine the flow into the arterial system, then clearly the representation of the change of chamber volume is critical. For larger arteries the issues are more subtle. The aorta changes volume by approximately 10 % over the cardiac cycle. One important consequence of the distensibility of the aorta is that the flow out of the domain is not equal to the flow in at each instant in time. Some of the blood mass is stored in the aorta during systole and gradually released during diastole, therefore acting

like a reservoir and secondary pump, smoothing out the flow distribution to the organs and distal circulation. A corollary is that there is a finite pressure (and flow) wave-speed in the aorta. The rise of pressure at the inlet, in the region of the aortic valve, is not immediately transmitted to more distal locations. Typically, the wave-speed in the human aorta is in the region of 5–10 m s⁻¹. The pressure pulse in the abdominal aorta will typically lag behind the pressure pulse at the valve by approximately 100 ms, which is a significant portion of the cardiac cycle and particularly of systole. In a rigid walled domain, any change in velocity at the inlet is immediately manifested at the outlet and the pressure per unit of acceleration is concurrently high. In a non-rigid walled domain, the temporal gradients of pressure are much lower. However, the computational cost of a rigid model might be an order of magnitude, or more, lower than that of a model with elastic walls. These issues are discussed in more depth by Brown et al. (2012).

Many clinically meaningful questions can be answered by rigid walled models, especially if the primary interest concerns local haemodynamics and/or average measures. However, if wall motion is important, for example, because the change of volume of the system is significant, then it is necessary to include its representation in the model.

There are fundamentally two approaches to the determination of wall motion: (a) measure it and impose this motion directly as a boundary condition, or (b) compute it using another model.

Depending on the application, wall motion can be measured using medical imaging such as ultrasound, MRI or cardiac-gated CT. However, small measurement errors in the displacement of the wall can lead to very large local pressure fluctuations in an incompressible fluid. The more desirable approach is to incorporate vessel elasticity into the model. This requires coupling of a flow model (CFD) and a solid model (FEA) into a single modelling regime. This is called ‘fluid structure interaction’ (FSI). Modelling regimes are considered further in Chap. 11.

10.4.3 Material Properties

An important limitation facing the solid mechanics component of the model is the lack of knowledge of material properties. In vivo material properties are difficult to obtain non-invasively. While tissue stiffness may be measured in vivo using elastography (Chaps. 9 and 11), measurements in the

cardiovascular system, especially in arteries and veins are not well developed at the time of writing. It is therefore common to assume that every person has the same mechanical properties for the region under investigation.

In almost all cardiovascular applications it is reasonable to assume that blood is incompressible with a fixed density of approximately 1056 kg m^{-3} . However, as described in Chap. 3, blood is a non-Newtonian fluid. It is more viscous at low shear rates than it is at high shear rates. As the shear rate increases the viscosity approaches asymptotically a value of approximately 0.004 Pa s , or four times that of water. For most analyses of the larger vessels, down to 0.5 mm diameter and even lower, it is reasonable to take this asymptotic limit and to treat blood as a Newtonian fluid. For smaller vessels it is more appropriate to use one of the empirically fitted shear–stress/shear-rate curves, perhaps a power law approximation. Blood is primarily a suspension of disc-shaped red cells, approximately $7 \text{ }\mu\text{m}$ in diameter, in plasma. In the very small vessels, $<100 \text{ }\mu\text{m}$, down to the capillaries, a more comprehensive model would explicitly represent the multi-phase nature of the fluid, including the deformable bodies of the red cells (Krüger et al. 2013).

10.5 Heart Models in 3D

The representation of the heart and its interactions with the cardiovascular system is one of the most complex challenges in physiological modelling. Major interdisciplinary research efforts aim to better understand and model the system in multi-dimensional (0D, 1D, 3D), multi-scale (molecular, cellular, organ, system), multi-physics (electrical, structural, fluid) and multi-science (physics, chemistry, biology) analysis processes. Smith et al. (2011) describes the current state-of-the-art and the major euHeart initiative (www.euHeart.eu) aimed at developing a ‘full’ heart model that integrates:

- *The propagation of an electrical wave through the myocardium.* This is partly an active process, with the cells responding to the electrical stimulus to generate an action potential, and partly a passive process representing the diffusion of the voltage through the myocardium. The active part requires a description of the electrochemical cellular processes, which ultimately are described by systems of ordinary differential equations. These are zero dimensional models that are

embedded locally into 3D tissue models.

- *The structural contraction of the myocardium induced by the electrical wave, combined with the stresses generated within the myocardium by the pressures in the heart chambers.* This is the least numerically stable and most difficult part of the model. The tissue is anisotropic (both electrically and structurally), as well as nonlinear in its constitutive equations.
- *The ejection of fluid from the heart chambers, caused by the contraction and resulting pressure elevation, working against the impedance of the cardiovascular system.*

There are generally three reasons for modelling the heart in 3D:

- Representation of 3D vortex structures within the ventricles to evaluate the haemodynamic efficiency of the ejection processes, viscous losses, acceleration profiles and energy consumption.
- Representation of local jets through normal, diseased and prosthetic valves (usually aortic and/or mitral, but there are studies of tricuspid valves) to evaluate pressure gradients and sometimes leakage characteristics. If the motion of the valve is important (i.e. the details of the opening and closing phases) then the model has to include either fluid–solid interaction and/or an imposed valve motion.
- Identification of regions of slow flow potentially associated with a propensity for the formation of thrombus. These are typically quantified by evaluation of residence times for blood elements (including activated platelets). This type of analysis can be very valuable, for example, in the study of the connection of a ventricular assist device into the apex of the left ventricle.

10.6 Multi-dimensional Models

In the context of cardiovascular biomechanics, the term multi-dimensional model typically refers to a computational model that spans more than one spatial dimension. So in this case, the region of interest is modelled in 3D, but the rest of the system is modelled with a lower dimensional model. A key challenge is the coupling of a 3D model with a lower dimensional model as

the former contains more information at the boundary than the latter, e.g. information about the distribution of velocity. This can be especially challenging for FSI models in which the boundary domain itself might be changing size. Information and advice on multi-dimensional coupling can be found in Formaggia et al. (2011).

A typical stylised cartoon, illustrating a multi-dimensional cardiovascular model from EurValve is illustrated in Fig. 10.3. A simplified version of this model was used in the euHeart project to estimate pressure gradients in sixteen cases with aortic coarctation. The aorta was modelled in 3D based on CT image data, the heart model was removed and in its place a proximal boundary condition of transient flow in the ascending aorta was prescribed, based on measured phase-contrast MRI data. The distal boundary condition on each outlet was a 0D RCR Windkessel model (resistor, R; capacitor, C). Windkessel parameters were tuned to produce measured flow in the descending aorta and a distribution of mean flow in the supra-aortic vessels based on Murray's Law using the measured vessel diameters. The results are sensitive to the values of these parameters and they must be chosen to reflect as closely as possible the measured conditions.

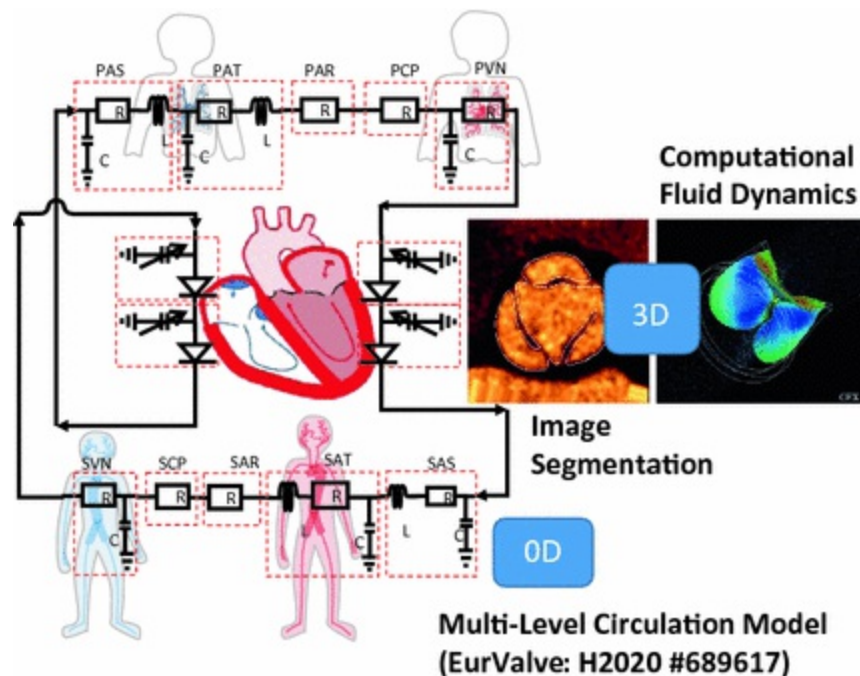


Fig. 10.3 Example of a multi-dimensional model of aortic coarctation (www.euheart.eu)

References

Brown AG, Shi Y, Marzo A, Staicu C, Valverde I, Beerbaum P, Lawford PV, Hose DR. Accuracy vs. computational time: translating aortic simulations to the clinic. *J Biomech.* 2012;45:516–23.

Canic S, Kim EH. Mathematical analysis of quasilinear equations in a hyperbolic model of blood flow through compliant axi-symmetric vessels. *Math Meth Appl Sci.* 2003;26:1161–86.
[CrossRef]

Formaggia L, Gerbeau JF, Nobile F, Quarteroni A. On the coupling of 3D and 1D Navier-Stokes equations for flow problems in compliant vessels. *Comput Methods Appl Mech Eng.* 2011;191:561–82.
[CrossRef]

Hughes AD, Parker KH, Davies JE. Waves in arteries: a review of wave intensity analysis in the systemic and coronary circulations. *Artery Res.* 2008;2:51–9.
[CrossRef]

Krüger T, Gross M, Raabe D, Varnik F. Crossover from tumbling to tank-treading-like motion in dense simulated suspensions of red blood cells. *Soft Matter.* 2013;9:9008–15.
[CrossRef][PubMed]

Landau LD, Lifshitz EM. *Fluid mechanics.* Oxford: Pergamon Press; 1959.

Qureshi MU, Vaughan GD, Sainsbury C, Johnson M, Peskin CS, Olufsen MS, Hill NA. Numerical simulation of blood flow and pressure drop in the pulmonary arterial and venous circulation. *Biomech Model Mechanobiol.* 2014;13:1137–54.
[CrossRef][PubMed][PubMedCentral]

Shi Y, Lawford P, Hose R. Review of zero-D and 1-D models of blood flow in the cardiovascular system. *BioMed Eng OnLine.* 2011;10:33. doi:10.1186/1475-925X-10-33.
[CrossRef][PubMed][PubMedCentral]

Smith N, de Vecchi A, McCormick M, Nordsletten D, et al. euHeart: personalized and integrated cardiac care using patient-specific cardiovascular modelling. *Interface Focus.* 2011;1:349–64.
[CrossRef][PubMed][PubMedCentral]

van de Vosse F, Stergiopoulos N. Pulse wave propagation in the arterial tree. *Ann Rev Fluid Mech.* 2011;43:467–99.
[CrossRef]

11. Patient Specific Modelling

Peter R. Hoskins¹✉, Noel Conlisk¹, Arjan J. Geers¹ and
Barry J. Doyle²✉

- (1) Edinburgh University, Edinburgh, UK
- (2) University of Western Australia, Perth, Australia

✉ **Peter R. Hoskins (Corresponding author)**
Email: P.Hoskins@ed.ac.uk

✉ **Barry J. Doyle**
Email: barry.doyle@uwa.edu.au

Learning outcomes

1. Define the term ‘patient specific modelling’.
2. Discuss the history of patient specific modelling.
3. Discuss the reasons for patient specific modelling gaining momentum since around 2000.
4. Describe the steps in computational mechanics (digital computation, discretization, solver).
5. Describe the steps in the patient specific modelling processing chain (imaging, segmentation, geometry preparation, meshing, computational

modelling, constitutive model, boundary conditions, post-processing and display of data).

6. Describe specific examples of patient specific modelling in practice.

11.1 Introduction

11.1.1 Introduction to Patient Specific Modelling

Patient specific modelling (PSM) is concerned with the integration of data from the patient with computational modelling. The process may be imagined as a black box in which computational modelling occurs. Data from the patient is fed into the box and different types of data are outputted from the box. In the context of this book, computational modelling refers to modelling of physical phenomena, mainly mechanical and electromagnetic forces. Similarly, inputs to computational modelling are concerned with physical phenomena; medical imaging data provides information on geometry and motion, data is provided on electrical activity from electrophysiological recordings. Other types of data concerned with patient history and ‘omics’ (genomics, proteomics etc.) fall under the ever growing area of big data and are not considered in this book. In the context of this book PSM may be divided into the following:

- *Electrical activity models.* These relate to modelling of electrical activity in the heart and are covered in Chap. 6.
- *0D, 1D patient specific models.* These use reduced-order models of pressure/flow in the cardiovascular system for which the 3D properties are not considered and are covered in Chap. 10.
- *3D patient specific models.* This is concerned with the integration of 3D imaging data with computational modelling of mechanical phenomena related to blood flow and cardiovascular wall motion.

This chapter is concerned with the last of these three areas; the integration of 3D imaging with computational modelling for estimation of blood flow and cardiovascular wall motion. Patient specific modelling involves a series of steps starting with image data and ending with displayed data from the modelling. These steps are referred to as a ‘processing chain’, ‘pipeline’ or

‘workflow’; on the basis that information is fed in at one end of the processing chain and a great deal more information is produced at the other end of the chain. The details of the processing chain form the majority of the content of this chapter. As an introduction, the patient specific modelling processing chain can be divided into three main steps:

1. Acquisition and processing of medical imaging data
2. Computational analyses
3. Data post-processing

The computational modelling usually falls into one of two different categories; fluid mechanics or solid mechanics. Fluid mechanics applications in the cardiovascular system usually concern blood, so here PSM involves estimation of the 3D flow field. Solid mechanics applications in the cardiovascular system concern the tissues of the heart and arteries, so here PSM involves estimation of the deformation and wall stresses arising from pressure changes. Articles which review the development of PSM are by Taylor and Figueroa (2009), Hoskins and Hardman (2009), Neal and Kerckhoffs (2010) and Morris et al. (2015).

11.1.2 Terminology

As the area of PSM continues to evolve, so does the terminology. Below is a list of various terms which are used in this chapter:

Term	Definition	Comment
Idealised	Simplified representation which captures key features	Relevant for studies involving general trends
Patient specific	Values from measurement or modelling which are relevant to the individual patient	Hence can be used in diagnosis and surgical planning
Image guided modelling	Integration of imaging with computational modelling	Image data may be idealised or patient specific
Patient specific modelling	Image guided modelling which provides data relevant to the individual patient	Input data is relevant to the individual patient; hence output data can be used in diagnosis and surgical planning of the individual patient

11.1.3 History and Motivation

Numerical modelling was pioneered in the early 1950s in an attempt to better understand the vibration response of new aircraft wing designs under loading (Turner et al. 1956). The first numerical simulations involving stress in biological tissues were applied to idealised geometries in bone and teeth (Rybicki et al. 1972; Thresher and Saito 1973). The first numerical simulations of blood flow were based on idealised 2D geometries (Perktold et al. 1984; Friedman and Ehrlich 1984). The first numerical simulations to estimate cardiovascular stress were in 2D idealised arteries (Richardson et al. 1989; Loree et al. 1992; Cheng et al. 1993). Patient specific modelling has been gaining momentum since around 2000. There are four main reasons for this which are briefly outlined in this section.

Improvements in computer power. There is no doubt that the principal reason for the spread of computational modelling, not just for biomedical applications but throughout engineering and industry, has been the continued increase in computer power. Moore's law, which is that the number of transistors on an integrated circuit doubles every 2 years, has been applicable for 40 years from 1971 to 2011, with only a brief change to every 2.5 years, since 2011. In parallel to the improvements in processing power there have been reductions in price. The cost of a high-end workstation has decreased to the point where these are affordable for the individual researcher. In 2016, a high-end workstation (32-core) costs around £5000 (\$8000, €7000). Three-dimensional simulations involving 500,000 nodes with time-resolved output have run times of just a few hours.

Improvements in modelling software. Early work on numerical modelling used software developed in-house. While some groups still use in-house software, commercial packages are now widely used in image guided modelling and patient specific modelling. These packages have undergone extensive validation and have options specifically designed for biomedical applications.

Availability of high-resolution medical imaging. At the beginning of the PSM processing chain is medical imaging. The modern medical imaging department has a number of 3D imaging systems with spatial resolution of around 1 mm suitable for acquiring high quality geometries for PSM.

Potential of biomechanical measurements for clinical decision-making and surgical planning. Major clinical events such as aneurysm rupture or rupture of atherosclerotic plaque are associated with mechanical failure of

tissues, where tissue stress exceeds tissue strength. Growth of atherosclerotic plaque and aneurysm is associated with changes in both tissue stress and wall shear stress. This has led many groups around the world to think that measurements related to the biomechanical status of disease may provide improved diagnosis and selection of patients for treatment. Medical imaging systems are unable to measure mechanical stress, whereas stress is one of the main outputs of PSM. This has provided a key rationale for the development of PSM as a potential diagnostic tool for use in cardiovascular disease. In parallel, there has been the realisation that PSM may be used as an aid to surgical planning where, for example, the effect of different surgical approaches on the haemodynamics may be investigated in the computer first.

11.2 Computational Mechanics

11.2.1 Introduction and Rationale

It has been noted in previous chapters that there are governing equations which describe the behaviour between strain and stress in a solid and between strain rate and shear rate in a fluid. There are a very few geometries for which exact solutions of these equations exist. For a fluid, the governing equations are the ‘Navier–Stokes equations’. Exact solutions of the Navier–Stokes equations may be found for simple geometries such as motion of an infinite plate and steady or pulsatile flow in a cylinder. For more complex geometries, computational mechanics provides a framework to allow the governing equations in a fluid and a solid to be solved. The mathematics of computational mechanics is complex and outside the scope of this book, but is available in standard texts and review articles for interested readers (Zienkiewicz 2004; Zienkiewicz et al. 2005; Chapra and Canale 2014). The basic steps involved in computational mechanics are detailed below:

Digital computation. The governing equations are applicable to a continuous media (i.e. all x, y, z, t). Computational mechanics operates using a digital or discrete model in which equations are solved at many specific values of x, y, z, t . This digital model is then suitable for calculation using a computer. The set of points is referred to as the ‘mesh’ or ‘grid’. The smallest unit of the mesh is called an ‘element’ which consists of a number of nodes. Each node of the mesh has a number of values related to the variables in the governing equations.

Discretization. The governing equations are broken down into simpler equations which are suitable for an iterative solution using a computer. This process is called ‘discretization’. There are a number of different discretization methods; ‘finite element method’, ‘finite volume method’, ‘finite difference method’, ‘spectral element method’. These all have slight differences in the mathematical formulation and some are more suited to solid modelling while others are more suited to flow modelling.

Solver. An initial set of values is assigned to each node of the mesh. The computer programme operates in an iterative manner in which the equations at each node are solved and the set of values at each node adjusted. After several iterations, the set of values will be stabilised and the solution will be reached. It should be noted that not all solutions are physically realistic. An experienced fluid or solid mechanics specialist is required to design the mesh and prepare the simulation to avoid physically unrealistic solutions.

11.2.2 Flow and Solid Modelling

Estimation of flow field data using computational mechanics is referred to as ‘computational fluid dynamics’ or CFD. Commonly the finite difference and finite volume discretization methods are used in CFD software packages. Estimation of stresses in solids usually involves finite element discretization, so that solid modelling is usually referred to as ‘finite element analysis’ or FEA. A number of commercial packages are available for flow and solid modelling including CFX and Fluent (ANSYS, Canonsburg, PA, USA) and Abaqus (Dassault Systemes, Simulia, Rhode Island, Providence, USA). For use in blood flow, several groups have developed their own CFD packages (for example, Mineev and Ethier 1998; Ethier et al. 1999; Sherwin and Karniadakis 1995; Witherden et al. 2014).

11.3 Processing Chain

This section describes the PSM processing chain (Fig. 11.1). The sections below describe each component of the chain in detail. An example of a full PSM processing chain has been described by Antiga et al. (2008).

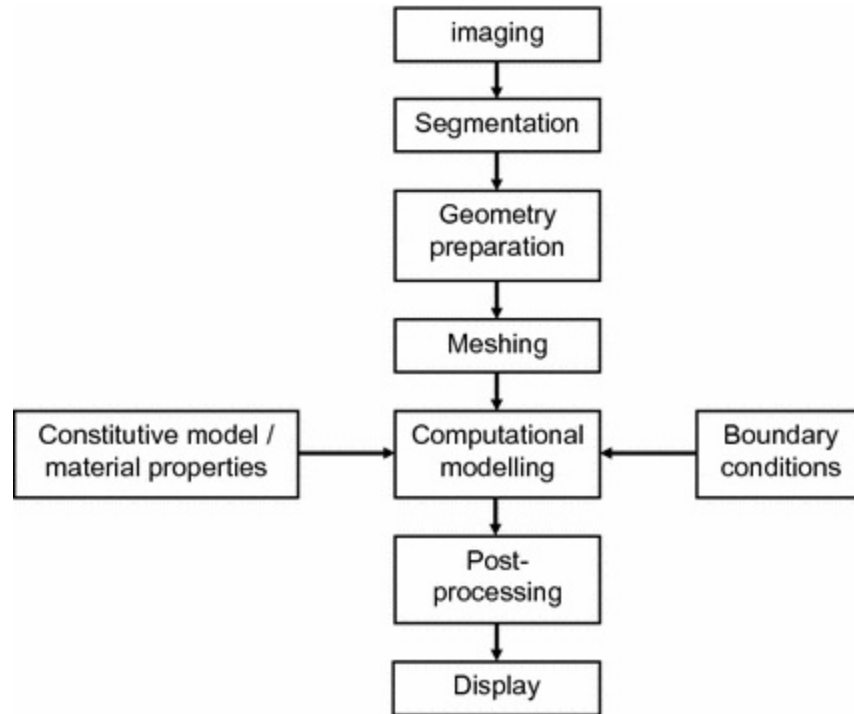


Fig. 11.1 Patient specific modelling processing chain

11.3.1 Imaging

The starting point of the PSM processing chain involves the acquisition of medical imaging data. Medical imaging systems were described in Chap. 9, where it was noted that a number of imaging modalities provide high-resolution 3D data. The medical imaging dataset provides 3D data on the tissues of interest in the patient. In the case of arteries this will be the arterial wall, any thrombus (e.g. present in clinically relevant aneurysms) and the vessel lumen. The ideal imaging modality for PSM should have the following features: high resolution, low noise, artefact-free, high contrast between tissues. A brief summary of the use of different imaging modalities in PSM is described below:

Computed tomography (CT). This is the imaging modality which comes closest to the set of criteria listed above. It has been widely used in PSM of the larger arteries and of aneurysms. With multislice scanning it is possible to acquire gated 3D cardiac data from which coronary artery geometries may be obtained. Using CT it is possible to distinguish the thrombus from the lumen in aneurysms. The main limitation is the inability to measure wall thickness; this arises due to resolution limitations (around 0.6 mm) and due to

insufficient contrast between the wall and surrounding soft tissue. For use in atherosclerosis, the resolution is insufficient to distinguish the detailed structure within the plaque.

Magnetic resonance imaging (MRI). Image contrast is high which enables different soft tissues to be distinguished. The good soft tissue contrast also enables some visualisation of the aortic wall, which is often not possible on CT. For use in atherosclerosis, MRI has been used to acquire 2D and 3D data in atherosclerotic plaque, where its excellent soft tissue discrimination enables visualisation of the different plaque components. However, MRI has a number of limitations for PSM. Acquisition times for 3D data can be long. For data acquired from the thorax and upper abdomen, the patient must hold their breath to limit the displacement of the chest. Image registration tools are required to register the images together and remove this motion. MRI has much larger slice intervals compared to CT, typically around 5–6 mm for abdominal imaging protocols. So although, MRI has excellent in-plane (x, y) pixel resolution, <1 mm, the resulting geometries may lack detail in z -direction and be unsuitable for PSM.

Ultrasound. In principle, 3D ultrasound data may be acquired using externally applied transducers. However, in practice, there are problems associated with registration, low resolution, loss of data due to calcifications and bowel gas (Hammer et al. 2009). These problems are mostly resolved by the use of intravascular ultrasound where the transducer is much higher frequency (resulting in much improved spatial resolution of 50–100 μm), and where the transducer images the tissues from inside the vessel. IVUS has been used to provide 3D geometries for PSM since the very early days of PSM (Chandran et al. 1996; Krams et al. 1997). The position and orientation of the IVUS scan-plane needs to be known so that the IVUS data can be positioned within a 3D geometry. Krams et al. (1997) used an angiography system to obtain this information; the overall system was known as ANGUS (ANGiography and UltraSound).

Optical coherence tomography (OCT). This is also an invasive technique which can be used for imaging arteries and has very good spatial resolution of 10–20 μm . It was noted in Chap. 9 that the critical thickness of the cap in atherosclerotic plaque is around 70 μm , far below the resolution of CT, MRI or transcutaneous ultrasound, and the only technique capable of providing accurate measurements of cap thickness in vivo is OCT.

11.3.2 Segmentation

Segmentation is the process whereby the surfaces of the organ of interest are identified. Segmentation may also involve defining the boundaries between different regions in the organ. Typically for fluid modelling the inner lumen of the vessel is required. For solid modelling ideally both inner and outer lumen of the vessel wall should be identified. For abdominal aortic aneurysms the region of thrombus is required. For atherosclerosis, the regions need to be identified corresponding to different plaque constituents. Segmentation concerns the detection of edges in an image and is commonly used in 3D imaging for visualisation of structures. For example, in CT imaging in the Radiology Department, the soft tissues can be ‘peeled back’ to reveal underlying organs, skeleton etc. Segmentation can be manual, automated or semi-automated.

Manual segmentation consists of a trained operator laboriously going through each image defining the boundaries by hand. This is extremely time-consuming for the operator. Manual segmentation is still used, often when image quality is low and automated methods fail.

Threshold methods. These are the simplest automated segmentation methods and involve looking for differences in intensity values between adjacent voxels. Figure 11.2 shows a threshold-based method in operation for identification of the inner lumen of an abdominal aortic aneurysm in a CT dataset. The algorithm starts in the middle of the lumen and works outwards radially. When the intensity value exceeds a threshold value, the edge has been found. These simple methods work best when image noise is low. Some commercial software such as Mimics (Materialise, Belgium) allows manual definition of the organ boundaries which are then smoothed to produce a 3D surface mesh suitable for modelling.

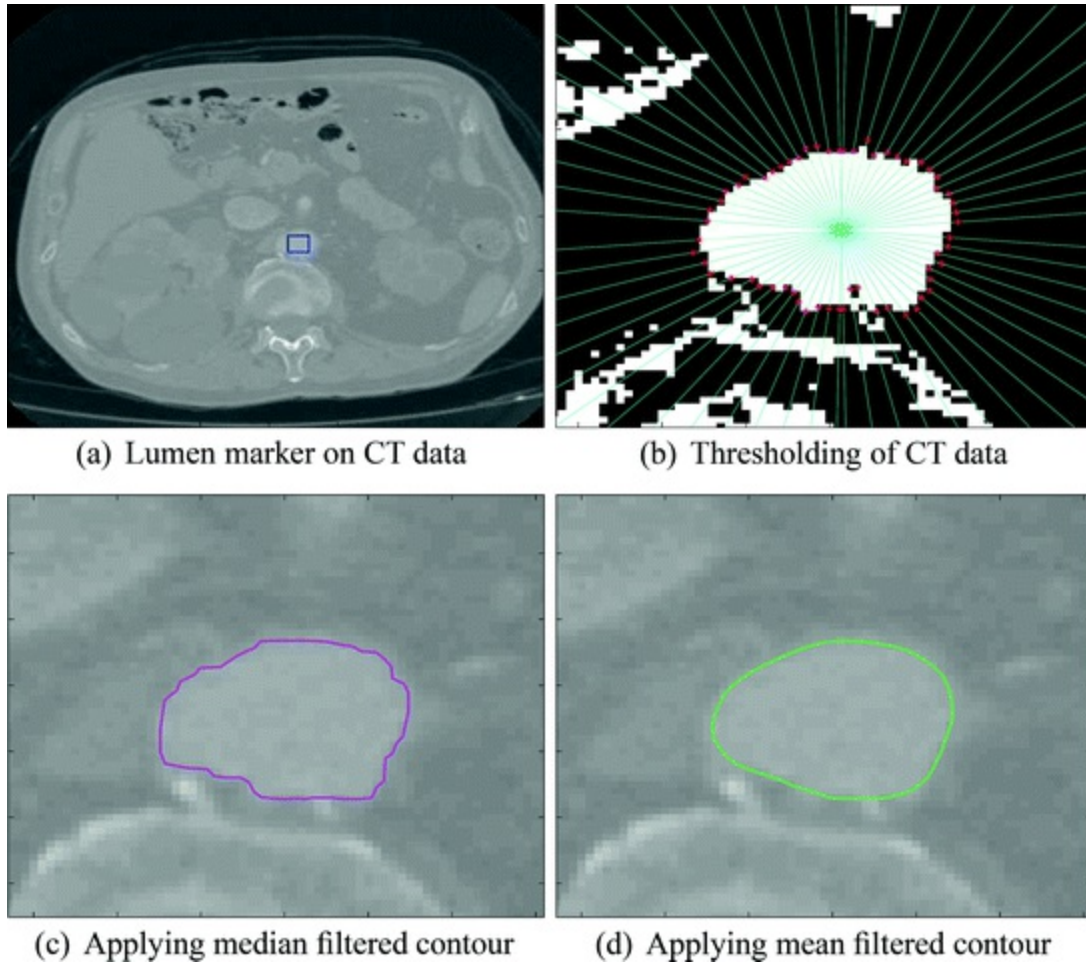


Fig. 11.2 Segmentation of the lumen of an abdominal aortic aneurysm. **a** Lumen marker is placed on the CT scan. **b** A simple threshold method is used to identify the lumen. **c** A median filter is applied to smooth the contour. **d** The contour is further smoothed using a mean filter

Deformable models. These are often referred to as ‘active contours’ (2D), ‘active surfaces’ (3D) or ‘snakes’ (Xu et al. 2000). These provide a widely used and powerful segmentation technique. The snake is a connected set of points which can deform dependent on the local image content. Typically an initial contour is seeded and grows outwards until it reaches the organ boundary. Local image measures which have high values where there is an edge are used to constrain the snake. The snake will often be ‘trained’ from learning datasets to exhibit some sort of geometrical behaviour, e.g. when segmenting the left ventricle the snake knows roughly what shape a typical left ventricle is and this is used as a constraint in the process. The result from this approach is a robust 3D reconstruction with good reproducibility.

Automatic segmentation methods represent the ideal scenario for the

operator. These work best when the image quality is very good such as for CT images. Automated segmentation techniques can be difficult to develop, especially when the image quality is poor. If the information required for segmentation is not present in the image then no amount of processing will help and the best that can be done is a 'best guess', either by the automated software or by the operator. Usually segmentation in PSM is done as a combination of automated and manual input.

11.3.3 Geometry Preparation

Prior to meshing, the surfaces obtained from segmentation must be prepared. For flow modelling, the blood is only in contact with the inner surface of the vessel. In this case, a single layer surface will suffice. For solid modelling in a vessel both an inner and outer surface are required. Due to imaging constraints, especially in CT, it is often not possible to identify the outer surface of the vessel. In this case, it is commonly assumed that the vessel has a particular wall thickness. In the case of abdominal aortic aneurysm, it is common to assume that the wall has a constant thickness of 1.9 mm (Raghavan et al. 2000), or that the wall thickness varies between 1.5 and 1.13 mm at thrombus-free and covered sites respectively (Gasser et al. 2010). The surfaces of resulting geometries must be smoothed to remove artefacts of the reconstruction algorithm and to ensure that surfaces do not cause undesirable issues during the meshing or modelling stages.

11.3.4 Meshing

Meshing is the process where the 3D segmented geometry is divided into many elements (Figs. 11.3 and 11.4). Mesh generation is one of the critical parts of the patient specific modelling process. Increased solution accuracy is produced with a larger number of elements, but at the expense of increased processing time. The total number of elements employed for a given model is a balance between solution accuracy and processing time. While the mesh is generated using a specialist computer programme, the operator has considerable input in defining element types and element sizes. For example, when there are large velocity gradients or stress gradients then the mesh density needs to be higher. The process of mesh optimisation is therefore essential and involves adjusting the local mesh following examination of the solution. In practice, several iterations between mesh and solution may be

required.

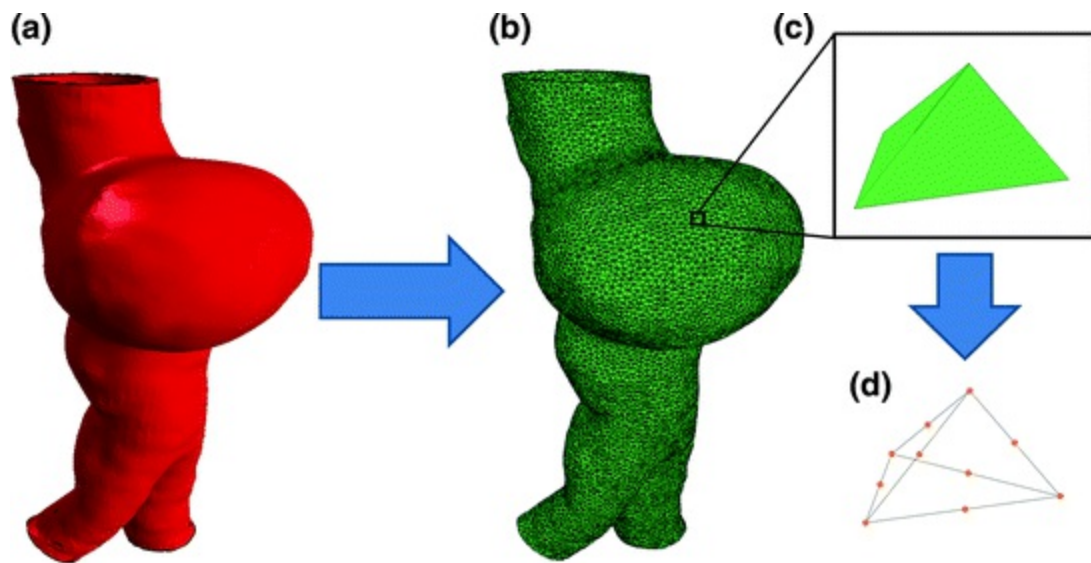


Fig. 11.3 Meshing of an abdominal aortic aneurysm geometry. **a** Reconstructed geometry from CT data. **b** Volume mesh. **c** Tetrahedral element. **d** Close up showing position of the 10 nodes

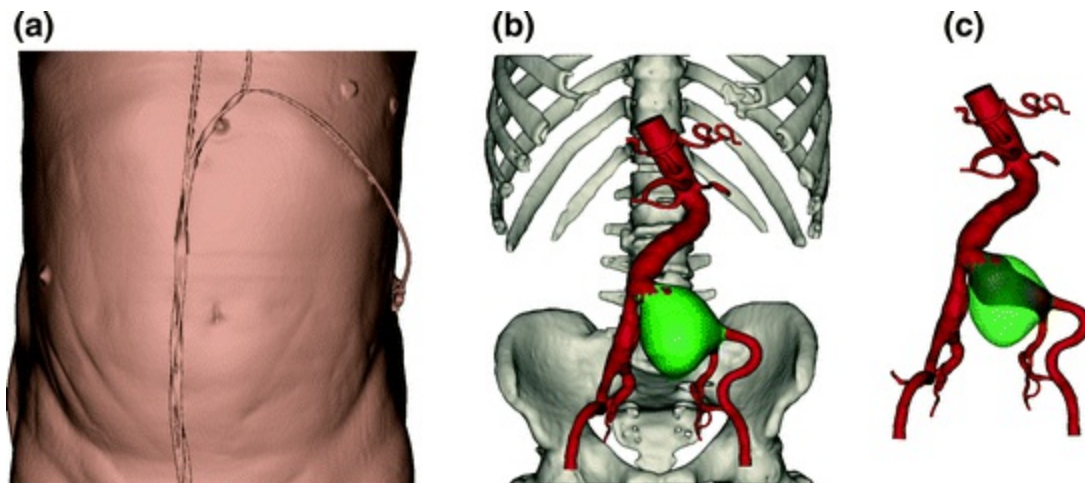


Fig. 11.4 Typical 3D reconstruction based on the marching squares/cubes algorithm in Mimics v18 (Materialise, Belgium). **a** The entire torso with external leads. **b** The main features of the skeleton. **c** The abdominal aorta with infrarenal and renal branches, iliac bifurcation, common iliac arteries and internal/external iliac arteries. This case shows a 91 year old female with an isolated common iliac artery aneurysm and thrombus (*green*)

Different types of element may be used. Common elements are tetrahedron (shaped like a pyramid) or hexahedron (shaped like a brick). Meshes may involve both types of elements. Hexahedral elements are generally more suited to structures with straight edges, hence in PSM the use

of tetrahedral elements is more common. For CFD, some codes such as STAR-CCM+ (CD-adapco Group) use polyhedral elements which offer improved computation time over tetrahedral elements, while maintaining the flexibility of tetrahedral elements to mesh complex geometries.

11.3.5 Computational Modelling

The next stage is computational modelling in which the solution is produced after several iterations. A number of different modelling regimes can be adopted. Computational fluid dynamics can be performed using a rigid-walled approach, which is simple and sufficient for providing output data on basic haemodynamics. A moving-wall method can be adopted with input of moving-wall geometry data. Solid modelling is used for estimation of tissue stress. Solid modelling alone is suitable for estimation of tissue stress in abdominal aortic aneurysms and for 2D studies in atherosclerotic plaque. Combined solid-fluid modelling is called fluid structure interaction or FSI. This is needed when the pressure distribution is not uniform within the 3D geometry and is essential for 3D studies of tissue stress in stenosed arteries.

More advanced modelling regimes have been developed for use in research. These include inverse methods which have been used to account for pre-stressing (Gee et al. 2009) and to estimate patient specific material properties (Chandran et al. 2003; Baldewsing et al. 2008).

11.3.6 Constitutive Model

The computational model needs to account for the governing physical behaviour of the solid or fluid. For blood, it is common to assume that blood is Newtonian, especially in the larger arteries. However, non-Newtonian behaviour can also be assigned. For modelling of the vessel wall, it is common to use a hyperelastic model (described in Chap. 1).

11.3.7 Boundary Conditions

The boundary conditions are the set of additional constraints which are required for modelling.

For CFD in a rigid-walled non-bifurcating vessel, it is sufficient to specify the inlet flow-time waveform; pressure is not needed. It is common to add an extension pipe to the inlet to allow the flow to become fully developed

at the true inlet to the vessel. Information on blood velocity in the individual patient can be obtained from Doppler ultrasound or MRI (Figs. 11.5 and 11.6). For Doppler ultrasound, the maximum velocity–time waveform may be obtained and converted to a flow–time waveform using Womersley equations (Blake et al. 2008). For MRI, a 2D velocity profile may be obtained, with either 1 or 3 velocity components. The use of 3 components allows rotational flow at the inlet to be accounted for. The use of different inlet flows does have a significant impact on the calculated flow patterns as shown in Fig. 11.7.

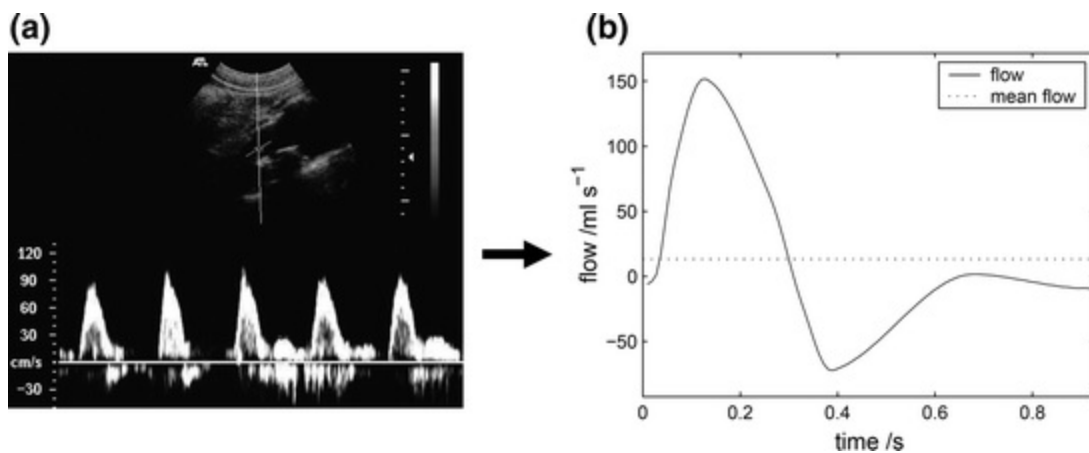


Fig. 11.5 Use of Doppler ultrasound to obtain inlet flow data. This example is from a patient with an abdominal aortic aneurysm. **a** Doppler ultrasound velocity–time waveforms and **b** estimated flow–time waveform

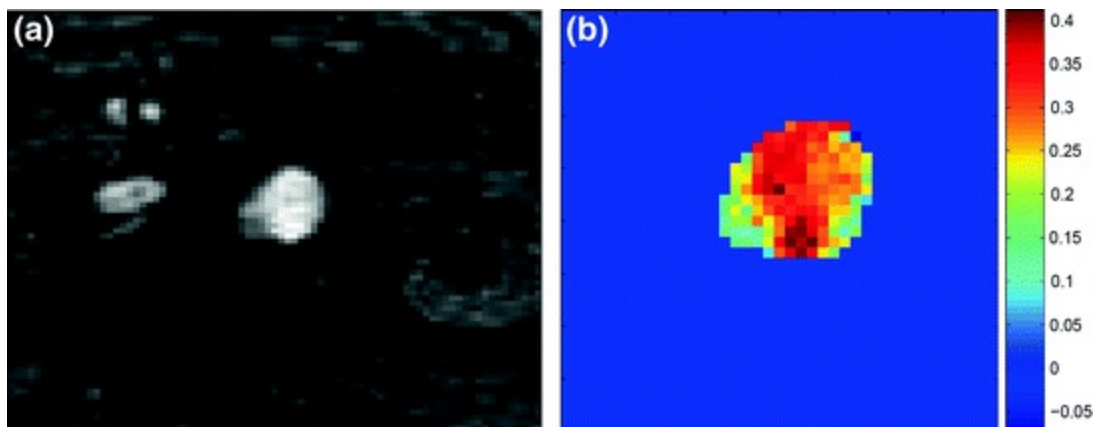


Fig. 11.6 Measurement of the 2D velocity profile using MRI in the abdominal aorta. **a** MRI images and **b** 2D velocity profile

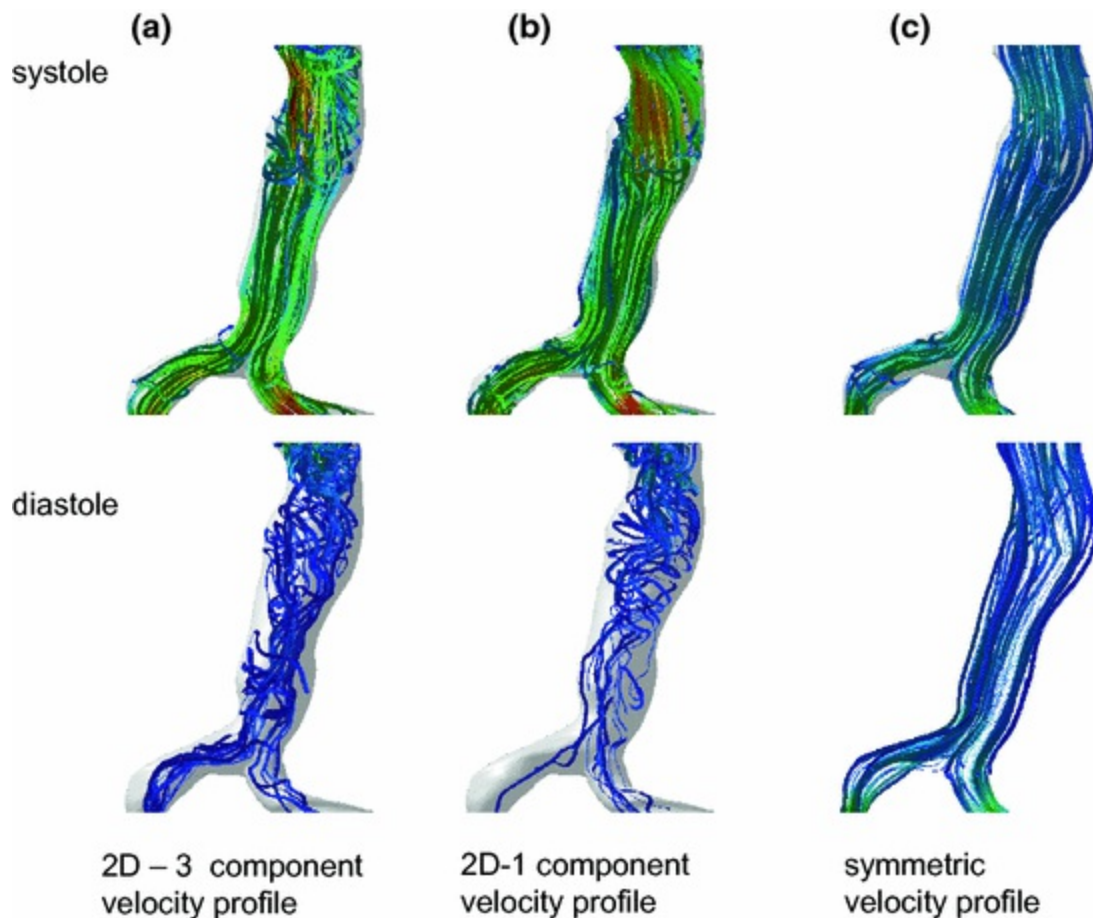


Fig. 11.7 Differences in flow patterns arising from different inlet flows. **a** 2D velocity profile with 3 velocity components, **b** 2D velocity profile with 1 velocity (z) component and **c** axisymmetric profile generated from maximum velocity data

Further information is needed for CFD if there is a bifurcation. Ideally, 3D-models should be coupled to 0D- or 1D-models representing the rest of the circulation in order to obtain accurate estimations of the pressure field (Blanco et al. 2009; Kim et al. 2010). In some fields of research, however, simulations still predominantly make use of a rigid wall assumption, a flow rate waveform at the inlet, and zero pressure conditions at the outlets. This has led to a strong emphasis on wall shear stress over pressure in hemodynamic studies of, for example, cerebral aneurysms (Taylor and Figueroa 2009).

Pressure information may be obtained non-invasively using a monitor with an arm cuff which is applicable for PSM in the brachial artery. Obtaining pressure information for other arteries non-invasively is more difficult and it is common to make assumptions; e.g. simply using the

pressure from the arm cuff.

Additional information on the pattern of loading is also required for the purposes of solid modelling. Loading can be static or dynamic and may be uniformly distributed over the faces of multiple elements in the mesh or applied as concentrated forces at a select group of nodes. For example, in FEA models of abdominal aortic aneurysms loading representative of peak systolic blood pressure, 120 mm Hg (0.016 MPa), is typically applied as an outward facing uniformly distributed pressure load acting on the inner luminal surface of the aneurysm

Consideration of realistic geometry, material properties, boundary conditions and loading are essential in order to obtain accurate results from any FE analysis.

11.3.8 Post-processing

Post-processing is concerned with calculation of relevant quantities from the data. Examples would be wall shear stress or particle paths. Post-processing also involves the creation of image and video files for display.

11.3.9 Display of Data

The final data is displayed on the computer screen, as a video for time-resolved data or as individual images. As the data is 3D the display may be a projection of the 3D dataset from one viewpoint. Several different displays may be used. Figure 11.8 shows display modes for CFD; streamlines for visualisation of overall flow patterns, velocity profiles to examine for asymmetry of flow and wall shear stress.

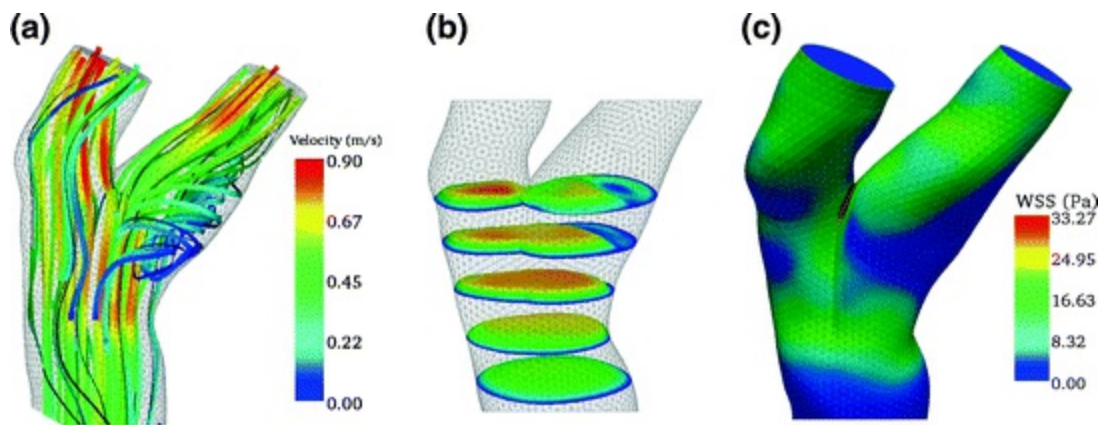


Fig. 11.8 Different display modes for CFD; **a** streamlines, **b** 2D velocity profiles **c** wall shear stress. Reprinted from *Ultrasound in Medicine and Biology*, Vol. 35(12), Hammer S, Jeays A, MacGillivray TJ, Allan PL, Hose R, Barber D, Easson WJ, Hoskins PR; Acquisition of 3D arterial geometries and integration with computational fluid dynamics; pp. 2069–2083, Copyright (2009), with permission from the World Federation for Ultrasound in Medicine & Biology

11.4 Patient Specific Modelling in Practice

This section will describe specific examples of PSM in different vessels drawn from the literature. It is noted that the technical level of material in this section is higher than the rest of the book in order to show how PSM is performed in practice.

11.4.1 Flow in a Cerebral Aneurysm

Patient specific modelling of cerebral aneurysms has focused on the role of haemodynamics in the development and rupture of cerebral aneurysms and the haemodynamic effect of endovascular treatment (Cebal et al. 2011; Larrabide et al. 2013). To illustrate the typical modelling pipeline of this application, we will discuss the details of the pipeline used in Geers et al. (2011). The main steps are visualised in Fig. 11.9.

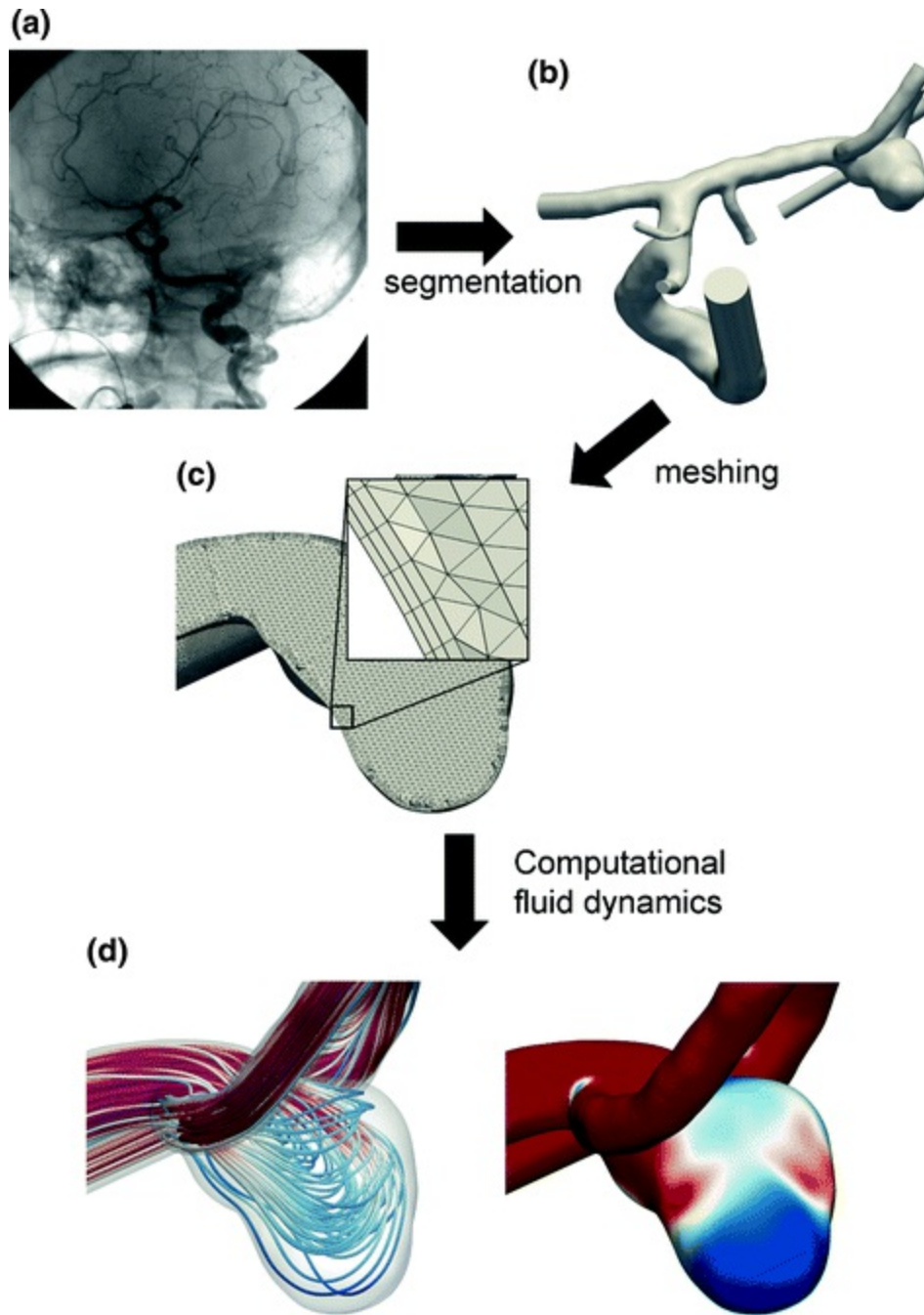


Fig. 11.9 Cerebral aneurysm CFD. **a** Rotational angiography image of the skull. Cerebral aneurysm, **b** Segmented geometry, **c** Meshed geometry close up **d** Flow streamlines and wall shear stress

Patient specific vascular models, represented by triangular surface meshes, were constructed by segmenting 3D rotational angiography (3DRA) images using a geodesic active regions approach (Bogunovic et al. 2011). Manual post-processing operations were applied to separate touching vessels, extrude poorly segmented in- and outlets, smooth the surface and improve the

mesh quality. Operations were performed in ReMESH v2.0 (IMATI-GE/CNR, Genova, Italy) (Attene et al. 2006).

Unstructured volumetric meshes were created with ICEM CFD 13.0 (ANSYS, Canonsburg, PA, USA) using an octree approach. Meshes were composed of tetrahedral elements with a side length of 0.2 mm and three prism layers with a total height of 0.15 mm. The prism layers covered the vessel wall to locally ensure an accurate definition of the velocity gradient for the computation of the wall shear stress.

CFD simulations were created with CFX 13.0 (ANSYS), which is a commercial vertex-centered finite volume solver. Blood was modelled as an incompressible Newtonian fluid with density of 1060 kg m^{-3} and viscosity of 4 mPa s . Vessel walls were assumed rigid with a no-slip boundary condition. A straight inlet extension was added to the image-based vasculature, and a parabolic velocity profile was imposed at the inlet of the extension.

Since patient specific flow information was unavailable the flow rate waveform at the inlet was estimated, and zero pressure boundary conditions were imposed at all outlets. The shape of the flow rate waveform was obtained from phase-contrast MR data of a healthy volunteer. The time-averaged flow rate was chosen to obtain a physiologically realistic mean wall shear stress of 1.5 Pa near the inlet. The cardiac cycle was discretised in time steps of 0.003 s around peak systole, when the time-derivative of the flow rate is relatively large, and 0.02 s elsewhere. Figure 11.10 shows the swirling flow patterns and reduced shear stress within the aneurysm.

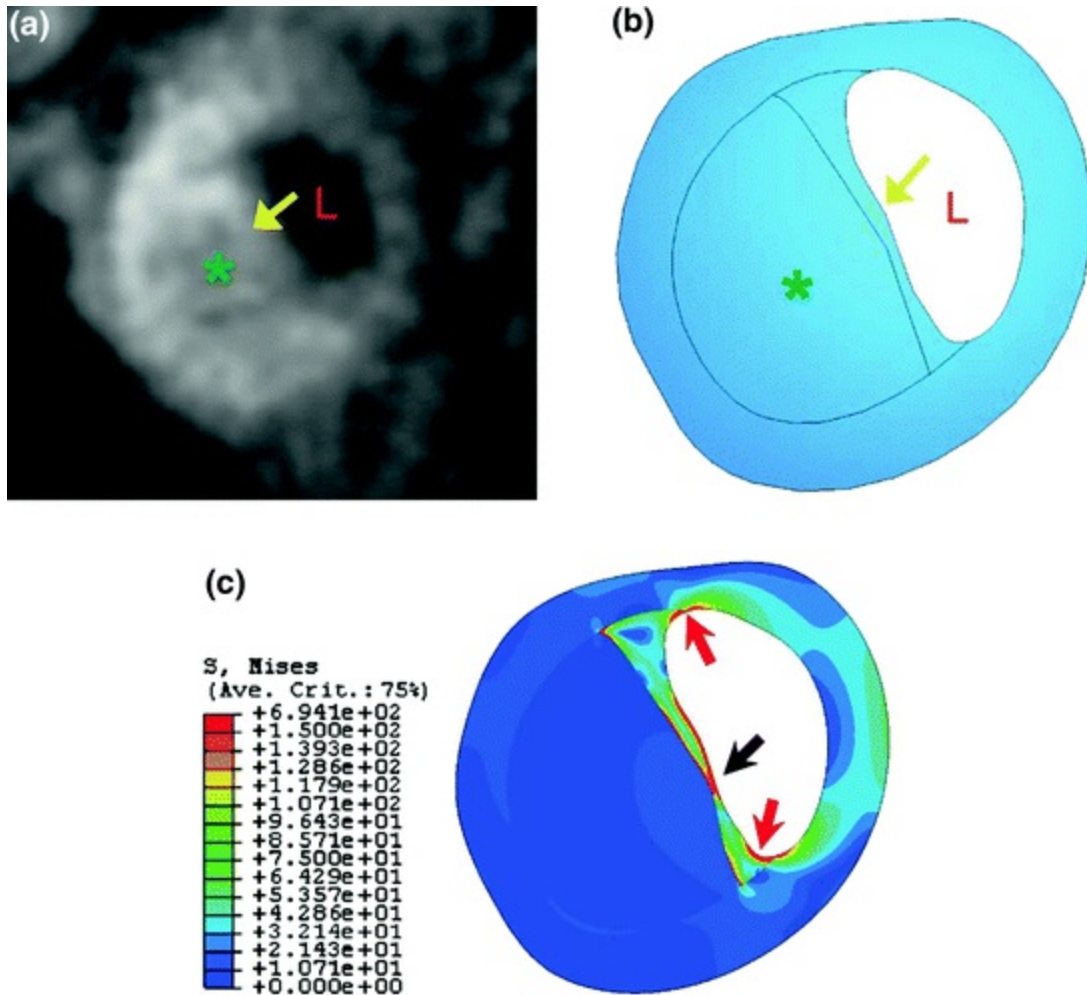


Fig. 11.10 Estimation of 2D stress in an atherosclerotic plaque with the lumen (L), cap (arrow) and lipid pool highlighted (*). **a** MRI scan of the plaque, **b** Segmented image **c** Image of von Mises stress. Reprinted from Journal of Biomechanics, Vol. 39(14), Li ZY, Howarth S, Trivedi RA, U-King-Im JM, Graves MJ, Brown A, Wang L, Gillard JH; pp. 2611–2622, Copyright (2006), with permission from Elsevier

11.4.2 2D Stress Estimation in an Atherosclerotic Plaque

Early work on patient specific modelling of stress in atherosclerotic plaque obtained 2D cross sectional microscopy images from autopsy specimens (Cheng et al. 1993). These showed stress ‘hot spots’ in the thin fibrous cap, leading to the hypothesis that plaque rupture where stress is high (further discussed in Chap. 15). In vivo PSM of stress estimation in plaque involves the use of high-resolution non-invasive imaging. MRI was used to obtain 2D data on plaque composition and estimated tissue stress using FEA (Li et al.

2006). The artery was segmented manually into four regions (wall, lumen, lipid pool, fibrous cap), and a B-spline fitting procedure used to generate the final geometry for meshing. Material properties were assigned based on a 2-term strain energy model:

$$W = \sum_{i=1}^N \frac{\mu_i}{\alpha_i} J^{-\frac{\alpha_i}{3}} (\lambda_1^{\alpha_i} + \lambda_2^{\alpha_i} + \lambda_3^{\alpha_i} - 3) + 4.5 \left(K^{-\frac{1}{3}} - 1 \right)^2,$$

where N is the number of terms taken to be 2. λ_1 is the principle stretch ratio, J is the determinant of the deformation gradient tensor and K the bulk modulus. μ_i are moduli constants and $\mu_1 = -\mu_2$. α_i are exponent constants and $\alpha_1 = -\alpha_2$. Values used are shown in Table 11.1.

Table 11.1 The parameters used for the plaque components and the vessel wall in the Ogden model

Tissues properties	μ_1	μ_2	α_1	α_2	K (Mpa)
Vessel wall	0.0008	-0.0008	30	-30	1600
Fibrous cap	0.0015	-0.0015	30	-30	3000
Lipid pool	0.0001	-0.0001	27	-27	200

Tonometry was used to obtain an uncalibrated pressure waveform. Pressure values were assigned corresponding to 115 mmHg mean pressure and 60 mmHg pulse pressure. Meshes were generated with an average element dimension of 0.1 mm. Solid modelling was performed using an FEA package (Abaqus software V6.5, Rhode Island, Providence, USA). Von Mises stress was displayed using Abaqus post-processing.

Figure 11.10 shows a cross section of the artery from MRI, the segmented geometry and the tissue stress distribution with hot spots at the shoulders of the fibrous cap and in the mid section.

11.4.3 3D Stress Estimation in an AAA

Early work on 3D stress estimation in abdominal aortic aneurysms was performed by Raghavan et al. (2000). Since then several groups have reported 3D stress estimation, discussed in detail in Chap. 16. The workflow described here is based on work undertaken in Edinburgh.

Computed tomography (CT) was used to obtain a high-resolution image stack of a patient specific abdominal aortic aneurysm (AAA) from the MA³RS clinical trial database (McBride et al. 2015). The region of interest

spanned from above the renal arteries to just below the iliac bifurcation (Aquilion One, Toshiba Medical Systems Ltd, UK), the slice thickness was 1 mm, with a pixel size of 0.625 mm.

Segmentation and 3D reconstruction was performed using commercial software (A4 Clinics Research Edition, VASCOPS GmbH, Sweden). The luminal region was segmented automatically using a 2D snake approach, and the outer wall was segmented using a 3D deformable balloon model initiated from the luminal surface. Manual correction of the outer wall contours was carried out on slices, where the automatic algorithms failed to distinguish a clear boundary with the surrounding tissue. Following generation of the outer wall the software then captures the wall-thrombus interface. Rather than assuming a uniform wall thickness of 1.5 mm, this package employs a specialist algorithm to calculate a more physiological aneurysm wall thickness distribution, which varies between 1.5 and 1.13 mm at the thrombus-free and covered sites, respectively (Gasser et al. 2010).

Finite element (FE) meshes were then created from the three-dimensional aneurysm geometry using the A4 clinics research software (VASCOPS), after suitable refinement the meshes typically consisted of >140,000 hexahedral elements (C3D8H). The refined meshes were then exported to Abaqus 6.10-1 (Dassault Systemes, Simulia, Providence, RI, USA) for analysis.

In the present study, both the aortic wall and intraluminal thrombus regions were modelled as hyperelastic, homogeneous, incompressible and isotropic materials, using well established constitutive models with material constants based on population data (Raghavan et al. 2000; Wang et al. 2001). Loading representative of peak systolic blood pressure, 120 mm Hg (0.016 MPa), was applied as an outward facing uniformly distributed pressure load acting on the luminal surface of the aneurysm. The effect of wall shear stress due to blood flow was not considered due to its negligible magnitude. Residual stresses in the aortic wall itself, and the interaction of the aorta with the surrounding structures of the body (e.g. organs and spine), were also not considered; however, displacements at the distal and proximal most regions of each aneurysm were restrained, in all degrees of freedom, to model attachment of the AAA to the rest of the aorta.

Contour plots of the resulting von Mises stress distributions were then visualised using Abaqus/CAE, as shown in Fig. 11.11.

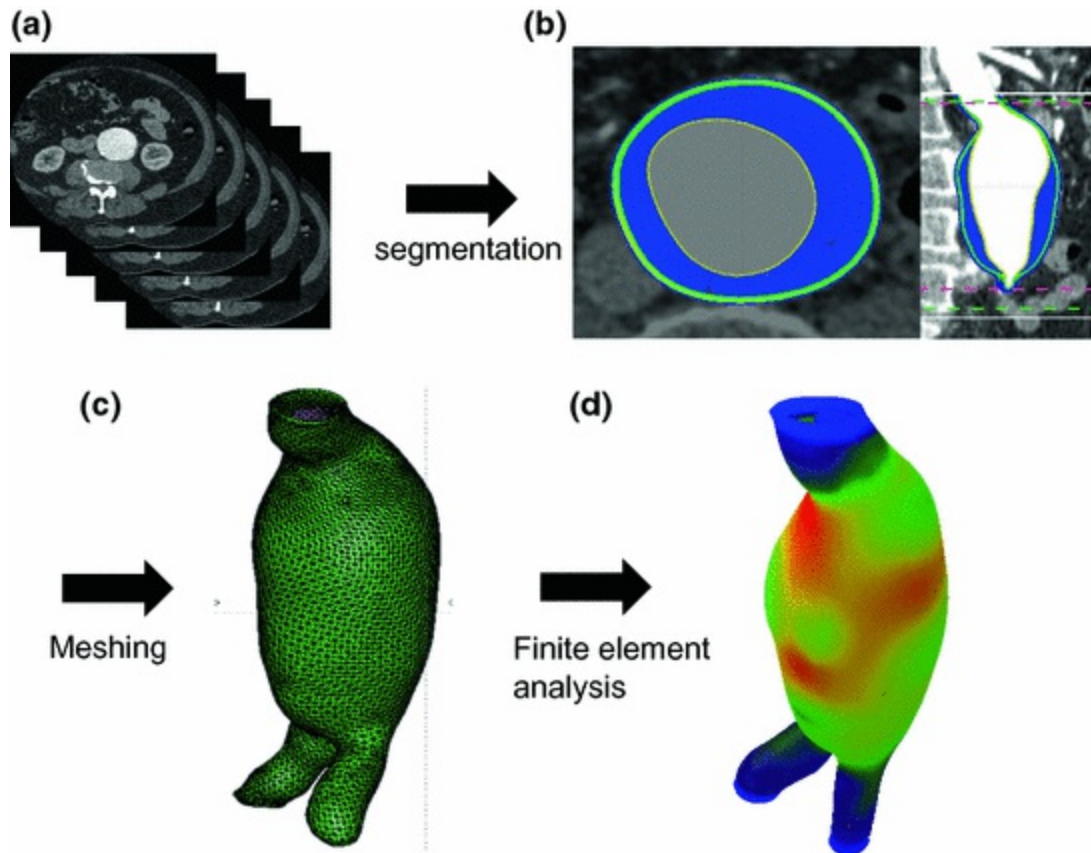


Fig. 11.11 Abdominal aortic aneurysm FEA. **a** CT slices of the aneurysm, **b** Wall and thrombus segmented, **c** Volume mesh **d** Stress estimated using FEA

11.4.4 3D Stress Estimation in an Atherosclerotic Plaque

Section 11.4.2 described 2D stress estimation. Later work from the same group described 3D PSM of atherosclerotic plaque in the carotid bifurcation (Gao et al. 2011). 3D ECG-gated data was obtained from MRI, along with inlet time-varying velocity data. In-house software was created with Matlab to perform manual segmentation on a series of 2D slices; segmenting the lipid core, the arterial wall and lumen (Fig. 11.12). A 3D plaque geometry was constructed from the segmented 2D slices using Solidworks with surface smoothing. A 10 % shrinkage was applied to mimic the stress-free state. An FSI modelling regime was used. For the solid model assumptions were made of incompressibility, isotropy and nonlinearity for the carotid wall. A nonlinear strain energy function was used with parameters described in Gao et al. (2011). The solid modelling mesh consisted of 90,000 10-node

tetrahedral elements. For fluid modelling, the mesh consisted of 1 million 4-node tetrahedral elements. Blood was modelled as a Newtonian incompressible fluid with a viscosity of 4 mPa s with a density of 1067 kg m⁻³. Mass flow rates at the common (CCA) and internal carotid artery (ICA) were obtained from MRI. Mass flow rate in the external carotid artery (ECA) was obtained as the difference between CCA and ICA. CFD simulations were performed to obtain pressure–time curves which were scaled with a physiologic range of 80–110 mmHg. Fully coupled FSI was undertaken for stress analysis; CFD was used to estimate pressure values which were passed to FEA from which displacement was estimated. Displacement values were used to adjust the 3D geometries and a further iteration of CFD/FEA performed. This continued until all fields and loads converged. The final output was the 3D pressure and stress (Fig. 11.13).

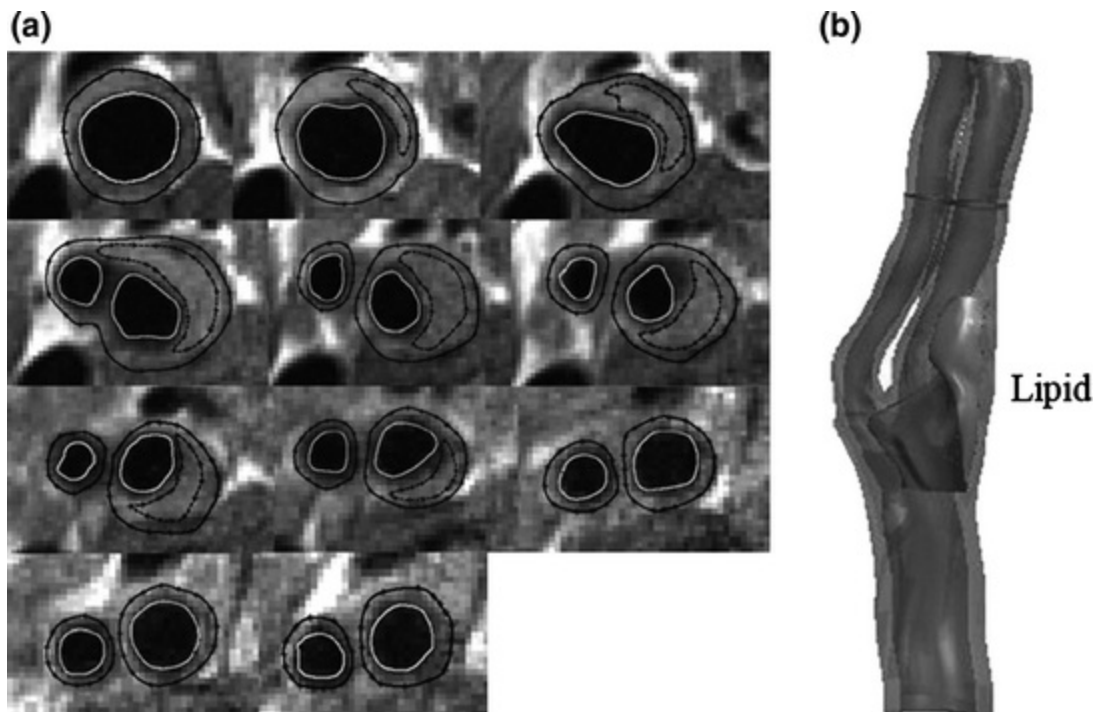


Fig. 11.12 a Sequential MRI slices from a carotid bifurcation with atherosclerosis with segmentation of inner and outer lumen and lipid pool. b Reconstructed geometry of the carotid bifurcation. Reprinted from *Journal of Biomechanics*, Vol. (44), Gao H, Long Q, Kumar Das S, Halls J, Graves M, Gillard JH, Li ZY; Study of carotid arterial plaque stress for symptomatic and asymptomatic patients; pp. 2551–2557, Copyright (2011), with permission from Elsevier

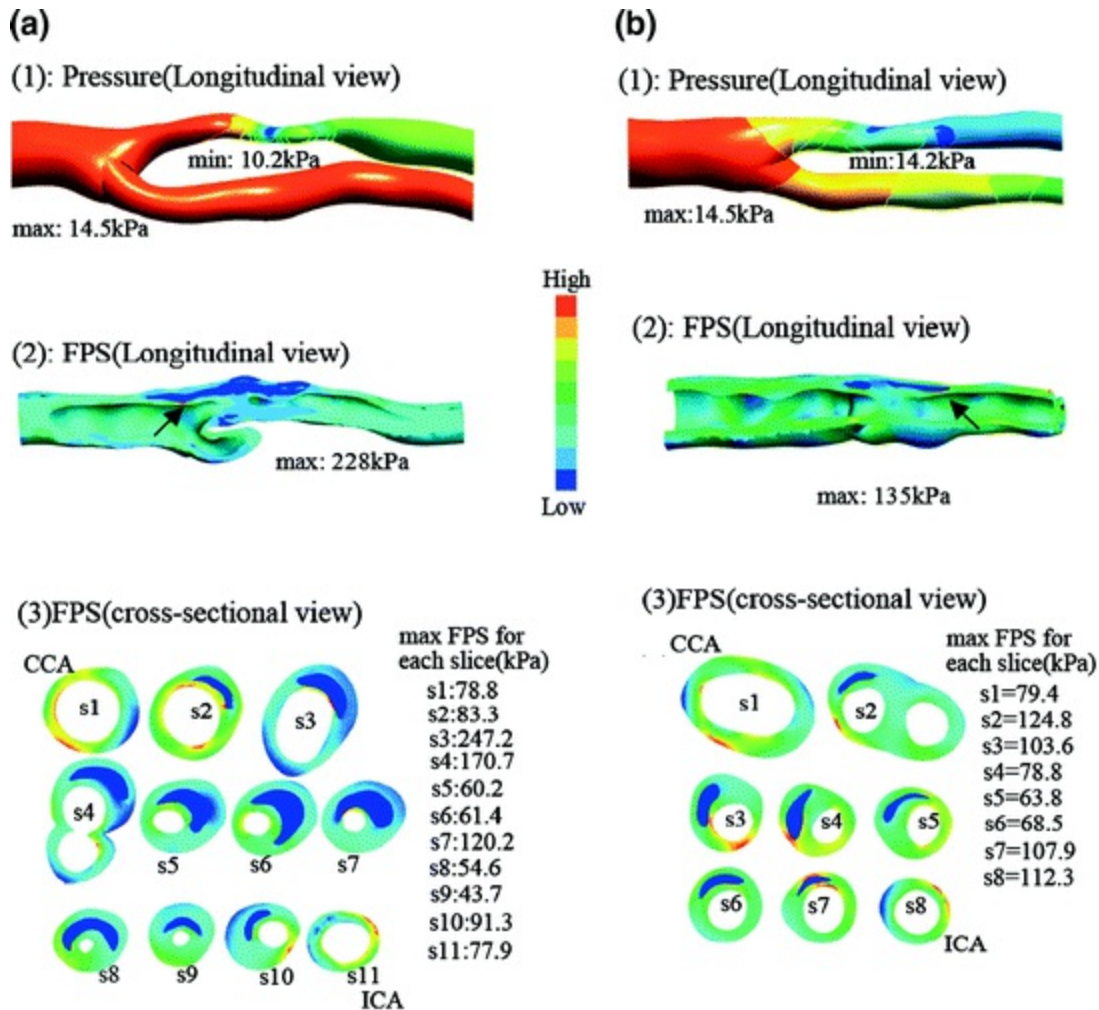


Fig. 11.13 Pressure and wall stress in the carotid bifurcation estimated using computational modelling, where there is atherosclerotic narrowing in the internal carotid artery using the geometries shown in Fig. 11.12. Reprinted from Journal of Biomechanics, Vol. (44), Gao H, Long Q, Kumar Das S, Halls J, Graves M, Gillard JH, Li ZY; Study of carotid arterial plaque stress for symptomatic and asymptomatic patients; pp. 2551–2557, Copyright (2011), with permission from Elsevier

11.4.5 Patient Specific Modelling Without PSM-Specific Material Properties

There is considerable variation between material properties measured from patient to patient, and the typical assumptions used in stress modelling that patients have similar material properties impacts the usefulness of the approach. Readers with a background in engineering mechanics may be familiar with statically determinate structures. Such structures are ones in which the reactions and internal forces can be solely determined from equations of equilibrium. What this means is that results of stress analyses are

independent of material properties. In practice, this means that computational models reconstructed from medical images of a living patient are reconstructions of a loaded geometry as the vessel is already subjected to internal pressurisation. Taking advantage of this enables stress analysis to be performed on multi-material vessel structures, so long as sensible ratios of stiffness between materials is maintained. This approach eliminates the inter-patient variability of material properties. This is an emerging area of research and applicable to a wide range of patient specific modelling scenarios (Miller and Lu 2013; Joldes et al. 2009).

References

Antiga L, Piccinelli M, Botti L, Ene-Iordache B, Remuzzi A, Steinman DA. An image-based modeling framework for patient-specific computational hemodynamics. *Med Biol Eng Comput.* 2008;46:1097–112.

[\[CrossRef\]](#)[\[PubMed\]](#)

Attene M, Falcidieno B. ReMESH: an interactive environment to edit and repair triangle meshes. In: *Proceedings IEEE international conference on shape modeling and applications 2006 (SMI'06)*; 2006. p. 271–6.

Baldewsing RA, Danilouchkine MG, Mastik F, Schaar JA, Serruys PW, van der Steen AFW. An inverse method for imaging the local elasticity of atherosclerotic coronary plaques. *IEEE Trans Informat Technol Biomed.* 2008;12:277–89.

[\[CrossRef\]](#)

Blanco PJ, Pivello MR, Urquiza SA, Feijoo RA. On the potentialities of 3D-1D coupled models in hemodynamics simulations. *J Biomech.* 2009;42:919–30.

[\[CrossRef\]](#)[\[PubMed\]](#)

Blake JR, Meagher SC, Fraser KH, Easson WJ, Hoskins PR. A method to estimate wall shear rate with clinical ultrasound scanners. *Ultrasound Med Biol.* 2008;34:760–74.

[\[CrossRef\]](#)[\[PubMed\]](#)

Bogunovic HJ, Pozo M, Villa-Uriol MC, Majoie CB, van den Berg R, van Andel HAFG, Macho JM, Blasco J, San Roman L, Frangi AF. Automated segmentation of cerebral vasculature with aneurysms in 3DRA and TOF-MRA using geodesic active regions: an evaluation study. *Med Phys.* 2011;38:210–22.

Cebal JR, Mut F, Weir J, Putman CM. Quantitative characterization of the hemodynamic environment in ruptured and unruptured brain aneurysms. *AJNR Am J Neuroradiol.* 2011;32:145–51.

[\[CrossRef\]](#)[\[PubMed\]](#)

Chandran KB, Vonesh MJ, Roy A, Greenfield S, Kane B, Greene R, McPherson DD. Computation of vascular flow dynamics from intravascular ultrasound images. *Med Eng Phys.* 1996;18:295–304.

[\[CrossRef\]](#)[\[PubMed\]](#)

Chandran KB, Mun JH, Choi KK, Chen JS, Hamilton A, Nagaraj A, et al. A method for in-vivo analysis for regional arterial wall material property alterations with atherosclerosis: preliminary results. *Med Eng Phys.* 2003;25:289–98.

[\[CrossRef\]](#)[\[PubMed\]](#)

Chapra S, Canale R. *Numerical methods for engineers.* 7th ed. New York: McGraw-Hill; 2014.

Cheng GC, Loree HM, Kamm RD, Fishbein MC, Lee RT. Distribution of circumferential stress in ruptured and stable atherosclerotic lesions—a structural-analysis with histopathological correlation. *Circulation.* 1993;87:1179–87.

[\[CrossRef\]](#)[\[PubMed\]](#)

Ethier CR, Steinman DA, Ojha M. Comparisons between computational hemodynamics, photochromic dye flow visualization and magnetic resonance velocimetry. In: Collins MW, Xu Y, editors. *Hemodynamics of internal organs.* Southampton: WIT Press; 1999. p. 131–83.

Friedman MH, Ehrlich LW. Numerical simulation of aortic bifurcation flows: the effect of flow divider curvature. *J Biomech.* 1984;17:881–8.

[\[CrossRef\]](#)[\[PubMed\]](#)

Gao H, Long Q, Kumar Das S, Halls J, Graves M, Gillard JH, Li ZY. Study of carotid arterial plaque stress for symptomatic and asymptomatic patients. *J Biomech.* 2011;44:2551–7.

Gasser TC, Auer M, Labruto F, Swedenborg J, Roy J. Biomechanical rupture risk assessment of abdominal aortic aneurysms: model complexity versus predictability of finite element simulations. *Eur J Vasc Endovasc Surg.* 2010;40:176–85.

[\[CrossRef\]](#)[\[PubMed\]](#)

Gee MW, Reeps C, Eckstein HH, Wall WA. Prestressing in finite deformation abdominal aortic aneurysm simulation. *J Biomech.* 2009;42:1732–9.

[\[CrossRef\]](#)[\[PubMed\]](#)

Geers AJ, Larrabide I, Radaelli AG, Bogunovic H, Kim M, van Andel HAFG, Majoie CB, VanBavel E, Frangi AF. Patient-specific computational hemodynamics of intracranial aneurysms from 3D rotational angiography and CT angiography: an in vivo reproducibility study. *Am J Neuroradiol.* 2011;32:581–6.

[\[CrossRef\]](#)[\[PubMed\]](#)

Hammer S, Jeays A, MacGillivray TJ, Allan PL, Hose R, Barber D, Easson WJ, Hoskins PR. Acquisition of 3D arterial geometries and integration with computational fluid dynamics. *Ultrasound Med Biol.* 2009;35(12):2069–83.

[\[CrossRef\]](#)[\[PubMed\]](#)

Hoskins PR, Hardman D. 3D imaging and computational modelling for estimation of wall stress in diseased arteries. *Brit J Radiol.* 2009;82:S3–17.

[\[CrossRef\]](#)[\[PubMed\]](#)

Joldes GR, Miller K, Wittek A, Doyle BJ. A simple, effective and clinically-applicable method to compute abdominal aortic aneurysm wall stress. *J Mech Behav Biomed Mat.* 2016;58:139–48

Kim HJ, Vignon-Clementel IE, Coogan JS, Figueroa CA, Jansen KE, Taylor CA. Patient-specific modeling of blood flow and pressure in human coronary arteries. *Ann Biomed Eng.* 2010;38:3195–209.

[CrossRef][PubMed]

Krams R, Wentzel JJ, Oomen JAF, Vinke R, Schuurbiens JCH, de Feyter PJ, Serruys PW, Slager CJ. Evaluation of endothelial shear stress and 3D geometry as factors determining the development of atherosclerosis and remodeling in human coronary arteries in vivo—combining 3D reconstruction from angiography and IVUS (ANGUS) with computational fluid dynamics. *Arterioscler Thromb Vasc Biol.* 1997;17:2061–5.

[CrossRef][PubMed]

Larrabide I, Aguilar ML, Morales HG, Geers AJ, Kulcsar Z, Rufenacht DA, Frangi AF. Intra-aneurysmal pressure and flow changes induced by flow diverters: relation to aneurysm size and shape. *Am J Neuroradiol.* 2013;34:816–22.

[CrossRef][PubMed]

Li ZY, Howarth S, Trivedi RA, U-King-Im JM, Graves MJ, Brown A, et al. Stress analysis of carotid plaque rupture based on in vivo high resolution MRI. *J Biomech.* 2006;39(14):2611–22.

Loree HM, Kamm RD, Stringfellow RG, Lee RT. Effects of fibrous cap thickness on peak circumferential stress in model atherosclerotic vessels. *Circ Res.* 1992;71:850–8.

[CrossRef][PubMed]

McBride OMB, Berry C, Burns P, Chalmers RTA, Doyle B, Forsythe R, Garden OJ, Goodman K, Graham C, Hoskins P, Holdsworth R, MacGillivray TJ, McKillop G, Murray G, Oatey K, Robson JMJ, Roditi G, Semple S, Stuart W, van Beek EJ, Vesey A, Newby DE. MRI using ultrasmall superparamagnetic particles of iron oxide in patients under surveillance for abdominal aortic aneurysms to predict rupture or surgical repair: MRI for abdominal aortic aneurysms to predict rupture or surgery—the MA3RS study. *Open Heart* 2015;2:2. doi:10.1136/openhrt-2014-000190.

Miller K, Lu J. On the prospect of patient-specific biomechanics without patient-specific properties of tissues. *J Mech Behav Biomed Mater.* 2013;27:154–66.

[CrossRef][PubMed][PubMedCentral]

Minev PD, Ethier CR. A characteristic/finite element algorithm for the Navier-Stokes equations using unstructured grids. *Comput Meth Appl Mech Engng.* 1998;178:39–50.

[CrossRef]

Morris PD, Narracott AJ, von Tengg-Koblingk H, Silva Soto DA, Hsiao S, Lungu A, Evans P, Bressloff NW, Lawford PV, Hose DR, Gunn JP. Computational fluid dynamics modelling in cardiovascular medicine. *Heart* 102;18–28. doi:10.1136/heartjnl-2015-308044.

Neal ML, Kerckhoffs R. Current progress in patient-specific modeling. *Brief Bioinform.* 2010;11:111–26.

[CrossRef][PubMed]

Perktold K, Gruber K, Kenner T, Florian H. Calculation of pulsatile flow and particle paths in an aneurysm-model. *Basic Res Cardiol.* 1984;79:253–61.

[CrossRef][PubMed]

Raghavan ML, Vorp DA, Federle MP, Makaroun MS, Webster MW. Wall stress distribution on three-dimensionally reconstructed models of human abdominal aortic aneurysm. *J Vasc Surg.* 2000;31:760–9.

[CrossRef][PubMed]

Richardson PD, Davies MJ, Born GVR. Influence of plaque configuration and stress-distribution on fissuring of coronary atherosclerotic plaques. *Lancet*. 1989;2:941–4.

[\[CrossRef\]](#)[\[PubMed\]](#)

Rybicki EF, Weis EB, Simonen FA. Mathematical analysis of stress in human femur. *J Biomech*. 1972;5:203–15.

[\[CrossRef\]](#)[\[PubMed\]](#)

Sherwin SJ, Karniadakis GE. A triangular spectral element method—applications to the incompressible Navier-Stokes equations. *Comput Methods Appl Mech Eng*. 1995;123:189–229.

[\[CrossRef\]](#)

Taylor CA, Figueroa CA. Patient-specific modeling of cardiovascular mechanics. *Ann Rev Biomed Eng*. 2009;11:109–34.

[\[CrossRef\]](#)

Thresher RW, Saito GE. The stress analysis of human teeth. *J Biomech*. 1973;6:443–4411.

[\[CrossRef\]](#)[\[PubMed\]](#)

Turner MJ, Clough RW, Martin HC, Topp LJ. Stiffness and deflection analysis of complex structures. *J Aeronaut Sci*. 1956;23:805–23.

[\[CrossRef\]](#)

Wang DHJ, Makaroun M, Webster MW, Vorp DA. Mechanical properties and microstructure of intraluminal thrombus from abdominal aortic aneurysm. *J Biomech Eng*. 2001;123:536–9.

[\[CrossRef\]](#)[\[PubMed\]](#)

Witherden FD, Farrington AM, Vincent PE. PyFR: an open source framework for solving advection–diffusion type problems on streaming architectures using the flux reconstruction approach. *Comput Phys Comm*. 2014;185:3028–40.

[\[CrossRef\]](#)

Xu C, Pham DL, Prince JL. 2000. Image segmentation using deformable models. In: Fitzpatrick JM, Sonka M, editors. *Handbook of medical imaging, volume 2, Medical image processing and analysis*. SPIE Press: Bellingham, USA; 2000. pp. 129–74.

Zienkiewicz OC. The birth of the finite element method and of computational mechanics. *Int J Num Meth Eng*. 2004;60:3–10.

[\[CrossRef\]](#)

Zienkiewicz OC, Taylor RL, Zhu JZ. *The finite element method: its basis and fundamentals*. 7th ed. Oxford: Butterworth-Heinemann; 2005.

12. Flow Phantoms

Peter R. Hoskins¹ 

(1) Edinburgh University, Edinburgh, UK

 **Peter R. Hoskins**
Email: P.Hoskins@ed.ac.uk

Learning outcomes

1. Discuss the rationale for the design and use of flow phantoms.
2. Describe optical techniques for visualisation and measurement of flow-fields in flow phantoms (flow visualisation, PI, PTV, LDA).
3. Describe methods of construction of phantoms based on 3D printing, corrosion casting and mould manufacture from milling.
4. Describe the design requirement for phantoms designed for different types of medical imaging.
5. Describe common materials used for the construction of phantoms.
6. Describe methods for formulation of tissue mimic, blood mimic and vessel mimic for flow phantoms used in MRI and ultrasound.

7. Describe the design and use of endothelial flow phantoms.

8. Describe the design and use of whole-artery flow phantoms.

12.1 Introduction to Flow Phantoms

A brief discussion will be presented on the rationale for design and use of flow phantoms. This underpins the remainder of the chapter, however the reader may wish to return to this section once specific examples of flow phantoms have been described.

Flow phantoms are used in the laboratory to mimic the flow of blood in some part of the cardiovascular system in such a manner which allows experiments to be undertaken which would be difficult, or impossible, in the living human. The flow phantom typically consists of a central construct which mimics the geometry of part of the cardiovascular system through which a blood mimic is pumped (Fig. 12.1). An imaging device is used to record information on fluid velocity and related quantities within the central construct.

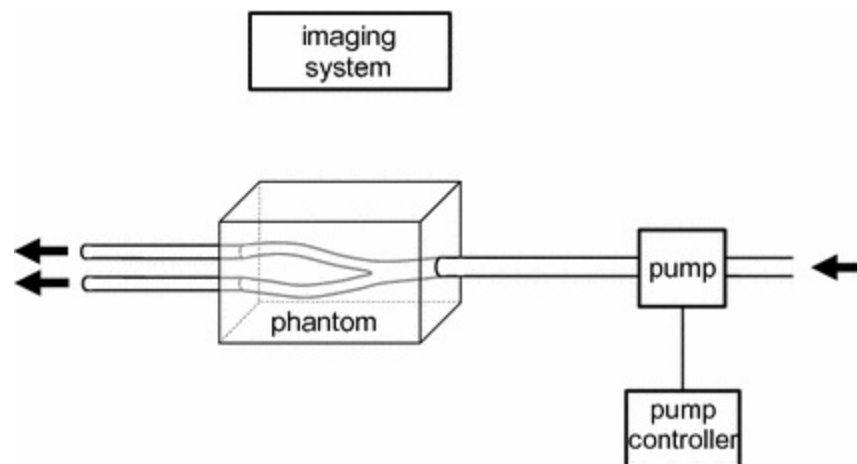


Fig. 12.1 Components of a flow phantom. The phantom mimics the cardiovascular geometry and is connected to a pump by tubing. A pump controller, usually a computer, enables programming of specific flow waveforms. An imaging system is used to record information on blood mimic velocities within the phantom

There are various terms used in the literature including ‘experimental flow system’, ‘phantom’ and ‘flow phantom’. In this chapter, the term

‘phantom’ will be used to describe the central cardiovascular construct, and ‘flow phantom’ used to describe the entire apparatus consisting of pump, pump controller, tubing, reservoirs and the phantom. The phantom consists of components which mainly mimic 2 tissues; the blood (blood mimic) and the soft tissue (tissue mimic). For phantoms mimicking flow in vessels the soft tissue may be further divided into the artery or vein (vessel mimic) and the surrounding soft tissue consisting of fat, muscle, liver, kidney, etc. (tissue mimic).

The advantages of using a flow phantom over an in vivo experiment are:

- *Control.* High degree of control over experimental conditions including vessel geometry and flow rates.
- *Reproducibility.* Ability to undertake repeated experiments with identical experimental conditions.
- *Licensing and safety.* Avoidance of the use of biological material (e.g. blood, arteries, animal models) which may be difficult to obtain, require specialist biological facilities and use-licenses and which may be hazardous.
- *Optical transparency.* Ability to create phantoms which can be used with imaging systems with high temporal and spatial resolution (i.e. optical imaging systems).

The main disadvantage of using a flow phantom over an in vivo experiment is

- *Inadequate mimicking.* The phantom may not adequately mimic the characteristics of the cardiovascular system (e.g. vascular geometry, arterial wall properties, haemodynamics) hence conclusions from experiments may not be applicable in vivo.

The flow phantom replicates or mimics key aspects of the cardiovascular system. The flow phantom cannot mimic in detail all aspects of the cardiovascular system. One might then ask: how complicated does the flow phantom need to be? As with computational models discussed earlier (Chap. 10), the flow phantom needs to be sufficiently complex to allow a specific research question to be answered. This rationale then dictates that the research question comes first, and the flow phantom design follows the research question. If the research question changes then this may require

redesign of aspects of the flow phantom. Another way of expressing this rationale is that the flow phantom is a simplified version of reality. The design of the flow phantom needs to be as complicated as necessary and no more complicated than that. An overcomplicated flow phantom will mean unnecessary effort in construction. It is noted that a similar rationale was discussed in Chap. 10 on the complexity of the computational model.

There are three main uses of flow phantoms:

- *Investigation of flow-field velocity data and associated phenomena.* Optical imaging systems such as PIV (particle image velocimetry) and LDA (laser Doppler anemometry) have high spatial and temporal resolution and have been mostly used for measurement of flow-field velocity data and associated phenomena.
- *Validation of flow-field data obtained using medical imaging.* Medical imaging systems such as MRI and ultrasound can be used to measure blood velocity and associated quantities. Validation of measured velocity is commonly undertaken using flow phantoms.
- *Investigation of the relationship between flow and aspects of biological function of the vessel wall.* These flow phantoms are mostly concerned with endothelium which is cultured on the walls of a flow chamber where the relationship between wall shear rate and endothelial function is of interest.

12.2 Optically Transparent Phantoms

The use of an optically transparent phantom allows direct visualisation of flow patterns and measurement using optical techniques. This section will describe phantom construction and the associated optical imaging techniques. Further reading of optical techniques with respect to use in medical applications is given in the reviews by Hoskins (2008) and Vennemann et al. (2007).

12.2.1 Flow Visualisation

This is the simplest method for investigating flow patterns. The flow is seeded with a material which ideally is neutrally buoyant and can be visualised. Materials which have been used include injected dyes and inks,

hydrogen bubbles, hollow glass spheres and a variety of solid particles. The seeded material will follow the flow-streamlines allowing the observer to visualise flow patterns. A video camera can be used to record the progress of the seeded material. In Fig. 1.18 a simple straight tube phantom with dye injection illustrated the difference between laminar flow and turbulence. Phantoms with anatomical geometry provided early evidence of complex flow patterns in bifurcations, including flow recirculation and helical flow (Ku and Giddens 1983; Zarins et al. 1983) (Fig. 12.2). Flow visualisation as its name implies is only concerned with qualitative visualisation of flow patterns, not quantitative measurement of velocities.

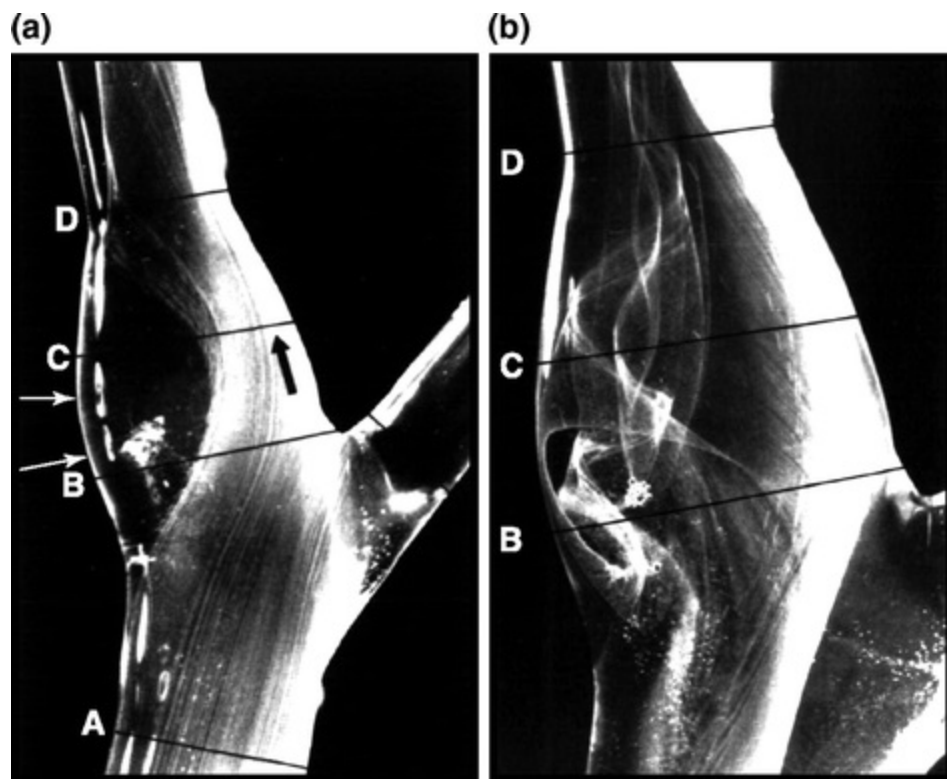


Fig. 12.2 Flow visualisation in a model of the carotid bifurcation. From;Zarins CK, Giddens DP, Bharadvaj BK, Sottiurai VS, Mabon RF, Glagov S; Carotid bifurcation atherosclerosis. Quantitative correlation of plaque localization with flow velocity profiles and wall shear stress; *Circulation Research* 1983;53(4):502–514; reprinted with permission by Wolters Kluwer Health, Inc. *Circulation Research* is an official journal of the American Heart Association

12.2.2 Particle Image Velocimetry (PIV) and Particle Tracking Velocimetry (PTV)

Quantitative measurement of the velocity field may be undertaken using

particle image velocimetry (PIV). In PIV the fluid is seeded with particles at low concentration of typically less than 1 % by volume. A pulsed laser is used to illuminate a single plane within the flow. A video camera is used to record sequential images of the illuminated particles. Between images the particles move a small distance. Image processing algorithms applied to groups of particles are used to estimate the distance the particles have moved; this distance is divided by the time between images to obtain the local velocity. Figure 12.3 shows an example of PIV data taken in a stenosis phantom. A related technique is particle tracking velocimetry (PTV) in which individual particles are tracked rather than groups of particles. Further details of PIV and PTV technology are provided by Adrian (1991), Westerweel (1997) and Prasad (2000).

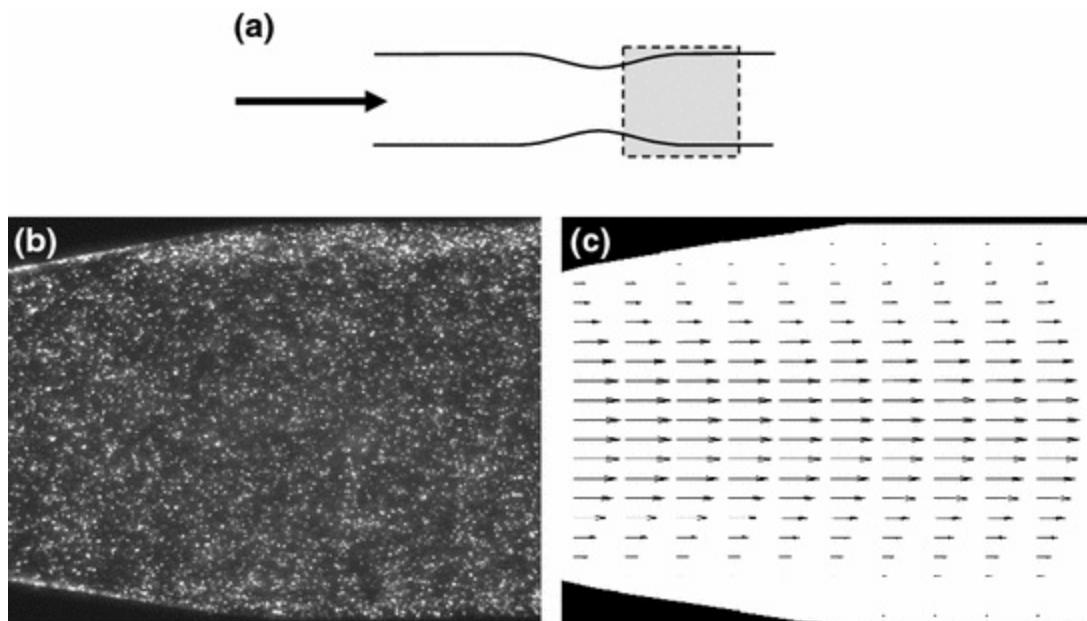


Fig. 12.3 PIV in a stenosis model. **a** The interrogation region is shown as shaded in the schematic. **b** A typical PIV image; each bright dot represents a particle or group of particles. **c** Estimated velocity field

PIV provides high accuracy high resolution data on the velocity field. Due to its simplicity, accuracy and robustness it is regarded as providing gold-standard data, which is useful in validation of flow-field data obtained from CFD or from medical imaging.

12.2.3 Laser Doppler Anemometry (LDA)

Quantitative measurement of velocity may also be undertaken using laser

Doppler anemometry (LDA). Two laser beams of the same frequency overlap producing a set of interference fringes within the overlap region. Particles moving through the interference fringes scatter light. The scattered light is detected by a photodetector. The frequency of the scattered light is dependent on the velocity of the particle and also on the angle between the direction of motion and the laser interference wave direction. This is very similar to Doppler ultrasound in that the motion of a particle produces a Doppler frequency shift. Common positions for the detector are on the opposite side to the laser or on the same side. Use of a single detector enables measurement of one velocity component whereas use of multiple detectors allows measurement of two or three velocity components. Information is gathered at a single point, however 3D information may be obtained by scanning the interrogation region through the flow field. Information is gathered continuously so that LDA may be used to study high frequency changes in the flow field associated with turbulence. Further details of LDA technology are provided by Tropea (1995); Liepsch et al. (1998) reviews the use of LDA in carotid artery phantoms.

12.2.4 Phantom Construction

Materials which are optically transparent and which have been used for phantom manufacture include glass, acrylic, polyester and silicone elastomers. The use of glass is challenging requiring phantom manufacture using glass-blowing. Most optically transparent phantoms with complex vascular geometries are manufactured using polyester, acrylic or silicone elastomers using a casting technique involving pouring and setting of the liquid. A simple straight tube model may be manufactured using metal rods which are joined together. These rods are positioned in a box and the liquid is poured into the box, allowed to set and the rods removed (Fig. 12.4).

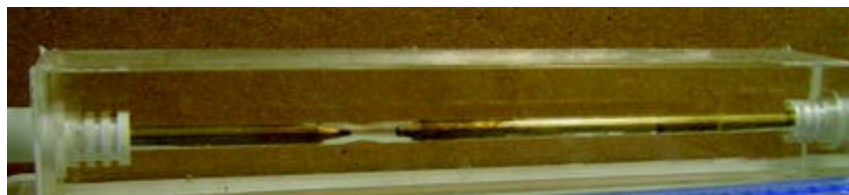


Fig. 12.4 Straight-tube stenosis phantom for use in PIV. The metal rods used in construction are shown positioned within the phantom

3D cardiovascular geometries such as bifurcations require a more complicated manufacturing approach. Phantom manufacture is increasingly dominated by recent developments in rapid-prototyping (3D printing). Figure 12.5 summarises the steps which have been taken in published studies and are described below.

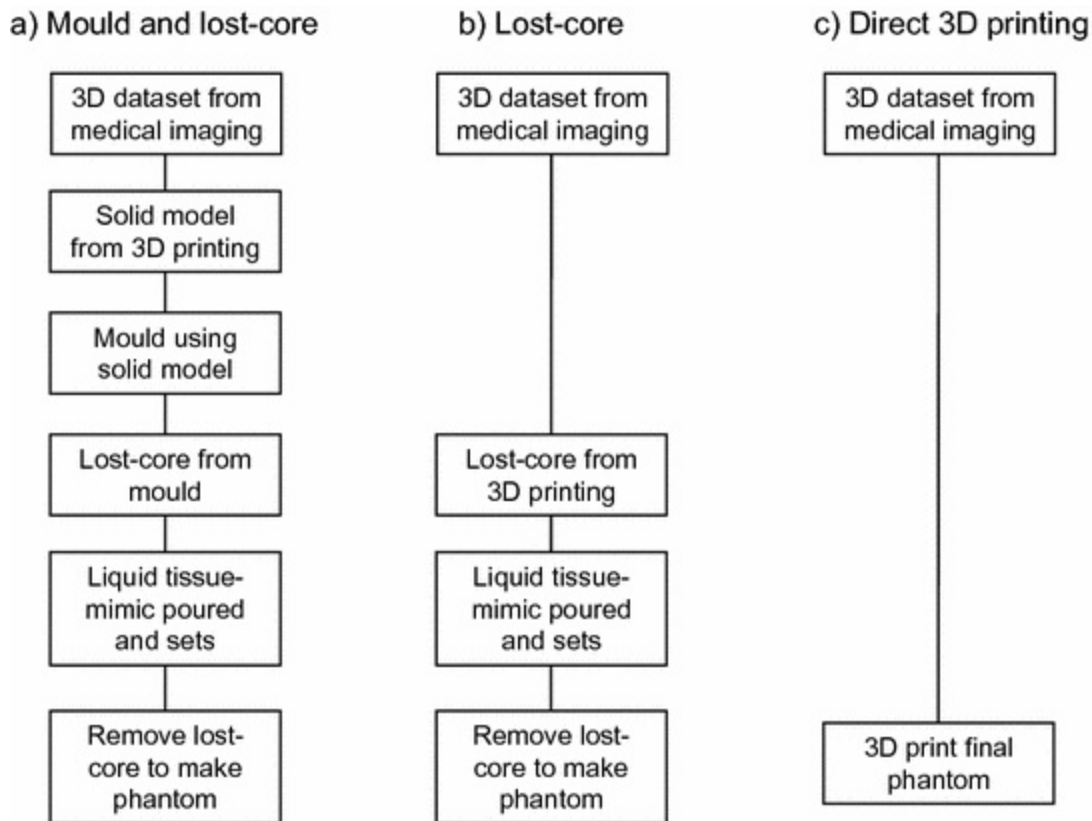


Fig. 12.5 Steps in the manufacture of 3D phantoms using 3D printing. **a** Mould and lost core. **b** Lost core. **c** Direct 3D printing

- *Mould and lost core.* This method is exemplified by Watts et al. (2007). A 3D dataset of the carotid bifurcation is obtained from a volunteer using MRI. This is used to generate an idealised CAD (computer-aided design file) in which surfaces are smoothed and some arterial segments straightened (Fig. 12.6a). A solid model of the bifurcation is 3D printed. This is used to make a mould consisting of silicone. A low melting point alloy is poured into the mould. After cooling, the metal core is removed (Fig. 12.6b) and incorporated into a container with suitable inlet and outlet connections. Liquid silicone elastomer is poured into the box and allowed to set. Once set the container is heated resulting in melting of

the metal core which can then be poured out leaving the final phantom containing the anatomical geometry (Fig. 12.6c). Doyle et al. (2008) also describes this process step by step for use in creating abdominal aortic aneurysm phantoms.

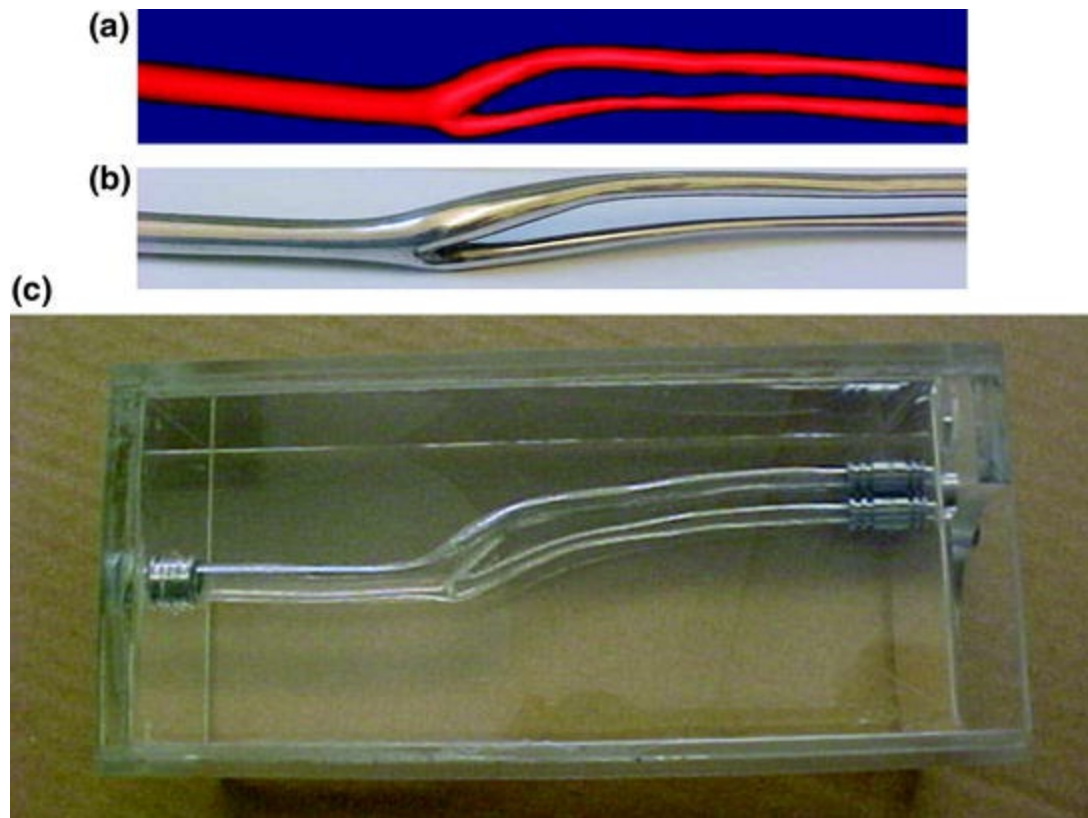


Fig. 12.6 Bifurcation phantom for use in optical studies manufactured using the ‘mould and lost core’ approach. **a** CAD image. **b** Lost core. **c** Final phantom. See Watts et al. (2007) for more detail

- **Lost core.** This method is exemplified by Geoghegan et al. (2012). The procedure is similar to that described above except the steps involving the mould are missing. The lost core is 3D printed directly. The lost core is composed of water-dissoluble plaster powder. This is coated with PVA which provides smoothness, strength and acts to prevent ingress of the liquid silicone elastomer. After the elastomer has set the core is removed through a combination of water and physical erosion with a soft scraper, producing the final phantom (Fig. 12.7).



Fig. 12.7 Carotid artery bifurcation rigid flow phantom. The phantom is for use in optical studies manufactured using the ‘lost core’ approach. From; *Experiments in Fluids; Fabrication of rigid and flexible refractive-index-matched flow phantoms for flow visualisation and optical flow measurements*; Vol. 52, 2012, pp. 1331–1347, Geoghegan P, Buchmann N, Spence C, Moore S, Jermy M; © Springer-Verlag 2012, with permission of Springer

- *Direct 3D printing.* This represents one of the goals in phantom manufacture as the number of steps is reduced to the minimum; direct 3D printing of the phantom in final form. Cloonan et al. (2014) describes the use of 3D printing for phantom manufacture.

Other methods have been used to acquire 3D geometries and create phantoms:

- *Corrosion casting* of arteries involves injection of a liquid into autopsy or excised tissues. The liquid hardens in the artery and the tissues are chemically removed. Early studies on anatomical optical phantoms used injected silicone rubber which then formed the lost core in a phantom consisting of transparent plastic (Friedman et al. 1987; Friedman 1993). Resin-based corrosion casting is commonly used producing a high-resolution stiff model of the vascular system. Whilst this could not be removed using a lost core method, the model geometry could be scanned using a laser scanning system to provide a 3D CAD file suitable for 3D printing. 3D geometry data obtained from corrosion casting of arteries is extremely high quality.
- *Mould manufacture from milling.* Planar anatomical phantoms have been manufactured based on the lost core method (Smith et al. 1999) which have been used in flow visualisation (Steinman et al. 2000). An

idealised planar carotid bifurcation was used from which a mould was made in aluminium using a milling machine. The mould was used to produce a lost core in low melting point alloy from which the phantom was produced in silicone.

Once the phantom has been produced, the blood mimic must be designed to match the refractive index of the material of the phantom (Nguyen et al. 2004; Miller et al. 2006; Yousif et al. 2011) otherwise there will be visualisation artefacts (Fig. 12.8) and velocity measurement errors.

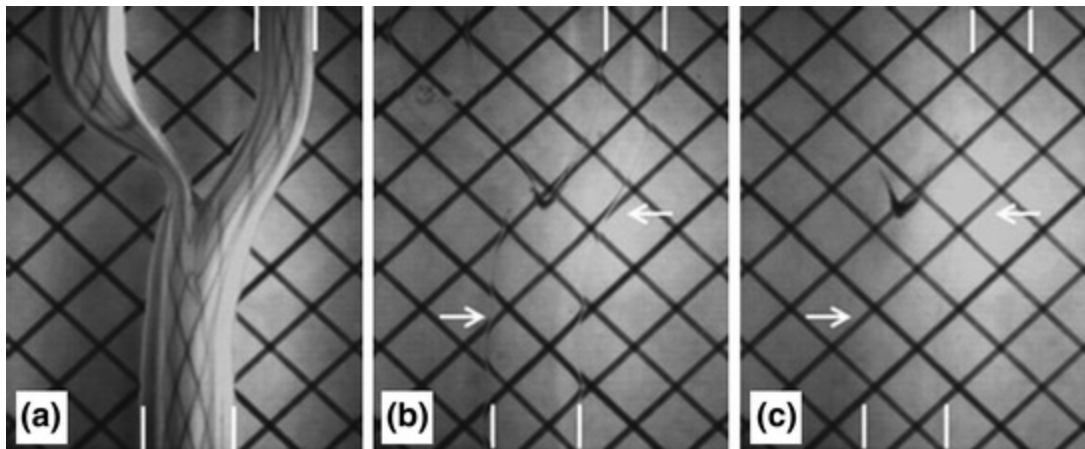


Fig. 12.8 Visual monitoring of the match in optical refractive index based on distortion of grid lines beneath a carotid bifurcation phantom fabricated from polydimethylsiloxane (PDMS) polymer. The phantom is filled with **a** air, showing high distortion, **b** nearly matched fluid ($n = 1.4112 \pm 0.0001$), still showing minor distortion as indicated by the *arrows*, and **c** optimally matched fluid ($n = 1.4140 \pm 0.0001$) with no distortion, as indicated by the *arrows*. Note the *vertical white markers*, denoting the flow lumen, and the unintentional stain at the bifurcation apex, which provides a convenient landmark here. From Yousif et al. (2011); © Springer-Verlag 2010, with permission of Springer. Image kindly provided by Prof. Tamie Poepping

12.3 Flow Phantoms for Medical Imaging

12.3.1 Medical Imaging Flow Phantom Design Requirements

Flow phantoms for medical imaging should mimic key features of the cardiovascular system which, as discussed above will depend on the application. Features might include cardiovascular geometry, blood viscous behaviour, wall stiffness and wall motion. In addition flow phantoms should mimic key properties of tissue relevant to the imaging modality. This ensures

that images produced from the phantom are a good representation of images from the cardiovascular system in vivo. Tissue-mimicking also enables conclusions (e.g. on quantification of measurement errors) to be applicable in vivo. Construction of flow phantoms for medical imaging therefore requires choice or formulation of materials with the correct physical properties.

Materials which mimic the relevant imaging properties of tissues are referred to as being ‘tissue equivalent’. The relevant imaging properties are summarised in Table 12.1.

Table 12.1 Relevant physical properties of materials relevant to flow phantom design

Imaging system	Physical properties relevant to imaging
MRI	T1, T2, proton density
Ultrasound	Speed of sound, acoustic attenuation, acoustic backscatter coefficient
CT	X-ray attenuation coefficient
PET	Gamma-ray attenuation coefficient

12.3.2 Tissue and Vessel Mimics

The most commonly used phantoms consist of a length of tubing bought from a laboratory supplier. Stiff tubing includes acrylic, glass, PTFE and polypropylene, whilst softer tubing is mostly based on latex rubber. These simple vessel phantoms may be used to produce idealised flow to validate MRI velocity measurement methods; with the implication that the MR properties of the tube are unimportant as they have little effect on the measurement of velocity. Simple tube models have been used in ultrasound, however the tube has a large effect due to refraction and attenuation of the ultrasound beam within the vessel wall. C-flex tubing (Cole Parmer, Vernon Hills, IL, USA) has been used as its speed of sound (1556 m s^{-1}) is close to the standard speed of 1540 m s^{-1} (Hoskins 2008).

Off-the-shelf materials can also be used to construct medical imaging phantoms with more complicated geometries. For CT and PET solid materials such as acrylic provide similar X-ray and gamma-ray attenuation characteristics to human tissue. This is convenient as phantoms can easily be constructed by milling or by casting. For MRI solid materials such as polyester, acrylic or silicone have been used to construct phantoms (e.g. Smith et al. 1999). Essentially these phantoms are identical to those used for optical imaging (Sect. 12.1). Figure 12.9 shows bifurcation phantoms and the

associated MRI images of flow.

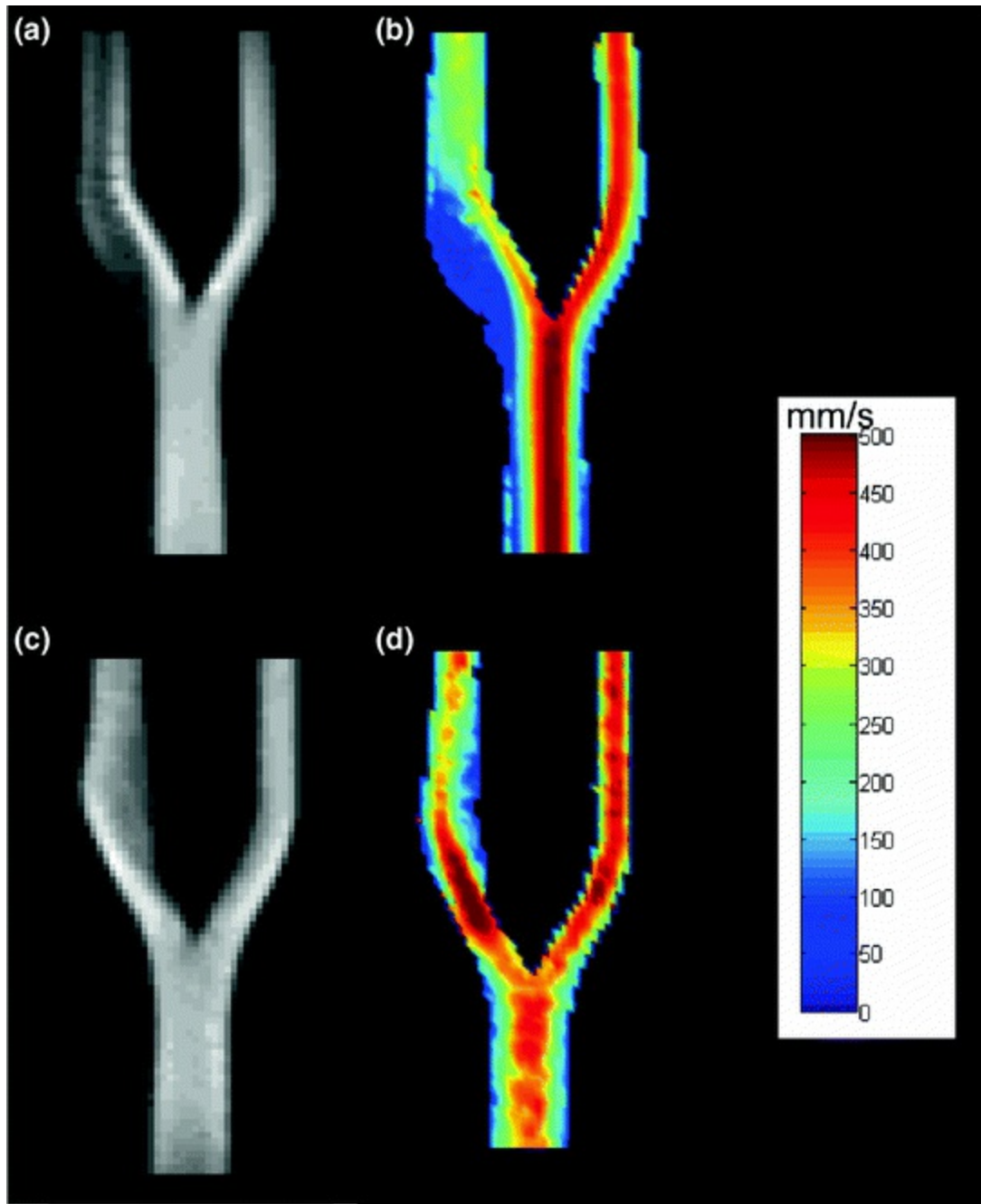


Fig. 12.9 MRI images from bifurcation phantoms. **a** Normal phantom—MRI intensity. **b** Normal phantom—MRI velocity. **c** 30 % stenosis phantom—MRI intensity. **d** 30 % stenosis phantom—MRI velocity. From; Marshall I. Computational simulations and experimental studies of 3D phase-contrast imaging of fluid flow in carotid bifurcation geometries. *Journal of Magnetic Resonance Imaging*. 2010;31:928–934; © 2010 Wiley-Liss, Inc., with permission from John Wiley and Sons. Images kindly provided by Prof. Ian Marshall

Solid materials such as polyester do not return an MRI signal which leads to unrealistic image appearance (Smith et al. 1999). This is an issue if the effect of surrounding tissue on velocity measurement is of interest. Solid materials such as acrylic have high speed of sound compared to soft tissue and are unsuitable for use in ultrasound phantoms. Ultrasound phantoms are available commercially based on urethane as the acoustic properties provide a reasonable match for soft tissue (Table 12.2).

Table 12.2 MRI properties of selected tissue mimics, vessel mimics and blood mimics

Mimic/Tissue	Main composition	T1 (ms) @1.5T	T2 (ms) @1.5T	T1 (ms) @3T	T2 (ms) @3T	Reference
Tissue/Vessel	PVAc (10 %)	718– 1034 ^a	108– 175 ^a	–	–	Surry et al. (2004)
Tissue	Agar	1150	50	1504	40	Smith et al. (1999), King et al. (2011)
Tissue	Sodium polyacrylate	–	–	1077– 2406	74–602	Hellerbach et al. (2013)
Tissue	Carrageenan/Agarose	202– 1904	38–423	395– 2601	29–334	Kato et al. (2005), Hattori et al. (2013)
Soft tissues	–	576– 1124	44–95	812– 1820	42–99	Selwyn (2014)
Blood	–	1441	290	1932	275	Selwyn (2014)
Blood	60:40 by vol water/glycerol	900	125	–	–	Summers et al. (2005)

^aValues depend on number of freeze-thaw cycles

Use of off-the-shelf materials is unlikely to lead to tissue mimics with the correct MRI or acoustic properties simply because these materials are not primarily designed for use as tissue mimics. Better success has been achieved by formulating recipes based on chemicals. Recipes based on agar have been used for both MRI and ultrasound tissue mimics which have good matching of acoustic and MRI properties (Tables 12.2 and 12.3). For use in MRI the agar is doped with a paramagnetic ion such as gadolinium, manganese, copper or nickel. The agar mixture is cooked for several hours, allowed to cool and poured. As it sets cross-linking of polymer molecules occurs which stabilises the agar. The cross-linking also leads to thermal irreversibility in that the melting temperature is higher (by 10–20 °C) than the setting temperature. This feature is essential when agar is used in lost core phantom

construction; the liquid agar tissue mimic must not melt the alloy core; yet when the temperature is raised the alloy core must melt while the agar tissue mimic remains solid. The widely used agar tissue mimic developed by Tierlinck et al. (1998) has very good acoustic matching to soft tissue but is mechanically weak which can lead to phantom rupture (Meagher et al. 2007). A recipe based on konjac and carrageenan leads to higher mechanical strength enabling phantoms to be built without rupture (Meagher et al. 2007; Kenwright et al. 2015).

Table 12.3 Acoustic properties of selected tissue mimics, vessel mimics and blood mimics. Values reported for clinical frequency range (5–15 MHz). FT—free-thaw cycle

Mimic	Main composition	Velocity (m s^{-1})	Attenuation coefficient ($\text{dB cm}^{-1} \text{MHz}^{-1}$)	Reference
Tissue	Agar	1551	0.52	Tierlinck et al. (1998)
Tissue	Konjac-carrageenan	1549	0.47	Kenwright et al. (2015)
Tissue/Vessel	PVAc	1543–1583 ^a	0.18–0.42 ^a (at 5 MHz)	Dineley et al. (2006)
Tissue	Urethane	1465	0.9 (at 5 MHz)	Browne et al. (2003)
Vessel	C-flex (Cole-Parmer)	1556	5.6 (at 5 MHz)	Hoskins (2008)
Vessel	Photopolymer	1802	1.58	Lai et al. (2013)
Ideal tissue ^b	–	1540	0.5	IEC 61685
Ideal blood ^b	–	1570	<0.1	IEC 61685
Blood mimic	Glycerol-water-nylon	1548	0.05	Ramnarine et al. (1998)

^aValue depend on number of freeze-thaw cycles

^bIEC specification for standard tissue and blood mimic (IEC 2001); allowed tolerances are 1 % for speed of sound and 10 % for attenuation coefficient

A second approach for the formulation of tissue mimics for MRI and ultrasound is the use of polyvinyl alcohol (PVA). This is initially prepared as a gel (Mano et al. 1986; Chu and Rutt 1997) which then undergoes a series of freeze-thaw cycles producing a white elastic material known as PVA cryogel or PVAc. The process of freeze-thawing results in cross-linking of the PVA polymer molecules. The number of freeze-thaw cycles is used to control

acoustic and MRI properties (Tables 12.2 and 12.3). The PVAc tissue mimic has high mechanical strength and is capable of withstanding physiologic pressure. PVAc is suitable for manufacture of a vessel wall mimic (Surry et al. 2004; Dineley et al. 2006).

12.3.3 Blood Mimics

It is common practice to design blood mimics with a viscosity of 3–4 mPa s with the intention that these behave in a Newtonian manner. For MRI a mixture of liquids with a high water content such as a 40/60 solution by mass of glycerol/water provide good blood mimicking (Smith et al. 1999; Summers et al. 2005). For ultrasound use of pure fluid does not work as particles are required to generate acoustic scatter. The blood mimic developed by Ramnarine et al. (1998) has been widely used. This is a glycerol/water fluid mixture with 5 µm nylon particles added in low concentration (1.8 % by volume) to mimic red blood cells and dextran to ensure matching of viscosity to blood.

12.3.4 Phantom Construction

In principle all of the methods described in Sect. 12.2.4 can be used for the construction of medical imaging phantoms. A summary of methods used for phantoms of increasing geometric complexity is shown in Table 12.4, concentrating on MRI and ultrasound.

Table 12.4 Methods for manufacture of MRI and ultrasound phantoms at increasing levels of complexity

	MRI	Ultrasound
Straight tube: (not tissue equivalent)	^a Off-the-shelf vessel ¹	^a C-flex tubing ²
Straight tube: (tissue equivalent)	^b PVAc vessel mimic ³	^b PVAc vessel mimic ⁴
		^b Agar block with channel ⁵
Planar bifurcation: (not tissue equivalent)	^b Machined acrylic ⁶	Not applicable
	^b Lost core made in planar mould, silicone elastomer tissue mimic ⁷	
Planar bifurcation: (tissue equivalent)	^c Lost core made in planar mould, agar based tissue mimic ⁷	^c Lost core made in planar mould, agar based tissue mimic ⁷

Nonplanar bifurcation phantom: (not tissue equivalent)	^c Direct 3D printing of vessel mimic in photopolymer tissue, embedded in agar tissue mimic ⁸	Not applicable
Nonplanar bifurcation geometry: (tissue equivalent)	^c Lost core made by 3D printing, agar based tissue mimic	^c Lost core made by 3D printing, konjac-carogeenan tissue mimic ⁹
	^d Direct 3D printing	^d Direct 3D printing

Difficulty ^avery easy (commercially available), ^beasy (commercially available or specialist in-house facilities), ^cdifficult (specialist in-house facilities), ^dvery difficult (very few/no reports)

References ¹Robertson et al. (2001), ²Blake et al. (2008), ³Surry et al. (2004), ⁴Dineley et al. (2006), ⁵Ramnarine et al. (2001), ⁶Kohler et al. (2001), ⁷Smith et al. (1999), ⁸Lai et al. (2013), ⁹Watts et al. (2007), Meagher et al. (2007)

The simplest phantom, and the most widely used, consists of off-the-shelf tubing bought from laboratory suppliers. For ultrasound, as noted above, C-flex tubing provides adequate acoustic matching. Off-the-shelf tubing can be arranged to be straight, and provided the inlet is sufficiently long, the flow is fully developed. This allows comparison of measured velocities with the true velocity within the vessel (Robertson et al. 2001; Blake et al. 2008). The next level of complexity also involves straight tube phantoms but with tissue equivalence of the vessel. PVAc may be used for both MRI and ultrasound phantoms (Surry et al. 2004; Dineley et al. 2006), or a wall-less approach may be used involving agar tissue mimic for ultrasound (Ramnarine et al. 2001). Figure 12.10 shows ultrasound images taken from a wall-less stenosis phantom.

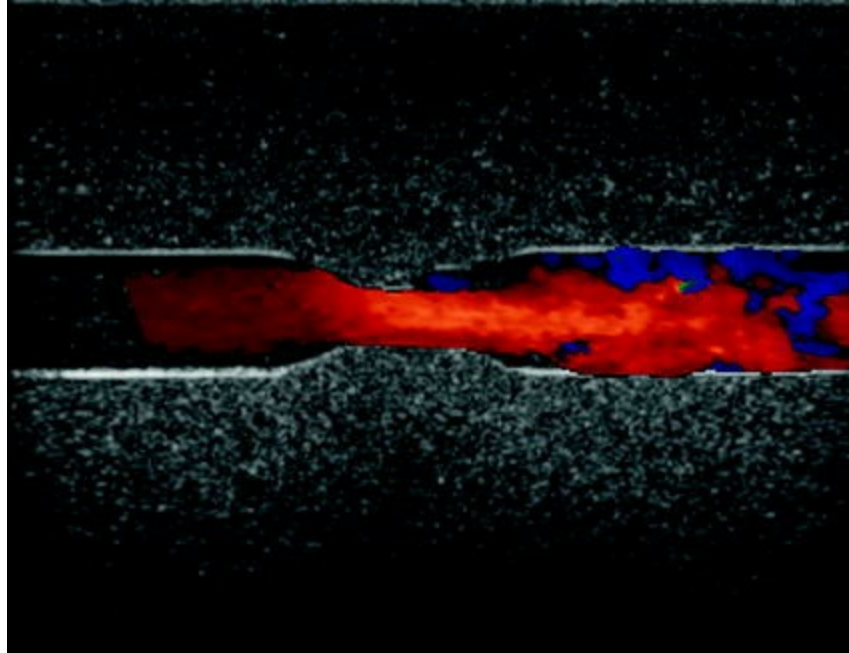


Fig. 12.10 Straight tube wall-less stenosis phantom. *Colour Doppler* image showing increase in velocity in the stenosis with turbulent flow in the post-stenosis region

Planar bifurcations may be manufactured for MRI using machined acrylic; i.e. circular holes are bored which meet at the bifurcation (Kohler et al. 2001), or using a lost core mould as described in Sect. 12.2.4 (Smith et al. 1999). Tissue equivalent versions of these phantoms can be made by using agar (a jelly-like substance derived from a naturally occurring complex polysaccharide) (Smith et al. 1999).

The final level of complexity concerns 3D anatomical phantoms and involves the use of 3D printing (Watts et al. 2007; Meagher et al. 2007; Lai et al. 2013) as shown in Figs. 12.11 and 12.12. Direct 3D printing of 3D anatomical phantoms for ultrasound and MRI would require materials suitable for 3D printing.

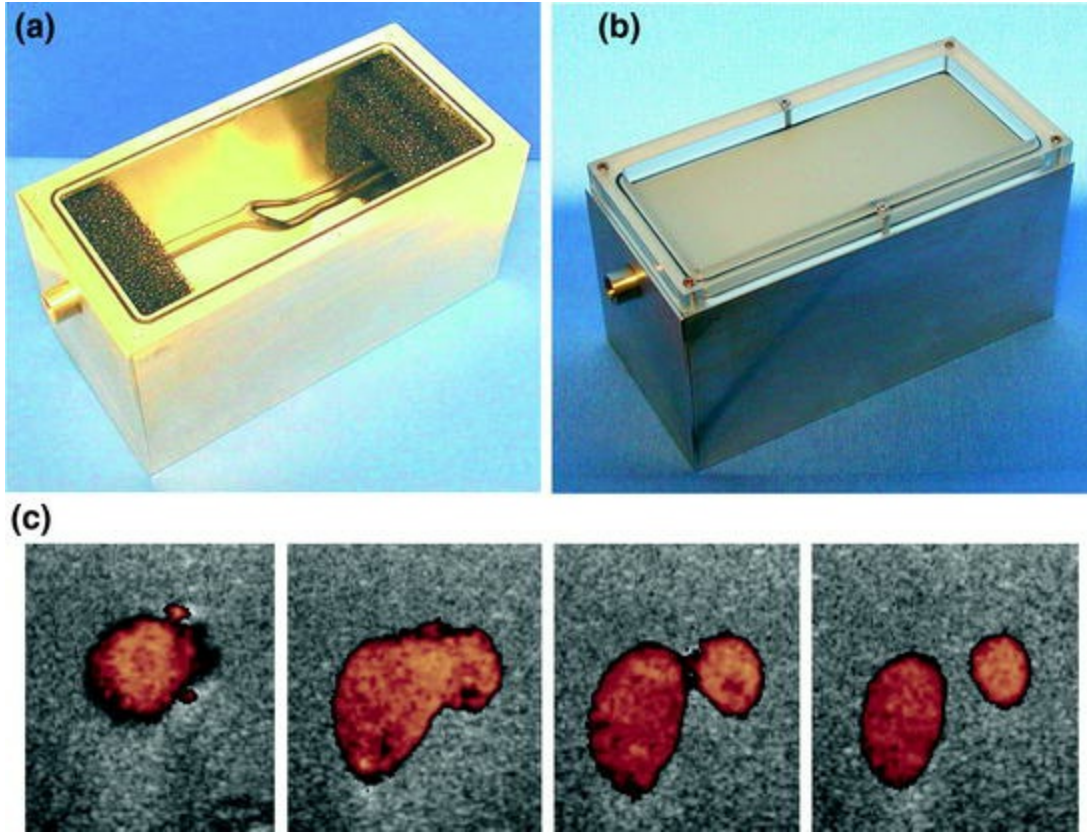


Fig. 12.11 Ultrasound carotid bifurcation phantom. **a** The lost core in a container with inlet and outlet connections in place. **b** Final phantom with solid tissue mimic after the metal core has been removed. **c** Cross-sectional colour flow images at 4 locations. Further details in Meagher et al. (2007) and Watts et al. (2007)

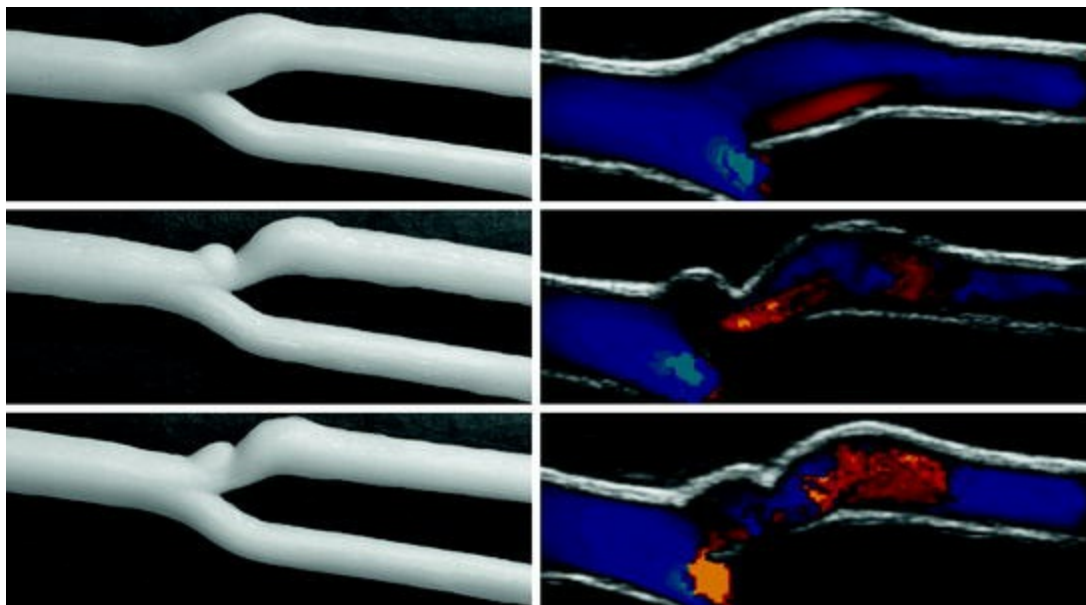


Fig. 12.12 **a** 3D-printed carotid bifurcations vessel mimics. **b** *Colour* flow images from the phantoms. Reprinted from Lai et al. (2013), copyright (2013), with permission from the World Federation for Ultrasound in Medicine & Biology

12.4 Biological Flow Phantoms

This class of flow phantoms incorporates biological tissues and allows exploration of the relationship between biological function and local haemodynamic and mechanical conditions. As with the other sections in this chapter, we will concentrate on the design and construction of the phantoms.

12.4.1 Brief History of Endothelial Flow Phantoms

It has been recognised for over 150 years that the endothelium senses haemodynamic forces (Virchow 1856). Flow systems for the systematic study of these effects in the laboratory date back to the 1970s (Krueger et al. 1971; Rosen et al. 1974). Studies in the early 1980s demonstrated alignment of endothelial cells with the direction of wall shear stress (Dewey et al. 1981; Levesque and Nerem 1985). The basis for these studies was a flow chamber in which endothelial cells were cultured on one wall. Flow through the chamber subjected the cells to a controllable shear stress. The transparent walls of the chamber allowed optical visualisation using microscopy which enabled examination of the behaviour of the endothelial cells under different shear conditions. Since these early studies cultured endothelial flow chambers have become by far the most widely used method for investigating endothelial response to shear stress. The terms ‘endothelial flow cell’ and ‘cell culture flow system’ are also used to describe the flow apparatus. For the purposes of consistency the term ‘endothelium flow phantom’ is used in this chapter. Reviews of the design of endothelial flow phantoms are provided by Young and Simmons (2010) and Davis et al. (2015), and of biological use are provided by Davies (1995, 2009).

12.4.2 Endothelial Flow Phantom Design

The components of an endothelial flow phantom are shown in Fig. 12.13 based on the popular parallel plate flow chamber. The flow chamber consists of three layers, a lower plate on which the endothelial cells are seeded, a gasket which defines a flow channel and an upper plate which seals the flow channel.

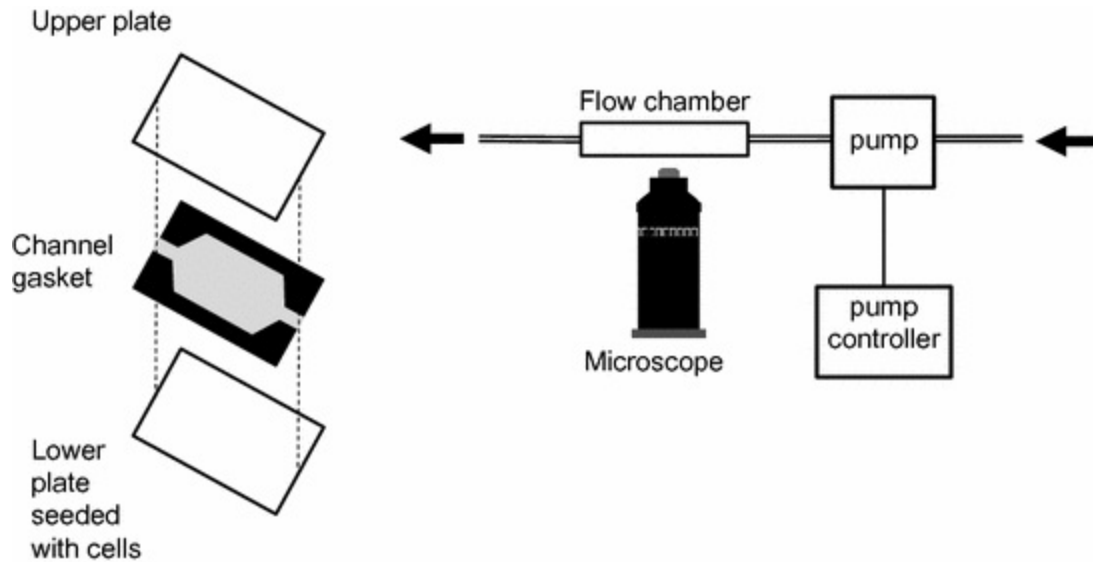


Fig. 12.13 Components of a parallel plate endothelial flow phantom

The components of a simple parallel plate flow phantoms are described in more detail below.

- *Endothelial plate.* The endothelial cells are most commonly seeded onto glass or glass-like materials which are rigid. If coated direct onto the glass the endothelial cells need time to lay down their own matrix to allow adherence to the glass. The use of a plate surface coating such as fibronectin, collagen or gelatin assists with cell adherence. The endothelial cells form a single-cell layer in which there are no gaps (called a ‘confluent layer’).
- *Opposite plate.* In simple flow chambers the opposite plate is constructed of glass to allow optical access.
- *Flow chamber geometry.* The basic flow chamber is designed so that fully developed flow is present. A step may be introduced into the flow to simulate the complex flow regions seen in atherosclerosis. More complex geometries may be constructed such as the Y-shaped geometry available from Ibidi GmbH (Martinsried, Germany) (Fig. 12.14). It is important to have good knowledge of the shear stress. This may be calculated for different flow rates using simple equations for simple geometries such as rectangular cross sections. For more complex geometries CFD may be used to estimate the shear stress distribution (Fig. 12.14).

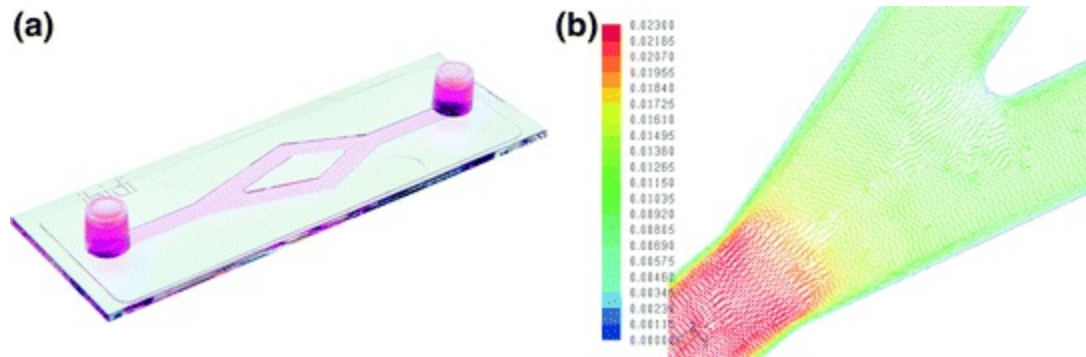


Fig. 12.14 **a** Y-shaped parallel plate endothelial flow phantom. **b** Velocity field estimated using CFD. Images provided courtesy of Ibidi GmbH (Martinsried, Germany)

- *Pump.* Simple experiments may be performed using steady flow, for example produced using a syringe pump. Physiological flow involving pulsatile flow requires a more sophisticated system with computer control of the pump speed.
- *Fluid.* The fluid used in endothelial flow phantoms is designed to replicate the osmotic and ion concentrations of fluid in the body, in this case of the plasma component of blood. Typically a general purpose fluid used in biological research called ‘phosphate buffered saline’ is used. This fluid mimics the osmolarity and pH of tissue fluid.
- *Microscope.* Simple visualisation of endothelial cells may be performed using an optical microscope. More detailed information on biological processes may be obtained using a variety of fluorescence techniques.

There have been many variants of the simple endothelial flow phantom described, some of which are detailed below (reviewed in Young and Simmons 2010).

- *Cone-plate phantom.* The cone-plate viscometer described in Chap. 3 provides a uniform shear distribution and also enables variation of shear over a wide range. This methodology can be included in an endothelial flow phantom. The cone may be optically transparent allowing microscope visualisation of the endothelial layer through the cone.
- *Combined flow-stretch-pressure phantom.* In vivo endothelial cells are subject to simultaneous changes in pressure, stretch and shear. Endothelial phantoms have been described in which the endothelial cells are subjected to two or three of these variables. To allow for stretching,

endothelial cells are seeded onto nonrigid materials such as silicone.

- *Co-culture phantom.* In vivo endothelial behaviour in an artery is affected by smooth muscle cells. In a co-culture phantom the endothelial cells and smooth muscle cells are both seeded and cultured. For example, separation of endothelial and smooth muscle cells is achieved by culturing them on opposite sides of a membrane.
- *Microfluidics.* Microfluidics refers to the set of techniques concerned with construction of devices which utilise movement of tiny amounts of fluid. These techniques are increasingly used to construct endothelial flow phantoms. There are two main reasons for this; one is the ability to run several experiments in parallel, all with either the same or slightly different conditions (hence vastly speeding up the process of experimentation). The second reason is the large reduction in the volume of consumables which are needed (hence reducing cost). A typical endothelial flow phantom constructed using microfluidic procedures might have a 100-fold reduction in endothelial surface area compared to a conventional phantom; with typical dimensions of 1 by 10 mm.

12.4.3 Whole-Artery Phantoms

These phantoms are composed of sections of excised artery which are plumbed into a flow network which can replicate key aspects of the in vivo haemodynamic and mechanical environment, including pressure, stretch and wall shear. These phantoms have several advantages over in vivo experiments

- *Biological behaviour.* The biological behaviour should be very similar to that in vivo as the artery is composed of the same cells that exist in vivo. It has been noted above that there is biological signalling between endothelial cells and smooth muscle cells which is naturally replicated in a whole-artery phantom. It has been argued that endothelial cells used in endothelial flow phantoms may have a nontypical phenotype hence their behaviour differs to the in vivo situation (Bergh et al. 2005)
- *Independent control of mechanical environment.* In vivo endothelial cells are subject to simultaneous changes in pressure, stretch and shear. In a whole-artery phantom it is possible to have independent control of pressure, stretch and shear. It is noted that this argument is also

applicable to endothelial phantoms.

The principal disadvantage is that the artery is not optically transparent hence use of conventional microscopy techniques which image through the container wall is not possible.

The metabolic activity of the artery is maintained by immersion in a fluid which has appropriate levels of ions, glucose, oxygen and carbon dioxide. Dextran may be added to the blood mimic to control viscosity. Whole-artery flow phantoms have been described by Gan et al. (1999), Han and Ku (2001), Bergh et al. (2005), Gambillara et al. (2006), Thacher et al. (2010), Ozaki and Karaki (2002) provides a review of work to 2001.

References

- Adrian RJ. Particle-imaging techniques for experimental fluid-mechanics. *Ann Rev Fluid Mech.* 1991;23:261–304.
[CrossRef]
- Bergh N, Ekman M, Ulfhammer E, Andersson M, Karlsson L, Jern S. A new biomechanical perfusion system for ex vivo study of small biological intact vessels. *Ann Biomed Eng.* 2005;33:1808–18.
[CrossRef][PubMed]
- Blake JR, Meagher SC, Fraser KH, Easson WJ, Hoskins PR. A method to estimate wall shear rate with clinical ultrasound scanners. *Ultrasound Med Biol.* 2008;34:760–74.
[CrossRef][PubMed]
- Browne JE, Ramnarine KV, Watson AJ, Hoskins PR. Assessment of the acoustic properties of common tissue-mimicking test phantoms. *Ultrasound Med Biol.* 2003;29:1053–60.
[CrossRef][PubMed]
- Chu KC, Rutt BK. Polyvinyl alcohol cryogel: An ideal phantom material for MR studies of arterial flow and elasticity. *Magn Res Med.* 1997;37:314–9.
[CrossRef]
- Cloonan A, Shammirzadi D, Li RX, Doyle BJ, Konoafagou EE, McGloughlin TM. 3D-printed tissue mimicking phantoms for medical imaging and computational validation studies. *3D Printing Add Manuf.* 2014;1:14–23.
- Davies PF. Flow-mediated endothelial mechanotransduction. *Physiol Rev.* 1995;75:519–60.
[PubMed][PubMedCentral]
- Davies PF. Hemodynamic shear stress and the endothelium in cardiovascular pathophysiology. *Nat Clin Pract Cardiovasc Med.* 2009;6:16–26.
[CrossRef][PubMed]
- Davis CA, Zambrano S, Anumolu P, Allen AC, Sonoqui L, Moreno MR. Device-based in vitro

techniques for mechanical stimulation of vascular cells: a review. *J Biomech Eng.* 2015;137:040801. doi:[10.1115/1.4029016](https://doi.org/10.1115/1.4029016). Epub 5 Feb 2015.

Dewey CF, Bussolari SR, Gimbrone MA Jr, Davies PF. The dynamic response of vascular endothelial cells to fluid shear stress. *J Biomech Eng.* 1981;103:177–85.
[CrossRef][PubMed]

Dineley J, Meagher S, Poepping TL, McDicken WN, Hoskins PR. Design and characterisation of a wall motion phantom. *Ultrasound Med Biol.* 2006;32:1349–57.
[CrossRef][PubMed]

Doyle BJ, Morris LG, Callanan A, Kelly P, Vorp DA, McGloughlin TM. 3D reconstruction and manufacture of real abdominal aortic aneurysms: from CT scan to silicone model. *J Biomech Eng.* 2008;130:034501.
[CrossRef][PubMed]

Friedman MH. Arteriosclerosis research using vascular flow models—from 2-d branches to compliant replicas. *J Biomech Eng.* 1993;115:595–601.
[CrossRef][PubMed]

Friedman MH, Barger CB, Deters OJ, Hutchins GM, Mark FF. Correlation between wall shear and intimal thickness at a coronary artery branch. *Atherosclerosis.* 1987;68:27–33.
[CrossRef][PubMed]

Gambillara V, Chambaz C, Montorzi G, Roy S, Stergiopoulos N, Silacci P. Plaque-prone hemodynamics impair endothelial function in pig carotid arteries. *Am J Physiol Heart Circ Physiol.* 2006;290:H2320–8.
[CrossRef][PubMed]

Gan L, Sjögren LS, Doroudi R, Jern S. A new computerized biomechanical perfusion model for ex vivo study of fluid mechanical forces in intact conduit vessels. *J Vasc Res.* 1999;36:68–78.
[CrossRef][PubMed]

Geoghegan P, Buchmann N, Spence C, Moore S, Jermy M. Fabrication of rigid and flexible refractive-index-matched flow phantoms for flow visualisation and optical flow measurements. *Exp Fluids.* 2012;52:1331–47.
[CrossRef]

Han HC, Ku DN. Contractile responses in arteries subjected to hypertensive pressure in seven-day organ culture. *Ann Biomed Eng.* 2001;29:467–75.
[CrossRef][PubMed]

Hattori K, Ikemoto Y, Takao W, Ohno S, Harimoto T, Kanazawa S, Oita M, Shibuya K, Kuroda M, Kato H. Development of MRI phantom equivalent to human tissues for 3.0-T MRI. *Med Phys.* 2013;40(3):032303. doi:[10.1118/1.4790023](https://doi.org/10.1118/1.4790023).
[CrossRef][PubMed]

Hellerbach A, Schuster V, Jansen A, Sommer J. MRI phantoms—are there alternatives to agar? *PLoS ONE.* 2013;8:e70343. doi:[10.1371/journal.pone.0070343](https://doi.org/10.1371/journal.pone.0070343).
[CrossRef][PubMed][PubMedCentral]

Hoskins PR. Simulation and validation of arterial ultrasound imaging and blood flow. *Ultrasound Med*

Biol. 2008;34:693–717.

[\[CrossRef\]](#)[\[PubMed\]](#)

IEC 61685. Ultrasonics—flow measurement systems: flow test object. International Electrotechnical Commission, Geneva, Switzerland, 2001.

Kato H, Kuroda M, Yoshimura K, Yoshida A, Hanamoto K, Kawasaki S, Shibuya K, Kanazawa S. Composition of MRI phantom equivalent to human tissues. *Med Phys*. 2005;32:3199–208.

[\[CrossRef\]](#)[\[PubMed\]](#)

Kenwright DA, Laverick N, Anderson T, Moran CM, Hoskins PR. A wall-less flow phantom for high-frequency ultrasound applications. *Ultrasound Med Biol*. 2015;41:890–7.

[\[CrossRef\]](#)[\[PubMed\]](#)[\[PubMedCentral\]](#)

King DM, Fagan AJ, Moran CM, Browne JE. Comparative imaging study in ultrasound, MRI, CT, and DSA using a multimodality renal artery phantom. *Med Phys*. 2011;38:565–73.

[\[CrossRef\]](#)[\[PubMed\]](#)

Kohler U, Marshall I, Robertson MB, Long Q, Xu Y, Hoskins PR. MRI measurement of wall shear stress in bifurcation models and comparison with CFD predictions. *J Magn Reson Imaging*. 2001;14:563–73.

[\[CrossRef\]](#)[\[PubMed\]](#)

Krueger JW, Young DF, Cholvin NR. An in vitro study of flow response by cells. *J Biomech*. 1971;4:31–6.

[\[CrossRef\]](#)[\[PubMed\]](#)

Ku DN, Giddens DP. Pulsatile flow in a model carotid bifurcation. *Arteriosclerosis*. 1983;3:313–9.

[\[CrossRef\]](#)

Lai SS, Yiu BY, Poon AK, Yu AC. Design of anthropomorphic flow phantoms based on rapid prototyping of compliant vessel geometries. *Ultrasound Med Biol*. 2013;39:1654–64.

[\[CrossRef\]](#)[\[PubMed\]](#)

Levesque MJ, Nerem RM. The elongation and orientation of cultured endothelial cells in response to shear stress. *J Biomedl Eng*. 1985;107:341.

Liepsch D, Pflugbeil G, Matsuo T, Lesniak B. Flow visualization and 1- and 3-D laser-Doppler-anemometer measurements in models of human carotid arteries. *Clin Hemorheol Microcirc*. 1998;18:1–30.

[\[PubMed\]](#)

Mano I, Goshima H, Nambu M, Iio M. New polyvinyl-alcohol gel material for MRI phantoms. *Magn Reson Med*. 1986;3:921–6.

[\[CrossRef\]](#)[\[PubMed\]](#)

Marshall I. Computational simulations and experimental studies of 3D phase-contrast imaging of fluid flow in carotid bifurcation geometries. *J Magn Reson Imaging*. 2010;31:928–34.

[\[CrossRef\]](#)[\[PubMed\]](#)

Meagher S, Poepping TL, Ramnarine KV, Black RA, Hoskins PR. Anatomical flow phantoms of the nonplanar carotid bifurcation, part II. Experimental validation. *Ultrasound Med Biol*. 2007;33:303–10.

[\[CrossRef\]](#)[\[PubMed\]](#)

Miller P, Danielson K, Moody G, Slifka A, Drexler E, Hertzberg J. Matching index of refraction using a diethyl phthalate/ethanol solution for in vitro cardiovascular models. *Exp Fluids*. 2006;41:375–81.

[\[CrossRef\]](#)

Nguyen TT, Biadillah Y, Mongrain R, Brunette J, Tardif JC, Bertrand OF. A method for matching the refractive index and kinematic viscosity of a blood analog for flow visualization in hydraulic cardiovascular models. *J Biomech Eng*. 2004;126:529–35.

[\[CrossRef\]](#)[\[PubMed\]](#)

Ozaki H, Karaki H. Organ culture as a useful method for studying the biology of blood vessels and other smooth muscle tissues. *Jpn J Pharmacol*. 2002;89:93–100.

[\[CrossRef\]](#)[\[PubMed\]](#)

Prasad AK. Particle image velocimetry. *Curr Sci*. 2000;79:51–60.

Ramnarine KV, Nassiri DK, Hoskins PR, Lubbers J. Validation of a new blood mimicking fluid for use in Doppler flow test objects. *Ultrasound Med Biol*. 1998;24:451–9.

[\[CrossRef\]](#)[\[PubMed\]](#)

Ramnarine KV, Anderson T, Hoskins PR. Construction and geometric stability of physiological flow rate wall-less stenosis phantoms. *Ultrasound Med Biol*. 2001;32:245–50.

[\[CrossRef\]](#)

Robertson MB, Kohler U, Hoskins PR, Marshall I. Quantitative analysis of PC MRI velocity maps: pulsatile flow in cylindrical vessels. *Mag Res Imag*. 2001;19:685–95.

[\[CrossRef\]](#)

Rosen L, Hollis TM, Sharma MG. Document Alterations in bovine endothelial histidine decarboxylase activity following exposure to shearing stresses. *Exp Molec Path*. 1974;20:329–43.

[\[CrossRef\]](#)[\[PubMed\]](#)

Smith RF, Rutt BK, Holdsworth DW. Anthropomorphic carotid bifurcation phantom for MRI applications. *J Magn Reson Imaging*. 1999;10:533–44.

[\[CrossRef\]](#)[\[PubMed\]](#)

Selwyn R. Phantoms for magnetic resonance imaging. In: DeWerd LA, Kissick M, editors. *The phantoms of medical and health physics: devices for research and development*. New York: Springer; 2014. p. 181–200.

[\[CrossRef\]](#)

Surry KJM, Austin HJB, Fenster A, Peters TM. Poly(vinyl alcohol) cryogel phantoms for use in ultrasound and MR imaging. *Phys Med Biol*. 2004;49:5529–46.

[\[CrossRef\]](#)[\[PubMed\]](#)

Steinman DA, Poepping TL, Tambasco M, Rankin RN, Holdsworth DW. Flow patterns at the stenosed carotid bifurcation: effect of concentric versus eccentric stenosis. *Ann Biomed Eng*. 2000;28:415–23.

[\[CrossRef\]](#)[\[PubMed\]](#)

Summers PE, Holdsworth DW, Nikolov HN, Rutt BK, Drangova M. Multisite trial of MR flow measurement: phantom and protocol design. *J Magn Reson Imaging*. 2005;21:620–31.

[\[CrossRef\]](#)[\[PubMed\]](#)

Teirlinck CJPM, Bezemer RA, Kollman C, Lubbers J, Hoskins PR, Fish P, Fredfeldt KE, Schaarschmidt UG. Development of an example flow test object and comparison of five of these test objects in various laboratories. *Eur J Ultrasound*. 1998;36:653–60.

Thacher TN, Silacci P, Stergiopoulos N, da Silva RF. Autonomous effects of shear stress and cyclic circumferential stretch regarding endothelial dysfunction and oxidative stress: an ex vivo arterial model. *J Vasc Res*. 2010;47:336–45.

[\[CrossRef\]](#)[\[PubMed\]](#)

Tropea C. Laser Doppler anemometry: recent developments and future challenges. *Meas Sci Technol*. 1995;6:605–19.

[\[CrossRef\]](#)

Vennemann P, Lindken R, Westerweel J. In vivo whole-field blood velocity measurement techniques. *Exp Fluids*. 2007;42:495–511.

[\[CrossRef\]](#)

Virchow R. Der atheromatose Prozess der Arterien. *Wien Med Wochenshr*. 1856;6:825–41.

Watts DM, Sutcliffe CJ, Morgan RH, Ramnarine KV, Bastin M, Marshall I, Wardlaw J, Connell M, Hoskins PR, Black RA. Anatomical flow phantoms of the nonplanar carotid bifurcation I. Design. *Ultrasound Med Biol*. 2007;33:296–302.

[\[CrossRef\]](#)[\[PubMed\]](#)

Westerweel J. Fundamentals of digital particle image velocimetry. *Meas Sci Technol*. 1997;8:1379–92.

[\[CrossRef\]](#)

Young EW, Simmons CA. Macro- and microscale fluid flow systems for endothelial cell biology. *Lab Chip*. 2010;10:143–60.

[\[CrossRef\]](#)[\[PubMed\]](#)

Yousif MY, Holdsworth DW, Poepping TL. A blood-mimicking fluid for particle image velocimetry with silicone vascular models. *Exp Fluids*. 2011;50:769–74.

[\[CrossRef\]](#)

Zarins CK, Giddens DP, Bharadvaj BK, Sottiurai VS, Mabon RF, Glagov S. Carotid bifurcation atherosclerosis. Quantitative correlation of plaque localization with flow velocity profiles and wall shear stress. *Circ Res*. 1983;53:502–14.

[\[CrossRef\]](#)[\[PubMed\]](#)

13. Measurement of the Mechanical Properties of Biological Tissues

Barry J. Doyle¹✉, Ryley A. Macrae¹ and
Peter R. Hoskins²✉

- (1) University of Western Australia, Perth, WA, Australia
- (2) Edinburgh University, Edinburgh, Scotland

✉ **Barry J. Doyle (Corresponding author)**
Email: barry.doyle@uwa.edu.au

✉ **Peter R. Hoskins**
Email: P.Hoskins@ed.ac.uk

Learning outcomes

1. Understand the experimental considerations when mechanically testing ex vivo cardiovascular tissue.
2. Understand the various mechanical test methods used to measure mechanical properties in cardiovascular tissue.
3. Understand imaging based methods for measurement of mechanical properties in cardiovascular tissue.
4. Gain knowledge of the application areas of imaging based methods of

estimation of mechanical properties in vivo.

13.1 Introduction

Knowledge of the mechanical behaviour of biological tissue is fundamental to understanding both health and disease, and this is particularly true in the cardiovascular system. For example, arterial tissue stiffens with age and the most conclusive way to measure stiffness is through mechanical testing. This chapter will describe some of the methods used to measure mechanical properties of cardiovascular tissue both in the laboratory and in vivo using medical imaging.

13.2 General Considerations for Ex Vivo Methods

13.2.1 Species and Physiology

Animal models have long been used in medical research with the more common models being mouse, rat, rabbit, canine, swine and bovine. There are several considerations needed depending on the animal model, ranging from equipment design to appropriate loading conditions. When performing uniaxial or biaxial testing, the load ranges should conform to those observed in vivo and can be typically inferred from the physiological range of blood pressure and heart rate (e.g. see Table 13.1).

Table 13.1 Physiological values of human and animal models

Source	Heart rate (Reece 2004)	Pressure	Artery	Axial stretch		
Human	60	120/80 mmHg	Aorta	(1.12–1.30)	Learoyd and Taylor (1966)	
			Carotid	1.10	Delfino et al. (1997)	
Pig	70–120	150/115 mmHg	Aorta	1.4 (1.2–1.5)	Han and Fung (1995)	
			Mésangeau et al. (2000)	Carotid	1.5	Han and Ku (2001)
				Renal	1.232	Rachev and Shazly (2013)
Dog	70–120	140/70 mmHg	Aorta	1.4 (1.2–1.5)	Han and Fung (1995)	
			Höglund et al. (2012)	Carotid	1.72	Holzappel et al. (2000)

Rabbit	180–350	130/65 mmHg (Carli 1974)	Carotid	1.4	Matsumoto et al. (1999)
Mouse	450–750	120/80 mmHg	Aorta	1.4 (1–1.6)	Guo and Kassab (2003)
		Gleason et al. (2004)	Carotid	1.8	Dye et al. (1985)

13.2.2 Storage and Tissue Environment

Testing fresh tissue immediately after excision is not always possible. Therefore, storage of the sample is important as tissue degrades (often due to autolysis, which is the self-digestion of or destruction of cells by its own enzymes or microbial activity) over time if not stored in appropriate conditions. Studies have shown that neither refrigeration (Adham et al. 1996) nor freezing (O’Leary et al. 2014a) affect material properties of aortic tissue. However, it is generally recommended that samples be tested within 24 h of excision if possible, otherwise, be immediately frozen. Depending on the tissue type and water content, it may be necessary to use sophisticated techniques to control the rate of freezing to prevent the formation of ice crystals.

Tissue is at approximately 37 °C in vivo and some material properties of arterial tissue change with temperature (Humphrey 2003; Guinea et al. 2005). Heated baths of physiological solution (e.g. phosphate buffer solution) are used to ensure that material testing is performed at the same temperature as that in vivo.

13.2.3 Preconditioning

Soft tissue exhibits variation (softening) in the loading-unloading curves over the initial series of cycles. This is also observed in filled rubbers and is known as the Mullins effect (Mullins 1969). Preconditioning is performed to overcome this and involves subjecting the sample to a series of loading-unloading cycles until a repeatable curve is obtained. The pre-conditioning protocol should match the desired testing protocol in terms of strain rate so as not to influence the test data. To ensure repeatability, at least 10 cycles should be performed prior to testing.

13.2.4 Tissue Morphology

Microscopy is used to image morphology and structure. After mechanical testing, it is typical to fix the tissue sample in physiological fixative solution

(a 4 % buffered solution of formaldehyde), embed in paraffin and sectioned into thin slices (e.g. 5 μm) using a microtome. Many histological stains are available depending on the desired biological component to be imaged; the common stains used in cardiovascular biomechanics being Haematoxylin and Eosin (H&E) to see the cell distribution, or picro-sirius red which stains collagen fibres. There are also specific stains (e.g. Verhoeff-van Gieson's stain that enables the elastin distribution to be visualised). Microscopy can determine changes to the microstructure from different stretch protocols. Furthermore, Scanning Electron Microscopy (SEM) or Transmission Electron Microscopy (TEM) can be used to examine failure regions of the tested sample, such as in the presence of calcified tissue (O'Leary et al. 2015) or during dissection as delamination occurs (Sommer et al. 2008).

13.3 Ex Vivo Measurement of Mechanical Properties

These methods all use samples of excised tissue. The tissues are subject to a known stress causing them to stretch, and the measurement system measures the resulting deformation enabling calculation of strain. From this, the stress-strain behaviour can be determined from which mechanical properties related to elasticity and viscoelasticity can be calculated. In this section a number of methods are described.

13.3.1 Uniaxial Extension

This is the most common mechanical test method and involves controlled stretching of a regular shaped sample in a single direction, often until failure. Dimensions of the sample are precisely measured beforehand particularly in the gauge length (i.e. the length over which data will be extracted). The force and displacement in the direction of elongation is measured throughout the test and used to infer behaviour of the tissue. The techniques used to test cardiovascular tissue have evolved from international industry standards used to test rubber (ASTM International 2013).

Typically, the sample is cut into dumbbell or rectangular shapes, selecting areas of uniform thickness, and mounted in the jaws of the tensile testing system. All dimensions are measured at least three times using either callipers or optical methods (see O'Leary et al. (2013) for the influence of thickness measurement error on data). The samples are mounted to the test machine

using flat clamps at both ends of the specimen so as to exert a uniform force over the clamped area. To account for anisotropy (i.e. tissue can behave differently in both the circumferential and longitudinal direction), the orientation of the sample's origin is noted. The sample is preconditioned until repeatable mechanical behaviour is observed (e.g. 10 cycles), then elongated until failure. The applied force is measured by the test machine using a load cell. The tissue displacements are measured, either by taking the displacement of the machine head or gauge region markers, or optically via marker tracking (Shazly et al. 2015) or digital image correlation techniques (Zhang et al. 2002; Zhang and Arola 2004). Optical tracking is the preferred option as it measures the true strain of the sample.

The resulting data is a plot of the stress versus the stretch. In mathematical terms, the stretch λ is defined as the fractional change in length of the sample in the unloaded, l_o , and loaded, l , configurations:

$$\lambda = \frac{l}{l_o} \quad (13.1)$$

The stress can be found with reference to the undeformed geometry, known as the first Piola-Kirchoff stress, P , (or often called the 'engineering stress') or with reference to the deformed geometry, known as the Cauchy stress, σ , (often called the 'true stress'). In the case of uniform deformation, these stresses can be found via:

$$P_x = \frac{f_x}{tw} \quad (13.2)$$

$$\sigma_x = \frac{f_x \cdot \lambda_x}{tw} \quad (13.3)$$

where f_x is the applied load, t and w are the reference thickness and width of the specimen in the gauge region, and Eq. 13.3 is derived from the assumed incompressibility of vascular tissue (Chuong and Fung 1984).

The most common parameter describing the mechanical behaviour is the Young's modulus, which is the ratio of stress over strain. This is applicable when the stress-strain behaviour is linear. However, it was noted in Chap. 1 that many biological materials exhibit a non-linear stress-strain relationship. The mechanical behaviour can be characterised by the incremental Young's modulus, which is the slope of the stress/strain curve. More commonly, the stress-strain behaviour is characterised by a non-linear constitutive model containing two or more parameters (the details of such models are beyond the

scope of this book; however see Chap. 1 for a brief description).

Uniaxial extension is the most common measurement undertaken to measure mechanical properties related to stiffness. There is measurement of displacement in only one direction (as opposed to two directions in the biaxial system described in the next section); hence, the instrumentation costs are relatively low. For materials, which are anisotropic the stress-strain behaviour will be different depending on the orientation of the material. For example, in arteries the mechanical behaviour is different in the longitudinal and circumferential directions.

13.3.2 Planar Biaxial Extension

This involves stress-strain measurements in a single plane. Simple biaxial testing involves stretching in two directions (x, y) at 90° to each other. More complex systems have the capability of stretching along multiple different directions. Figure 13.1 shows a simple schematic of this test, whereas Fig. 13.2 shows an actual image of a sample of intraluminal thrombus (ILT) under equi-biaxial extension (O'Leary et al. 2013).

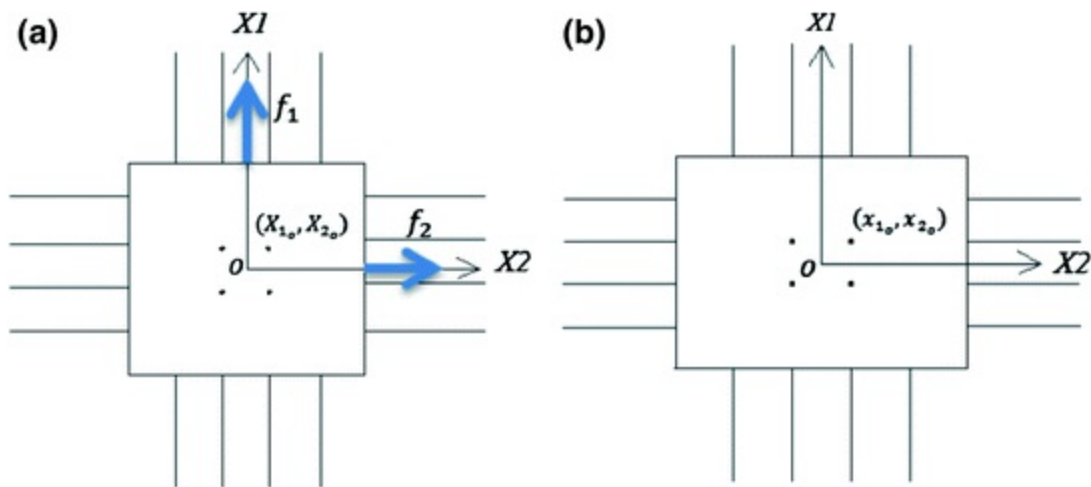


Fig. 13.1 Schematic of planar biaxial tension test, with coordinate system $O(X_1, X_2)$, in the **a** reference and **b** deformed configurations

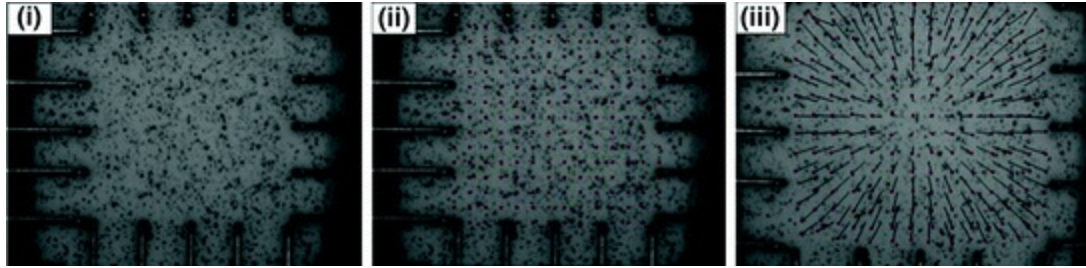


Fig. 13.2 Biaxial testing of intraluminal thrombus. **i** A speckle pattern is applied to the sample surface or **ii** an evenly dispersed grid of virtual points is used by the optical tracking algorithm to produce, **iii** displacement vectors

Typically, a square specimen is cut from a larger tissue sample. The sample dimensions are measured; sample dimensions are typically much bigger than in uniaxial tests (e.g. 14×14 mm in Fig. 13.2). The sample is mounted to the biaxial test machine. Instead of clamps used in uniaxial tests, hooks, barbs and tines are often used. Hooks and barbs can damage the tissue, especially under high strain, and samples can be lost due to failure at the boundaries. Evenly spread tines are the preferred option (as in Fig. 13.2). Loading is applied along each axis and is independently controlled, enabling variable loading rates or different stretch ratios in each direction. The displacement of marks on the central region of the specimen surface is tracked optically (see Fig. 13.2) or by using full-field methods like Electronic Speckle Pattern Interferometry (ESPI) or Digital Image Correlation (DIC). It is important to only examine the central region to avoid the effects present from the attachment area. This is known as Saint-Venant's principle and become negligible beyond a critical distance (decay length) from the grips. For cardiovascular tissue, this central area varies from 16 (Sun et al. 2005) to 25 % (O'Leary et al. 2013, 2014b). The measured positions are expressed in a coordinate system (x_1, x_2) and the axial forces are measured using load cells.

The principles for estimation of elastic moduli are similar to that for uniaxial testing in that these are ratios of stress/strain; however, the mathematics is more complex involving tensor equations and hence is provided in the appendix. The reader is referred to Macrae et al. (2016) for more detail.

Biaxial testing is used to obtain data on mechanical properties, which exhibit anisotropy. While planar biaxial testing enables some characterisation of anisotropic behaviour, it does not provide full 3D characterisation;

Holzapfel and Ogden (2009) discusses the issue of full 3D characterisation of mechanical properties in detail.

Biaxial testing systems are more expensive than uniaxial testing (in 2016 around £100 k as opposed to £15 k for uniaxial testing), so are less commonly used.

13.3.3 Inflation Testing

Inflation testing is an alternative to tensile testing on excised samples of tissues. The whole vessel is inflated under a controlled pressure and the resulting change in dimensions is measured (Fig. 13.3). This method allows the vessel to maintain the same overall shape as it had in the body, including any pre-stressing, and therefore provides a measurement environment more similar to that in vivo than is possible using tensile testing. The widely cited work on the mechanical properties of whole arteries by Learoyd and Taylor (1966) and Bergel (1961a, b) involved an inflation methodology.

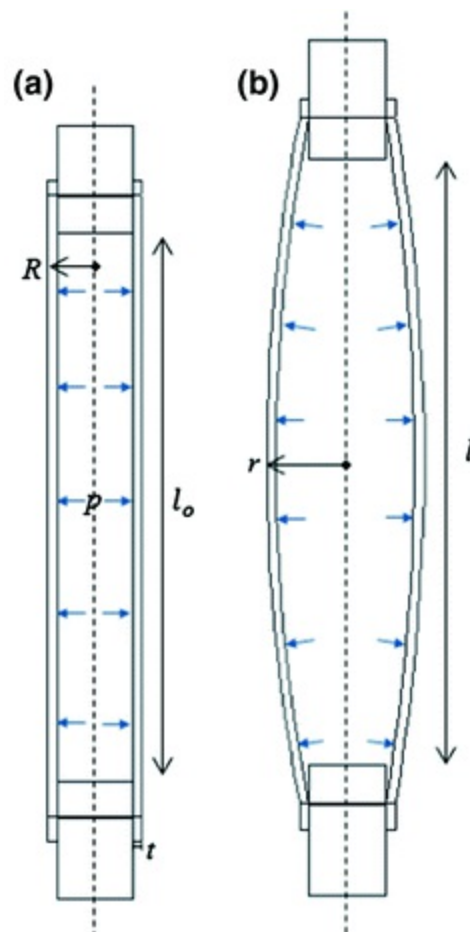


Fig. 13.3 Schematic of inflation-extension test for a cylindrical vessel, in **a** the reference configuration and **b** the deformed configuration

The method involves excising a whole artery and incorporating this into a pressurisation system. Any side branches are tied off to prevent leakage. The artery is stretched to its *in vivo* length and filled with a fluid such as isotonic saline. Pressure and force measurements are continuously recorded by transducers as the pressure increases/decreases, and the changes in geometry are measured with non-contact methods, such as a Charged Coupled Device (CCD) camera, DIC or by measuring the outer diameter with a precise laser micrometer. The wall thickness can be measured by cutting the vessel into slices after testing or by performing Computed Tomography (CT) imaging on the whole sample prior to testing (Doyle et al. 2010). The incremental Young's modulus, E_{inc} can be found from the following equation (from Learoyd and Taylor 1966) which is based on a thin-walled model:

$$E_{inc} = \frac{P_3 - P_1}{R_{O3} - R_{O1}} \cdot \frac{2(1 - \sigma^2)R_{I2}^2 \cdot R_O^2}{(R_{O2}^2 - R_{I2}^2)} \quad (13.4)$$

where σ is the Poisson ratio taken as 0.5; P is the pressure, R_O the outer radius, R_I the inner radius. The subscripts 1, 2, 3 refer to successive measurements at equal pressure differences (e.g. 10 mmHg).

It is important to note that in many cardiovascular applications the sample will be inhomogeneous, thick-walled and anisotropic in behaviour, which leads to significantly more complicated mathematics.

13.3.4 Bioreactor Studies

Bioreactors enable the study of vascular response to transmural pressure, flow rate and axial extension, and often employ inflation-extension tests within a bioreactor chamber. Early experiments involved culturing artery segments in a custom rig, where wall tension was applied via steel wires or by being cultured around a needle (De Mey et al. 1989; Lindqvist et al. 1997) before being subjected to mechanical testing. However, designs have since evolved (McFetridge et al. 2007; Tondreau et al. 2015) and can now accommodate cylindrical specimens (Zaucha et al. 2009) and even much more complicated geometries (e.g. tissue engineered heart valves (Engelmayr et al. 2003)).

13.4 In Vivo Measurement of Mechanical Properties

Measurement of the mechanical properties of tissues may be undertaken in vivo using medical imaging. This section provides some details of work in this area relevant to cardiovascular tissues. Further details on the technology of medical imaging are provided in Chap. 9.

13.4.1 Measurement of Arterial Stiffness from Wall Motion

In Chap. 4 it was described how the elasticity of arteries gives rise to change in diameter through the cardiac cycle associated with the change in blood pressure. Several stiffness indices can be estimated from diameter and pressure changes described in this section. In each case the underlying physical model is that the artery is a uniform homogeneous elastic cylinder.

The Young's modulus E of the arterial wall can be estimated in vivo from these measurements using Eq. 13.5.

$$E = \frac{d_d (P_s - P_d)}{2h(d_s - d_d)/d_d} \quad (13.5)$$

where h is wall thickness; P_s and P_d are the pressure, and d_s and d_d the diameter, at systole and end-diastole. The elastic modulus is an example of material stiffness.

An index was formulated by Peterson et al. (1960) to provide a stiffness index, which could be used when it was not possible to measure wall thickness. This is called the pressure-strain elastic modulus E_p and is an example of an index of structural stiffness.

$$E_p = \frac{(P_s - P_d)}{(d_s - d_d)/d_d} \quad (13.6)$$

The third index described here is the 'stiffness index' β formulated by Hayashi et al. (1980) to account for the non-linear stress-strain behaviour of arteries. This is also an example of an index of structural stiffness.

$$\beta = \frac{\ln(P_s/P_d)}{(d_s - d_d)/d_d} \quad (13.7)$$

All three quantities above require measurement of the diameter distension and the blood pressure. Typically, an ultrasound system is used to measure diameter distension, an arm cuff is used to measure pressure at systole and

diastole and in some arteries (such as the carotid), the ultrasound system can also be used to measure wall thickness. Figure 13.4 shows ultrasound images showing distension and wall thickness measurements.

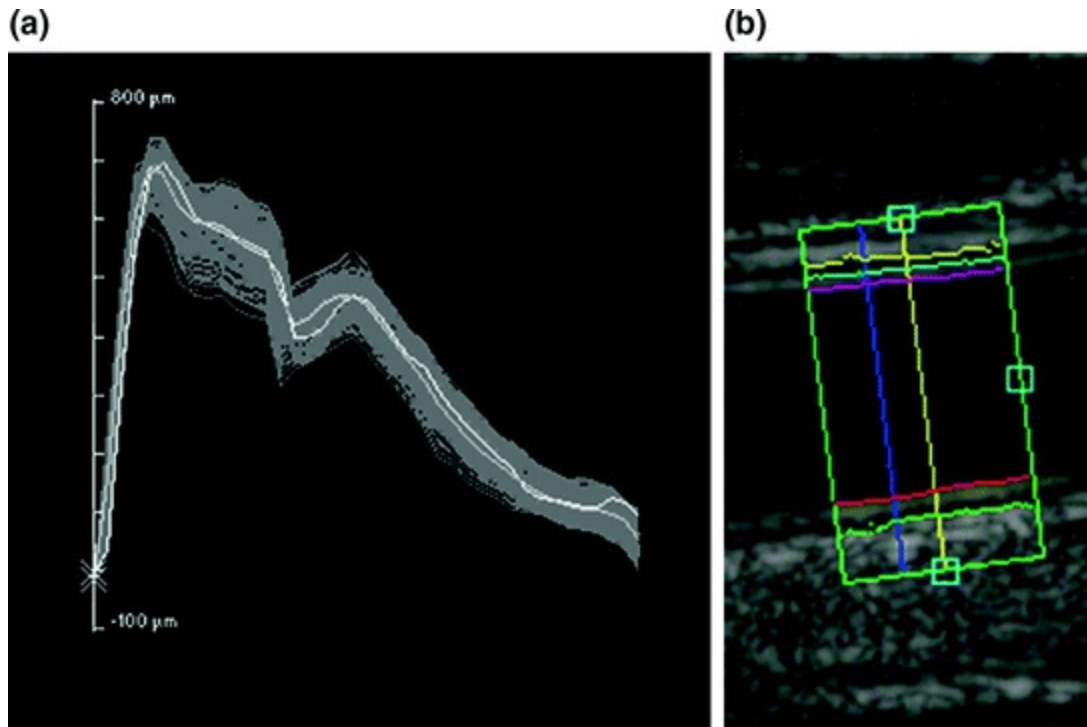


Fig. 13.4 Measurement made using ultrasound for estimation of elastic properties of arteries in vivo; images taken using a Philips HDI 5000 with analysis in HDILab. **a** Diameter-time waveform. **b** Wall thickness (purple and red—blood/wall interface; yellow and green—media/adventitia interface)

In abdominal aortic aneurysms, there was no overall difference between E_p in a rupture group and a non-rupture group (Wilson et al. 2003). In patients with atherosclerosis both E and E_p were higher in the contralateral artery in patients with carotid stenosis compared to normal arteries (Claridge et al. 2009). Further reading is provided in Hoskins and Bradbury (2012).

13.4.2 Measurement of Arterial Stiffness from Pulse Wave Velocity

The Moens-Korteweg equation described in Chap. 4 and below (Eq. 13.8) shows that the pulse wave velocity (PWV) is related to Young's modulus E .

$$PWV = \sqrt{\frac{Eh}{d\rho}} \quad (13.8)$$

The Young's modulus may be measured from PWV by rearrangement of the above equation:

$$E = \frac{d\rho}{h}(PWV)^2 \quad (13.9)$$

The PWV may be estimated from the difference in arrival time of the pressure or flow wave at different points in the arterial tree, divided by the distance between points. Commonly the PWV in the aorta is measured from the carotid artery and the femoral artery. These are accessible arteries from which pressure waveforms may be obtained using pressure tonometry or velocity-time flow waveforms obtained using Doppler ultrasound. The distance between the two sites is measured using a tape measure on the patient. When PWV is measured in this manner, it provides a global assessment related to stiffness.

Local measurement of PWV may be performed by simultaneous measurement of pressure and blood velocity, using the 'water hammer' Eq. (13.10).

$$\frac{dP}{dV} = \rho c \quad (13.10)$$

where P is pressure, V is blood velocity, ρ is blood density and c is PWV.

Early measurements of local PWV were invasive involving flowmeters and pressure transducers positioned on or in the artery (Khir et al. 2001). Non-invasive measurement of local PWV may be performed using tonometry for pressure and Doppler ultrasound for blood velocity (Zambanini et al. 2005), or distension measurement as a surrogate for pressure and Doppler ultrasound for blood velocity (Rabben et al. 2004). The measured velocity and distension produce a loop as shown in Fig. 13.5. The water hammer equation is valid in the region of the curve where there are no reflected waves, so in early systole. The region highlighted shows the curve in early systole from which measurements are made of the slope and from which the PWV may be calculated.

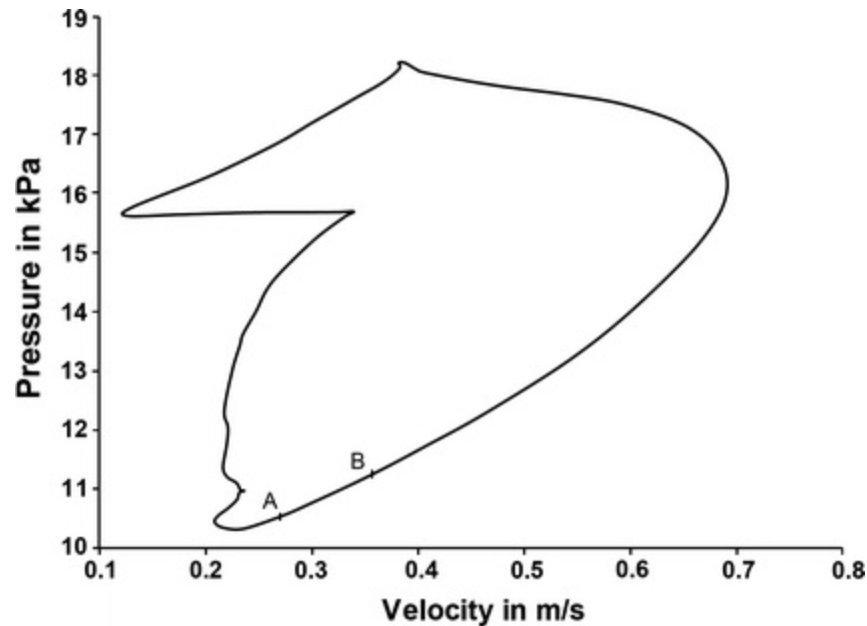


Fig. 13.5 Measurement of local pulse wave velocity from the pressure-velocity loop. Measurement of PWV from a diameter-velocity loop. The start and end points (*A–B*) of the linear portions used for the calculation of wave speed. Reprinted from *Ultrasound in Medicine and Biology* Vol. (35); Rakebrandt et al. (2009), Copyright (2009), with permission from the World Federation for Ultrasound in Medicine and Biology

In principle, measurement of PWV could be combined with measurement of wall thickness h and diameter d to estimate local elastic modulus E using Eq. 13.9.

13.4.3 Elastography

Elastography concerns the measurement and imaging of stiffness. In practice, this area is sub-divided into ‘strain elastography’ and ‘shear wave elastography’. A description of the principles of these techniques was given in Chap. 9 where it was noted that strain elastography (as its’ name implies) is concerned with the measurement of strain. Strain is used as a surrogate for stiffness on the basis that stiff lesions generally exhibit low strain when a load is applied. True measurement of tissue stiffness *in vivo* involves the use of shear wave elastography. Briefly shear wave elastography may be undertaken using ultrasound or MRI (where its called ‘magnetic resonance elastography’ or MRE) and involves the following steps; induction of shear waves in the tissues, use of the imaging system to track the shear waves; measurement of local shear wavelength; estimation of local stiffness E using

Eq. 13.11 where c_s is the shear wave velocity and ρ is the local tissue density (the manufacturers assume a value for density).

$$E = 3\rho c_s^2 \quad (13.11)$$

Applications in cardiovascular tissues have mainly concentrated on the heart and used MRI (Kolipaka et al. 2010; Elgeti et al. 2014), see Fig. 13.6. There are a small number of references, which mention shear wave imaging in arteries. Ultrasound shear wave imaging has demonstrated regions of increased stiffness in patients with atherosclerotic plaque (Garrard and Ramnarine 2014; Ramnarine et al. 2014). However, the shear wavelength is long (centimeters) compared to the plaque dimensions (millimetres) so it is unclear whether these measurements are quantitatively correct. Using MRE, images have been produced of the aorta (Woodrum et al. 2006; Kolipaka et al. 2012). However, these are not typical MRE studies in that the propagation of the shear waves in the tissues (in this case the aorta wall) is not measured directly due to spatial resolution limitations. Instead, the shear waves induce a pressure wave in the blood in the aorta. The velocity of this wave is dependent on the thickness and elastic modulus of the aorta, hence stiffness values are actually a composite of these two quantities. At the time of writing, it is unclear whether shear wave elastography is a useful investigative or clinical technique for measurement of cardiovascular tissue stiffness.

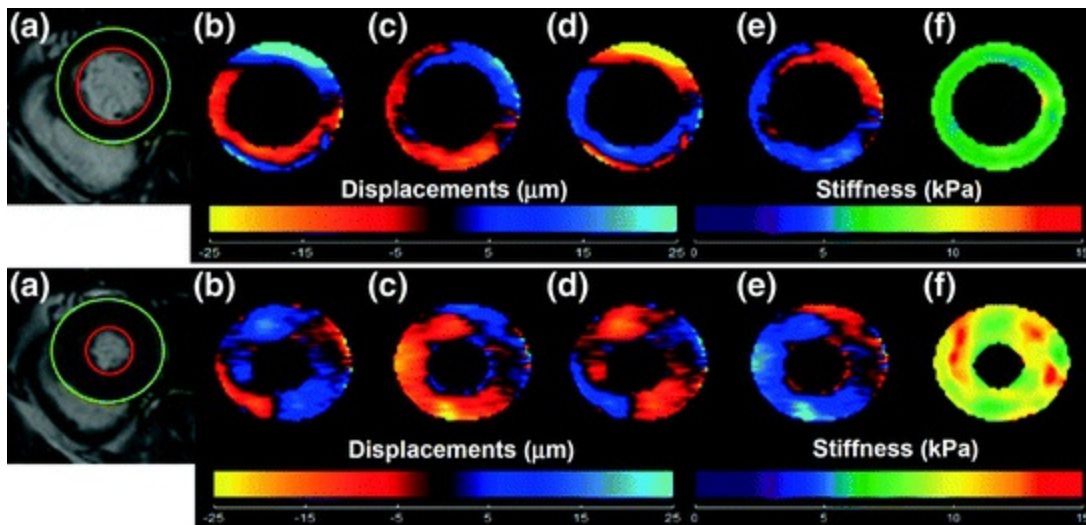


Fig. 13.6 MRE of the heart. *Upper:* images taken at end-diastole. **a** Short-axis magnitude image of the myocardium with epicardial (*green*) and endocardial (*red*) contours. **b–e** The four phases of the through-plane component of the propagating waves. **f** Weighted stiffness map from 3 encoding

directions with a mean stiffness of 6.5 ± 0.6 kPa. *Lower*: images taken at end-systole. **a** Short-axis magnitude image of the myocardium. **b–e** The four phases of the through-plane component of the propagating waves and **f** Weighted stiffness map from three encoding directions with a mean stiffness of 9.8 ± 1.5 kPa. Reproduced from Kolipaka et al. (2010); with permission from the International Society for Magnetic Resonance in Medicine (ISMRM), Concord, USA

References

Adham M, Gournier JP, Favre JP, De La Roche E, Ducerf C, Baulieux J, Barral X, Pouyet M. Mechanical characteristics of fresh and frozen human descending thoracic aorta. *J Surg Res.* 1996;64:32–4.

[CrossRef][PubMed]

ASTM International. ASTM D412–06a. Standard test methods for vulcanized rubber and thermoplastic elastomers—tension. West Conshohocken: ASTM International; 2013.

Bergel DH. The static elastic properties of the arterial wall. *J Physiol London.* 1961a;156:445–57.

[CrossRef][PubMed][PubMedCentral]

Bergel DH. The dynamic elastic properties of the arterial wall. *J Physiol London.* 1961b;156:458–69.

[CrossRef][PubMed][PubMedCentral]

Carli G. Blood pressure and heart rate in the rabbit during animal hypnosis. *Electroencephalogr Clin Neurophysiol.* 1974;37:231–7.

[CrossRef][PubMed]

Chuong CJ, Fung YC. Compressibility and constitutive equation of arterial wall in radial compression experiments. *J Biomech.* 1984;17:35–40.

[CrossRef][PubMed]

Claridge MW, Bate GR, Hoskins PR, Adam DJ, Bradbury AW, Wilmink AB. Measurement of arterial stiffness in patients with peripheral arterial disease: are changes in vessel wall more sensitive than intima-media thickness? *Atherosclerosis.* 2009;205:477–80.

[CrossRef][PubMed]

De Mey JG, Uitendaal MP, Boonen HC, Vrijdag MJ, Daemen MJ, Struyker-Boudier HA. Acute and long-term effects of tissue culture on contractile reactivity in renal arteries of the rat. *Circ Res.* 1989;65:1125–35.

[CrossRef][PubMed]

Delfino A, Stergiopoulos N, Moore JE Jr, Meister JJ. Residual strain effects on the stress field in a thick wall finite element model of the human carotid bifurcation. *J Biomech.* 1997;30:777–86.

[CrossRef][PubMed]

Doyle BJ, Cloonan AJ, Walsh MT, Vorp DA, McGloughlin TM. Identification of rupture locations in patient-specific abdominal aortic aneurysms using experimental and computational techniques. *J Biomech.* 2010;43:1408–16.

[CrossRef][PubMed][PubMedCentral]

Dye WW, Gleason RL, Wilson E, Humphrey JD. Altered biomechanical properties of carotid arteries in two mouse models of muscular dystrophy. *J Appl Physiol*. 1985;2007(103):664–72.

Elgeti T, Knebel F, Hättasch R, Hamm B, Braun J, Sack I. Shear-wave amplitudes measured with cardiac MR elastography for diagnosis of diastolic dysfunction. *Radiology*. 2014;271:681–7.
[CrossRef][PubMed]

Engelmayr GC Jr, Hildebrand DK, Sutherland FW, Mayer JE Jr, Sacks MS. A novel bioreactor for the dynamic flexural stimulation of tissue engineered heart valve biomaterials. *Biomaterials*. 2003;24:2523–32.
[CrossRef][PubMed]

Garrard JW, Ramnarine KV. Shear-wave elastography in carotid plaques: comparison with grayscale median and histological assessment in an interesting case. *Ultraschall Med*. 2014;35:1–3.
[CrossRef][PubMed]

Gleason RL, Gray SP, Wilson E, Humphrey JD. A multiaxial computer-controlled organ culture and biomechanical device for mouse carotid arteries. *J Biomech Eng*. 2004;126:787–95.
[CrossRef][PubMed]

Guinea GV, Atienza JM, Elices M, Aragoncillo P, Hayashi K. Thermo-mechanical behaviour of human carotid arteries in the passive state. *Am J Physiol Heart Circulatory Physiol*. 2005. doi:[10.1152/ajpheart.01099.2004](https://doi.org/10.1152/ajpheart.01099.2004).

Guo X, Kassab GS. Variation of mechanical properties along the length of the aorta in C57bl/6 mice. *Am J Physiol Heart Circ Physiol*. 2003;285:H2614–22.
[CrossRef][PubMed]

Han HC, Fung YC. Longitudinal strain of canine and porcine aortas. *J Biomech*. 1995;28:637–41.
[CrossRef][PubMed]

Han HC, Ku DN. Contractile responses in arteries subjected to hypertensive pressure in seven-day organ culture. *Ann Biomed Eng*. 2001;29:467–75.
[CrossRef][PubMed]

Hayashi K, Handa H, Nagasawa S, Okumura A, Moritake K. Stiffness and elastic behavior of human intra-cranial and extra-cranial arteries. *J Biomech*. 1980;13:175–85.
[CrossRef][PubMed]

Höglund K, Hanås S, Carnabuci C, Ljungvall I, Tidholm A, Häggström J. Blood pressure, heart rate, and urinary catecholamines in healthy dogs subjected to different clinical settings. *J Vet Intern Med*. 2012;26:1300–8.
[CrossRef][PubMed]

Holzapfel GA, Ogden RW. On planar biaxial tests for anisotropic nonlinearly elastic solids. A continuum mechanical framework. *Math Mech Solids*. 2009;14:474–89.
[CrossRef]

Holzapfel GA, Gasser T, Ogden R. A new constitutive framework for arterial wall mechanics and a comparative study of material models. *J Elast Phys Sci Solids*. 2000;61:1–48.
[CrossRef]

Hoskins PR, Bradbury AW. Wall motion analysis. In: Nicolaides A, Beach KW, Kyriakou E, Pattichis CS, editors. *Ultrasound and carotid bifurcation atherosclerosis*. Springer, 2012. pp. 325–339.

Humphrey JD. Continuum thermomechanics and the clinical treatment of disease and injury. *Appl Mech Rev*. 2003;56:231–60.

[[CrossRef](#)]

Khiri AW, O'Brien A, Gibbs JSR, Parker KH. Determination of wave speed and wave separation in the arteries. *J Biomech*. 2001;34:1145–55.

[[CrossRef](#)][[PubMed](#)]

Kolipaka A, Araoz PA, McGee KP, Manduca A, Ehman RL. In vivo cardiac MR elastography in a single breath hold. *Proc Int Soc Magn Reson Med*. 2010;18:591.

Kolipaka A, Woodrum D, Araoz PA, Ehman RL. MR elastography of the in vivo abdominal aorta: a feasibility study for comparing aortic stiffness between hypertensives and normotensives. *J Magn Reson Imaging*. 2012;35:582–6.

[[CrossRef](#)][[PubMed](#)]

Learoyd BM, Taylor MG. Alterations with age in viscoelastic properties of human arterial walls. *Circ Res*. 1966;18:278–92.

[[CrossRef](#)][[PubMed](#)]

Lindqvist A, Nilsson BO, Hellstrand P. Inhibition of calcium entry preserves contractility of arterial smooth muscle in culture. *J Vasc Res*. 1997;34:103–8.

[[CrossRef](#)][[PubMed](#)]

Macrae RA, Miller K, Doyle BJ. Methods in mechanical testing of arterial tissue: a review. *Strain*. 2016;52:380–99.

Matsumoto T, Okumura E, Miura Y, Sato M. Mechanical and dimensional adaptation of rabbit carotid artery cultured in vitro. *Med Biol Eng Comput*. 1999;37:252–6.

[[CrossRef](#)][[PubMed](#)]

McFetridge PS, Abe K, Horrocks M, Chaudhuri JB. Vascular tissue engineering: bioreactor design considerations for extended culture of primary human vascular smooth muscle cells. *ASAIO J*. 2007;53:623–30.

[[CrossRef](#)][[PubMed](#)]

Mésangeau D, Laude D, Elghozi JL. Early detection of cardiovascular autonomic neuropathy in diabetic pigs using blood pressure and heart rate variability. *Cardiovasc Res*. 2000;45:889–99.

[[CrossRef](#)][[PubMed](#)]

Mullins L. Softening of rubber by deformation. *Rubber Chem Technol*. 1969;42:339–62.

[[CrossRef](#)]

O'Leary SA, Doyle BJ, McGloughlin TM. Comparison of methods used to measure the thickness of soft tissues and their influence on the evaluation of tensile stress. *J Biomech*. 2013;46:1955–60.

[[CrossRef](#)][[PubMed](#)]

O'Leary SA, Doyle BJ, McGloughlin TM. The impact of long term freezing on the mechanical

properties of porcine aortic tissue. *J Mech Behav Biomed Mater.* 2014a;37:165–73.

[[CrossRef](#)][[PubMed](#)]

O’Leary SA, Healey DA, Kavanagh EG, Walsh MT, McGloughlin TM, Doyle BJ. The biaxial biomechanical behavior of abdominal aortic aneurysm tissue. *Ann Biomed Eng.* 2014b;42:2440–50.

[[CrossRef](#)][[PubMed](#)]

O’Leary SA, Mulvihill JJ, Barrett HE, Kavanagh EG, Walsh MT, McGloughlin TM, Doyle BJ. Determining the influence of calcification on the failure properties of abdominal aortic aneurysm (AAA) tissue. *J Mech Behav Biomed Mater.* 2015;42:154–67.

[[CrossRef](#)][[PubMed](#)]

Peterson LH, Jensen RE, Parnell J. Mechanical properties of arteries in vivo. *Circ Res.* 1960;8:622–39.

[[CrossRef](#)]

Rabben SI, Stergiopoulos N, Hellevik LR, Smiseth OA, Slørdahl S, Urheim S, Angelsen B. An ultrasound-based method for determining pulse wave velocity in superficial arteries. *J Biomech.* 2004;37:1615–22.

[[CrossRef](#)][[PubMed](#)]

Rachev A, Shazly T. A preliminary analysis of the data from an in vitro inflation-extension test can validate the assumption of arterial tissue elasticity. *J Biomech Eng.* 2013;135:84502. doi:[10.1115/1.4024665](#).

[[CrossRef](#)][[PubMed](#)]

Rakebrandt F, Palombo C, Swampillai J, Schon F, Donald A, Kozakova M, Kato K, Fraser AG. Arterial wave intensity and ventricular-arterial coupling by vascular ultrasound: rationale and methods for the automated analysis of forwards and backwards running waves. *Ultrasound Med Biol.* 2009;35:266–77.

Ramnarine KV, Garrard JW, Kanber B, Nduwayo S, Hartshorne TC, Robinson TG. Shear wave elastography imaging of carotid plaques: feasible, reproducible and of clinical potential. *Cardiovasc Ultrasound.* 2014;12:49.

[[CrossRef](#)][[PubMed](#)][[PubMedCentral](#)]

Reece WO (ed). *Duke’s physiology of domestic animals*, 12th ed. Sage House, 512 East State Street, Ithaca, New York 14850, Cornell University Press. 2004.

Shazly T, Rachev A, Lessner S, Argraves W, Ferdous J, Zhou B, Moreira AM, Sutton M. On the uniaxial ring test of tissue engineered constructs. *Exp Mech.* 2015;55:41–51.

[[CrossRef](#)]

Sommer G, Gasser TC, Regitnig P, Auer M, Holzapfel GA. Dissection properties of the human aortic media: an experimental study. *J Biomech Eng.* 2008;130:021007. doi:[10.1115/1.2898733](#).

[[CrossRef](#)][[PubMed](#)]

Sun W, Sacks MS, Scott MJ. Effects of boundary conditions on the estimation of the planar biaxial mechanical properties of soft tissues. *J Biomech Eng.* 2005;127:709–15.

[[CrossRef](#)][[PubMed](#)]

Tondreau MY, Laterreur V, Gauvin R, Vallières K, Bourget JM, Lacroix D, Tremblay C, Germain L,

Ruel J, Auger FA. Mechanical properties of endothelialized fibroblast-derived vascular scaffolds stimulated in a bioreactor. *Acta Biomater.* 2015;18:176–85.

[\[CrossRef\]](#)[\[PubMed\]](#)

Wilson KA, Lee AJ, Lee AJ, Hoskins PR, Fowkes FG, Ruckley CV, Bradbury AW. The relationship between aortic wall distensibility and rupture of infrarenal abdominal aortic aneurysms. *J Vasc Surg.* 2003;37:112–7.

[\[CrossRef\]](#)[\[PubMed\]](#)

Woodrum DA, Romano AJ, Lerman A, Pandya UH, Brosh D, Rossman PJ, Lerman LO, Ehman RL. Vascular wall elasticity measurement by magnetic resonance imaging. *Magn Reson Med.* 2006;56:593–600.

[\[CrossRef\]](#)[\[PubMed\]](#)

Zambanini A, Cunningham SL, Parker KH, Khir AW, McG Thom SA, Hughes AD. Wave-energy patterns in carotid, brachial, and radial arteries: a noninvasive approach using wave-intensity analysis. *Am J Physiol Heart Circulatory Physiol.* 2005;289:H270–6.

[\[CrossRef\]](#)

Zaucha MT, Raykin J, Wan W, Gauvin R, Auger FA, Germain L, Michaels TE, Gleason RL Jr. A novel cylindrical biaxial computer-controlled bioreactor and biomechanical testing device for vascular tissue engineering. *Tissue Eng Part A.* 2009;15:3331–40.

[\[CrossRef\]](#)[\[PubMed\]](#)[\[PubMedCentral\]](#)

Zhang D, Arola DD. Applications of digital image correlation to biological tissues. *J Biomed Opt.* 2004;9:691–9.

[\[CrossRef\]](#)[\[PubMed\]](#)

Zhang D, Eggleton C, Arola D. Evaluating the mechanical behavior of arterial tissue using digital image correlation. *Exp Mech.* 2002;42:409–16.

[\[CrossRef\]](#)

14. Hypertension

Peter R. Hoskins¹✉ and Ian B. Wilkinson²

- (1) Edinburgh University, Edinburgh, UK
- (2) Cambridge University, Cambridge, UK

✉ **Peter R. Hoskins**
Email: P.Hoskins@ed.ac.uk

Learning outcomes

1. Define hypertension.
2. Describe the causes, risk factors and treatment of hypertension.
3. Describe isolated and mixed hypertension and the relationship with age.
4. Describe the typical change in blood pressure which occurs with ageing, as a result of arterial stiffening.
5. Describe arterial remodelling following a medium-term (weeks) change in blood pressure.
6. Describe invasive and non-invasive methods for the measurement of blood pressure.
7. Describe estimation of central pressure from a radial artery tonometry.

Hypertension is an elevated blood pressure which arises as a result of a number of haemodynamic changes. Ageing can also lead to elevated blood pressure. This chapter will consider hypertension and the effect of ageing on blood pressure.

14.1 Hypertension

As blood pressure is a continuous variable and is normally distributed in the population, any definition of hypertension is purely arbitrary. This is compounded by the fact that epidemiological data indicate a continuous relationship between blood pressure and the risk of stroke/heart attack. However, a level of ≥ 140 mmHg systolic and/or ≥ 90 mmHg diastolic, measured in the arm, is commonly used to 'define' hypertension, as it is a level above which we know that lowering blood pressure brings benefit. 'Ideal' blood pressure is considered to be $< 120/80$ mmHg.

Hypertension is common, affecting up to a third of the adult population in the UK. In the majority of cases (90–95 %), there is no clear underlying cause—so-called primary or 'essential' hypertension. This is thought to result from a combination of life style factors including excess salt intake, reduced level of exercise and stress in genetically susceptible individuals. In rare cases, causes can be identified—so-called secondary hypertension and this offers the possibility of a cure. Causes of secondary hypertension include kidney disease, rare endocrine disorders such as Conn's syndrome, pregnancy and drugs including the oral contraceptive pill, antidepressants and cocaine.

Hypertension is a major risk factor for stroke, heart attack, kidney disease and aneurysm formation. Increased central pressure (i.e. pressure in the ascending aorta) means that the heart must work harder to eject blood into the aorta which if sustained over many years can lead to diminished heart function and eventually heart failure. Increased blood pressure in arteries is associated with increased circumferential stress which leads to a reduction in nitric oxide production, promoting plaque formation, with greater risk of rupture of atherosclerotic plaque and aneurysm. Overall, hypertension is the most common modifiable risk factor for premature death across the world. This is the reason that there is considerable clinical attention on reduction of blood pressure in the population.

Treatment of hypertension mostly involves changes to lifestyle (increased

exercise, reduction in salt content of food) and medication.

Physiologically, it is important to think about the two components of blood pressure when trying to identify the underlying pathophysiological causes of hypertension (Fig. 14.1).

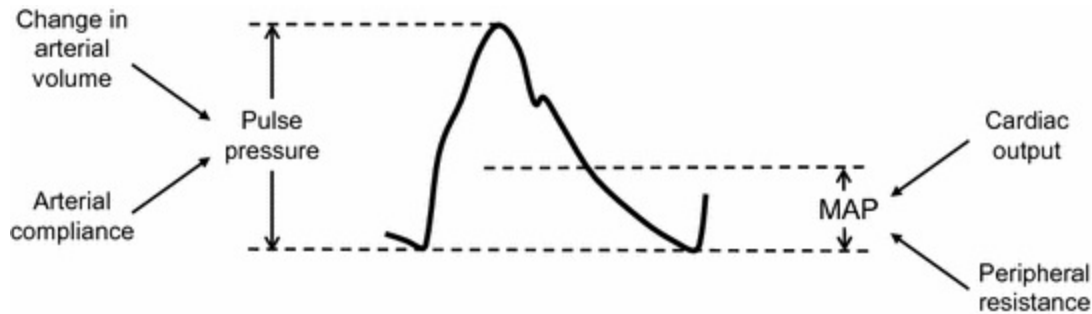


Fig. 14.1 Haemodynamic influences on pulse pressure and mean pressure. From; Koeppen BM, Stanton BA; Berne & Levy Physiology, Updated Edition, 6th Edition; Berne RM et al. Physiology. Philadelphia, PA: Copyright Elsevier (2010), with permission from Elsevier

- Pulsatile—i.e. the pulse pressure (difference between systolic and diastolic blood pressure). The principal determinants of pulse pressure are the stroke volume and the stiffness of the large arteries.
- Static or ‘steady-state’—represented by the mean arterial pressure. The determinants of the mean arterial pressure are cardiac output and peripheral vascular resistance:

$$\text{mean arterial pressure} = \text{cardiac output} \times \text{peripheral vascular resistance} \quad (14.1)$$

Essential hypertension is characterised by changes in one or more of the haemodynamic determinants of blood pressure. Interestingly, which of these components is responsible for hypertension is strongly influenced by age. In adolescents and young adults (<30 years), the principal haemodynamic disturbance is an increased stroke volume. Peripheral vascular resistance is relatively normal, as is arterial stiffness. The result is that young people tend to present with an elevated pulse pressure—so-called isolated systolic hypertension (high systolic but normal or low diastolic pressure) (Fig. 14.2). Over time, cardiac output falls to normal or subnormal levels, and peripheral vascular resistance rises, probably due to remodelling of small resistance vessels. Consequently, pulse pressure is relatively normal, but mean pressure is elevated, and this gives rise to elevation in systolic and diastolic pressures—so-called ‘mixed’ systolic/diastolic hypertension (Fig. 14.2), which is by far the most common form of hypertension in middle-aged individuals.

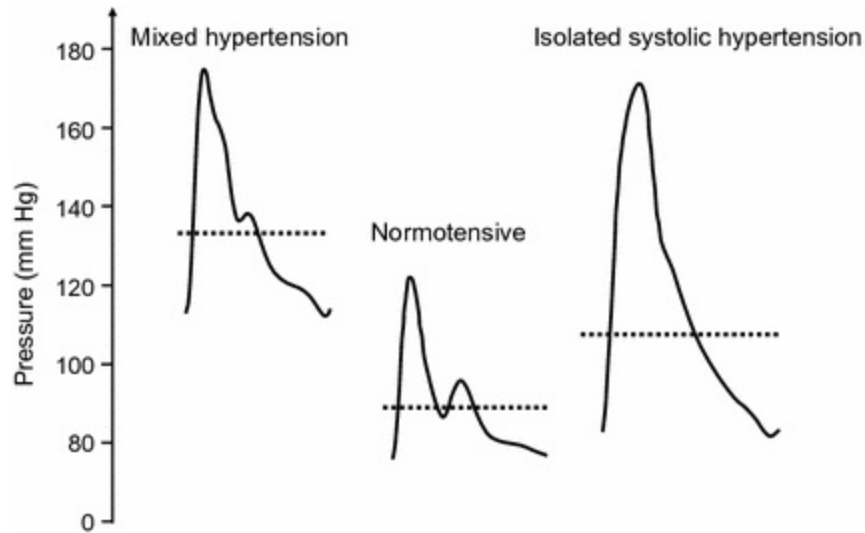


Fig. 14.2 Pressure waveforms for typical examples of mixed hypertension and isolated systolic hypertension; compared to normotension. Reproduced with permission from; McEniery CM, Wilkinson IB, Avolio AP; Age, hypertension and arterial function; *Clinical and Experimental Pharmacology and Physiology*. 2007;34:665–671; reproduced with permission. © 2007 The Authors Journal compilation © 2007 Blackwell Publishing Asia Pty Ltd., with permission from John Wiley and Sons

In older adults (>50 years), isolated systolic hypertension is again the most common form of hypertension, but arterial stiffening is the principal haemodynamic disturbance, causing an exaggerated increase in pulse pressure as the large arteries can no longer effectively buffer the cyclical changes in blood pressure during each cardiac cycle. Indeed, this demonstrates the importance of normal arterial compliance. Table 14.1 summarises the relationship between haemodynamics and hypertension with age.

Table 14.1 summarises the relationship between haemodynamics and hypertension with age

Age	Principal haemodynamic disturbance	Predominant form of hypertension
<30 years	Increased stroke volume	Isolated systolic hypertension
30–50 years	Increased peripheral resistance	Mixed (systolic/diastolic) hypertension
>50 years	Increased arterial stiffness	Isolated systolic hypertension

It is important to understand that systolic pressure is not constant along the arterial tree. Moving from the aorta to the peripheral arteries, where we tend to measure blood pressure, systolic pressure rises by up to 30 mmHg due to increased vessel stiffness and wave reflections. In contrast, diastolic pressure falls by 1–2 mmHg. This difference between aortic and brachial

pressure is important because the heart, brain and other major organs are exposed to aortic not brachial pressure, and certain drug therapies exert differential effects on peripheral and central pressure.

14.2 Ageing and Blood Pressure

With increasing age arteries get stiffer. This is illustrated in Fig. 14.3, and this leads to an increase in systolic central blood pressure as shown in Fig. 14.7. Published data on brachial pressure with age is given in Burt et al. (1995) for a USA population (Fig. 14.4). Herbert et al. (2014) present data on change in central pressure with age from data collected worldwide. Data on the change in the rate of hypertension with age for different parts of the world is provided by Kearney et al. (2005). They note lower overall rates (15–27 %) in Eastern and some developing countries. The highest rates were in established market economies (37 %), former socialist economies (37 %) and Latin America and the Caribbean (37 %). Wilkinson and McEniery (2012) noted that some populations have a much lower change of pressure with age identifying a rural community in China (Avolio et al. 1985), and a tribe in Cameroon living a hunter-gatherer lifestyle (Lemogoum et al. 2012) in this context. This leads to the idea that there is stiffening as a natural consequence of ageing and stiffening as a pathological process associated with disease (Wilkinson et al. 2012). This is illustrated in Fig. 14.5. The 2 processes are the following:

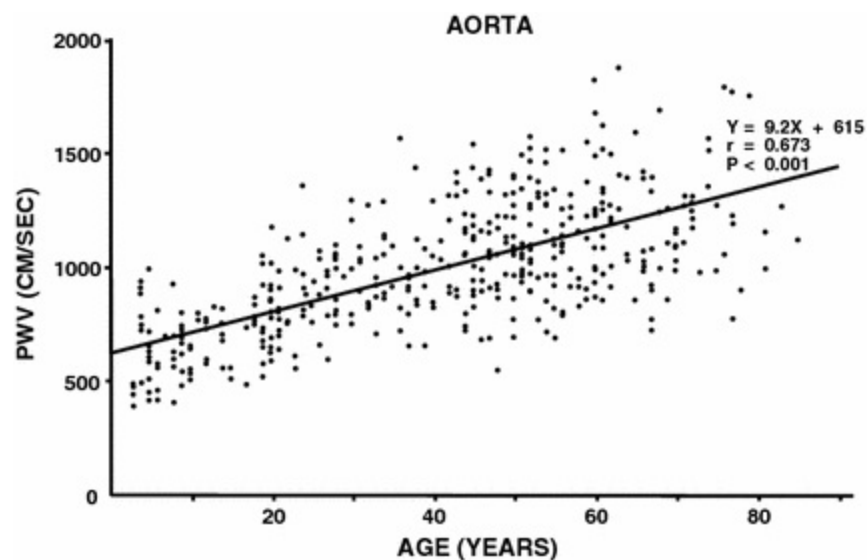


Fig. 14.3 Aortic PWV, measured between base of the neck and groin for all subjects (both male and female subjects) between ages 3 and 89 years. Individual values were determined as the average of 10 pairs of pulses simultaneously recorded with identical transcutaneous Doppler transducers. From; Avolio AP, Chen SG, Wang RP, Zhang CL, Li MF, O'Rourke MF; Effects of aging on changing arterial compliance and left ventricular load in a northern Chinese urban community. *Circulation*. 1983;68:50–58; with permission from Wolters Kluwer Health, Inc.

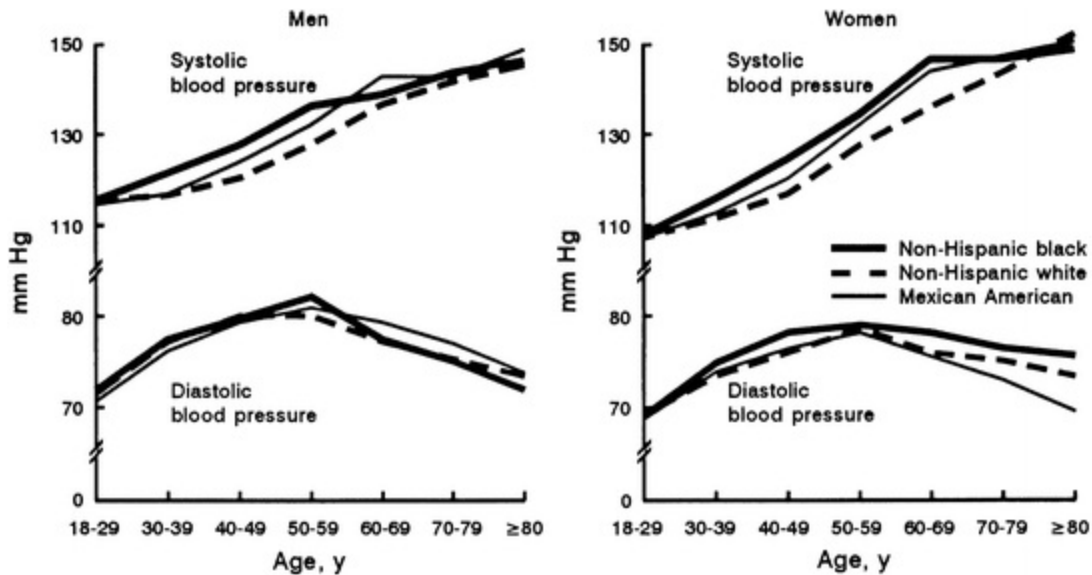


Fig. 14.4 Mean systolic and diastolic blood pressures by age and race/ethnicity for men and women, US population 18 years of age and older. From; Burt VL, Whelton P, Roccella EJ, Brown C, Cutler JA, Higgins M et al.; Prevalence of hypertension in the US population. Results from the Third National Health and Nutrition Examination Survey. 1988–1991. *Hypertension*. 1995;25:305-313; © 1995 American Heart Association, Inc., with permission from Wolters Kluwer Health, Inc.

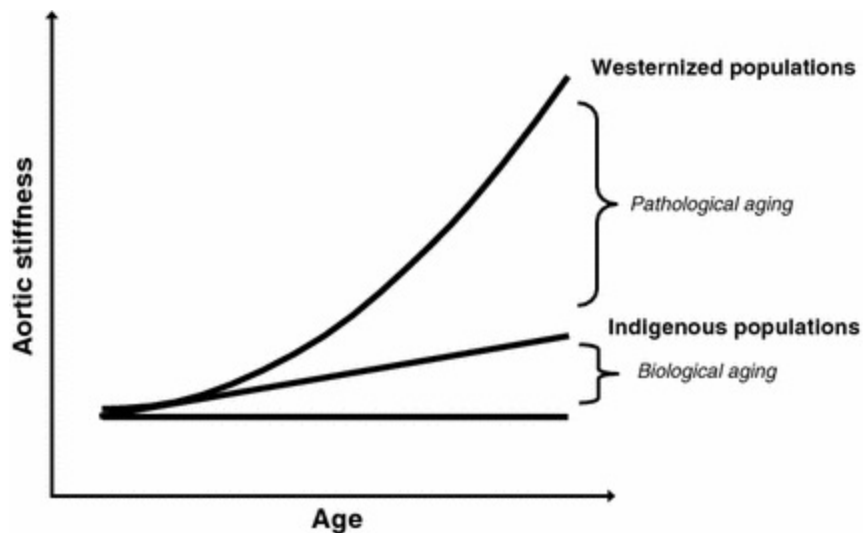


Fig. 14.5 Schema demonstrating pathological versus biological vascular ageing. From; Wilkinson IB, McEniery CM. Arteriosclerosis: inevitable or self-inflicted? *Hypertension*. 2012;60:3–5; © 2012

- *Biological increase in stiffness with age.* The repeated cyclic stress on the elastic fibres in the arterial wall leads to fibre fracture and loss of elasticity (O'Rourke 1990). Cyclic fatigue is commonly seen in engineering where repeated stretching and unstretching of materials many millions of times eventually lead to fracture of the material. In the human over a single decade, the elastic fibres in the artery wall will stretch and unstretch over 300 million times. This effect is also more marked at higher pressures. A measure of the degree of cyclic stretch fatigue is the product of age times pulse pressure times heartrate.
- *Pathological increase in stiffness with age.* Diseases such as diabetes and aspects of Western lifestyle such as high salt intake, along with genetic predisposing factors, lead to biological changes in the vessel wall and increase in stiffness.

Biological and pathological factors form a vicious circle in which there continues to be increase in stiffness and pressure over time (Fig. 14.6) both of which contribute to the formation of atherosclerosis.

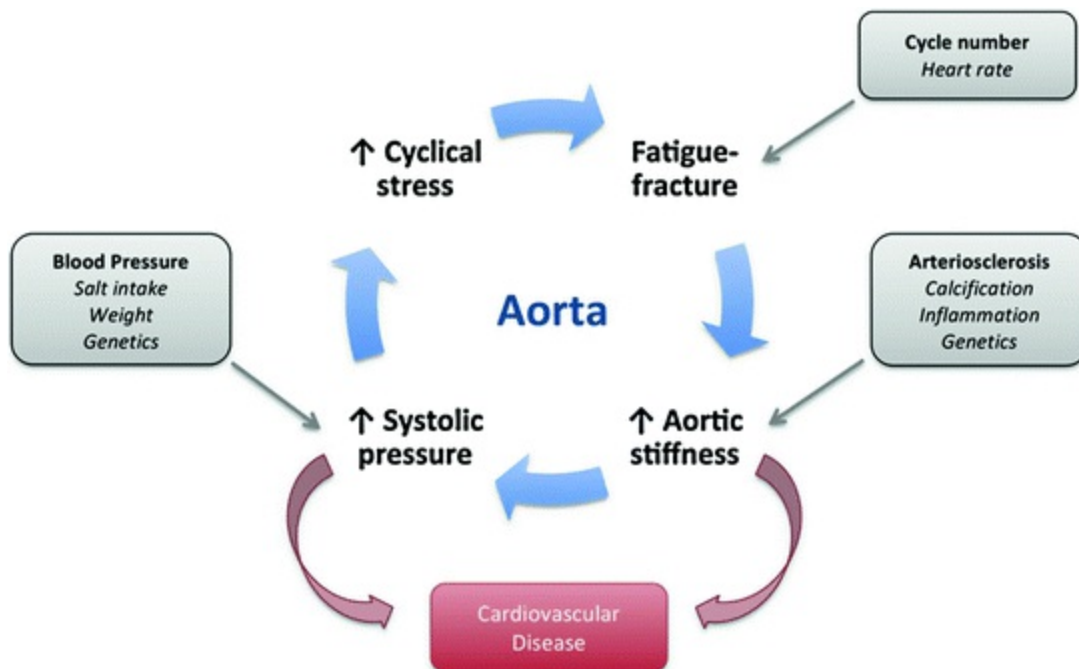


Fig. 14.6 The vicious circle of arteriosclerosis. Fatigue fracture of the elastic elements in the aorta leads to elevated systolic pressure and thus increased cyclic stress—setting up a vicious circle. Factors driving blood pressure elevation lead to increased systolic pressure, thereby accelerating the process, as

do the factors driving arteriosclerosis. Ultimately, elevated systolic pressure and increased stiffness both lead to cardiovascular disease. From McEniery CM, Wilkinson IB. The pressures of ageing. *Hypertension* 2013;62:823–824. © 2013 American Heart Association, Inc., with permission from Wolters Kluwer Health, Inc.

14.3 Pressure and Stiffness

Blood pressure is inextricably linked to arterial stiffness, mainly stiffness of the aorta. This section will examine what happens to blood pressure as the stiffness of the aorta increases.

14.3.1 Role of PWV in Determining Pressure

It will be recalled from Chap. 4 that the blood pressure waveform (pressure–time) is a composite of the forward going pressure wave and the reverse going pressure wave. The pressure wave from the heart travels down the aorta and returns after being reflected from the distal arteriolar beds. The time at which the reverse going wave returns is determined by the pressure wave speed (the pulse wave velocity, PWV) in the aorta. The PWV is in turn determined by the stiffness, wall thickness and diameter of the aorta through the Moens–Korteweg equation described in Chap. 4 and reproduced below.

$$\text{PWV} = \sqrt{\frac{Eh}{d\rho}}, \quad (14.2)$$

where E is elastic modulus of the artery, h is wall thickness, d is diameter and ρ is density of blood.

The effect of increased stiffness on the pressure waveform is illustrated in Fig. 14.7. In this example, increasing stiffness arises through ageing (discussed in Sect. 14.2). At higher stiffness, the amplitude of the reverse going pressure wave is greater and the reverse wave returns earlier in the cardiac cycle leading to augmentation of the overall pressure.

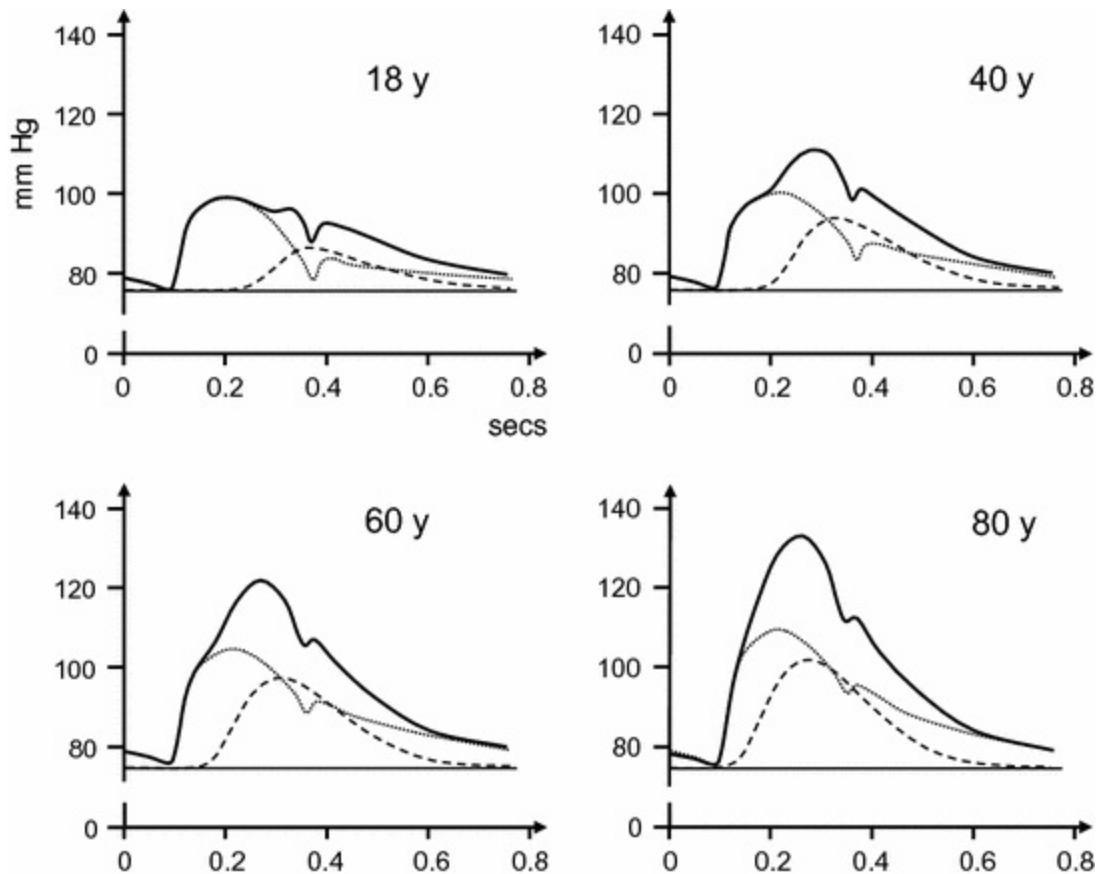


Fig. 14.7 Changes in the central pressure waveform with age. This is divided into forward (*dotted lines*) and reflected (*dashed lines*) pressure waves. The resultant pressure (*solid lines*) is the summation of forward and reflected waves. The reflected wave component increases in amplitude with age and also returns earlier, both effects leading to increase in systolic pressure. Redrawn with permission from images from Atcor Medical, West Ryde, NSW 2114, Australia

14.3.2 Pressure and Remodelling

Let us consider the case where there is a medium-term (weeks to months) increase in blood pressure as a result of disease or lifestyle. Figure 14.8 shows the pressure–stiffness curve of the aorta. The resting pressure of this particular individual is 95/65; well within what is classified as the ‘normal’ range. During the cardiac cycle the aorta stiffness will change as pressure changes from 2.2 to 2.6 units in Fig. 14.8. Suppose that the pressure increases due to some change in lifestyle or due to disease; this is shown in an exaggerated manner where the new blood pressure is 175/100. The artery is now operating in the stiffer part of the curve with the new stiffness changing from 2.7 to 3.1 units during the cardiac cycle. There is an associated increase in PWV which acts to exacerbate the increase in systolic pressure through the

processes mentioned above. If the blood pressure increase is sustained long-term, then the artery will remodel to normalise circumferential stress. However, this is achieved through wall thickening which itself will lead to long-term increase in stiffness, in PWV and in systolic pressure. A medium-term decrease in blood pressure, through medication, exercise or reduction in psychological stress will result in the opposite. These processes are illustrated in Fig. 14.9.

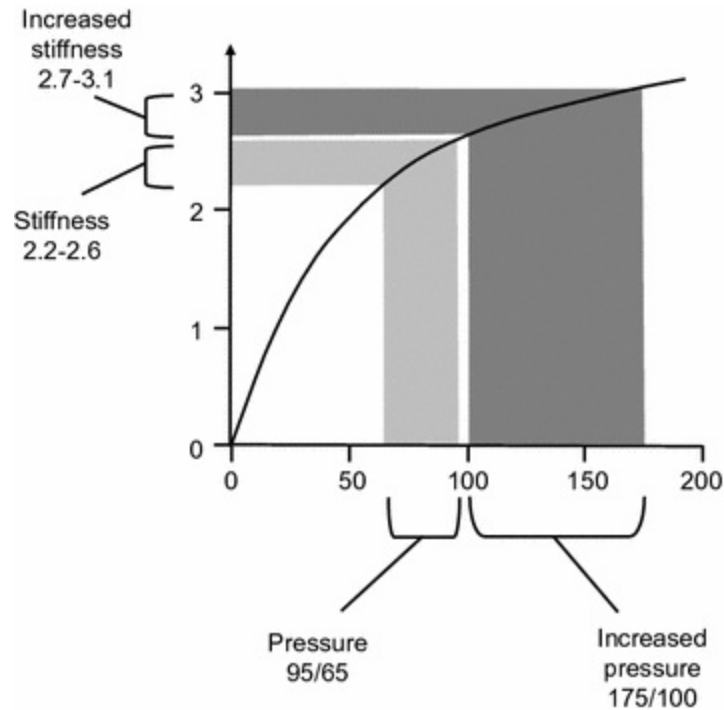


Fig. 14.8 Pressure–stiffness curve for an artery. In this example, pressure of 95/65 is associated with stiffness of 2.2–2.6 units. Increase in pressure to 175/105 is associated with stiffness of 2.7–3.1 units

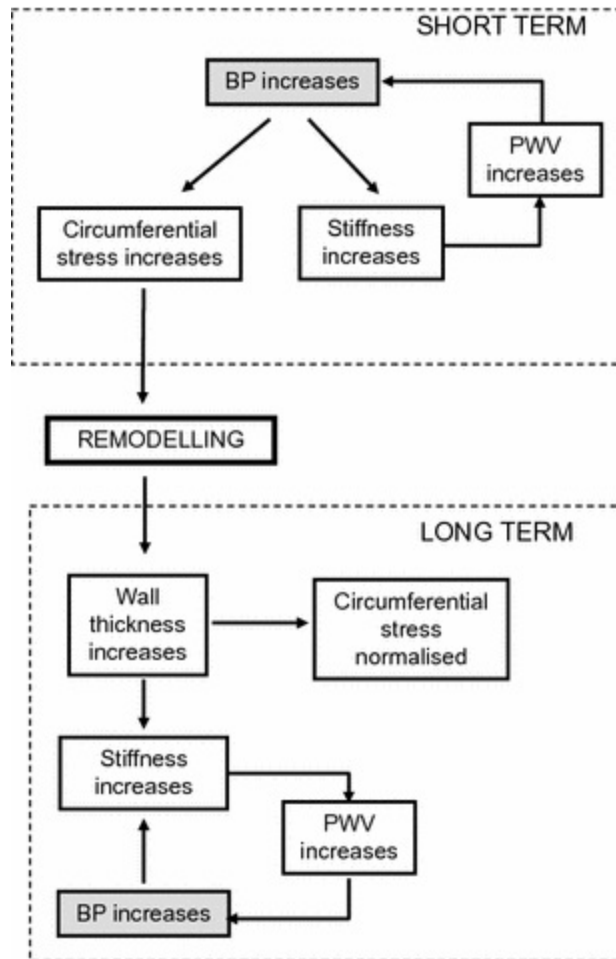


Fig. 14.9 Changes to the artery resulting from medium-term (weeks–months) change in blood pressure

14.4 In Vivo Measurement of Pressure

14.4.1 Invasive Measurement

Direct measurement of blood pressure requires an arterial puncture and insertion of a catheter. The tip of the catheter is directed by the operator to the site of interest (e.g. the coronary artery), usually under X-ray guidance. The original methodology was based on a flexible membrane within the catheter tip with pressure variations transmitted along a fluid-filled column to a pressure sensor which was located in a control unit into which the catheter was plugged. These have several disadvantages including the need to flush the vessel to remove air bubbles and motion artefacts. There is also signal attenuation and overshoot leading to an inaccurate pressure trace. Modern catheters used in clinical practice have used measurement of pressure at the

catheter tip using, for example, a piezoelectric transducer (Millar Instruments) (Fig. 14.10). The direct measurement enables an improved frequency response and more accurate recording of pressure (Fig. 14.11). An early paper which described catheter-tip pressure measurement is Millar and Baker (1973). Reviews of invasive pressure measurement are provided by Zimmer and Millar (1998) and Papaioannou et al. (2009).

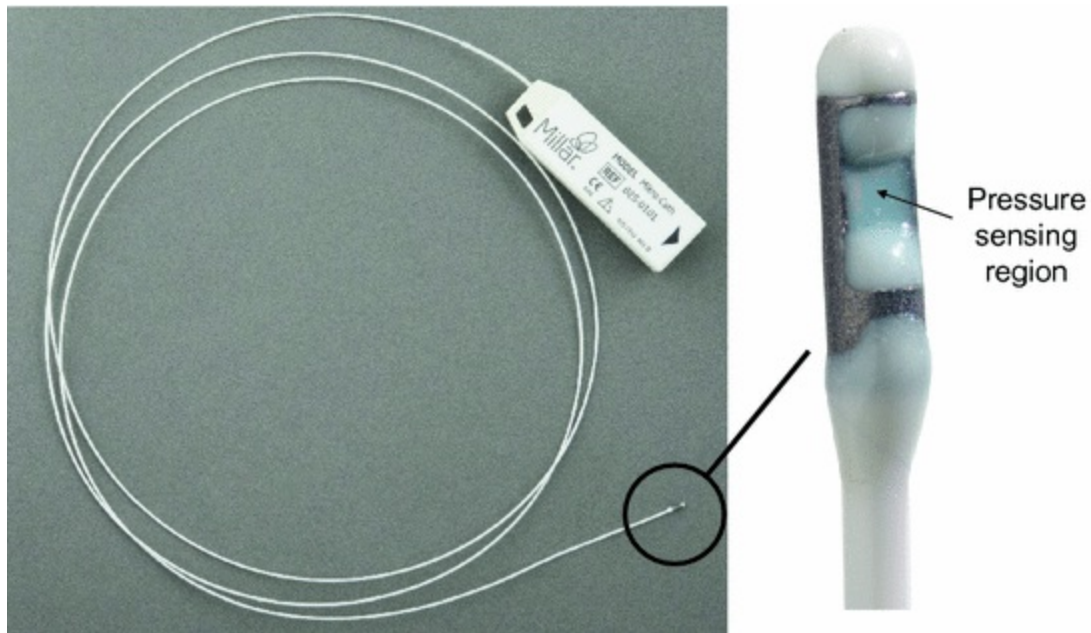


Fig. 14.10 Pressure catheter for measurement in arteries. The catheter tip showing the pressure measuring region is shown. This is the Mikro-Cath pressure catheter; images kindly provided by Millar Inc. (Houston, Texas, USA)

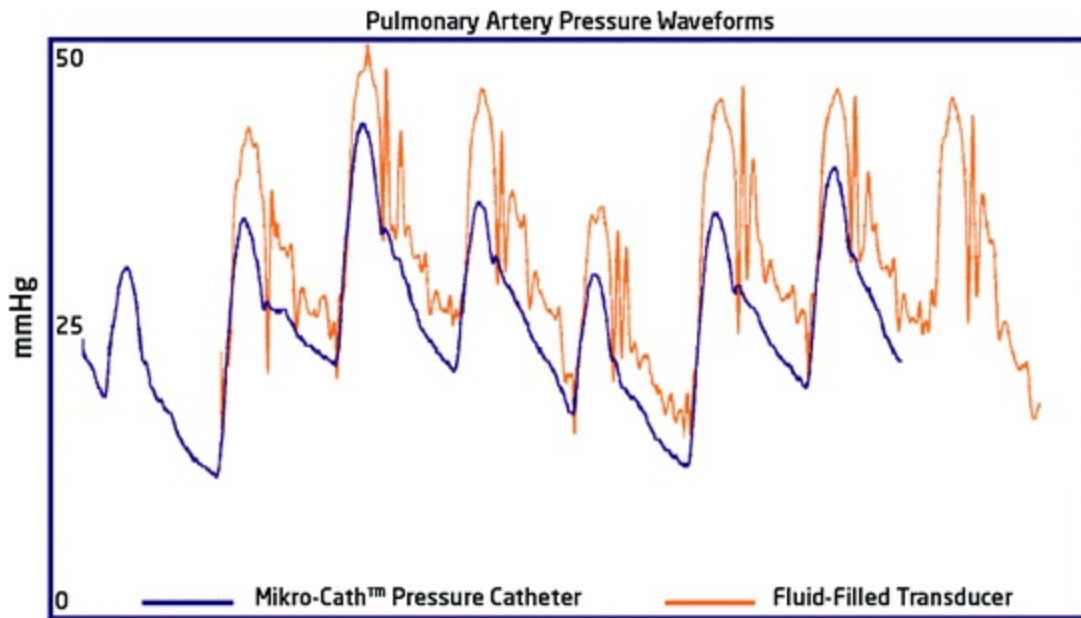


Fig. 14.11 Comparison of pressure waveforms measured using a fluid-filled transducer and a solid-state transducer (Mikro-Cath, Millar Inc.). Images kindly provided by Millar Inc. (Houston, Texas, USA)

14.4.2 Non-invasive Measurement—Pressure Cuff

Measurement of blood pressure in the brachial artery is undertaken using a cuff wrapped around the arm. The cuff is inflated to above systolic blood pressure then gradually deflated allowing blood to flow in the artery. The pressure in the cuff is traditionally measured using a mercury manometer with a stethoscope used to monitor the sounds arising from the occlusion and re-establishment of blood flow. Using this method the systolic and diastolic pressure can be identified. Blood flow may also be measured using Doppler ultrasound allowing identification of the point of systole (where blood just begins to flow) but not diastole.

Automated monitoring of blood pressure may be performed by examining the pressure oscillations in the cuff as the cuff pressure is released. A pressure sensor is used to monitor cuff pressure and signal processing is used to extract the systolic and diastolic blood pressures. These are referred to as NIBP (non-invasive blood pressure) devices.

Though cuffs are mostly used in the arm they can also be used in the leg, though this is not commonly done outside of a few research labs.

14.4.3 Non-invasive Measurement—Applanation Tonometry

The term ‘tonometry’ refers to measurement of pressure, the term ‘applanation’ means to flatten. Applanation tonometry concerns the measurement of arterial pressure using a probe containing a pressure sensor in which the probe is pressed onto the skin over the artery causing (at least to some degree) flattening of the surface of the artery against the probe and against the bone. The pressure variations from the artery are transmitted through the overlying tissues and detected by the pressure sensor. This technique is applicable to arteries which are close to the surface, so the radial and brachial arteries in the arm, the carotid artery in the neck and the common femoral artery in the leg. The blood pressure is obtained as a function of time; however, this is uncalibrated. In the brachial or radial artery, the blood pressure may be calibrated using pressure measurements taken using an arm cuff.

The main interest for applanation tonometry has been the estimation of the central pressure waveform from the radial waveform. The central pressure waveform is estimated using a transfer function approach developed by O’Rourke and colleagues (Karamanoglu et al. 1993). This has been validated against invasive measurements (Pauca et al. 2001; Chen et al. 1997; Gallagher et al. 2004). Reviews of the development and clinical application of applanation tonometry are provided by O’Rourke and Gallagher (1996), O’Rourke et al. (2001), Wilkinson et al. (1998), Nelson et al. (2010) and Kim and Braam (2013).

Figure 14.12 shows typical radial artery waveforms and the calculated central pressure waveforms. An index ‘augmentation index’ may be measured (Fig. 14.13) which describes the increase in pressure arising from the reflected wave component:

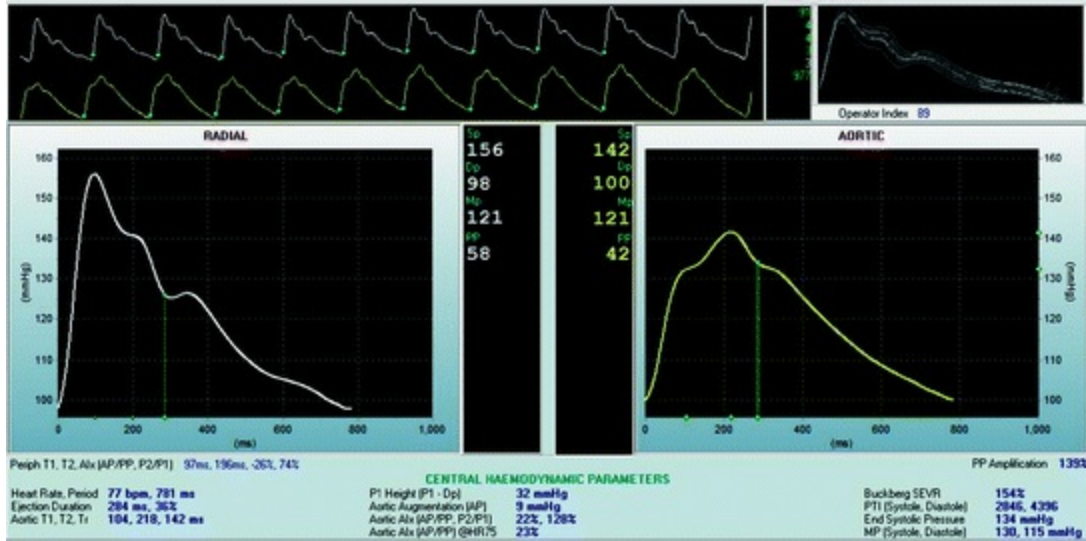


Fig. 14.12 Radial artery pressure waveform obtained using a Sphygmocor applanation tonometry system and the calculated central pressure waveforms

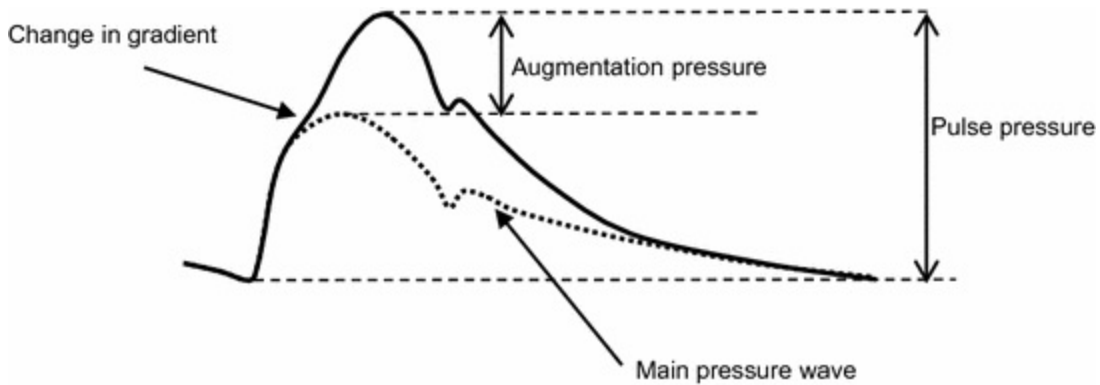


Fig. 14.13 Measurement of pressure required in calculation of augmentation pressure

Augmentation index = augmentation pressure/pulse pressure

The augmentation pressure is the difference between the peak pressure which would have occurred in the absence of reflected waves and peak pressure in practice (Fig. 14.13). These are often referred to as the first and second peaks. In some cases, these peaks can be clearly distinguished allowing estimation of the augmentation pressure from the pressure waveform. However in most cases there is no second peak. Instead, there is a slight change in the pressure gradient (labelled on Fig. 14.13) which may be difficult to detect with accuracy. In practice, commercial devices such as the Sphygmocor (AtCor Medical, Sydney, Australia) calculate the main and reflected pressure components and use these to estimate the augmentation

pressure.

References

Avolio AP, Chen SG, Wang RP, Zhang CL, Li MF, O'Rourke MF. Effects of aging on changing arterial compliance and left ventricular load in a northern Chinese urban community. *Circulation*. 1983;68:50–8.

[CrossRef][PubMed]

Avolio AP, Deng FQ, Li WQ, Luo YF, Huang ZD, Xing LF, O'Rourke MF. Effects of aging on arterial distensibility in populations with high and low prevalence of hypertension: comparison between urban and rural communities in China. *Circulation*. 1985;71:202–10.

[CrossRef][PubMed]

Burt VL, Whelton P, Roccella EJ, Brown C, Cutler JA, Higgins M, et al. Prevalence of hypertension in the US population. Results from the Third National Health and Nutrition Examination Survey. 1988–1991. *Hypertension*. 1995;25:305–13.

[CrossRef][PubMed]

Chen CH, Nevo E, Fetics B, Pak PH, Yin FC, Maughan WL, Kass DA. Estimation of central aortic pressure waveform by mathematical transformation of radial tonometry pressure. Validation of generalized transfer function. *Circulation*. 1997;95:1827–36.

[CrossRef][PubMed]

Gallagher D, Adji A, O'Rourke MF. Validation of the transfer function technique for generating central from peripheral upper limb pressure waveform. *Am J Hypertens*. 2004;17:1059–67.

[CrossRef][PubMed]

Herbert A, Cruickshank JK, Laurent S, Boutouyrie P. Reference values for arterial measurements collaboration. Establishing reference values for central blood pressure and its amplification in a general healthy population and according to cardiovascular risk factors. *Eur Heart J*. 2014;35:3122–33.

[CrossRef][PubMed]

Karamanoglu M, O'Rourke MF, Avolio AP, Kelly RP. An analysis of the relationship between central aortic and peripheral upper limb pressure waves in man. *Eur Heart J*. 1993;14:160–7.

[CrossRef][PubMed]

Kearney PM, Whelton M, Reynolds K, et al. Global burden of hypertension: analysis of worldwide data. *Lancet*. 2005;365:217–23.

[CrossRef][PubMed]

Kim DH, Braam B. Assessment of arterial stiffness using applanation tonometry. *Can J Physiol Pharmacol*. 2013;91:999–1008.

[CrossRef][PubMed]

Lemogoum D, Ngatchou W, Janssen C, Leeman M, Van Bortel L, Boutouyrie P, Degaute JP, Van de Borne P. Effects of hunter-gatherer subsistence mode on arterial distensibility in Cameroonian pygmies. *Hypertension*. 2012;60:123–8.

[\[CrossRef\]](#)[\[PubMed\]](#)

McEniery CM, Wilkinson IB. The pressures of ageing. *Hypertension*. 2013;62:823–4.

[\[CrossRef\]](#)[\[PubMed\]](#)

McEniery CM, Wilkinson IB, Avolio AP. Age, hypertension and arterial function. *Clin Exp Pharmacol Physiol*. 2007;34:665–71.

[\[CrossRef\]](#)[\[PubMed\]](#)

Millar HD, Baker LE. A stable ultraminiature catheter-tip pressure transducer. *Med Biol Eng*. 1973;11:86–9.

[\[CrossRef\]](#)[\[PubMed\]](#)

Nelson MR, Stepanek J, Cevette M, Covalciuc M, Hurst RT, Tajik AJ. Noninvasive measurement of central vascular pressures with arterial tonometry: clinical revival of the pulse pressure waveform? *Mayo Clin Proc*. 2010;85:460–72.

[\[CrossRef\]](#)[\[PubMed\]](#)[\[PubMedCentral\]](#)

O'Rourke M. Arterial stiffness, systolic blood pressure, and logical treatment of arterial hypertension. *Hypertension*. 1990;15:339–47.

[\[CrossRef\]](#)[\[PubMed\]](#)

O'Rourke MF, Gallagher DE. Pulse wave analysis. *J Hypertens Suppl*. 1996;14:S147–57.

[\[CrossRef\]](#)[\[PubMed\]](#)

O'Rourke MF, Pauca A, Jiang XJ. Pulse wave analysis. *Brit J Clin Pharmacol*. 2001;51:507–22.

[\[CrossRef\]](#)

Papaoiannou TG, Protogerou AD, Stamatelopoulos KS, Vavuranakis M, Stefanadis C. Non-invasive methods and techniques for central blood pressure estimation: procedures, validation, reproducibility and limitations. *Curr Pharm Des*. 2009;15:245–53.

[\[CrossRef\]](#)[\[PubMed\]](#)

Pauca AL, O'Rourke MF, Kon ND. Prospective evaluation of a method for estimating ascending aortic pressure from the radial artery pressure waveform. *Hypertension*. 2001;38:932–7.

[\[CrossRef\]](#)[\[PubMed\]](#)

Wilkinson IB, McEniery CM. Arteriosclerosis: inevitable or self-inflicted? *Hypertension*. 2012;60:3–5.

[\[CrossRef\]](#)[\[PubMed\]](#)

Wilkinson IB, Cockcroft JR, Webb DJ. Pulse wave analysis and arterial stiffness. *J Cardiovasc Pharmacol*. 1998;32:S33–7.

[\[PubMed\]](#)

Zimmer HG, Millar HD. Technology and application of ultraminiature catheter pressure transducers. *Can J Cardiol*. 1998;14:1259–66.

[\[PubMed\]](#)

15. Atherosclerosis

Peter R. Hoskins¹✉ and Patricia V. Lawford²✉

- (1) Edinburgh University, Edinburgh, UK
- (2) Sheffield University, Sheffield, England, UK

✉ **Peter R. Hoskins (Corresponding author)**

Email: P.Hoskins@ed.ac.uk

✉ **Patricia V. Lawford**

Email: p.lawford@sheffield.ac.uk

Learning outcomes

1. Describe, in brief, atherosclerosis; the natural history, the clinical consequences for different end-organs and treatment.
2. Describe the effect of a stenosis on haemodynamic quantities; velocity, flow, pressure and wall shear stress.
3. Discuss the variation of flow and blood velocity with degree of stenosis in terms of changes in arteriolar resistance.
4. Describe the mechanical properties of atherosclerotic plaque.
5. Discuss the role of wall shear stress and related phenomena on plaque initiation and growth.

6. Discuss the role of peak cap stress in plaque rupture.
7. Describe in vivo measurements made on atherosclerotic plaque.
8. Describe briefly the treatment of carotid atherosclerosis and of coronary atherosclerosis.

The World Health Organisation reported that in 2012 cardiovascular diseases were responsible for 31 % of all world deaths. The largest contributor to deaths from cardiovascular disease is atherosclerosis. This chapter will explore atherosclerosis, its development, biomechanics and clinical treatment.

15.1 Atherosclerosis

Atherosclerosis is a disease characterised by the build up of fatty deposits in the arterial wall. The disease begins in early childhood and progresses through the entire adult life. There are several stages of atherosclerosis (Lusis 2000) illustrated in Figs. 15.1 and 15.2. Early disease is associated with deposition of fatty deposits (atheroma) within the intimal layer of the wall, initially these are seen as fatty streaks on the inner lumen of the wall (Fig. 15.1b). This is followed by thickening of the intimal layer which may be associated with lipid deposits and the presence of foam cells (Fig. 15.1b). As the disease progresses there is further lipid deposition and an atherosclerotic plaque is formed (Fig. 15.1d). In these initial phases, which may last for many decades, there is preservation of the inner lumen (Glagov et al. 1987). In other words formation of the plaque is associated with outward remodelling of the vessel wall. Later stages of plaque formation are associated with encroachment of the lumen. The degree of narrowing (stenosis) increases with time and there is flow reduction at higher degrees of stenosis. Figure 15.1e, f show late-stage plaque, one with a thick cap (Fig. 15.1e) and one with a thin cap (Fig. 15.1f). It will be described below that cap thickness is a principle determinant of rupture risk. If the plaque ruptures there is spillage of thrombogenic (clot-promoting) plaque contents into the bloodstream which are then carried downstream and can cause blockage of downstream vessels. The ruptured plaque may also become

thrombosed further exacerbating reduction in flow.

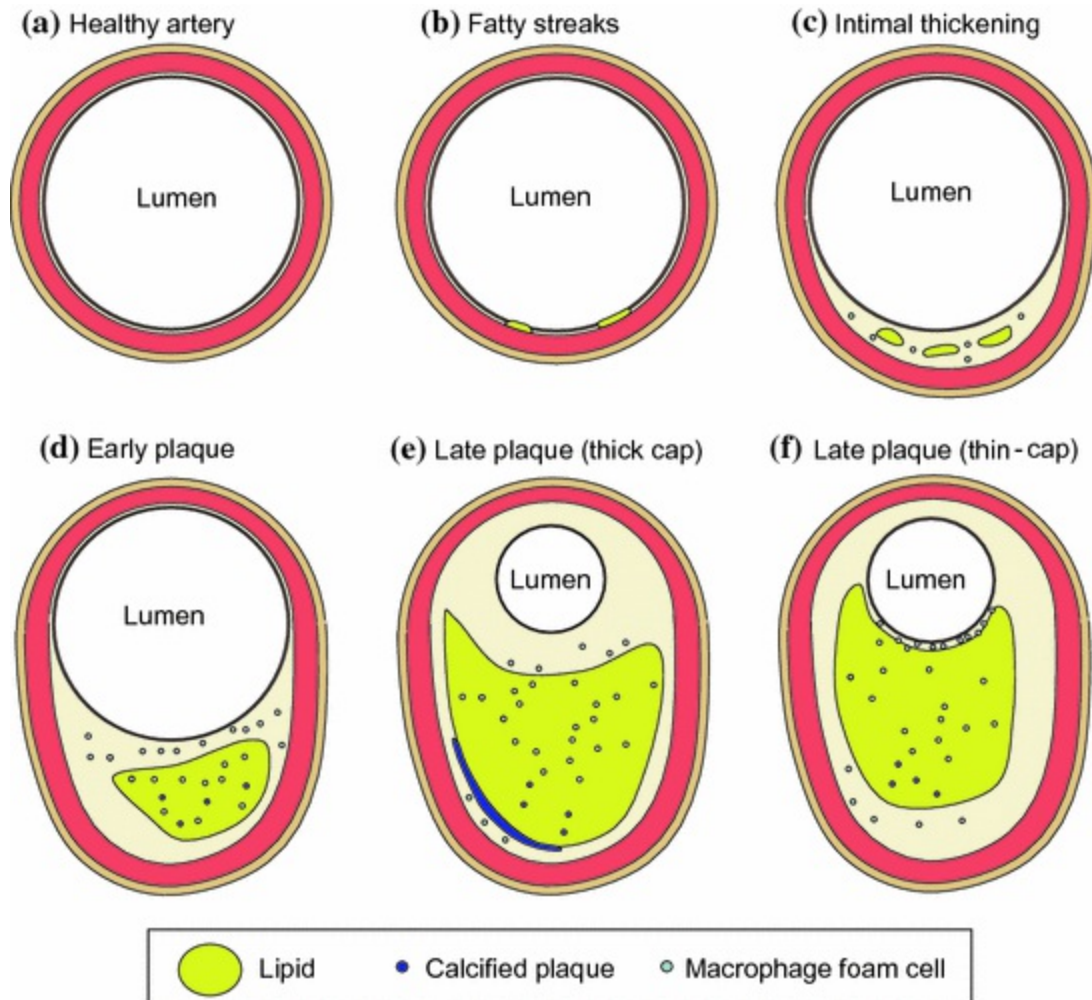


Fig. 15.1 Progression of atherosclerosis with time. **a** Healthy artery showing the various layers, from the outside these are the adventitia, media and intima. **b** The first sign of disease is fatty streaks seen in the intima; these usually appear from about the first decade of life. **c** As the disease progresses there is thickening of the intimal layer; often associated with lipid deposition and the presence of foam cells. **d** An early plaque is formed consisting of a lipid pool, and there are calcified regions, foam cells and cholesterol clefts. The inner lumen is unaffected due to outward remodelling. Early plaque appear from about the third decade of life. **e** and **f** Late plaque is associated with reduction in the lumen diameter; there may be larger regions of calcification. The wall between the lumen and the lipid pool (the cap) is of variable size. In **(e)** the cap is thick, in **(f)** the cap is thin—thin cap plaque are at higher risk of rupture. Late plaque appear from about the fourth decade of life

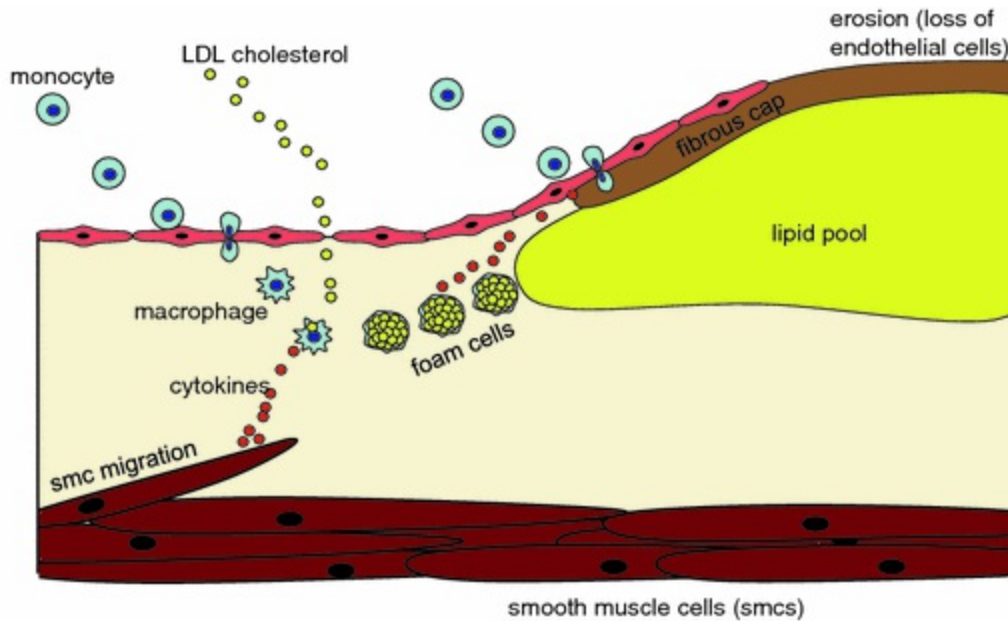


Fig. 15.2 Plaque biology basics. This involves; adhesion of monocytes to the endothelial surface (1), migration into the vessel wall (2), differentiation into macrophages (scavenger cells) (3). Movement of LDL cholesterol between the endothelial cells and into the subendothelial space (4) where they are oxidised and ingested by macrophages (5) forming foam cells (6) which reach a certain size and then rupture depositing their lipids in the vessel wall (7) which attracts more monocytes (8). Migration of vascular smooth muscle cells (smcs) from the media into the intima (9) and smc proliferation under the control of cytokines (10)

All these phenomena (local lumen reduction, spillage of contents and local thrombosis) combine to cause reduced perfusion to the tissues supplied by the artery. If perfusion reduces below a critical amount then there is tissue death. The tissue which is affected may have an alternative supply from a different artery in which case perfusion may be impaired but still sufficient for tissue viability. Often plaque rupture is the event that triggers symptoms in the patient. Plaque rupture in the carotid arteries typically leads to death of brain tissue (stroke). Plaque rupture in the coronary arteries typically leads to death of cardiac tissue (heart attack).

For arteries supplying the legs (aorta, iliac, femoral), the effects of atherosclerosis are often less dramatic. As atherosclerosis progresses then a secondary (collateral) circulation develops which enables blood to bypass the affected artery. The first sign of disease is claudication which is pain in the calf after walking. The distance the patient can walk (the claudication distance) gradually decreases until the patient has pain at rest. Any further deterioration leads to inadequate blood supply which if untreated can lead to

tissue death and gangrene.

Treatment of disease is usually associated with re-establishing adequate perfusion, and in some cases surgical removal of dead tissue through amputation. Re-perfusion treatment can involve bypassing the affected artery using a vein taken from the patient or using an artificial graft. The atherosclerotic plaque may be surgically removed if the artery is accessible, such as the carotid artery. The artery may be rebored using catheter techniques under X-ray guidance. Stents may be used in an attempt to stop re-stenosis.

15.2 Biomechanics

Atherosclerosis causes considerable changes to the elastic properties of the vessel wall and to blood flow and pressure which are described in this section.

15.2.1 The Flow-Field in Stenoses

The effect of a stenosis on local blood velocities is illustrated in Fig. 15.3. This is an idealised 70 % stenosis by diameter with steady flow. As the blood flows through the stenosis there is an increase in velocity. This may be understood in that, as the cross-sectional area A decreases, the velocity v increases. The flow rate is the product of the cross-sectional area and the mean velocity

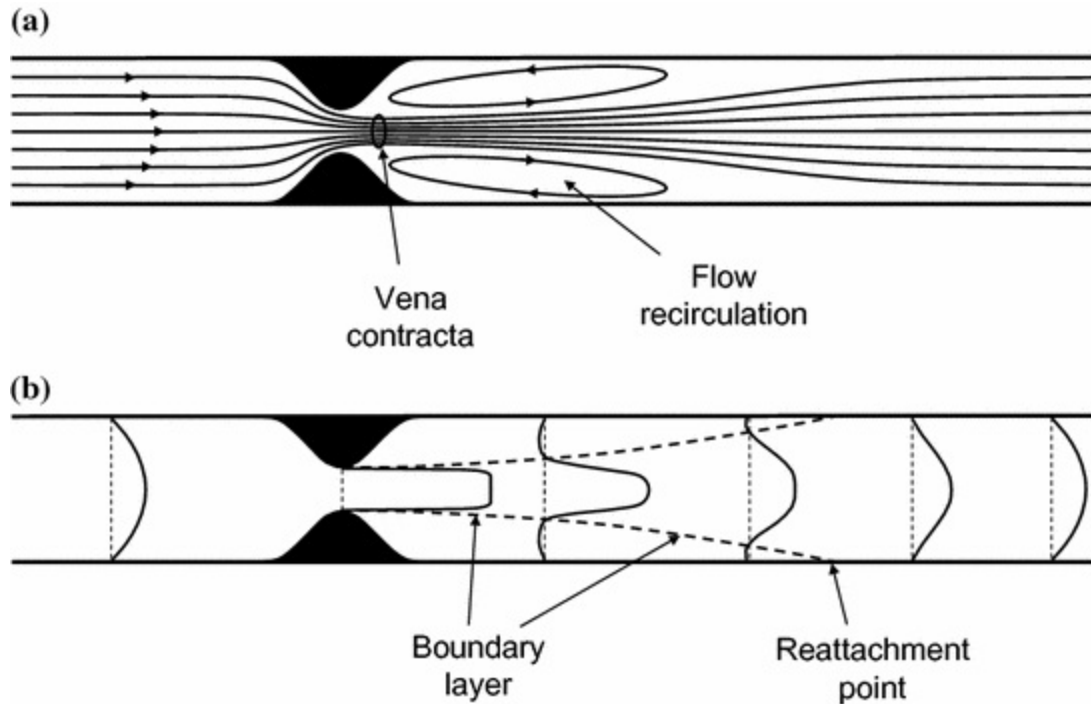


Fig. 15.3 Schematic of flow characteristics in an idealised 70 % stenosis in which turbulence is ignored. Velocity increases within the stenosis and a jet is formed. In the immediate post-stenosis region there is boundary separation with an area of recirculating flow. Fully developed flow is re-established some diameters downstream

$$Q = Av \quad (15.1)$$

Flow rate is constant at all cross sections along the vessel so that a decrease in A must lead to an increase in v . It might be thought that the maximum velocity would be located at the point of minimum lumen however this is not the case. The convergence of the flow streamlines which occur in the immediate pre-stenotic region continues and the minimum diameter of the flow stream is located just downstream of the minimum lumen; this region is called the 'vena contracta'. The maximum velocity is located at the vena contracta, not at the point of minimum lumen. Immediately downstream of the stenosis there is a region of flow recirculation. Flow separation occurs and there is a boundary layer separating the two flow regions. The boundary layer reattaches to the vessel wall downstream as shown in Fig. 15.3b

Changes in the velocity profiles are shown in Fig. 15.3b. The velocity profile which is initially parabolic becomes almost flat within the stenosis. In the post-stenotic region the velocity profile has small regions of reverse flow. Due to viscosity, the effect of the stenosis on the flow patterns diminishes with distance. After several diameters downstream the jet dies out and the

parabolic velocity profile resumes. In this idealised example the effect of turbulence has not been considered, and the region of recirculation is stable. In real stenoses in arteries the post-stenotic region may be highly unstable with turbulence and detachment of the post-stenotic vortices which are swept downstream. Figure 15.4 shows examples of flow-field data taken in simulated stenoses.

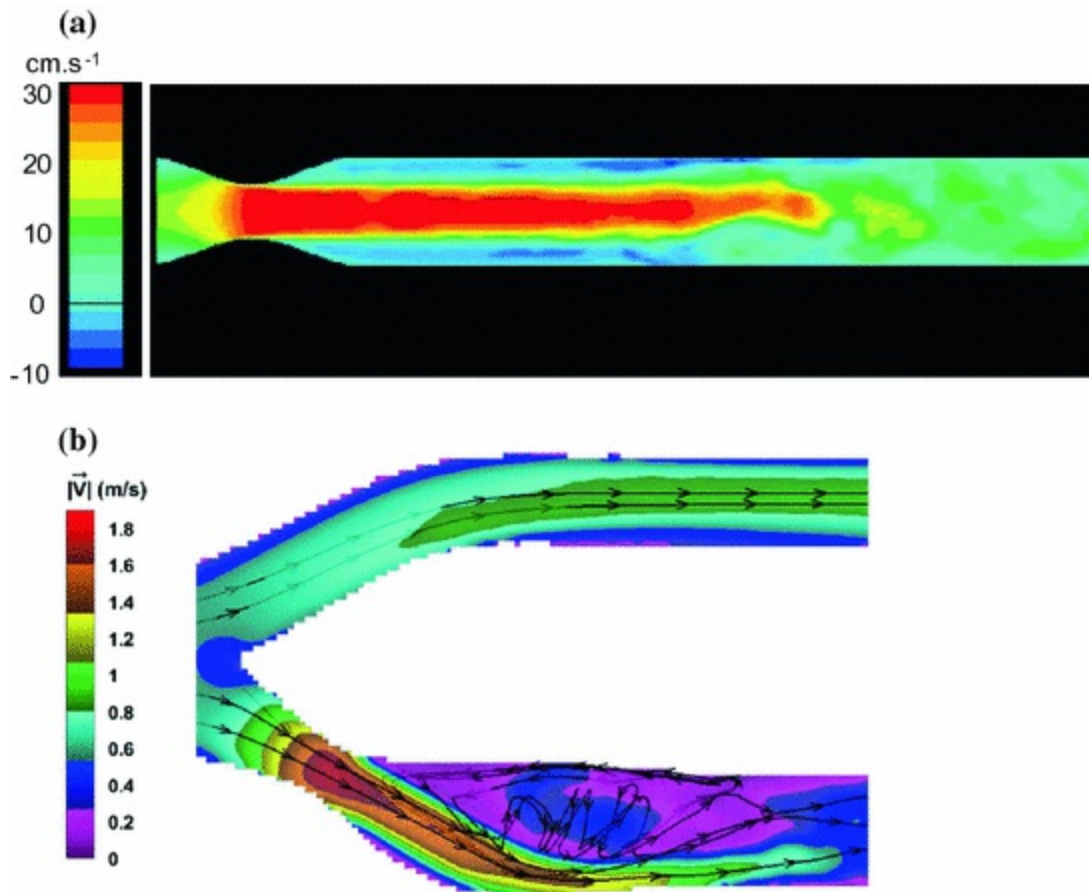


Fig. 15.4 Flow-field data in idealised stenoses. **a** 50 % stenosis with velocities estimated using CFD with an LES model of turbulence. The jet is seen in red with recirculating flow in blue and turbulence several diameters downstream. **b** Planar carotid bifurcation model with a 50 % stenosis with velocities estimated using PIV. The jet is seen in red with recirculation of flow in purple and blue. Figure 15.4b reprinted from; Journal of Biomechanics, Vol. 47(1); Kefayati S, Holdsworth DW, Poepping TL; Turbulence intensity measurements using particle image velocimetry in diseased carotid artery models: Effect of stenosis severity, plaque eccentricity, and ulceration; pp. 253–263, Copyright (2014); with permission from Elsevier

The changes which the stenosis makes on the velocity field will cause changes to the wall shear stress patterns (Fig. 15.5). The maximum wall shear stress is located just before the minimum lumen. The post-stenotic region has

low wall shear stress values. The peak wall shear stress in the tighter stenosis is 180–200 Pa. These high values of wall shear stress are thought to be responsible for the endothelial stripping which commonly occurs in tight stenoses in vivo. The distribution of wall shear stress is relevant in terms of the growth of atherosclerotic plaque as described in Sect. 15.3.

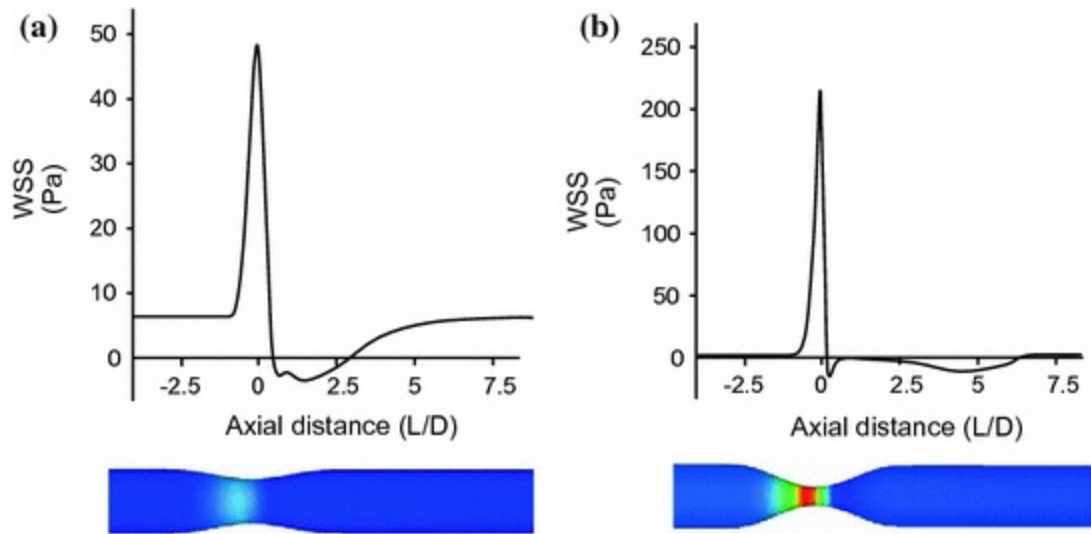


Fig. 15.5 Wall shear stress in idealised stenosed straight arteries estimated using CFD, with **a** 30 % stenosis and **b** 70 % stenosis. In each case the peak wall shear stress occurs just before the point of minimum lumen and there is negative shear stress in the immediate post-stenotic region. WSS images from; Li (2007); reprinted with permission from the author

15.2.2 Pressure Changes Across Stenoses

To investigate the change in pressure as blood flows through a stenosis we will initially consider flow of an idealised fluid in which there is no loss of energy in which case the simplified version of Bernoulli's equation can be used

$$P + h\rho g + \frac{\rho v^2}{2} = \text{constant} \quad (15.2)$$

where P is pressure, h is height, ρ is density, g is the gravitational constant and v is velocity.

Assuming that the effects of gravity can be ignored, this gives, equation, 15.2

$$P + \frac{\rho v^2}{2} = \text{constant} \quad (15.3)$$

In Eq. 15.2 an increase in velocity is associated with a reduction in pressure, and vice versa. As blood flows through a stenosis there will be an increase in velocity and consequently a reduction in pressure (Fig. 15.6b). The point of maximum velocity and minimum pressure is located at the vena contracta. Downstream from the vena contracta the velocity decreases and so pressure increases, eventually recovering to its pre-stenosis value. This may be explained in terms of energy. The energy of the blood is shared between energy associated with pressure and kinetic energy (associated with movement of the blood). In this simplified example the total energy is constant so a reduction in pressure energy is associated with an increase in kinetic energy and vice versa.

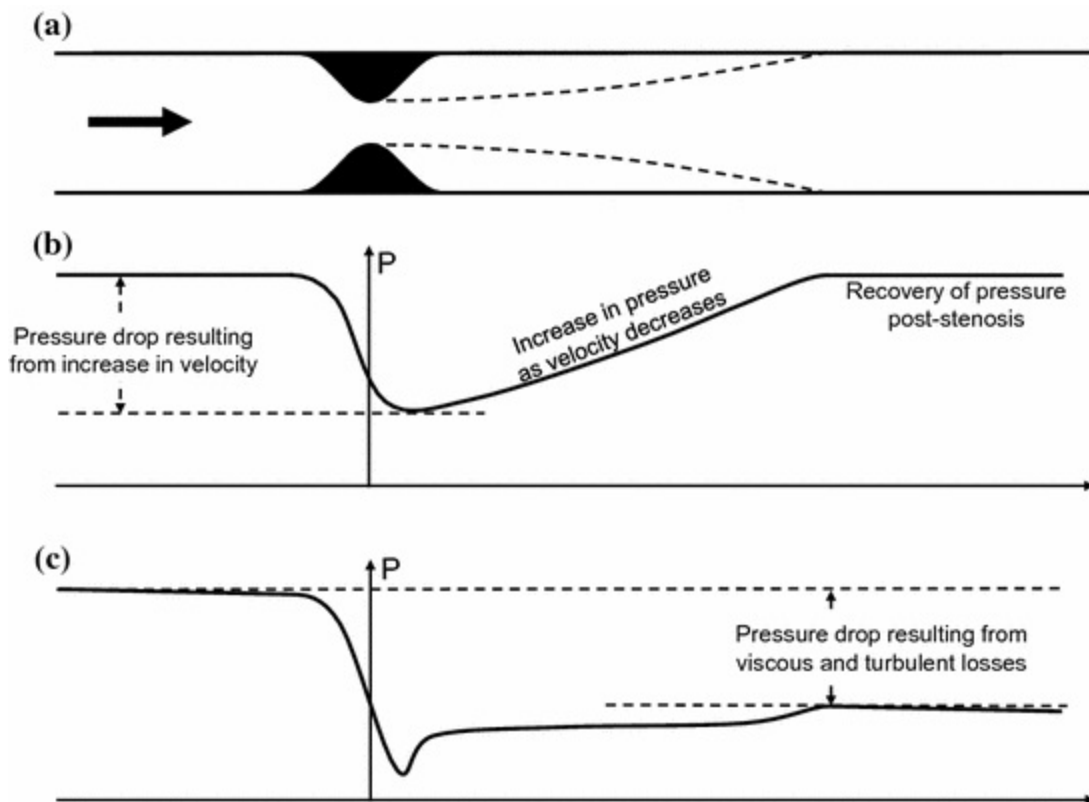


Fig. 15.6 Pressure as a function of axial distance in an artery with a 70 % stenosis (same geometry as Fig. 15.3). **a** Vessel geometry. **b** Flow of blood with no viscosity or turbulence (i.e. no energy losses). The pressure falls reaching a minimum value corresponding to the point of minimum lumen (at the vena-contracta); with increasing distance from the stenosis there is increase in pressure with full recovery to the pre-stenotic value. **c** Flow of blood including energy losses due to viscosity and turbulence. There is some recovery of pressure in the post-stenosis region but overall there is a pressure drop resulting from viscous and turbulent energy losses

In reality there are energy losses due to viscosity and turbulence. This leads overall to a pressure drop as the blood passes through the stenosis as shown in Fig. 15.6c.

Measurements of the pressure drop are widely used in cardiology in the coronary arteries where decisions are made as to which stenosis to treat and whether the effect of treatment has been successful (Sect. 15.5.2).

15.2.3 Flow Rate and Velocity as a Function of Degree of Stenosis

It might be expected that even a small reduction in artery diameter would cause some reduction in flow rate in the artery. However studies on animals with artificial stenosis and flow monitoring probes have shown that the flow is unaffected until the degree of stenosis reaches about 70 % by diameter (91 % by area), (Berguer and Hwang 1974). The value of lumen reduction after which flow decreases is called the 'critical stenosis'. Figure 15.7 shows the effect of stenosis value on flow rate and blood velocity. The velocity increases from $20 \text{ cm}\cdot\text{s}^{-1}$ in an unstenosed artery to a maximum value of $600 \text{ cm}\cdot\text{s}^{-1}$ at 84 % stenosis. It will be described in Sect. 15.4, in terms of clinical measurement of the degree of stenosis, that it is velocity which is used as flow rate does not distinguish different degrees of stenosis.

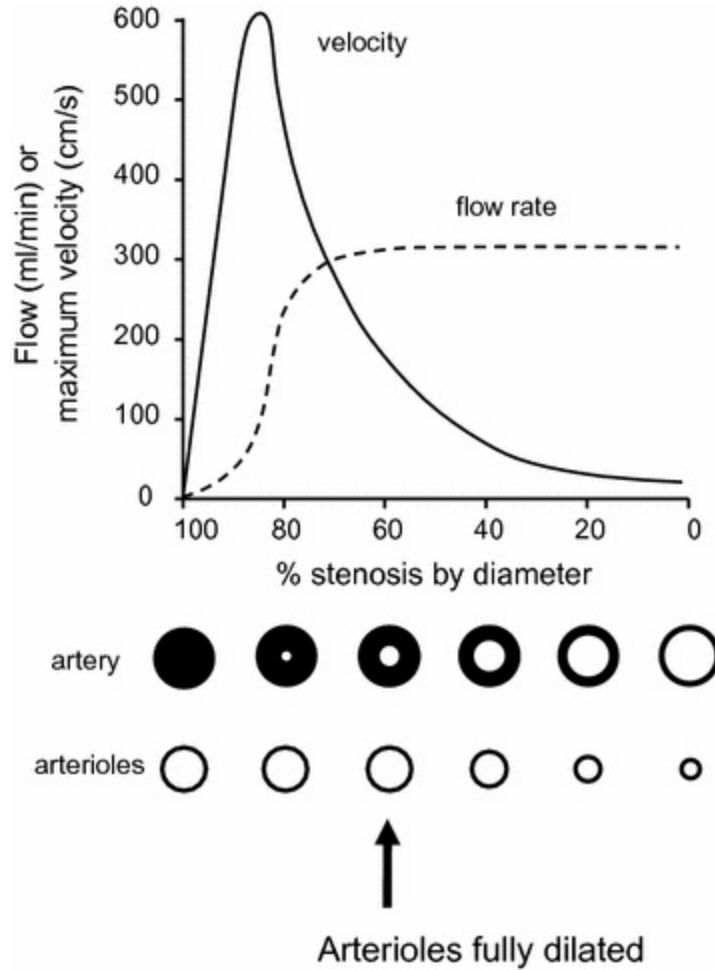


Fig. 15.7 Flow rate and velocity as a function of degree of stenosis. Flow rate is maintained constant up to 70 % by diameter after which flow reduces. The diameter of the artery and downstream arterioles are illustrated. As disease progresses the arterioles compensate by dilating in order to maintain flow constant. At 70 % stenosis the arterioles are fully dilated. Further increase in disease cannot be compensated by further arteriolar dilation and flow reduces. Drawn from data in Spencer and Reid (1979)

This data may be explained using the simple model of the arterial system described in Chap. 5, which is shown in Fig. 15.8. The flow rate is determined by the pressure gradient and by the overall resistance. The overall resistance is a combination of the resistance in the large arteries and in the arterioles. When a stenosis develops, the resistance in the large arteries increases. This is compensated by a reduction of resistance in the arterioles which is caused by dilation of the arterioles. Hence the overall resistance is maintained constant and the flow rate is also maintained constant. The arterioles are fully dilated when the stenosis value is 70 % by diameter (Fig. 15.7). Further increase in the degree of stenosis leads to increase in

overall resistance and the flow rate decreases.

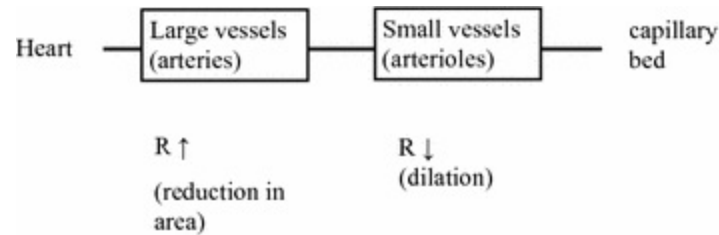


Fig. 15.8 Simple model of flow consisting of a heart, an artery and a downstream arterioles. Disease in the artery increases resistance. This is compensated by decrease in resistance of the arterioles

The concept of critical stenosis is useful in understanding the haemodynamic effects of stenosis, however in practice other mechanisms come into play to help preserve perfusion to the organ. The organ may be perfused by several arteries so that flow reduction in one artery does not have a drastic effect on perfusion. In the brain, the Circle of Willis acts to connect the different arteries which supply the brain. If the Circle of Willis is complete, then a stenosis in one artery (e.g. left internal carotid artery) may have a relatively minor impact on perfusion of the brain as the supply of blood can be taken over by other arteries. However if the Circle of Willis has missing connections then this resupply from other arteries is less effective and there will be reduced perfusion to the relevant area of the brain which may lead to a stroke. Atherosclerosis in arteries in the leg leads to reduction in flow rate in the artery. However, downstream (distal) tissues may be supplied by a collateral circulation which bypasses the diseased region. The collateral circulation consists of many small arteries which grow in size as the degree of stenosis in the main artery increases. The severity of symptoms (claudication, gangrene) depends to a large extent on how well the collateral circulation matures. Patients may have complete occlusion of both superficial femoral arteries and be unaware of this as they have very well developed collateral circulations.

15.2.4 Plaque Stiffness and Wall Stress

From a mechanical point of view an atherosclerotic plaque has two main regions; a lipid pool surrounded by a fibrous region (Fig. 15.9). The region of the plaque between the lipid pool and the lumen is called the ‘cap’, and rupture of the cap triggers clinical events such as stroke and heart attack.

Plaque rupture occurs when the mechanical stress within the cap exceeds the mechanical strength of the plaque. The first studies on the stress distribution within the cap were performed by Richardson et al. (1989), Loree et al. (1992) and Cheng et al. (1993). There have been many subsequent studies which are reviewed in Cardoso and Weinbaum (2014). Figure 15.10 illustrates typical findings from computational stress modelling. The presence of the lipid pool leads to stress concentrations within the cap. The thickness of the fibrous cap also plays a role; thin caps have increased stress. This has led to the idea that vulnerable plaque (those with high risk of rupture) have high cap stress as a result of thin cap, whilst stable plaque (those with low risk of rupture) have low cap stress as a result of thick fibrous cap. Microcalcifications within the cap are also thought to play a role in that these act to locally increase the stress due to the differing gradients of stiffness between these microcalcifications and the surrounding fibrous tissue. Early attempts to quantify risk suggested that plaque with a cap thickness less than 65 μm were at risk of rupture (Loree et al. 1992), and that plaque with a peak wall stress greater than 300 kPa were at risk of rupture (Cheng et al. 1993).

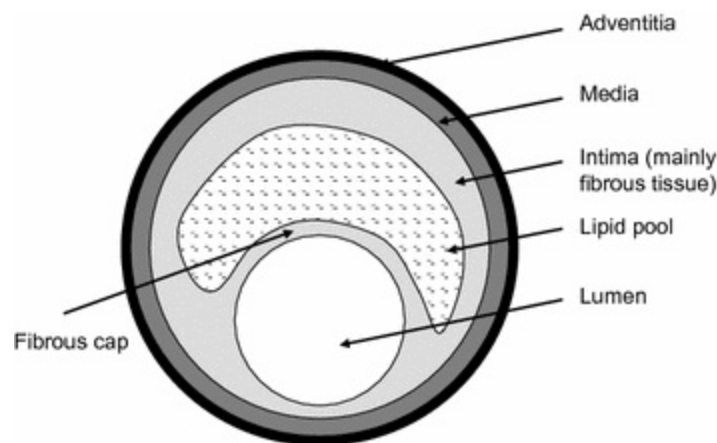


Fig. 15.9 Constituents of an atherosclerotic plaque from a mechanical perspective

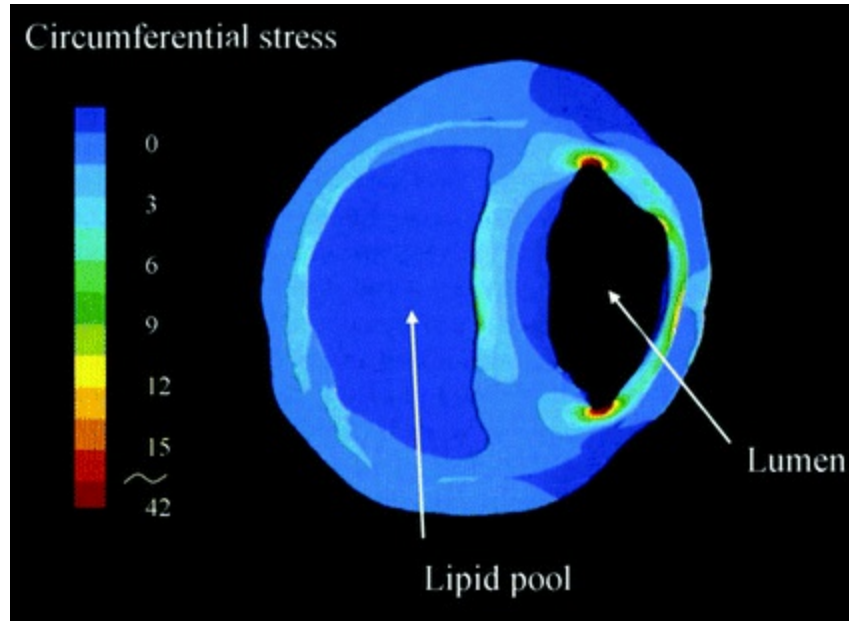


Fig. 15.10 Display of tissue stress (labelled circumferential stress) in a two-dimensional (2D) cross-section of a plaque. The 2D geometry was taken from microscopy of a section of an excised artery. Elastic moduli were taken from the literature and solid modelling used to estimate stress. Stress hot spots are shown at the shoulders of the fibrous cap. From Rohde L, Lee RT. Mechanical stress and strain and the vulnerable atherosclerotic plaque. In: Fuster V, editor. The vulnerable atherosclerotic plaque: understanding, identification and modification. New York: Futura Publishing Company, 1999: p. 305–316. © Futura Publishing Company. Reprinted with permission from John Wiley & Sons

The material properties of the individual components of the plaque are required for stress modelling. Table 15.1 shows a summary of indicative values for elastic modulus of plaques as a whole and of the individual components in order to show differences in stiffness of the different components. In practice there are a wide range of values in the literature associated with the variability of plaques, the measurement conditions, and whether a linear or nonlinear stress-strain model is used. The overall stiffness of a plaque will strongly depend on the relative size of the lipid pool. Stable plaque with small or no lipid pool will be stiffer than vulnerable plaque with large lipid pool. This goes some way to explaining the large variation in the overall stiffness of plaque in Table 15.1.

Table 15.1 Elastic moduli of atherosclerotic plaque and plaque components; value (range)

Component	Elastic modulus (kPa)	Reference
Whole plaque	530 (1–2300)	Cardoso et al. (2013)
Lipid	50 (1–202) ^a	Baldewsing et al. (2004)

Smooth muscle cells	1000 ^b	Baldewsing et al. (2004)
Collagen	1500 ^c	Baldewsing et al. (2004)

^aMean of 1, 0.5, 16.4 and 202 kPa, values taken from Cheng et al. (1993), Lee et al. (1996), Veress et al. (2000) and de Korte et al. (2000)

^bFrom Lee et al. (1996)

^cMean of 630 and 2310 kPa, from Mozersky et al. (1972) and Gow and Hadfield (1979)

The reader is referred to the article by Cardoso and Weinbaum (2014) for a review of plaque stress modelling, mechanical properties of plaque and components, and the thickness of the cap in relation to risk of rupture.

15.2.5 Stenosis Wall Dynamics

Atherosclerotic plaque is associated with local changes in the arterial stiffness. These cause alterations to the local motion of the arterial wall. Figure 15.11 shows the wall motion measured using ultrasound in a normal artery and in an artery with atherosclerotic plaque. The normal artery shows uniform displacement as a function of longitudinal position which is expected. The atherosclerotic plaque shows different parts of the wall moving in different directions at the same time. This causes a longitudinal strain which itself may be a potential source of rupture risk.

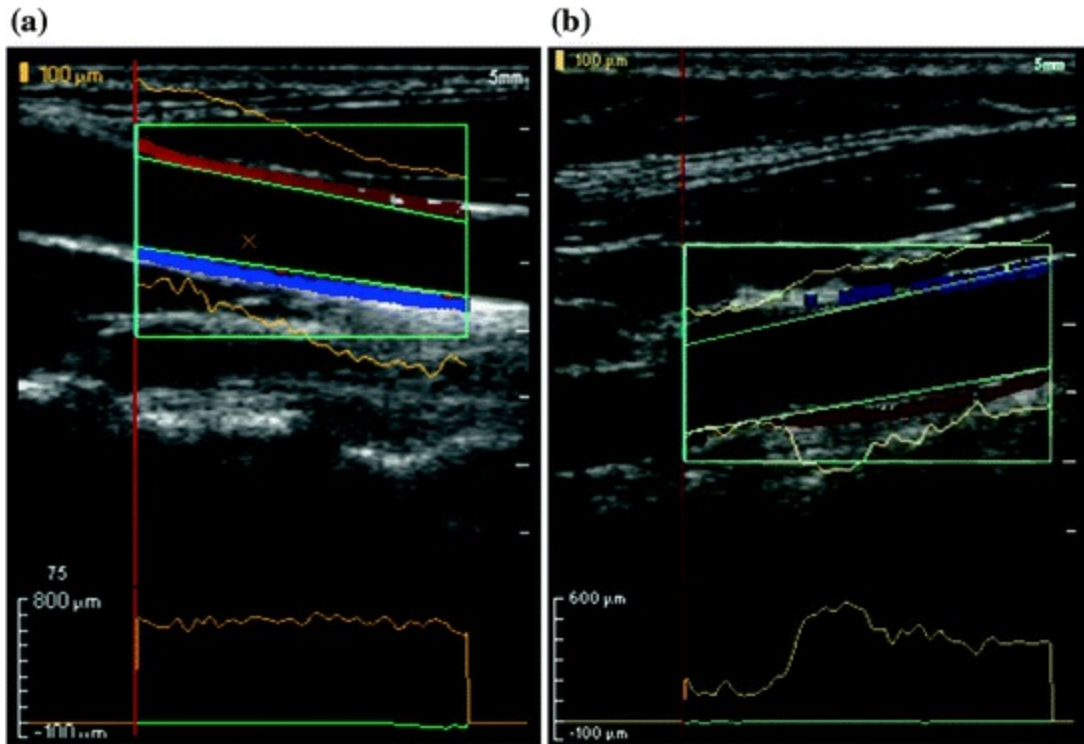


Fig. 15.11 Multi-line wall motion. Top: TDI images and instantaneous wall displacement (magnified). Bottom: maximum wall distension. **a** Healthy carotid showing no change in maximum distension with position along the vessel axis. **b** Stenosed artery showing restriction of movement within the region of the stenosis. From; Dineley JA. Doppler ultrasound measurement of arterial wall motion; Ph.D. thesis; Edinburgh: Edinburgh University Library; 2006; reprinted with permission from the author

15.3 Plaque Initiation, Growth and Rupture

This section describes the development of atherosclerosis from initiation through plaque growth and eventual rupture, concentrating on the role of forces.

15.3.1 Initiation of Atherosclerosis

In previous sections it has been noted that the arterial system detects wall shear stress and remodels in an attempt to maintain mean wall shear stress within a narrow bound. Wall shear stress plays a central role in the initiation of atherosclerosis. It was proposed that atherosclerosis is initiated at regions of low wall shear stress (Caro et al. 1971) and regions where the wall shear stress direction changes during the cardiac cycle (Ku et al. 1985). The oscillatory index (OSI) was formulated to capture the pattern of changing direction (He and Ku 1996). Common sites for the initiation of

atherosclerosis are on the inner curve of arteries and bifurcations (Figs. 15.12 and 15.13), which are associated with low wall shear stress.

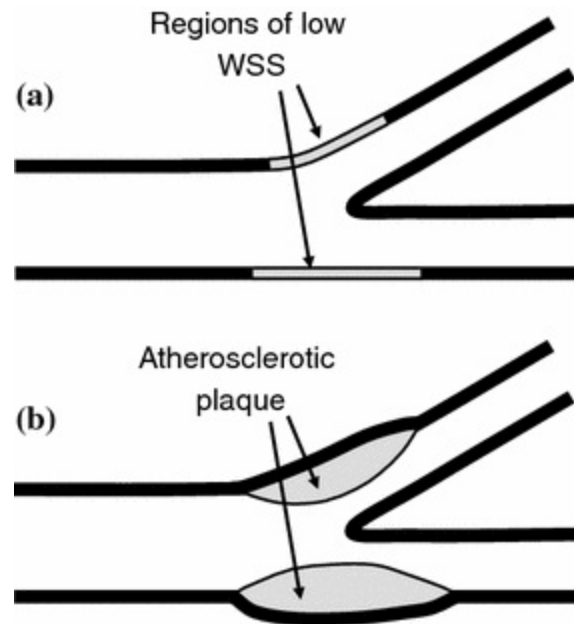


Fig. 15.12 Schematic of a bifurcation showing **a** low shear regions in the undiseased artery, **b** the development of atherosclerotic plaque several decades later

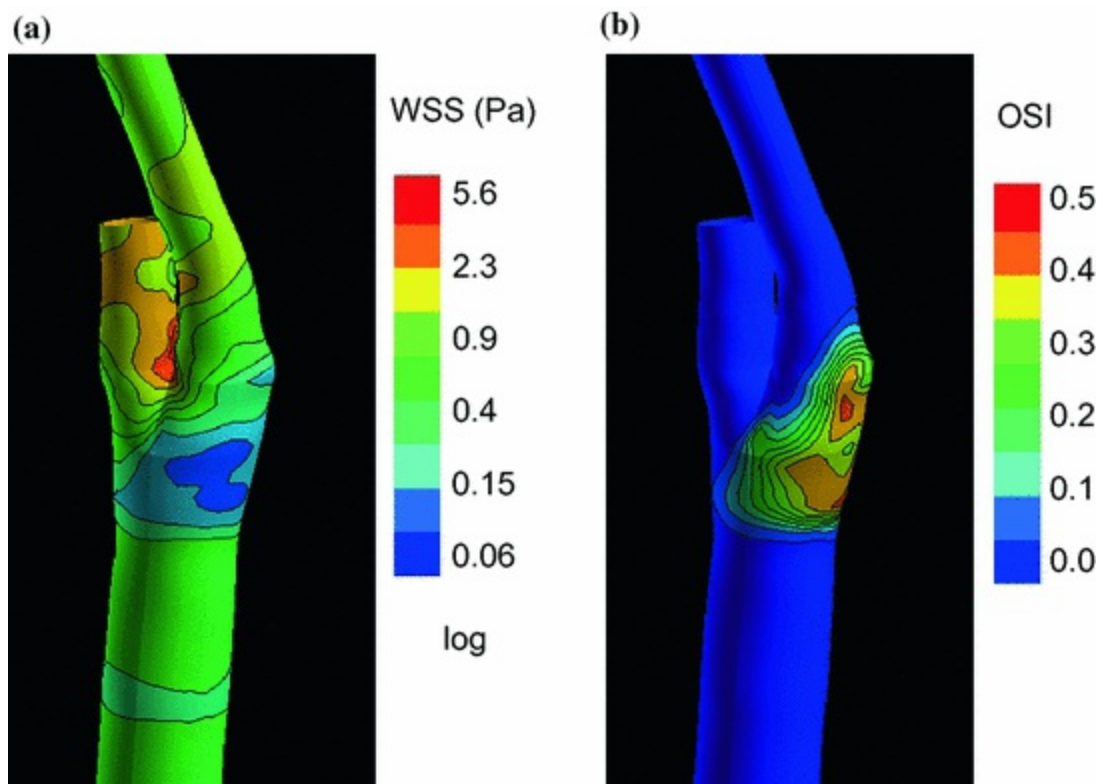


Fig. 15.13 Carotid bifurcation showing **a** mean wall shear stress, **b** oscillatory index. Images kindly provided by Prof. Yun Xu, Imperial College, London

The low WSS / high OSI model has underpinned this area for the last 30 years. A systematic review demonstrated that the actual evidence to support this hypothesis is not strong (Peiffer et al. 2013a) and they proposed that multidirectional wall shear stress is the important initiating feature (Mohamied et al. 2014). The Trans-WSS index was formulated to quantify multidirectional wall shear stress (Peiffer et al. 2013b). A summary of this area is provided by Mohamied et al. (2014).

15.3.2 Plaque Growth and Rupture

Plaque growth is initially associated with preservation of the lumen; that is the plaque grows outwards. This phenomenon was discovered by Glagov et al. (1987). He hypothesised that there is compensatory expansion of the vessel in order to maintain the lumen at a constant diameter. This compensatory expansion is almost certainly as a result of control of mean wall shear stress. In early growth the medial layer increases in size increasing the stiffness of the artery and reducing diameter. The overall flow remains constant but blood velocity and wall shear stress increase as a result of decrease in cross-sectional area. The endothelium, which in this stage of disease is still intact, detects the increase in wall shear stress. The endothelium initiates signalling events which result in increase in diameter to maintain wall shear stress constant. In practice there is a limit to this process. Outward remodelling continues till the relative plaque area reaches 40 % after which there is lumen reduction and formation of a stenosis. The reasons for this 40 % threshold are unclear (Slager et al. 2005a, b).

As the plaque continues to grow so the degree of stenosis continues to increase. The wall shear stress on the upstream (proximal) side of the plaque increases whilst the WSS on the downstream side of the plaque decreases (Figs. 15.5 and 15.14). These upstream and downstream regions have a different haemodynamic environment and biological behaviour. The following is based on hypotheses formulated by Slager et al. (2005a, b).

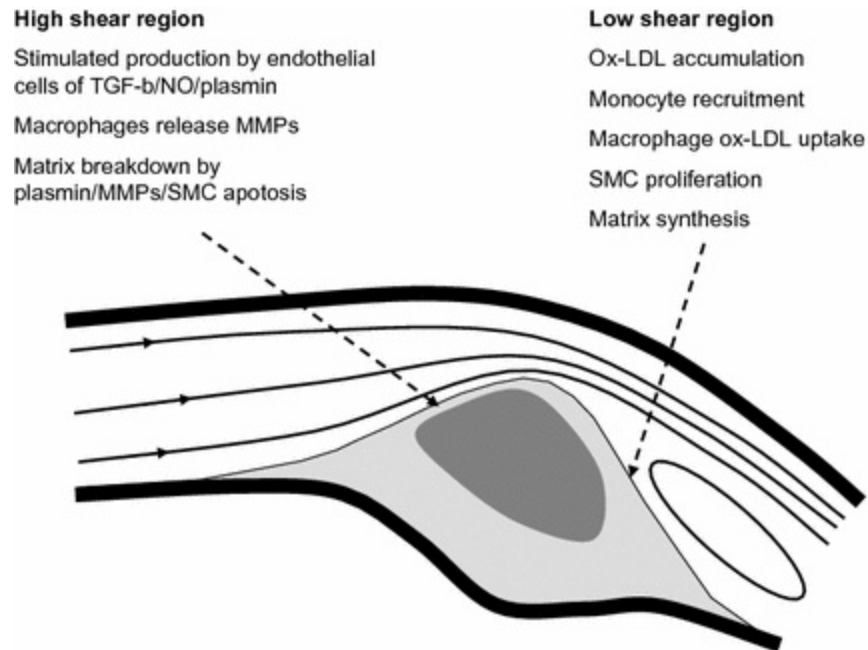


Fig. 15.14 Schematic of an atherosclerotic plaque showing high and low shear regions

In the upstream region of the plaque the high WSS stimulates the endothelium to induce thinning of the fibrous cap. A number of biological processes are triggered including stimulation of macrophages to release MMPs (matrix metalloproteinases) which degrade collagen leading to cap thinning. This is significant in that the cap is then at risk of rupture through high tissue stress. The WSS itself is a tiny force that could not cause cap rupture.

In the downstream region, there is reduced WSS and there may be flow recirculation. In this low shear region there is enhanced recruitment of monocytes (which pass into the wall converting to macrophages). There is also increased residence time of LDL cholesterol and consequently increased transport of LDL into the vessel wall where it is taken up by macrophages, contributing to growth of the plaque.

Overall the haemodynamic environments lead to plaque erosion on the upstream side and plaque growth on the downstream side. It has been observed that in practice plaques tend to grow in the downstream direction (Smedby 1997).

15.4 In Vivo Measurement

This section will provide details of measurement techniques related to arterial mechanics drawing on the principles described in previous sections.

15.4.1 Degree of Stenosis

The degree of stenosis may be estimated from measurements of lumen diameter made from a variety of medical imaging systems, including ultrasound, MRI, CT and X-ray angiography. In clinical practice the degree of stenosis may also be estimated from the maximum blood velocity within the stenosis measured using Doppler ultrasound. The reasons for this are partly historical; early ultrasound systems had insufficiently high image quality to allow visualisation of the lumen. With the improved image quality of modern ultrasound systems lumen may be measured direct in most cases, however estimation via blood velocity remains widely used.

The rationale for using blood velocity is illustrated in Fig. 15.7 where the velocity continuously increases as the degree of stenosis increases, reaching a peak at typically 85 % stenosis by diameter. Figure 15.15 shows a typical image in which maximum velocity is measured. This is then converted to a % stenosis using a standard table; Table 15.2 (e.g. Oates et al. 2009).

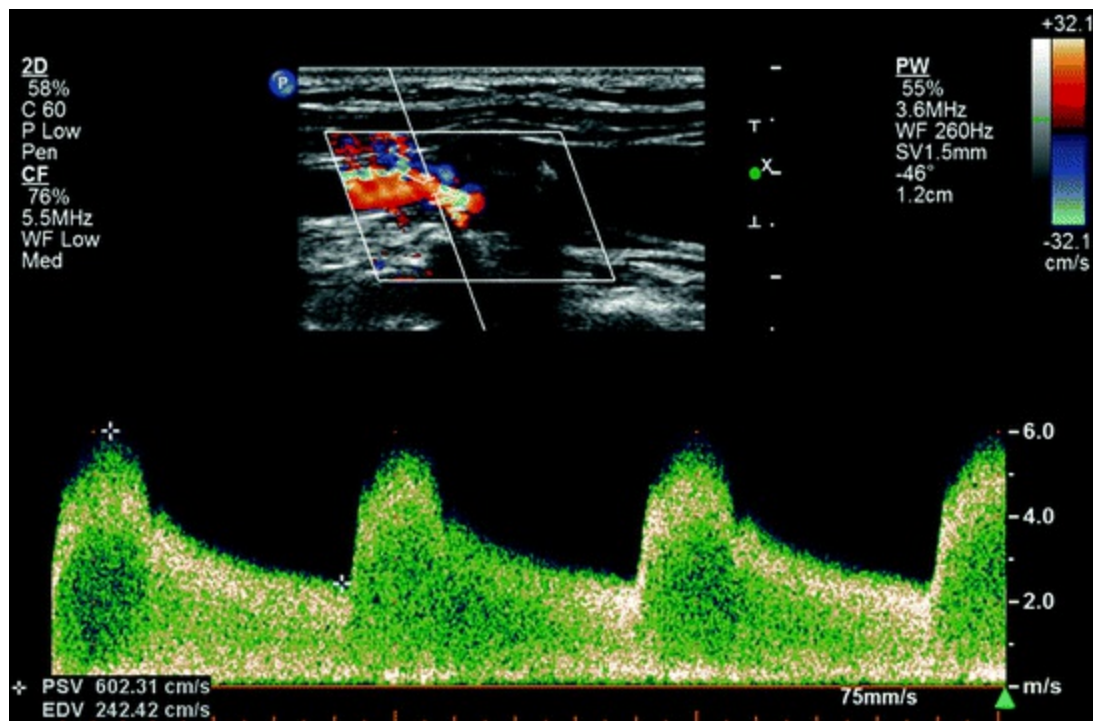


Fig. 15.15 Ultrasound image of a diseased carotid artery. The *upper* image is a composite B-mode image of tissue geometry and a colour image of blood velocity showing increased velocity in the

stenosis. The *lower* image show the time-velocity flow waveform. In the example shown the peak velocity is 602 cm.s^{-1}

Table 15.2 Criteria to convert velocity to % stenosis (from Oates et al. 2009)

Peak velocity (cm.s^{-1})	% stenosis (NASCET)
<125	<50
>125	50–69
>230	70–89
>400	>90
Near occlusion	High, low- string flow
No flow	Occlusion

15.4.2 Pressure Drop Across Stenoses

The Bernoulli equation for flow across a small orifice may be written

$$P_1 + \frac{\rho v_1^2}{2} = P_2 + \frac{\rho v_2^2}{2} \quad (15.4)$$

If the velocity v_1 within the orifice is much higher than the velocity v_2 then the v_2 term can be ignored, and the equation becomes

$$P_1 - P_2 = \frac{\rho v_1^2}{2} \quad (15.5)$$

This expression is mostly used to estimate pressure drop across stenosed cardiac valves. It has been used to estimate pressure drop in arterial stenoses but there is poor agreement with invasive measurements and it has been concluded that the simplified Bernoulli equation is not applicable in arteries (de Smet et al. 2000; Illig et al. 1996).

15.4.3 Stiffness

Circumferential stiffness E (Eq. 15.6) and pressure strain elastic modulus E_p (Eq. 15.7) may be estimated from the radial wall motion measured using ultrasound, pressure measured using an arm cuff, and (where possible) wall thickness measured using ultrasound; see Sect. 13.4.1.

$$E = \frac{d_d (P_s - P_d)}{2h(d_s - d_d)/d_d} \quad (15.6)$$

where h is wall thickness; P_s and P_d are the pressure, and d_s and d_d the

diameter, at systole and end-diastole. The elastic modulus is an example of material stiffness.

$$E_p = \frac{(P_s - P_d)}{(d_s - d_d)/d_d} \quad (15.7)$$

The underlying physical model used in Eqs. 15.6 and 15.7 is an isolated homogeneous ring of uniform stiffness and diameter. This method has been applied to estimate stiffness in patients with atherosclerosis. For example Claridge et al. (2009) identified patients with atherosclerotic plaque in one carotid artery and measured stiffness in the opposite (contralateral) carotid artery. They demonstrated an increase in stiffness in the patients with atherosclerosis compared with normal controls (Fig. 15.16). The assumptions used by the underlying physical model become invalid in advanced atherosclerotic plaque where assumptions of uniformity are untrue.

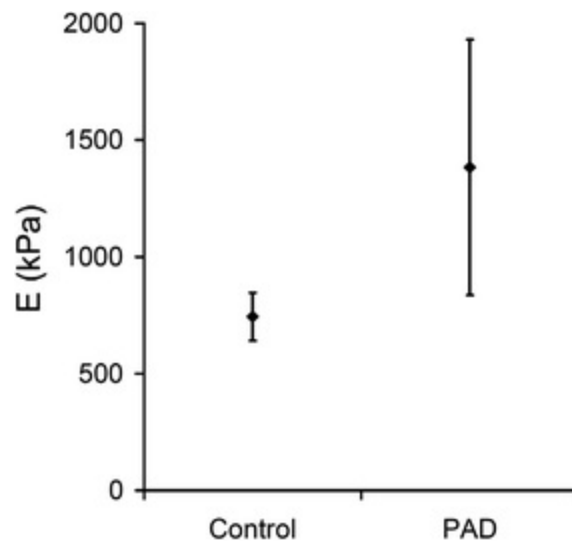


Fig. 15.16 Increase in Young's modulus in carotid arteries in patients with peripheral arterial disease (PAD) compared to controls. Data from Claridge et al. (2009)

Stiffness in tissues in vivo may be measured using elastography. This technique was described in Chaps. 9 and 13 where it was noted that the speed of propagation of the shear waves is related to the stiffness of the tissues. This technique has been applied in arteries where images of atherosclerotic plaque show regional changes which are thought to be due to features such as lipid pools.

15.4.4 Stress

The use of patient specific modelling to estimate stress in vivo in carotid plaque was described in Chap. 11; Fig. 11.13, from Gao et al. (2011). The critical cap thickness below which rupture is thought to be likely is 65 μm (see Sect. 15.2.4). This is well below the spatial resolution of an MRI system which is around 250–500 μm . In fact no noninvasive medical imaging system has sufficiently good spatial resolution to adequately resolve the fibrous cap which leads to underestimation of the peak wall stress. Invasive imaging techniques such as intravascular ultrasound and optical coherence tomography have improved spatial resolutions of 50 and 10–15 μm , respectively, and are used in research studies in plaque visualisation.

15.5 Treatment

The effects of plaque rupture were described in Sect. 15.1. If there is sufficient reduction in blood supply to downstream tissues there will be tissue death (called an ‘infarction’), such as occurs in a heart attack or stroke. These events require immediate treatment in order to restore blood flow and prevent tissue damage.

If disease is identified sufficiently early then treatment may be offered before rupture occurs. Patients who have not yet had a major clinical event can be identified by several ways. First they may present to their doctor with more minor symptoms, associated with plaque rupture but which do not lead to infarction. A ‘transient ischaemic attack’ (TIA) or mini-stroke is a brief episode (<24 h) of neurological dysfunction. This includes loss of sight in one or both eyes; lack of coordination; slurring of speech; weakness, numbness or paralysis of one side of the face, arm or leg. A TIA is a warning sign of a possible future stroke. A mini-heart attack is associated with symptoms including difficulty in breathing, chest pains, fainting and vomiting. The second method whereby at-risk patients are identified is through a screening programme if this exists (there are none in the UK for atherosclerosis). The third method is as chance findings whilst the patient is being investigated for other symptoms. In all cases the patient is referred for a series of tests to identify the location and severity of disease and to help decide on the treatment options.

15.5.1 Carotid Disease

Treatment of carotid atherosclerosis is by surgical removal of the plaque; the operation is called 'carotid endarterectomy'. The operation itself carries a risk of stroke so the operation is only offered when the benefit outweighs the risk. Clinical trials were undertaken in the 1990s to establish criteria for selection of patients based on risk. The European Carotid Surgery Trial (ECST collaborators 1998) and the North American Symptomatic Carotid Endarterectomy Trial (NASCET collaborators 1991) both used the degree of stenosis as their diagnostic measure of risk. The measurement methods were slightly different so that current clinical practice (NICE68 2008) is based on surgery if the degree of stenosis is 50–99 % according to NASCET criteria or 70–99 % using ECST criteria. The use of stenting as an alternative to carotid surgery is also undertaken in some patients.

If the degree of stenosis is nonsignificant (<50 % NASCET or <70 % ECST) the patient is offered a combination of medication and advice on changes to lifestyle aimed at reducing the risk of plaque rupture. Medication includes antiplatelet agents and cholesterol reducing medication (statins). Lifestyle advice includes quitting smoking, changes in diet to reduce cholesterol and increase in exercise.

15.5.2 Coronary Disease

The terms 'coronary artery disease' and 'ischaemic heart disease' describe a single pathology. Ischaemic heart disease is the consequence of a restriction in the flow of blood to the myocardium due to the presence of coronary artery plaque and occurs when the oxygen demands of the heart muscle outstrips the supply. Where ischaemic heart disease is suspected, coronary anatomy is assessed using invasive angiography. Patients with coronary artery disease frequently (but not always) complain of chest pain (angina) and management aims to both to reduce symptoms and to improve outcomes. A first line treatment approach is pharmacological reduction of cardiac parameters such as the preload and afterload. These in turn reduce the workload for the heart and hence myocardial oxygen demand. Vasodilators, betablockers, aspirin and statins can also be used to maximise coronary dilatation, reduce myocardial work, reduce the progression of plaque and to stabilise existing plaque, respectively. When this approach fails, patients with uncontrolled angina are offered angioplasty. This technique involves widening of the narrowed artery using a balloon, and often includes the introduction of a metal frame (stent) to support the vessel wall over the longer term. This technique is discussed in

more detail in Chap. 17. Patients with severe disease at many different sites within the arteries may be offered surgery (coronary bypass grafting).

A subgroup of patients with ischaemic heart disease will have acute coronary syndrome. These are patients who have already had a myocardial infarction (MI), i.e. an occlusion, and have a high risk of further plaque rupture and associated MI.

The best management strategies for these different subgroups of patients with cardiac ischaemia, taking account of available evidence, risks and benefits, are incorporated into Guidelines offered by expert groups. An example of these is the widely used European Guidelines (Windecker et al. 2014).

Whilst coronary angiography has become established as the gold standard investigative technique for the diagnosis of coronary artery disease, the decision to treat or not treat individual lesions is often based on the clinician's visual appraisal of angiographic images. Measurement of the fractional flow reserve (FFR) provides a more objective measure of lesion severity (Pijls et al. 1996). The FFR is defined as the ratio of the pressure downstream of the stenosis to the pressure immediately upstream. Pressures can be measured invasively by introducing a catheter with a pressure-sensitive wire into the coronary artery under investigation via the femoral or radial arteries. Recordings are made during maximal flow (hyperaemia). This is achieved by administering a vasoactive drug to dilate the arteries.

$$\text{FFR} = P_d/P_a \quad (15.8)$$

where P_d is the distal (downstream) pressure and P_a is the proximal (upstream) pressure.

As a general rule an FFR of 0.8 or less is taken as an indication that the stenosis requires treatment.

References

Baldewising RA, de Korte CL, Schaar JA, Mastik F, van der Steen AFW. A finite element model for performing intravascular ultrasound elastography of human atherosclerotic coronary arteries. *Ultrasound Med Biol.* 2004;30:803–13.

[CrossRef][PubMed]

Berguer R, Hwang NHC. Critical arterial stenosis: a theoretical and experimental solution. *Ann Surg.* 1974;180:39–50.

[CrossRef][PubMed][PubMedCentral]

Cardoso L, Weinbaum S. Changing views of the biomechanics of vulnerable plaque rupture: a review. *Ann Biomed Eng.* 2014;42:415–31.

[\[CrossRef\]](#)[\[PubMed\]](#)

Caro CG, Fitz-Gerald JM, Schroter RC. Atheroma and arterial wall shear; observation, correlation and proposal of a shear dependent mass transfer mechanism for atherogenesis. *Proc Royal Soc Lond B Biol Sci.* 1971;177:109–59.

Cheng GC, Loree HM, Kamm RD, Fishbein MC, Lee RT. Distribution of circumferential stress in ruptured and stable atherosclerotic lesions—a structural-analysis with histopathological correlation. *Circulation.* 1993;87:1179–87.

[\[CrossRef\]](#)[\[PubMed\]](#)

Claridge MW, Bate GR, Hoskins PR, Adam DJ, Bradbury AW, Wilmink AB. Measurement of arterial stiffness in patients with peripheral arterial disease: are changes in vessel wall more sensitive than intima-media thickness? *Atherosclerosis.* 2009;205:477–80.

[\[CrossRef\]](#)[\[PubMed\]](#)

de Korte CL, Pasterkamp G, van der Steen AFW, Woutman HA, Bom N. Characterization of plaque components with intravascular ultrasound elastography in human femoral and coronary arteries in vitro. *Circulation.* 2000;102:617–23.

[\[CrossRef\]](#)[\[PubMed\]](#)

de Smet AA, Tetteroo E, Moll FL. Noninvasive evaluation before and after percutaneous therapy of iliac artery stenoses: the value of the Bernoulli-predicted pressure gradient. *J Vasc Surg.* 2000;32:153–9.

[\[CrossRef\]](#)[\[PubMed\]](#)

Dineley JA. Doppler ultrasound measurement of arterial wall motion; Ph.D. thesis; Edinburgh: Edinburgh University Library; 2006.

ECST (European Carotid Surgery Trial) collaborators. Randomised trial of endarterectomy for recently symptomatic carotid stenosis: final results of the MRC European Carotid Surgery Trial (ECST). *Lancet.* 1998;351:1379–87.

Gao H, Long Q, Kumar Das S, Halls J, Graves M, Gillard JH, Li ZY. Study of carotid arterial plaque stress for symptomatic and asymptomatic patients. *J Biomech.* 2011;44:2551–7.

[\[CrossRef\]](#)[\[PubMed\]](#)

Glagov S, Weisenberg E, Zarins CK, Stankunavicius R, Kolettis GJ. Compensatory enlargement of human atherosclerotic coronary arteries. *New Eng J Med.* 1987;316:1371–5.

[\[CrossRef\]](#)[\[PubMed\]](#)

Gow BS, Hadfield CD. Elasticity of canine and human coronary arteries with reference to postmortem changes. *Circ Res.* 1979;45:588–94.

[\[CrossRef\]](#)[\[PubMed\]](#)

He X, Ku DN. Pulsatile flow in the human left coronary artery bifurcation: average conditions. *J Biomech Eng.* 1996;118:74–82.

[\[CrossRef\]](#)[\[PubMed\]](#)

Illig KA, Ouriel K, DeWeese JA, Holen J, Green RM. Measurement of carotid bifurcation pressure gradients using the Bernoulli principle. *Cardiovasc Surg.* 1996;4:130–4.

[CrossRef][PubMed]

Ku DN, Giddens DP, Zarins CK, Glagov S. Pulsatile flow and atherosclerosis in the human carotid bifurcation. Positive correlation between plaque location and low oscillating shear stress. *Arteriosclerosis.* 1985;5:293–302.

[CrossRef][PubMed]

Lee RT, Schoen FJ, Loree HM, Lark MW, Libby P. Circumferential stress and matrix metalloproteinase 1 in human coronary atherosclerosis—implications for plaque rupture. *Arterioscler Thromb Vasc Biol.* 1996;16:1070–3.

[CrossRef][PubMed]

Li M. Numerical simulation of blood flow and wall stresses in stenosed arteries; Ph.D. thesis; Edinburgh: Edinburgh University Library; 2007.

Loree HM, Kamm RD, Stringfellow RG, Lee RT. Effects of fibrous cap thickness on peak circumferential stress in model atherosclerotic vessels. *Circ Res.* 1992;71:850–8.

[CrossRef][PubMed]

Lusis AJ. Atherosclerosis. *Nature.* 2000;407:233–41.

[CrossRef][PubMed][PubMedCentral]

Mohamied Y, Rowland EM, Bailey EL, Sherwin SJ, Schwartz MA, Weinberg PD. Change of direction in the biomechanics of atherosclerosis. *Ann Biomed Eng.* 2014;43:16–25.

[CrossRef][PubMed][PubMedCentral]

Mozersky DJ, Strandness DE, Sumner DS, Hokanson DE. Transcutaneous measurement of elastic properties of human femoral artery. *Circulation.* 1972;46:948–55.

[CrossRef][PubMed]

NASCET (North American Symptomatic Carotid Endarterectomy Trial) Collaborators. Beneficial effect of carotid endarterectomy in symptomatic patients with high-grade carotid stenosis. North American Symptomatic Carotid Endarterectomy Trial Collaborators. *N Engl J Med.* 1991;325:445–53.

NICE68. Clinical guideline 68. Stroke: Diagnosis and initial management of acute stroke and transient ischaemic attack (TIA). July 2008; available from: www.nice.org.uk/guidance/CG68.

Oates CP, Naylor AR, Hartshorne T, Charles SM, Fail T, Humphries K, Aslam M, Khodabakhsh P. Joint recommendations for reporting carotid ultrasound investigations in the United Kingdom. *Eur J Vasc Endovasc Surg.* 2009;37:251–61.

[CrossRef][PubMed]

Peiffer V, Sherwin SJ, Weinberg PD. Does low and oscillatory wall shear stress correlate spatially with early atherosclerosis? A systematic review. *Cardiovasc Res.* 2013a;99:242–50.

[PubMed][PubMedCentral]

Peiffer V, Sherwin SJ, Weinberg PD. Computation in the rabbit aorta of a new metric—the transverse wall shear stress—to quantify the multidirectional character of disturbed blood flow. *J Biomech.* 2013b;46:2651–8.

[CrossRef][PubMed][PubMedCentral]

Pijls NH, De Bruyne B, Peels K, et al. Measurement of fractional flow reserve to assess the functional severity of coronary artery stenoses. *N Engl J Med*. 1996;334:1703–8.

[\[CrossRef\]](#)[\[PubMed\]](#)

Richardson PD, Davies MJ, Born GVR. Influence of plaque configuration and stress-distribution on fissuring of coronary atherosclerotic plaques. *Lancet*. 1989;2:941–4.

[\[CrossRef\]](#)[\[PubMed\]](#)

Rohde L, Lee RT. Mechanical stress and strain and the vulnerable atherosclerotic plaque. In: Fuster V, editor. *The vulnerable atherosclerotic plaque: understanding. Identification and modification*. New York: Futura Publishing Company; 1999. pp. 305–16.

Slager CJ, Wentzel JK, Gijssen FJH, Schuurbiers JCH, van der Wal AC, van der Steen AFW, Serruys PW. The role of shear stress in the generation of rupture-prone vulnerable plaques. *Nat Clin Pract Cardiovasc Med*. 2005a;2:401–7.

[\[CrossRef\]](#)[\[PubMed\]](#)

Slager CJ, Wentzel JJ, Gijssen FJH, Thury A, van der Wal AC, Schaar JA, Serruys PW. The role of shear stress in the destabilization of vulnerable plaques and related therapeutic implications. *Nat Clin Pract Cardiovasc Med*. 2005b;2:456–64.

[\[CrossRef\]](#)[\[PubMed\]](#)

Smedby O. Do plaques grow upstream or downstream? An angiographic study in the femoral artery. *Arterioscler Thromb Vasc Biol*. 1997;17:912–8.

[\[CrossRef\]](#)[\[PubMed\]](#)

Spencer MP, Reid JM. Quantitation of carotid stenosis with continuous wave (CW) Doppler ultrasound. *Stroke*. 1979;10:326–330

Veress AI, Vince DG, Anderson PM, Cornhill JF, Herderick EE, Kuban BD, Greenberg NL, Thomas JD. Vascular mechanics of the coronary artery. *Z Kardiol*. 2000;89(Suppl 2):92–100.

[\[CrossRef\]](#)[\[PubMed\]](#)

Windecker S, Kolh P, Alfonso F, Collet J-P, Cremer J, Falk V, Filippatos G, Hamm C, Head SJ, et al. 2014 ESC/EACTS Guidelines on myocardial revascularisation. *Euro Heart J*. 2014;35:2541–619.

[\[CrossRef\]](#)

16. Aneurysms

Barry J. Doyle¹✉ and Peter R. Hoskins²✉

- (1) University of Western Australia, Perth, WA, Australia
- (2) Edinburgh University, Edinburgh, UK

✉ **Barry J. Doyle (Corresponding author)**
Email: barry.doyle@uwa.edu.au

✉ **Peter R. Hoskins**
Email: P.Hoskins@ed.ac.uk

16.1 Aneurysms

16.1.1 Introduction to Aneurysms

An aneurysm is a localised increase in the diameter of an artery; an outpouching of the wall. In an aneurysm there is increase in both inner and outer wall diameter, as opposed to atherosclerotic plaque where the outer wall diameter increases due to outward remodelling but the inner wall diameter (at least initially) remains unchanged.

There are 2 main types of aneurysm; the fusiform aneurysm and the saccular aneurysm (Fig. 16.1). The saccular aneurysm is often referred to as a berry aneurysm. Fusiform aneurysms most commonly occur in the abdominal aorta and to a lesser extent in popliteal arteries and in cerebral arteries. Saccular aneurysms most commonly occur in cerebral arteries, where they represent 80–90 % of all cerebral aneurysms (CAs).

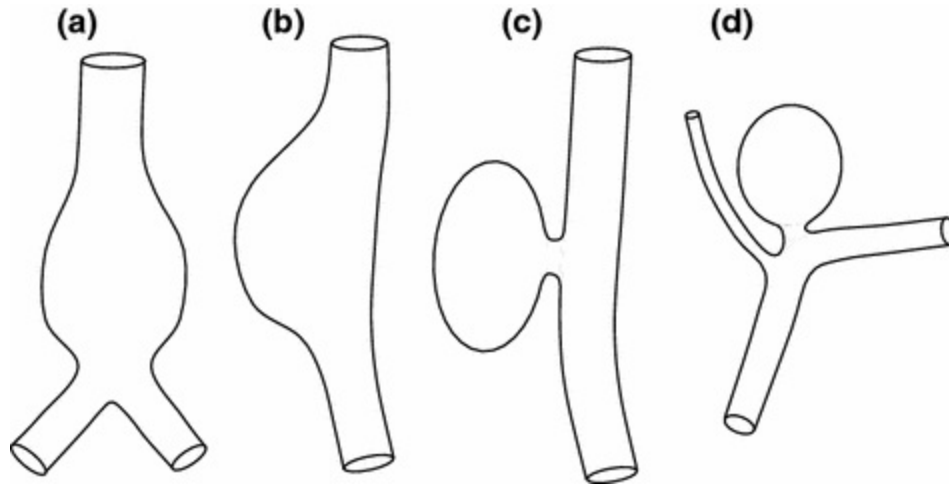


Fig. 16.1 Types of aneurysm; **a** and **b** fusiform aneurysms; **c** and **d** saccular or berry aneurysms

Factors leading to susceptibility for aneurysm formation include both genetic and environmental factors. Hereditary conditions such as Marfan's and Ehlers-Danlos syndromes are associated with collagen disorders leading to arterial wall weakening and both these syndromes have a predisposition to aneurysms. Environmental risk factors include hypertension, cigarette smoking, family history of aneurysmal disease and oestrogen deficiency in the postmenopausal female (Mehra et al. 2011, Lasheras 2007). These risk factors translate into biological processes in the arterial wall. Development and growth of an aneurysm is an interplay between these biological processes and the mechanical environment.

Development and growth of aneurysms is associated with weakening of the wall through loss of elastin with subsequent remodelling of the wall in an attempt to renormalise forces on and within the wall. The interplay between the local mechanical environment and the local biology is thought to be paramount in the initiation and growth of aneurysms, but the exact details of this relationship remain the subject of research. Once established, the aneurysm continues to grow and for some aneurysms there comes a point when the stress within the wall exceeds the wall strength and the aneurysm will rupture. Most aneurysms give no symptoms prior to rupture. The subsequent bleeding into the surrounding tissues is associated with a high mortality rate; 90 % for abdominal aortic aneurysm (AAA) rupture and 45 % for cerebral aneurysm rupture.

This chapter will concentrate on the 2 most common types of aneurysm; the abdominal aortic aneurysm and the saccular cerebral aneurysm. Further

reading is provided by Lasheras (2007), Sforza et al. (2009), Humphrey and Taylor (2008), Humphrey and Holzapfel (2012), Vorp (2007), McGloughlin and Doyle (2010), Penn et al. (2011), Wong and Poon (2011) and Meng et al. (2014).

16.1.2 Aneurysms and the Law of Laplace

A simple understanding of aneurysm mechanics involves the Law of Laplace which was introduced in Chap. 5. Equations 16.1 and 16.2 describe the tension in the wall of a thin-walled cylinder and a thin-walled sphere respectively. In each case the tension T increases with diameter d .

$$T = \frac{Pd}{2} \quad (16.1)$$

$$T = \frac{Pd}{4} \quad (16.2)$$

In biomechanics it is more common to use circumferential stress H rather than tension. Equations 16.3 and 16.4 are for a thin-walled cylinder and a thin-walled sphere respectively, where w is wall thickness.

$$H = \frac{Pd}{2w} \quad (16.3)$$

$$H = \frac{Pd}{4w} \quad (16.4)$$

An artery may be considered as a thin-walled cylinder, a saccular aneurysm resembles a sphere and a fusiform aneurysm has a shape between a cylinder and a sphere. These equations suggest that the circumferential stress, and hence the risk of rupture, increases with diameter. This helps understand why diameter is the current clinical method for evaluating risk of rupture in both abdominal aortic aneurysm and in saccular CAs.

In practice there are limitations to this simple model. Arteries are not just pipes and will remodel in an attempt to normalise stresses. In practice this means that there will be changes in wall thickness as the aneurysm grows. Rupture represents mechanical failure of the tissues where circumferential stress exceeds tissue strength. The tissue strength will depend on the local tissue composition which will vary from point to point around the wall. Aneurysms have a complex geometry which does not correspond to either a cylinder or a sphere. In evaluation of rupture risk all these factors need to be

accounted for, which is the aim of patient specific modelling as described in Chap. 14.

16.2 Cerebral Aneurysms

16.2.1 Cerebral Aneurysm Disease

Cerebral aneurysms are localised increases in diameter of arteries supplying the brain. These are also referred to as intracranial aneurysms. Some 4–6 % of the population aged greater than 30 years have a CA (Wardlaw and White 2000). The main clinical complication is rupture leading to bleeding. The blood accumulates beneath the arachnoid membrane which surrounds the brain, producing a subarachnoid haemorrhage. The risk of rupture of a CA is low at 0.1–1 % per year (Juvela 2004). However the consequences of rupture are severe for the patient. Mortality following aneurysm rupture is 45 %, 30 % of survivors demonstrate moderate to severe disability, and the remainder have increased risk of re-bleeds and stroke (Brisman et al. 2006). Most CAs are asymptomatic so that the first knowledge of the presence of a CA is the symptoms associated with subarachnoid haemorrhage ('thunderclap headache', nausea, vomiting, altered consciousness of varying degree from drowsiness to complete loss of consciousness, and disturbance of vision). In some cases larger CAs may themselves produce similar symptoms immediately prior to rupture. Treatment of CAs involves a variety of procedures concerned with sealing off the aneurysm and these are considered further in Sect. 16.5.

CAs are of 2 main types, saccular and fusiform. Saccular aneurysms are round in shape and also referred to as 'berry aneurysms'; these usually occur at the branching point of arteries of the Circle of Willis and are the most common type of CA (80–90 %). Fusiform aneurysms involve an overall widening of the artery and usually do not rupture. Saccular aneurysms are also classified by size; small (<15 mm diameter), large (15–25 mm), giant (25–50 mm) and super-giant (>50 mm). The remainder of Sect. 16.2 will be concerned with saccular CAs.

16.2.2 Haemodynamics

Saccular CAs are not conduit vessels; blood flow enters and exits the aneurysm via the neck. The flow pattern within the aneurysm depends on its

orientation with respect to the parent artery (Moftakher et al. 2007) (Fig. 16.2). Figure 16.2a shows a sidewall aneurysm. Flow in the aneurysm recirculates, often through the entire cardiac cycle. Blood velocity is very low, wall shear stress is very low and there is low pressure on the dome (far wall) of the aneurysm. In the case of a bifurcation aneurysm 2 flow patterns are seen. The most common is illustrated in Fig. 16.2b. Here flow enters the aneurysm from the parent artery through a channel within the aneurysm neck, circulates around the aneurysm, and exits through a separate channel in the neck. Velocities, wall shear and pressure at the dome are low. The second flow pattern seen in bifurcation aneurysms is illustrated in Fig. 16.2c. Here flow from the parent artery enters the aneurysm as a jet which impacts on the dome, flow then exits in a random manner through the neck. The impact of the jet causes local high wall shear and pressure on the dome. Because of the persistent flow through the cardiac cycle most CAs have no thrombus, as opposed to AAAs where thrombus is common.

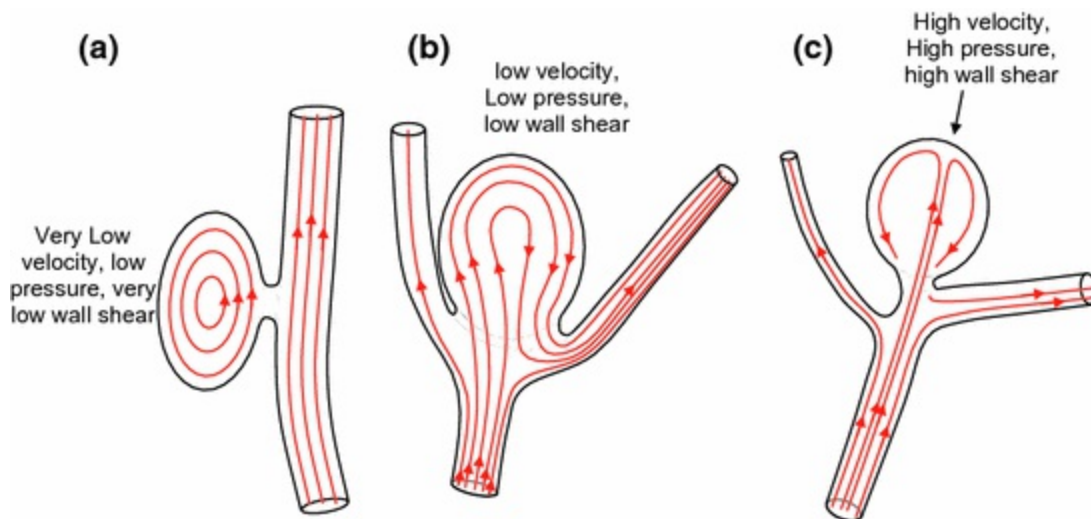


Fig. 16.2 Schematic of flow within saccular cerebral aneurysms, with indications of blood velocity, dome pressure gradient (with respect to the neck) and wall shear stress. **a** *Recirculation* recirculating flow in a side-aneurysm. **b** *Jet impact* flow from the parent artery forms a jet which impacts on the aneurysm wall. **c** *Circulating flow* flow from the parent artery enters the aneurysm through a channel in the neck, circulates as a result of the geometry of the aneurysm, and exits through a separate channel in the neck

16.2.3 Initiation, Growth and Rupture

The composition of cerebral arteries is different to that of systemic arteries. Cerebral arteries possess much less elastin in the medial layer, the external

elastic lamina is absent, and there are structural abnormalities at the apex of bifurcations, all of which are thought to make cerebral arteries prone to saccular aneurysms. Cerebral aneurysms are characterised by loss of elastin and smooth muscle cells with consequent thinning of the medial layer (Frösen et al. 2012). Collagen fibres remodel, probably in an attempt to mechanically stabilise the aneurysm. The result is an increase in wall stiffness, with the main load-bearing performed by the adventitia rather than the media.

Initiation, growth and rupture of the CA are governed by an interplay between the mechanical environment and the local biology. The exact details of this remain the subject of research for CAs, though central to this will be presence of an intact endothelial layer. Unruptured aneurysms lack an endothelial layer (Frösen et al. 2004), and prior to this there is endothelial dysfunction. An intact endothelial layer is essential for an artery to adapt to its mechanical environment. This suggests that as the CA evolves, initially the endothelial layer is intact and the aneurysm will remodel in an attempt to normalise its mechanical environment. Later there is endothelial dysfunction with impairment in the aneurysms ability to maintain the mechanical environment. Finally there is loss of the endothelial layer and the aneurysm's ability to remodel is largely absent. Reviews of this area are provided by Sforza et al. (2009), Meng et al. (2014), Penn et al. (2011) and Selimovic et al. (2013) from which the analysis below is derived. The latter paper (Selimovic) describes computational models of aneurysm growth.

16.2.3.1 Initiation of Saccular CAs

- High wall shear stress hypothesis. Meng et al. (2014) proposed a high WSS hypothesis discussed here. At a bifurcation, flow from the parent artery impacts on the bifurcation apex producing high WSS and also a positive WSS gradient along the flow. The endothelium detects these WSS abnormalities, and a series of biological events occurs resulting in degradation of elastin, medial thinning and formation of a bulge, which constitutes the early aneurysm.
- Low wall shear stress hypothesis. Meng et al. (2014) also proposed a low WSS hypothesis discussed in this section. In the paper on computational modelling of aneurysm growth, Selimovic et al. (2013) report that when elastin degradation was associated with high WSS this

led to aneurysm formation, but of the fusiform type rather than the saccular type. Linking low WSS to elastin degradation resulted in formation of a saccular aneurysm. Selimovic et al. note that a possible mechanism for low-WSS initiation is the release of matrix-metalloproteinases (MMPs) by inflammatory cells, which degrade elastin.

- Flow instability hypothesis. In their study on computational modelling of aneurysms Selimovic et al. note that it may actually not be the magnitude of the WSS which is important, but the nature of the flow including flow oscillation and instability.

16.2.3.2 Growth of Saccular CAs

- High wall shear stress hypothesis. In an established aneurysm with impact of a jet on the dome (Fig. 16.2c), there will be a region of high WSS. This high WSS is detected by the endothelium, which in the early stages of aneurysm development is still intact, leading to release of MMPs and matrix degradation. There may be a local bleb formed at the region of impact. Remodelling of collagen stabilises the aneurysm.
- Low wall shear stress hypothesis. In an established aneurysm where there is recirculating flow (Fig. 16.2b) the wall shear stress will be low. This low WSS is sensed by the endothelium, which in the early stages of aneurysm development, is still intact. This also leads to release of MMPs, but by an inflammatory route, which also leads to matrix degradation.

16.2.3.3 Rupture of Saccular CAs

A possible sequence of events concerning rupture is described here. Rupture occurs when the circumferential stress exceeds the local wall strength. Wall shear stress itself is too small a force to cause rupture. However the growth of the aneurysm is effected by WSS, causing changes to the wall which leave the aneurysm vulnerable to rupture. Following on from the above subsection, where there is loss of matrix material, the aneurysm remodels in an attempt to achieve mechanical stability. This process must rely on an intact endothelium in order to drive remodelling. It is however noted above that aneurysms are commonly associated with loss of endothelium which must

mean that at some point the remodelling apparatus is also lost. With loss of endothelium driven remodelling the aneurysm is unable to mechanically stabilise itself and after this point the aneurysm is at risk of rupture.

16.2.4 In Vivo Imaging and Patient Specific Modelling

Traditional visualisation of CAs was undertaken using angiography which involved an arterial puncture. A number of non-invasive techniques have been used to diagnose the presence of CAs including CT angiography (CTA), rotational angiography (RA) and magnetic resonance angiography (MRA). All these techniques provide 3D data from which measurements may be made of aneurysm dimensions. In addition the 3D geometries may be used to derive indices describing shape and as the input to patient specific modelling. Ultrasound systems may also be used for visualisation of CAs. Further reading on the imaging of cerebral aneurysm is provided in Hoskins et al. (2011).

16.2.4.1 Measurements of Size

The measurements commonly made on a saccular aneurysm are illustrated in Fig. 16.3. The diameter of a saccular aneurysm is measured as the largest of the height (H), and the 2 orthogonal widths. As noted above the aneurysm is classified according to diameter (small <15 mm diameter, large 15–25 mm, giant 25–50 mm, super-giant >50 mm); and risk of rupture increase with diameter (Wermer et al. 2007).

H – aneurysm height

W – aneurysm width

N – neck width

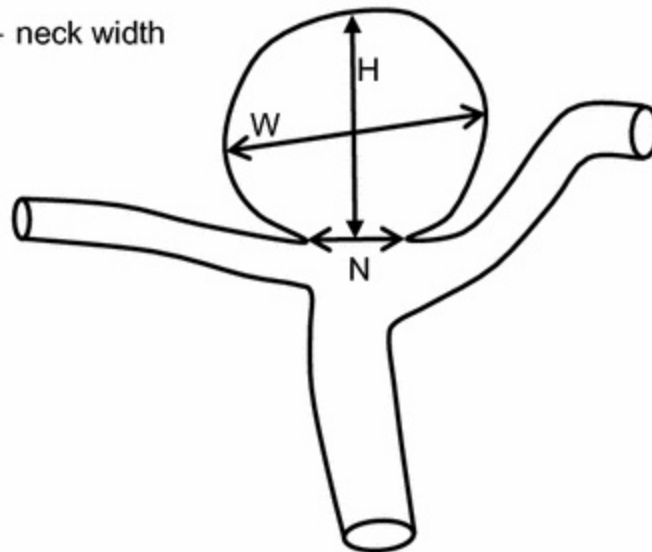


Fig. 16.3 Definition of dimensions of a saccular aneurysm measured from medical imaging data

The aspect ratio is the ratio of aneurysm height to neck width (Eq. 16.5).

$$\text{Aspect ratio} = \frac{\text{aneurysm height}}{\text{neck width}} \quad (16.5)$$

Aneurysms with a higher aspect ratio are at greater risk of rupture (Dhar et al. 2008; Ujiie et al. Ujiie et al. 1999; Weir et al. 2003; Nader-Sepahi et al. 2004), so this measurement may be used for clinical evaluation. The aspect ratio may also be used to help plan therapy; a ratio of >2 is considered as favourable for coil occlusion (Meyers et al. 2009). Measurement of aneurysm volume helps define the size of coil or balloon needed in therapeutic treatment. More complex shape descriptors involving the whole 3D geometry have been developed in research studies, whose details are outside the scope of this book (Millán et al. 2007).

16.2.4.2 Pulsatility

The aneurysm will change volume during the cardiac cycle as a result of the change in blood pressure. Dynamic CTA has been used to measure this change in volume (Hayakawa et al. 2005; Ishida et al. 2005; Krings et al. 2009). Ishida et al. (2005) noted pulsation in 9 of 28 saccular aneurysms and in 3 of 5 non-saccular aneurysms. Hayakawa et al. (2005) investigated 23

patients with ruptured aneurysms, of which 4 showed pulsation whose location corresponded to the site of rupture in all 4 cases. It was hypothesised in these studies that the pulsation occurred where the wall was thin, and that this was a site at risk of rupture.

16.2.4.3 Haemodynamics and Wall Stress

MRI may be used to measure blood velocities from which 3D data on haemodynamic flow patterns and wall shear stress may be calculated (Moftakhar et al. 2007). Haemodynamics may also be obtained as the output from patient specific modelling (see Chap. 11). Figure 16.4 shows examples of flow streamlines and wall shear stress in a saccular aneurysm. Patient specific modelling may also be used to estimate the distribution of circumferential wall stress (Fig. 16.5).

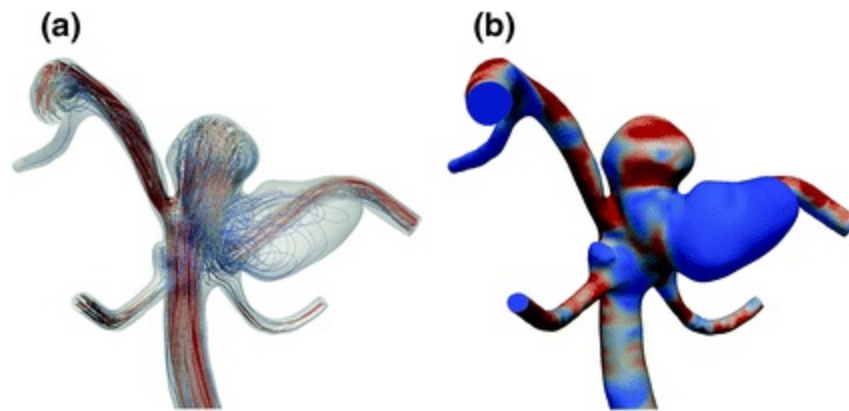


Fig. 16.4 Haemodynamics in a Basilar tip aneurysm with two lobes calculated from patient specific modelling. The basilar artery enters from the bottom of the image and is nearly vertical. **a** Flow streamlines; the velocity range is $0\text{--}2\text{ ms}^{-1}$. **b** Wall shear stress; the range is $0\text{--}50\text{ Pa}$. Images kindly provided by Dr. Arjan Geers (Edinburgh University). In both figures, red is ‘high’ and blue is ‘low’ ends of the range

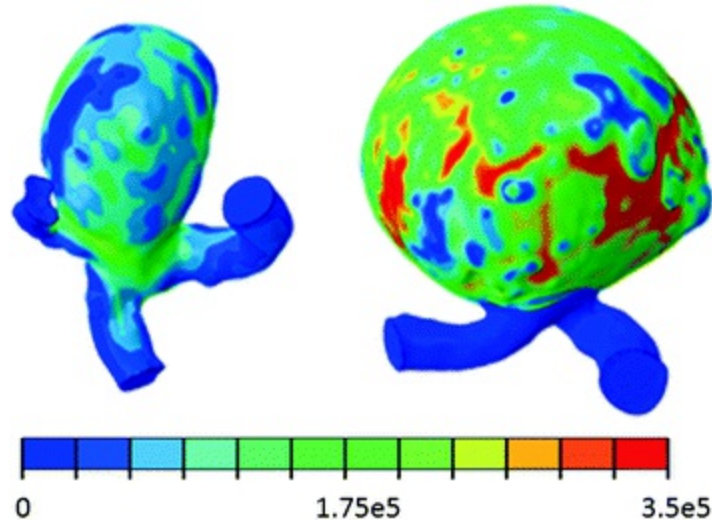


Fig. 16.5 von Mises stress (Pa) in cerebral aneurysms calculated from patient specific modelling. Image kindly provided by Dr. Noel Conlisk (Edinburgh University)

16.2.5 Treatment

This section presents a very brief description of the treatment of CAs. Further reading on diagnostic and treatment pathways are provided in Wardlaw and White (2000) and Mehrar et al. (2011). Most CAs that rupture are undiagnosed at the time of rupture and present as an emergency. Treatment of the ruptured aneurysm involves exclusion of the aneurysm from the circulation. The decision to treat the unruptured aneurysm is based on aneurysm diameter. Treatment is considered if the diameter is greater than 7 mm, however if there are other risk factors then treatment is considered if the diameter is greater than 3 mm diameter. Historically surgical clipping of the aneurysm was the preferred method for treatment of a cerebral aneurysm. This is highly invasive involving open surgery with placement of a clip across the aneurysm neck to separate the aneurysm from the main arterial flow channel. It is much more common to perform intervention by catheter based techniques under fluoroscopic guidance (White et al. 2015). The most common technique is the insertion of coils in the aneurysm which are thrombogenic, so that the aneurysm is sealed off by the presence of thrombus. Increasingly coiling is combined with the placement of a stent. The stent helps prevent ingress of the coil into the main arterial channel, hence allowing more aggressive coil placement, and provides a mesh on which an endothelium can grow. Other devices and methods which are used in interventional treatment include balloon remodelling, flow diverters and

intrasaccular flow disruptors.

16.3 Abdominal Aortic Aneurysms

16.3.1 Abdominal Aortic Aneurysm Disease

As the name implies, AAAs are localised increases in the diameter of the abdominal aorta (see Fig. 16.6), however they can often extend distally beyond the iliac bifurcation, or begin above the abdominal aorta. They are defined as a maximum aortic diameter ≥ 3.0 cm with the un-diseased diameter being around 2 cm. The incidence rates of AAAs range from 2 to 8 % for men over 65 years and the prevalence is 4 times lower in women. Over recent years, the incidence rates appear to be falling, with this being attributed to the change in smoking habits in developed countries (Lederle 2011).

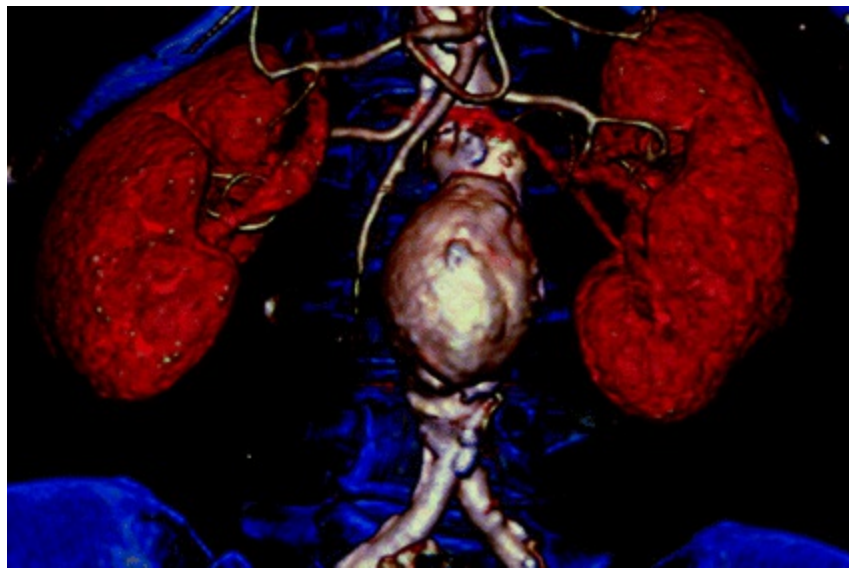


Fig. 16.6 CT reconstruction of an abdominal aortic aneurysm

Most AAAs are asymptomatic so that the first time the patient is aware of an aneurysm is after rupture. The most common symptom is sudden pain in the abdomen; other symptoms include low blood pressure, loss of consciousness and a pulsatile mass in the abdomen. Following rupture there is usually considerable internal bleeding and this is the main cause of death. If an unruptured AAA is detected, usually with medical imaging, the primary criterion determining surgical intervention is the size of the AAA, more specifically, the maximum diameter. If the maximum anterior-posterior

diameter of the AAA exceeds 5.5 cm in men or 5.0 cm in women, and the patient is fit for surgery, repair is offered. Risk of rupture increases with maximum AAA diameter. The annual rupture risk increases from 0.5 to 5 % for diameter of 4.0–4.9 cm, 3–5 % for 5.0–5.9 cm, 10–20 % for 6.0–6.9 cm, and 20–40 % for 7.0–7.9 cm (Brewster et al. 2003).

A minority of AAA are symptomatic in that the patient develops a variety of symptoms associated with imminent rupture. These symptoms include abdominal pain, lower back pain and a pulsatile abdominal mass. Generally symptomatic patients are offered urgent repair of their AAA (De Martino et al. 2010).

16.3.2 Mechanics and Haemodynamics

The healthy aorta is often approximated as a cylinder; however, AAAs can develop into highly irregular shapes with regions of high curvature and highly tortuous centrelines. As such, the mechanics used to determine the stresses and strains cannot be approximated using the Law of Laplace (see Chap. 5.1.5). It is these stresses and strains that contribute to the growth, remodelling and eventual rupture of the AAA, hence the large research focus aimed at accurately predicting them (see Chap. 11.4.3). A material will fail when the local stress exceeds the local strength, and although there are many biological processes also at play, this general understanding also applies to AAA. Using patient specific modelling (PSM—discussed in detail in Chap. 11), it is possible to estimate the stress acting on the AAA wall in vivo (Fillinger et al. 2002, 2003; Truijers et al. 2007; Doyle et al. 2009; Gasser et al. 2010; Doyle et al. 2014). By coupling this data with knowledge of the AAA wall strength (Thubrikar et al. 2001; Raghavan et al. 2011, 2006), it is possible to determine the likelihood of rupture. However, predicting in vivo wall strength remains a significant challenge (vande Geest et al. 2006; Reeps et al. 2013).

Loss of elastin and increase in collagen content as the AAA grows leads to overall stiffening of the AAA vessel wall. The wall motion (difference in diameter between diastole and systole) is typically 10 % of the diameter in healthy arteries, so for a 20 mm diameter normal abdominal aorta the wall motion is around 2 mm. In a study performed on patients with AAA the average wall motion measured using an ultrasound system was only 1 mm (Wilson et al. 2003).

The majority (~75 %) of clinically-relevant AAAs have intraluminal

thrombus (ILT) in the sac region. This ILT is a complex fibrin structure, with a continuous network of canaliculi, platelets, red blood cells and other haematopoietic cells, and its' role in AAA mechanics is still poorly understood. ILT starves the AAA wall of oxygen and thus weakens it (Vorp et al. 2001), yet appears to 'anchor' the wall and reduce wall deformation over the cardiac cycle. However, it allows the transmittance of the full pressure load to the wall (Schurink et al. 2000). The mechanical problem is further compounded by the fact that ILT develops in a patient-specific manner and can range from a relatively structured material to an unstructured one (see Fig. 16.7).

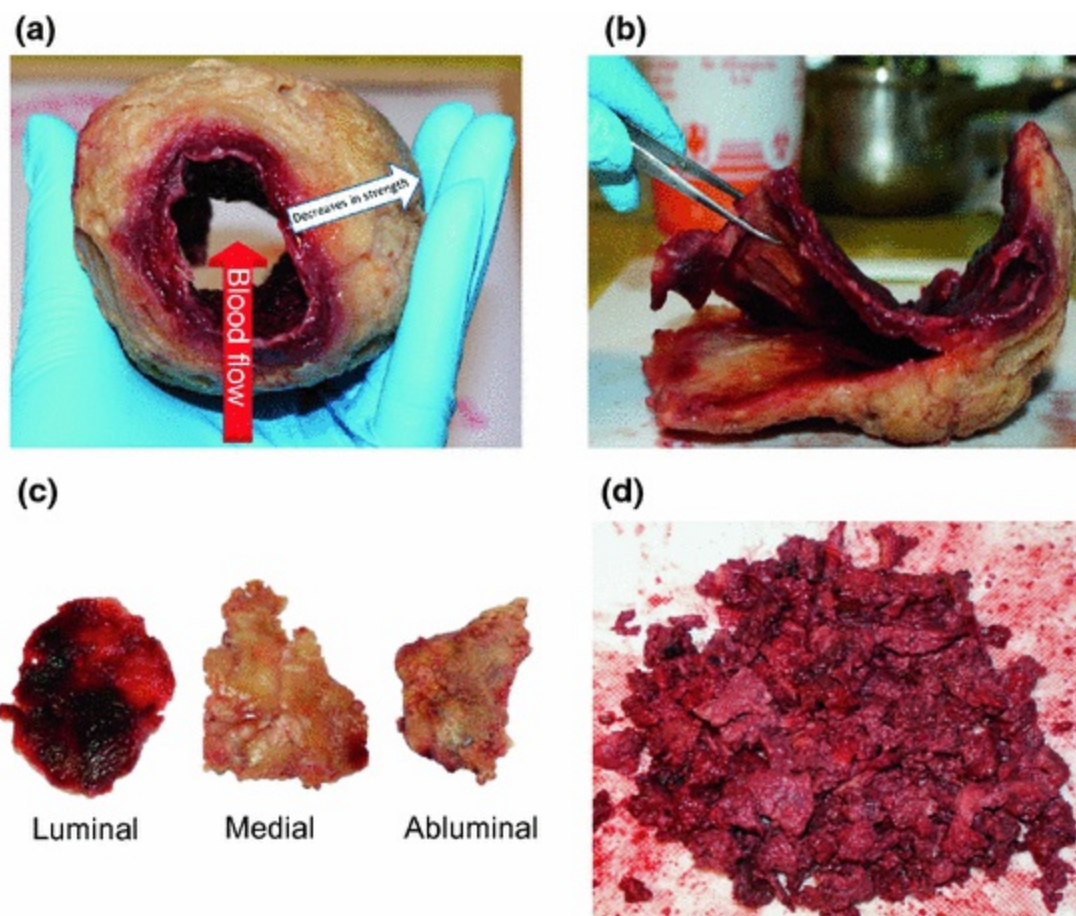


Fig. 16.7 The morphology of intraluminal thrombus (ILT). **a** Gross appearance of excised ILT, **b** separation of a structured ILT specimen into **c** the various layers (luminal, medial and abluminal), and **d** an unstructured ILT

Information on the detailed mechanical properties of AAA tissues including thrombus arises from tensile testing performed on specimens of

material gathered when surgery is performed. These properties are of interest in themselves for understanding of the progression of AAA, and essential for PSM where assumed mechanical properties are imposed in a finite element analysis (FEA) framework. Material constants for a hyperelastic, homogeneous, incompressible, and isotropic constitutive model were provided by fitting experimental data; for the vessel wall (Raghavan and Vorp 2000) and for the thrombus (Wang et al. 2001). More sophisticated biaxial test methods are also possible, as discussed in Chap. 13. Further details of research studies on the mechanical properties of AAA thrombus and vessel wall are provided by Vorp (2007).

In conjunction with the structural mechanics at play, the haemodynamics in AAA are also crucial. As the aneurysm gradually expands, the geometry can become highly irregular, whereby the blood flow is complex. Flow into a tube where diameter increases causes an adverse pressure gradient leading to vortex formation at the edge of the tube. Curvature leads to changes in direction of flow including helical flow. In addition it is clear that there is already helical flow at the inlet to the AAA, which further enhances helical tendencies (Hardman et al. 2013); see Fig. 11.7a, d in Chap. 11. The nature of the flow contributes to the development of ILT and it has been shown that the residence time of platelets, red blood cells and other particles suspended in the blood, as well as the presence of vortical structures, calculated using PSM techniques, predicts the location of ILT build up (Biasetti et al. 2010, 2011; Basciano et al. 2011; Di Achille et al. 2014). In particular, the lumen of the AAA (that is, the blood channel) can form pockets surrounded by ILT (see Fig. 16.8). These pockets harbour stagnant, recirculating flow that contributes to further build-up of ILT and other biological processes.

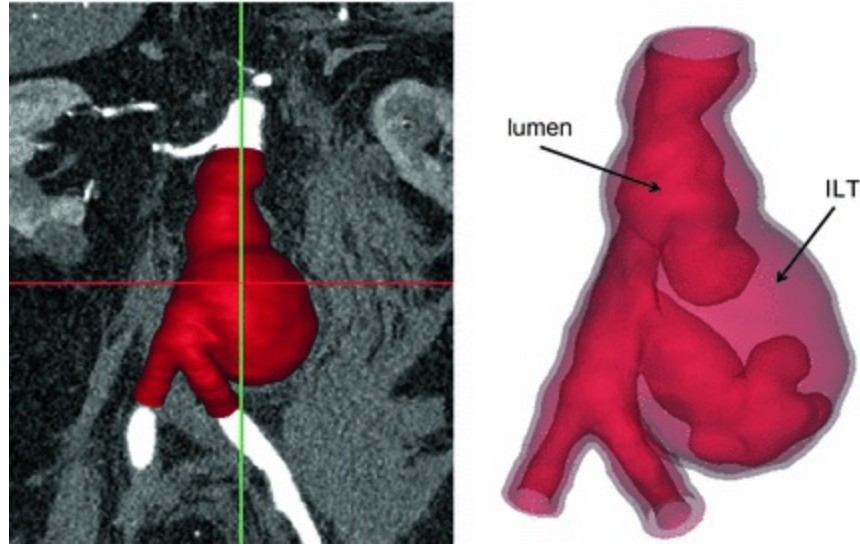


Fig. 16.8 (Left) 3D reconstructions of AAA from CT data and (right) the complicated lumen geometry as a result of ILT formation

16.3.3 Initiation, Growth and Rupture

As with CAs, the initiation, growth and rupture of AAA is a complex interplay of mechanical forces and biology. The exact cause of an aneurysm is still not known, however, it is widely accepted that the role of haemodynamics and wall shear stresses in the aorta, contribute to the initiation. In the healthy aorta, the innermost layer is the endothelium. As discussed in Chap. 5.4, haemodynamic forces in the aorta can upset this layer (as with all cardiovascular disease), especially in regions of abnormal flow. The continued exposure of the abdominal aorta to disturbed flow and the change in arterial microstructure with age, is thought to contribute to aneurysm initiation, and furthermore, growth.

As mentioned earlier, AAA is associated with a loss of elastin. Potential causes of elastin degradation are discussed by Lasheras (2007):

- Ageing. Over time repeated cycling of the elastin fibres during the cardiac cycle will lead to fibre fracture. Compensatory collagen deposition leads to stiffening of the aorta and a local increase in systolic pressure further exacerbating elastin fibre degradation.
- Wall shear. The normal abdominal aorta will increase in diameter over time as a response to stiffening of the aorta. This may lead to increased tortuosity, which will give rise to regions of abnormal wall shear; for

example low wall shear has been associated with elastin loss.

Studies which describe models of AAA initiation and growth are described by Sheidaei et al. (2011), and this growth and remodelling (G&R) of AAA is a highly active research area (Watton et al. 2004; Humphrey 2008; Sheidaei et al. 2011; Zeinali-Davarani et al. 2011; Humphrey and Holzapfel 2012; Grytsan et al. 2015). The growth of AAA is largely due to the change in microstructure. AAAs are characterised by a thinning medial layer with a reduction in elastin and an increased turnover of collagen. This knowledge has led to computational models of G&R that account for microstructural changes and result in AAA expansion due to the haemodynamic load (Fig. 16.9).

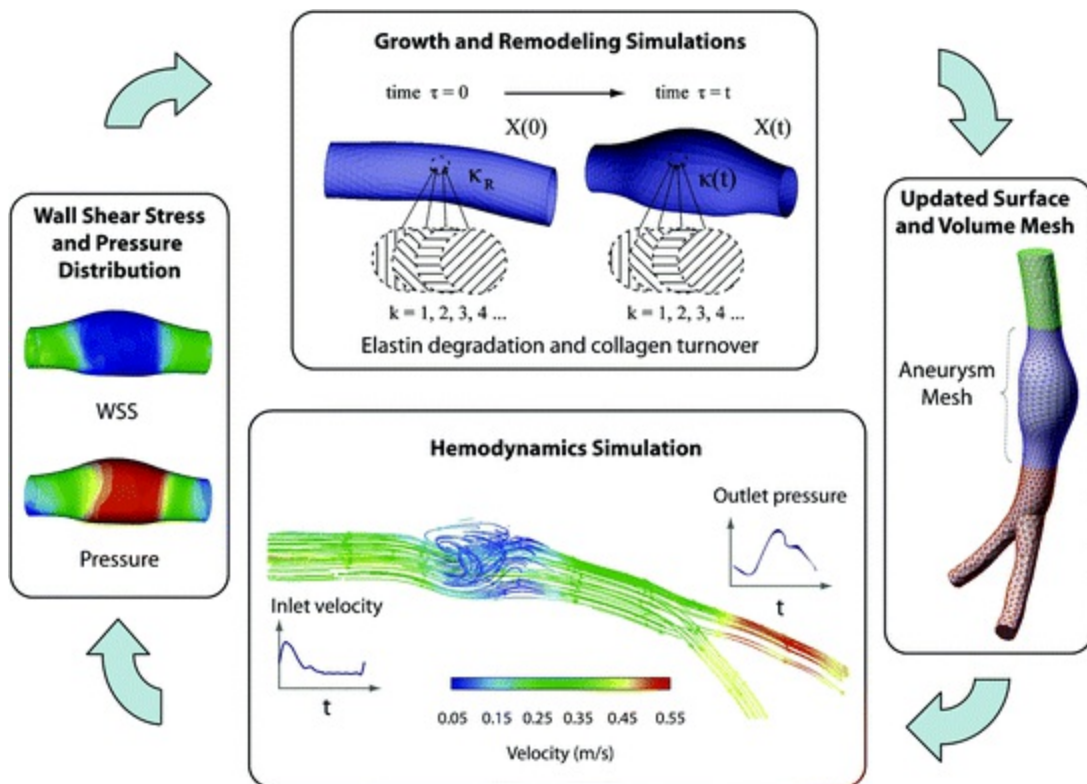


Fig. 16.9 A computational growth and remodelling (G&R) framework. Iterative loop and information transfer in the coupling between the haemodynamics and G&R simulations. Reprinted from Medical Engineering & Physics, Vol. 33(1), Sheidaei A, Hunley SC, Zeinali-Davarani S, Ragun LG, Baek S; Simulation of abdominal aortic aneurysm growth with updating hemodynamic loads using a realistic geometry. pp. 80–88, Copyright (2011), with permission from the Institute of Physics and Engineering in Medicine and Biology

The likely chain of events leading to rupture is shown in Fig. 16.10.

Although fundamentally, the AAA will rupture when stress exceeds strength, the chain of events leading to wall weakening (and thus, increases in stress) is not trivial. For a detailed review of the biological factors influencing AAA rupture, see (Choke et al. 2005).

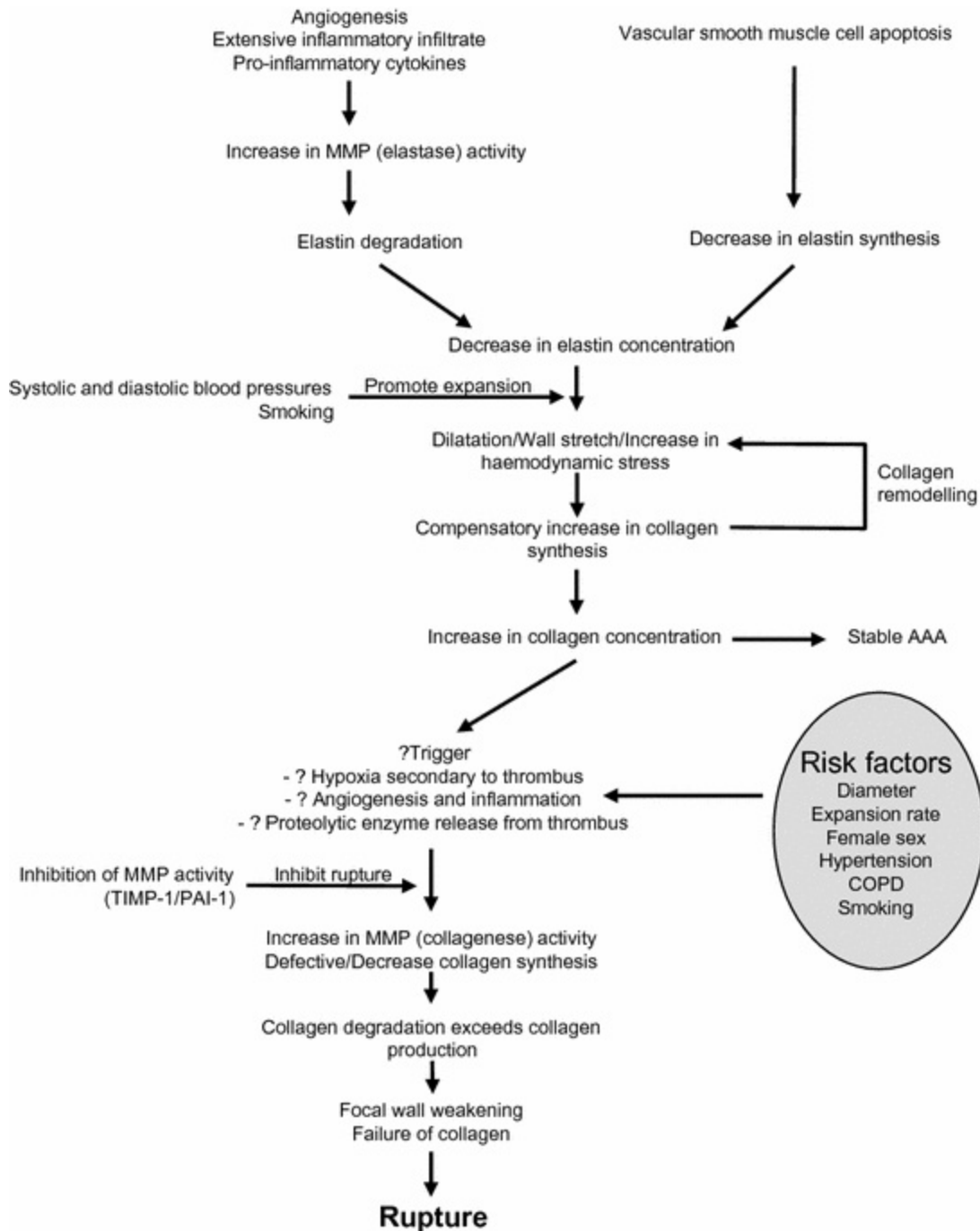


Fig. 16.10 Chain of biological events leading to AAA rupture. Reprinted from European Journal of Vascular and Endovascular Surgery, Vol. 30(3), Choke E, Cockerill G, Wilson WR, Sayed S, Dawson

16.3.4 In Vivo Imaging and Patient Specific Modelling

In clinical practice, ultrasound imaging is the most common method of evaluating the size of an AAA. The maximum diameter is measured using B-mode imaging (Fig. 16.11). CT scanning is performed to evaluate if the AAA has ruptured, or to assist in planning of surgical intervention. For use in patient specific modelling, 3D geometry is provided from CT or MRI, as discussed in Chap. 11.

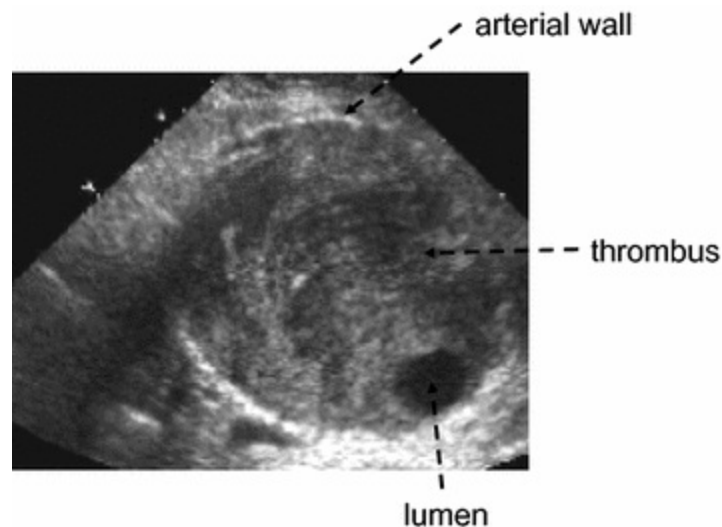


Fig. 16.11 In vivo ultrasound image of AAA

16.3.4.1 AAA Symmetry

As described earlier, the decision to undertake elective surgery is mostly based on maximum diameter. In the research literature, shape descriptors have been formulated based on an analysis of the 3D data from CT. One such descriptor is the asymmetry index as illustrated in Fig. 16.12 (Doyle et al. 2009). The analysis starts with identification of the centre of the vessel for each slice of the CT scan. The inlet and the outlet centre points are connected with a straight line. The deviation from the centreline is measured and plotted. The asymmetry index is defined as the maximum deviation. It has been argued that the asymmetry index is a surrogate for peak wall stress; in

that AAA which are more asymmetric have higher peak wall stress.

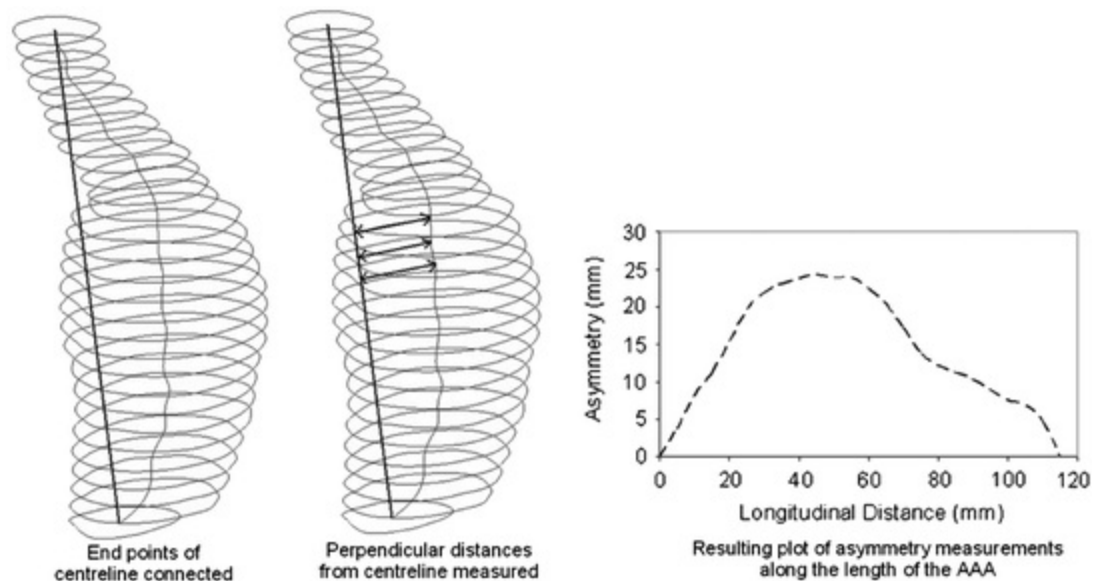


Fig. 16.12 The asymmetry method for AAA. Reprinted from Journal of Vascular Surgery, Vol. 49(2), Doyle BJ, Callanan A, Burke PE, Grace PA, Walsh MT, Vorp DA, McGloughlin TM. Vessel asymmetry as an additional diagnostic tool in the assessment of abdominal aortic aneurysms. pp. 443–454, Copyright (2009), with permission from The Society for Vascular Surgery

In general shape indices rely only on information from the CT scan so could be implemented easily in clinical practice whereas biomechanics-based rupture risk requires a patient specific modelling workflow.

16.3.4.2 Wall Motion and Pressure Strain Elastic Modulus

The radial motion of the vessel wall during the cardiac cycle may be measured using ultrasound. A number of different techniques have been used (Hoeks et al. 1999) of which correlation of the RF data from consecutive image lines is probably the most widely used. Using these techniques displacements in the range 1–10 micron can easily be measured. This is sufficient to provide good accuracy for typical AAA diameter changes of 0.5–3 mm. From the measured wall motion, a measure of wall stiffness may be measured called the ‘pressure strain elastic modulus’ E_p , first formulated by Peterson et al. (1960).

$$E_p = \frac{P_s - P_d}{(d_s - d_d)/d_d} \quad (16.6)$$

where P_s and P_d are systolic and diastolic pressure, d_s and d_d are systolic and diastolic diameter.

Pressure values within the AAA are difficult to obtain and in practice, pressure values taken with an arm cuff are used. Stiffness of AAA using this methodology was measured in AAA by Wilson et al. (2003) where it was shown that there was no difference between in stiffness in patients who ruptured, compared to patients who did not.

In this approach the assumed physical model is that the artery consists of an elastic cylinder of uniform wall thickness and uniform elasticity. In reality, an AAA is a complex 3D structure with variations in wall thickness and mechanical properties, suggesting that more complex methods able to account for these 3D variations are needed.

16.3.4.3 Haemodynamics and Wall Stress

MRI techniques may be used to estimate flow-field data from which wall shear stress may, in principle, be estimated. In practice, it is more common to use a patient specific modelling approach involving computational fluid dynamics for the estimation of wall shear stress (Fig. 16.13). Outward expansion of the lumen is associated with regions of low wall shear stress and high residence time for blood particles, such as platelets.

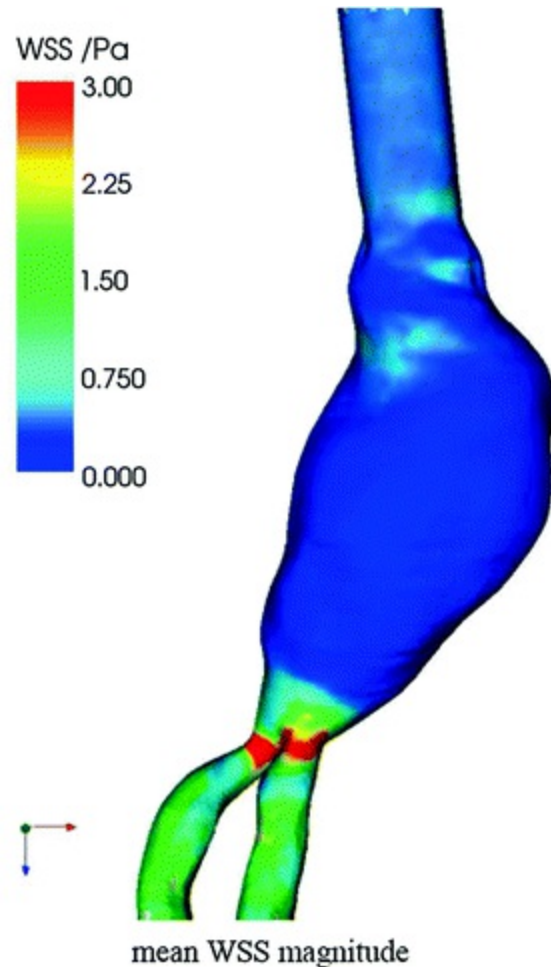


Fig. 16.13 Distribution of wall shear stress (WSS) in AAA

Patient specific modelling, using FEA, may also be used for the estimation of stress within the wall; see Chap. 11. Typically the von-Mises stress is calculated which is a composite of the various stresses estimated using FEA. Surprisingly in this area there are few clinical studies.

Figure 16.14 shows peak wall stress in different groups of AAA patients from Fillinger et al. (2003). In the lowest risk group patients have AAA with diameter <5.5 cm and attend a surveillance programme. The group with the next highest risk have diameters greater than 5.5 cm and are being considered for elective surgery. The highest risk group are those who went on to rupture or presented with symptoms of imminent rupture such as severe back pain. Diameter increases with risk, as would be expected. Also peak wall stress increases with risk. The ROC plot shows that overall categorisation is performed better by peak wall stress.

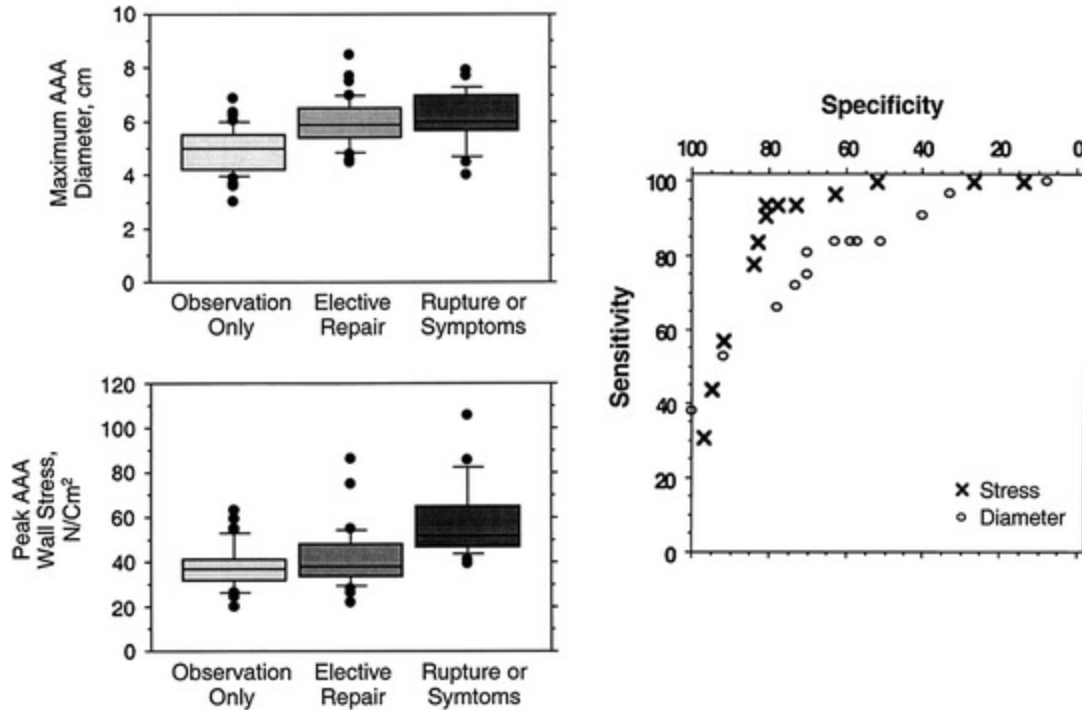


Fig. 16.14 Top left box plot for AAA diameter demonstrates that 90 % of AAAs under observation have diameter larger than the lowest recorded diameter for an AAA that subsequently ruptured or became symptomatic, which was 4.4 cm in maximum diameter. Bottom left box plot for peak AAA wall stress demonstrates that 75 % of AAAs under observation have stress lower than the lowest recorded stress for an AAA that subsequently ruptured or became symptomatic. Right receiver operating characteristic curves shows superior sensitivity and specificity of peak wall stress in comparison with diameter throughout the clinically important range. Reprinted from Journal of Vascular Surgery, Vol. 37(4), Fillinger MF, Marra SP, Raghavan ML, Kennedy FE. Prediction of rupture risk in abdominal aortic aneurysm during observation: wall stress versus diameter. pp. 724–732, Copyright (2003), with permission from The Society for Vascular Surgery and The American Association for Vascular Surgery

16.3.5 Diagnosis and Treatment

In the absence of a screening programme, most AAA are diagnosed following rupture or through chance findings during imaging investigations for other medical problems. A UK-wide AAA screening programme has been in operation since 2013 with men aged over 65 years are offered an ultrasound scan to measure the diameter of their abdominal aorta. If an AAA is found (diameter >3 cm) the patient is put on a surveillance programme with measurements every 6 months. Generally AAA grow in size. When the diameter exceeds 5.5 cm the patient is considered for elective surgery. The measure of risk of rupture of an AAA is based largely on the maximum diameter. This diameter criterion stems from early autopsy data (Darling et

al. 1977) that noted cases over 5.0 cm (~40 %) are more likely to rupture. However, the same report also showed many larger AAAs were still intact after death and many smaller ones did not burst (~13 %). The criteria of 5.5 cm was set following clinical trials performed in the 1990s (UKSAT 1998). In addition the growth rate (i.e. change in diameter over time) is also recorded and a growth rate of greater than ≥ 1.0 cm/year is considered an indicator of imminent rupture.

Traditional repair of an AAA involved open surgery and replacement of the AAA with a synthetic graft, which is connected to the aorta with stitches. The operation involves removal of the thrombus, if present. The original AAA wall is trimmed to allow the wall to be wrapped around the graft. This traditional open repair is increasingly being replaced by a less invasive method involving endovascular stenting (endovascular aneurysm repair or EVAR). Access is gained through the femoral artery and an expanding stent graft is located within the AAA under fluoroscopic guidance.

More details of AAA diagnosis, imaging and treatment are provided in Hoskins et al. (2011).

References

Basciano C, Kleinstreuer C, Hyun S, Finol EA. A relation between near-wall particle-hemodynamics and onset of thrombus formation in abdominal aortic aneurysms. *Ann Biomed Eng.* 2011;39:2010–26.

[CrossRef][PubMed][PubMedCentral]

Biasetti J, Gasser TC, Auer M, Hedin U, Labruto F. Hemodynamics of the normal aorta compared to fusiform and saccular abdominal aortic aneurysms with emphasis on a potential thrombus formation mechanism. *Ann Biomed Eng.* 2010;38:380–90.

[CrossRef][PubMed]

Biasetti J, Hussain F, Gasser TC. Blood flow and coherent vortices in the normal and aneurysmatic aortas: a fluid dynamical approach to intra-luminal thrombus formation. *J R Soc Interface.* 2011;8:1449–61.

[CrossRef][PubMed][PubMedCentral]

Brewster DC, Cronenwett JL, Hallett JW Jr, et al. Guidelines for the treatment of abdominal aortic aneurysms. Report of a subcommittee of the Joint Council of the American Association for Vascular Surgery and Society for Vascular Surgery. *J Vasc Surg.* 2003;37:1106–17.

[CrossRef][PubMed]

Brisman JL, Song JK, Newell DW. Cerebral aneurysms. *New Eng J Med.* 2006;355:928–39.

[CrossRef][PubMed]

Choke E, Cockerill G, Wilson WR, Sayed S, Dawson J, Loftus I, Thompson MM. A review of biological factors implicated in abdominal aortic aneurysm rupture. *Eur J Vasc Endovasc Surg*. 2005;30:227–44.

[\[CrossRef\]](#)[\[PubMed\]](#)

Darling RC, Messina CR, Brewster DC, Ottinger LW. Autopsy study of unoperated abdominal aortic aneurysms. The case for early resection. *Circulation*. 1977;56(3 Suppl):II 161–164.

De Martino RR, Nolan BW, Goodney PP, Chang CK, et al. Outcomes of symptomatic abdominal aortic aneurysm repair. *J Vasc Surg*. 2010;52:5–12.

[\[CrossRef\]](#)[\[PubMed\]](#)[\[PubMedCentral\]](#)

Dhar S, Tremmel M, Mocco J, Kim M, Yamamoto J, Siddiqui AH, Hopkins LN, Meng H. Morphology parameters for intracranial aneurysm rupture risk assessment. *Neurosurgery*. 2008;63:185–96.

[\[CrossRef\]](#)[\[PubMed\]](#)[\[PubMedCentral\]](#)

Di Achille P, Tellides G, Figueroa CA, Humphrey JD. A haemodynamic predictor of intraluminal thrombus formation in abdominal aortic aneurysms. *Proc Royal Soc Lond A Math Phys Eng Sci*. 2014;470:0163.

Doyle BJ, Callanan A, Burke PE, Grace PA, Walsh MT, Vorp DA, McGloughlin TM. Vessel asymmetry as an additional diagnostic tool in the assessment of abdominal aortic aneurysms. *J Vasc Surg*. 2009;49:443–54.

[\[CrossRef\]](#)[\[PubMed\]](#)

Doyle BJ, McGloughlin TM, Miller K, Powell JT, Norman PE. Regions of high wall stress can predict the future location of rupture of abdominal aortic aneurysm. *Cardiovasc Intervent Radiol*. 2014;37:815–8.

[\[CrossRef\]](#)[\[PubMed\]](#)

Fillinger MF, Raghavan ML, Marra SP, Cronenwett JL, Kennedy FE. In vivo analysis of mechanical wall stress and abdominal aortic aneurysm rupture risk. *J Vasc Surg*. 2002;36:589–97.

[\[CrossRef\]](#)[\[PubMed\]](#)

Fillinger MF, Marra SP, Raghavan ML, Kennedy FE. Prediction of rupture risk in abdominal aortic aneurysm during observation: wall stress versus diameter. *J Vasc Surg*. 2003;37:724–32.

[\[CrossRef\]](#)[\[PubMed\]](#)

Frösen J, Piippo A, Paetau A, Kangasniemi M, Niemelä M, Hernesniemi J, Jääskeläinen J. Remodeling of saccular cerebral artery aneurysm wall is associated with rupture: histological analysis of 24 unruptured and 42 ruptured cases. *Stroke*. 2004;35:2287–93.

[\[CrossRef\]](#)[\[PubMed\]](#)

Frösen J, Tulamo R, Paetau A, Laaksamo E, Korja M, Laakso A, Niemelä M, Hernesniemi J. Saccular intracranial aneurysm: pathology and mechanisms. *Acta Neuropathol*. 2012;123:773–86.

[\[CrossRef\]](#)[\[PubMed\]](#)

Gasser TC, Auer M, Labruto F, Swedenborg J, Roy J. Biomechanical rupture risk assessment of abdominal aortic aneurysms: model complexity versus predictability of finite element simulations. *Eur J Vasc Endovasc Surg*. 2010;40:176–85.

[\[CrossRef\]](#)[\[PubMed\]](#)

Grytsan A, Watton PN, Holzapfel GA. A thick-walled fluid-solid-growth model of abdominal aortic aneurysm evolution: application to a patient-specific geometry. *J Biomech Eng.* 2015;137. doi:[10.1115/1.4029279](https://doi.org/10.1115/1.4029279).

Hardman D, Semple SIK, Richards JMJ, Hoskins PR. Comparison of patient specific inlet boundary conditions in the numerical modelling of blood flow in abdominal aortic aneurysm disease. *Int J Num Meth Biomed Eng.* 2013;29:165–78.

[\[CrossRef\]](#)

Hayakawa M, Katada K, Anno H, Imizu S, Hayashi J, Irie K, Negoro M, Kato Y, Kanno T, Sano H. CT angiography with electrocardiographically gated reconstruction for visualizing pulsation of intracranial aneurysms: identification of aneurysmal protuberance presumably associated with wall thinning. *Am J Neuroradiol.* 2005;26:1366–9.

[\[PubMed\]](#)

Hoeks APG, Brands PJ, Willigers JM, Reneman RS. Noninvasive measurement of mechanical properties of arteries in health and disease. *J Eng Med.* 1999;213:195–202.

[\[CrossRef\]](#)

Hoskins PR, Semple S, White P, Richards J. Imaging of aneurysms. In: McGloughlin T, editor. *Biomechanics and mechanobiology of aneurysms*. Berlin: Springer; 2011. p. 35–65.

[\[CrossRef\]](#)

Humphrey JD. Vascular adaptation and mechanical homeostasis at tissue, cellular, and sub-cellular levels. *Cell Biochem Biophys.* 2008;50:53–78.

[\[CrossRef\]](#)[\[PubMed\]](#)

Humphrey JD, Taylor CA. Intracranial and abdominal aortic aneurysms: similarities, differences, and need for a new class of computational models. *Annu Rev Biomed Eng.* 2008;10:221–46.

[\[CrossRef\]](#)[\[PubMed\]](#)[\[PubMedCentral\]](#)

Humphrey JD, Holzapfel GA. Mechanics, mechanobiology, and modeling of human abdominal aorta and aneurysms. *J Biomech.* 2012;45:805–14.

[\[CrossRef\]](#)[\[PubMed\]](#)

Ishida F, Ogawa H, Simizu T, Kojima T, Taki W. Visualizing the dynamics of cerebral aneurysms with four-dimensional computed tomographic angiography. *Neurosurgery.* 2005;57:460–470.

Juvela S. Treatment options of unruptured intracranial aneurysms. *Stroke.* 2004;35:372–4.

[\[CrossRef\]](#)[\[PubMed\]](#)

Krings T, Willems P, Barfett J, Ellis M, Hinojosa N, Blobel J, Geibprasert S. Pulsatility of an intracavernous aneurysm demonstrated by dynamic 320-detector row CTA at high temporal resolution. *Cen Eur Neurosurg.* 2009;70:214–8.

[\[CrossRef\]](#)

Lasheras JC. The biomechanics of arterial aneurysms. *Ann Rev Fluid Mech.* 2007;39:293–319.

[\[CrossRef\]](#)

Lederle FA. The rise and fall of abdominal aortic aneurysm. *Circulation.* 2011;124:1097–9.

[\[CrossRef\]](#)[\[PubMed\]](#)

McGloughlin TM, Doyle BJ. New approaches to abdominal aortic aneurysm rupture risk assessment: engineering insights with clinical gain. *Arterioscler Thromb Vasc Biol.* 2010;30:1687–94.

[\[CrossRef\]](#)[\[PubMed\]](#)

Mehra M, Spilberg G, Gounis MJ, Wakhloo AK. Intracranial aneurysms: clinical assessment and treatment options. In: T McGloughlin, editor. *Biomechanics and mechanobiology of aneurysms.* Springer: Berlin; 2011. pp. 331–372.

Meng H, Tutino VM, Xiang J, Siddiqui A. High WSS or low WSS? Complex interactions of hemodynamics with intracranial aneurysm initiation, growth, and rupture: toward a unifying hypothesis. *Am J Neuroradiol.* 2014;35:1254–62.

[\[CrossRef\]](#)[\[PubMed\]](#)

Meyers P, Schumacher HC, Higashida RT, Derdeyn C, Nesbit GM, Sacks D, Wechsler L, Bederson J, Lavine S, Rasmussen P. Reporting standards for endovascular repair of saccular intracranial cerebral aneurysms. *Stroke.* 2009;40:e366–79.

[\[CrossRef\]](#)[\[PubMed\]](#)

Millán RD, Dempere-Marco L, Pozo JM, Cebal JR, Frangi AF. Morphological characterization of intracranial aneurysms using 3-D moment invariants. *IEEE Trans Med Imag.* 2007;26:1270–82.

[\[CrossRef\]](#)

Moftakhar R, Aagaard-Kienitz B, Johnson K, et al. Noninvasive measurement of intra-aneurysmal pressure and flow pattern using phase contrast with vastly undersampled isotropic projection imaging. *Am J Neuroradiol.* 2007;28:1710–4.

[\[CrossRef\]](#)[\[PubMed\]](#)

Nader-Sepahi A, Casimiro M, Sen J, et al. Is aspect ratio a reliable predictor of intracranial aneurysm rupture? *Neurosurgery.* 2004;54:1343–8.

[\[CrossRef\]](#)[\[PubMed\]](#)

Penn DL, Komotar RJ, Connolly ES. Hemodynamic mechanisms underlying cerebral aneurysm pathogenesis. *J Clin Neurosci.* 2011;18:1435–8.

[\[CrossRef\]](#)[\[PubMed\]](#)

Peterson LH, Jensen RE, Parnell R. Mechanical properties of arteries in vivo. *Circ Res.* 1960;8:622–639.

Raghavan ML, Vorp DA. Toward a biomechanical tool to evaluate rupture potential of abdominal aortic aneurysm: identification of a finite strain constitutive model and evaluation of its applicability. *J Biomech.* 2000;33:475–82.

[\[CrossRef\]](#)[\[PubMed\]](#)

Raghavan ML, Kratzberg J, de Tolosa EMC, Hanaoka MM, Walker P, da Silva ES. Regional distribution of wall thickness and failure properties of human abdominal aortic aneurysm. *J Biomech.* 2006;39:3010–6.

[\[CrossRef\]](#)[\[PubMed\]](#)

Raghavan ML, Hanaoka MM, Kratzberg JA, de Higuchi ML, da Silva ES. Biomechanical failure properties and microstructural content of ruptured and unruptured abdominal aortic aneurysms. *J Biomech.* 2011;44:2501–7.

[\[CrossRef\]](#)[\[PubMed\]](#)

Reeps C, Maier A, Pelisek J, Härtl F, Grabher-Meier V, Wall WA, Essler M, Eckstein HH, Gee MW. Measuring and modeling patient-specific distributions of material properties in abdominal aortic aneurysm wall. *Biomech Model Mechanobiol*. 2013;12:717–33.

[\[CrossRef\]](#)[\[PubMed\]](#)

Schurink GW, van Baalen JM, Visser MJ, van Bockel JH. Thrombus within an aortic aneurysm does not reduce pressure on the aneurysmal wall. *J Vasc Surg*. 2000;31:501–6.

[\[CrossRef\]](#)[\[PubMed\]](#)

Selimovic A, Ventikos Y, Watton PN. Modelling the evolution of cerebral aneurysms: Biomechanics, mechanobiology and multiscale modelling. *Procedia IUTAM*. 2013;10:396–409.

[\[CrossRef\]](#)

Sforza DM, Putman CM, Cebal JR. Hemodynamics of cerebral aneurysms. *Ann Rev Fluid Mech*. 2009;41:91–107.

[\[CrossRef\]](#)

Sheidaei A, Hunley SC, Zeinali-Davarani S, Raguin LG, Baek S. Simulation of abdominal aortic aneurysm growth with updating hemodynamic loads using a realistic geometry. *Med Eng Phys*. 2011;33:80–8.

[\[CrossRef\]](#)[\[PubMed\]](#)

Thubrikar MJ, Labrosse M, Robicsek F, Al-Soudi J, Fowler B. Mechanical properties of abdominal aortic aneurysm wall. *J Med Eng Technol*. 2001;25:133–42.

[\[CrossRef\]](#)[\[PubMed\]](#)

Truijers M, Pol JA, Schultzekool LJ, van Sterkenburg SM, Fillinger MF, Blankensteijn JD. Wall stress analysis in small asymptomatic, symptomatic and ruptured abdominal aortic aneurysms. *Eur J Vasc Endovasc Surg*. 2007;33:401–7.

[\[CrossRef\]](#)[\[PubMed\]](#)

Ujiie H, Tachibana H, Hiramatsu O. Effects of size and shape (aspect ratio) on the hemodynamics of saccular aneurysms: a possible index for surgical treatment of intracranial aneurysms. *Neurosurgery*. 1999;45:119–30.

[\[PubMed\]](#)

vande Geest JP, Wang DHJ, Wisniewski SR, Makaroun MS, Vorp DA. Towards a noninvasive method for determination of patient-specific wall strength distribution in abdominal aortic aneurysms. *Ann Biomed Eng*. 2006;34:1098–2006.

[\[CrossRef\]](#)[\[PubMed\]](#)

Vorp DA. Biomechanics of abdominal aortic aneurysm. *J Biomech*. 2007;40:1887–902.

[\[CrossRef\]](#)[\[PubMed\]](#)[\[PubMedCentral\]](#)

Vorp DA, Lee PC, Wang DH, Makaroun MS, Nemoto EM, Ogawa S, Webster MW. Association of intraluminal thrombus in abdominal aortic aneurysm with local hypoxia and wall weakening. *J Vasc Surg*. 2001;34:291–9.

[\[CrossRef\]](#)[\[PubMed\]](#)

Wang DHJ, Makaroun MS, Webster MW, Vorp DA. Mechanical properties and microstructure of

intraluminal thrombus from abdominal aortic aneurysm. *J Biomech Eng.* 2001;123:536–9.
[\[CrossRef\]](#)[\[PubMed\]](#)

Wardlaw JM, White PM. The detection and management of unruptured intracranial aneurysms. *Brain.* 2000;123:205–21.
[\[CrossRef\]](#)[\[PubMed\]](#)

Watton PN, Hill NA, Heil M. A mathematical model for the growth of the abdominal aortic aneurysm. *Biomech Model Mechanobiol.* 2004;3:98–113.

Weir B, Amidei C, Kongable G, et al. The aspect ratio (dome/ neck) of ruptured and unruptured aneurysms. *J Neurosurg.* 2003;99:447–51.
[\[CrossRef\]](#)[\[PubMed\]](#)

Wermer MJ, van der Schaaf IC, Algra A, Rinkel GJ. Risk of rupture of unruptured intracranial aneurysms in relation to patient and aneurysm characteristics: an updated meta-analysis. *Stroke.* 2007;38:1404–10.
[\[CrossRef\]](#)[\[PubMed\]](#)


White P, duPlessis J, Jayakrishnan V, Mitrac D. An overview of the endovascular treatment of intracranial aneurysms. In: Lanzer P, editor. *Pan vascular medicine.* Berlin: Springer; 2015. p. 2497–535.

Wilson KA, Lee AJ, Lee AJ, Hoskins PR, Fowkes FGR, Ruckley CV, Bradbury AW. The relationship between aortic wall distensibility and rupture of infrarenal abdominal aortic aneurysms. *J Vasc Surg.* 2003;37:112–7.
[\[CrossRef\]](#)[\[PubMed\]](#)

Wong GK, Poon WS. Current status of computational fluid dynamics for cerebral aneurysms: the clinician's perspective. *J Clin Neurosci.* 2011;18:1285–8.
[\[CrossRef\]](#)[\[PubMed\]](#)

Zeinali-Davarani S, Sheidaei A, Baek S. A finite element model of stress-mediated vascular adaptation: application to abdominal aortic aneurysms. *Comput Methods Biomech Biomed Eng.* 2011;14:803–17.
[\[CrossRef\]](#)

17. Cardiovascular Prostheses

Patricia V. Lawford¹ 

(1) Sheffield University, Sheffield, England, UK

 **Patricia V. Lawford**
Email: p.lawford@sheffield.ac.uk

Learning outcomes

1. Describe the difference between active and passive devices.
2. Describe the main failure modes for vascular grafts.
3. Discuss the benefits of stenting over balloon angioplasty alone.
4. Discuss the basic categories of heart valve and their relative advantages and disadvantages.
5. Discuss the factors which are used to determine valve performance.
6. Describe the fundamental components of a pacemaker.
7. Discuss the basic principle of a ‘safety-critical’ device.

17.1 Requirement for Cardiovascular Devices

Cardiovascular diseases remain the major cause of death in Europe, the USA, and in many developing countries, accounting for over 50 % of all deaths. The management of cardiovascular disease is a significant challenge to healthcare systems. Its prevalence increases with age. This is important given that more people are living to an older age. Furthermore, as treatments improve there is a steady increase in the number of patients discharged from hospital with chronic cardiovascular problems requiring long-term management.

For clinicians treating patients with symptomatic cardiovascular disease, the first line of approach is to use appropriate drugs in an attempt to restore normal physiological balance. If this fails, and the patient's condition deteriorates, then the clinician may have the option of either correctional surgery, as discussed briefly in Chaps. 15 and 16, or of using an implantable device. Depending on the type of device, these are introduced into the body using a minimally invasive (under local anaesthetic) or open surgical approach.

Devices are available to treat a range of different cardiovascular diseases including; vessel blockage (occlusion) or narrowing (stenosis), abnormal vessel enlargement (aneurysm) or dissection (partial tearing and delamination of the vessel wall), valvular disease, abnormal heart beat (arrhythmia), or heart failure.

17.1.1 Types of Cardiovascular Devices

A wide range of different types of cardiovascular implants are available. Examples include; stents, vascular grafts, prosthetic heart valves, pacemakers/implantable cardiac defibrillators and cardiac pumps (ventricular assist devices—VADs). These can be sub-divided into two overarching categories; active implantable devices and passive implantable devices. Active devices require a power source, i.e. an energy supply. Examples of these include pacemakers, powered by a small battery implanted under the skin, and VADs which demand significant power and typically have an energy source outside the body. Passive devices have no requirement for energy over and above that supplied by gravity or by movement of the human body. Examples of these include stents and prosthetic heart valves.

The basic principles, current state of the art and specific issues associated with these are discussed below.

17.2 Vascular Grafts

As indicated in Chaps. 15 and 16 arterial diseases can compromise blood flow to the downstream vascular territory or can lead to vessel expansion and weakening of the wall. Vascular grafts can be used to replace/repair/or bypass, damaged segments of vessels. Vascular grafts are relatively simple in terms of their structure and the major bioengineering challenges relate to the connection between graft and the natural vessel and the ‘suturability’ of the graft, i.e. How easy it is for the surgeon to create the join between graft and natural vessel (anastomosis) and how stable is the mechanical stability of the join.

17.2.1 Classification of Graft Type

Vascular grafts can be classified as biological or synthetic.

Biological grafts are harvested from the patient’s own tissues (autografts). Saphenous vein (from the leg) and internal mammary artery (a long straight artery which runs along the internal surface of the breast bone) are the most commonly used examples. Chemically treated bovine artery has also been used but with poorer results.

Synthetic grafts are typically made from woven or knitted fabrics (e.g. Dacron or PTFE) or expanded polymer (e.g. ePTFE). Figure 17.1 shows two examples, an aortic graft and a femoral artery graft. The critical material properties are biocompatibility, flexibility and resistance to biological and mechanical degradation. The material must also be capable of being sterilised without alteration to its properties. Some knitted grafts have a velour (velvet-like) luminal surface. This enables fibrin and cells from the blood to attach more easily encouraging a layer of endothelium to form thus providing a natural biocompatible surface.

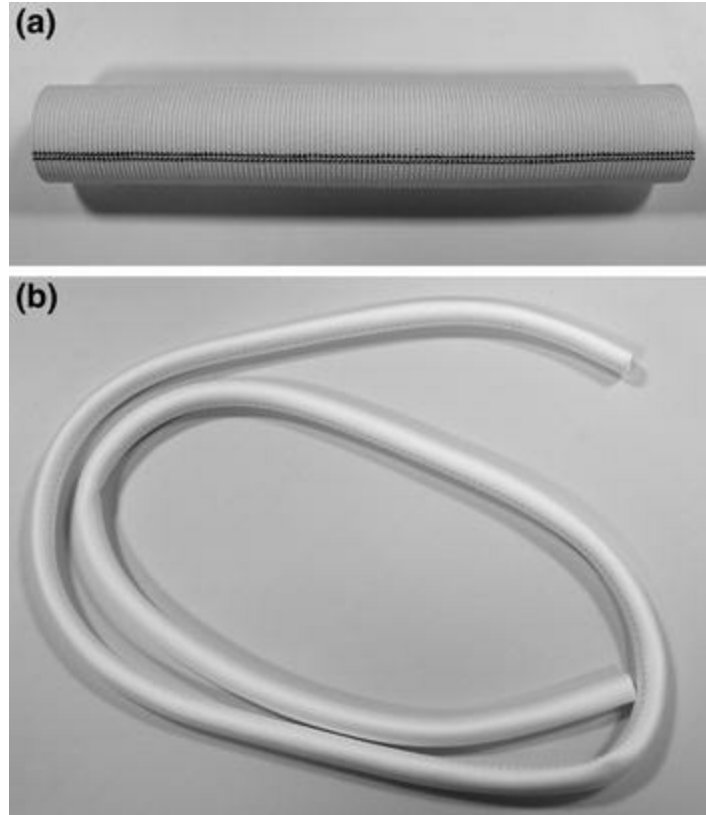


Fig. 17.1 Example vascular grafts. **a** 300 mm diameter aortic graft made from woven polyester. The graft has a crimped structure which helps to prevent collapse of the lumen. Both external and internal surfaces are textured (velour) which enhances integration into the surrounding tissues and promotes the adhesion and growth of endothelium on the luminal surface. **b** 6 mm expanded PTFE graft for femoral artery bypass

17.2.2 Complications and Failure Modes

Large diameter grafts are generally regarded as successful but problems arise with medium and small diameter prostheses. This is a significant issue since vessels of the leg (e.g. femoral artery circa 6 mm diameter) and the coronary arteries (circa 3 mm diameter) are commonly affected by atheroma.

Thrombosis is reported to be a complication in the early post-operative period but, in the medium- to long-term there is growth of a fibrous lining within the graft. This is called neointimal hyperplasia (NH) and is due to proliferation and migration of smooth muscle cells and increased production of extracellular matrix. NH can lead to a significant reduction of lumen diameter and loss of patency (becoming obstructed). Compliance mismatch between the natural vessel and the graft is believed to play a role due to both mechanical strain and wall shear stress (WSS) effects as described by

Salacinski et al. (2001). The sensitivity of the natural vessel to variations in WSS is discussed in Chap. 5. The most commonly used graft materials are, in general, stiffer than the natural vessel. In addition most grafts are secured to the host vessel using sutures. This damages the natural vessel wall and also introduces local stiffening. Computational fluid dynamic (CFD) studies of typical graft/vessel geometries have shown that the anastomotic sites (the sites of surgical joining of the two vessels) can result in altered WSS. Natural pulsatile changes in arterial diameter will also affect the WSS close to the stiffer anastomosis. Whilst, as discussed in Chap. 5, arteries respond to changes in WSS by a change in diameter, the diameter of the graft remains unchanged.

17.3 Vascular Stents

A vascular stent is an expandable tube which is inserted into an artery to correct a narrowing or support a weakness in the vessel wall. Stents are commonly used to improve flow in diseased coronary arteries but they are also used in the carotid, iliac, and femoral arteries. Stents can also be used in conjunction with a fabric graft (stented graft) which can be placed within the aorta, for example, to provide a strong repair for an aneurysm or, as will be described later, to introduce a heart valve into the aorta.

Here, we will focus on coronary stents. In the treatment of coronary artery stenosis, stenting provides a less invasive alternative to bypass surgery using a graft.

17.3.1 Balloon Angioplasty and Stent Deployment

Percutaneous Transluminal Angioplasty (PCTA) was first introduced in 1977 (Meier et al. 2003). This procedure involves the introduction of a catheter, via a thin guidewire, into the radial or femoral artery. The guidewire is advanced through the circulation to the coronary arteries under angiographic guidance with the aid of a radio-opaque contrast medium allowing the catheter to be positioned at the site of the occlusion. The end of the catheter carries a collapsed non-compliant balloon. This is aligned with the plaque and inflated with saline and contrast medium using a hand pump to carefully apply the pressure. The balloon displaces the plaque and restores the vessel lumen.

There are two major drawbacks to what at first appears to be a relatively

simple process. First, there is a risk of immediate elastic recoil of the vessel wall when the balloon is removed resulting in narrowing the lumen. Second, injury to the vessel wall caused by balloon inflation may lead to an adverse biological response involving the proliferation and migration of smooth muscle cells from the vessel media into the lumen and the deposition of extracellular matrix. This remodelling process is known as neointimal hyperplasia (NH). The magnitude of the biological response has been shown to be related to the degree of injury and may result in the gradual restenosis of the diseased vessel. Restenosis affects an estimated 40 % of cases within 3–6 months of ballooning (Dangas and Kuepper 2002).

Elastic recoil can be prevented by introducing a stent into the vessel via the balloon. Expansion of the stent (stent deployment) provides a scaffold to support the vessel wall maintaining patency. The first balloon-expandable stents were proposed by Palmaz et al. in (1985) and a range of different designs have been used in clinical practice since the 1990s and are now used by cardiologists across the world. More detail is available in a review by Iqbal et al. (2013). A catheter, balloon with stent and pump are shown in Fig. 17.2 and the balloon and stent are shown in greater detail in Figs. 17.3 and 17.4.



Fig. 17.2 PCTA system for the delivery of a coronary artery stent comprising; balloon-tipped catheter with non-compliant balloon and mounted stent and a hand pump for inflating the balloon. The same system without the stent can be used for PCTA alone



Fig. 17.3 Balloon and mounted stent are shown in greater detail prior to inflation

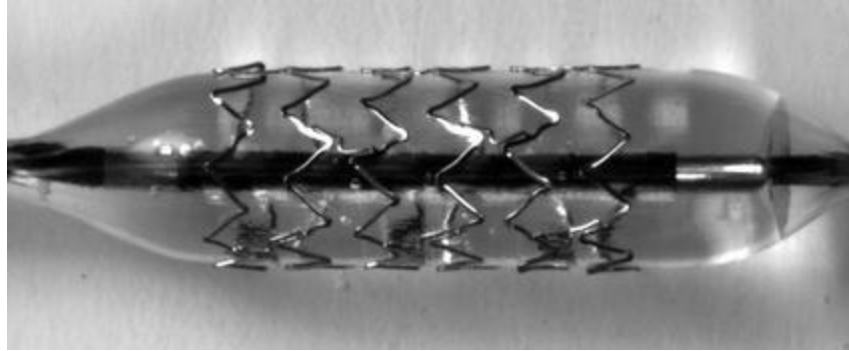


Fig. 17.4 Detail of the inflated balloon and expanded stent

An ideal stent should be flexible and have good radiographic trackability and radial strength, have low radial and longitudinal recoil and be able to be expanded symmetrically (reducing the likelihood of high local wall strain and deep injury to the vessel wall with local penetration of the stent struts).

Whilst NH remains the primary complication, stenting has been shown to halve the number of cases experiencing restenosis (from 40 % reported with ballooning alone to 25 %, Serruys et al. 1994). NH formation has been shown to be related to changes in stress and strain distribution in the artery wall due to the force of the deployed stent. Thicker struts offer better support to the arterial wall but are associated with increased neointimal response. This is thought to be due to the greater degree of injury imposed (Zahedmanesh and Lally 2001). There is a clear link between the magnitude of the NH response and the magnitude of stresses and strains during stent deployment as shown by Gunn et al. (2002).

17.3.2 Types of Stent

The first stents were manufactured from 316L stainless steel. 316L Stainless steel has the benefit of acceptable material properties with adequate corrosion-resistance and good biocompatibility but it has some limitations in terms of the thickness of strut needed to ensure adequate radio-opacity, and radial strength which can have a negative effect on the flexibility of the overall device. Recent designs use cobalt chromium alloy or, more recently still, platinum chromium alloy (Jorge and Dubois 2015), giving the required radial strength, improved flexibility and radio-opacity in designs with thinner struts. Despite the known risk of NH and restenosis, *bare-metal* stents (BES) are used in 15–20 % of procedures (Alfonso et al. 2014).

Drug-eluting stents (DES) offer a potential solution to the problem of NH. Restenosis can be significantly reduced or even prevented by local controlled release of an anti-proliferative drug. The drug is incorporated into a thin polymer carrier material coated onto a bare-metal stent (Nabil and Braunwald 2012).

Although clinical experience with DES indicates clear benefits in terms of reduced incidence of restenosis, it also reveals drawbacks. The mechanical impact of deploying the stent partially or completely removes the protective anti-thrombotic layer of endothelium in the vicinity of the stent. Reports show that, whilst mitigating against NH, the anti-proliferative drug also prevents re-endothelialisation of the stented segment. This can lead to late thrombosis (McFadden et al. 2004). Clinical guidelines recommend antiplatelet therapy is administered for 1 month after using a bare-metal stent but a period of more than 6 months is recommended for DES.

In addition to balloon-expandable stents self-expanding stents are also available. These are constructed from shape memory alloy, typically nitinol. Nitinol, an alloy of nickel and titanium, has unique properties; it has the ability to undergo deformation at one temperature and then return to its original, un-deformed shape when heated above its “transformation temperature”. This enables a stent to be introduced into the artery in its compact shape, constrained by a sheath. Removal of the sheath enables the stent to spring back to its expanded shape. The force generated by the expansion is sufficient to restore the lumen in a blocked vessel. More information on the properties of nitinol and the design of self-expanding stents can be found in Stoeckel et al. (2004).

17.3.3 The Future

Work is already under way to develop a fully resorbable stent. These are intended to perform the same mechanical scaffolding function of a traditional metal stent but for a controlled period of time. This offers the possibility that the natural vasomotor function of the vessel can be re-established (Tamburino et al. 2015). Polymers such as polylactic acid (this has the advantage of breaking down into a naturally occurring molecule—lactic acid) and metals such as magnesium are under consideration. Other novel target areas under consideration are methods to accelerate re-endothelialisation of the stented segment using growth factors or cells delivered on the stent.

17.4 Heart Valves

The heart contains four major valves. These maintain the flow of blood in the forward direction, opening and closing passively in response to pressure changes generated by cardiac contraction. Two valves (aortic and pulmonary) are located at the outflow of the major arteries (aorta and pulmonary trunk) leaving the left and right ventricles, respectively. The aortic and pulmonary valves are semi-lunar valves; they have three, thin, flexible, crescent-shaped leaflets which are strengthened by strong collagen cords. Two further valves (right and left atrioventricular (AV) valves) are located between the upper and lower chambers of the heart. These have a more complex structure; the leaflets are 'flap-like'. Strong cords of collagen spanning between the free edges of each leaflet and the walls of the ventricles act as 'guy-lines' tethering the leaflets and preventing them from turning inside out under the back pressure which is applied as the ventricle contracts.

17.4.1 Disease of Natural Valves

In the open position, healthy valves provide minimal resistance to forward flow. Closure is also very effective with little backflow or leakage. In contrast, diseased valves can result in major haemodynamic disturbances which cause increased workload for the heart. Valve disease has a number of potential underlying causes including congenital defects (present at birth), infection or age-related degeneration. More than 10 % of the population aged 70 or over have diseased valves. An introduction to valve disease and current treatment guidelines can be found in Morris et al. (2015). Whilst all valves in the heart can be affected by disease, in reality those in the left side of the heart (the aortic and left AV valves) are most frequently affected. This is related to the greater load experienced due to the pressure regime in the systemic circulation.

Valve disease can be categorised as;

- Stenotic—leaflets are stiff, restricting the open orifice and presenting increased resistance to forward flow. More energy must be expended by the heart to maintain forward flow.
- Regurgitant—the leaflets fail to close or leak allowing regurgitation (backflow of blood) as blood is able to flow back upstream the heart must work harder to maintain the same level of cardiac output.

- A combination of stenosis and regurgitation is also possible.

The *pressure difference (pressure gradient)* across the open valve provides a measure of stenosis whilst the *regurgitant fraction* (percentage of the stroke volume leaking back through the valve) provides a measure of leakage. Quantitative evaluation of valve haemodynamics can be made clinically using trans-oesophageal echocardiography (TOE-Chap. 9). Haemodynamic diagnostic markers of severe disease include a stenotic valve area $<1 \text{ cm}^2$ or a regurgitation fraction of $>50 \%$. Ultimately, for the individual, the physiological impact of valve failure will depend on the ability of the heart to adapt to the increasing workload. If the physiological impact becomes severe the diseased valve can be replaced by an artificial valve.

There are a number of requirements for a successful replacement valve. First and foremost, it must have adequate durability, i.e. withstand opening and closing 40 million times a year, ideally for the life-time of the patient. It must also have good haemodynamic characteristics including; a large orifice area to offer minimal resistance to forward flow, allow minimal backflow, create minimal flow disturbance and not cause regions of high shear stress (which could lead to blood cell damage, see Chap. 3). In addition, the materials used must be non-thrombogenic (i.e. not cause activation of the blood).

17.4.2 Types of Artificial Heart Valves

Two different types of replacement valves are available; mechanical valves which are made from man-made materials and biological (tissue) valves which are made from a combination of synthetic materials and chemically stabilised collagen-based animal tissues. A support structure and a fabric cuff, enabling the valve to be sutured in place within the heart are common features of both types of valve. More information on the range of designs and their evolution can be found in Gott et al. (2003).

Mechanical valves have one, or more commonly 2, moving components (occluder(s)) trapped within a rigid metal or pyrolytic carbon frame (housing), these are free to rotate in response to the changes in pressure field as the heart contracts and relaxes. The components of many of the current generation of mechanical valves are made from pyrolytic carbon, a material that is extremely durable and, importantly, does not cause blood clotting.

Biological valves are made from animal tissue supported on a frame (stented valves) or mounted in a conduit of synthetic fabric or fixed tissue (stentless valves). The tissue component has 3 flexible leaflets (formed from a natural pig aortic valve or fashioned from bovine pericardium, the sac of fibrous tissue that surrounds the heart). These tissues need to be treated with a chemical fixative agent to enhance their mechanical and biological durability. Issues relating to durability are discussed in more detail by Hofmans et al. (2008). Examples of valve models of different designs are shown in Fig. 17.5.

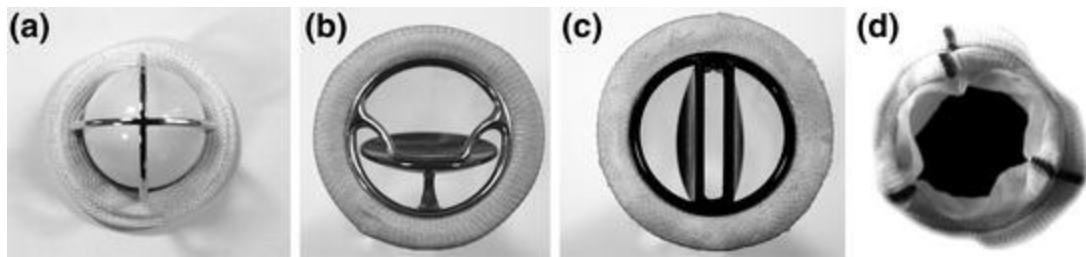


Fig. 17.5 Four different valve designs in the open configuration. **a** Caged ball mechanical valve with silicone ball and metal housing. **b** Tilting disc valve with single pyrolytic carbon occluder captured in a metal housing. **c** Bileaflet valve with two semi-circular pivoting pyrolytic carbon occluders. **d** Bioprosthetic valve, chemically stabilised porcine valve mounted on a fabric covered frame

Valve replacement, although now routine, is a major undertaking as it involves opening the heart; the damaged valve is excised and a suitable artificial valve is sutured in its place. The specific valve type is chosen based on factors such as patient age, and the ability to comply with anticoagulation treatment. Tissue valves are susceptible to calcification in the young, but in adults the expected durability of the most recent designs is in excess of 12 years. Mechanical valves are associated with haemodynamic disturbances which may increase the risk of thromboembolism.

Concerns about the high risks associated with surgery have driven the development of percutaneous (meaning ‘through the skin’) valve implantation. This more recently introduced procedure (currently only for aortic replacement) is also known as trans-catheter aortic valve implantation (TAVI). A review of TAVI and the current state of the art is provided by Collas et al. (2014). In TAVI valves tissue leaflets are mounted on an expandable wire stent and delivered into the aorta on a catheter. A number of different approaches can be used including introduction via the femoral artery in the thigh to the site of the damaged aortic valve. This procedure is guided

by fluoroscopy (Chap. 9). Stents are either balloon-expandable or self-expanding, and once correctly located, the stent is expanded by inflating a balloon on a catheter within the orifice or by removing a constraining sheath releasing the self-expanding stent.

17.4.3 Valve Performance

All replacement valves present some degree of obstruction to flow. From Fig. 17.6 which illustrates three different occluder configurations of mechanical valves, it can be seen that the early ball and cage design, first introduced in the 1960s, is much more obstructive than the tilting disc and bileaflet designs which are in current use. Whilst tissue valves should present less obstruction due to the central flow, the supporting frame and cover adds bulk to the design, limiting the size of the valve that can be implanted. For this reason, stentless valves have been introduced. Stentless valves lack a stiff supporting frame which means that they can only be implanted in the aortic position.

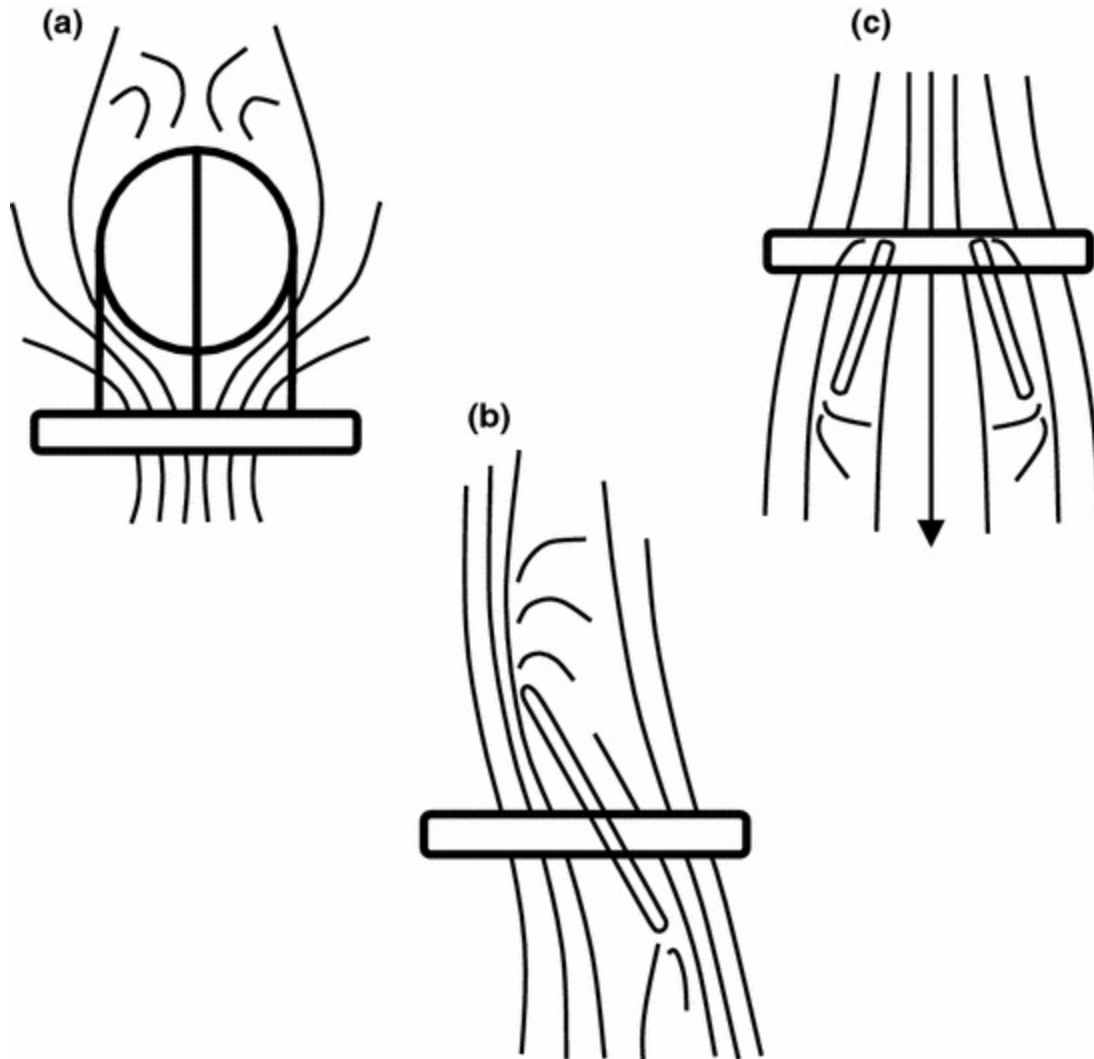


Fig. 17.6 Schema illustrating the primary flow paths through three different configurations of mechanical valve. **a** Ball and cage valve. Annular flow path around the occluder with flow disturbance at the apex of the cage. **b** Orifice of tilting disc valve is split into minor and major orifices with some recirculation in the wake of the disc. **c** Bileaflet valve has three approximately equal flow paths, presenting less disturbance to flow

All valves allow some regurgitation. This backflow has two components (see Fig. 17.7); the first is due to the sweeping action of the occluders or leaflets as they close. This is the closing volume. The second, the leakage volume, is due to flow through gaps in the closed valve. Both tissue and mechanical designs have small closing volumes. The highly flexible leaflets of tissue valves close tightly under backpressure, preventing backflow. In contrast, in mechanical valves blood is able to flow back through the gaps between the occluder and housing. Indeed, some degree of leakage is built

into the design specifications to prevent deposition of blood clot.

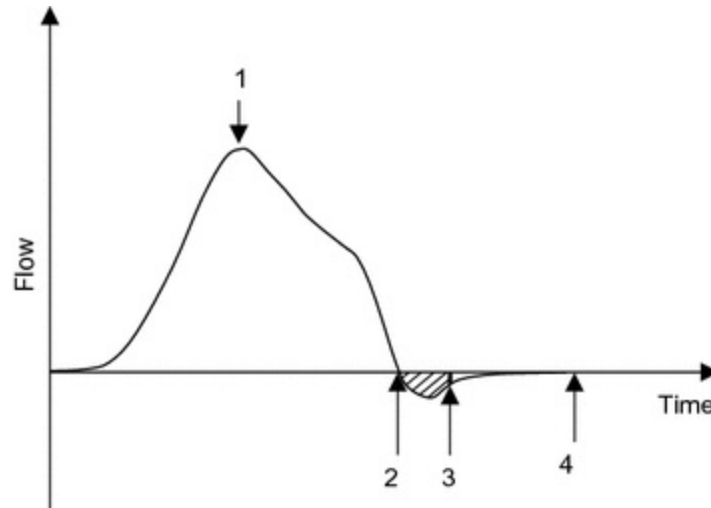


Fig. 17.7 Flow through a mechanical valve over the cardiac cycle. The period of forward flow (1) comes to an end (2) and, as the occluder closes a volume of fluid is swept back (2–3). This is the closing volume which for a given model, is related to valve size. As the occluder comes to rest within the housing a small volume of blood will continue to leak through the gaps between the occluder and the housing. This provides an important wash out action to prevent accumulation of thrombus and is particularly important for the hinge regions of bileaflet valves

Valve performance can be evaluated in the laboratory using hydrodynamic test rigs, i.e. a pulse duplicator/cardiac flow simulator. There are many different pulse duplicator designs of different levels of sophistication, and their aim is to mimic the flow regime in the left side of the heart. Routine measurements performed include the mean pressure difference across the open valve during the phase of forward flow and the amount of leakage associated with valve closure/when the valve is closed.

Calculation of the effective orifice area (EOA) is used to provide an indication of the degree of obstruction presented by a specific valve (Yoganathan et al. 1984).

$$EOA = \frac{Q_{rms}}{51.6 \sqrt{\overline{\Delta P}}} \quad (17.1)$$

where Q_{rms} is the root mean square flow rate in cm^3s^{-1} over the cardiac cycle and $\overline{\Delta P}$ is the mean pressure difference over the open valve during forward flow.

These are useful measures but both the degree of obstruction and the amount of leakage are important determinants of the impact of valve function on the heart, i.e. the load presented by the valve. Whilst it may be

advantageous to implant the valve with the largest possible orifice in order to minimise the pressure difference, for mechanical valves, the degree of regurgitation increases with valve size as both the closing volume and the leakage volume increase with valve size. Calculation of the valve's energy loss can be a useful indicator of valve performance as it represents the combined effect of pressure difference and leakage. Energy loss is a well-established concept in engineering. For an artificial heart valve the total energy loss is can be calculated as the sum of the energy losses in the forward and regurgitant energy losses.

$$\text{Energy consumption/unit time} = Q_f(\overline{\Delta P_f} + \overline{\Delta P_{\text{reg}}}\cdot\text{RF}) \quad (17.2)$$

where, Q_f is the forward flow, $\overline{\Delta P_f}$ is the pressure drop across the valve during forward flow, $\overline{\Delta P_{\text{reg}}}$ is the pressure drop through the closed valve and RF is the regurgitant fraction.

The theory behind the concept of energy loss and its application to both natural and replacement heart valves has been reviewed by Akins et al. (2008).

In vitro techniques such as flow visualisation, laser Doppler anemometry (LDA), and particle image velocimetry (PIV) can be used to characterise the flow field downstream of the valve (Kini et al. 2001; Akutsu and Fukuda 2005). Flow velocities can be used to derive information on the shear field, providing insight into the likelihood of blood cell damage and the relative thrombogenic potential of different designs.

In vitro testing can be expensive in terms of both time and equipment and there is increasing reliance by valve designers on CFD analyses for evaluation of valve designs. The potential benefits are clear; in vitro analyses are expensive in terms of both time and equipment and an accurate physical prototype is needed each time a design is modified, whereas modifications are relatively simple to implement in a computational model. However, whilst simple models (e.g. valve open/closed) are routine to run, complex dynamic simulations, particularly for the flexible leaflets of tissue valves, remain challenging with current methodology (see Tio et al. (2013) for detail).

Durability is very important for these safety critical devices. A basic evaluation of durability can be carried out in the laboratory but it is important to note that these mechanical tests do not address the impact of the biological

environment. It is impractical to run tests in real time and accelerated rates of up to 20 Hz are used. Standard tests are usually run for the equivalent of ten years which equates to 8 months in vitro testing (ISO Cardiac valve standard; ISO 5840-2:2015). Valve components are examined for signs of fracture and wear (mechanical valves) or tissue abrasion and tearing (tissue valves).

17.4.4 Complications and Failure Modes

Common failure modes for biological valves are associated with leaflet tearing and calcification (which may in turn also lead to tearing). Significant improvements have been made as each new generation of valve emerges and reports of early failures due to poor leaflet mounting techniques, leaflet contact with the stent resulting in abrasion and stent fractures are no longer a concern. There are also new tissue treatments which slow or prevent calcification leading to improved durability. Nevertheless as it is fixed (in a similar way in which animal skins are preserved as leather) the tissue is unable to regenerate, and with time the collagen is subject to fatigue.

Similarly, improvements in the design of mechanical valves mean that failures are very rare. The major complications are associated with the thrombogenic potential of these valves and the need to carefully monitor and control anticoagulant therapy.

At present the use of TAVI valves is restricted to patients for whom open heart surgery is considered too risky. Reported issues for TAVI are related to deployment of the device and include conduction disturbances due to compression of the SV node by the stent and potential dislodgement of plaque or calcification as the catheter carrying the valve is navigated through the circulation. Their long-term durability is not yet known.

17.4.5 The Future

If the long-term durability of percutaneous valves can be established these valves are likely to become the treatment of choice for a wider population of patients with aortic valve disease (Hamm et al. 2015). Percutaneous valves are being developed for the mitral position (De Backer et al. 2014). The use of new polymers is being investigated for valve leaflets. In parallel, tissue engineering solutions are being explored. Advances in CFD methodology will continue to be incorporated into evaluation tools helping to smooth the pathway to improvement in designs. Work on developing a tissue engineering

solution is underway but as yet there is no immediate prospect for this (Mack 2014).

17.5 Pacemakers

Cardiac pacemakers are active medical devices which are used to correct problems arising from arrhythmias (abnormalities of the heart rhythm) or conduction defects. Most commonly a pacemaker is used to treat an abnormally slow heart rate (bradycardia).

In a healthy individual, the normal rhythmic contraction of the heart (sinus rhythm) is maintained by action potentials originating from natural pacemaker cells (specialised myocardial cells located in the sinoatrial node in the wall of the right atrium). The normal activation sequence associated with sinus rhythm, and conduction abnormalities leading to arrhythmias are discussed in Chap. 6. Failure of sinus rhythm may compromise cardiac output and, depending on its exact nature, the consequences of arrhythmia may be mild or life-threatening. The primary purpose of a pacemaker is to regulate the beating of the heart which in turn improves cardiac output and ameliorates symptoms. Typical symptoms include; fainting, light-headedness, fatigue, and breathlessness.

The simple principle behind the use of a cardiac pacemaker, reported by John Alexander McWilliam as early as 1889, is that the heart can be stimulated by applying a short, controlled, burst of electrical current and that a chosen rhythm can be maintained by repeating this process about once every second (McWilliam 1899).

The first cardiac pacemakers, introduced in the 1950s, were external devices with an electrical current applied through electrodes on the surface of the patient's chest. Whilst this was effective in bringing about cardiac contraction, the level of current which had to be used with these early devices was sufficiently high to cause pain to the patient and could also result in local burns to the skin beneath the electrodes. The solution to this problem was to apply the current to the surface of the heart using implantable electrodes. By applying the current directly to the surface of the heart only a few milliamps are required and furthermore this can be supplied by a battery. The first implantable cardiac pacemaker was used in 1958 (Jeffrey and Parsonnet 1998). Whilst these were effective, implantation of these early devices required major surgery. In the intervening years, there have been numerous

developments in terms of both technology and implantation techniques but the basic principles behind the therapy remain unchanged.

17.5.1 Components of a Pacemaker

Pacemakers have two basic elements; a pulse generator and a lead system.

The *pulse generator* contains electronic circuit for sensing, pacing and communication and, in an implantable device, the bulk of the volume of this module may be occupied by the battery.

The lead system transmits pulses from the generator to the heart and, depending on the type of device, may also monitor the electrical activity of the heart. The lead is fundamentally a flexible conductive core (electrode) insulated, except at the tip where it is in electrical contact with the heart, by a non-conductive coating. It is important that the coating is non-toxic and remains both mechanically and chemically stable within the relatively hostile environment found within the body. Medical grade silicone is often used for this purpose. The electrode must also be made from a stable, non-toxic material and is usually manufactured from corrosion-resistant wire (i.e. stainless steel, platinum, silver, titanium, or alloys) which is coiled rather than straight to increase its flexibility and protect against fatigue due to the motion of the heart.

The current produced by the pulse generator, after passing through the myocardium, must return to the pulse generator completing the conduction path. This is normally achieved in one of two ways depending whether a single or dual lead conductor is used. For single conductors, the metal housing of the pulse generator acts as the second electrode and the current is conducted through the patient's tissues to complete the circuit. Dual conductor systems have both active and return conductors encased within the lead system.

17.5.2 Types of Pacemaker

There are three types of devices: external, transcutaneous, and implantable.

External and transcutaneous devices are used temporarily to control the heart rate during surgery, if the arrhythmia is expected to resolve (during recovery from heart surgery, or from a heart attack, for example) or as a 'bridge' until a permanent device can be implanted.

The key features of each type are summarised below;

In *external pacemakers* the pulse generator remains outside the body but the lead between the pulse generator and the myocardium is either placed in contact with the surface of the heart (for open heart surgery) or inserted via the venous system into the right chamber of the heart.

Transcutaneous pacemakers are also known as external non-invasive pacemakers. These sit entirely outside the body. The electrical stimulation from the pulse generator is passed through two large adhesive gel electrodes which are applied to the skin on front and back of the chest. They have the advantage that they are quick and easy to apply making this an appropriate emergency treatment. However, as the pacing energy required is relatively high this method of stimulation may be uncomfortable for the patient and may also lead to severe twitching in skeletal muscles in the vicinity of electrode placement.

Implantable pacemakers. Most pacemakers are implanted and the entire device is located inside the body. The pulse generator is placed into a surgically created pocket under the skin on one side of the chest below the clavicle (collar bone) and, under X-ray guidance (fluoroscopy), the lead system is advanced, through the venous system travelling from the subclavian vein (the principal vein draining the arm, accessed below the clavicle) to the cephalic vein on the surface of the heart, and via this to the right atrium or ventricle. Placement of a single lead pacemaker with a ventricular pacing lead is illustrated schematically in Fig. 17.8.

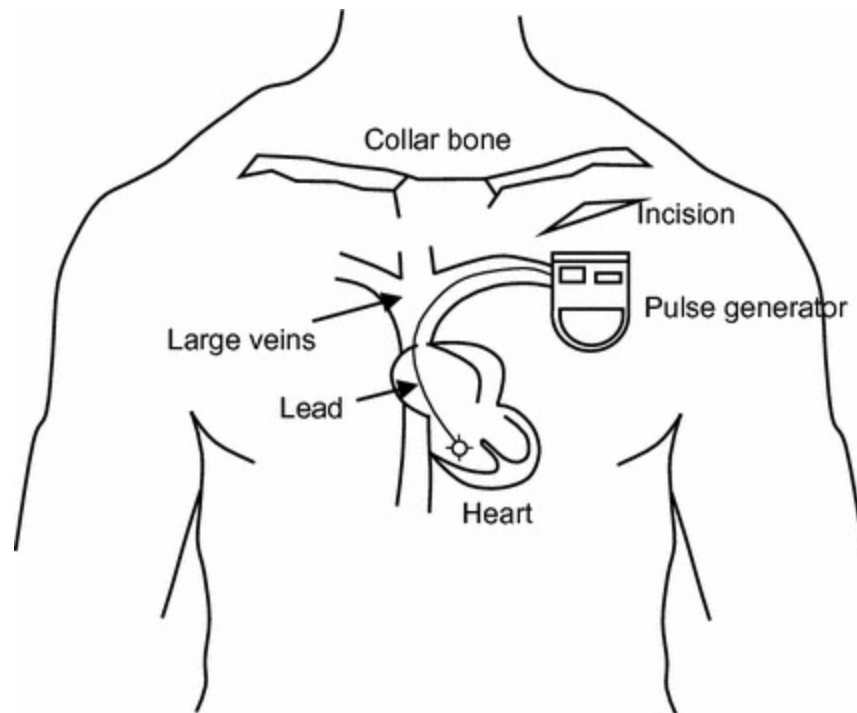


Fig. 17.8 Schema showing main components of a conventional (single chamber) pacemaker system with ventricular pacing lead and the relative anatomical location of the main components

17.5.3 Permanent Pacemakers

Implantable pacemakers are intended for long-term use and are thus regarded as permanent implants.

There are 3 types of permanent devices which are categorised by the chambers of the heart stimulated:

Conventional (single chamber) pacemakers have a single lead which stimulates a single cardiac chamber (either the right atrium or right ventricle) and the stimulus is transmitted to the remaining chambers via the myocardium.

Dual chamber pacemakers have two leads (typically, one to the right atrium and one to the right ventricle). Dual pacing is more likely to restore the natural rhythm as it more closely replicates the natural co-ordination of the upper and lower chambers.

Triple chamber pacemakers have three leads, typically stimulating the right atrium, the right ventricle and the left ventricle. As both ventricles are simulated this is commonly known as biventricular or simultaneous pacing. This is specifically used for patients whose hearts are failing with the aim of ‘resynchronising’ the ventricles and improving the efficiency of contraction.

Whilst some patients benefit from this therapy placement of the leads is complex and the devices are expensive.

17.5.4 Operation Modes

There are three basic pacemaker operating modes; asynchronous, demand and rate modulated.

Asynchronous pacing; the simplest pacemakers produce a continuous stream of pulses at about 70 bpm. These fixed rate devices are unable to synchronise with naturally occurring beats. This may not be an issue when a patient has suffered a complete heart block but in others it may compromise cardiac performance.

Demand pacing; operating in demand mode the pacemaker records the ECG produced by the heart and produces an output based on this. The trigger can come from the atrium (*P* wave of the ECG) or the ventricle (*R* wave—triggered). Depending on the particular pacemaker, output may only be produced in the absence of an *R* wave or an output is for every *R* wave replacing any missing *R* waves.

Rate modulation; here the pacemaker has sensors which can detect changes in the patient's physical activity and the rate is automatically adjusted to meet the body's needs.

Most pacemakers are programmable in terms of mode, pacing rate, pulse amplitude and duration, upper pacing rate, rate changes that will occur under exercise condition, and so on. As unnecessary pacing can be detrimental to the heart, there is increasing focus on giving just the right amount of pacing. Many also incorporate microprocessors that store diagnostic information which can then be downloaded by the clinician. Communication between the device and a programmer or receiver on the surface of the skin is achieved through telemetry (electromagnetic coupling); this may also allow the pacemaker status to be monitored at routine intervals over the internet or by telephone.

17.5.5 Power Supply

Whilst a number of solutions have been offered to providing durable battery power, including the use of thermoelectric batteries powered by plutonium-238 (Parsonnet 2007), current implantable systems are usually powered by light-weight lithium/carbide mono-fluoride batteries. If the battery requires

replacement the whole pulse generator is replaced in a small operation and the leads are transferred to the new device.

17.5.6 Complications and Failure Modes

These devices are generally reliable. A fail-safe mechanism can be incorporated in the design to ensure that the device reverts to a simple mode of operation if a fault occurs. The majority of problems reported relate to leads with broken wires, poor connections or insulation failures resulting in intermittent or continuous interruption of the sensing or pacing. There is also a risk of perforation of the heart wall by a broken lead. Whilst it is a relatively simple process to replace the generator with its battery, the leads become integrated into the patient's tissues and are thus much more complex and potentially risky to remove. For this reason, damaged leads are often disconnected from the generator, capped, and left within the body when replacement leads are implanted. In common with implants of all types infection can be an issue and, if this occurs, the generator and leads must be removed.

Pacemakers can be susceptible to electromagnetic interference from other medical equipment including MRI systems and from mobile phones and security checking devices. This is gradually being addressed; for example, significant interference from mobile phones is no longer considered an issue for the latest models. Manufacturers now offer MR-compatible devices but, as yet, MR scanning protocols must be carefully tailored for these patients.

17.5.7 The Future

The immediate focus is on designs with lower power demands, better lead construction, novel pacing algorithms and improving rate responsiveness using input data from a wider range of physiological sensors. Future devices will benefit from technology being developed for mobile phones and laptops.

Leadless pacemakers are now approved for use in Europe and are in clinical trials within the USA (Sperzel et al. 2015). These tiny devices (dimensions of a few mm) can be introduced into the chest via a catheter and fixed to the surface of the heart by a tiny screw. Another solution to the challenge of providing leadless devices includes the design of an implantable generator which produces acoustic energy at ultrasound frequencies. This is directed to a receiver delivered to the ventricle wall by a catheter introduced

in the aorta. The receiver is able to convert the acoustic signal into an electrical impulse thus producing a pacing pulse.

17.6 Device Regulation

The majority of cardiovascular devices, including those discussed above, are safety critical devices; failure of such a device carries a significant risk of harm or even death for the patient. Whilst absolute safety is impossible to guarantee, procedures are needed to ensure that the risk of harm is monitored carefully and minimised. Complex regulatory frameworks are in place within the USA (Food and Drug Administration—FDA) and across Europe through the incorporation of the EU Medical Devices Directives into national law in each EU member state. For countries outside these systems (particularly developing countries) the World Health Organisation World Health Organisation has published a document ‘Medical Device Regulations Global Overview and Guiding Principles’ outlining a common framework and aims to move towards Global Harmonization.

The underpinning principles of device regulation are to,

- eliminate or reduce risks as far as possible by incorporating safety considerations into both the design and construction of the device,
- take adequate protection measures to ensure safety, and
- ensure that the device users are informed of residual risks through information presented with the device (directions for use) and thorough training programmes.

17.6.1 Device Classification

Device classification determines the level of assessment that is required and definition of the intended purpose is critical.

Devices are classified through;

- the intended duration of contact with the patient since the longer the contact period the greater the potential for harm. Thus a device that is in continuous use is considered to have a higher risk of harm than a device which is only used for a few hours.
- the degree of invasiveness; implants are categorised as high risk devices

since if they fail it is not a simple task to remove them.

- anatomical site; failure of a vascular graft will be more immediately harmful than a that of a prosthetic joint for example.
- active or non-active device with the expectation that active devices offer higher risk than passive devices. However, this may not be the case and depends on the exact failure mode. For example fracture of a heart valve may result in heart failure whilst failure of a pacemaker to respond to demand might not be immediately life-threatening.

17.6.2 Possibilities for the Future

Developers of medical devices have a dilemma when proposing a new device do they create a novel design and face the major regulatory challenge or build a ‘me too’ device with small modifications to an existing clinical implant? The advent of low-cost 3D printing and the potential for on-site manufacture of patient tailored devices will present a similar dilemma for the regulators. How can quality and safety be ensured?

References

Akins CW, Travis B, Yoganathan AP. Energy loss for evaluating heart valve performance. *J Thorac Cardiovasc Sur.* 2008;136:820–33.

[\[CrossRef\]](#)

Akutsu T, Fukuda T. Time-resolved particle image velocimetry and laser Doppler anemometry study of the turbulent flow field of bileaflet mechanical mitral prostheses. *J Artif Organs.* 2005;8(3):171–83.

[\[CrossRef\]](#)[\[PubMed\]](#)

Alfonso F, Byrne RA, Rivero F, Kastrati A. Current treatment of in-stent restenosis. *J Am Coll Cardiol.* 2014;63(24):2659–73.

[\[CrossRef\]](#)[\[PubMed\]](#)

Collas V, Philipsen T, Rodrigus I, Vrints C, Paelinck BP, Bosmans J. Transcatheter aortic valve implantation: review and current state of the art. *EMJ Int Cardiol.* 2014;1:52–61.

Dangas G, Kuepper F. Restenosis: Repeat narrowing of a coronary artery prevention and treatment. *Circulation.* 2002;105(22):2586–7.

[\[CrossRef\]](#)[\[PubMed\]](#)

De Backer O, Piazza N, Banai S, Lutter G, Maisano F, Herrmann HC, Franzen OW, Søndergaard L. Percutaneous trans-catheter mitral valve replacement. An overview of devices in preclinical and early clinical evaluation. *Circ Cardiovasc Interv.* 2014;7:400–409.

Gott VL, Aljeo DE, Cameron DE. Mechanical heart valves: 50 years of evolution. *Ann Thorac Surg*. 2003;6:S2230–9.

[\[CrossRef\]](#)

Gunn J, Arnold N, Chan L, Shepherd L, Cumberland DC, Crossman DC. Coronary artery stretch versus deep injury in the development of in-stent neointima. *Heart*. 2002;88(4):401–5.

[\[CrossRef\]](#)[\[PubMed\]](#)[\[PubMedCentral\]](#)

Hamm CW, Arsalan M, Mack MJ. The future of trans-catheter aortic valve implantation. *W Eur Heart J*. 2015;37(10):803–10.

[\[CrossRef\]](#)

Hoffmans G, Lutter G, Cremmer J. Durability of bioprosthetic cardiac valves. *Deutsches Arzteblatt Int*. 2008;105(8):143–8.

Iqbal J, Gunn J, Serruys PW. Coronary stents: historical development, current status and future directions. *Br Me Bull*. 2013;106(1):193–211.

[\[CrossRef\]](#)

ISO 5840-2:2015 Cardiovascular valve prostheses—Part 2: Surgically implanted heart valve substitutes.

Jeffery K, Parsonnet V. Cardiac pacing 1960–1985. *Circulation*. 1998;97(19):1978–91.

[\[CrossRef\]](#)

Jorge C, Dubois C. Clinical utility of platinum chromium bare-metal stents in coronary heart disease. *Med Dev Evid Res*. 2015;8:359–67.

Kini V, Bachmann C, Fontaine A, Deutsch S, Tarbell JM. Integrating particle image velocimetry and laser Doppler velocimetry measurements of the regurgitant flow field past mechanical heart valves. *Artif Organs*. 2001;25(2):136–45.

[\[CrossRef\]](#)[\[PubMed\]](#)

Mack M. Progress toward tissue-engineered heart valves. *J Am Coll Cardiol*. 2014;63(13):1330–1.

[\[CrossRef\]](#)[\[PubMed\]](#)

McFadden EP, Stabile E, Regar E, Cheneau E, Ong AT, Kinnaird T, Suddath WO, Weissman NJ, Torguson R, Kent KM, Pichard AD, Satler LF, Waksman R, Serruys PW. Late thrombosis in drug-eluting coronary stents after discontinuation of antiplatelet therapy. *Lancet*. 2004;364(444):1519–21.

[\[CrossRef\]](#)[\[PubMed\]](#)

McWilliam JA. Electrical stimulation of the heart in man. *Br Med J* 1899;1(1468):348–50.

Meier B, Bachmann D, Lüscher T. 25 years of coronary angioplasty: almost a fairy tale. *Lancet Feb* 2003;361(9356):527.

Morris P, Warriner D, Morton A. Cardiovascular medicine. JP medical. 2015. ISBN 978-1-907816-82-6 (Chapter 7: Valvular Heart Disease).

Nabil EG, Braunwald EA. A tale of coronary artery disease and myocardial infarction. *N Engl J Med*.

2012;366(1):54–63.

[\[CrossRef\]](#)

Palmaz JC, Sibbitt RR, Reuter SR, Rice WJ. Expandable intraluminal graft: a preliminary study. *Radiology*. 1985;156(1):73–7.

[\[CrossRef\]](#)[\[PubMed\]](#)

Parsonnet V. A lifetime pacemaker revisited. *N Engl J Med*. 2007;357:2638–9.

[\[CrossRef\]](#)[\[PubMed\]](#)

Salacinski HJ, Goldner S, Giudiceandrea A, Hamilton G, Seifalian AM, Edwards A, Carson RJ. The mechanical behaviour of vascular grafts: a review. *J Biomater Appl*. 2001;15(3):241–78.

[\[CrossRef\]](#)[\[PubMed\]](#)

Serruys PW, de Jaegere P, Kiemeneij F, Macaya C, Rutsch W, Heyndrickx G, Emanuelsson H, Marco J, Legrand V, Materne P, Belardi J, Sigwart U, Colombo A, Goy JJ, van den Heuvel P, Delcan J, Morel M-A. A comparison of balloon-expandable-stent implantation with balloon angioplasty in patients with coronary artery disease. *N Engl J Med*. 1994;331:489–95.

[\[CrossRef\]](#)[\[PubMed\]](#)

Sperzel J, Burri H, Gras D, Tjong FVY, Knops RE, Hindricks G, Steinwender C, Defaye P. State of the art leadless pacing. *Europace*. 2015;17:1508–13.

[\[CrossRef\]](#)[\[PubMed\]](#)[\[PubMedCentral\]](#)

Stoeckel D, Pelton A, Duerig T. Self-expanding nitinol stents: material and design considerations. *Eur Radiol*. 2004;14(2):292–301.

[\[CrossRef\]](#)[\[PubMed\]](#)

Tamburino C, Latib A, van Geuns RJ, Sabate M, Mehilli J, Gori T, Achenbach S, Alvarez MP, Nef H, Lesiak M, Di Mario C, Colombo A, Naber CK, Caramanno G, Capranzano P, Brugaletta S, Geraci S, Araszkievicz A, Mattesini A, Pyxaras SA, Rzeszutko L, Depukat R, Diletti R, Boone E, Capodanno D, Dudek D. Contemporary practice and technical aspects in coronary intervention with resorbable scaffolds. A European perspective. *Eurointervention*. 2015;10:1–16.

[\[CrossRef\]](#)

Tio FO, Votta E, Le T B, Stevanella M, Fusini L, Caiani EG, Redaelli A, Sotiropoulos F. Toward patient-specific simulations of cardiac valves: state-of-the-art and future directions. *J Biomech*. 2013;46(2):217–228.

World Health Organisation 2003. Medical device regulations global overview and guiding principles. 2003. ISBN 92 4 154618 2.

Yoganathan AP, Chaux A, Gray RJ, Woo Y-R, DeRobertis M, Williams FP, Matloff JM. Bileaflet, tilting disc and porcine aortic valve substitutes: in vitro hydrodynamic characteristics. *JACC*. 1984;3(2):313–20.

[\[CrossRef\]](#)[\[PubMed\]](#)

Zahedmanesh H, Lally C. Determination of the influence of stent strut thickness using the finite element method: implications for vascular injury and in stent restenosis. *Med Biol Eng Comput*. 2001;47(4):385–93.

[\[CrossRef\]](#)

Appendix A: Questions

This chapter contains questions which the reader may find useful in preparing for exams. Teachers may also find these questions useful as the basis for setting exam questions. The questions are based on the text in the book. There are 3 types of questions, multiple-choice questions (MCQs), short-answer questions (SAQs) and long-answer questions (LAQs). The answers to the MCQs are provided in a list at the end of this chapter. A typical exam might be 2 h long with 30 min MCQs, 30 min SAQs and 60 min LAQs.

Multiple-choice questions (MCQs) . These consist of a statement followed by 5 choices which are true or false. The reader should select the statements which are true. There is at least 1 true statement, with a maximum of 5 statements true. For example:

Question 1. Concerning red cells.

- (a) These have a biconcave shape.
- (b) These are spherical in shape.
- (c) Their function is concerned with immune defence.
- (d) Their function is the transport of oxygen from lungs to tissues.
- (e) Have an effective diameter of 5.5 mm.

Answer is: a, d

As a rough guide an exam might have 20 MCQs which must be completed in 30 min.

Short-answer questions . These consist of a short question. The answer typically should be less than half a page of A4. It is acceptable to include simple diagrams. These typically might take 7–8 min to complete. An exam might require the answering of 4 short-answer questions from a choice of 8 in 30 min.

Long-answer questions . These are essay questions which typically would require a 2–3 page answer including simple diagrams as necessary. These typically take 30 min to complete. An exam might require answering 2 long-

answer questions from a choice of 6 in 1 h.

Chapter 1 Questions; Introduction to Solid and Fluid Mechanics

Chapter 1 MCQs

1. A solid:
 - (a) is characterised by viscosity and shear rate.
 - (b) continually deforms under an applied shear.
 - (c) will flow to assume the shape of the container.
 - (d) will sustain an applied shear force.
 - (e) always has a density of 1025 kg/m^3 .

2. The Young's modulus:
 - (a) is measured using a tensile testing system.
 - (b) is a measure of elasticity.
 - (c) is the ratio of tension divided by area.
 - (d) is a measure of viscosity.
 - (e) is the ratio of stress divided by strain.

3. The Poisson ratio:

- (a) has a value of 0.7 for incompressible materials.
- (b) is the ratio of flow rate to velocity.
- (c) has a value of 0.5 for most soft biological tissues.
- (d) is the ratio of the fractional change in lengths in z and x,y directions.
- (e) is relevant for fluids.

4. Which of the following is not a modulus of mechanical behaviour:

- (a) Young's modulus.
- (b) Bulk modulus.
- (c) Shear modulus.
- (d) Poisson ratio.
- (e) density.

5. A viscoelastic material:

- (a) has linear stress–strain behaviour.
- (b) may be described by an elastic modulus and a viscosity.
- (c) continually deforms under an applied shear force.

(d) has a time lag between the applied stress and the resulting strain.

(e) has no time lag between the applied stress and the resulting strain.

6. For an isotropic linear elastic material with a Poisson ratio of 0.5:

(a) the shear modulus is 3 times the elastic modulus.

(b) the shear modulus is 9 times the elastic modulus.

(c) the Poisson ratio is 0.7.

(d) the mechanical behaviour is different for different directions.

(e) there is no time lag between the applied stress and the resulting strain.

7. A fluid:

(a) is a substance which changes shape while shear is applied but returns to its original shape when the shear is withdrawn.

(b) is a substance which continually deforms under an applied shear.

(c) is characterised by density and viscosity.

(d) is characterised by elastic modulus and density.

(e) is characterised by magnetic moment and elastic modulus.

8. Hydrostatic pressure:

- (a) is the pressure in a fluid arising as a result of the weight of the fluid.
- (b) is the pressure in a fluid arising as a result of the volume of the fluid.
- (c) is equal to (elastic modulus) \times (density) \times (depth) $E\rho d$.
- (d) is equal to (gravitational constant) \times (density) \times (depth) $g\rho d$.
- (e) is equal to (gravitational constant) \times (mass) \times (depth) gmd .

9. In a moving fluid:

- (a) a fixed object such as a wall will give rise to change in velocity with distance from the wall.
- (b) a fixed object such as a wall has no effect on local velocity.
- (c) the velocity at every point in the fluid is the same.
- (d) the shear at every point in the fluid is the same.
- (e) the fluid flows as a result of a pressure gradient within the fluid.

10. Which of the following is true for viscosity:

- (a) there is an upper limit to the value of viscosity which a fluid can hold of 400 Pa.s.
- (b) pitch is a fluid with a viscosity value 2×10^{11} that of water.
- (c) viscosity is a measure of the resistance of the fluid to deformation by shear stress.
- (d) there is a lower limit to the value of viscosity which a fluid can hold of 0.001 Pa.s.
- (e) blood has a viscosity 3–4 times that of water.

11. Which of the following is true for Poiseuille flow:

- (a) the velocity profile is parabolic.
- (b) the resistance to flow is inversely proportional to diameter to the fourth power.
- (c) concerns flow of a fluid in a tube with a square cross section.
- (d) the resistance to flow is inversely proportional to radius to the third power.
- (e) the velocity profile is described by a cube law.

12. The inlet length:

- (a) is the distance from the entrance of a pipe at which the flow

becomes turbulent.

- (b) is the diameter of the pipe at the entrance.
- (c) is the diameter of the pipe divided by the peak velocity.
- (d) is the distance from the entrance of a pipe at which flow has a parabolic velocity profile for steady flow.
- (e) is the distance after which flow is fully developed.

13. Concerning the boundary layer:

- (a) it separates regions of turbulent flow from regions of laminar flow.
- (b) it separates regions of flow dominated by viscous forces from regions where flow is dominated by inertial forces.
- (c) it is absent for fully developed flow.
- (d) it separates laminar from non-laminar flow.
- (e) it separates regions of flow with $Re < 2300$ from areas with $Re > 2600$.

14. Reynolds number of flow of a fluid in a cylinder:

- (a) is proportional to diameter.

- (b) is proportional to viscosity.
- (c) is the ratio of inertial forces to viscous forces.
- (d) is the ratio of viscous forces to inertial forces.
- (e) is inversely proportional to velocity.

15. Turbulent flow:

- (a) does not occur in low viscosity fluids.
- (b) is associated with movement of fluid elements along well defined pathways.
- (c) usually occurs at Re less than about 2300.
- (d) is associated with movement of fluid elements along erratic pathways.
- (e) usually occurs at Re greater than about 2300.

16. Concerning a time-varying pressure gradient for flow in a cylinder:

- (a) the pressure lags the flow by a certain time period due to the inertia of the fluid.
- (b) the flow is steady.
- (c) the flow lags the pressure by a certain time period due to the

inertia of the fluid.

(d) in a cylinder the velocity profile is always parabolic.

(e) the flow is time-varying.

17. Steady flow of a Newtonian fluid in a long straight tube with stiff walls:

(a) has a velocity profile skewed to one wall.

(b) is associated with no change in velocity with time.

(c) has a parabolic velocity profile.

(d) is associated with huge changes in velocity with time.

(e) has maximum velocity in the centre of the vessel.

Chapter 1 SAQs

1. Describe the key differences between a solid and a fluid.
2. What is Young's modulus?
3. What is meant by viscoelasticity?
4. Describe why collagen leads to biological materials having a nonlinear stress–strain behaviour.
5. What does the Poisson ratio refer to?

6. What is hydrostatic pressure?
7. Estimate (with working) the head-toe pressure difference in the cardiovascular system for a person of height 1.4 m ($g = 9.81 \text{ m.s}^{-2}$, density of blood = 1025 kg m^{-3}).
8. Illustrate stress–strain behaviour for the following fluids; Newtonian, shear-thinning, shear-thickening.
9. Describe a simple way of measuring fluid viscosity using a funnel.
10. Describe flow states and their relationship to Reynolds number.
11. What is Bernoulli's principle?

Chapter 1 LAQs

1. Describe and define Young's modulus and its measurement for a section of soft tissue such as arterial wall; illustrate the answer with typical stress–strain curves
 2. Describe viscoelasticity and what methods may be used to characterise viscoelastic behaviour
 3. Describe viscosity and how it might be measured for a typical fluid to give data on viscosity-shear rate behaviour. Illustrate with data for different types of viscous behaviour.
 4. Describe flow of a Newtonian fluid in a rigid cylinder discussing the relation between pressure and flow rate, resistance, velocity profile, and steady and unsteady flow.
-

Chapter 2 Questions; Introduction to Mechanics of the Cardiovascular System

Chapter 2 MCQs

1. Concerning the systemic circulation:
 - (a) blood is pumped from the left ventricle.
 - (b) returns oxygenated blood to the right atrium.
 - (c) blood is pumped from the right ventricle.
 - (d) involves vessels in the head, legs and arms.
 - (e) involves the lungs.

2. Concerning the pulmonary circulation:
 - (a) blood is pumped from the left ventricle.
 - (b) returns oxygenated blood to the right atrium.
 - (c) blood is pumped from the right ventricle.
 - (d) involves vessels in the head, legs and arms.
 - (e) involves the lungs.

3. The intima:

- (a) is the outermost layer in the arterial wall.
- (b) is not present in capillaries.
- (c) contains a single layer of endothelial cells.
- (d) contains elastin.
- e) contains collagen.

4. Concerning the layers of vessels:

- (a) the adventitia is the outermost layer.
- (b) the media is the middle layer.
- (c) the intima is the inner layer in contact with flowing blood in the vessel.
- (d) there is no medial or adventitial layer in capillaries.
- (e) there is no intima present in capillaries.

5. Concerning the different types of vessel:

- (a) systemic arteries have relatively thick walls in order to withstand high pressure.
- (b) capillaries have larger diameter than venules and arterioles.
- (c) veins have thicker walls than arteries in order to withstand low pressures.

- (d) backflow of blood along medium sized veins is prevented by valves.
- (e) backflow of blood along medium sized arteries is prevented by valves.

6. Concerning transport of molecules in the cardiovascular system:

- (a) oxygenated blood is transported from the lungs to the rest of the body.
- (b) deoxygenated blood is transported from the lungs to the rest of the body.
- (c) carbon dioxide is transported from the rest of the body to the lungs where it is discharged.
- (d) carbon dioxide is transported from the lungs to the liver where it is consumed.
- (e) several types of molecule enter and exit the cardiovascular system via capillaries.

7. Concerning the distribution of blood in the systemic cardiovascular system:

- (a) all the blood is contained in the arteries.
- (b) most of the blood (2/3) is contained in the venous system.
- (c) most of the blood (2/3) is contained in the arterial system.

- (d) most of the blood ($2/3$) is contained in the capillaries.
- (e) there is no blood in the systemic cardiovascular system.

8. Concerning the dimensions of vessels:

- (a) arteries and veins have diameters from 1 to 30 mm.
- (b) arterioles and venules have dimensions of 1–30 mm.
- (c) arterioles and venules have dimensions of 15–300 micron.
- (d) capillaries have dimensions of 50–100 micron.
- (e) most capillaries have dimensions of 5–10 micron.

9. Concerning mean pressure in the systemic circulation:

- (a) is typically 90 mm Hg in the aorta.
- (b) is typically 90 mm Hg in the aorta.
- (c) continuously falls from the aorta to the capillaries.
- (d) continuously increases from the aorta to the capillaries.
- (e) has a value of 22 mm Hg in capillaries.

10. Concerning blood velocity in the systemic circulation:

- (a) mean velocity is the same in all vessels.
- (b) mean velocity in the aorta and other large arteries is around 10–25 cm s^{-1} .
- (c) mean velocity in the aorta and other large arteries is around 10–25 m s^{-1} .
- (d) mean velocity is 0.04 cm s^{-1} in the capillaries.
- (e) mean velocity is 400 cm s^{-1} in the capillaries.

Chapter 2 SAQs

1. Describe the different layers in an artery.
2. Describe the three different types of capillary.
3. Describe the difference between muscular and elastic arteries.
4. Describe the role of the cardiovascular system in oxygen transport.
5. Draw the major components of the pulmonary circulation.
6. Draw the major components of the system circulation.
7. Describe briefly the three main functions of the cardiovascular system.
8. Illustrate the change in pressure in the different vessels of the systemic

system.

9. Describe and illustrate pressure in the capillary with reference to osmotic pressure and trans-wall flow.

Chapter 2 LAQs

1. Describe the organisation of the cardiovascular system into systemic and pulmonary systems with reference to transport of oxygen and other molecules.
 2. Discuss the composition of the wall for different types of vessel.
 3. Describe and illustrate the variation in pressure, diameter and blood velocity in the different vessels in the systemic circulation.
-

Chapter 3 Questions; Blood and Blood Flow

Chapter 3 MCQs

1. The main particles in blood are:
 - (a) red cells (40–50 % by volume).
 - (b) red cells (0.7 % by volume).
 - (c) white cells (40–50 % by volume).
 - (d) white cells (0.7 % by volume).
 - (e) platelets (0.3 % by volume).

2. Concerning particles in blood; the role of:
 - (a) white cells is immune defence.
 - (b) red cells is to transport oxygen.
 - (c) red cells is to fight infection.
 - (d) platelets is blood clotting.
 - (e) platelets is osmotic balance.

3. Concerning red cells:
 - (a) These have an effective diameter of 5.5 mm.

- (b) These are shaped like plates (hence the term 'erythrocyte').
- (c) These are rigid (i.e. cannot be deformed).
- (d) These maintain a constant surface area on deformation.
- (e) These have a biconcave shape.

4. Concerning white cells:

- (a) These are all the same size at 10 micron diameter.
- (b) Monocytes migrate to tissues where they become macrophages which consume foreign bodies.
- (c) White cell volume fraction decreases in infection.
- (d) White cells take longer than red cells to traverse the capillaries due to their greater stiffness.
- (e) They are all shaped like plates (hence the term 'white cell').

5. Concerning platelets:

- (a) The usual form of platelets is in the activated form to assist blood clotting.
- (b) These are spherical.
- (c) In the unactivated form these are shaped like plates (hence the term 'platelet').

- (d) These have a maximum diameter of 2–3 microns.
 - (e) These are activated in regions of damaged endothelium and high shear.
6. The following roll along the arterial wall:
- (a) red cells.
 - (b) leukocytes.
 - (c) monocytes.
 - (d) LDL cholesterol.
 - (e) nicotine.
7. For flow of a dense (50 % by volume) suspension of identical particles, the particles:
- (a) are subject to forces which cause them to travel laterally.
 - (b) are always distributed uniformly.
 - (c) have a tendency to move away from the wall leaving a region near the wall depleted of particles.
 - (d) do not flow as the volume fraction is too high.
 - (e) have non-uniform distribution, especially at low shear rates.

8. The Segre–Silberberg effect:

- (a) occurs at high Reynolds number.
- (b) occurs at high magnetic field strength.
- (c) is associated with a uniform distribution of particles.
- (d) is associated with particles migrating from the centre and from the wall.
- (e) occurs at low Reynolds number.

9. Concerning electrostatic forces:

- (a) these are not relevant in blood.
- (b) red and white cells and platelets have negative charge and attract each other leading to thrombosis.
- (c) red and white cells and platelets have negative charge and repel each other helping prevent thrombosis.
- (d) these are shear forces.
- (e) these are drag forces.

10. Concerning chemical forces on particles in blood:

- (a) Shear induced lateral movement arises through a chemical force.

- (b) Chemical forces concern the binding of one biological cell or molecule with another cell or molecule.
- (c) red cells will attach to the endothelium through chemical bonding.
- (d) leukocytes will attach to the endothelium through chemical bonding.
- (e) activated platelets will bond through electrostatic attraction.

11. Identify the three types of forces arising from collisions of particles in a fluid:

- (a) Brownian motion.
- (b) electrostatic force.
- (c) depletion force.
- (d) particle–particle forces.
- (e) fluid drag.

12. Brownian motion:

- (a) produces steady linear motion of the particle.
- (b) is an example of a force between the fluid and particles.
- (c) is more significant for small particles.
- (d) is more significant for large particles.

(e) produces erratic random motion.

13. For flow of a suspension of identical particles in a straight tube:

(a) collisions between particles gives rise to lateral displacement.

(b) particles are distributed homogeneously.

(c) particles are distributed inhomogeneously with greater concentration at the vessel centre.

(d) particles are distributed inhomogeneously with greater concentration at the vessel wall.

(e) there are no collisions between particles.

14. Collisions between particles in blood leads to:

(a) reduced concentration of platelets at the vessel wall.

(b) reduced concentration of white cells at the vessel wall.

(c) increased concentration of platelets at the vessel wall.

(d) increased concentration of white cells at the vessel wall.

(e) change in packed cell volume.

15. Rouleaux:

- (a) are formed at shear rates below about 1 s^{-1} .
- (b) are formed at shear rate above 100 s^{-1} .
- (c) are clumps of white cells.
- (d) lead to decrease in blood viscosity.
- (e) at sufficiently low shear ($<0.01 \text{ s}^{-1}$) form an interlocking structure like a solid.

16. At high shear ($>1000 \text{ s}^{-1}$):

- (a) there is considerable red cell aggregation.
- (b) the viscosity value in whole blood is about 3–4 mPa s.
- (c) there is no red cell aggregation.
- (d) red cells are deformed with a stretched appearance.
- (e) the viscosity of blood reaches asymptotic value of about 100 mPa s.

17. Farhaeus–Lindqvist effect:

- (a) occurs for a pure fluid (i.e. no particles).

- (b) occurs in large (>5 mm) vessels.
- (c) is lowering of the effective viscosity of blood in small diameter (0.1–0.3 mm) vessels.
- (d) is associated with the presence of a cell-free layer near the vessel wall.
- e) is associated with a uniform distribution of red cells.

18. Regions free of red cells may occur in arteries:

- (a) at regions of low shear.
- (b) in the centre of the artery.
- (c) at regions of high shear.
- (d) at regions of high wall shear.
- (e) in the post-stenosis region near the wall.

19. Non-Newtonian flow:

- (a) means that the viscosity is dependent on shear rate.
- (b) means that the viscosity is independent of shear rate.
- (c) occurs in arteries in vivo in humans.
- (d) does not occur in arteries in vivo in humans.

(e) leads to no change in observed flow patterns compared to Newtonian flow.

20. Concerning flow in arteries and veins:

(a) some arteries (e.g. aorta) have periods of turbulent flow.

(b) red cell aggregation is present in normal arteries.

(c) red cells are mostly distributed uniformly in arteries.

(d) red cell aggregation is present in normal veins.

(e) some veins have periods of turbulent flow.

Chapter 3 SAQs

1. List the major particles in the blood and their function.
2. Describe drag force and its effect on a particle.
3. Describe shear induced lift force and its effect on a particle.
4. Describe wall induced lift force and its effect on a particle.
5. Describe electrostatic force and its effect on particles in blood.
6. Describe Rouleaux formation.
7. Describe leukocyte adhesion.

8. Briefly describe the three types of forces arising from collision.
9. Describe what margination is in the context of blood.
10. Describe and explain the behaviour of a single red cell in a shear field at low shear ($<10 \text{ s}^{-1}$).

Chapter 3 LAQs

1. Describe the different types of forces on particles at low Reynolds number (<30) and their effect on particle distribution.
 2. Describe the viscous behaviour of whole blood with shear and explain the shape of the viscosity-shear curve.
 3. Discuss whether red cells are distributed uniformly in arteries.
 4. Describe the Fahraeus and Fahraeus–Linqvist effects and discuss whether these are relevant for flow in the cardiovascular system.
 5. Compare characteristics of flow such as turbulence and viscosity in different parts of the cardiovascular system.
-

Chapter 4 Questions; Mechanics of Arteries

Chapter 4 MCQs

1. Which of the following statements are true concerning arterial structure:
 - (a) the outermost layer is the endothelium.
 - (b) the outermost layer is the adventitia.
 - (c) elastin fibres are only present within the adventitia.
 - (d) elastin fibres are laid down as parallel sheets.
 - (e) collagen fibres are arranged in a helical pattern.

2. The stress–strain relationship for arteries:
 - (a) is J-shaped.
 - (b) is linear.
 - (c) is S-shaped.
 - (d) is dominated by collagen behaviour at low strain (or low radius).
 - (e) is dominated by elastin behaviour at high strain (or high radius).

3. The Windkessel model of the arterial system:

- (a) consists of a heart, a compliant chamber and a resistance outflow.
- (b) predicts a flow waveform with a period of reverse flow.
- (c) predicts a flow waveform with monophasic flow.
- (d) accounts for pressure pulse propagation.
- (e) does not account for pressure pulse propagation.

4. Pressure pulse propagation speeds in healthy arteries:

- (a) is in the range 500–600 m/s.
- (b) is the same as the blood velocity.
- (c) is 5–15 m/s.
- (d) is 1540 m/s.
- (e) is infinitely fast.

5. Reverse going pressure waves:

- (a) are pressure waves which travel towards the heart rather than away from the heart.
- (b) combine in a subtractive manner with forward going pressure waves.
- (c) arise mainly from the distal arteriolar bed.

- (d) are pressure waves which travel away from the heart.
- (e) combine in an additive manner with forward going pressure waves.

6. Concerning blood flow-time and velocity-time waveforms:

- (a) have quasi-steady flow in arteries supplying the brain (carotid) and kidney (renal).
- (b) usually exhibit a period of reverse flow in arteries supplying muscle at rest.
- (c) are a plot of pressure versus time.
- (d) have typical peak velocities in the range 5–15 m/s in health.
- (e) have typical peak velocities in the range 0–1 m/s in health.

7. Flow in real arteries may exhibit the following flow characteristics:

- (a) laminar flow.
- (b) spiral flow.
- (c) skewing of the velocity profile in curved arteries.
- (d) change in velocity profile with time.
- (e) change in flow rate with time.

8. Vortices:

- (a) cannot be detected using colour-flow ultrasound.
- (b) commonly occurs in the carotid bulb region.
- (c) refers to regions of circulating flow.
- (d) does not occur in the arterial system.
- (e) commonly occurs in the post-stenosis region.

9. Rotational flow:

- (a) leads to mixing of blood in arteries.
- (b) is induced by curvature and bifurcations.
- (c) cannot be visualised using MRI.
- (d) does not occur in the arterial system.
- (e) is not induced by the heart.

10. If an artery is long and straight:

- (a) there is no rotational flow.
- (b) flow is fully developed.

- (c) the velocity profile is parabolic.
- (d) the velocity profile is axially symmetric.
- (e) maximum velocity is located in the centre of the vessel most of the time.

Chapter 4 SAQs

1. Describe the main layers of the artery wall and their composition.
2. Discuss the role elastin and collagen play in the stress–strain behaviour of an artery
3. Describe the Windkessel model of the arterial system.
4. Describe the origin of reflected pressure waves and their effect on overall pressure in the aorta.
5. What is the origin of rotational flow in arteries?
6. What is recirculating flow (vortices) and where in the arterial system does it commonly occur?
7. Describe when the velocity profile is likely to be symmetric in an artery?

Chapter 4 LAQs

1. Describe the origin of pressure-time and flow-time blood waveforms in arteries, explaining the shape of waveforms for arteries supplying muscle at rest and arteries supplying brain and kidney.

2. Discuss the general characteristics of flow in arteries

Chapter 5 Questions; Biomechanics of Arteries

Chapter 5 MCQs

1. Concerning wall shear stress:
 - (a) wall shear stress is equal to longitudinal stress.
 - (b) wall shear stress is the viscous drag of blood on the adventitia.
 - (c) wall shear stress is the viscous drag of blood on the arterial wall.
 - (d) wall shear stress is always aligned with the arterial axis.
 - (e) wall shear stress has values in healthy arteries in the human of typically 1–20 Pa.

2. Concerning the forces on the arterial wall:
 - (a) the wall shear stress is the stress within the wall in the direction parallel to the vessel axis.
 - (b) the mean circumferential stress is typically 1–2 Pa.
 - (c) the circumferential stress is the stress within the wall in the direction perpendicular to the vessel axis.
 - (d) the mean blood pressure is typically 12,000 Pa.
 - (e) the mean blood pressure is typically 1–2 Pa.

3. Concerning forces within the arterial wall:
 - (a) an artery is prestressed both longitudinally and from inner to outer wall.
 - (b) an artery is prestressed longitudinally but not from inner to outer wall.
 - (c) an artery is prestressed from inner to outer wall but not longitudinally.
 - (d) an excised artery will be around 40 % greater in length than its native length in the body.
 - (e) an excised artery will be around 40 % less in length than its native length in the body.

4. Concerning Murray's law and wall shear stress in the human:
 - (a) Murray's law is concerned with the circumferential stress.
 - (b) Murray's law implies that mean wall shear stress is constant for all arteries (i.e. independent of diameter).
 - (c) In practice mean wall shear stress is the same in different arteries.
 - (d) Murray's law implies that mean wall shear stress is proportional to diameter.
 - (e) In practice mean wall shear stress is different in different arteries.

5. Concerning circumferential tension and stress for thin-walled cylinders:

- (a) the law of Laplace is: tension equals pressure divided by radius.
- (b) the law of Laplace is concerned with blood flow.
- (c) the law of Laplace is: tension is equal to pressure times radius.
- (d) circumferential stress is proportional to wall thickness.
- (e) circumferential stress is inversely proportional to wall thickness.

6. Concerning lamellar unit:

- (a) the unit of circumferential stress values is called the lamellar abbreviated La.
- (b) the tension per lamellar unit in the aorta is 1–3 N/m for all mammals.
- (c) a lamellar unit is a structure consisting of muscle, elastin and collagen in the arterial wall.
- (d) the number of lamellar units in the wall increases with age from birth to death.
- (e) the number of lamellar units in the wall increases during gestation (i.e. before birth).

7. Concerning the vessel wall:

- (a) Increase in blood pressure leads to increase in wall thickness.
- (b) Increase in blood pressure leads to increase in number of lamellar units during gestation.
- (c) Increase in blood pressure leads to increase in the thickness of each lamellar unit after birth.
- (d) Decrease in blood pressure leads to increase in the thickness of each lamellar unit after birth.
- (e) Increase in wall shear stress leads to increase in wall thickness.

8. Concerning control mechanisms; changes in:

- (a) wall shear stress lead to changes in arterial length.
- (b) circumferential stress lead to changes in wall thickness.
- (c) wall shear stress lead to changes in vessel diameter.
- (d) longitudinal stress lead to changes in vessel length.
- (e) circumferential stress lead to changes in diameter.

9. Mechanotransduction is the process where:

- (a) mechanical forces are translated in biological behaviour.

- (b) magnetic forces are translated into biological behaviour.
- (c) electrical forces are translated into biological behaviour.
- (d) where biological behaviour is translated into magnetic forces.
- (e) where biological behaviour is translated in mechanical forces.

10. Concerning mechanosensing:

- (a) mechanosensors reside on the endothelium and on no other cell type.
- (b) this is the process where the biological response from a mechanical stimulus is produced.
- (c) an example of a mechanosensor is the stretch-sensitive ion channel.
- (d) this is the process where the mechanical stimulus is detected.
- (e) the main underlying physical basis for mechanosensing is changes in protein conformation.

11. Mechanosignalling:

- (a) via the cytoskeleton results in more rapid propagation of information compared to chemical signalling.
- (b) via the cytoskeleton results in less rapid propagation of

information compared to chemical signalling.

- (c) is the process where the biological response from a mechanical signal is produced.
- (d) concerns the propagation of gravitational waves.
- (e) does not occur in endothelial cells.

12. Concerning the endothelium:

- (a) mechanosensors are only distributed on the lumen adjacent to blood.
- (b) the endothelium aligns itself perpendicular to the shear stress direction.
- (c) mechanosensors are distributed throughout the endothelial cell.
- (d) the endothelium contains no mechanosensors.
- (e) the endothelium is capable of detecting changes in wall shear stress.

Chapter 5 SAQs

1. What are the main forces arising from blood on the arterial wall?
2. What is the functioning of prestressing of the artery wall from inner to outer lumen?

3. Describe Murray's Law.
4. List the principal determinants of artery diameter, wall thickness and arterial length?
5. Describe the effect on diameter when wall shear stress increases long term and explain the control mechanism.
6. Describe the effect of increasing blood pressure on artery wall thickness during gestation and during childhood.
7. Describe why diameter of the aorta increases with age in childhood.
8. Describe why and how wall thickness increases with age in gestation.
9. Describe what is meant by the decentralised model of mechanotransduction and illustrate this.
10. Describe the main steps in the process of mechanotransduction.
11. Describe four responses to a long term increase in wall shear stress in an artery and include timescales.
12. Describe four examples of candidate mechanosensors for the endothelium.

Chapter 5 LAQs

1. Describe the forces on the arterial wall of the adult human and how changes to these forces give rise to changes in arterial structure.

2. Describe the role of wall shear stress in the remodelling of arteries; drawing examples from gestation, childhood, adulthood and intervention.
 3. Describe the principle steps of mechanotransduction in the general cell.
 4. Describe the principle steps of mechanotransduction in the endothelial cell in relationship to wall shear stress.
-

Chapter 6 Questions; Biomechanics of the Heart

Chapter 6 MCQs

1. In which region of the heart is a normal heart beat initiated?
 - (a) The sinoatrial node.
 - (b) The atrioventricular node.
 - (c) The Purkinje system.
 - (d) The bundle of His.

2. Which of the following act to regulate transmembrane current in cardiac myocytes?
 - (a) Ion channels, ion pumps, and ion exchangers.
 - (b) Ion channels and the t-tubule system.
 - (c) Ion pumps and ion exchangers.
 - (d) Ion channels and the sarcoplasmic reticulum.

3. Which part of the normal electrocardiogram is generated by slow conduction of the action potential through the atrioventricular node?
 - (a) The ST segment.
 - (b) The QRS complex.

- (c) The PQ interval.
 - (d) The QT interval.
4. Which of the following features associated with an action potential initiate mechanical contraction in cardiac myocytes?
- (a) Changes in membrane voltage.
 - (b) Influx of Ca^{2+} ions.
 - (c) Influx of Na^{+} ions.
 - (d) Influx of K^{+} ions.
5. Which part of the normal electrocardiogram is generated by slow conduction of the action potential through the atrioventricular node?
- (a) The ST segment.
 - (b) The QRS complex.
 - (c) The PQ interval.
 - (d) The QT interval.
6. What role is played by the sarcoplasmic reticulum in a cardiac myocyte?

- (a) Sink for Na^+ .
 - (b) Buffer for Ca^{2+} .
 - (c) Mechanical support for contractile proteins.
 - (d) Store for Ca^{2+} .
7. Under normal physiological conditions, which of following quantities does not contribute to the active isometric tension developed by a myocyte?
- (a) Afterload.
 - (b) Intracellular Ca^{2+} concentration
 - (c) Preload.
 - (d) Sarcomere length.
8. Which of the following quantities contributes to afterload?
- (a) Ventricular volume.
 - (b) Ventricular pressure.
 - (c) Venous pressure.
 - (d) Arterial pressure.

9. Which expression describes the mechanical work done by the left ventricle during a normal beat?
- (a) Total change in LV volume.
 - (b) Change in LV pressure multiplied by change in LV volume.
 - (c) Change in LV pressure multiplied by heart rate.
 - (d) Arterial pressure multiplied by change in LV volume.
10. How does the Frank–Starling mechanism compensate for a transient increase in right ventricular output?
- (a) Increased volume in the systemic circulation, increased RV preload, and hence a decrease in RV output.
 - (b) Decreased volume in the pulmonary circulation, increased LV preload, and hence an increase in LV output.
 - (c) Increased volume in the pulmonary circulation, increased LV preload, and hence an increase in LV output.
 - (d) Decreased volume in the systemic circulation, decreased LV preload, and hence an decrease in RV output.

Chapter 6 SAQs

1. Describe the main anatomical features of the human heart, explaining the functional role played by each.

2. Enumerate the different phases of the cardiac action potential, and describe the direction of the dominant transmembrane current at each phase along with the ionic species that carries the current.
3. Using a sketch of pressure and volume changes during the cardiac cycle, show how the electrical activation sequence of the whole heart is related to the mechanical activation sequence.
4. Compare and contrast preload and afterload.
5. Summarise the main mechanisms responsible for cardiac remodelling.

Chapter 6 LAQs

1. Describe how the cardiac action potential acts to initiate and synchronise mechanical contraction in each part of the heart, focusing on both the subcellular and whole organ mechanisms.
 2. Explain how the sliding filaments in myofibrils influence the way that cardiac tissue responds to preload and afterload.
 3. Describe the cardiac cycle using the pressure–volume relation, and show how this relation is altered in conditions of reduced and increased contractility.
-

Chapter 7 Questions; Biomechanics of the Venous System

Chapter 7 MCQs

1. The veins:
 - (a) Take blood from the heart to the lungs.
 - (b) Return de-oxygenated blood from the periphery to the heart.
 - (c) Have thinner walls than the arteries.
 - (d) Store 60–80 % of total blood volume.
 - (e) Contain more smooth muscle than the arteries.

2. The transmural pressure in the veins:
 - (a) depends only on the posture of the subject.
 - (b) is important in definition of the tube law.
 - (c) is determined by the thickness of the surrounding tissue.
 - (d) is given by the difference between internal and external venous pressure.
 - (e) depends on the bending stiffness of the vessel.

3. The tube law during vessel collapse:

- (a) becomes stiffer when self-contact occurs.
- (b) describes the relationship between transmural pressure and cross-sectional area.
- (c) is nonlinear.
- (d) is linear.
- (e) becomes softer when self-contact occurs.

4. Super-critical flow:

- (a) occurs when the local speed of the fluid, u , is greater than the pulse wave transmission speed, c .
- (b) occurs when the Reynolds number exceeds 2000.
- (c) occurs when the local speed of the fluid, u , is less than the pulse wave transmission speed, c .
- (d) results in more complex flow effects.
- (e) is more likely in vessels which are partially collapsed.

5. Venous return is increased by:

- (a) decrease in venous resistance.
- (b) the activation of the respiratory pump.

- (c) compression of the vena cava.
- (d) the activation of the calf muscle pump.
- (e) an increase in pressure gradient along the venous circulation.

6. As the calf muscle pump relaxes:

- (a) the proximal deep vein valves open and the distal valves close.
- (b) blood flows from the deep to the superficial venous system.
- (c) blood ejected from the calf returns under the influence of gravity.
- (d) the deep veins are re-filled as a result of arterial inflow.
- (e) the deep veins are re-filled as a result of flow from the superficial veins.

7. The venous valves:

- (a) open and close during respiration and muscular contractions.
- (b) include leaflets which are thick relative to the vessel wall.
- (c) are generally found to be bicuspid.
- (d) are always observed to be tricuspid.
- (e) resist venous flow away from the heart.

8. The number of valves in the veins:
 - (a) generally increase with distance from the central circulation.
 - (b) is greater where the muscle pump is more active.
 - (c) is greater in the vena cava than in the deep veins of the leg.
 - (d) is the same for all individuals.
 - (e) is greater than in the arterial circulation.

9. The geometry of the venous valves:
 - (a) is associated with a reduction in venous diameter in the sinus region.
 - (b) causes recirculation of blood in front of the valve leaflets.
 - (c) results in a narrowing of the lumen at the location of the valve leaflets.
 - (d) causes recirculation of blood behind the valve leaflets.

 - (e) is associated with an increase in venous diameter in the sinus region.

10. Following change in posture from seated to standing:

- (a) The change in pressure takes around 20 s to establish.
- (b) Venous pressure in the neck increases.
- (c) Local changes in venous volume occur.
- (d) Venous pressure in the foot increases.
- (e) The change in hydrostatic pressure in the veins occurs immediately.

11. Deep vein thrombosis:

- (a) can result in potentially fatal pulmonary embolism.
- (b) is linked to the formation of vortices in the region of the valve.
- (c) has been observed to form at the sites of venous valves.
- (d) has been associated with periods of prolonged activity.
- (e) can result in symptoms including swelling of the limb and change in pigmentation.

Chapter 7 SAQs

1. What proportion of the blood volume is stored in the venous system, what factors influence the venous volume and why?
2. Describe factors that will influence the form of venous collapse, giving examples of two veins where the collapse behaviour will differ.

3. Define the conditions under which sub-critical and super-critical flow occurs.
4. Describe the phases of the respiratory pump, with reference to the abdomen, thorax and vena cava.
5. What non-invasive technique can be used to assess the degree of venous valve reflux and how would this be applied in practice?
6. Sketch the venous valve geometry identifying key features and describe the role of these valves within the circulation.

Chapter 7 LAQs

1. Describe the nonlinear pressure/area response observed during collapse of an unsupported vein with use of appropriate diagrams; identify physiological conditions under which venous collapse might occur.
 2. Describe the purpose and mechanism of action of the calf muscle pump including the role of the venous valves. Illustrate your description with a diagram indicating typical venous anatomy in the calf.
 3. Describe the phases of action of the venous valve, including discussion of the associated fluid dynamics. Discuss the implications of the fluid dynamics during the open equilibrium phase for the formation of thrombosis local to the valve site.
-

Chapter 8 Questions; Biomechanics of the Microcirculation

Chapter 8 MCQs

1. Which of the following statements is not true concerning microcirculation vessels:
 - (a) molecular exchange primarily occurs through arteriolar walls.
 - (b) venules have a diameter in the range 15–300 μm .
 - (c) a metarteriole is connected directly to a venule allowing flow to bypass the capillary bed.
 - (d) most capillaries have a diameter of 5–10 μm .
 - (e) arterioles are vasoactive.

2. Concerning viscosity in the microcirculation; viscosity is:
 - (a) constant in all vessels with a value of 3.5 mPa s.
 - (b) primarily determined by the number and distribution of white cells.
 - (c) primarily determined by the number and distribution of red blood cells.
 - (d) increased in capillaries compared to that in major vessels.
 - (e) increased in vessels where red cell concentration is reduced at the vessel wall.

3. Concerning the myogenic effect; an increase in input pressure to the arterioles leads to:
- (a) relaxation of smooth muscle in order to constrict arterioles.
 - (b) short-term increase in pressure in the capillary.
 - (c) constriction of smooth muscle in order to increase the diameter of arterioles.
 - (d) short-term decrease in pressure in the capillary.
 - (e) constriction of smooth muscle in order to decrease arteriolar diameter.
4. Concerning vasomotion:
- (a) This is the regular change in flow rate in capillaries from 3 to 30 nL s^{-1} .
 - (b) This is the movement of blood through vessels at a speed of 3–30 cm s^{-1} .
 - (c) This is a general term associated with movement of blood or vessel wall.
 - (d) This is regular change in diameter of arterioles at a frequency of 3–30 min^{-1} .

(e) This is the regular change in viscosity in capillaries from 3 to 30 mPa s.

5. Most cells in the body are within what distance from a capillary:

(a) 1 μm .

(b) 10 μm .

(c) 100 μm .

(d) 1 mm.

(e) 10 mm.

6. In Starling's equation transcapillary flow is related to:

(a) net hydrostatic pressure plus net colloid osmotic pressure.

(b) net hydrostatic pressure.

(c) net colloid osmotic pressure.

(d) intravascular pressure minus intervascular colloid osmotic pressure.

(e) net hydrostatic pressure minus net colloid osmotic pressure.

7. Which of the following is not a form of molecular movement across the capillary wall?

- (a) Diffusion of glucose through fenestrations and pores in the capillary wall.
- (b) Quantum tunnelling of H^+ .
- (c) Bulk flow through pores and clefts in the walls of sinusoidal capillaries.
- (d) Diffusion across the lipid bilayer for CO_2 and O_2 .
- (e) Vesicular transport of antibodies.

8. The purpose of autoregulation of perfusion is to:

- (a) ensure that tissues remain ischaemic most of the time.
- (b) maintain adequate perfusion for a wide range of arterial pressure.
- (c) maintain adequate wall shear stress for a wide range of arterial pressure.
- (d) ensure that arteriolar resistance is maintained at a constant level regardless of perfusion values.
- (e) ensure that central blood pressure is maintained constant for a wide range of perfusion values.

Chapter 8 SAQs

1. List the main components of the microcirculation.

2. Describe briefly the origin of red blood cell margination in arterioles and venules.
3. Describe why effective viscosity is lower in the arterioles and venules than in larger vessels.
4. Describe plasma skimming and its cause.
5. Describe and illustrate the Bayliss effect.
6. Describe what is meant by vasomotion.
7. Write down Starling's equation with definitions of each term of the equation.
8. List three mechanisms for transport of molecules across the capillary wall with a sentence explaining each one.
9. Describe briefly metabolic control of perfusion.
10. Briefly explain the meaning of the term 'angiogenesis' and give 3 examples of when this occurs.

Chapter 8 LAQs

1. Describe how viscosity varies in different vessels in the microcirculation and explain why it has such a wide variation in values in different vessels.
2. Describe the Bayliss effect and how this might lead to vasomotion.
3. Explain why capillary intravascular pressure needs to be kept constant and explain the principle mechanism for achieving this.

4. Describe what is meant by flow autoregulation and explain the mechanisms by which local perfusion is controlled.
-

Chapter 9 Questions; In Vivo Imaging

Chapter 9 MCQs

1. Concerning structural imaging:
 - (a) uses an ingested, inhaled or injected tracer.
 - (b) gives information on biological function.
 - (c) PET is an example of a structural imaging technique.
 - (d) gives information on geometry and motion.
 - (e) CT is an example of a structural imaging technique.

2. Concerning functional imaging:
 - (a) may use an ingested or injected tracer.
 - (b) gives information on physiological function.
 - (c) PET is an example of a functional imaging technique.
 - (d) this primarily provides information on organ geometry.
 - (e) may only be performed by PET.

3. Concerning X-ray imaging:

- (a) involves the use of ionising radiation.
- (b) MRI uses X-rays.
- (c) X-ray images show information related to X-ray attenuation of tissues.
- (d) X-ray images show information related to X-ray speed of propagation.
- (e) X-ray images show information related to T1 and T2 values.

4. Catheter placement in angiography:

- (a) may be undertaken using projection radiography.
- (b) can only be undertaken using a CT scanner.
- (c) may be undertaken using a fluoroscopy system.
- (d) involves injection of an iodine contrast agent.
- (e) involves injection of a barium contrast agent.

5. Concerning CT scanning:

- (a) Only produces 2D images.
- (b) May be obtained using a standard projection radiography system.
- (c) Involves the collection of X-ray data at multiple angles around the

patient.

- (d) Has a data acquisition time of 20–60 min.
- (e) Involves production of the 3D dataset using tomographic reconstruction.

6. A contrast agent in X-ray imaging:

- (a) is not used in angiography.
- (b) is usually based on barium or iodine.
- (c) is usually based on arsenic or uranium.
- (d) is based on iron.
- (e) is used to improve image quality by improving image contrast between tissues.

7. MRI:

- (a) has typical imaging times of 1–2 min.
- (b) is usually undertaken using a 0.15T or 9T magnet.
- (c) mostly concerns imaging of the hydrogen nucleus.
- (d) is usually undertaken using a 1.5T or 3T magnet.
- (e) mostly concerns imaging of the nitrogen nucleus.

8. The Larmor frequency:

- (a) is the frequency of the transmitted ultrasound.
- (b) is the rate of rotation of the magnetic axis of the proton around the magnetic field.
- (c) is equal to 42 MHz per tesla.
- (d) is the rate of rotation of the magnetic axis of the electron around the magnetic field.
- (e) is equal to 420 MHz per tesla.

9. The T1 relaxation time:

- (a) is also called the spin-lattice relaxation time.
- (b) is a measure of the rate of decay of the transverse magnetization.
- (c) is usually longer than the T2 relaxation time.
- (d) is equal to 0.15 s for all tissues.
- (e) is a measure of the rate of energy exchange between the protons and the neighbouring molecules.

10. Concerning the various coils in an MRI scanner:

- (a) Radiofrequency receiver coils are used to detect the RF ultrasound

signals from the patient.

- (b) Radiofrequency receiver coils are used to detect the RF signal from the patient.
- (c) Gradient coils are used to produce small changes in magnetic field along x, y and z.
- (d) Gradient coils are not needed for 3T MRI.
- (e) Radiofrequency transmitting coils are used to change the direction of magnetisation of protons.

11. Ultrasound for medical imaging diagnosis:

- (a) involves transmission and reception of ultrasound along a narrow beam.
- (b) uses low frequency sound waves in the range 2–20 kHz.
- (c) uses high frequency sound waves in the frequency range 2–20 MHz.
- (d) does not involve real-time imaging.
- (e) is designed to cause extensive tissue damage.

12. Concerning the ultrasound B-mode image:

- (a) this is a display of received Doppler mean frequency.
- (b) this is built up by sweeping of the ultrasound beam through the

tissues.

- (c) involves measurement of echo depth by timing between pulse transmission and echo reception.
- (d) this is a display of the received ultrasound amplitude.
- (e) this is a display of the received ultrasound frequency.

13. Concerning Doppler ultrasound:

- (a) spectral Doppler is a real-time display of Doppler frequency shift versus time.
- (b) the Doppler shift is proportional to the square of the blood velocity.
- (c) spectral Doppler is a real-time 2D display of mean Doppler frequency of blood flow.
- (d) may be used to estimate blood velocity.
- (e) the Doppler shift is proportional to the cosine of the angle between beam and direction of motion.

14. Concerning ultrasound contrast agents:

- (a) these are based on the use of high atomic number elements such as iodine.
- (b) these have a diameter of 2–6 μm .

- (c) these consist of gas encapsulated by a thin shell.
- (d) these have a typical diameter of 2–6 micron.
- (e) these are based on the use of paramagnetic elements such as iron.

15. In PET imaging, radioactive atoms disintegrate:

- (a) releasing an electron, which collides with another electron producing 2 X-rays.
- (b) releasing a positron, which collides with an electron producing 2 gamma rays.
- (c) releasing a positron, which collides with another positron producing 2 gamma rays.
- (d) releasing an electron, which collides with another electron producing 2 gamma rays.
- (e) releasing a positron, which collides with an electron producing 2 X-rays.

16. For PET imaging of the human:

- (a) spatial resolution is typically 4–6 micron.
- (b) spatial resolution is typically 4–6 mm.
- (c) spatial resolution is typically 0.4–0.6 mm.
- (d) acquisition time is typically 20–60 min.

- (e) PET is a real-time technique with a frame rate of 20–60 frames per second.

17. In PET imaging:

- (a) pairs of gamma rays are created which travel in the same direction and are detected by sensors.
- (b) pairs of alpha rays are created which travel in opposite directions and are detected by sensors.
- (c) pairs of X-rays are created which travel in opposite directions and are detected by sensors.
- (d) pairs of X-rays are created which travel in the same direction and are detected by sensors.
- (e) pairs of gamma rays are created which travel in opposite directions and are detected by sensors.

18. Blood velocity is commonly measured using:

- (a) PET.
- (b) CT.
- (c) Doppler ultrasound.
- (d) MRI.
- (e) projection radiography.

19. In shear wave elastography tissue stiffness is:

- (a) proportional to the square of shear wave velocity.
- (b) inversely proportional to local tissue density.
- (c) proportional to shear wave velocity.
- (d) proportional to local tissue density.
- (e) inversely proportional to shear wave velocity.

20. Concerning shear wave elastography:

- (a) shear waves may be induced by means of a high-output acoustic pulse.
- (b) typically travel at 1–20 m/s in soft tissues.
- (c) shear waves may be induced by an external actuator in contact with the skin of the patient.
- (d) is applicable to CT and rotational angiography.
- (e) typically travel at 1540 m/s in soft tissues.

Chapter 9 SAQs

1. Describe briefly what is meant by structural imaging and functional imaging and gives examples of each.

2. Describe the principle of X-ray imaging for the projection radiograph.
3. Describe the principles of X-ray imaging when used in angiography.
4. Describe briefly why MRI mostly concerns imaging of hydrogen nuclei.
5. Describe briefly the origin of the MRI signal from hydrogen nuclei following application of an RF pulse.
6. Describe what is meant by T1 and T2 in MRI.
7. Describe the pulse-echo technique for ultrasound imaging.
8. Describe how ultrasound is commonly used to measure blood velocity.
9. Describe briefly the different types of contrast agents used in CT and ultrasound.
10. Describe briefly the principles of imaging for PET.
11. Describe the principles of ultrasound elastography.
12. Describe briefly the principles of magnetic resonance elastography.

Chapter 9 LAQs

1. Describe the different types of X-ray imaging techniques; which are suitable for 3D imaging?
2. Describe the principle of formation of an MRI image.
3. Describe the basic principles of formation of the B-mode image and give

examples of measurements that may be made using B-mode imaging.

4. Compare and contrast the measurement of blood velocity and volumetric flow using Doppler ultrasound and using MRI.
-

Chapter 10 Questions; Modelling of the Cardiovascular System

Chapter 10 MCQs

1. Concerning models and modelling, which statements below do you think are correct?
 - (a) A model must always be as near to physical reality as possible.
 - (b) A model of the cardiovascular system should be 3D to be useful.
 - (c) A model is a simplified version of reality.
 - (d) A model should be just complicated enough in order to answer a specific question.
 - (e) The model complexity should always be the same regardless of the problem to be solved.

2. Which of these is not required in computational modelling e.g. biomechanical arterial applications?
 - (a) Output data.
 - (b) Boundary conditions.
 - (c) Model.
 - (d) Input data.
 - (e) General physical properties of arteries unrelated to the model.

3. Concerning reduced order models:

- (a) A reduced order model does not account for 1 or more of x , y , z .
- (b) 0D (t) models may be used to investigate pulse wave propagation in arteries.
- (c) 1D (x , t) models may be used to investigate pulse wave propagation in arteries.
- (d) 3D models (x , y , z , t) may be used to investigate pulse wave propagation in arteries.
- e) Computational run time is likely to be greater for reduced order models.

4. Incorporation of 3D geometry in modelling:

- (a) Requires a 0D modelling regime.
- (b) Requires a 1D modelling regime.
- (c) Requires a 3D modelling regime.
- (d) May involve idealised geometry creation in CAD.
- (e) May involve patient specific geometry creation in CAD.

5. Concerning rigid and moving-wall models used in arterial modelling:

- (a) A rigid wall model considers the wall to be compliant.
- (b) Moving walls can be modelled using an FSI approach.
- (c) Moving walls can be measured direct from medical imaging and included into a CFD-only approach.
- (d) A moving-wall model considers the wall to be infinitely stiff.
- (e) Modelling of pulse wave propagation can be undertaken using a rigid walled model.

6. Concerning inlet flow data for CFD modelling in arteries.

- (a) The use of a plug flow profile at the inlet accurately represents velocity profiles in all arteries.
- (b) The use of a parabolic flow profile at the inlet accurately represents velocity profiles in all arteries.
- (c) A Womersley based approach may be used to account for flow assymetry and spiral flow at the inlet.
- (d) The use of a development length may be used to account for flow assymetry and spiral flow at the inlet.
- (e) The use of a time-varying 2D velocity profile with all 3 velocity components from MRI may be used to account for flow asymmetry and spiral flow at the inlet.

7. For modelling of blood flow it would be necessary to account for deformable red cells in:

(a) Major arteries (1–20 mm diameter).

(b) Major veins (1–20 mm diameter).

(c) Minor arteries (0.3–1 mm diameter).

(d) Minor veins (0.3–1 mm diameter).

(e) Microcirculation vessels $<100 \mu\text{m}$.

Chapter 10 SAQs

1. Describe briefly what a model is and how complex the model should be.
2. Illustrate the modelling process explaining briefly what each of the components are.
3. Explain what a reduced order model is and why these are used rather than full 3D models.
4. Explain the difference between a rigid walled model and a compliant model used in arterial modelling.
5. For inlet flow conditions for arterial CFD, explain how asymmetric spiral-flow would be accounted for.
6. Explain what assumptions are commonly made concerning the physical properties of blood in CFD in larger arteries and veins.

7. Explain what a multidimensional model is and why these are used.

Chapter 10 LAQs

1. Describe the modelling process, explaining what a model is, how complex it should be in general terms, and illustrate this with an example.
 2. Describe rigid and moving-wall models used in arterial modelling and when each model might be used.
 3. Describe 3D heart models including the type of data which is simulated and the applications of interest.
-

Chapter 11 Questions; Patient Specific Modelling

Chapter 11 MCQs

1. Patient specific modelling:
 - (a) is the combination of computational modelling with idealised organ geometries.
 - (b) is the combination of computational modelling with organ geometries obtained from 3D medical imaging on the patient.
 - (c) involving CFD should use patient specific inlet flow data.
 - (d) aims to provide data relevant to the individual patient.
 - (e) aims to provide data which is relevant to a group of patients.

2. Which of the following has contributed to the growth of patient specific modelling in recent years?
 - (a) Improvements in computer power.
 - (b) The need for improved methods for diagnosis.
 - (c) Improvements in the availability of commercial computational modelling software.
 - (d) Availability of high-resolution medical imaging.
 - (e) Improvements in data on material properties.

3. Computational mechanics:
 - (a) involves a continuum description of tissues.
 - (b) involves discretisation of space and time.
 - (c) provides an exact solution to the governing equations.
 - (d) commonly uses simplified equations involving iteration.
 - (e) applies to fluid mechanics but not solid mechanics.

4. Which of the following are ideal characteristics for medical imaging when used to collect data for PSM?
 - (a) high noise.
 - (b) low tissue contrast.
 - (c) high resolution.
 - (d) long image acquisition times.
 - (e) being MRI.

5. Concerning segmentation:
 - (a) in the PSM processing chain segmentation is performed after

computational modelling.

- (b) automated segmentation works best when image quality is worst.
- (c) is concerned with identifying boundaries in imaging data.
- (d) manual segmentation does not require any input from the operator.
- (e) is often concerned with the detection of edges in the image.

6. Which of the following are not in the PSM processing chain?

- (a) boundary condition data.
- (b) computational modelling.
- (c) post processing.
- (d) 3D imaging.
- (e) patient consent.

7. Concerning the mesh used in computational modelling:

- (a) The number of mesh elements should always be as large as possible.
- (b) Is commonly composed of tetrahedral or hexahedral elements.
- (c) The number of mesh elements is 100,000 for FEA and 1 million for CFD.

- (d) The number of mesh elements is chosen to balance solution accuracy with processing time.
 - (e) Mesh generation is usually a fully automated process.
8. For CFD in a stiff walled artery with no branches, the following information is needed:
- (a) Circumferential elastic modulus of the artery wall.
 - (b) Inlet flow.
 - (c) Viscosity of blood.
 - (d) Inlet pressure.
 - (e) Density of blood.
9. For estimation of tissue stresses in an abdominal aortic aneurysm commonly involves the following:
- (a) An FSI modelling regime.
 - (b) An FEA-only modelling regime.
 - (c) Information on wall thickness from MRI.
 - (d) A CFD only modelling regime.
 - (e) An assumption of constant wall thickness of typically 1.55 mm.

10. An FSI modelling regime:

- (a) is needed for estimation of the 3D flow field in a stiff walled artery.
- (b) is commonly used for estimation of tissue stress in an abdominal aortic aneurysm.
- (c) does not involve CFD.
- (d) involves both CFD and FEA.
- (e) is needed for estimation of flow field or tissue stress data in an artery with a tight stenosis.

Chapter 11 SAQs

1. Describe briefly what is meant by patient specific modelling.
2. Describe briefly the basic steps in computational mechanics.
3. Describe briefly the basic steps in patient specific modelling.
4. Discuss the choice of imaging modality for patient specific modelling of tissue stress in an abdominal aortic aneurysm.
5. Discuss the choice of imaging modality for patient specific modelling of tissue stress in the carotid bifurcation.
6. Describe how images may be segmented for patient specific modelling.
7. Describe what information can be obtained from the patient for use in

patient specific modelling of blood flow in the abdominal aortic aneurysm, and what assumptions have to be made.

8. Describe what information can be obtained from the patient for use in patient specific modelling of tissue stress in the abdominal aortic aneurysm and what assumptions have to be made.
9. Describe what is meant by FSI and when this might be needed.

Chapter 11 LAQs

1. Describe the steps of patient specific modelling for estimation of tissue stress in an abdominal aortic aneurysm.
 2. Describe the steps of patient specific modelling for estimation of tissue stress in the carotid bifurcation.
 3. Describe the steps of patient specific modelling for estimation of flow field data in a non-diseased carotid bifurcation.
 4. Describe the steps of patient specific modelling for estimation of flow field data in a cerebral aneurysm.
-

Chapter 12 Questions; Flow Phantoms

Chapter 12 MCQs

1. Which of these are not components of a typical flow phantom?
 - (a) the central construct which mimics the geometry of part of the cardiovascular system.
 - (b) blood mimic.
 - (c) ultrasound system.
 - (d) tissue mimic.
 - (e) pump.

2. Which technique can be used to measure blood-mimic velocity in a suitable flow phantom?
 - (a) LDA.
 - (b) flow visualisation using a video camera.
 - (c) CT.
 - (d) PIV.
 - (e) Doppler ultrasound.

3. Phantoms for PIV and LDA:

- (a) can be constructed from glass or silicone elastomer.
- (b) are optically transparent.
- (c) are optically opaque.
- (d) require seeding with low concentrations of particles.
- (e) are suitable for use with ultrasound imaging.

4. PIV:

- (a) does not require the use of seeded particles.
- (b) uses seeded particles at a typical concentration of $<1\%$.
- (c) uses ultrasound to measure the particle velocity by a Doppler shift.
- (d) involves a laser to illuminate the particles.
- (e) involves a laser to measure the particle velocity by a Doppler shift.

5. In lost-core phantom construction:

- (a) the lost-core may be manufactured from a mould.
- (b) the tissue mimic is removed once the lost-core has set.
- (c) the lost-core is commonly composed of a low-melting point alloy.

- (d) the lost-core is removed once the tissue mimic has set.
 - (e) the lost-core is discarded immediately after it has been manufactured.
6. Phantom materials which attempt to match the imaging properties of tissues are referred to as:
- (a) tissue mimicking (for soft tissue).
 - (b) tissue-equivalent (in general).
 - (c) blood mimicking (for blood).
 - (d) vessel mimicking (for vessel).
 - (e) flow phantoms.
7. Solid tissue mimicking materials used in ultrasound phantoms include:
- (a) acrylic.
 - (b) agar.
 - (c) Urethane.
 - (d) PVAc.
 - (e) water.
8. A commonly used blood-mimicking fluid for MRI is:

- (a) 60:40 water:glycerol solution by mass containing nylon particles.
 - (b) water (100 %).
 - (c) 60:40 water:glycerol solution by mass.
 - (d) 10 % solution of ethyl alcohol by volume.
 - (e) 90:10 water:glycerol solution by mass.
9. A blood-mimicking fluid for ultrasound should have the following properties:
- (a) acoustic velocity of $1570 \text{ cm/s} \pm 10 \%$.
 - (b) attenuation coefficient $< 0.1 \text{ dB cm}^{-1} \text{ MHz}^{-1}$.
 - (c) acoustic velocity of $1540 \text{ cm/s} \pm 10 \%$.
 - (d) blood equivalent backscatter.
 - (e) viscosity of 3–4 mPa s.
10. Which of the following are components of a parallel plate endothelial flow phantom:
- (a) microscope.
 - (b) cone viscometer.

- (c) confluent endothelial cell layer.
- (d) blood mimic composed of 60:40 water:glycerol by mass.
- (e) optically transparent window.

Chapter 12 SAQs

1. Describe the advantages and disadvantages of using a flow phantom over an in vivo experiment.
2. Describe three uses of flow phantoms.
3. Briefly describe the principles of PIV.
4. Briefly describe the principles of LDA.
5. Briefly describe the steps for 3D printing of a phantom using the mould and lost-core technique.
6. Describe how corrosion casting might be used to manufacture a 3D anatomical phantom.
7. Describe how PVA may be used to make phantom components for MRI and ultrasound.
8. Describe components of a tissue-equivalent ultrasound phantom incorporating a vessel.
9. Describe components of a tissue-equivalent MRI phantom of an artery.

10. Describe how a low-melting point lost-core may be used to make a vascular phantom for MRI or ultrasound.
11. Describe the design and construction of a parallel plate endothelial flow phantom.

Chapter 12 LAQs

1. Describe the techniques used for visualisation and measurement of the velocity field in optically transparent flow phantoms.
 2. Describe how 3D printing may be used to manufacture phantoms for use in flow phantoms.
 3. Describe the design, construction and components of a flow phantom incorporating a planar carotid phantom for use with MRI.
 4. Describe the design, construction and components of a flow phantom incorporating a non-planar carotid phantom for use with ultrasound.
 5. Compare the design and advantages/disadvantages of a parallel plate endothelial flow phantom and a whole artery flow phantom.
-

Chapter 13 Questions; Measurement and Imaging of the Mechanical Properties of Biological Tissues.

Chapter 13 MCQs

1. In tensile testing of excised tissues the load:
 - (a) Should produce the range of stress values in the tissue sample relevant for all biological tissues *in vivo*.
 - (b) Should range from 1 to 10^6 kPa.
 - (c) Should be set to zero.
 - (d) Should produce the range of stress values in the tissue sample relevant for that tissue *in vivo*.
 - (e) Is adjusted so that there is tissue failure.

2. In uniaxial tensile testing for measurement of stress–strain properties of tissues:
 - (a) the sample is compressed until failure.
 - (b) the tissue is cut into dumbbell- or rectangular-shaped samples.
 - (c) stretching causes reduction in area in the lateral direction.
 - (d) the tissue is cut into J-shaped samples.
 - (e) the sample is elongated until failure.

3. The mechanical properties such as Young's modulus may be measured by:
 - (a) uniaxial tensile testing on a sample of excised artery in the shape of a rectangle or dumbbell.
 - (b) biaxial tensile testing on a sample of excised section of artery in the shape of a rectangle.
 - (c) inflation testing on an excised section of whole artery.
 - (d) in vivo from measurements of wall motion, wall thickness and pressure.
 - (e) in vivo from measurement of pulse wave velocity, wall thickness and diameter.

4. Planar biaxial testing of the mechanical properties of excised tissue samples:
 - (a) typically uses dumbbell-shaped samples of tissue.
 - (b) enables characterisation of anisotropic behaviour.
 - (c) concerns loading in 2 or more directions in a 2D plane.
 - (d) enables characterisation of 3D behaviour.
 - (e) typically uses square samples of tissue.

5. Which of these equations is the correct formulation for the stiffness index β measured in arteries?

(a) $\beta = \frac{d_d (P_s - P_d)}{2h (d_s - d_d) / d_d}$

(b) $\beta = \frac{(P_s - P_d)}{(d_s - d_d) / d_d}$

(c) $\beta = \frac{\ln(P_s / P_d)}{(d_s - d_d) / d_d}$

(d) $\beta = \sqrt{\frac{Eh}{d\rho}}$

(e) $\beta = \frac{d\rho}{h} (\text{PWV})^2$

6. For measurement of the pressure-strain elastic modulus in the carotid artery the following are needed:

(a) systolic and diastolic diameter from ultrasound.

(b) Young's modulus from shear wave imaging.

(c) wall thickness from ultrasound.

(d) pulse wave velocity from tonometry.

(e) systolic and diastolic pressures from an arm cuff.

7. Concerning elastography; which of the following are not steps that are needed in shear wave elastography:

- (a) Use of MRI or ultrasound to measure the shear wavelength or frequency in vivo.
- (b) Induction of compressional waves.
- (c) Induction of shear waves.
- (d) Measurement of local stress from local strain using finite element analysis.
- (e) Estimation of local Young's modulus from the equation: $E = 3\rho c_s^2$.

Chapter 13 SAQs

1. Describe three steps in sample preparation in uniaxial testing of stress–strain behaviour of an excised artery.
2. List and describe briefly three methods for estimation of the circumferential Young's modulus of an artery.
3. Write down the equation for pressure-strain elastic modulus E_p in terms of diameter and pressure and state how ultrasound may be used to estimate E_p .
4. Describe the main steps in shear wave elastography leading to the calculation of local Young's modulus.

Chapter 13 LAQs

1. Describe how uniaxial testing may be used to estimate the stress–strain behaviour of a sample of excised tissue and how Young's modulus may

be measured from the output data.

2. Describe how shear waves may be used to measure local Young's modulus in vivo giving reference to both ultrasound and MRI methods.
-

Chapter 14 Questions; Hypertension and Ageing

Chapter 14 MCQs

1. The definition of hypertension is:
 - (a) systolic blood pressure ≥ 90 mmHg and/or diastolic pressure ≥ 140 mmHg measured in the arm.
 - (b) systolic blood pressure ≥ 160 mmHg measured in the arm.
 - (c) diastolic blood pressure ≥ 100 mmHg measured in the arm.
 - (d) systolic blood pressure ≥ 140 mmHg and/or diastolic pressure ≥ 90 mmHg measured in the arm.
 - (e) systolic blood pressure ≥ 140 mmHg and/or diastolic pressure ≥ 90 mmHg measured in the thigh.

2. Primary hypertension:
 - (a) constitutes 5–10 % of all hypertension cases.
 - (b) has no clear underlying cause.
 - (c) is caused by anti-depressants and cocaine.
 - (d) is caused by kidney disease.
 - (e) has the same origins as secondary hypertension.

3. Mixed hypertension:

- (a) involves increase in both systolic and diastolic pressure.
- (b) involves decrease in systolic and increase in diastolic pressure.
- (c) is the most common pattern of hypertension >50 years.
- (d) is the most common pattern of hypertension in age 30–50.
- (e) involves increase in systolic pressure and no change in diastolic pressure.

4. Concerning blood pressure and ageing:

- (a) Systolic blood pressure decreases with age.
- (b) The biological cause of blood pressure increasing with age is cyclic fatigue fracture of elastin.
- (c) Systolic blood pressure increases with age.
- (d) Biological ageing is the main cause of increasing blood pressure with age in the Western world.
- (e) Biological ageing is the main cause of increasing blood pressure with age in primitive societies.

5. Stiffening of arteries:

- (a) leads to decrease in the return-time of reflected pressure waves in

the aorta.

- (b) is associated with a decrease in pulse wave velocity in the aorta.
- (c) leads to increase in the return time of reflected pressure waves in the aorta.
- (d) can lead to increase in the systolic pressure in the aorta.
- (e) can lead to reduction in systolic pressure in the aorta.

6. Medium-term increase in mean blood pressure leads to:

- (a) decrease in PWV.
- (b) increase in wall thickness to normalise circumferential stress.
- (c) increase in PWV.
- (d) decrease in wall thickness to normalise circumferential stress.
- (e) no change in PWV.

7. Modern invasive measurement of blood pressure involves:

- (a) use of a catheter containing a flexible membrane and fluid-filled column.
- (b) use of a catheter containing a piezoelectric transducer.
- (c) use of an arm cuff.

(d) use of a tonometry system.

(e) use of an NIBP.

8. Concerning applanation tonometry:

(a) This produces a pressure-time waveform.

(b) This produces a blood velocity-time waveform.

(c) Produces measurements of pressure which require calibration using another device (e.g. arm cuff).

(d) This is applicable to deep arteries (e.g. aorta).

(e) This is applicable to arteries near the surface (e.g. carotid, brachial, radial).

9. Central blood pressure:

(a) is estimated from a calibrated femoral pressure waveform using a transfer function.

(b) is the blood pressure in the radial artery.

(c) may be estimated using an arm cuff.

(d) is the blood pressure in the ascending aorta.

(e) is estimated from a calibrated radial pressure waveform using a

transfer function.

10. Concerning augmentation pressure:

- (a) is the additional systolic pressure in the ascending aorta arising from reflected waves.
- (b) is the systolic pressure in the ascending aorta.
- (c) the augmentation index is the augmentation pressure divided by the pulse pressure.
- (d) may be estimated using an arm cuff.
- (e) the augmentation index is the augmentation pressure multiplied by the pulse pressure.

Chapter 14 SAQs

1. Define hypertension and discuss the prevalence and origins of primary and secondary hypertension.
2. Illustrate the change in stiffness with age and discuss biological and pathological contributions.
3. How do reflected waves lead to increase in central pressure?
4. Describe what happens to the aorta following a medium-term (weeks) increase in blood pressure.
5. Compare the performance of fluid-filled and piezoelectric catheter systems for measuring pressure.

6. Describe the principle of measurement of blood pressure using an arm cuff.
7. Describe the process whereby central pressure is estimated using a tonometry system.
8. Describe what is meant by augmentation and how central pressure augmentation index is calculated.

Chapter 14 LAQs

1. Describe what is meant by hypertension and discuss the causes of hypertension, including the effect of ageing.
 2. Describe the relationship between arterial stiffness and central blood pressure and how this is measured using tonometry.
 3. Describe 3 methods by which arm blood pressure may be measured.
-

Chapter 15 Questions; Atherosclerosis

Chapter 15 MCQs

1. Cardiovascular disease are responsible for what percentage of world deaths;
 - (a) 1 %.
 - (b) 11 %.
 - (c) 31 %.
 - (d) 61 %.
 - (e) 81 %.

2. Atherosclerosis;
 - (a) does not occur in the carotid arteries.
 - (b) begins in old age.
 - (c) is associated with deposition of fatty deposits in the medial layer.
 - (d) is concerned with increase in diameter of the inner lumen.
 - (e) leads to lumen reduction in advanced disease.

3. For an isolated 50 % stenosis by diameter in an artery;

- (a) blood velocity is maximum where cross-sectional area is minimum.
- (b) flow rate at the point of minimum lumen is 4 times flow rate in the pre-stenotic region.
- (c) blood velocity is maximum a small distance downstream from the point of minimum area.
- (d) wall shear stress is highest in upstream part of the stenosis.
- (e) there is a pressure drop associated with viscous and turbulent energy losses.

4. With increasing degree of stenosis;

- (a) flow rate gradually increases reaching a peak value at around 70 % stenosis by diameter.
- (b) blood velocity gradually increases reaching a peak at around 84 % stenosis by diameter.
- (c) flow rate is maintained constant until around 70 % stenosis.
- (d) the downstream arteriolar bed dilates until it is fully dilated at around 70 % stenosis.
- (e) the downstream arteriolar bed resistance to flow is maintained constant.

5. Concerning atherosclerotic plaque:

- (a) stable cap are associated with thin cap walls and large lipid pools.
 - (b) rupture occurs when the mechanical stress within the cap exceeds the cap strength.
 - (c) high wall shear stress leads to cap thickening.
 - (d) rupture occurs when the wall shear stress exceeds the cap strength.
 - (e) plaque tend to grow downstream through a process of upstream erosion and downstream growth.
6. In the conventional model of atherosclerosis disease is initiated at regions of:
- (a) low wall shear stress and/or low oscillatory index.
 - (b) high wall shear stress.
 - (c) high blood velocity.
 - (d) low wall shear stress and/or high oscillatory index.
 - (e) high circumferential stress.
7. In the early stages of atherosclerosis:
- (a) plaque volume increases.
 - (b) lumen is maintained constant.

- (c) there is inward remodelling.
 - (d) there is outward remodelling.
 - (e) there is no remodelling.
8. Estimation of the degree of stenosis using ultrasound is based mainly on measurement of:
- (a) intima-media thickness from the B-mode image.
 - (b) diameter from the B-mode image.
 - (c) peak systolic velocity from spectral Doppler.
 - (d) flow rate using the B-mode image and spectral Doppler.
 - (e) mean velocity from spectral Doppler.
9. The decision to offer carotid surgery for patients with atherosclerosis is based on:
- (a) flow rate below a critical value of 50 ml/min (NASCET) or 70 ml/min (ECST).
 - (b) degree of stenosis above a critical value of 50 % (NASCET) or 70 % (ECST).
 - (c) wall shear stress above a critical value of 50 Pa (NASCET) or 70 Pa (ECST).
 - (d) maximum velocity is above a critical value of 500 cm/s

(NASCET) or 700 cm/s (ECST).

(e) plaque volume above a critical value of 0.5 cm^3 (NASCET) or 0.7 cm^3 (ECST).

10. Quantitative information on the severity of a coronary artery stenosis can be obtained from:

(a) a knowledge of the upstream and downstream pressure.

(b) the angiogram.

(c) the diameter of the artery.

(d) the severity of chest pain.

(e) body mass index.

Chapter 15 SAQs

1. Describe briefly the progression of atherosclerosis from initiation to rupture.

2. Describe the relationship between velocity, flow rate and degree of stenosis.

3. Describe the changes in pressure across a stenosis.

4. Describe what is meant by stable and vulnerable plaque and their typical composition.

5. Describe the role of wall shear stress in atherosclerosis initiation and

progression.

6. Explain the phenomenon of outward remodelling and explain why this occurs.
7. Explain how ultrasound may be used to estimate the degree of stenosis.
8. Describe the typical warning signs of imminent plaque rupture in carotid and coronary arteries.
9. Describe the typical clinical management of a patient who is suspected of a carotid stenosis.
10. Describe the typical clinical management of a patient who is suspected of a coronary stenosis.

Chapter 15 LAQs

1. Describe the physical characteristics of the flow-field for a stenosis.
 2. Describe the progression of atherosclerosis from initiation to rupture, the clinical consequence of atherosclerosis in the patient, and the management of the patient with examples from 1 of heart, brain or lower limb.
 3. Describe and explain the relationship between velocity, flow rate and degree of stenosis and describe how ultrasound is used to estimate the degree of stenosis.
 4. Describe the role of wall shear stress and tissue stress in the initiation, progression and rupture of atherosclerotic plaque.
-

Chapter 16 Questions; Aneurysms

Chapter 16 MCQs

1. Aneurysms:

- (a) Occur only in the abdominal aorta.
- (b) Involve a reduction in the diameter of the inner-wall of an artery.
- (c) Are associated with loss of elastin leading to increased stiffness.
- (d) Can rupture causing spillage of plaque contents into the bloodstream.
- (e) Involve an increase in the inner and outer wall diameter of an artery.

2. Concerning tension and stress within the wall of a thin-walled sphere or cylinder (Law of Laplace):

- (a) Tension is proportional to pressure.
- (b) Tension is proportional to wall thickness.
- (c) Circumferential stress is inversely proportional to pressure.
- (d) Circumferential tension is proportional to diameter.
- (e) Circumferential stress is proportional to (diameter)².

3. In the early stages of disease local loss of elastin from the artery wall may:
 - (a) lead to formation of an aneurysm.
 - (b) lead to formation of an atherosclerotic plaque.
 - (c) lead to remodelling involving laying down collagen fibres to mechanically stabilise the artery.
 - (d) lead to degradation of collagen fibres in order to mechanically stabilise the artery.
 - (e) lead to loss of the endothelium.

4. Concerning rupture of a saccular cerebral aneurysm:
 - (a) Rupture occurs when wall shear stress exceeds wall strength.
 - (b) Risk of rupture increases with aspect ratio.
 - (c) Never occurs when the aneurysm diameter is less than 3 mm.
 - (d) Risk of rupture decreases with aneurysm diameter.
 - (e) Rupture occurs when circumferential stress exceeds wall strength.

5. For an unruptured saccular aneurysm:
 - (a) Treatment is not considered to be cost effective or worthwhile.
 - (b) Treatment is normally considered if the diameter is less than 2 mm.

- (c) Treatment is normally considered if the diameter is greater than 7 mm.
- (d) If there are other risk factors treatment is considered if the diameter is greater than 3 mm.
- (e) If there are other risk factors treatment is considered if the diameter is greater than 7 mm.

6. For unruptured abdominal aortic aneurysm, surgical repair is considered if:

- (a) the maximum diameter is greater than 5.5 cm for men.
- (b) the patient has symptoms of imminent rupture, such as abdominal pain, lower back pain or a pulsatile mass in the abdomen.
- (c) the maximum peak wall stress is greater than 0.50 MPa.
- (d) the maximum diameter is greater than 5.5 mm for men.
- (e) treatment is not considered worthwhile.

7. An abdominal aortic aneurysm generally:

- (a) is a Berry aneurysm.
- (b) is stiffer than a normal artery.
- (c) does not contain intraluminal thrombus.

- (d) has greater elastin content as a result of laying down of elastin sheets.
- (e) has greater collagen content as a result of collagen synthesis in the wall.

8. Concerning rupture of an abdominal aortic aneurysm:

- (a) Aneurysms whose diameter is less than 5.5 cm never burst.
- (b) Mortality rate is only 10 %.
- (c) Risk of rupture increases with diameter.
- (d) Survival rate is only 10 %.
- (e) Risk of rupture decreases for greater peak wall stress.

Chapter 16 SAQs

1. Describe what an aneurysm is and where in the body these typically occur.
2. Describe the law of Laplace and how this relates to risk of rupture of an aneurysm.
3. Describe two different flow patterns in a saccular cerebral aneurysm and state the blood velocity, wall shear stress and dome pressure compared to the parent artery.
4. Describe and illustrate measurement of diameter and aspect ratio of a saccular cerebral aneurysm.

5. Describe briefly modern methods for treating a saccular cerebral aneurysm.
6. Describe modern clinical practice for patient-selection and repair of abdominal aortic aneurysm.
7. Describe changes to elastin and collagen in an abdominal aortic aneurysm and how these relate to changes in stiffness.
8. Describe the relationship between haemodynamics and thrombus formation in a growing abdominal aortic aneurysm.

Chapter 16 LAQs

1. Describe prevalence, causes, diagnosis and treatment of a saccular cerebral aneurysm.
 2. Describe theories on the role of wall shear stress in the initiation, development and rupture of a saccular cerebral aneurysm.
 3. Describe the measurement or estimation of diameter, asymmetry index and peak wall stress on an abdominal aortic aneurysm.
 4. Describe theories on the role of mechanical forces and growth of abdominal aortic aneurysm.
-

Chapter 17 Questions; Cardiovascular Prostheses

Chapter 17 MCQs

1. A clinician's first line approach to the treatment of chronic cardiovascular disease is:
 - (a) correctional surgery.
 - (b) surgical implantation of an appropriate cardiovascular device.
 - (c) introduction of a device using a minimally invasive approach.
 - (d) use of one or more appropriate drugs.
 - (e) to advise the patient to stop all exercise with immediate effect.

2. Which procedures can be carried out using a minimally invasive approach?
 - a) replacing an aortic heart valve.
 - (b) balloon angioplasty.
 - (c) balloon angioplasty with stenting.
 - (d) femoral bypass grafting.
 - (e) pacemaker implantation.

3. Which of the following are classified as active implantable devices?

- (a) vascular graft.
- (b) mechanical heart valve.
- (c) ventricular assist device.
- (d) vascular stent.
- (e) balloon catheter.

4. The following are used as biological grafts:

- (a) saphenous vein.
- (b) fabric grafts with velour surface for endothelial attachment.
- (c) Dacron grafts.
- (d) autologous internal mammary artery.
- (e) chemically stabilised bovine artery.

5. Neointimal hyperplasia involves:

- (a) proliferation of smooth muscle cells.
- (b) migration of smooth muscle cells.
- (c) formation of extracellular matrix.
- (d) restoration of the natural vessel wall.

(e) movement of lipid into the vessel wall.

6. Nitinol is:

(a) an alloy of nickel and titanium.

(b) 316L Stainless steel.

(c) a polymer.

(d) a shape-memory metal.

(e) resorbed in the body.

7. The following are types of mechanical heart valve:

(a) bileaflet.

(b) TAVI.

(c) tilting disc.

(d) stentless.

(e) porcine.

8. The following are used to characterise the flow field downstream of a replacement valve:

(a) pressure difference.

- (b) percentage backflow.
- (c) flow visualisation.
- (d) root mean square flow.
- (e) laser Doppler anemometry.

9. Implantable pacemakers have the following basic components:

- (a) pulse generator.
- (b) lead system.
- (c) an external power source.
- (d) gel electrodes.
- (e) an alarm system.

10. The following are pacemaker operation modes:

- (a) transcutaneous.
- (b) dual chamber.
- (c) asynchronous.
- (d) removable.

(e) demand.

Chapter 17 SAQs

1. Describe the steps involved in delivering and deploying a coronary artery stent to the site of vessel occlusion.
2. What are the failure modes associated with artificial heart valves? Describe the underlying design issues.
3. Cardiovascular devices are considered to be safety critical devices. Explain why this is the case giving a specific example.
4. List the factors which need to be considered when classifying a device in order to determine the level of assessment required for regulatory compliance.

Chapter 17 LAQs

1. Discuss the major bioengineering challenges to be considered when developing implantable cardiovascular devices. Illustrate your answer with examples of different types of devices.
2. Describe how the performance of an artificial heart valve can be assessed in vitro. Explain the measures that can be calculated and indicate their clinical significance.
3. Describe the use of cardiac pacemakers including the clinical indications for their use, the types of devices available and their modes of operation.

Answers to MCQs

Chapter 1 Answers

1: d	2: a, b, e	3: c, d	4: e	5: b, d
6: a, e	7: b, c	8: a, d	9: a, e	10: b, c, e
11: a, b	12: d, e	13: b, c	14: a, c	15: d, e
16: c, e	17: b, c, e			

Chapter 2 Answers

1: a, d	2: c, e	3: c	4: a, b, c, d	5: a, d
6: a, c, e	7: b	8: a, c, e	9: b, c, e	10: b, d

Chapter 3 Answers

1: a, d, e	2: a, b, d	3: d, e	4: b, d	5: c, d, e
6: b, c	7: a, c, e	8: d, e	9: c	10: b, d
11: a, c, d	12: b, c, e	13: a, c	14: c, d	15: a, e
16: b, c, d	17: c, d	18: a, e	19: a, c	20: a, c, d

Chapter 4 Answers

1: b, d, e	2: a	3: a, c, e	4: c	5: a, c, e
6: a, b, e	7: a, b, c, d, e	8: b, c, e	9: a, b	10: a, b, d, e

Chapter 5 Answers

1: c, e	2: c, d	3: a, e	4: b, e	5: c, e
6: b, c, e	7: a, b, c	8: b, c, d	9: a, e	10: c, d, e
11: a	12: c, e			

Chapter 6 Answers

1: a	2: a	3: c	4: b	5: c
6: d	7: a	8: d	9: b	10: c

Chapter 7 Answers

1. b, c, d	2. b, d	3. a, b, c	4. a, d, e	5. a, b, d, e
6. b, d, e	7. a, c, e	8. a, b, e	9. c, d, e	10. a, c, d
11. a, b, c, e				

Chapter 8 Answers

1: a	2: c, d	3: b, e	4: d	5: c
6: e	7: b	8: b		

Chapter 9 Answers

1: d, e	2: a, b, c	3: a, c	4: c, d	5: c, e
6: b, e	7: c, d	8: b, c	9: a, c, e	10: b, c, e
11: a, c	12: b, c, d	13: a, d, e	14: c, d	15: b
16: b, d	17: e	18: c, d	19: a, d	20: a, b, c

Chapter 10 Answers

1: c, d	2: e	3: a, c, d	4: c, d	5: b, c
6: e	7: e			

Chapter 11 Answers

1: b, c, d	2: a, b, c, d, e	3: b, d	4: c	5: c, e
6: e	7: b, d	8: b, c, e	9: b, e	10: d, e

Chapter 12 Answers

1: c	2: a, d, e	3: a, b, d	4: b, d	5: a, c, d
6: a, b, c, d	7: b, c, d	8: c	9: a, b, d, e	10: a, c, e

Chapter 13 Answers

--	--	--	--	--

1: d, e	2: b, c, e	3: a, b, c, d, e	4: b, c, e	5: c
6: a, e	7: b, d			

Chapter 14 Answers

1: d	2: b	3: a, d	4: b, c, e	5: a, d
6: b, c	7: b	8: a, c, e	9: d, e	10: a, c

Chapter 15 Answers

1: c	2: c, e	3: c, d, e	4: b, c, d	5: b, e
6: d	7: a, b, d	8: c	9: b	10: a

Chapter 16 Answers

1: c, e	2: a, d	3: a, c	4: b, e	5: c, e
6: a, b	7: b, e	8: c, d		

Chapter 17 Answers

1: d	2: a, b, c, e	3: c	4: a, d, e	5: a, b, c
6: a, d	7: a, c	8: c, e	9: a, b	10: c, e

Appendix B: Glossary

0D model

Computational model where there is no spatial variation of relevant quantities within model compartments

1D model

Computational model in which there are spatial variations of relevant quantities in only 1 spatial dimension; e.g., for PWV propagation in arteries

2D ultrasound

Ultrasound where the data is collected in 2D, and displayed in 2D

2D velocity profile

Referring to measurement of the velocity profile in which the velocity is measured at each point within a 2D cross section

3D model

Computational model in which there are spatial variations of relevant quantities in all 3 spatial dimensions; e.g., for patient-specific modelling

3D printing

Technologies which enable manufacture of a 3D model from a computer design; usually involving building up the object in layers in a manner similar to printing

3D ultrasound

Ultrasound where 3D data is collected

7D imaging

Measurement of blood velocity in which there is measurement of the full flow-field data; i.e. all 3 velocity components (v_x, v_y, v_z) within a volume of space (x, y, z) and with time

α

Womersley number; relating to pulsatile (time-varying) flow of a fluid in a vessel

β

Arterial stiffness index

μ

Abbreviation of 'micro' meaning one millionth or 10^{-6} ; e.g. μm

Abdominal aortic aneurysm

Aneurysm of the lower aorta

Acoustic impedance

Fundamental property of a medium in the context of sound wave propagation

Acoustic matching (phantoms)

Ensuring that the ultrasound properties of the phantom material are similar to those in the relevant human tissue

Acrylic (phantom material)

Material used in construction of phantoms; the most common acrylic is perspex; see 'perspex'

Activated platelet

Platelet which has become more sticky leading to accumulation at sites of endothelial injury

Active contour

Another name for a 2D deformable model

Active surface

Another name for a 3D deformable model

Actuator (MRE)

Device which produces shear waves which travel through the body

Adaptability (cardiovascular)

Ability of the cardiovascular system to change in terms of heart and vessel geometry, flow rates and pressures

Adhesion protein

Proteins in the cell membrane to which the cytoskeleton is connected; see 'focal adhesion site'

Adhesion site

See 'focal adhesion site'

Adulthood

Time after childhood; from 20 years to death at age up to around 100 years

Adventitia

Outermost layer of the artery wall mainly consisting of collagen fibres

Afterload

Tension generated by the left (or right) ventricle during the ejection phase of the cardiac cycle

Agar (for tissue mimic)

Jelly-like organic material used in the construction of MRI and ultrasound phantoms

Aggregation (red cell)

Accumulation of red cells into a single larger structure which occurs at very low shear ($<10 \text{ s}^{-1}$); consists of rouleaux

Albumin

Protein present in blood whose function is concerned with maintenance of osmotic pressure

Alpha

See 'Womersley number'

Ammonia

One of the waste products of metabolism

Anaemia

Abnormally low haematocrit and/or haemoglobin level leading to lowered ability of the blood to carry oxygen; leading to tiredness and related symptoms

Aneurysm

Localised increase in diameter of an artery characterised by loss of elastin
Aneurysm rupture

Tearing of the wall of an aneurysm leading to leakage of blood into the surrounding tissues

Angiography

X-ray imaging techniques which are aimed at producing images of blood vessels

Angioplasty

Procedure used to widen arteries which have become occluded or narrowed as a result of atherosclerosis; usually performed under imaging guidance such as fluoroscopy

Anisotropic

Physical properties in a material are different in different directions

Annihilation

Complete conversion of the mass of a particle and its anti-particle into energy

Anti-particle

Fundamental particle of matter but with opposite charge and magnetic moment; every sub-atomic particle has an anti-particle; e.g. positron is the anti-particle of the electron; extremely short lived in this universe due to collision and annihilation

Aorta

The main artery in the systemic circulation originating at the heart and ending in the lower abdomen where it divides into the left and right common iliac arteries

Aortic valve

Heart valve between the left ventricle and the aorta preventing backflow of blood into the left ventricle

Applanation tonometry

Measurement of pressure using a probe pressed against the skin

Arachnoid membrane

One of the membranes which surrounds the brain

Arrhythmia

Disturbance to normal heart rhythm

Arterial biomechanics

Study of the structure and function of arteries using the methods of mechanics

Arterial mechanics

Synonymous with the term 'arterial biomechanics'

Arterial remodelling

Change in diameter or shape of an artery; e.g. in response to changes in wall shear stress, changes in longitudinal stress or circumferential stress

Arteriolar resistance

The resistance offered by the arteriolar bed; this affects flow rate and pressure drop across the arteriolar bed (see 'resistance to flow')

Arteriole

Small vessel connecting arteries to capillaries; diameter 10–100 μm

Artery

Large vessels involved in transport of blood from the heart; diameter 1–30 mm

Aspect ratio

Ratio of the longest to shortest side in a mesh element; a metric used in evaluation of mesh quality; ratios near 1 are ideal

Aspect ratio

The ratio of the neck width to height for a saccular cerebral aneurysm

Atherosclerosis

A common disease of arteries in which lipid deposits (atheroma) accumulate in the vessel wall

Atherosclerotic plaque

Later stage of atherosclerosis in which, for a localised region of an artery, the intimal layer contains a mix of lipid, fibrous tissue, white cells, smooth muscle cells and calcifications

Atria

Chambers of the heart which receive blood from the venous system; left atrium receives blood from the pulmonary venous system, right atrium receives blood from the systemic venous system

Atrioventricular node

Component of the electrical conduction system of the heart, which provides an activation pathway from atria to ventricles

Augmentation index

The ratio of augmentation pressure divided by pulse pressure

Augmentation pressure

Difference between the peak pressure which would have occurred in the absence of reflected waves and peak pressure in practice

Autocrine molecules

Signalling molecules produced by a cell which act on the same cell

Autolysis

Self-digestion of or destruction of cells by its own enzymes

Axial

Relating to a vessel, in the direction of the vessel

Axial accumulation

Increase in the concentration of cells near the centre of a vessel; e.g. red cells in arterioles

Axial flow

Relating to flow in a vessel in which the velocity vectors are all in the axial direction, with no transverse flow component (i.e. no secondary or rotational flow)

Axisymmetric flow

Flow in a tube or vessel where the velocity profile is not radially symmetric; there is some skewing to one wall and the maximum velocity is not located at the centre of the vessel

Back-projection

Method used in CT to reconstruct the image

Balloon angioplasty

Angioplasty which uses a balloon catheter to widen the artery the balloon is inflated to high pressure which widens the artery

Balloon catheter

Catheter used in angioplasty which has an inflatable balloon near the distal end of the catheter which can be inflated for the purpose of widening diseased arteries

Barium contrast agent

Liquid containing barium used to improve image contrast in X-ray imaging of the gastrointestinal system

Basement membrane

Part of the intima, a layer of extracellular matrix on which the endothelial cells are attached

Bayliss effect

Myogenic effect in arterioles

Bernoulli equation

Equation for flow of an inviscid fluid; an expression of conservation of energy in a streamline whereby gravitational potential energy plus pressure energy plus kinetic energy is a constant

Bernoulli principle

For an inviscid flow (i.e. no viscosity), an increase in fluid velocity is associated with decrease in pressure

Berry aneurysm

See 'saccular aneurysm'

Biaxial testing

Mechanical testing of materials with stretching in 2 or more directions

Biconcave

Having surfaces which are concave (curving in) on both sides

Bicuspid valve

A valve with two leaflets

Bifurcation

Splitting of a vessel into 2 or more branches

Bilipid membrane

Cell membrane formed from two layers of lipid molecules

Binding site

Region (site) of a protein to which specific molecules can attach (bind)

Bingham plastic

Fluid which has a yield stress before it will flow

Biomechanics

Study of the structure and function of biological systems using the methods of mechanics

Bioreactor

Laboratory device which supports biological activity

Black blood imaging

MRI technique in which blood in vessels appears dark

Blood

Fluid pumped around the cardiovascular system

Blood mimic

See blood-mimicking fluid

Blood-mimicking fluid

Fluid used in a flow phantom to mimic the blood; mimicking viscous properties and relevant imaging properties

Blood velocity

Velocity of blood; different quantities include maximum velocity (during the cardiac cycle), mean velocity at a particular time (averaged over a vessel) mean velocity (average over the vessel and the cardiac cycle). Common

units are cm s^{-1} , m s^{-1}

Blunt profile

Velocity profile which is flattened apart from near the wall

BMF

Abbreviation for 'blood-mimicking fluid'

B-mode

Ultrasound imaging mode in which the received echo amplitude is displayed in 2D, usually in grey scale; short for 'brightness mode'

Boundary conditions

Set of additional constraints used in computational modelling in order that a unique solution can be obtained

Boundary conditions

Set of constraints required for execution of a computational model

Boundary layer

Region between flow dominated by viscous effects (e.g. near the vessel wall) and flow dominated by inertial effects (e.g. in the vessel centre near an inlet)

Bright blood imaging

MRI technique in which blood in vessels appears bright

Brightness-mode

See B-mode

Brownian motion

Random variations in collisions between the fluid molecules and a particle lead to erratic movements called Brownian motion

Bulk modulus

Property of a solid or liquid describing elastic behaviour, concerned with changes in volume; defined as the negative ratio of change in pressure divided by change in volume

Buoyant force

Force on an object in a fluid (e.g. particle) arising from hydrostatic pressure

C-11

See carbon-11

Calcium ion channel

Ion channel for the passage of calcium ions (Ca^{2+}) into or out of the cell

Calcium wave

An influx of calcium ions via the calcium ion channel pass through the cell in the form of a wave; this is one type of mechanosignalling

Calf muscle pump

The muscular anatomy in the region of the deep veins which acts to expel blood from the deep venous circulation during muscle contraction

Capillary

Smallest vessels of the cardiovascular system where there is exchange of oxygen and other molecules with the surrounding tissues (diameter 4–10 μm , up to 40 μm in sinusoidal capillaries)

Carbon dioxide

Molecule produced as a consequence of metabolic activity; transported in blood and discharged via the lungs

Carbon-11

Isotope of carbon which is unstable, decaying to boron-11 (B-11) and also producing a positron; half life of 20.3 min, used in PET

Cardiac action potential

Transient electrical activation and recovery of a cardiac cell, manifest as an excursion of membrane potential

Cardiac output

Flow rate of blood leaving the heart, usually averaged over the cardiac cycle; units are usually L min^{-1}

Cardiovascular biomechanics

Study of the structure and function of the cardiovascular system using the methods of mechanics

Cardiovascular disease

Umbrella term for a range of diseases of the cardiovascular system

Cardiovascular system

Organs in the body which are concerned with pumping and transport of blood; consisting of heart, arteries, arterioles, capillaries, venules and veins; divided into the systemic circulation and the pulmonary circulation

Carotid endarterectomy

Removal of the inner layers of the carotid arteries including any atherosclerotic plaque

Catheter

Flexible tube inserted into the body; e.g. along an artery via an arterial puncture

Catheter based imaging

Medical imaging systems in which a miniature imaging system mounted on the end of a catheter passed along the arterial system to the point of

interest

Cell alignment

See 'endothelial cell alignment'

Central pressure

Pressure of blood in the aorta near the heart

Central pressure waveform

Variation of blood pressure with time in the aorta near the heart

Cerebral aneurysm

Aneurysm of a cerebral artery (usually involving the Circle of Willis)

CFD

See 'computational fluid dynamics'

C-flex (vessel mimic)

Commercially available tube which has similar speed of sound to that in soft tissue and has been used in ultrasound flow phantoms

Childhood

From birth to adulthood in which there is increase in the child's height and growth of organs; 0–20 years in the human

Circulation

Abbreviation of 'circulatory system'; another name for the cardiovascular system

Circulatory system

Another name for the cardiovascular system

Circumferential stress

Stress within the vessel wall in the circumferential direction (i.e. in the direction perpendicular to the vessel axis)

Circumferential wall stress

See 'circumferential stress'

Claudication

Pain in the calf after walking for a certain distance, caused by atherosclerosis in the arteries of the leg

Claudication distance

Distance that a person can walk before claudication develops. See 'claudication'

Cleaving

Splitting into 2 parts; e.g. cleaving a molecule

Clinical ultrasound

Sound with frequencies in the range used in clinical scanning; commonly 2–

20 MHz for non-invasive use, 20–60 MHz for invasive use in the form of intravascular ultrasound

Clip

Metallic device surgically placed at the neck of a saccular cerebral aneurysm to seal it from the parent artery

Clotting

Normal coagulation of blood at sites of vascular damage to prevent bleeding

Co-culture phantom

Example of an endothelial flow phantom in which there are adjacent layers of endothelial cells and smooth cells

Coil

Coiled metal wire of small dimensions inserted into a saccular cerebral aneurysm to induce thrombosis within the aneurysm

Collagen

A protein with high tensile strength, in vessels of the cardiovascular system it is present mainly in the adventitial layer of the artery wall

Collagen/elastin ratio

Ratio of collagen to elastin content in the vessel wall is an indicator of vessel stiffness

Collateral circulation

Network of small arteries in parallel to the main artery; as main artery atherosclerosis progresses the collateral vessels enlarge and may be able to take over blood supply to the tissues

Colloid osmotic pressure

Osmotic pressure exerted by albumin in the blood (equal to around 22 mm Hg); also called ‘oncotic pressure’

Colour flow (ultrasound)

General term describing a range of techniques which are used for 2D imaging of blood flow using methods based on the Doppler equation

Competent venous valve

A venous valve which is able to resist flow of blood away from the heart due to closure of the leaflets

Compliant-wall model

Model used in arterial CFD in which vessel walls are compliant (rather than stiff) and hence allowed to move during the cardiac cycle

Composite

Relating to materials or biological tissues; containing 2 or more types of

material or tissue with different physical properties

Computation time

Length of time it takes for completion of a single run of a computer programme

Computational fluid dynamics

Numerical method for calculation of flow-field data in complex geometries (generally used where analytical solutions are not available)

Computational fluid dynamics

A branch of computational mechanics, concerned with estimation of flow-field data

Computational mechanics

The area concerned with the solution of mechanical problems by the use of computers, in which the governing equations are solved at discrete points within the 3D volume

Computational modelling

General term referring to the use of computers to simulate complex phenomena where behaviour is summarised by governing equations; in which the governing equations are replaced by simpler equations and a process of iteration

Computed tomography

See CT

Computer simulation

See 'computational modelling'

Conductance

Measure of the movement of electrical charge through an ion channel, pump, or exchanger

Conduction defect

Disturbance to the normal sequence of electrical activation in the heart

Cone plate viscometer

Device for measuring the viscosity of a fluid as a function of shear rate; consisting of a fixed flat plate and a rotating plate in the shape of a cone

Conformation

3D arrangement of atoms within a molecule; e.g. a protein

Constitutive equations

Equations of a solid which govern the relationship between stress and strain, or of a liquid which govern the relationship between shear stress and shear strain rate

Constitutive model

The set of equations which describe the governing physical behaviour of the fluid or solid

Continuous capillary

The most common type of capillary in which the endothelium is continuous (with no gaps or pores)

Continuous elastic compression

Compression applied with constant pressure, typically to the lower limb, using elastic bandages

Continuous media

A material which has physical or mechanical properties at all positions in space (x, y, z) and time (t)

Contrast agent

A material which when injected into the patient provides a significant change (increase or decrease) in the imaged quantity enabling improved visualisation of particular structures; or in other words an agent which improves image contrast

Contrast agent (MRI)

Contrast agent used for improving image quality in MRI; mostly based on gadolinium or iron; see 'contrast agent', 'gadolinium (contrast agent)', 'iron (contrast agent)'

Contrast agent (targetted)

See 'Targetted contrast agent'

Contrast agent (ultrasound)

Contrast agent used for improving image quality in ultrasound; based on the use of microbubbles. See 'contrast agent', 'microbubble'

Contrast agent (X-ray)

Contrast agent used for improving image quality in X-ray imaging; based on the use of iodine or barium. See 'contrast agent', 'iodine contrast agent', 'barium contrast agent'

Coronary sinus

Part of the venous system that drains myocardial tissue

Corrosion casting

Process for creating a cast of the vasculature in which a material (e.g. resin) is injected into the vasculature, allowed to set, and the tissues are chemically removed

Crack

Localised fracture of a material as result of high stress

Crack propagation

Increase in size and extent of a crack with time

Critical stenosis

For flow in an artery; the value of lumen reduction above which flow decreases

Cross-correlation

Technique used in ultrasound strain imaging in which consecutive A-lines are taken and cross-correlation undertaken to estimate local displacement from which local strain is calculated

Cross-linking

Formation of chemical bonds between molecules; e.g. between polymer molecules

CT

X-ray imaging technique involving collection of data around the patient followed by image reconstruction in the computer

Cultured endothelium

Laboratory preparation in which a layer of endothelial cells is prepared on substrate such as glass; typically the cultured endothelium is incorporated into a flow phantom which allows experiments to be performed on the response of the endothelial cells to changes in flow conditions (e.g. changes in wall shear rate)

Cyclic fatigue

Reduction in strength of a material which is subject to repeated stretching and unstretching

Cyclic fatigue (wrt pressure)

Increase in arterial stiffness associated with elastin fibre fracture arising from repeated stretching and unstretching over many years

Cyclic stress (wrt pressure)

See 'cyclic fatigue (wrt pressure)'

Cyclic stretch fatigue (wrt pressure)

See 'cyclic fatigue (wrt pressure)'

Cyclic stretching

Repeated stretching and unstretching of the vessel wall (in both circumferential and longitudinal directions) as a result of variations in blood pressure during the cardiac cycle

Cyclotron

Device for the production of radioactive isotopes, for use in PET

Cytoskeleton

Structure within a cell that allows the cell to maintain its shape and internal structure, and allows transmission of force; composed of microtubules and filaments

Dashpot

In the context of viscoelastic models; purely viscous component where stress is proportional to strain rate

Decentralised model (of endothelial mechanotransduction)

Model of endothelial mechanotransduction in which mechanosensors are distributed throughout the endothelial cell rather than just being on the luminal surface

Deep Vein Thrombosis (DVT)

Formation of thrombus in the deep veins, typically in the calf

Deep venous circulation

The venous circulation which lies beneath the fascial boundary

Deformable model

A type of segmentation method in which a line (2D) or surface (3D) is deformed so that it matches the boundary within an image

Deformable particle

Particle which can be deformed; e.g. red cell

Deformation

Alteration in shape of a structure

Deformation (red cell)

Change in the shape of the red cell at high shear

Degree of stenosis

The reduction in lumen diameter or area of an artery, usually arising through atherosclerotic disease

Density

Property of a liquid or solid; mass divided by volume; unit kg m^{-3}

Deoxygenated blood

Blood depleted of oxygen

Depletion force

Concerning a fluid in which there are larger particles (e.g. red cells) and smaller particles (e.g. macromolecules). Random reductions in the concentration of the smaller particles causes the larger particles to be in close contact which is equivalent to a force called a 'depletion force'

Deployment

The action of placing and expanding a stent

Depolarisation

Initial phase of the cardiac action potential where membrane voltage changes from around -85 mV to around $+20$ mV

Destruction imaging (ultrasound)

Ultrasound imaging technique used with contrast agents in which bubbles accumulate within tissue and are caused to destruct by use of a high power pulse; this produces a Doppler shift signal allowing bubbles to be visualised

Development (fetal and embryo)

Process by which the organ systems are laid down and grow from fertilisation to birth

Dialysis fistula

Fistula created to provide a high-flow allowing blood to be drawn for the purposes of cleansing using a dialysis system; usually created in the arm

Diameter

Distance of a circle from one side to another where the distance passes through the centre of the circle

Diastole

The portion of the cardiac cycle in which the heart is not contracting

Diastolic pressure

The lowest pressure in an artery during the cardiac cycle

Diffusion tensor imaging

MRI technique which images the Brownian motion of water molecules

Digital model

A model of a material which has physical or mechanical properties at discrete locations in space and time, see 'mesh'

Dilatant

Another word for 'shear thinning'

Discrete model

See 'digital model'

Discretization

The process of approximation of the governing equations by simpler equations which are suitable for iterative solution using a computer

Dislocation

Irregularity in the structure of a material, especially those with a regular

crystal structure

Dissection of a vessel wall

Partial tearing or delamination

Disturbed flow

Flow state in which vortices are produced which may travel downstream

Dome (of cerebral aneurysm)

Relating to a saccular cerebral aneurysm; the rear wall of the aneurysm

Doppler equation

Equation describing the relationship between the Doppler shift frequency, the target velocity and the direction of motion of the blood or tissue

Doppler frequency

See Doppler shift

Doppler shift (ultrasound)

Difference in frequency between reception and transmission of ultrasound arising due to motion of the object

Doppler ultrasound

(a) Term used to describe ultrasound systems whose design is based on use of the Doppler equation. (b) Ultrasound which has been frequency shifted as a result of scattering from a moving target

Drag force

Relating to an object in a fluid; force on the object when there is relative motion between the fluid and the object, arising from inertial and viscous effects

DTI

Diffusion tensor imaging; MRI technique concerned with the diffusion of molecules; used for investigation of orientation of fibres in the body

Ductus arteriosus

Hole between the pulmonary artery and the aorta connecting the pulmonary and systemic circulations in the fetus

ECST

Abbreviation for the European Carotid Surgery Trial

ECST criteria

Criteria for selection of patients for carotid surgery arising from the ECST trial

Ectopic beat

Abnormal heart beat, not arising from the sinoatrial node

Ehlers–Danlos syndrome

Genetic disorder of connective tissues, including tissues in arteries

Ejection fraction

Stroke volume as a fraction of the total volume of the left ventricle

Elastic

Description of a solid material which recovers its original shape fully after release of the applied stress

Elastic-linear

Concerning the stress–strain graph which is linear in the elastic region (i.e. before the yield point)

Elastic-nonlinear

Concerning the stress–strain graph which is nonlinear in the elastic region (i.e. before the yield point)

Elastic instability

Instability of equilibrium in elastic systems, including elastic buckling of thin structures

Elastic modulus

See ‘modulus’

Elastin

Protein with high elasticity; in vessels of the cardiovascular system it is present mainly in the medial layer of the artery wall

Elastography

Medical imaging techniques for measurement of the stiffness of tissues in vivo

Elective surgery

Surgery which is planned in advance but which is not an emergency

Electrocardiogram (ECG)

Electrical potential on the body surface arising from electrical activation of the heart

Electrolytes

Ions present in blood, including calcium ion (Ca^{2+}), chloride (Cl^{-}), potassium (K^{+}) and sodium (Na^{+})

Electromagnetic flow probe

Device for measurement of flow rate in a vessel; requires exposure of the vessel and placement of the probe around the vessel; the device operates by inducing a magnetic field; a voltage field is produced in the flow (proportional to flow rate) which is measured

Electromagnetic spectrum

The range of frequencies of all electromagnetic radiation; from radio waves, microwaves, infrared, light (visible radiation), ultraviolet to X-rays and gamma rays

Electron

One of the fundamental particles of matter, charge of -1 , orbits the nucleus, mass is $1/1837$ of the mass of a proton

Electrostatic force

Force between two objects which carry an electric charge; opposite charges (positive/negative) attract, identical charges (positive/positive or negative/negative) repel

Element

Building block of a mesh used in computational modelling

Embryo

An unborn mammal from conception and before the fetal stage (i.e. from fertilisation to 8 weeks in humans)

Embryogenesis

Formation of the embryo

Endarterectomy

Removal of the inner layers of an artery including any atherosclerotic plaque

Endocardial

Inner surface of the heart

Endoscope

Long flexible instrument which is inserted into a body orifice such as the oesophagus for examination of the tissues from the inside

Endothelial cell alignment

Alignment of the cell direction with the wall shear stress vector

Endothelial cell culture phantom

See 'endothelial flow phantom'

Endothelial flow cell

See 'endothelial flow phantom'

Endothelial flow phantom

Flow phantom incorporating a layer of endothelial cells used for investigation of the relationship between endothelial behaviour and mechanical forces

Endothelium

A single cell layer of specialised cells in contact with flowing blood; important because of their role in mechanotransduction

Enzyme

Molecule which increases the rate of a chemical reaction occurring in the body

Epicardial

Outer surface of the heart

Epidemiology

The study of the causes, distribution and control of disease in populations

Erythrocyte

Another name for 'red cell'

Erythrocyte volume fraction

See 'haematocrit'

Essential hypertension

Elevated blood pressure where there is no clear underlying cause

Euheart

See www.euheart.eu

Experimental flow system

Another name for 'flow phantom'

Expiration

Concerning lungs, breathing out

Ex-vivo

From the Latin 'outside of the living', referring to experiments on tissues or organs which have been removed from a living subject and kept metabolically alive

F-18

See fluorine-18

Fahraeus effect

Fahraeus effect is that the haematocrit of blood in a tube of small diameter is less than the haematocrit of blood in the receiving tank (after the 1929 paper by Fahraeus)

Fahraeus-Lindqvist effect

The Fahraeus–Lindqvist effect is that the viscosity in the tube (measured from pressure and flow) depends on tube diameter, reaching a minimum viscosity at a tube diameter of 7 μm ; after the paper by Fahraeus and Lindqvist in 1931

Fascia

The sheet of connective tissue which separates muscle groups within the lower limb

Fatty streak

Small yellow area on the inner lumen of an artery consisting of white blood cells and lipid deposits in the intimal layer; the first stage of atherosclerosis

FDG

Abbreviation for fluorodeoxyglucose; used in PET

FEA

See 'finite element analysis'

Fenestrated capillary

Type of capillary cell which contains fenestrations (pores) to allow the passage of certain molecules

Fenestrations

Pores present in the wall of some capillaries which allow the passage of certain molecules

Fetus

An unborn mammal after the embryonic stage (i.e. from 9 weeks after fertilisation in humans)

Fibrinogen

Large molecule present in blood; part of the clotting system

Fibroblast

Connective tissue cell that provides mechanical support within heart tissue

Fibrous cap (plaque)

Layer between the arterial lumen (where blood flows) and the lipid pool in an atherosclerotic plaque.

Fibrous cap thickness (plaque)

Thickness of the fibrous cap

Fibrous tissue (plaque)

Component of atherosclerotic plaque

Filaments

See cytoskeleton

Filtered back projection

See 'back projection'

Finite difference method

One type of discretization method; commonly used in fluid modelling

Finite element analysis

Solid modelling which uses the finite element discretization method

Finite element method

One type of discretization method; commonly used in solid modelling

Finite element model

A numerical model which captures complex behaviour through solution of a system of equations describing the interaction of many small regions (elements)

Finite volume method

One type of discretization method; used in fluid modelling

Fistula

Connection between an artery and a vein, bypassing the microcirculation

Flash pulse

High peak pressure ultrasound pulse used to cause bubble destruction, used as the basis for 'destruction imaging'; see 'destruction imaging'

Flow diverter

Device placed in the parent artery of a cerebral aneurysm to reduce flow within the aneurysm (which eventually thromboses)

Flow limitation

An effect where flow ceases to increase with increasing pressure gradient due to dynamic increase in resistance

Flow phantom

Apparatus for mimicking the flow of blood in a part of the cardiovascular system; consisting of pump, pump controller, tubing, reservoirs and a central construct which mimics the cardiovascular geometry

Flow probe

Device for measurement of flow rate in a vessel; usually by exposure of the vessel (e.g. electromagnetic flowmeter, transit time flowmeter)

Flow rate

Volume of fluid flowing through a cross section per unit time; e.g. flow of blood in an artery; common units in blood flow are ml min^{-1} , ml s^{-1} , L min^{-1}

Flow recirculation

Flow which goes around in a circle; e.g. in the post-stenosis region

Flow separation

May occur where there is flow in a tube where the cross-sectional area increases, e.g. post-stenosis; there are two adjacent regions of flow with little mixing of fluid

Flow state

Term describing the behaviour of fluid elements in time and space; see 'laminar flow', 'transitional flow', 'disturbed flow', 'turbulence'

Flow visualisation

Visualisation of flow in a flow phantom; by eye or by recording using a video camera

Flow waveform

The plot of flow rate versus time; e.g. in an artery

Flow-field

The 7D dataset of velocity within a 3D volume consisting of all 3 velocity components (v_x, v_y, v_z) at each location (x, y, z) and as a function of time t

Fluid

A liquid; formally a material unable to maintain a shear force at rest

Fluid kinematics

Behaviour of fluids which are in motion

Fluid mechanics

The branch of mechanics which studies the behaviour of fluids

Fluid modelling

See 'computational fluid dynamics'

Fluid statics

Behaviour of fluids which are not in motion

Fluid-particle force

See Brownian motion

Fluorine-18

Isotope of fluorine which is unstable, decaying to oxygen-18 (O-18) and also producing a positron, half life of 110 min, used in PET

Fluorodeoxyglucose

See FDG

Fluoroscopy

X-ray imaging technique in which X-rays are produced and detected continuously forming a 2D real-time image sequence

fMRI

Functional MRI; technique that provides information on brain activity

Focal adhesion

See 'focal adhesion site'

Focal adhesion site

Structures within the cell membrane to which the cytoskeleton connects on the inner side, and on the outer side the extracellular matrix connects

Foramen ovale

Hole between the left and right atria connecting the left and right sides of the heart in the fetus

Force

A physical effect which gives rise to change in motion or deformation

Force-extensional

Force acting perpendicular to a surface causing extension of the material

Force-shear

Force acting parallel to a surface causing shearing of the material

Force-compression

Force acting perpendicular to a surface causing compression of the material

Force-extension graph

Concerning the stretching of a sample of a solid material; the graph of applied force versus the length in the direction of the force

Forward wave (flow)

Blood flow where the flow direction is away from the heart

Forward wave (pressure)

Pressure wave which travels along arteries away from the heart

Fracture

Concerning stretching of a material; the point (stress) above which the material breaks

Frame rate

(a) General: number of frames displayed per second for a display monitor. (b)

Ultrasound: number of image frames acquired per second

Frank–Starling law

Relates the stroke volume to preload of the heart

Free energy

A measure of chemical potential energy; useful in describing chemical reactions; also called ‘Gibb’s free energy’

Frequency

Property of a wave; the number of oscillations passing a given point per second; unit is hertz or Hz

Friction

The force between 2 moving surfaces (e.g. between a fluid layer and a solid wall, between 2 fluid layers)

Fully developed flow

Relating to flow in a tube; flow in which the velocity profile (for steady flow) or the change in velocity profile with time (for pulsatile flow) does not

change with distance along the tube. More formally—flow in which the boundary layer reaches to the centre of the tube

Functional imaging

Medical imaging techniques which provide information related to physiological function, including regional blood flow (perfusion), chemical and biological function

Fusiform aneurysm

Aneurysm in which there is widening at all points around the entire artery

G

Abbreviation of ‘giga’ meaning one billion or 10^9 ; e.g. GPa

Gadolinium (contrast agent)

Metallic element which is strongly paramagnetic and used as a contrast agent for MRI

Gamma camera

Imaging system used in nuclear medicine in which gamma rays from radioactive atoms are detected

Gamma ray

Photon produced by radioactive decay or by positron-electron annihilation

Gangrene

Death of tissues commonly caused by inadequate blood supply followed by decay and decomposition

Gap junction

Pore in the intercalated disc that connects the intracellular space of two adjacent myocytes

Gauge length

Length over which data will be extracted in relationship to mechanical testing

Generator

Device used in nuclear medicine in which a short half-life isotope is produced by radioactive decay of a longer half-life parent (e.g. Mo-99, Tc-99 m generator)

Ghost

See ‘red cell ghost’

Gigapascal

One billion (10^9) Pa, abbreviated GPa

Glass (phantom material)

Material which is optically transparent and has been used in the construction of optically transparent phantoms

Globulins

Family of proteins in the blood including albumin

Glycerol (for blood mimic)

Liquid with high viscosity; component of blood mimics for MRI and ultrasound

Glycocalyx

Network of molecules covering the endothelium, typically 0.2–4.5 μm depending on vessel type, probable role in mechanosensing

Governing equations

The equations which summarise the behaviour of a complex system

Gradient coil

Part of an MRI system; provides a smooth change in field strength along x , y and z ; enabling positional information to be encoded into the received MRI signal

Granulocyte

Type of white cell; responsible for absorbing and digesting bacteria, viruses and other parasites

Gravitational force

Force on an object arising from gravity; in a fluid will lead to particles sinking

Grid

See 'mesh'

Gridding

See 'meshing'

Ground

substance

Haematocrit

Volume fraction of red cells in blood, typically 40–50 %

Half life

Time it takes for the number of atoms of a particular radioactive isotope to halve in number

Hard tissue

General term referring to biological tissues with high calcium content and/or high stiffness (e.g. bone, enamel, ligaments)

Heart

Organ responsible for pumping blood round the circulation

Heart rate

Frequency of heart beats, usually given as beats per minute

Helical flow

Flow which has a rotational component so that particle streamlines have a helical appearance

Helical scanning

Scanning method used in a CT scanner in which data is collected continuously with continuous rotation of the tube-detector around the patient and continuous movement of the patient through the CT system

High WSS hypothesis (cap thinning)

Theory that high wall shear stress in a stenosis leads to thinning of the cap, leaving the cap prone to rupture

Homogeneous

Generally; the same value of a physical property throughout a volume; in the context of red cell concentration; the same red cell concentration throughout the vessel

Hoop stress

See 'circumferential stress'

Hydrogen nucleus

Nucleus of hydrogen consisting of just one proton

Hydrostatic pressure

The pressure gradient which arises due to the weight of a column of fluid

Hyperaemia

Increased blood flow associated with dilation of the arteriolar bed; mechanism for increasing local flow rate

Hyperelastic

Constitutive model for a purely elastic material derived by considering the strain energy density function

Hypertension

Abnormally high blood pressure

Idealised (general)

Simplified representation which captures key features

ILT

See 'intraluminal thrombus'

Image

2D or 3D representation of a 2D or 3D object; in colour or greyscale; for which local image values are related to some property of the object

Image formation

The process by which an image is produced from the object

Image guided modelling

Integration of imaging with computational modelling

Image noise

Generally, any feature of the image which is unwanted which obscures the feature of interest; see 'photon noise', 'speckle'

Imaging

Process of recording/acquiring an image. See 'image'

Immune system

The systems in the body which deal with defence against disease including bacteria, viruses and other pathogens

Impedance

Generally, property of a material which leads to wave reflection when there is a discontinuity in impedance

Impedance (acoustic)

See 'acoustic impedance'

Incremental elastic modulus

Referring to the graph of stress versus strain obtained using a tensile testing system, the slope of the stress-strain curve when the stress-strain curve is not linear

Inertial force

Force on a fluid element arising from the mass of adjacent fluid elements

Infarction

Local tissue death caused by reduction in blood supply below a critical value

Inferior vena cava

Large vein which delivers deoxygenated blood from the lower body to the right atrium

Inflammation (imaging)

Imaging methods which provide information on the degree of inflammation in tissues

Inflation testing

Method for mechanical testing of cylinders involving inflation under pressure and measurement of changes in diameter and wall thickness

Inhomogeneous

Generally, differences in the value of a physical property throughout a volume; in the context of red cell concentration, differences in red cell concentration in a vessel (e.g. depletion near the wall)

Inlet

Relating to the entrance to a tube (e.g. from a large reservoir); region at the beginning of the tube where flow is not fully developed (see 'inlet length')

Inlet length

Distance from the entrance to a tube beyond which flow is fully developed

Inner diameter

Relating to a tube/vessel, the diameter of the lumen (i.e. diameter of the region occupied by the fluid/blood flowing within the tube/vessel)

Input data

In relation to computational modelling; data which is provided as input to a computational model

Inspiration

Concerning lungs, breathing in

Intercalated disc

End to end connections between myocytes

Intermittent pneumatic compression

Compression applied with varying pressure, typically to the lower limb, using a cuff inflated with air

Internal elastic membrane

Layer of elastic material which forms the outer part of the intimal layer

Intervertebral disc

Shock absorber between vertebral discs in the vertebral column; the intervertebral discs thin (reduce in thickness) with age leading to reduction in height later in life

Intima

Innermost layer of the artery wall including a layer of endothelial cells in contact with flowing blood

Intima-media layer

Term for the intimal and medial layers, whose combined thickness can be measured using ultrasound imaging

Intima-media thickness

Combined thickness of the intima and media measured using ultrasound imaging

Intracranial aneurysm

See 'cerebral aneurysm'

Intraluminal thrombus

Thrombus present within the lumen of some aneurysms

Intrasaccular flow disruptor

Device placed in the sac of a saccular aneurysm to seal the aneurysm

Invasive imaging

Medical imaging technique which does lead to some damage (temporary or long term) to the organism; see IVUS, OCT

Inviscid

No viscosity

Inviscid flow

Flow in which there are no viscous effects

In-vitro

From the Latin 'in glass' (a reference to use of a glass test-tube); referring to experiments undertaken in the lab on tissue samples which are no longer living, or on cultured cells

In vitro imaging

Imaging of an organism or part of an organism which is kept metabolically alive but is no longer connected to the rest of the organism. See 'in vitro'

In vivo

From the Latin 'in the living'; referring to experiments or tests undertaken on a living subject

In vivo imaging

Imaging of the living organism; i.e. imaging which can be undertaken on an organism (human, animal) while the organism is alive (see 'Medical imaging')

Iodine contrast agent

Injectable liquid containing iodine used to improve image contrast in X-ray imaging of vessels and heart chambers

Ion channel

Protein embedded in a cell membrane which enables ions to move into or out of a cell under concentration or electrical gradients

Ion exchanger

Protein embedded in a cell membrane, which actively pumps ions into or out of a cell, while pumping another ion out of or into the cell

Ion pump

Protein embedded in a cell membrane, which actively pumps ions into or out of a cell

Ionising radiation

Radiation which causes ionisation (creation of ions); causes damage to tissues; examples of ionising radiation include alpha, beta and gamma rays

Iron (contrast agent)

Metallic element which is strongly paramagnetic and used as a contrast agent for MRI

Ischaemia

Metabolic disturbance resulting from interruption of blood supply

Isolated systolic hypertension

Elevated blood pressure characterised by an increase in systolic pressure

Isotonic

A fluid with the same concentration of sodium chloride as occurs in blood

Isotropic

Physical properties in a material are the same in all directions (i.e. same along x , y and z)

IVUS

Abbreviation for 'intravascular ultrasound'; an IVUS system produces a cross-sectional image of an artery using a high frequency ultrasound transducer mounted on the distal end of a catheter

k

Abbreviation of 'kilo' meaning one thousand or 10^3 ; e.g. kPa

Kelvin model

Model of viscoelastic behaviour consisting of a Maxwell model and a spring in parallel

kilopascal

One thousand (10^3) Pa, abbreviated kPa

Kinetic energy

Energy arising from motion

Konjac-carrageenan (for tissue mimic)

Combination of 2 organic chemicals used in the construction of ultrasound flow phantoms

Lamellar unit

Unit of structure within the medial layer of an artery; consisting of smooth muscle, elastin and collagen

Laminar flow

Flow state where fluid elements follow clearly defined paths and there is little mixing between adjacent layers of fluid

Laplace's law

See 'Law of Laplace'

Larmor frequency

Rate of precession for a hydrogen nucleus in a magnetic field; equal to the field strength in tesla (T) times 4.2×10^7

Laser Doppler anemometry

Method for estimation of fluid velocity involving overlapping laser beams and the Doppler effect

Laser sheet

Referring to a laser which is swept back and forth in a 2D plane; e.g. for the purpose of illumination of particles in PIV

Law of Laplace

For a thin-walled cylinder the circumferential tension is equal to pressure times radius; modern version is that circumferential stress equals pressure times radius divided by wall thickness

LDA

Abbreviation for 'laser Doppler anemometry'

LDL cholesterol

Low density lipoprotein (LDL) or 'LDL cholesterol' is a molecule which is ingested from foods and is associated with atherosclerosis

Leukaemia

Cancer resulting in over-production of white cells

Leukocyte

Another name for 'white cell'

Leukocyte adhesion

Attachment of leukocytes to endothelial cells arising from molecular binding between ligands on the leukocyte and selectin molecules on the endothelial cell surface

Lift force

Relating to fluid flowing past an object; force on the object perpendicular to the direction of fluid motion

Ligand

A molecule whose function is to bind to another specific molecule (e.g. see leukocyte adhesion)

Lipid core (plaque)

The region of an atherosclerotic plaque composed mainly of lipid

Lipid pool (plaque)

See 'lipid core'

Loading

Gradual increase in stress applied to a solid

Longitudinal relaxation

Magnetisation in the direction of the main magnetic field

Longitudinal wall stress

Stress in a vessel in the longitudinal direction

Lost-core

Method of manufacture of a complex object (e.g. anatomical phantom) in which a core is created, placed in a box, liquid (e.g. TMM) is poured in and allowed to set and the core is removed by melting or by physical action

Low melting point alloy

Alloy of various metals which has a low melting point (around 50–99 °C); see 'lost-core'

Low wall shear hypothesis (atherogenesis)

Theory that atherosclerosis develops at regions of low wall shear stress

Lumen

The inner part; e.g. of an artery or vein; the part through which blood flows

Lumen

The space bounded by the vessel wall in which the blood flows

Lymphocyte

Type of white cell; responsible for attacking invading bacteria and viruses; also help destroy cells in the body which have become diseased through virus infection or cancer

m

Abbreviation of 'milli' meaning one thousandth or 10^{-3} ; e.g. mm

M

Abbreviation of 'mega' meaning one million or 10^6 , e.g. MPa

Macromolecule

Large molecule; blood contains a number of macromolecules including globulins, albumin, fibrinogen, vitamins, hormones and waste products; make up 9 % of plasma volume

Macrophage

Type of white cell which engulfs and removes microorganisms and damaged or diseased cells

Magnetic axis

The line joining the two poles of a magnet

Magnetic field

The region of space near a magnet over which the effects of the magnet are experienced

Magnetic resonance elastography

MRI technique in which the stiffness of tissues is estimated from measurements of the local speed of propagation of shear waves

Magnetic resonance imaging

See MRI

Magnus effect

One of a number of wall induced inertial lift forces

Malaria

Disease spread by mosquitoes in which a parasite enters the bloodstream; potentially fatal; common in tropical areas

Marfan's syndrome

Genetic disorder of connective tissue, including tissues in arteries

Margination

Increase in the concentration of cells near the wall; e.g. platelets and white cells flowing in whole blood

Maxwell model

Model of viscoelastic behaviour in which the spring and dashpot are in series

Mean arterial pressure

Average arterial pressure during the cardiac cycle

Mean pressure

Average pressure during the cardiac cycle

Mean velocity

Velocity of blood averaged over space (e.g. over the cross section of a vessel), or more commonly over space (cross section) and time (cardiac cycle). Common units are cm s^{-1} , m s^{-1}

Mechanics

Science which covers the forces on and subsequent motions of solids and liquids

Mechanobiology

Field relating the mechanical forces on tissues to the biology of tissues

Mechanoresponse

The final step of mechanotransduction in which a biological change is effected as a result of the detected mechanical signal

Mechanosensing

One step of mechanotransduction in which sensors within the cell detect a transmitted force

Mechanosensor

Biological sensors which detect mechanical forces; leading to some change in biological behaviour

Mechanosignalling

One step of mechanotransduction in which the detected force results in events which are transmitted elsewhere in the cell

Mechanotransduction

The process whereby mechanical forces are translated into biological behaviour and vice versa

Mechanotransmission

One step of mechanotransduction involving transmission of a force to mechanosensors within the cell

Media

Middle layer of the artery wall mainly consisting of elastin and smooth muscle

Medical image

2D or 3D representation of a 2D or 3D object; in colour or greyscale; for which local image values are related to some property of the object; used for diagnosis or treatment planning (see X-ray, CT, MRI, nuclear medicine, ultrasound, IVUS, OCT)

Medical imaging

Process of recording/acquiring a medical image. See 'medical image'

Megapascal

One million (10^6) Pa, abbreviated MPa

Mesenteric circulation

Circulation supplying the mesentery which is part of the abdominal region

Mesh

The set of points which represents a 3D volume in computational mechanics

Mesh quality

Characteristics of a computational modelling mesh concerned with accuracy and speed of solution (see 'mesh size', 'skewness', 'aspect ratio')

Mesh size

Number of elements in a mesh used for computational modelling

Meshing

The process in which the mesh is created for computational modelling

Metabolism

Chemical activity which sustains life

Metarteriole

An arteriole which is directly connected to a venule allowing the capillary bed to be bypassed

MI

See 'myocardial infarction'

Microbubble

Contrast agent used for ultrasound; an individual bubble consists of gas encapsulated by a thin shell, diameter 2–6 micron

Microcalcification

Small calcium deposit within tissue, a sign of early disease

Microcalcification (imaging)

Imaging methods which provide information on the degree of microcalcification in tissues

Microcalcifications (plaque.)

Component of atherosclerotic plaque

Microcirculation

Term describing the part of the cardiovascular system consisting of arterioles, capillaries and venules

Microfluidics

Branch of science concerned with devices which rely on the flow of fluids through small channels

Micron-sized particles of iron oxide

See MPIO

Microtome

Cutting tool used to generate very thin slices used for mechanical testing or microscopy

Microtubules

See cytoskeleton

Mini-stroke

See 'Transient ischaemic attack'

Mitral valve

Heart valve between the left atrium and left ventricle, preventing backflow of blood into the left atrium

Mixed (systolic/diastolic) hypertension

Elevated blood pressure characterised by an increase in diastolic and systolic blood pressure

Model

Simplified version of reality, often in the form of a set of equations, designed to answer a specific question

Modelling

See 'computational modelling'

Modulus

Property of a material describing elastic behaviour; there are 3 main elastic moduli; Young's modulus E shear modulus G and bulk modulus K

Moens Korteweg equation

Equation allowing estimation of the pulse wave velocity from artery diameter, wall thickness, Young's modulus and density

Molecular binding force

Force between tissues arising from chemical bonds (e.g. ligand-receptor bond)

Molecular imaging

Medical imaging technique which primarily provides information related to biological function of tissues at the molecular and cellular level; see SPECT, PET, targetted ultrasound contrast imaging, targetted MR contrast imaging

Monocyte

Type of white cell; carried to different tissues where they transform into macrophages which engulf and remove microorganisms and damaged or diseased cells

Mooney-Rivlin model

A hyperelastic constitutive model

Moore's law

Predication made in 1965 by Gordon Moore that the density of transistors on an integrated circuit doubles every 2 years

Mould

Container which has been created with an internal shape into which a molten substance is poured and allowed to set; removal of the container leaves the solid substance in the desired shape

Moving-wall model

Model used in arterial CFD which allows movement of the wall during the cardiac cycle

MPIO

Abbreviation for micron-sized particles of iron oxide, referring to paramagnetic particles with a diameter of 0.75–1.75 μm , used as a contrast agent for MRI

MR fluoroscopy

MRI technique in which the beating heart is imaged

MRE

See magnetic resonance elastography

MRI

Medical imaging technique based on magnetisation of the nuclei of atoms (mostly hydrogen atoms)

MRI magnet

Large magnet in the form of a cylinder made from superconducting wire; cooled by liquid helium; typically 1.5T or 3T for clinical use

Mullin's effect

Variation in stress–strain data in loading–unloading during the first few cycles

Multidimensional model

A model that spans more than one spatial dimension

Multislice

Imaging detector for CT enabling acquisition of several imaging slices simultaneously

Murray's law

Law developed by Murray (1926) to describe the diameter relationship of arteries in a bifurcation; the diameter of the parent artery to the third power is equal to the sum of the diameters of the daughter arteries to the third power

Muscular tone

The degree of constriction of smooth muscle in the vascular wall

Myocardial infarction (MI)

Region of tissue death in the heart resulting from blockage of a coronary artery

Myocardial tagging

Technique used in MRI tracking of the motion of myocardial tissue, enabling measurement of local strain

Myocyte

Cardiac cell that generates tension following electrical activation

Myogenic effect

Response of small arteries and arterioles to a change in blood pressure; following an increase in blood pressure there is decrease in diameter caused by constriction of the smooth muscle cells in the media

n

Abbreviation of 'nano' meaning one billionth or 10^{-9} ; e.g. nm

N-13

See nitrogen-13

NASCET

Abbreviation for the North American Symptomatic carotid Surgery Trial

NASCET criteria

Criteria for selection of patients for carotid surgery arising from the NASCET trial

Navier Stokes equations

Equations which govern the motion of fluids

Neck (of cerebral aneurysm)

Relating to a saccular cerebral aneurysm; the inlet to the aneurysm

Neo-Hookean model

A hyperelastic constitutive model

Neointimal formation

Formation of new lining within a vessel- comprises smooth muscle cells and extracellular matrix

Nernst equation

Gives the potential difference arising from differences in ion concentration across a cell membrane

newton

Unit of force, abbreviated N

Newtonian fluid

Fluid in which the viscosity is constant as a function of shear rate

NIBP

See 'Non-invasive blood pressure monitor'

Nitric oxide

An important molecule concerned with the regulation of vascular function; abbreviated NO; NO is produced by the endothelium in response to a rise in wall shear stress and has vasodilatory properties; abnormalities in NO production are associated with abnormal endothelial function

Nitrogen-13

Isotope of nitrogen which is unstable, decaying to carbon-13 (C-13) and also producing a positron, half life of 10.0 min, used in PET

NO

Abbreviation for nitric oxide

Node

One point of a digital model

Noise (image)

See image noise

Non-axial flow

Flow which is non-axial, where there are components in the plane perpendicular to the vessel axis (i.e. rotational flow)

Non-invasive blood pressure device

Device for measurement of blood pressure using an arm cuff

Non-invasive imaging

Medical imaging technique which leads to negligible damage to the organism; see X-ray, CT, MRI, PET, ultrasound

Nonlinear imaging (ultrasound)

Ultrasound imaging based on display of higher frequency components generated from the tissue or from contrast agents

Non-Newtonian fluid

Fluid which is not Newtonian (i.e. viscosity is not constant as a function of shear rate)

Nuclear medicine

Techniques used to diagnose and treat clinical disorders using radioactive isotopes

Nucleus

Part of the cell which contains the DNA

Numerical modelling

See 'computational modelling'

O-15

See oxygen-15

Occlusion

Blockage or obstruction

Occluder

Moving part of a mechanical heart valve. Closes to prevent backflow

OCT

Abbreviation for optical coherence tomography; an OCT system produces a

cross-sectional image (e.g. of an artery) using infrared light

Oedema

Excess fluid in tissues arising from disturbances in the osmotic balance

One-D model

See '1D model'

Optically transparent phantom

Phantom which is transparent to visible light; used in flow visualisation, PIV and LDA

Orthotropic

Solid which is anisotropic along 3 perpendicular planes of symmetry

Oscillatory index

An index which describes the variation of shear stress magnitude through the cardiac cycle

OSI

See 'oscillatory index'

Osmotic balance

Concerning osmosis; when there is no net flow of liquid across the membrane separating fluids of different particle concentrations

Outer diameter

Relating to a tube/vessel; the diameter which includes the wall

Output data

In relation to computational modelling; data which is outputted from the computational model

Outward remodelling

Response of an artery to increasing degree of atherosclerotic material whereby the inner lumen diameter is maintained constant but the outer lumen diameter increases

Oxygen

Molecule required for metabolic activity, transported in blood via the lungs and taken up in tissues throughout the body

Oxygen-15

Isotope of oxygen which is unstable, decaying to nitrogen-15 (N-15) and also producing a positron, half life of 122 s, used in PET

Oxygenated blood

Blood rich in oxygen

Pacemaker

Origin of spontaneous electrical activation in the heart. The natural

pacemaker is the sinoatrial node

Packed cell volume

See 'haematocrit'

Parabolic profile

Velocity profile which has the shape of a parabola (associated with steady Poiseuille flow)

Paramagnetic

Material which becomes magnetised while placed in a magnetic field

Paramagnetism

Magnetism in which the material becomes magnetised while placed in a magnetic field

Particle

Molecule or cell which is not part of the main fluid; blood particles consists of red cells, white cells, platelets and macromolecules

Particle image velocimetry

Method for estimation of fluid velocity in a flow phantom; involving laser illumination of seeded particles and video capture of particle positions

Particle tracking velocimetry

Method for estimation of fluid velocity in a flow phantom; involving laser illumination of seeded particles and video capture of particle positions

Particle–particle force

Force arising from collisions between particles; has little effect at low volume concentrations but is the dominant effect on particle distribution at higher volume concentrations

pascal

Unit of force divided by area, abbreviated to Pa

Patency

Open, unobstructed

Pathway

Series of actions concerning molecules in a cell; for the purpose of metabolism, signalling or gene expression

Patient specific modelling

Integration of imaging with computational modelling which provides output data relevant to the individual patient

Patient-specific

Data from measurement or modelling which is relevant to a particular patient

Peak velocity (ultrasound)

Maximum blood velocity during the cardiac cycle; used in ultrasound imaging to estimate the degree of stenosis

Peak wall stress

The maximum value of wall stress in an organ (e.g. aneurysm); estimated using FEA

Perforating veins

Veins which run between the deep and superficial circulation

Permeability

Measure of the movement of ions through an ion channel, pump, or exchanger

Perspex

Material which is optically transparent; is used in the construction of phantoms

PET

Abbreviation for 'positron emission tomography'; medical imaging technique involving injection or inhalation of radioactive chemicals which undergo radioactive decay producing a positron, which then collides with an electron undergoing annihilation producing gamma rays which are detected

PET-CT

Combined imaging system in which there is both a PET scanner and a CT scanner

Phantom

In the context of a flow phantom this is the central construct which mimics the cardiovascular geometry

Photon

Particle of electromagnetic radiation; e.g. RF photon emitted from the nucleus following nuclear energy transitions, or light photon emitted as a result of changes in the energy level of an electron

Photon noise

Random noise in the image due to random variations in the number of photons detected in an area or volume

Photon-limited

Referring to medical imaging systems in which the image is built up from many individual photons; the significance being that the image noise is related to the number of photons and hence image quality is limited by the number of photons which are acquired

Physiological solution

Fluid which is isotonic; used in e.g. experiments involving tissue samples

Pipeline

See 'processing chain (PSM)'

PIV

Abbreviation for 'particle image velocimetry'

Pixel

'Picture element'; the smallest component of a 2D digital image; typically rectangular

Plaque

Local region of atherosclerosis within an artery

Plaque constituents

The different tissues present within an atherosclerotic plaque; i.e. Lipid, fibrous tissue, white cells, smooth muscle cells and calcifications

Plaque erosion

Decrease in volume of an atherosclerotic plaque with time

Plaque growth

Increase in volume of an atherosclerotic plaque with time

Plaque rupture

Fracture of the wall (cap) between the arterial lumen (where blood flow) and the lipid pool in the plaque

Plasma

The liquid constituent of blood consisting of water and a number of macromolecules

Plasma skimming

Phenomenon whereby flow in a side-branch contains little or no red cells as a result of cell depletion near the wall in the parent vessel

Plastic

Description of a solid material which does not recover its original shape after release of an applied stress but instead undergoes some permanent deformation

Platelet

Particles within blood concerned with clotting; 0.03 % by volume of blood; greatest diameter of 2–3 μm

Platelet activation

Process whereby a platelet becomes activated (more sticky); activation is effected through contact with collagen in regions of damaged vessel wall

Platelet adhesion

Attachment of activated platelets to tissues (e.g. Collagen exposed by vascular damage) in connection with thrombus formation

Platelet aggregation

Clumping of activated platelets, in connection with thrombus formation

PMMA

Abbreviation for ‘polymethyl methacrylate’; also known as perspex; see ‘perspex’

Poiseuille equation

Equation relating flow rate to pressure, diameter, length and viscosity for flow of a Newtonian fluid in a long straight stiff tube

Poiseuille flow

Flow of a Newtonian fluid in a long straight stiff cylindrical tube

Poisson ratio

The ratio of the fractional change in lengths in z and x, y directions (where z is the direction of compression)

Polyester (phantom material)

Type of polymer; can be manufactured transparent; used in construction of optically transparent phantoms

Polymethyl methacrylate

See Perspex

Polyurethane

See urethane

Polyvinyl alcohol

See PVA

Positron

One of the fundamental particles of matter, the anti-particle of the electron, charge of $+1$, mass is $1/1837$ of the mass of a proton, produced by radioactive decay, after production the positron combines with an electron annihilating producing 2 gamma rays

Positron emission tomography

See PET

Post-processing

Processing of the output data from modelling for the purposes of visualisation and estimation of particular quantities

Post-buckling behaviour

The form of the pressure/area relationship once the critical buckling pressure

has been exceeded; e.g. in veins

Potassium channel

Ion channel for the passage of potassium ions (K^+) into or out of the cell

Potassium channel activation

Process whereby the potassium channel is opened allowing potassium ions to flow through the channel

Potential energy

Energy arising from height (vertical position within a gravitational field)

Pre-capillary sphincter

Band of smooth muscle wrapped around arterioles which can constrict to reduce or stop flow into the capillary bed

Precess

Where the axis of rotation of an object sweeps out a cone around the direction of the relevant force field; e.g. a spinning top will precess around the gravitational field direction, the magnetic axis of rotation of the hydrogen nucleus will precess around a static magnetic field

Precession

See precess

Preconditioning

Concerning tensile testing protocols: initial load–unload cycles performed to achieve stability in the stress–strain data

Preferential channel

Channel formed by the metarteriole and a venule bypassing the capillary bed

Preload

Tension in the left (or right) ventricle at the end of the filling phase of the cardiac cycle

Pressure

Force divided by area; units are Pascals (Pa)

Pressure difference

The difference in pressure between 2 points

Pressure energy

Energy arising from pressure

Pressure gradient

Difference in pressure over a given distance between two regions of flow

Pressure measurement (catheter)

Blood pressure measured invasively using a catheter

Pressure measurement (cuff)

Blood pressure measured non-invasively using an arm cuff

Pressure waveform

Usually the plot of pressure versus time in an artery; also can mean the plot of pressure versus distance (e.g. along the aorta)

Pressure-stiffness graph

Graph of blood pressure plotted against the stiffness of an artery

Pressure-strain elastic modulus

Index of arterial stiffness which does not take account of wall thickness

Pre-stress

Internal stresses in a tissue when it is in an unloaded state

Primary cilia

Thin tubular structure which projects from the endothelium; probable role in mechanosensing

Primary hypertension

Elevated blood pressure where there is no clear underlying cause

Prism element

Type of mesh element used in computational modelling

Processing chain (for PSM)

Series of steps for patient specific modelling starting with image data and ending with displayed data

Projection radiograph

X-ray imaging technique in which a 2D image is produced with both tube and detector remaining fixed in position during the taking of the X-ray

Propagation model

Model of the arterial system which accounts for propagation and reflection of pressure and flow waves

Protein phosphorylation

Addition of a phosphate group to a protein

Proteins

Large molecules present in all living things; have the ability to change shape (conformation) which is important in mechanotransduction

Proton

One of the fundamental particles of matter, present in the nucleus of atoms; the hydrogen atom contains 1 proton

Pseudoplastic

Another words for 'shear thickening'

PSM

See ‘patient specific modelling’

PTV

Abbreviation for ‘particle tracking velocimetry’

Pullback

Method used in catheter based imaging to obtain 3D data in which the catheter is slowly pulled back while continuously acquiring 2D slices

Pulmonary artery

Main artery from the heart to the lungs; arises from the right ventricle and after about 5 cm divides into the left and right pulmonary arteries

Pulmonary circulation

Part of the cardiovascular system which transports blood to and from the lungs

Pulmonary valve

Heart valve between the right ventricle and the pulmonary artery preventing backflow of blood into the right ventricle

Pulse pressure

The difference between systolic and diastolic pressure in an artery

Pulse wave velocity

The speed of propagation of pressure waves in arteries; abbreviated to PWV

Pulse-echo

Technique used in ultrasound imaging to provide information on the depth from which received echoes arise, involving timing the delay between transmission and reception, dividing by 2, and multiplying this by the assumed average velocity of 1540 m s^{-1}

Purkinje fibres

Component of the electrical conduction system of the heart, which provides a fast activation pathway to ventricular tissue

Pushing beam

In ultrasound shear wave elastography, a high output beam which is used to produce deformation of tissue at the focal region, hence producing shear waves

PVA

Abbreviation for polyvinyl alcohol; used in the construction of MRI and ultrasound phantoms

PVAc (vessel mimic)

Abbreviation for polyvinyl alcohol cryogel; referring to PVA which has undergone 1 or more freeze-thaw cycles which causes cross-linking of the

polymer molecules

PWV

See 'pulse wave velocity'

QRS complex

ECG deflections that correspond to electrical activation of the ventricles

Radial pressure waveform

Variation of blood pressure with time in the radial artery

Radioactivity

Particles emitted from nuclei during radioactive decay; the 3 main particles are the alpha particle consisting of 2 protons and 2 neutrons; the beta particle is either an electron or a positron, the gamma particle is a high energy photon usually called the gamma ray; gamma rays are useful for medical imaging

Radiofrequency

Frequencies which are in the radio part of the electromagnetic spectrum; from 3 kHz to 300 GHz

Radioisotope

Version of an element which is unstable and hence radioactive; e.g. O-16 (8 neutrons, 8 protons) is the most abundant stable isotope of oxygen, O-15 (8 protons, 7 neutrons) is radioactive, decaying to N15 and a positron

Radius

Distance of a circle from one side to the centre (equal to half the diameter)

Rapid prototyping

Creation of a 3D object from a computer design quickly; first used in manufacturing industry to reduce the time for creation of a demonstration model (the prototype) which was traditionally time-consuming; the term rapid-prototyping has been superseded by '3D printing'. See '3D printing'

Reactive hyperaemia

Temporary increase in blood flow following a period of reduced or absent flow (e.g. Caused by application of an arm cuff)

Real-time

Occurring now, as in 'real-time ultrasound' which provides information with negligible delay between acquisition and visualisation; as opposed to off-line imaging such as CT where the data is acquired then visualised with a delay of a few seconds or minutes

Received frequency (ultrasound)

Frequency of the received ultrasound

Receiving coil

Part of an MRI system; involved in receiving the RF data from nuclei while they gain their original magnetisation

Reception (of ultrasound)

The process of detection of ultrasound echoes arriving at the face of the transducer, following transmission

Recirculation

See 'flow recirculation'

Red cell

Particle within blood concerned with oxygen transport; also called erythrocytes; 40–50 % by volume of blood, greatest diameter 7.5 μm

Red cell ghost

Red cells rendered optically transparent by removal of their haemoglobin

Reduced velocity

Ratio of blood velocity to vessel diameter, units s^{-1} , surrogate measure of wall shear rate

Reduced-order model

Model in which there are a reduced number of dimensions; reality is 3D (x, y, z) + time; a reduced order model might be 0D(t) or 1D(z, t)

Re-entry

Arrhythmia, in which electrical activation continually propagates into regions of tissue that are electrically recovering

Reflected waves

Generally, waves which travel towards their point of origin; in relation to arteries, pressure waves which travel towards the heart

Refraction (light)

Change in direction of light when passing from one material to another where the refractive index is different

Refractive index (light)

Ratio of the speed of light in a vacuum to the speed of light in the material

Refractive index matching (light)

Ensuring that the refractive index of 2 adjacent materials is the same, hence eliminating refraction of light

Refractory period

Period following depolarisation when an action potential cannot be elicited by a further stimulus

Regurgitation

Leakage or backflow

Relaxation

Change in the MRI signals with time following an RF transmission pulse

Remodelling

See 'arterial remodelling'

Repolarisation

Later phase of the cardiac action potential where membrane voltage returns to its resting value of around -85 mV

Resistance (to flow)

Ratio of pressure gradient to flow rate (e.g. in a tube)

Respiratory pump

The action of the respiratory system on the veins within the abdomen and thorax

Reverse wave (flow)

Blood flow where the flow direction is towards the heart

Reverse wave (pressure)

Pressure wave which travels along arteries towards the heart

Reynolds number

Dimensionless number used in fluid mechanics which is related to the flow state of the fluid (i.e. whether flow is laminar, disturbed, transitional or turbulent); formally the ratio of inertial to viscous forces

Rheology

Branch of science concerned with the study of the flow of matter

Rigid-wall model

Model commonly used in arterial CFD in which the walls are assumed to be rigid; i.e. not to move during the cardiac cycle

Rotational angiography

X-ray technique which uses a fluoroscopy system to acquire images around the patient enabling a 3D dataset to be obtained using CT reconstruction techniques; mostly used in cerebral imaging

Rotational flow

See 'helical flow'

Rouleaux

Clumps or aggregates of red cells in which the red cells are arranged face to face; only occurs at low shear (<10 s⁻¹)

Rupture

Breaking or bursting of an organ; tearing of a vessel with leakage of contents into the surrounding tissues; see 'plaque rupture', 'aneurysm rupture'

Saccular aneurysm

Aneurysm arising from one side of the artery; roughly spherical in shape; also referred to as a 'Berry aneurysm'

Sarcomere

Contractile unit within myocyte

Sarcoplasmic reticulum

Region inside myocytes that acts to store calcium

Scar tissue

Region of connecting tissue that forms following a myocardial infarction

Scattering (of ultrasound)

Generation of a wave which travels in all directions, after an incident wave has encountered a small object (dimensions \ll wavelength), where the object has an impedance different to the surrounding material

Screening programme

The process of identifying healthy people who may be at increased risk of disease, with the aim of offering treatment at an early stage

Secondary circulation

See collateral circulation

Secondary flow

Flow which is non-axial, where there are components in the plane perpendicular to the vessel axis (i.e. rotational flow)

Secondary hypertension

Elevated blood pressure arising from disease (e.g. kidney disease, endocrine disorders)

Secondary motion

Another name for 'secondary flow'. Also see 'helical flow'

Segmentation

Image processing method in which the boundaries of an organ or of a region within an organ are identified

Segre Silberberg effect

Relating to flow of neutrally buoyant particles in a tube for Reynolds number around 30; particles accumulate in a ring at a distance of 0.6 of the tube radius from the centre; named after the authors of the 1962 paper; also called the 'tubular pinch effect'

Selectin

Cell adhesion molecules found on white cells

Self-excited oscillations

Oscillations in a flexible structure which occur spontaneously without a time-varying loading condition

Set-point hypothesis

Concerning the control of wall shear stress in arteries; hypothesis that there is a value of wall shear stress which is maintained through a control mechanism involving wall shear stress sensors and arterial remodelling; it is noted that the set-point value is different in different arteries

Shear induced inertial lift

Relating to an object in a fluid at high Reynolds number where inertial forces dominate; force on the object arising from differences in shear on either side of the object; gives rise to transverse movement (across streamlines); in steady flow the particles move towards the wall

Shear modulus

Property of a solid describing elastic behaviour, concerned with the ability of a solid to withstand a shear force

Shear rate

Change in fluid velocity with perpendicular distance arising from a shear force; units s^{-1}

Shear strain

Relating to shearing of a liquid or solid; is the deformation in the direction of shear divided by the original length of the vertical; equal to the tangent of the shear angle θ

Shear-thickening fluid

Fluid where the viscosity increases with increasing shear rate

Shear-thinning fluid

Fluid where the viscosity decreases with increasing shear rate

Shear wave elastography

Techniques that provide information related to the elastic modulus of tissue in vivo, based on the measurement and display of shear wave velocity

Shear wave velocity

Velocity of shear waves (e.g. in tissues during elastography)

Sickle cell

Diseased red cell which has the shape of a sickle rather than the normal biconcave shape

Sickle cell disease

Disease associated with abnormally shaped red cells (sickle cells)

Silicone (phantom material)

Type of material with similar properties to rubber; can be manufactured optically transparent; used in the construction of optically transparent phantoms

Simulation (general)

See 'computational modelling'

Simulation (specific)

One run of a computational model; involving specification of input data and production of output data

Single photon emission computed tomography

See SPECT

Single-beam (ultrasound)

Ultrasound system where information on only 1 scan line is collected at a time

Sinus node

Natural pacemaker of the heart

Sinusoidal capillary

Type of capillary cell in which the basement membrane is incomplete allowing flow of molecules from the extracellular fluid into the blood stream

Skewness

A metric of mesh shape which characterises long thin elements

Slip process

Movement within a material of adjacent planes resulting in plastic deformation

Smooth muscle

Type of muscle cell found in the walls of arteries, mainly in the medial layer

Soft tissue

General term referring to biological tissues with low stiffness and low calcium content (e.g. artery, muscle, abdominal organs)

Solid

Material able to maintain a shear force at rest

Solid mechanics

The branch of mechanics which studies the behaviour of solids

Solid modelling

A branch of computational mechanics, concerned with estimation of

displacements and stresses within solids

Solid particle

Particle which cannot be deformed; rigid particle

Solver

The part of the computational modelling workflow which is concerned with finding a solution to the governing equations

Sound

Vibrations in the form of pressure waves which travel within a medium (solid, liquid or gas); divided into infrasound (frequency <20 Hz), audible sound (frequency 20 Hz–20 kHz), ultrasound (frequency >20 kHz)

Sound wave

Pressure waves within a medium such as a solid, liquid or gas; divided into infrasound (frequency <20 Hz), audible sound (frequency 20 Hz–20 kHz), ultrasound (frequency >20 kHz)

Spatial resolution

Minimum separation in space for which 2 separate point or line targets can be identified or, size on the image of a point object

Speckle

Noise appearing on ultrasound images, arising from variations in the position and scattering strength of the various scatterers within the beam

SPECT

Single photon emission computed tomography; method of using a gamma camera to produce 3D images

Spectral Doppler

Doppler ultrasound technique which produces Doppler frequency shift versus time waveforms with full Doppler frequency shift data estimated and presented at each time point

Spectral element method

One type of discretization method; used in fluid modelling

Spectrin

Protein which is the major component of the cytoskeletal structure that gives the red cell its biconcave shape

Speed of sound

Distance that the crest of the sound wave (or other similar point) travels per second. Values in soft tissue are 1400–1600 m s⁻¹, with an average value of about 1540 m s⁻¹

Spin (of nucleus)

Property of a nucleus of an atom concerned with its magnetic behaviour

Spin-lattice relaxation

See T2 relaxation

Spin-spin relaxation

See T1 relaxation

SPIO

Abbreviation for 'superparamagnetic iron oxide', referring to paramagnetic particles with a diameter of 4–50 nm, used as a contrast agent for MRI

Spiral flow

Another name for helical flow

Spring

In the context of viscoelastic models; purely elastic component with linear stress–strain behaviour

Starling's equation

Equation in which transcapillary flow is related to the net hydrostatic pressure minus the net colloid osmotic pressure

Statins

Medicine that is used to lower cholesterol and reduce the risk of plaque rupture

Stenosis

A local narrowing of the vessel lumen

Stenosis

Localised reduction in the cross-sectional area of an artery caused by an atherosclerotic plaque

Stent

Structure in the form of a tube inserted into an artery under imaging guidance to help keep the artery open

Stiffness

Property of a solid; describing the degree to which it will deform when subject to a force

Stiffness index (β)

Elastic modulus of a vessel which does not account for wall thickness

Stokes domain

Relating to a particle in a moving fluid; particular type of flow occurring at very low Reynolds number where flow is dominated by viscous forces

Strain

Ratio of extension divided by original length (for a material that has applied

stress)

Strain elastography

Measurement of strain in vivo using ultrasound imaging where strain is used as a surrogate for stiffness

Strain imaging

Measurement of strain in vivo using medical imaging

Streamline

Path followed by a fluid element

Stress

Ratio of force divided by area; units are pascals (Pa)

Stress–strain graph

Concerning the stretching of a sample of a solid material; the graph of stress versus strain

Stretch-sensitive ion channel

Ion channel which is opened as a result of stretching of the surrounding lipid bilayer (e.g. if there is swelling of the cell)

Stroke volume

Volume of blood ejected from left ventricle during each heart beat

Stroke work

Work performed by the left ventricle during each cardiac cycle

Structural imaging

Medical imaging technique which primarily provides information on geometry and motion; see X-ray, CT, ultrasound, MRI

Subarachnoid haemorrhage

Bleeding into the space beneath the arachnoid membrane, usually caused by rupture of a cerebral aneurysm

Sub-critical/ super-critical flow (vein)

Where the local speed of blood within the vein is less than/ greater than the speed of wave propagation

Suction pressure

Force associated with flow of a fluid into a low pressure region, whereby the low pressure acts to propel the fluid forward

Superficial venous circulation

The venous circulation which lies between the skin and the fascial boundary

Superior vena cava

Large vein which delivers deoxygenated blood from the upper body to the right atrium

Superparamagnetic iron oxide particles

See SPIO

Supine

Lying face upwards

Suspension

Fluid containing particles (i.e. not a pure fluid)

Symmetric flow

Flow in a tube or vessel where the velocity profile is radially symmetric; the maximum velocity is mostly located at the centre of the vessel apart from when flow changes direction where the maximum velocity is located off-centre

Systemic circulation

Part of the cardiovascular system which transports blood from the heart to the tissues of the body apart from the lungs

Systole

The portion of the cardiac cycle in which the heart is contracting

Systolic pressure

The highest pressure in an artery during the cardiac cycle

T1

In an MRI scanner, following a transmission pulse; T1 is the time for the longitudinal magnetization to achieve 63 % of its equilibrium value

T1 relaxation

In an MRI scanner, change in the T1 signal with time following an RF transmission pulse

T2

In an MRI scanner, following a transmission pulse; T2 is the time at which there is 37 % loss of the original transverse magnetization

T2 relaxation

In an MRI scanner, change in the T2 signal with time following an RF transmission pulse

Tachycardia

Rapid heart rate, often arising from an arrhythmia

Tank-treading

Relating to a deformable particle suspended in a moving fluid; the particle appears to be stationary but is in fact rotating; the membrane of the particle surface deforms in manner similar to the treads of a tank

Targetted contrast agent

Contrast agent which binds to specific biological sites

Targetted MR contrast imaging

Targetted contrast agent used in MRI

Targetted ultrasound contrast imaging

Targetted contrast agent used in ultrasound imaging

Tensegrity

Structural principle based on stiff components in compression linked by elastic components in tension

Tensile testing

Measurement of the stress–strain or force-extension behaviour of material, measured by gradually stretching the material until it breaks

Tension

Force within an object which is stretched

Tethering

See ‘tethering forces’

Tethering forces

Forces on a vessel as a result of the proximity of surrounding tissues

Tetrahedral element

Type of mesh element used in computational modelling

Thermal irreversibility

Process which is not thermally reversible; e.g. here the material setting temperature is higher than the melting temperature

Thermodilution

Method for measurement of flow rate in a vessel; requires insertion of a device into the vessel; liquid (e.g. saline) is injected at a higher temperature than blood at the proximal end of the device, at the distal end of the device the temperature is recorded and from this flow rate can be determined

Thermoregulation

Mechanism by which temperature is maintained at a constant level

Thick filament

Part of the contractile apparatus composed of myosin

Thin filament

Part of the contractile apparatus composed of titin

Thoroughfare channel

See ‘preferential channel’

Three-D model

See '3D model'

Thrombosis

Formation of a blood clot

Thrombus

Blood clot

TIA

See 'Transient ischaemic attack'

Tight junction

Region between two adjacent cells where cell membranes are connected which prevents fluid flow between the cells

Tissue mimic

See 'tissue mimicking material'

Tissue mimicking material

Component of a flow phantom which mimics the tissues; for which key imaging physical properties are matched to those in human tissues

TMM

Abbreviation for 'tissue mimicking material'

TOE

Transoesophageal echocardiography; method for imaging the heart using an endoscope

Tonometry

Measurement of pressure

Tortuous artery

Arteries which are more elongated than is normal and as a result twist and turn; may be due to reduction in height (through vertebral collapse with ageing), more commonly due to artery elongation because of a genetic defect

Tracer

In medical imaging; substance which mimics particular molecules in the body and which can be imaged

Transducer

Component of the ultrasound system which generates and receives the ultrasound beam, and sweeps the beam through the tissues to produce an image

Transient ischaemic attack

Symptoms of a stroke which last for less than 24 h

Transit time flow probe

Device for measurement of flow rate in a vessel; requires exposure of the vessel and placement of the probe around the vessel; the device operates by measuring the time of propagation of a pulse of ultrasound through the moving blood

Transitional flow

Flow state which oscillates between laminar and turbulent flow

Transmission (of ultrasound)

The process of production of ultrasound from the transducer

Transmitted frequency (ultrasound)

Frequency of the transmitted ultrasound

Transmitting coil

Part of an MRI system, involved in transmitting an RF pulse which causes change in the direction of magnetisation of nuclei

Transmural pressure

The difference between pressure acting on the wall from the inside (blood pressure) and the pressure acting on the wall from the outside

Transmural pressure

The pressure given by the internal pressure minus the external pressure acting on a vessel

Transoesophageal echocardiography

See TOE

Transverse magnetization

Magnetization in the plane 90° perpendicular to the main magnetic field direction

Trans-WSS

An index which describes the variation of shear stress direction through the cardiac cycle

Tricuspid valve

Heart valve between the right atrium and the right ventricle preventing backflow of blood into the right atrium

Tricuspid valve

A valve with three leaflets

Tube-law

The relationship used to define the pressure-area response of a vessel

Tubing (vessel mimic)

Commercially available tube used as a convenient vessel mimic in a flow phantom

Tubular pinch effect

See 'Segre Silberberg effect'

Turbulent flow

Flow state in which fluid elements follow erratic paths and there is mixing between adjacent layers of fluid

Ultimate strength

Concerning stretching of a material; the maximum stress which can be applied which does not result in fracture

Ultrasmall superparamagnetic iron oxide particles

See USPIO

Ultrasound

Sound with frequencies above the limit of hearing for humans; i.e. frequencies >20 kHz

Ultrasound elastography

Ultrasound technique in which the stiffness of tissues is estimated from measurements of the local speed of propagation of shear waves

Umbilical cord

Flexible cylindrical structure approximately 1 m in length connecting the embryo to the placenta; contains 2 umbilical arteries and 1 umbilical vein; oxygenated blood passes down the vein from placenta to fetus and deoxygenated blood along the arteries from fetus to placenta

Unactivated platelet

Platelet which has not been activated and is not sticky

Uniaxial testing

Mechanical testing of materials with stretching in a single direction

Unloading

Gradual decrease in stress applied to a solid

Upstream–downstream asymmetry

Difference in the flow-field upstream and downstream of an object such as a stenosis in an artery

Urea

One of the waste products of metabolism

Urethane (tissue mimic)

Material used as a TMM in ultrasound phantoms

USPIO

Abbreviation for 'ultrasmall superparamagnetic iron oxide', referring to paramagnetic particles with a diameter of 10–40 nm, used as a contrast

agent for MRI

Valve

Structure which prevents backflow of blood, present in medium sized veins and in the heart

Valve plane

Plane in which the main cardiac valves lie

Valve sinus

A local increase in diameter in the vein at the location of the venous valve

Valvular agger

A fibroelastic structure located at the base of the venous valve which connects the valve leaflets to the vessel wall

Varicose veins

Veins which have become enlarged and tortuous

Vascular graft

Vessel replacement—can be natural (e.g. Vein graft) or synthetic

Vasoconstriction

Contraction of the smooth muscle cells in the vessel wall causing slight decrease in lumen diameter for muscular arteries), large decrease in diameter (for arterioles)

Vasodilation

See 'vasorelaxation'

Vasomotion

Regular change in diameter of arterioles, occurring at a frequency of 3–30 min⁻¹

Vasorelaxation

Relaxation of the smooth muscle cells in the vessel wall causing slight increase in lumen diameter (for muscular arteries), large increase in diameter (for arterioles)

Vein

Large vessels involved in transport of blood to the heart; diameter 1–25 mm

Velocity

Distance travelled per unit time; units m s⁻¹

Velocity (shear wave)

See shear wave velocity

Velocity field

See 'flow field'

Velocity profile

Velocity as a function of radial position in a tube

Velocity waveform

The plot of blood velocity versus time; e.g. in an artery. Note 'velocity' may refer to maximum velocity or mean velocity

Vena cava

The 2 largest veins in the systemic circulation which deliver deoxygenated blood to the right atrium; consisting of inferior vena cava and superior vena cava

Vena contracta

Relating to flow in a vessel past a partial obstruction; region where the flow stream has minimum diameter, located just after (but not coinciding with) the point of minimum cross-sectional area

Venous insufficiency

Lack of reduction of pressure in the deep veins of the lower limb during exercise and is associated with a range of complications which present clinical symptoms associated with poor venous return from the lower limb

Venous reflux

Reverse flow of blood in the veins, typically observed following muscle pump activity if venous valves are incompetent

Venous return

The volume of blood returning to the right atrium from the systemic venous circulation

Venous valve

Valves present in medium sized veins preventing backflow of blood in the vein

Ventricles

Chambers of the heart concerned with pumping of blood into the arterial system; left ventricle pumps into systemic arterial system, right ventricle into pulmonary arterial system

Venule

Small vessel connecting veins to capillaries; diameter 10–200 μm

Vesicle

Fluid-filled structure formed from the lipid bilayer

Vesicular transport

Movement of molecules into and out of a cell by containment within vesicles

Vessel compliance

The degree to which a vessel distends following increase in transmural pressure

Vessel length

Longitudinal length of a vessel

Vessel lumen diameter

Diameter of the lumen (i.e. of the region occupied by the fluid/blood flowing within the tube/vessel)

Vessel mimic

See 'vessel mimicking material'

Vessel mimicking material

Component of a flow phantom which mimics the vessel wall; for which key imaging physical properties are matched to those in human vessels

Vessel wall thickness

Thickness of the wall of a vessel

Virtual histology

Method used in IVUS imaging involving identification of plaque component (e.g. fibrous, lipid, calcified) by analysis of the RF data

Viscoelastic

Term concerning a solid material whose stress–strain behaviour demonstrates both fluid (viscous) and solid (elastic) behaviour

Viscometer

Device for measuring the viscosity of a fluid

Viscometry

The science of measurement of viscosity

Viscosity

The ability of a fluid to resist deformation by a shear force

Viscous force

Force on a fluid element arising from friction with adjacent fluid elements or a surface

VMM

Abbreviation for 'vessel mimicking material'

Voigt model

Model of viscoelastic behaviour in which the spring and dashpot are in parallel

Volumetric flow rate

See 'flow rate'

Von Willebrand factor

A blood protein involved in thrombus formation

Vortex

Region of rotating flow; may be located to one region (e.g. post-stenosis) or may travel downstream

Vortex shedding

Term describing the creation of vortices (e.g. post-stenosis) which then travel downstream

Vortices

Regions in which the flow locally rotates around a point

Voxel

Volume element; smallest component of a 3D digital image

Wall induced inertial lift

Relating to an object in a fluid at high Reynolds number where inertial forces dominate; force on the object occurring when the object is near a wall; force is directed away from the wall; for flow in a tube the particles move away from the wall

Wall shear rate

Change in fluid velocity with perpendicular distance arising from a shear force measured at the wall; units s^{-1}

Wall shear stress

Viscous drag of a fluid on the wall of a vessel; e.g. viscous drag of blood on an arterial wall

Wall shear stress control

Control mechanism whereby the wall shear stress in an artery is maintained within a narrow bound; involves sensing of wall shear stress (mechanosensing) and change in arterial diameter (remodelling)

Wall thickness

Thickness of the wall of vessels in the cardiovascular system

Water hammer equation

Equation relevant for a fluid relating the variation of pressure with velocity to the pulse wave velocity

Wave inversion

In magnetic resonance elastography, method used to estimate the local stiffness from the measured displacement associated with passage of shear waves

Waveform

The plot of wave amplitude versus time or wave amplitude versus distance

(e.g. flow-time waveform)

Wavelength

Property of a wave; the distance between two consecutive crests or other similar points on the wave

White cell

Particles within blood concerned with immune defence; also called leukocytes; a variety of different white cells exist each with a different function; occupy 0.7 % of blood volume; diameter 7–15 μm

WHO

See ‘World Health Organisation’

Whole artery phantom

Flow phantom incorporating an excised section of an artery

Whole-body

Referring to medical imaging in which the entire body is imaged

Windkessel model

A simple model of the arterial system consisting of a pump, a chamber and an outflow resistance; provides estimates of the pressure-time waveform and the flow-time waveform; from the German word ‘Windkessel’ meaning ‘air chamber’

Wolff–Parkinson–White syndrome

Syndrome in which an additional electrical activation connection between atria and ventricles that together with the atrioventricular node provides a pathway for re-entry

Womersley number

Relating to the Womersley equations, α is the Womersley number; a dimensionless number for pulsatile flow equal to the square root of the ratio of inertial force to viscous force

Workflow

See ‘processing chain (PSM)’

Workflow

See ‘processing chain (PSM)’

World Health Organisation

Organisation concerned with directing and coordinating international health within the United Nations system

WSS

See ‘wall shear stress’

X-ray imaging

Medical imaging technique based on the use of X-rays; see projection radiograph, fluoroscopy, CT and rotational angiography

X-ray venogram

An X-ray examination using contrast medium to visualise the blood within the veins

Yeoh model

A hyperelastic constitutive model

Yield point

Concerning stretching of a material; the point (stress) above which the material behaves plastically

Young's modulus

Property of a solid describing elastic behaviour, concerned with deformation along one axis; ratio of stress divided by strain

Z-disk

End-to-end connections between sarcomeres

Zero-D model

See '0D model'

Index

0–9

0D model

1D model

2D ultrasound

2D velocity profile

3D model

3D printing

3D ultrasound

7D imaging

A

Abdominal aortic aneurysm

Acoustic impedance

Acoustic matching (phantoms)

Acrylic (phantom material)

Activated platelet
Active contour
Active surface
Actuator (MRE)
Adaptability, cardiovascular
Adhesion protein
Adhesion site
Adulthood
Adventitia
Afterload
Agar (for tissue mimic)
Aggregation, (red cell)
Albumin
Alpha. *See* Womersley number
Ammonia
Anaemia
Aneurysm rupture
Aneurysm
Angiography
Angioplasty
Anisotropic
Annihilation
Anti-particle
Aorta
Aortic valve
Applanation tonometry
Arachnoid membrane
Arrhythmia
Arterial biomechanics
Arterial mechanics
Arterial remodeling
Arteriolar resistance
Arteriole
Artery
Aspect ratio
Atherosclerosis
Atherosclerotic plaque

Atria
Atrio-ventricular node
Augmentation index
Augmentation pressure
Autocrine molecules
Autolysis
Axial
Axial accumulation
Axial flow
Axisymmetric flow

B

Back-projection
Balloon angioplasty
Balloon catheter
Barium contrast agent
Basement membrane
Bayliss effect
Bernoulli equation
Bernoulli principle
Berry aneurysm
Biaxial testing
Biconcave
Bicuspid valve
Bifurcation
Bilipid membrane
Binding site
Bingham plastic
Biomechanics
Bioreactor
Black blood imaging
Blood
Blood mimic
Blood mimicking fluid (BMF)
Blood velocity
B-mode
Boundary conditions

Boundary layer
Bright blood imaging
Brightness-mode. *See* B-mode
Brownian motion
Bulk modulus
Buoyant force

C

C-11
Calcium ion channel
Calcium wave
Calf muscle pump
Capillary
Carbon dioxide
Carbon-11
Cardiac action potential
Cardiac output
Cardiovascular biomechanics
Cardiovascular disease
Cardiovascular system
Carotid endarterectomy
Catheter
Catheter based imaging
Cell alignment
Central pressure
Central pressure waveform
Cerebral aneurysm
CFD
C-flex (vessel mimic)
Childhood
Circulation
Circulatory system
Circumferential stress
Circumferential wall stress
Claudication
Claudication distance
Cleaving

Clinical ultrasound
Clip
Clotting
Co-culture phantom
Coil
Collagen
Collagen/elastin ratio
Collateral circulation
Colloid osmotic pressure
Colour flow (ultrasound)
Competent venous valve
Compliant-wall model
Composite
Computation time
Computational fluid dynamics (CFD)
Computational mechanics
Computational modeling
Computed tomography
Computer simulation
Conductance
Conduction defect
Cone plate viscometer
Conformation
Constitutive equations
Constitutive model
Continuous capillary
Continuous elastic compression
Continuous media
Contrast agent (MRI)
Contrast agent (targetted)
Contrast agent (ultrasound)
Contrast agent (x-ray)
Coronary sinus
Corrosion casting
Crack propagation
Cracks
Critical stenosis

Cross-correlation
Cross-linking
CT
Cultured endothelium
Cyclic fatigue
Cyclic fatigue, pressure
Cyclic stress, pressure
 See also Cyclic fatigue
Cyclic stretch fatigue, pressure
 See also Cyclic fatigue
Cyclic stretching
Cyclotron
Cytoskeleton

D

Dashpot
Decentralised model, of endothelial mechanotransduction
Deep vein thrombosis (DVT)
Deep venous circulation
Deformable model
Deformable particle
Deformation (red cell)
Degree of stenosis
Density
Deoxygenated blood
Depletion force
Deployment
Depolarisation
Destruction imaging (ultrasound)
Development, fetal and embryo
Dialysis fistula
Diameter
Diastole
Diastolic pressure
Diffusion tensor imaging (DTI)
Digital model
Dilatant

Discrete model
Discretization
Dislocation
Dissection of a vessel wall
Disturbed flow
Dome, of cerebral aneurysm
Doppler equation
Doppler frequency
Doppler shift (ultrasound)
Drag force
Ductus arteriosus

E

ECST
ECST criteria
Ectopic beat
Ehlers-Danlos syndrome
Ejection fraction
Elastic instability
Elastic

- linear
- non-linear

Elastic modulus

- See also* Modulus

Elastin
Elastography
Elective surgery
Electrocardiogram (ECG)
Electrolytes
Electromagnetic flow probe
Electromagnetic spectrum
Electron
Electrostatic force
Element
Embryo
Embryogenesis
Endarterectomy

Endocardial
Endoscope
Endothelial cell alignment
Endothelial cell culture phantom
Endothelial flow cell
Endothelial flow phantom
Endothelium
Enzyme
Epicardial
Epidemiology
Erythrocyte
Erythrocyte volume fraction. *See* Haematocrit
Essential hypertension
euHeart
Experimental flow system
Expiration
Ex-vivo

F

Fahraeus effect
Fahraeus-Lindquist effect
Fascia
Fatty streak
FDG
FEA
Fenestrated capillary
Fenestrations
Fetus
Fibrinogen
Fibroblast
Fibrous cap thickness, plaque
Fibrous cap, plaque
Fibrous tissue, plaque
Filaments
Filtered back projection
Finite difference method
Finite element analysis

Finite element method
Finite element model
Finite volume method
Fistula
Flash pulse
Flow diverter
Flow limitation
Flow phantom
Flow probe
Flow rate
Flow recirculation
Flow separation
Flow state
Flow visualisation
Flow waveform
Flow-field
Fluid kinematics
Fluid mechanics
Fluid modeling
Fluid statics
Fluid
Fluid-particle force. *See* Brownian motion
Fluorine-18 (F-18)
Fluorodeoxyglucose
Fluoroscopy
fMRI
Focal adhesion
Focal adhesion site
Foramen ovale
Force
 compression
 extension graph
 extensional
 shear
Forward wave, flow
Forward wave, pressure
Fracture

Frame rate
Frank-Starling law
Free energy
Frequency
Friction
Fully developed flow
Functional imaging
Fusiform aneurysm

G

Gadolinium (contrast agent)
Gamma camera
Gamma ray
Gangrene
Gap junction
Gauge length
Generator
Ghost. *See* Red cell ghost
Gigapascal
Glass (phantom material)
Globulins
Glycerol (for blood mimic)
Glycocalyx
Governing equations
Gradient coil
Graft
Granulocyte
Gravitational force
Grid
Gridding
Ground substance

H

Haematocrit
Half life
Hard tissue

Heart
Heart rate
Helical flow
Helical scanning
High WSS hypothesis, cap thinning
Homogeneous
Hoop stress
Hydrogen nucleus
Hydrostatic pressure
Hyperaemia
Hyperelastic

I

Idealised (general)
Idealised (in image guided modelling)
ILT
Image
Image formation
Image guided modeling
Image noise
Immune system
Impedance (acoustic)
Impedance
Incremental elastic modulus
Inertial force
Infarction
Infarction
Inferior vena cava
Inflammation (imaging)
Inflation testing
Inhomogeneous
Inlet
Inlet length
Inner diameter
Input data
Inspiration
Intercalated disc

Intermittent pneumatic compression
Internal elastic membrane
Intervertebral disc
Intima
Intima-media layer
Intima-media thickness
Intracranial aneurysm
Intraluminal thrombus
Intrasaccular flow disruptor
Invasive imaging
In-vitro imaging
In-vivo
In-vivo imaging
Iodine contrast agent
Ion channel
Ion exchanger
Ion pump
Ionising radiation
Iron (contrast agent)
Ischaemia
Isolated systolic hypertension
Isotonic
Isotropic
IVUS

K

Kinetic energy
Konjac-carogeenan (for tissue mimic)

L

Lamellar unit
Laminar flow
Laplace's law
Larmor frequency
Laser Doppler Anemometry (LDA)
Laser sheet

Law of Laplace
LDL cholesterol
Leukaemia
Leukocyte
Leukocyte adhesion
Lift force
Ligand
Lipid core, plaque
Lipid pool, plaque
 See also Lipid core
Loading
Longitudinal relaxation
Longitudinal wall stress
Lost-core
Low melting point alloy
Low wall shear hypothesis, atherogenesis
Lumen
Lymphocyte

M

Macromolecule
Macrophage
Magnetic axis
Magnetic field
Magnetic resonance elastography (MRE)
Magnetic resonance imaging
Magnus effect
Malaria
Marfan's syndrome
Margination
Maxwell model
Mean arterial pressure
Mean pressure
Mean velocity
Mechanics
Mechanobiology
Mechanoresponse

Mechanosensing
Mechanosignalling
Mechanotransmission
Media
Medical image
Medical imaging
Mesenteric circulation
Mesh
Mesh quality
Mesh size
Metabolism
Metarteriole
Microbubble
Microcalcification
Microcalcification (imaging)
Microcalcifications, plaque
Microcirculation
Microfluidics
Micron-sized particles of iron oxide
Microtome
Microtubules
Mini-stroke. *See* Transient ischaemic attack
Mitral valve
Mixed (systolic/diastolic) hypertension
Model
Modeling
Modulus
Moens Korteweg equation
Molecular binding force
Molecular imaging
Monocyte
Mooney-Rivlin model
Moore's law
Mould
Moving-wall model
MPIO
MR fluoroscopy

MRI
MRI magnet
Mullin's effect
Multi-dimensional model
Multislice
Murray's law
Muscular tone
Myocardial infarction (MI)
Myocardial tagging
Myocyte
Myogenic effect

N

NASCET
NASCET criteria
Navier Stokes equations
Neck, of cerebral aneurysm
Neo-Hookean model
Neointimal formation
Nernst equation
Newton
Newtonian fluid
NIBP. *See* Non-invasive blood pressure device
Nitric oxide (NO)
Nitrogen-13 (N-13)
Node
Non-axial flow
Non-invasive blood pressure device
Noninvasive imaging
Non-linear imaging (ultrasound)
Non-Newtonian fluid
Nuclear medicine
Nucleus
Numerical modeling

O

Occluder
Occlusion
OCT
Oedema
One-D model
Optically transparent phantom
Orthotropic
Oscillatory index
OSI. *See* Oscillatory index
Osmotic balance
Outer diameter
Output data
Outward remodelling
Oxygen
Oxygen-15 (O-15)
Oxygenated blood

P

Pacemaker
Packed cell volume. *See* Haematocrit
Parabolic profile
Paramagnetic
Paramagnetism
Particle
Particle image velocimetry
Particle tracking velocimetry
Particle-particle force
Pascal
Patency
Pathway
Patient-specific
Patient specific modelling
Peak velocity, ultrasound
Peak wall stress
Perforating veins
Permeability
Perspex

PET
PET-CT
PGI
Phantom
Photon
Photon-limited
Photon noise
Physiological solution
Pipeline
PIV
Pixel
Plaque
 See also Atherosclerotic plaque
Plaque constituents
Plaque erosion
Plaque growth
Plaque rupture
Plasma
Plasma skimming
Plastic
Platelet activation
Platelet adhesion
Platelet aggregation
Platelet
Poiseuille equation
Poiseuille flow
Poisson ratio
Polyester (phantom material)
Polymethyl methacrylate (PMMA)
Polyurethane
Polyvinyl alcohol
Positron emission tomography
Positron
Post-buckling behavior
Post processing
Potassium channel
Potassium channel activation

Potential energy
Precapillary sphincter
Precess
Precession
Preconditioning
Preferential channel
Preload
Pressure
Pressure difference
Pressure energy
Pressure gradient
Pressure measurement, catheter
Pressure measurement, cuff
Pressure-stiffness graph
Pressure-strain elastic modulus
Pressure waveform
Pre-stress
Primary cilia
Primary hypertension
Prism element
Processing chain (for PSM)
Projection radiograph
Propagation model
Protein phosphorylation
Proteins
Proton
Pseudoplastic
PSM
PTV
Pullback
Pulmonary artery
Pulmonary circulation
Pulmonary valve
Pulse-echo
Pulse pressure
Pulse wave velocity
Purkinje fibres

Pushing beam
PVA
PVAc (vessel mimic)
PWV. *See* Pulse wave velocity

Q

QRS complex

R

Radial pressure waveform
Radioactivity
Radiofrequency
Radioisotope
Radius
Rapid prototyping
Reactive hyperaemia
Real-time
Received frequency (ultrasound)
Receiving coil
Reception (of ultrasound)
Recirculation. *See* Flow recirculation
Red cell
Red cell ghost
Reduced velocity
Reduced-order model
Re-entry
Reflected waves
Refraction
Refractive index
Refractive index matching
Refractory period
Regurgitation
Relaxation
Remodeling
Resistance, to flow
Respiratory pump

Reticulin
Reverse wave, flow
Reverse wave, pressure
Reynolds number
Rheology
Rigid-wall model
Rotational angiography
Rotational flow. *See* Helical flow
Rouleaux
Rupture

S

Saccular aneurysm
Sarcomere
Sarcoplasmic reticulum
Scar tissue
Scattering (of ultrasound)
Screening programme
Secondary circulation. *See* Collateral circulation
Secondary flow
Secondary hypertension
Secondary motion
Segmentation
Segre Silberberg effect
Selectin
Self-excited oscillations
Set-point hypothesis
Shear induced inertial lift
Shear modulus
Shear rate
Shear strain
Shear thickening fluid
Shear thinning fluid
Shear wave elastography
Shear wave velocity
Sickle cell
Sickle cell disease

Silicone (phantom material)
Simulation (general)
Simulation (specific)
Single-beam (ultrasound)
Single photon emission computed tomography (SPECT)
Sinus node
Sinusoidal capillary
Skewness
Slip process
Smooth muscle
Soft tissue
Solid
Solid mechanics
Solid modelling
Solid particle
Solver
Sound
Sound wave
Spatial resolution
Speckle
Spectral doppler
Spectral element method
Spectrin
Speed of sound
Spin (of nucleus)
Spin-lattice relaxation
Spin-spin relaxation
SPIO
Spiral flow
Spring
Starling's equation
Statins
Stenosis
Stent
Stiffness
Stiffness index (b)
Stokes domain

Strain
Strain elastography
Strain imaging
Streamline
Stress
Stress-strain graph
Stretch-sensitive ion channel
Stroke volume
Stroke work
Structural imaging
Subarachnoid haemorrhage
Subcritical / supercritical flow
Suction pressure
Superficial venous circulation
Superior vena cava
Superparamagnetic iron oxide particles
Supine
Suspension
Symmetric flow
Systemic circulation
Systole
Systolic pressure

T

T1
T1 relaxation
T2
T2 relaxation
Tachycardia
Tank-treading
Targetted contrast agent
Targetted MR contrast imaging
Targetted ultrasound contrast imaging
Tensegrity
Tensile testing
Tension
Tethering

Tethering forces
Tetrahedral element
Thermal irreversibility
Thermodilution
Thermoregulation
Thick filament
Thin filament
Thoroughfare channel
Thrombosis
Thrombus
TIA. *See* Transient ischaemic attack
Tight junction
Tissue mimic
Tissue mimicking material (TMM)
TOE. *See* Transoesophageal echocardiography
Tonometry
Tortuous artery
Tracer
Transducer
Transient ischaemic attack
Transit time flow probe
Transitional flow
Transmission (of ultrasound)
Transmitted frequency (ultrasound)
Transmitting coil
Transmural pressure
Transmural pressure
Transoesophageal echocardiography
Transverse magnetization
Trans-WSS
Tricuspid valve
Tube-law
Tubing (vessel mimic)
Tubular pinch effect. *See* Segre Silberberg effect
Turbulent flow

U

Ultimate strength
Ultrasmall superparamagnetic iron oxide particles
Ultrasound
Ultrasound elastography
Umbilical cord
Unactivated platelet
Uniaxial testing
Unloading
Upstream-downstream asymmetry
Urea
Urethane (tissue mimic)
USPIO

V

Valve
Valve plane
Valve sinus
Valvular agger
Varicose veins
Vascular graft
Vasoconstriction
Vasodilation
Vasomotion
Vasorelaxation
Vein
Vein graft
Velocity
Velocity field
Velocity profile
Velocity waveform
Vena cava
Vena contracta
Venous insufficiency
Venous reflux
Venous return
Venous valve
Ventricles

Venule
Vesicle
Vesicular transport
Vessel compliance
Vessel length
Vessel lumen diameter
Vessel mimic
Vessel mimicking material (VMM)
Vessel wall thickness
Virtual histology
Viscoelastic
Viscometer
Viscometry
Viscosity
Viscous force
Voigt model
Volumetric flow rate
von Willebrand factor
Vortices
Voxel

W

Wall induced inertial lift
Wall shear rate
Wall shear stress
Wall shear stress control
Wall thickness
Water hammer equation
Waveform
Wave inversion
Wavelength
White cell
WHO. *See* World Health Organisation
Whole artery phantom
Whole-body
Windkessel model
Wolff-Parkinson-White syndrome

Womersley number

Workflow

World Health Organisation

WSS. *See* Wall shear stress

X

X-ray imaging

X-ray venogram

Y

Yeoh model

Yield point

Young's modulus

Z

Z-disk

Zero-D model